TECHNICAL REPORT STANDARD TITLE PAGE

1. Report No.	2. Government Accession No.	3. Recipient's Catalog No.

4. Title and Subtitle
STRUCTURAL BEHAVIOR OF A SKEW TWO SPAN REINFORCED CONCRETE BOX GIRDER BRIDGE MODEL, VOL. II - REDUCTION, ANALYSIS AND INTERPRETATION OF RESULTS

5. Report Date
June 1980

6. Performing Organization Code

7. Author(s)
A.C. Scordelis, J.G. Bouwkamp, S.T. Wasti, D. Anicic

8. Performing Organization Report No.
UC SESM 80-2

9. Performing Organization Name and Address
Department of Civil Engineering
University of California
Berkeley, California 94720

10. Work Unit No.

11. Contract or Grant No.
D-4-156

12. Sponsoring Agency Name and Address
California Department of Transportation
Sacramento, California 95807

13. Type of Report and Period Covered
Final Report

14. Sponsoring Agency Code
RTA 13945-14134

15. Supplementary Notes
Prepared in cooperation with the State of California, Business and Transportation Agency, Department of Transportation and the U. S. Department of Transportation, Federal Highway Administration

16. Abstract

This is the second of a four volume sequence on the structural behavior of a skew two span four cell box girder bridge model as follows: Volume I - Design, Construction, Instrumentation and Loading; Volume II - Reduction, Analysis and Interpretation of Results; Volume III - Response during Ultimate Loading to Failure and Volume IV - Detailed Tables of Experimental and Analytical Results. In the present volume, a detailed presentation of the reduction, analysis and interpretation of the experimental and theoretical results obtained in testing a large scale 45° skew, two span, four cell, reinforced concrete box girder bridge model is given. The various computer programs used in obtaining theoretical results are described and compared. The methods and computer programs used for reduction of experimental data are also presented. Results, in terms of reactions, deflections, strains and moments, for the response of the bridge to dead load, working stress loads and at overload stress levels are given and comparisons between experimental and theoretical values are made. A review of the behavior under sustained dead load during the load history of the model is given with respect to strains, deflections and cracking. A comparison is made at all stages between the behavior of the skew bridge studied in this investigation, and of similar straight and curved bridges studied previously.

17. Key Words	18. Distribution Statement
Skew box girder bridge, continuous skew box girder; reinforced concrete model; large scale model; experimental study; dead load; live load; overloads; ultimate strength; measurement of reactions, deflections and strains.	Unlimited

19. Security Classif. (of this report)	20. Security Classif. (of this page)	21. No. of Pages	22. Price
Unclassified	Unclassified	407	

Form DOT F 1700.7 (8-69)

Structures and Materials Research
Department of Civil Engineering
Division of Structural Engineering
and
Structural Mechanics

UC-SESM Report No. 80-2

STRUCTURAL BEHAVIOR OF A SKEW TWO SPAN REINFORCED CONCRETE BOX GIRDER BRIDGE MODEL

VOL. II - REDUCTION, ANALYSIS AND INTERPRETATION OF RESULTS

by

A. C. Scordelis
J. G. Bouwkamp
Professors of Civil Engineering

S. T. Wasti
Research Engineer

and

D. Anicic
Associate Research Engineer

In cooperation with

State of California
Business and Transportation Agency
Department of Transportation
Under Research Technical Agreement
No. 13945-14134

and

U. S. Department of Transportation
Federal Highway Administration

College of Engineering
Office of Research Services
University of California
Berkeley, California

June 1980

DISCLAIMER

The contents of this report reflect the views of the authors who are reponsible for the facts and the accuracy of the data presented herein. The contents do not necessarily reflect the official views or policies of the State of California or the Federal Highway Administration. This report does not constitute a standard, specification or regulation.

ABSTRACT

This is the second of a four volume sequence on the structural behavior of a skew two span four cell box girder bridge model as follows: Volume I - Design, Construction, Instrumentation and Loading; Volume II - Reduction, Analysis and Interpretation of Results; Volume III - Response during Ultimate Loading to Failure and Volume IV - Detailed Tables of Experimental and Analytical Results. In the present volume, a detailed presentation of the reduction, analysis and interpretation of the experimental and theoretical results obtained in testing a large scale, 45° skew, two span, four cell, reinforced concrete box girder bridge model is given. The various computer programs used in obtaining theoretical results are described and compared. The methods and computer programs used for reduction of experimental data are also presented. Results, in terms of reactions, deflections, strains and moments, for the response of the bridge to dead load, working stress loads and at overload stress levels are given and comparisons between experimental and theoretical values are made. A review of the behavior under sustained dead load during the load history of the model is given with respect to strains, deflections and cracking. A comparison is made at all stages between the behavior of the skew bridge studied in this investigation and of similar straight and curved bridges studied previously.

KEYWORDS

Skew box girder bridge; continuous skew box girder; reinforced concrete model; large scale model; experimental study; dead load; live load; overloads; ultimate strength, measurements of reactions, deflections and strains.

TABLE OF CONTENTS

LIST OF TABLES

LIST OF FIGURES

List of Figures (Cont'd)

List of Figures (Cont'd)

List of Figures (Cont'd)

List of Figures (Cont'd)

List of Figures (Cont'd)

List of Figures (Cont'd)

List of Figures (Cont'd)

List of Figures (Cont'd)

List of Figures (Cont'd)

List of Figures (Cont'd)

1. INTRODUCTION

1.1 General Remarks

The present volume is the second of a four volume sequence on the "Structural Behavior of a Skew Two Span Reinforced Concrete Box Girder Bridge Model". The material included in each volume is as follows:

Vol. I - Design, Construction, Instrumentation and Loading

Vol. II - Reduction, Analysis and Interpretation of Results

Vol. III - Response During Ultimate Loading to Failure

Vol. IV - Detailed Tables of Experimental and Analytical Results

These volumes deal with the complete experimental and analytical study of a 1:2.82 scale skew box girder bridge model (Fig. 1.1) built and tested in the Structural Engineering Laboratory at Davis Hall at the University of California, Berkeley. The model was 72 ft (22 m) long, along the longitudinal centerline, 12 ft (3.66 m) wide and 1 ft 8 9/16 in. (0.52 m) in depth, and had an angle of skew of 45°. Bridge model dimensions; location and amounts of reinforcing steel; instrumentation and loading used for the model have been described in detail in Vol. I. For easy reference in the present volume, Figs. 1.2 and 1.3 depict the general dimensions of the model and the designation of transverse right and skew sections and longitudinal girder lines which are of pertinent interest.

1.2 Scope of Volume II

The present volume comprises the analysis of experimental data from the skew box girder bridge model and comparisons with theoretical

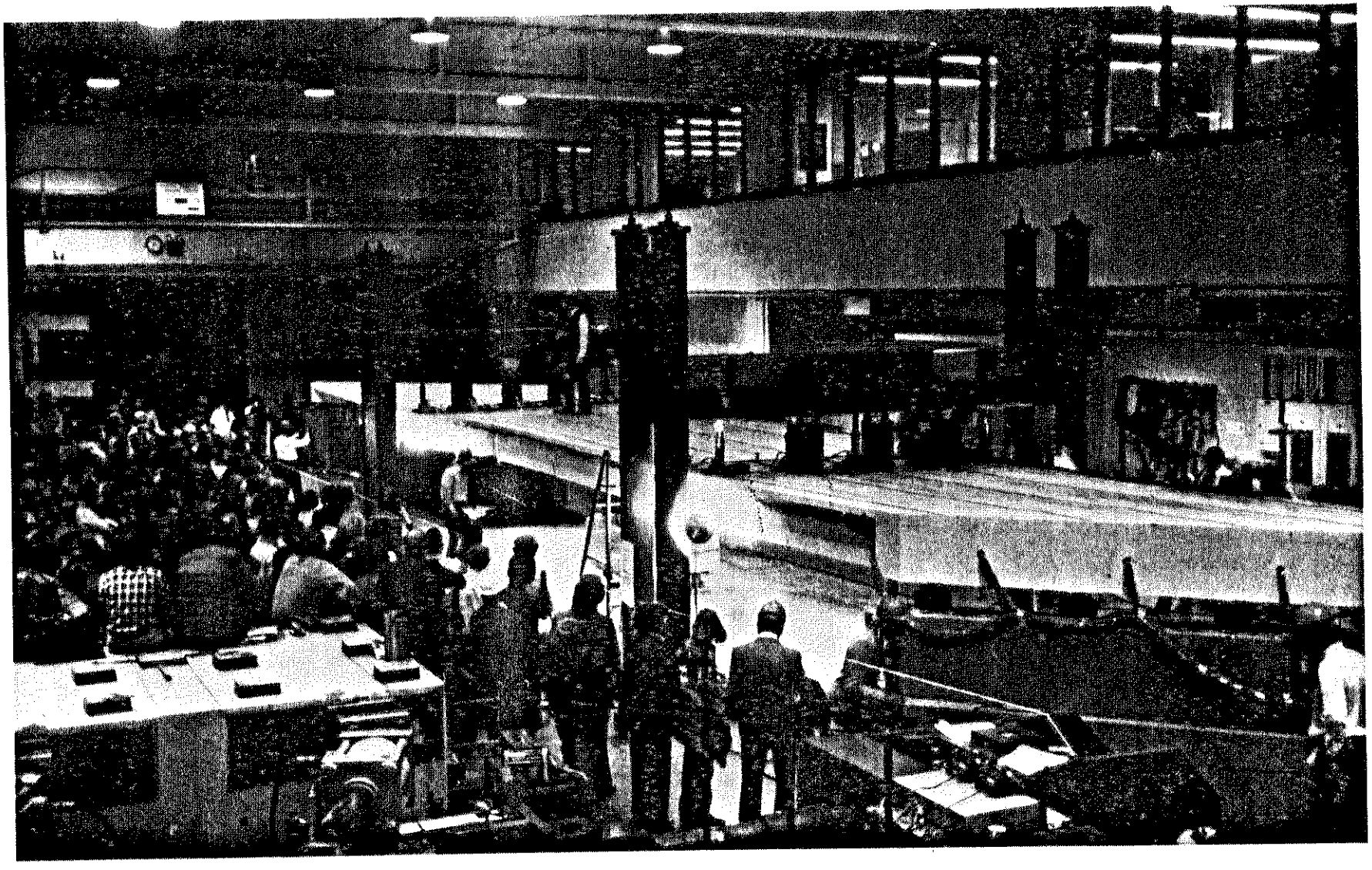

FIG. 1.1 FINAL LOAD TEST ON SKEW BOX GIRDER BRIDGE MODEL

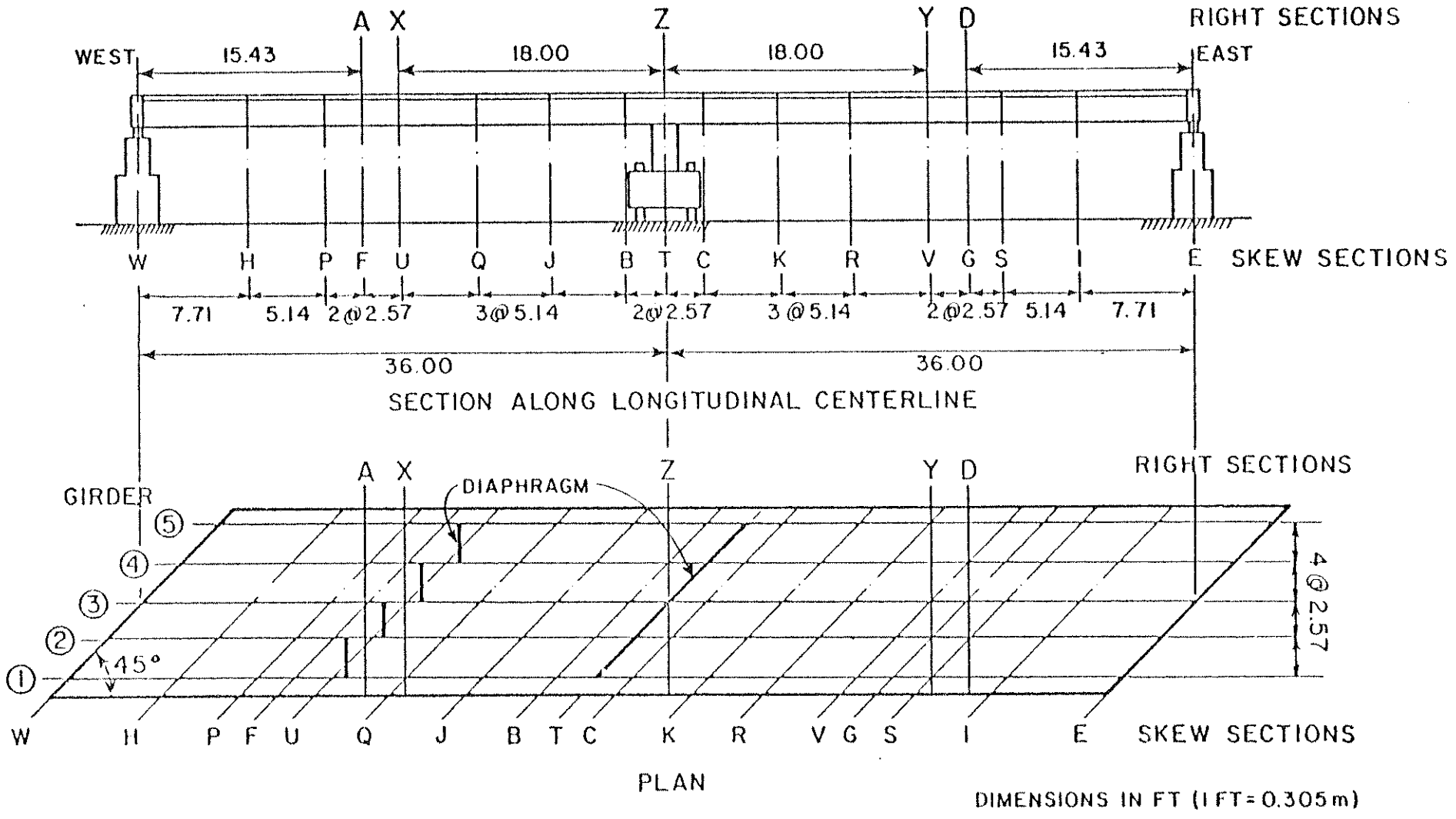

FIG. 1.2 DIMENSIONS OF SKEW BOX GIRDER BRIDGE MODEL WITH LOCATIONS OF TRANSVERSE SECTIONS AND LONGITUDINAL GIRDER LINES

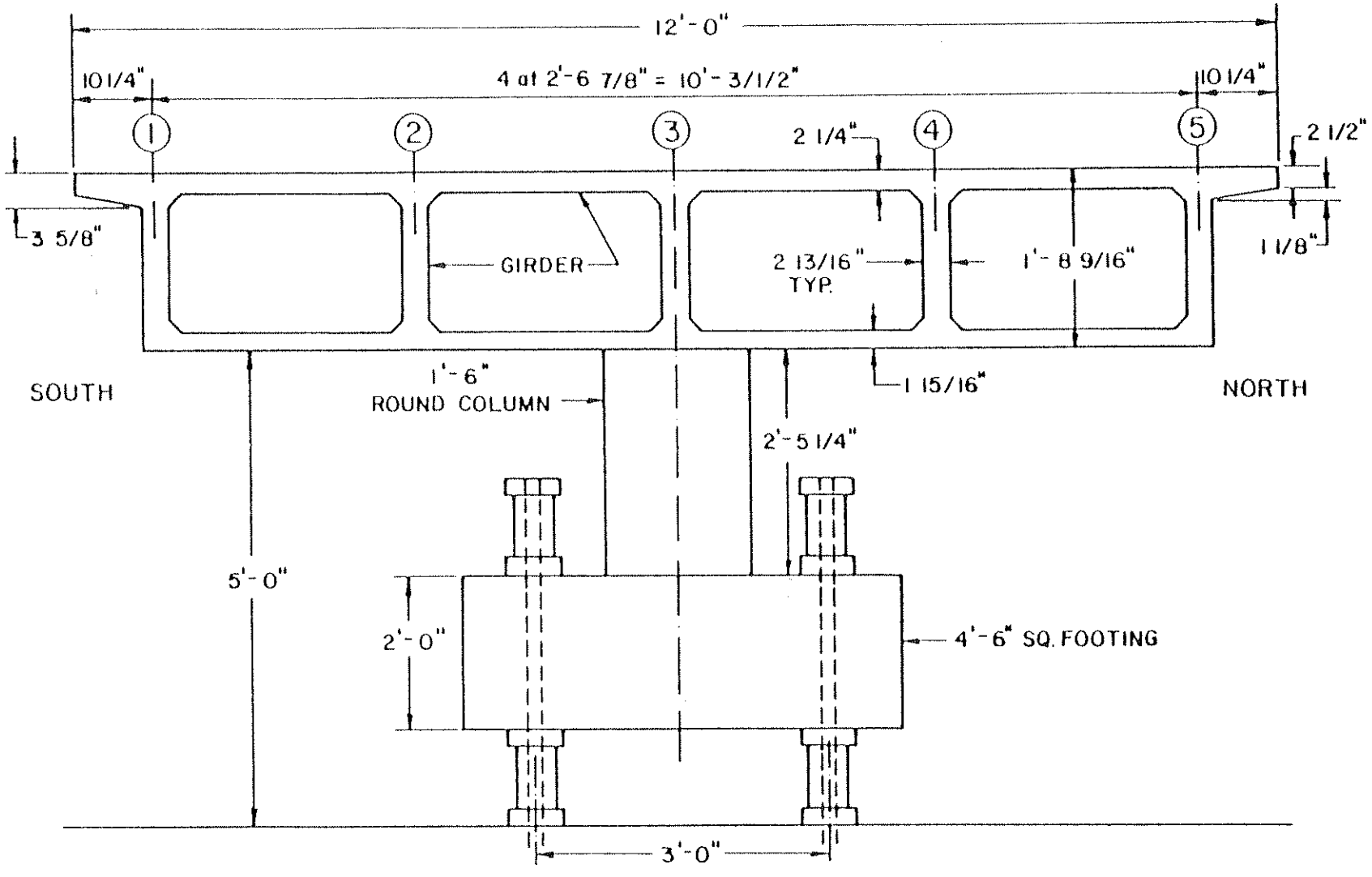

FIG. 1.3 TYPICAL SECTION OF BOX GIRDER BRIDGE MODEL

results obtained from the computer programs CELL [14] and SAP [49] as well as previously obtained data from the straight and curved bridge models investigated at the University of California, Berkeley [1 to 10].

While the main emphasis is placed on the part dealing with load distribution properties of the box girder bridge at working stresses, the dead load and overload cases and the whole history of the bridge are also treated in detail. Experimental data reduction is described, and data is presented for almost all loading cases of interest.

Each presentation of theoretical and experimental results is accompanied by interpretation and discussion with special reference to correlations and corroborations between the sets of results, checks for superposition and skew symmetry, evaluation of the effect of the midspan diaphragms,and comparisons with results from previous studies of similar straight and curved bridges [1 to 10]. Special attention is given to the effect of skewness of the bridge model and where possible, implications of the results with regard to design are considered.

Of particular interest from a load distribution standpoint at the working stress level is how accurately the proposed theoretical methods predict the results found in the experimental study with respect to the following three important items for a load anywhere on the bridge.

1. The total end support reactions consisting of a vertical reaction, a moment and a torque and their associated influence on the total midspan and center support external moments.

2. The total external and internal moments at the right midspan Sections A and D (Fig. 1.2).

3. The transverse distribution of these total moments at a section across the width of the bridge.

General detailed tables comparing theoretical and experimental results for reactions, deflections, strains, longitudinal stresses and moments are given in Volume IV for all load cases considered. Selected typical cases are taken from these tables and discussed in detail in the present volume. Results for dead load and for live loads producing a working stress of 30 ksi in the steel reinforcement are considered at length. Response of the bridge at and after overload stresses of 40, 50 and 60 ksi in the reinforcement is also examined. The linearity of the structural response during the overloading as well as afterwards is studied.

Attention is paid to the interpretation and applicability of theoretical results given by different analytical models. Different finite element meshes using the CELL program are studied and comparisons are made with results obtained by idealizing the box girder bridge model as a three dimensional frame composed of one dimensional beam and column members using the SAP program.

In addition, the whole scheme of cataloging, classifying and editing experimental data in several specially prepared computer post processing programs giving normalized results for comparison with theoretical values is also treated. These comparisons are made mainly for reactions, deflections, strains and moments. In most cases, pertinent theoretical and experimental data are presented in the text.

A study is also made of the shear behavior of the skew box girder bridge model with special interest paid to the transverse distribution

of the total shear force to the individual girders and the longitudinal variation of these individual girder shears.

A study of the time history experimental response of the bridge in terms of deflections and strains under sustained loading is presented covering both the construction phase and the entire testing period until loading to failure. The deterioration of the structure as indicated by cracking patterns after the completion of each successively increasing load phase is presented.

Finally, a summary, pertinent conclusions and general observations are presented covering the response of the bridge during the dead load, working load, and overload phases up to the 60 ksi stress level. The response during ultimate loading to failure is treated in Volume III.

2. EFFECTS OF SKEWNESS ON BOX GIRDER BRIDGE BEHAVIOR

2.1 General Remarks

The finite element computer program CELL provides a powerful tool for the analysis of box girder bridge systems and can be employed to assess the effects of skewness on the structural behavior of box girder systems. It is known that the introduction of skewness modifies the distribution of the reactions at the supports of a structure. From the CELL analysis, the reactions at the supports can be found and the external moment diagram drawn for a box girder bridge under a given loading. The longitudinal internal forces given by CELL can also be integrated over any section to yield the internal moment value at the section. The present chapter will consider the overall effects of skewness and skew diaphragms on the reactions and moments of box girder systems.

2.2 Simple Span Box Structure

For purposes of illustration, consider a simple, one-span, two cell box structure without skew, having the plan and cross-section shown in Fig. 2.1.a. The structure is simply supported at its two ends, and the loading consists of three midspan loads, one above each girder, of 1 kip (4.45 kN) each. The structural behavior of this box may now be compared with that of one which has the same loads and an identical cross-section, but with a 45° skew in plan, as shown in Fig. 2.1.b. Both straight and skew structures have, respectively straight and skew 0.1 ft (30.5 mm) thick diaphragms only at the two supported ends. For both structures, a homogeneous and isotropic material with $E = 432{,}000$ ksf (20,700 MPa) has been assumed. The reactions at the points of support may be calculated for the straight box as $R_A = R_B = R_C = R_D = 0.75$ k

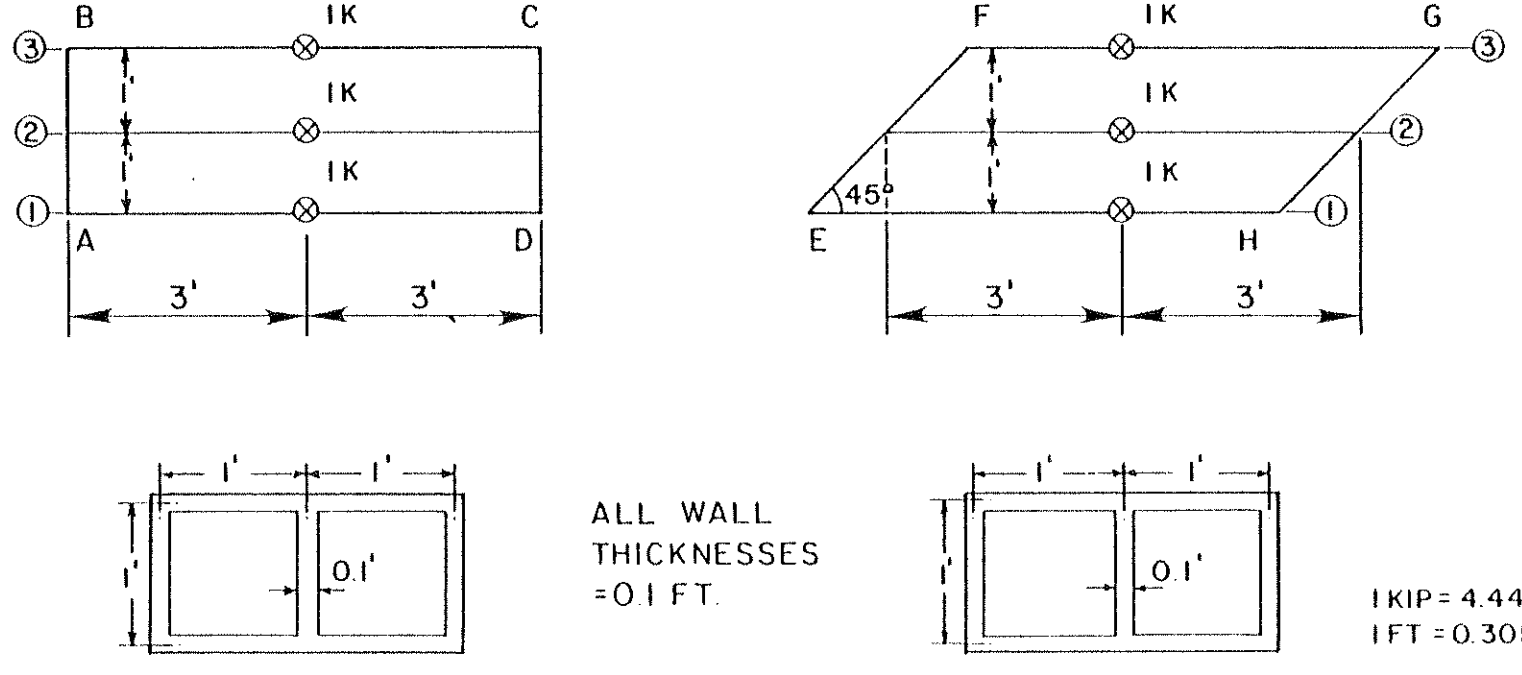

(a) PLAN AND SECTION OF SIMPLY SUPPORTED TWO CELL STRAIGHT BOX GIRDER

(b) PLAN AND SECTION OF SIMPLY SUPPORTED TWO CELL SKEW BOX GIRDER

FIG. 2.1 SINGLE SPAN STRAIGHT AND SKEW BOX GIRDERS

(3.34 kN) whereas for the skew box they are found from the computer program CELL to be $R_F = R_G = 0.096$ k (0.43 kN) and $R_F = R_H = 1.40$ k (6.23 kN) as shown in Fig. 2.2. The relatively large values of the reactions R_F AND R_H at the obtuse corners of the skew bridge indicate a tendency on the part of the bridge to span across FH and to carry the external load of 3 kips (13.3 kN) diagonally. Next, the midspan moments at the right sections X - X and X' - X' for the straight and skew boxes may be calculated from the external support reactions as $M_{X-X} = 4.50$ ft-kips (6.10 kN-m) and $M_{X'-X'} = 3.19$ ft-kips (4.33 kN-m) respectively. This dramatic drop in the midspan longitudinal moment varies with the angle of skew.

If it is desired to replace the loads and the reactions at the two ends of the straight box span by their resultants, i.e. a single load of 3 kips (13.3 kN) and two reactions of 1.5 kips (6.67 kN) each acting along the longitudinal centerline of the straight box, this presents no problem and the forces may simply be lumped as shown in Fig. 2.3(a). It may be verified that the external moment at any section of the structure has not changed. However, for the skew box it is observed that the resultant reactions and loads do not act along the longitudinal centerline of the structure but as shown in Fig. 2.3(b), with an eccentricity from the longitudinal centerline in the present case of 1.234 ft (0.38 m). When the reactions are shifted to the longitudinal centerline, end reaction torques and couples have to be introduced, as shown in Fig. 2.3(c). The effect of the skewness on the end reactions may thus be represented by the required additional presence of end torques and couples at both skew ends of the structure and also such reactions as would be needed for a similar straight structure under identical loading. Phrased differently,

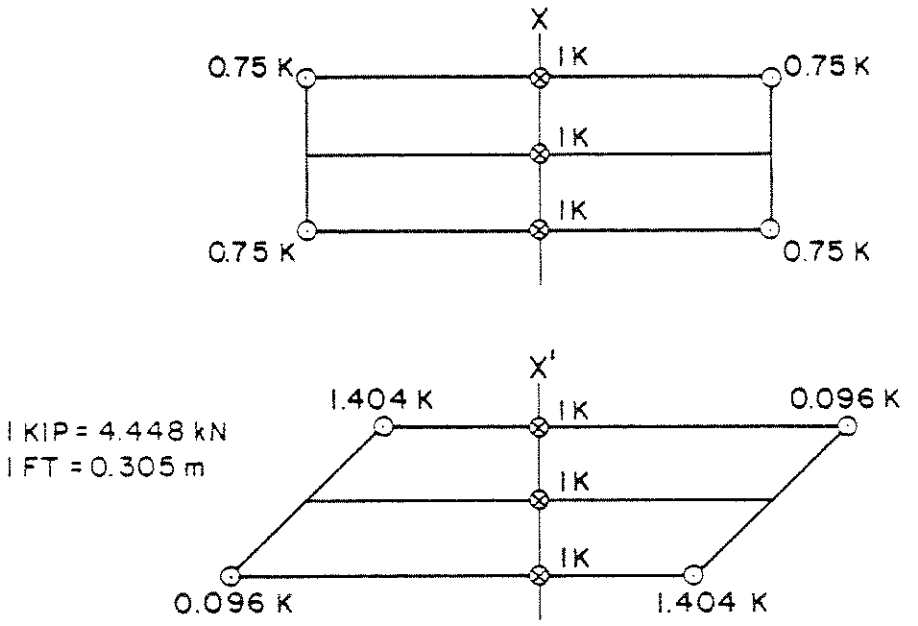

FIG. 2.2 SUPPORT REACTIONS FOR STRAIGHT AND SKEW BOX GIRDERS

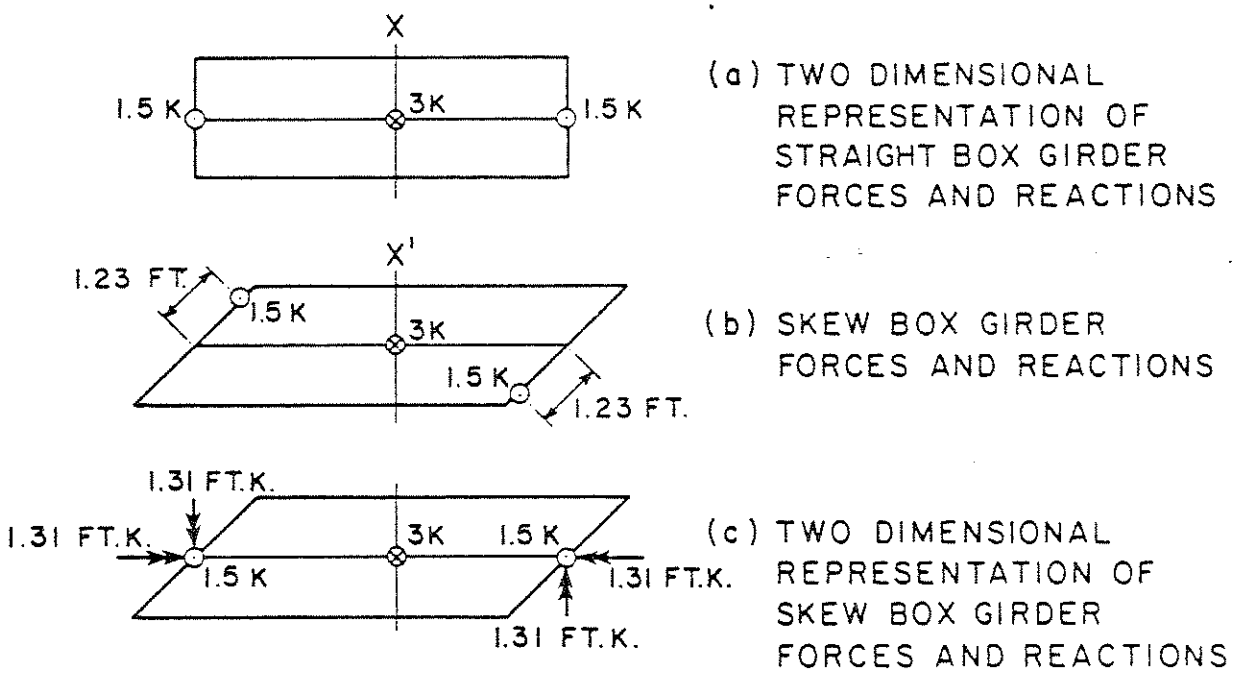

FIG. 2.3 CENTERLINE REACTIONS FOR STRAIGHT AND SKEW BOX GIRDERS

the skewness causes the reactions to be distributed longitudinally, thus materially altering the structural behavior.

With reference to the significant decrease in the value of the midspan moment, it might therefore be claimed that the diminution has been attained at the price of increasing torsional effects and negative bending effects. Given the high torsion resisting capacity and structural efficiency of the box section, however, these effects are not of primary importance when compared to the advantages of reducing the steel area required for the longitudinal reinforcement. In this connection it may be pointed out that in current design practice, the longitudinal reinforcement for skew box girders is usually designed as for straight bridges of similar span, thus not taking advantage of the reduction in longitudinal moment described above. However, it will be observed later that although the reduction is also obtained for the dead load case, it is not valid for point loads placed in those halves of skew bridges that include the acute support corners. For such loading cases the midspan moment is usually greater for skew box girder structures than for similar straight structures.

2.3 Continuous Two Span Two Cell Structure

In the case of a two span skew box girder structure, the effect of skewness is substantially the same: the reactions at the obtuse corners are high, and the midspan moments generally reduced. However, two additional factors have to be taken into account: the type of middle support, e.g. one or two columns, and the introduction of a center bent girder over (and often monolithic with) the middle support.

Two span, two cell straight and skew box girder structures shall now be analyzed for the same type of loading as before, i.e., a 1 kip

(4.45 kN) load over each girder at each midspan, as shown in Fig. 2.4. The cross-sections of the structures are identical with those of the single span box structures treated earlier. Each two span structure has a 0.1 ft. (31 mm) thick diaphragm at each end, and a 0.4 ft. (122 mm) thick center bent diaphragm with a support that prevents displacement but not rotation. Once again, the skew end and center bent diaphragms are placed at an angle of 45° with the longitudinal axis of the skew structure. The reactions for the two structures may be observed from Fig. 2.5. It is noticed that the sum of the two end reactions for the skew structure is now greater than that for the straight structure. However, the midspan moment M_X for the straight structure is calculated as 2.93 ft-kips (3.97 kN-m) as opposed to the value $M_{X'}$ equal to 2.45 ft-kips (3.32 kN-m) for the skew structure. When the two structures are treated as two dimensional structures based on the longitudinal centerline dimensions, the skew structure has the additional end moments and torques shown in Fig. 2.6. The diminution of midspan moment in the case of the two span skew box, while still marked, is not as great as that for the single simple span skew box of Fig. 2.1(b).

The effect of the center bent diaphragms on the structural behavior of the straight and skew boxes will next be assessed. If the center bent diaphragm is eliminated, and only the central column support remains, the reactions for the straight and skew boxes under the loading of 3 kips (13.3 kN) per span are as shown in Fig. 2.7. It is observed that the removal of the center bent diaphragm in both cases results in a smaller reaction at the central column and larger end reactions. The midspan moments at $X - X$ and $X' - X'$ increase to the values M_X = 3.40 ft-kips (4.61 kN-m) and $M_{X'}$ = 3.00 ft-kips (4.07 kN-m) respectively, indicating

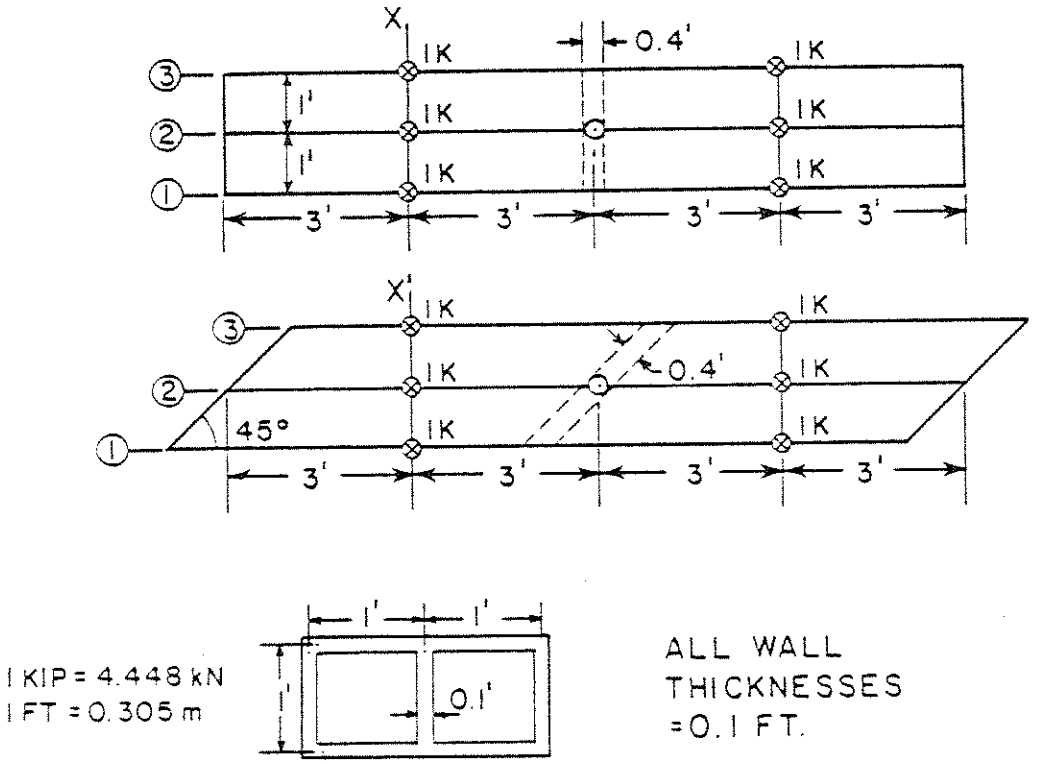

FIG. 2.4 DIMENSIONS OF TWO SPAN STRAIGHT AND SKEW BOX GIRDERS

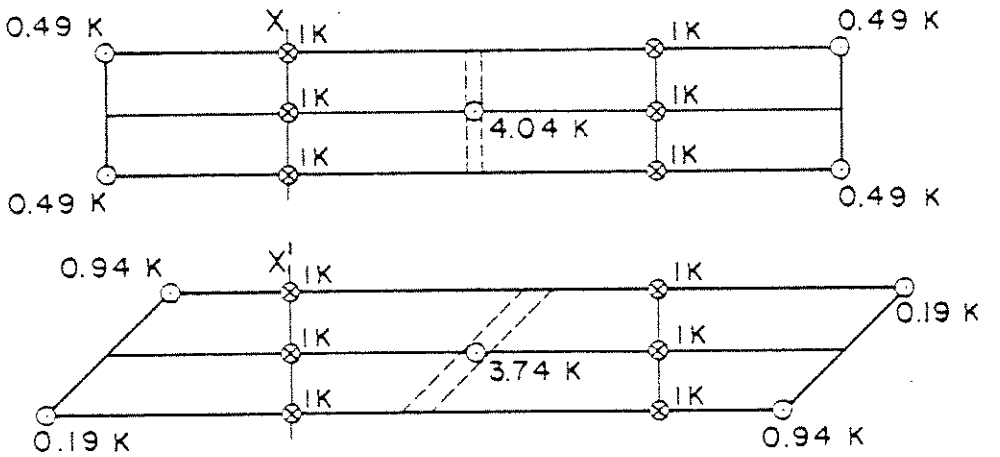

FIG. 2.5 SUPPORT REACTIONS FOR TWO SPAN STRAIGHT AND SKEW BOX GIRDERS

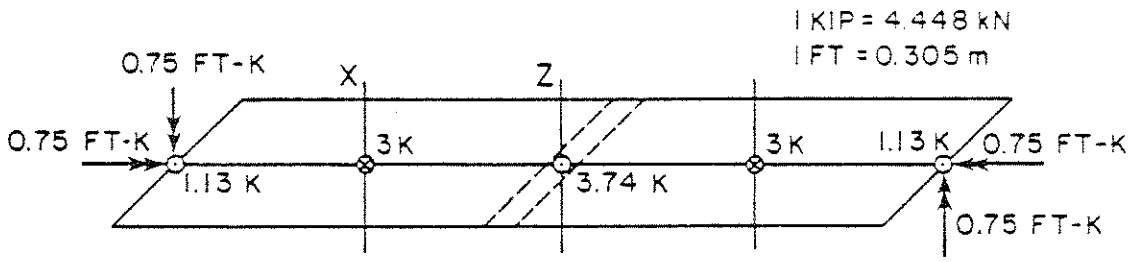

FIG. 2.6 CENTERLINE REACTIONS FOR TWO SPAN SKEW BOX GIRDER

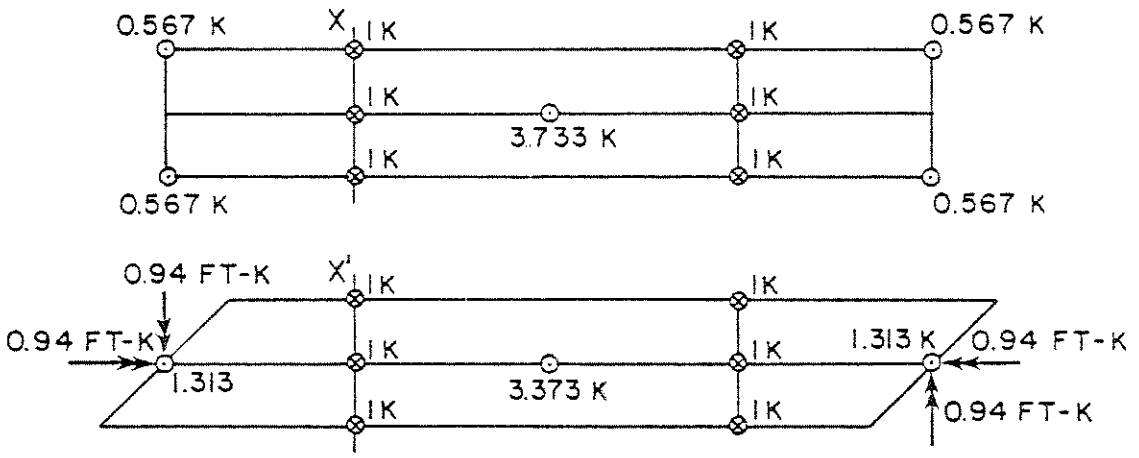

FIG. 2.7 REACTIONS FOR TWO SPAN STRAIGHT AND SKEW BOX GIRDERS WITHOUT CENTER BENT DIAPHRAGMS

that there is a relative reduction in the diminution of midspan moments without the center bent diaphragm for this case. The presence of the center bent diaphragm does, therefore, have the desirable effect of reducing the maximum positive midspan moments at section X and X'. Furthermore, as will be shown the center bent diaphragm has the even more favorable effect of lowering the center bent negative moment.

Figure 2.8 shows bending moment diagrams along the longitudinal axes for the straight and skew two span two cell boxes that have been treated in Figs. 2.4 to 2.7. The loading, as before consists of three loads of 1 kip (4.45 kN) each, one per girder at both right midspans. The reactions for the straight and skew box girders for this loading have already been calculated in Figs. 2.6 to 2.8 for the case of a 0.4 ft (122 mm) thick center bent diaphragm and for the case of no center bent diaphragm over the interior support. Using the above reaction values, the external moment diagrams for the two span straight and skew boxes have been plotted in Figs. 2.8(a) and 2.8(b) as shown by the dashed lines for the box without a center bent diaphragm and by the solid lines for the same box with a center bent diaphragm of 0.4 ft (122 mm) thickness. For the straight two span box with the center bent diaphragm it is observed that the midspan moment of 2.94 ft-kips (3.99 kN-m) is favorably smaller than the midspan moment of 3.40 ft-kips (4.61 kN-m) for the same box without the center bent diaphragm. As opposed to this, the moment at the center support as measured from the external reactions is -3.12 ft-kips (-4.23 kN-m) for the diaphragmed case as compared with -2.20 ft-kips (-2.98 kN-m) for the undiaphragmed case. When the internal moment from the CELL program is calculated at various right sections of the two span box, it is observed that the internal and external moments

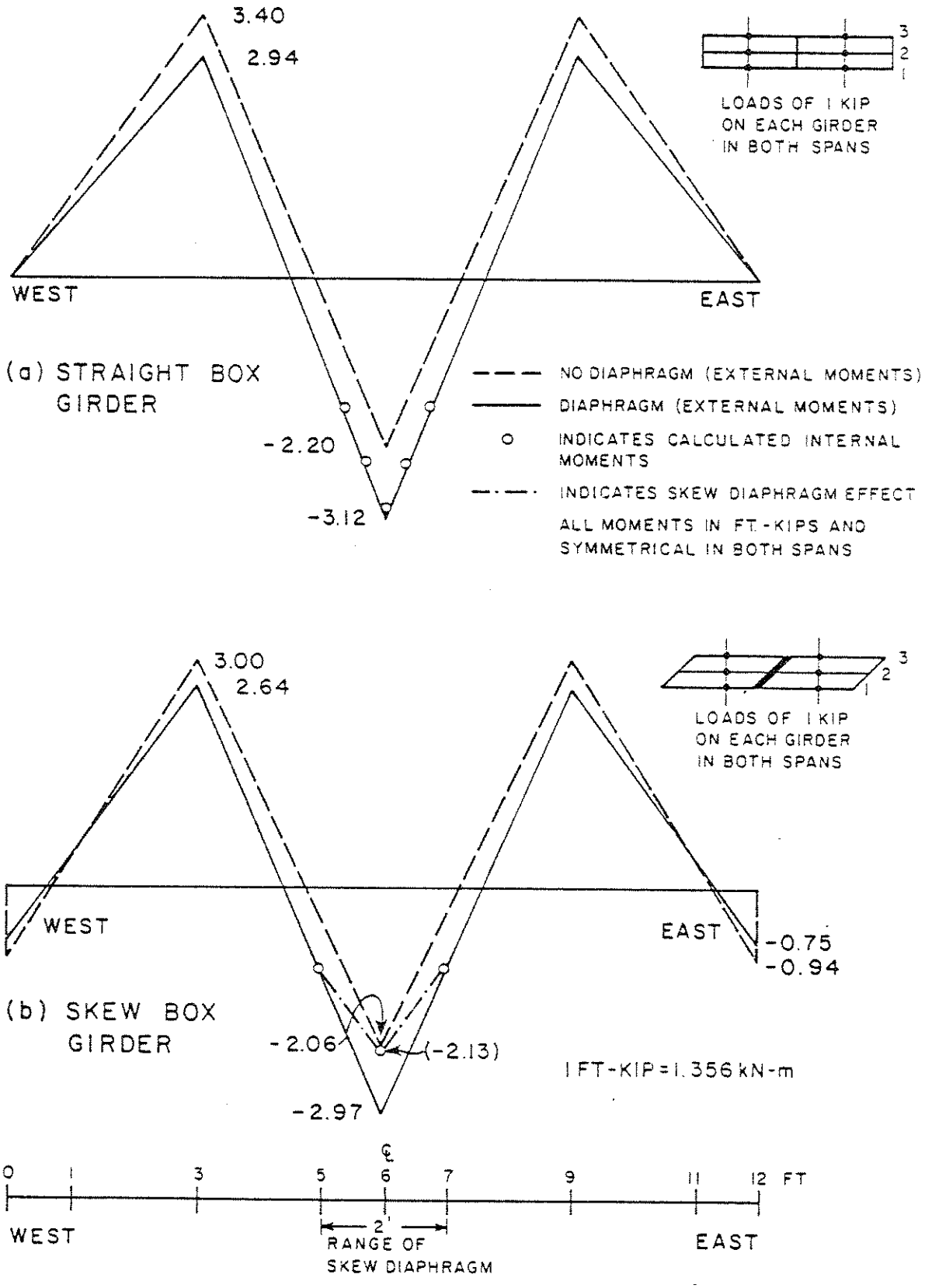

FIG. 2.8 EFFECT OF CENTER BENT DIAPHRAGM ON LONGITUDINAL MOMENT DISTRIBUTION FOR TWO SPAN STRAIGHT AND SKEW BOX GIRDERS

agree closely over the length of the two span box girder, as would be expected. The internal moments calculated at certain locations in the vicinity of the support diaphragm can be seen in Fig. 2.8(a), and show good agreement with the external moment values.

For the skew two span box, the presence of the center bent diminishes the midspan moment from 3.00 ft-kips (4.07 kN-m) to 2.64 ft-kips (3.58 kN-m) as shown in Fig. 2.8(b) by the dashed lines for the skew box without a diaphragm and by the solid lines for the skew box with a diaphragm of 0.4 ft. (122 mm) thickness. As in the case of the straight two span box, the moment at the center support measured from external reactions is higher for the diaphragmed case than for the undiaphragmed case: -2.97 ft-kips (-4.03 kN-m) versus -2.06 ft-kips (-2.79 kN-m). The external moments, however, are significantly larger than the internal moments calculated from the CELL program over the 2 ft. (0.61 m) range where the skew center bent diaphragm is located, and it is observed, as shown by the punctuated line in Fig. 2.8(b) that the support negative moment values are noticeably blunted by the presence of the skew diaphragm, with a maximum value for the internal moment at the center line calculated at -2.13 ft-kips (-2.89 kN-m). A comparison of Figs. 2.8(a) and 2.8(b) indicates clearly that the skewness of the center bent diaphragm has the substantially pronounced beneficial effect of causing the whole longitudinal region between the two ends of the skew diaphragm to act as a kind of broad support for the continuous box structure and the bending moment over this whole region is attenuated. The difference between the externally and internally evaluated moments in the center bent region, therefore, represents the contribution of the center bent diaphragm in carrying the support negative moment. A similar contribution

would be made by a skew center bent diaphragm in a straight box girder bridge.

It also needs to be pointed out that the presence of skew end diaphragms at the outer ends of the box girder bridge structure contributes to the higher reactions at the obtuse corner at the expense of the reactions at the acute corner. If the two end diaphragms are removed from the continuous two span skew box girder structure of Fig. 2.4, the reactions as given in Fig. 2.5 change from 0.94 kips (4.18 kN) at the obtuse corner to 0.76 kips (3.38 kN) and at the acute corner from 0.19 kips (0.85 kN) to 0.28 kips (1.25 kN). The center bent footing reaction changes from 3.74 kips (16.6 kN) to 3.92 kips (17.4 kN). While the construction of a box girder bridge structure without end diaphragms is not likely, their effect on the structural behavior of a skew box girder structure is to augment the difference between the reactions at the obtuse and acute corners.

2.4 Dead Load and Different Point Load Cases

Hitherto both the one and two span skew box girder structures have been analyzed for a loading case of equal point loads above each girder at midspan. In order to assess the effect of the load position on the structural behavior of skew structures, the skew, two span, two cell box structure of Fig. 2.5 with skew center bent and end diaphragms will now be analyzed using the CELL program for different load cases.

2.4.1 Dead Load

The support reactions for the dead load case for the straight and skew box girders, assuming a material density of 0.156 kips/ft^3 (2500 kg/m^3) are shown in Fig. 2.9. The reactions for the skew box girder

at the end abutments are observed to be smaller than those of the straight box girder. The midspan moments for the two box girders may then be calculated as 0.238 ft-kips (0.32 kN-m) at section X for the straight box girder and 0.177 ft-kips (0.24 kN-m) at the right midspan section X' for the skew structure. These results indicate that a 34% reduction in span moments due to skewness is valid for the case of dead load. The negative moment at the support section Z for the straight box girder will, however, be less than that for the skew box girder at the section Z'. The participation of the skew center bent diaphragm in the longitudinal bending will help to reduce the internal negative moment as earlier described, and thus a combination of favorable effects is possible. The dead load case is the most important and often the most severe load case in actual bridges and hence diminution in moment values is desirable.

2.4.2 Point Load on Exterior Girder in One Span

The reactions for both straight and skew box girders for a load of 1 kip (4.45 kN) on an exterior girder at one midspan section are shown in Fig. 2.10. When transferred to the respective centerlines of the two box girders the resultants are as given in Fig. 2.11. Although the vertical reaction at the west abutment of the skew box girder is less than that of the straight box girder, the external moment at section X of the straight box girder is M_X = 1.24 ft-kips (1.68 kN-m) whereas the moment at section X' for the skew box girder is $M_{X'}$ = 1.45 ft-kips (1.97 kN-m). The external moments at the support sections for the straight and skew box girders are calculated as M_Z = -0.52 ft-kips (-0.71 kN-m) and $M_{Z'}$ = -0.680 ft-kips (-0.92 kN-m).

Even though the internal moment at the support section Z' is reduced by the participation of the skew center bent in the bending

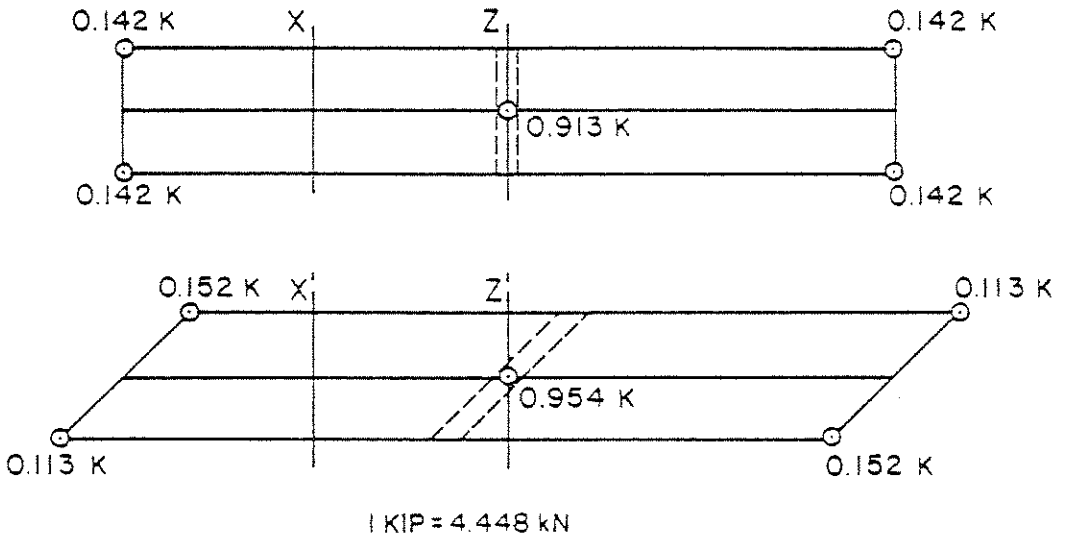

FIG. 2.9 SUPPORT REACTIONS FOR TWO SPAN STRAIGHT AND SKEW BOX GIRDERS UNDER SELF-WEIGHT

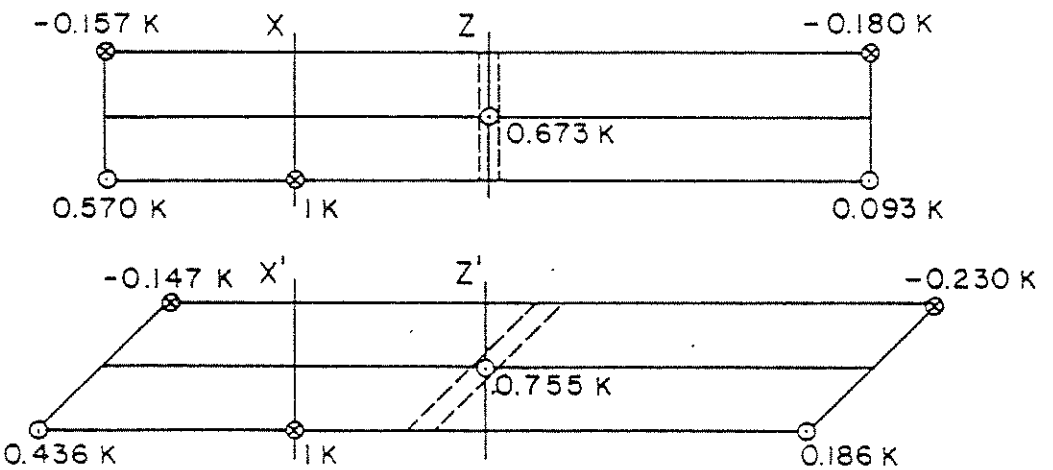

FIG. 2.10 SUPPORT REACTIONS FOR TWO SPAN STRAIGHT AND SKEW BOX GIRDERS UNDER POINT LOAD ON EXTERIOR GIRDER IN ONE SPAN

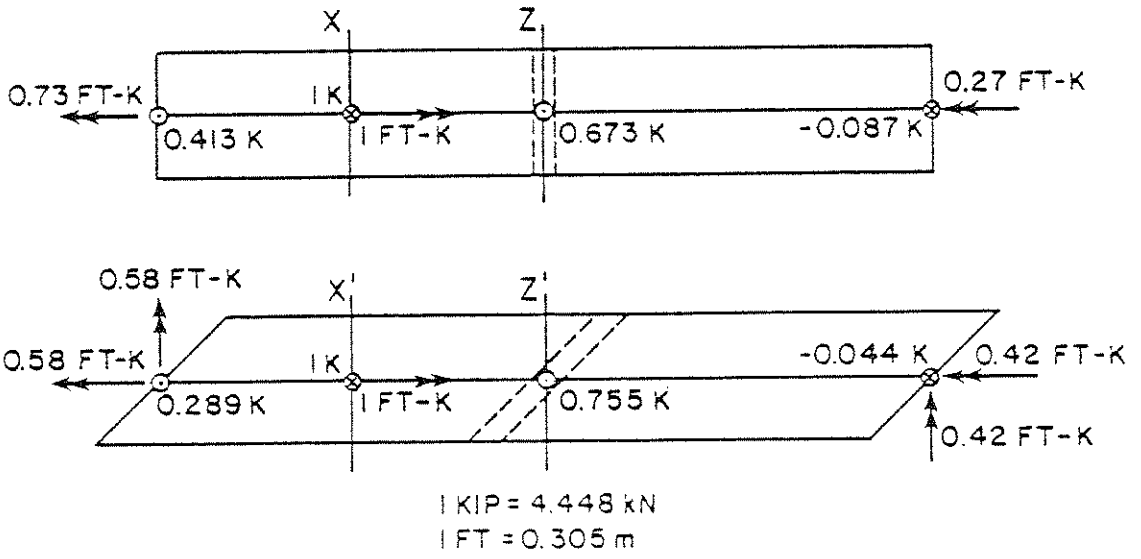

FIG. 2.11 CENTERLINE REACTIONS FOR TWO SPAN STRAIGHT AND SKEW BOX GIRDERS UNDER POINT LOAD ON EXTERIOR GIRDER IN ONE SPAN

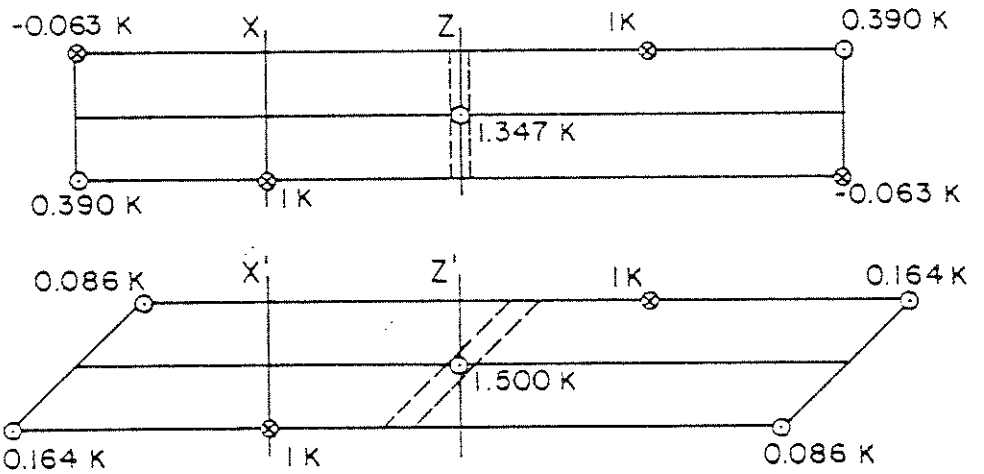

FIG. 2.12 SUPPORT REACTIONS FOR TWO SPAN STRAIGHT AND SKEW BOX GIRDERS UNDER SKEW-SYMMETRIC POINT LOADS

from -0.680 ft-kips (-0.92 kN-m) to -0.480 ft-kips (-0.65 kN-m), it is observed that the end abutment moment of 0.538 ft-kips (0.73 kN-m) augments the midspan moment for the case of the skew box girder. The skew has the effect of changing the sign of this external moment depending on the transverse position of the load, resulting in unfavorable increases in the span moment when the load is on an exterior girder in the half of the skew box girder that contains an acute angle support.

2.4.3 Skew-Symmetric Point Loads

On the basis of the above observations it can be concluded that a case such as the one shown in Fig. 2.12 is likely to yield unfavorable results for a skew box girder structure of the type considered, compared to a similar straight box girder, when the negative support moments are compared.

The reactions of Fig. 2.12 have been shifted to the centerline as resultants in Fig. 2.13. The external moments at the midspan sections are calculated as M_X = 0.981 ft-k (1.33 kN-m) and $M_{X'}$ = 0.828 ft-k (1.12 kN-m) whereby it is observed that the tendency of one load to increase the midspan positive moment is lessened by the other load in both the straight and skew box girders, and the skew box girder midspan moment is once again of smaller magnitude than the straight box girder midspan moment.

The negative support moments at sections Z and Z' may next be calculated from the external reactions to give M_Z = -1.038 ft-kips (-1.41 kN-m) and $M_{Z'}$ = -1.422 ft-kips (-1.93 kN-m). However, the internal moment at section Z' is calculated as -1.004 ft-kips (-1.36 kN-m), indicating that the relatively thick skew diaphragm of thickness 0.4 ft

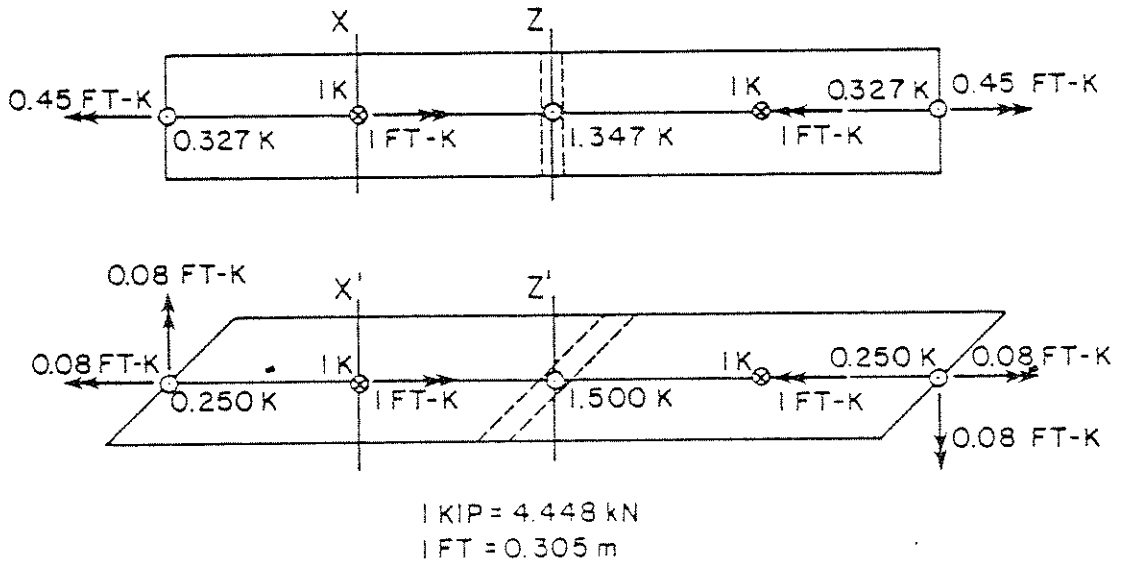

FIG. 2.13 CENTERLINE REACTIONS FOR TWO SPAN STRAIGHT AND SKEW BOX GIRDERS UNDER SKEW-SYMMETRIC POINT LOADS

(122 mm) as opposed to the girder thickness of 0.1 ft (31 mm) withstands a substantial moment.

2.5 Conclusions from CELL Analytical Study

The results of the preceding illustrative examples with fixed dimensions, span loads and skew angle can only provide a general indication of the effects of skewness and skew diaphragms on the structural behavior of box girder bridges and were carried out primarily in relation to the large scale skew, continuous box girder bridge model of the present study.

It is observed that the introduction of skewness favorably modifies the manner in which reactions both at the end supports and in the area of the skew center bent are distributed for the important cases of dead load and midspan loads over each girder in both spans. The skew center bent over its own range contributes to the longitudinal bending stiffness and as a result the internal moments in the box girder system within the range of the center bent are reduced. This modifies the shear, bending and torsional behavior of box girder bridges, and certain structural advantages also accrue from these changes.

The midspan moments are unfavorably modified when point loads are placed at the midspans of girders which lie in the bridge halves that include the acute support corners. With reference to the skew, continuous two span, four cell reinforced concrete box girder bridge model of the present investigation, detailed results for reactions, deflections and moments for dead load and all point loads are given in later chapters of this volume.

3. THEORETICAL ANALYSES

3.1 General Remarks

The theoretical analysis of the skew, reinforced concrete box girder bridge model of the present study was carried out using different linear elastic finite element models. In all cases the reinforced concrete box girder bridge was considered to be an elastic, homogeneous, isotropic and uncracked concrete structure in which the reinforcement was ignored. The computer programs SAP [49] and CELL [14] which were used for the analysis of these models are briefly summarized below:

SAP program (1972) [49]

The purpose of this versatile, general purpose program is to perform linear elastic analyses of three dimensional structural systems. These systems may be composed of a number of structural element types. For the bridge model studies, SAP was only used to analyze a simplified model of the bridge idealized as a three dimensional frame made up of one dimensional beam and column members. This simplified model was used for direct comparison with the CELL results.

CELL program (1970) [14]

This finite element program analyzes cellular structures of constant depth with arbitrary plan geometry. The structure must be made up of top and bottom decks and vertical webs and diaphragms. Two different finite element types incorporating both membrane and plate bending effects are used to capture the main behavior of the deck and web components. Each of these elements has five degrees of freedom at each corner node. Orthotropic plate properties and arbitrary loadings and boundary conditions can be treated.

CELL is one of a number of computer programs, which have been developed especially for box girder bridges at the University of California. A summary of the various analytical solutions and computer programs developed may be found in References [17,18]. Details of each

of these programs including input-output formats and Fortran source listings, are given in the research reports [1 to 20].

3.2 CELL Analyses

For the CELL analyses two finite element discretizations termed CELL COARSE and CELL FINE were used to model the skew box girder bridge. The mesh layouts for CELL COARSE and CELL FINE are shown in Fig. 3.1.

CELL COARSE was used for preliminary parameter studies, such as the assessment of the effect of various assumed support conditions at the end abutments and at the center bent. It was also used for the final results for the 40 load positions of the moving fork lift truck on the top deck from which theoretical influence lines were drawn. This was done to minimize computer costs.

CELL FINE was used for all other final analyses for dead load, block loads, conditioning loads and all points loads. Results of these final analyses are tabulated in Vol. IV and also used in this Vol. II of the present study for comparison with experimental results. It should be noted that in general, unless otherwise stated, results for conditioning loads and point loads have been normalized to 100 kip (445 kN) loads per span for ease of comparison.

3.2.1 CELL COARSE Model and Solutions

The CELL COARSE finite element model (Fig. 3.1) consists of 231 nodal points (one nodal point represents a pair of top and bottom nodes). Since each nodal point has 5 degrees of freedom, each load case analyzed involved the solution of $5(2)(231) = 2310$ simultaneous equations.

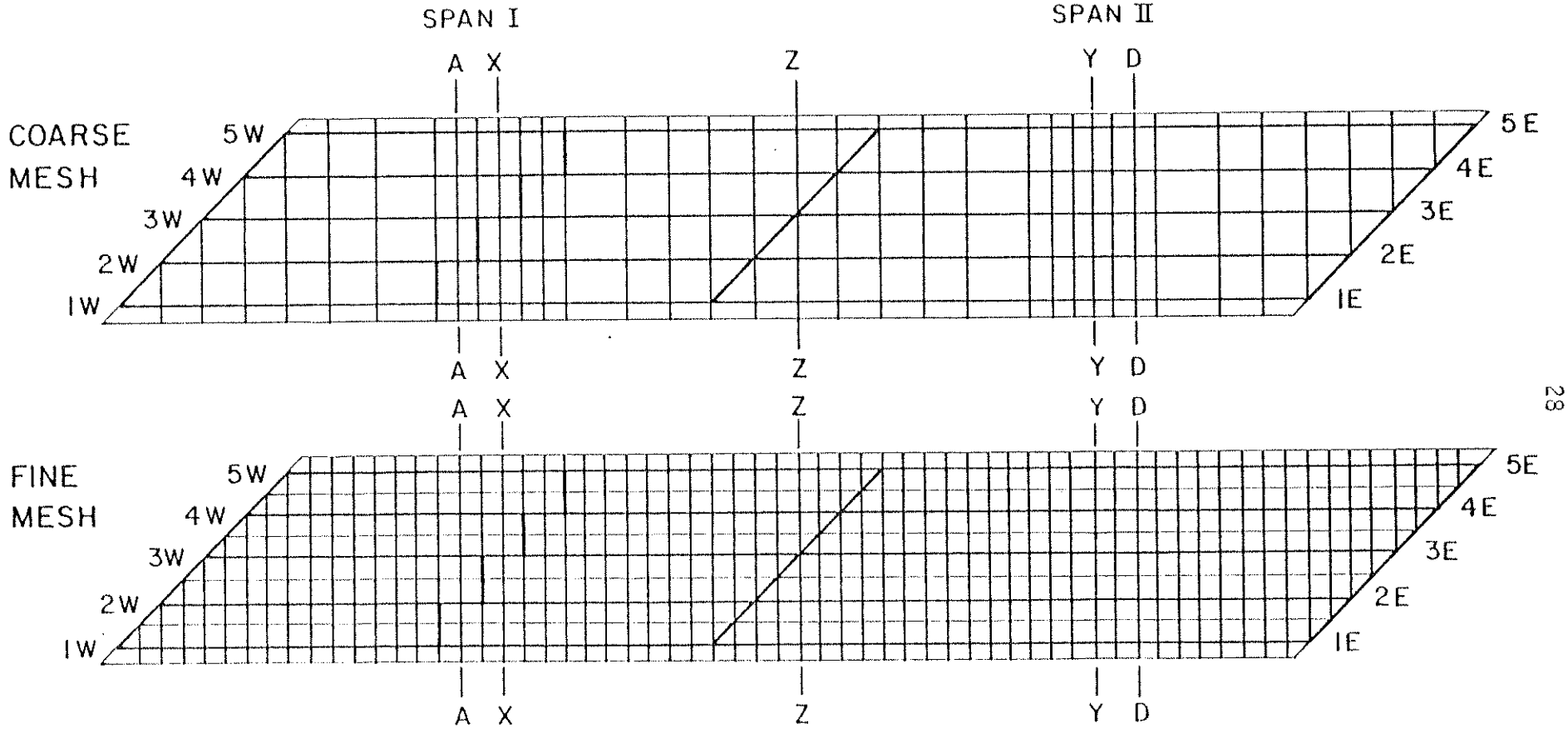

FIG. 3.1 MESH LAYOUTS FOR CELL FINITE ELEMENT ANALYSES

The top and bottom slab decks are composed of 200 elements. The side top deck cantilever portions of the bridge are modelled by assigning zero stiffness (zero thickness) to the corresponding bottom slab elements. A total of 176 vertical web elements were used to connect the top and bottom slabs. These were located along the five longitudinal girder webs, the center and end abutment diaphragms and the staggered midspan diaphragm in Span I. The stiffness of the vertical web elements is concentrated along the corresponding nodal line where the top and bottom slab are connected.

Because CELL does not have an automatic provision for introducing boundary conditions of arbitrary stiffness using boundary spring elements, the program was modified especially for the support conditions of the skew bridge model.

At the location of the center column the exact column stiffnesses were added to the global stiffness matrix at the location of the bottom deck where the column would be connected. The necessary quantities representing the column stiffness were calculated by assuming the column fixed at its base and then subjecting the top of the column to unit displacements for each of the 5 degrees of freedom involved. The 1.5 ft (0.46 m) diameter column had a length of 2.44 ft (0.74 m) from the top of the footing to the bottom of the bridge cross-section and a modulus of elasticity of 442,000 ksf (21,000 MPa).

At each end abutment the actual box girder bridge model was supported at 5 points on girder lines 1 to 5 by an assembly of steel plates, load cells and elastomeric pads. The measured stiffness of the elastomeric pads at the different support points varied between

3500 kips/ft (51,000 kN/m) and 6700 kips/ft (97,700 kN/m) with an average of 5700 kips/ft (83,100 kN/m) for all support points.

In an initial trial run, the CELL COARSE model was used with vertically rigid supports at the end abutments. The distribution of the five vertical and reactions for this case was found to be quite different from the experimental data, whereas the total vertical end reaction at each end abutment was in good agreement with the experimental data. In order to improve the analytical model, the rigid end supports in the CELL program were replaced by vertical springs, by incorporating the spring stiffness in the solution. A parametric study with the CELL COARSE mesh was made using the following assumptions for the end abutment support stiffnesses:

(1) end supports with individual spring stiffnesses equal to the measured stiffness of each elastomeric pad.

(2) end supports with a uniform spring stiffness of 5700 kips/ft (83,100 kN/m) equal to the mean stiffness of all ten elastomeric pads.

(3) vertically rigid supports

From this parameter study it was found that the distribution of the individual end reactions was virtually the same for the cases where individual or average spring stiffnesses for the elastomeric pads were used, indicating that either assumption could be used for the analysis. However, this distribution changed significantly for the case where rigid supports were used.

A comparison between the experimental reactions at the 30 ksi working stress level, CELL COARSE reactions for an average spring stiffness of 5700 kips/ft (83,100 kN/m) and CELL COARSE reactions for vertically rigid supports is shown in Table 3.1 for the conditioning load case of 100 kips (445 kN) per span and the load case 1X, i.e. a point load of 100 kips (445 kN) at location 1X.

Several points can be made from the results in Table 3.1:

(1) The total analytical resultant vertical reaction at the end and center supports are quite close for the rigid and spring end supports and they are in relatively good agreement with the experimental values.

(2) The distributions of the total analytical end reactions to the individual girder supports are quite different for the rigid and spring end supports with the latter case giving analytical results which are in better agreement with the experimental values.

(3) It is evident that in an actual bridge structure the distribution of the total end reaction would be very difficult to predict analytically without some knowledge of the spring stiffnesses of the supports.

As a result of this parameter study a spring stiffness of 5700 kips/ft (83,100 kN/m) was used for each of the end abutment support points for all the computer analyses with CELL. Details of the evaluation of the elastomeric pad stiffness are given in Chapter 6, Volume I of the present sequence of research reports.

TABLE 3.1 INFLUENCE OF END SUPPORT STIFFNESS k ON DISTRIBUTION OF REACTIONS

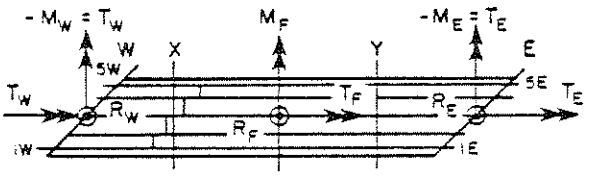

LOAD CASE	CONDITIONING LOAD			1X		
REACTION	CELL COARSE k = ∞	CELL COARSE k = 5700 kip/ft	EXPT. 30 KSI LEVEL	CELL COARSE k = ∞	CELL COARSE k = 5700 kip/ft	EXPT. 30 KSI LEVEL
1W	-0.4	-1.1	0.6	4.9	13.2	11.2
2W	1.8	2.1	3.5	19.3	16.4	17.2
3W	7.1	5.8	8.0	12.1	14.8	19.1
4W	1.2	10.8	9.7	39.6	4.9	3.0
5W	26.8	18.2	14.1	-43.7	-16.7	-16.9
TOTAL RW	36.6	35.8	35.8	32.2	32.6	33.6
1E	27.0	18.3	14.4	26.00	12.6	13.7
2E	0.9	10.7	10.7	-18.2	0.5	0.3
3E	7.0	5.7	3.9	-3.1	-5.3	-4.6
4E	2.0	2.1	4.8	-7.6	-6.8	-3.5
5E	-0.4	-1.1	1.2	-2.3	-6.2	-5.8
TOTAL RE	36.6	35.8	34.9	-5.2	-5.3	-6.0
RF	126.8	128.3	135.0	73.0	72.7	74.0
TOTAL R	200.0	200.0	205.7	100.0	100.0	101.7
MW	-139	-121	-86	197	184	181
ME	138	122	83	118	115	125

1 KIP = 4.448 kN
1 FT = 0.305 m

The actual bridge model was supported at the end abutments by the elastomeric pads and teflon coated steel plates, which theoretically permitted horizontal movement in any direction. Thus no horizontal supports could be applied to the finite element model at the end abutment nodes without introducing unrealistic restraints to the model. The only horizontal restraint for the bridge model was provided by the center bent column, and this was modeled analytically using the appropriate stiffnesses added to the bottom node of the cellular structure at the column location. However, no rotational stiffness about the column axis could be added, since this degree of freedom is not included in the CELL five degree of freedom per node finite element model. In order to prevent rigid body modes of displacement, additional horizontal restraints were necessary in the analytical model to prevent rotation about the center bent column axis. To model this situation as closely as possible a stiff horizontal spring was added to each of the two bottom nodes on either side of the center column node along the center bent diaphragm axis. This preserved the symmetry of the structure as well as the unrestrained horizontal movement at the two end abutments of the bridge.

3.2.2 CELL FINE Model and Solutions

The CELL FINE finite element model (Fig. 3.1) consists of 627 pairs of nodal points (top and bottom) and thus each load case analyzed involved the solution of $5(2)(627) = 6270$ simultaneous equations. The top and bottom slab decks are each composed of 576 deck elements, and a total of 312 vertical web elements were used to connect the top and bottom slabs. It should be noted in Fig. 3.1 that the discretization lines of CELL COARSE are included in the CELL FINE mesh and

therefore CELL FINE represents a refinement of CELL COARSE. In addition to this, CELL FINE also incorporates a modelling of the web flares by a stepped variation of the web element thickness along the girder lines, in order to model the actual bridge structure as closely as possible.

The CELL FINE support conditions incorporated the final added spring stiffnesses of 5700 kips/ft (83,100 kN/m) at each end abutment support and the column stiffness and horizontal springs at the center bent support described in Section 3.2.1 for CELL COARSE.

For both the CELL FINE and CELL COARSE analyses the following average values of moduli of elasticity, taken from the experimental data were used in the analysis of the gross uncracked concrete structure.

Top slab	= 434,000 ksf (20,800 MPa)
Bottom slab	= 442,000 ksf (21,100 MPa)
Webs	= 442,000 ksf (21,100 MPa)
Column	= 442,000 ksf (21,100 MPa)
Poisson's ratio	= 0.15

Detailed results of the material control tests, which form the basis for the above values are given in Chapter 6, Volume I.

3.2.3 Comparison of CELL COARSE and CELL FINE Results

Comparisons between the results for reactions, deflections, internal forces, internal moments and external moments as obtained using CELL COARSE and CELL FINE for several important load cases are shown in Tables 3.2 to 3.7. From these tables it can be seen that the refinement of the finite element mesh from CELL COARSE to CELL FINE yields results which do not differ significantly. One reason for the small differences encountered is the different modelling of the flares in CELL FINE.

TABLE 3.2 REACTIONS (KIPS OR FT-KIPS) FROM CELL FINE AND COARSE MESH ANALYSES

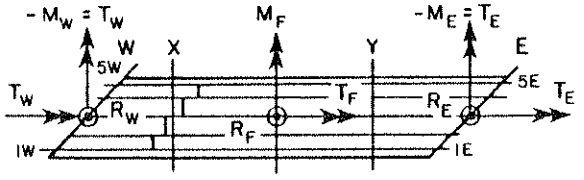

REACTIONS (KIPS OR FT-KIPS)								
LOAD CASE	CELL	WEST END		CENTER COLUMN			EAST END	
		RW	TW = -MW	RF	TF	MF	RE	TE = -ME
CL	COARSE	35.8	121	128.3	0	0	35.8	-122
	FINE	35.6	122	128.3	0	0	35.6	-122
DL	COARSE	16.6	19	46.4	0	0	16.3	-19
	FINE	16.7	19	48.2	0	0	16.4	-19
BLOCKS	COARSE	*	*	*	*	*	*	*
	FINE	25.0	37	46.7	0	0	25.0	-37
1X	COARSE	32.6	-184	72.7	-215	138	-5.4	-115
	FINE	32.5	-193	72.9	-196	117	-5.4	-125
3X	COARSE	42.5	98	64.1	-77	103	-6.7	-21
	FINE	42.5	93	64.4	-69	91	-6.9	-25
5X	COARSE	52.6	390	55.7	53	69	-8.3	72
	FINE	52.6	390	55.9	51	64	-8.5	73
1Y	COARSE	-8.2	-70	55.5	-53	-67	52.7	-391
	FINE	-8.4	-72	55.8	-51	-63	52.7	-392
3Y	COARSE	-6.7	20	64.2	76	-104	42.5	-96
	FINE	-6.9	24	64.5	68	-93	42.4	-92
5Y	COARSE	-5.3	112	72.7	217	-137	32.6	183
	FINE	-5.5	125	73.0	198	-117	32.5	192
1X + 5Y	COARSE	27.3	-69	145.4	1	0	27.3	67
	FINE	27.0	-68	145.9	1	0	27.1	67
1X +1Y	COARSE	24.4	-254	128.2	-269	71	47.4	-506
	FINE	24.1	-264	128.7	-247	54	47.3	-517

*Values not computed for CELL COARSE

1 KIP = 4.448 kN
1 FT = 0.305 m

TABLE 3.3 LONGITUDINAL DISTRIBUTION OF DEFLECTIONS ($FT \times 10^{-2}$) AT CENTER GIRDER 3

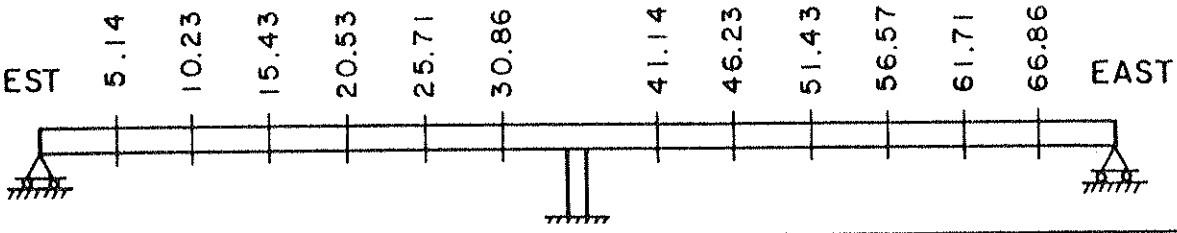

LOAD CASE	CELL	DEFLECTIONS ($FT \times 10^{-2}$) ALONG GIRDER 3											
		5.14	10.29	15.43	20.57	25.71	30.86	41.14	46.29	51.43	56.57	61.67	66.86
CL	COARSE	1.53	2.76	3.42	3.09	1.93	0.66	0.65	1.91	3.06	3.40	2.74	1.52
	FINE	1.51	2.74	3.42	3.08	1.88	0.63	0.63	1.87	3.06	3.40	2.73	1.51
DL	COARSE	0.39	0.63	0.72	0.70	0.42	0.16	0.14	0.39	0.59	0.67	0.60	0.37
	FINE	0.40	0.64	0.73	0.64	0.42	0.16	0.14	0.39	0.60	0.68	0.60	0.38
BLOCKS	COARSE	*	*	*	*	*	*	*	*	*	*	*	*
	FINE	0.76	1.22	1.37	1.18	0.75	0.26	0.25	0.74	1.16	1.35	1.22	0.76
1X	COARSE	3.40	5.70	6.75	6.18	4.50	2.20	-1.51	-2.45	-2.85	-2.76	-2.23	-1.32
	FINE	3.45	5.80	6.90	6.32	4.58	2.24	-1.58	-2.57	-3.00	-2.91	-2.36	-1.40
3X	COARSE	2.38	4.30	5.49	5.28	3.77	1.78	-1.08	-1.72	-1.93	-1.80	-1.39	-0.79
	FINE	2.41	4.36	5.58	5.37	3.79	1.79	-1.12	-1.79	-2.02	-1.89	-1.46	-0.83
5X	COARSE	1.15	2.43	3.33	3.51	2.64	1.24	-0.68	-1.02	-1.07	-0.89	-0.60	-0.27
	FINE	1.14	2.43	3.36	3.54	2.62	1.23	-0.69	-1.04	-1.09	-0.91	-0.51	-0.28
1Y	COARSE	-0.27	-0.59	-.088	-1.04	-1.00	-0.66	1.19	2.47	3.24	3.19	2.35	1.11
	FINE	-0.28	-0.60	-0.89	-1.06	-1.02	-0.67	1.18	2.46	3.26	3.22	2.36	1.10
3Y	COARSE	-0.78	-1.39	-1.80	-1.93	-1.72	-1.09	1.86	4.00	5.79	5.99	4.54	2.47
	FINE	-0.83	-1.46	-1.89	-2.02	-1.79	-1.13	1.86	4.01	5.86	6.08	4.59	2.50
5Y	COARSE	-1.32	-2.24	-2.77	-2.86	-2.45	-1.51	2.18	4.43	6.04	6.47	5.53	3.34
	FINE	-1.40	-2.37	-2.92	-3.00	-2.58	-1.58	2.22	4.52	6.18	6.62	5.64	3.40
1X + 5Y	COARSE	2.07	3.46	3.99	3.33	2.04	0.69	0.67	1.98	3.19	3.71	3.29	2.02
	FINE	2.05	3.43	3.98	3.31	2.00	0.66	0.65	1.95	3.18	3.70	3.28	2.00
1X + 1Y	COARSE	3.12	5.10	5.88	5.14	3.50	1.54	-0.33	0.22	0.39	0.43	0.12	-.22
	FINE	3.18	5.20	6.00	5.26	3.56	1.57	-0.40	-0.11	0.26	0.30	0	-.29

1 FT = 0.305 m

*Values not computed for CELL COARSE

TABLE 3.4 TRANSVERSE DISTRIBUTION OF DEFLECTIONS ($FT \times 10^{-2}$) AT MIDSPAN SECTIONS X AND Y

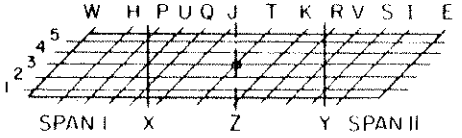

LOAD CASE	CELL	SECTION X					SECTION Y				
		GIRDERS					GIRDERS				
		1	2	3	4	5	1	2	3	4	5
CL	COARSE	4.08	3.72	3.41	3.11	2.83	2.86	3.10	3.39	3.72	4.09
	FINE	4.07	3.73	3.42	3.12	2.86	2.88	3.12	3.39	3.72	4.09
DL	COARSE	0.87	0.78	0.70	0.61	0.53	0.51	0.38	0.65	0.74	0.82
	FINE	0.88	0.79	0.71	0.62	0.54	0.52	0.58	0.66	0.76	0.83
BLOCKS	COARSE	*	*	*	*	*	*	*	*	*	*
	FINE	1.62	1.46	1.31	1.16	1.01	1.02	1.15	1.30	1.46	1.63
1X	COARSE	12.16	8.97	6.66	4.52	2.54	-0.75	-1.80	-2.86	-3.95	-5.07
	FINE	12.45	9.18	6.80	4.60	3.55	-0.98	-1.88	-3.02	-4.18	-5.38
3X	COARSE	6.66	6.15	5.67	4.60	3.55	-0.78	-1.43	-1.91	-2.39	-2.87
	FINE	6.80	6.27	5.77	4.66	3.58	-0.99	-1.48	-1.99	-2.50	-3.02
5X	COARSE	2.54	2.99	3.55	4.26	5.83	-1.22	-1.10	-1.00	-0.90	-0.77
	FINE	2.56	3.01	3.58	4.30	5.90	-1.24	-1.12	-1.03	-0.91	-0.78
1Y	COARSE	-0.75	-0.87	-0.98	-1.09	-1.22	6.44	4.46	3.32	2.68	2.33
	FINE	-0.76	-0.89	-0.99	-1.12	-1.24	6.51	4.51	3.35	2.70	2.34
3Y	COARSE	-2.86	-2.38	-1.90	-1.45	-1.00	3.32	4.48	6.26	6.03	6.43
	FINE	-3.02	-2.50	-1.99	-1.50	-1.02	3.35	4.54	6.35	6.15	6.57
5Y	COARSE	-5.07	-3.96	-2.87	-1.81	-0.77	2.33	4.20	6.43	9.18	12.81
	FINE	-5.38	-4.19	-3.02	-1.89	-0.77	2.34	4.28	6.58	9.42	13.10
1X + 5Y	COARSE	7.09	5.00	3.79	2.72	1.78	1.58	2.40	3.56	5.24	7.74
	FINE	7.07	5.00	3.78	2.72	1.78	1.58	2.40	3.55	5.24	7.73
1X + 1Y	COARSE	11.40	8.09	5.68	3.43	1.32	5.69	2.66	0.46	-1.27	-2.74
	FINE	11.69	8.30	5.80	3.49	1.32	5.75	2.63	0.33	-1.47	-3.03

*Values not computed for CELL COARSE

1 FT = 0.305 m

TABLE 3.5 TRANSVERSE DISTRIBUTION OF LONGITUDINAL MEMBRANE FORCES N_x (KIPS/FT) AT SECTION A

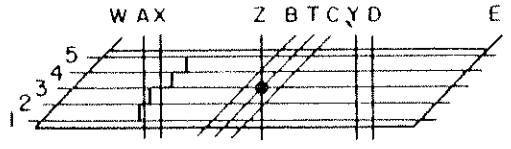

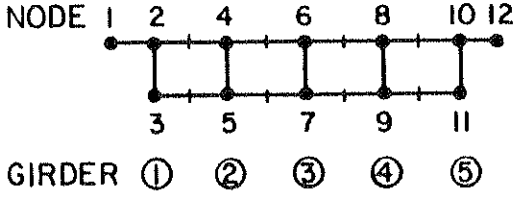

LOAD CASE	LOCATION	CELL	TOP NODES							BOTTOM NODES				
			1	2	4	6	8	10	12	3	5	7	9	11
DL	PLATE	COARSE	-4.5	-4.0	-3.6	-3.6	-3.4	-3.9	-4.4	2.0	3.9	3.8	3.7	1.9
		FINE	-4.5	-4.0	-3.5	-3.6	-3.4	-3.9	-4.4	1.9	3.9	3.8	3.7	1.9
	WEB	COARSE	-	-4.5	-4.7	-4.7	-4.5	-4.4	-	5.8	5.8	5.7	5.5	5.6
		FINE	-	-4.5	-4.7	-4.8	-4.5	-4.4	-	5.8	5.7	5.7	5.5	5.7
CL	PLATE	COARSE	-26.7	-23.4	-20.5	-20.5	-20.0	-23.0	-26.2	11.6	22.3	21.6	21.6	11.4
		FINE	-26.7	-23.2	-20.2	-20.4	-19.9	-22.9	-26.5	11.9	22.0	21.5	21.5	11.3
	WEB	COARSE	-	-26.2	-27.1	-27.1	-26.5	-25.8	-	34.5	33.2	32.1	32.2	34.0
		FINE	-	-25.9	-26.7	-26.9	-26.3	-25.6	-	34.0	32.6	32.0	32.0	33.8
1X	PLATE	COARSE	-45.0	-40.4	-36.8	-34.4	-28.0	-30.8	-36.9	19.0	41.0	36.8	30.0	14.3
		FINE	-45.7	-40.3	-36.7	-35.2	-28.6	-31.6	-37.5	18.6	40.8	37.7	30.8	14.7
	WEB	COARSE	-	-45.4	-49.5	-46.9	-37.7	-34.7	-	57.7	62.1	55.9	45.7	43.2
		FINE	-	-45.2	-49.3	-47.7	-38.4	-35.9	-	56.5	61.8	37.4	46.5	44.1

1 KIP = 4.448 kN
1 FT = 0.305 m

TABLE 3.6 - TRANSVERSE DISTRIBUTION OF TOTAL MOMENT AT SECTIONS A AND D TO EACH GIRDER (FT-KIPS AND PERCENT)

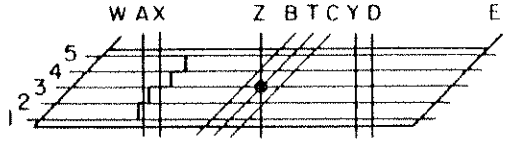

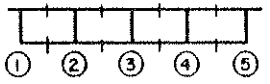

LOAD CASE	CELL	INTERNAL MOMENTS (FT-KIPS)						PERCENTAGE OF TOTAL INT. MOM.					
SECTION A		GIRDERS					TOTAL	GIRDERS					TOTAL
		1	2	3	4	5		1	2	3	4	5	
DL	COARSE	12	16	17	16	11	72	16.3	22.8	23.2	21.9	15.8	100
	FINE	12	17	17	16	12	74	16.4	22.7	22.8	22.0	16.1	100
CL	COARSE	69	95	96	93	68	421	16.4	22.6	22.8	22.1	16.1	100
	FINE	71	96	95	94	70	426	16.6	22.5	22.3	22.2	16.4	100
1X	COARSE	118	171	161	132	90	672	17.6	25.5	23.9	19.7	13.4	100
	FINE	124	176	162	136	95	693	17.9	25.4	23.4	19.7	13.7	100
SECTION D		GIRDERS					TOTAL	GIRDERS					TOTAL
		1	2	3	4	5		1	2	3	4	5	
DL	COARSE	11	15	16	16	11	68	15.6	21.9	23.0	22.9	16.7	100
	FINE	11	15	16	16	12	69	15.9	22.0	22.5	22.8	16.8	100
CL	COARSE	67	93	96	95	70	421	16.0	22.0	22.7	22.6	16.7	100
	FINE	69	94	95	96	72	426	16.3	22.1	22.2	22.6	16.8	100
1X	COARSE	-32	-43	-44	-43	-31	-192	16.4	22.5	22.9	22.3	16.0	100
	FINE	-35	-47	-47	-47	-34	-209	16.6	22.5	22.4	22.3	16.2	100

1 FT-KIP = 1.356 kN-m

TABLE 3.7 LONGITUDINAL DISTRIBUTION OF TOTAL INTERNAL MOMENTS (FT-KIPS) AT A SECTION COMPUTED FROM INTEGRATION OF INTERNAL FORCES AND TOTAL EXTERNAL MOMENTS (FT-KIPS) AT A SECTION COMPUTED FROM EXTERNAL REACTIONS

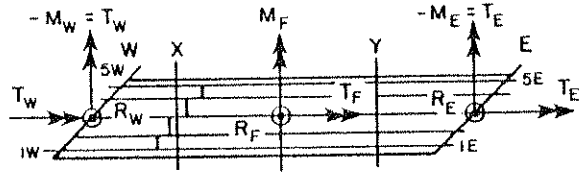

TYPE OF MOMENT	LOAD CASE	CELL	MOMENTS (FT-KIPS) AT SECTION				
			A	X	Z	Y	D
INTERNAL MOMENTS	DL	COARSE	72	67	-113	63	68
		FINE	73	68	-126	63	69
	CL	COARSE	421	477	-510	477	421
		FINE	426	484	-545	481	426
	1X	COARSE	672	713	-301	-205	-192
		FINE	693	744	-320	-203	-209
EXTERNAL MOMENTS	DL	COARSE	72	68	-146	63	68
		FINE	73	69	-156	64	69
	CL	COARSE	432	523	-632	523	431
		FINE	427	519	-614	519	427
	1X	COARSE	687	771	-442 -305	-212	-197
		FINE	694	778	-437 -321	-223	-209

For practical design purposes the CELL COARSE mesh would be adequate, however, for the present investigation the more accurate CELL FINE mesh was chosen for comparison with the experimental data for all load cases with the exception of the 40 load positions of the moving fork lift truck, for which CELL COARSE was used to develop theoretical influence lines.

3.3 Total Reactions, Moments, Torques and Centerline Deflections

Results obtained from the CELL FINE analyses are presented in Figs. 3.2 to 3.21 for all of the important load cases. Note that results for conditioning load and all point load cases are for 100 kips (445 kN) per span. These values of reactions, deflections, moments and torques as shown in Figs. 3.2 to 3.21 are a useful and convenient reference for defining the general structural behavior of the skew two span box girder bridge.

First considering the reactions, Figs. 3.2 to 3.6, the influence of the skewness of the bridge is clearly shown for single point loads placed successively on girders 1, 3 and 5 transversely across the midspans X and (or) Y of the bridge. Load positions where the load is close to the obtuse corner of the skew bridge will be termed as loaded on the "obtuse side" of the bridge while loads on the "acute side" of the bridge will be used when the loads are closer to the acute corner of the span under consideration. For loads shifting from the acute side of a span to the obtuse side, the total vertical reaction at the end abutment increases while the vertical reaction at the center bent decreases. It should be noted, that the reaction moment and torque at the end abutment even changes signs with the change in transverse position of the point loads across the midspan sections.

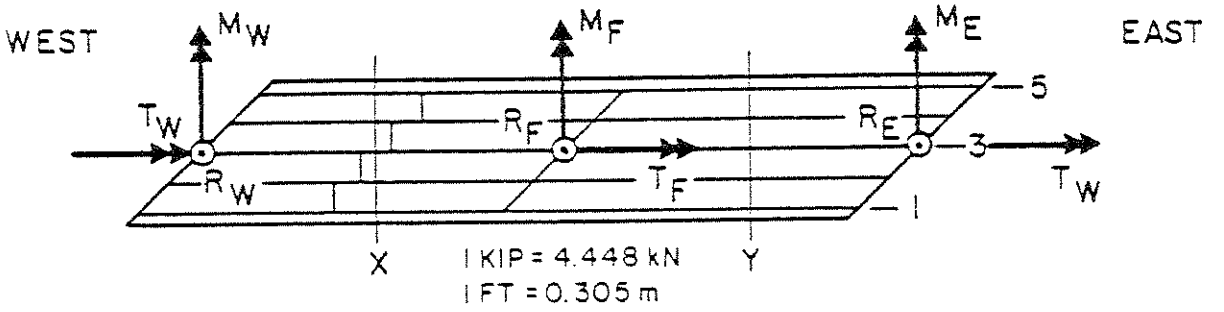

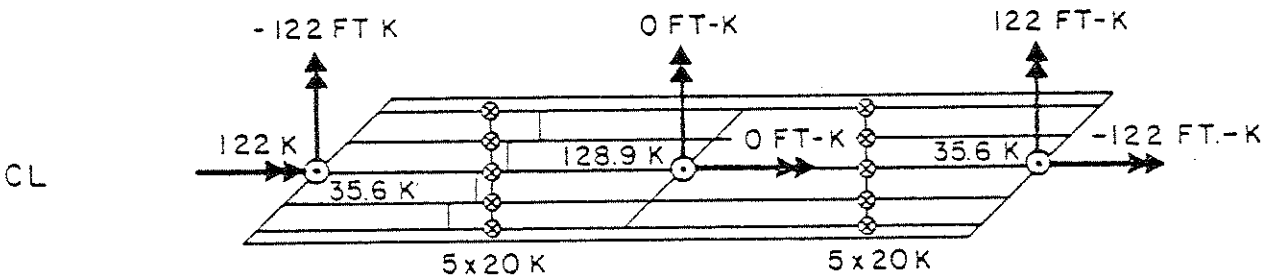

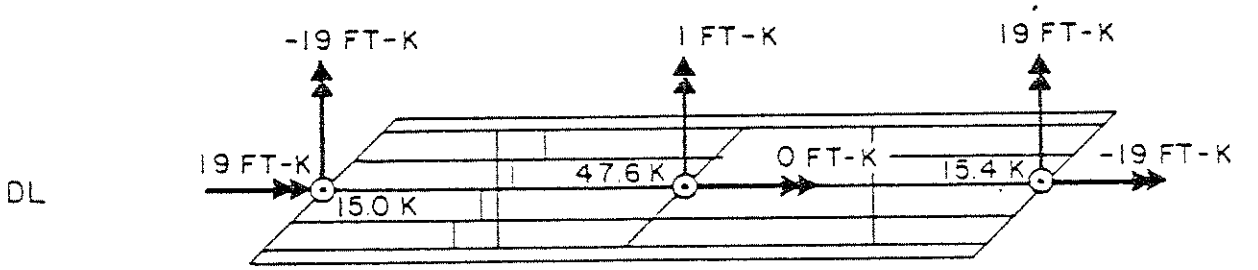

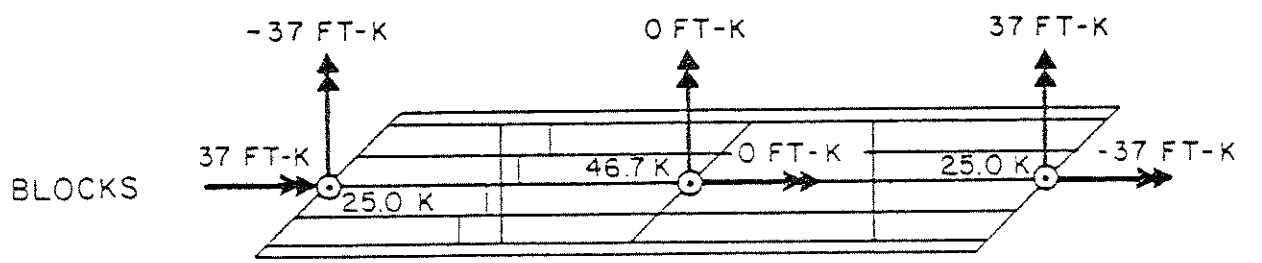

FIG. 3.2 CELL CENTERLINE REACTIONS FOR CONDITIONING LOADS, DEAD LOAD AND BLOCK LOADING

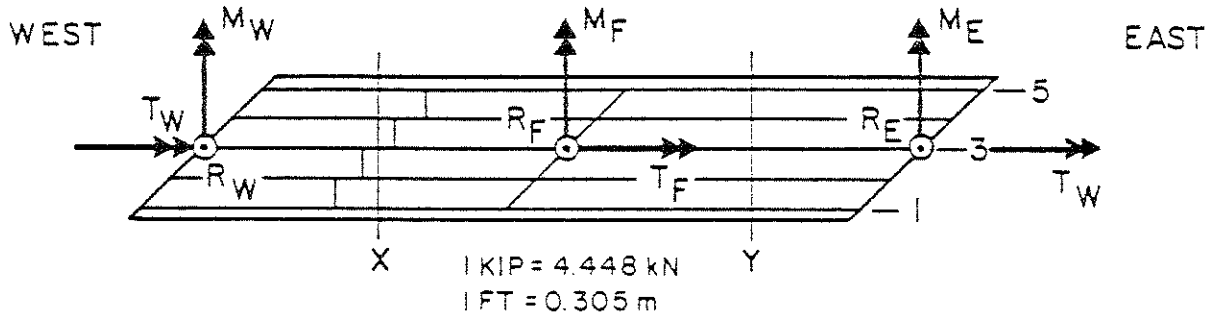

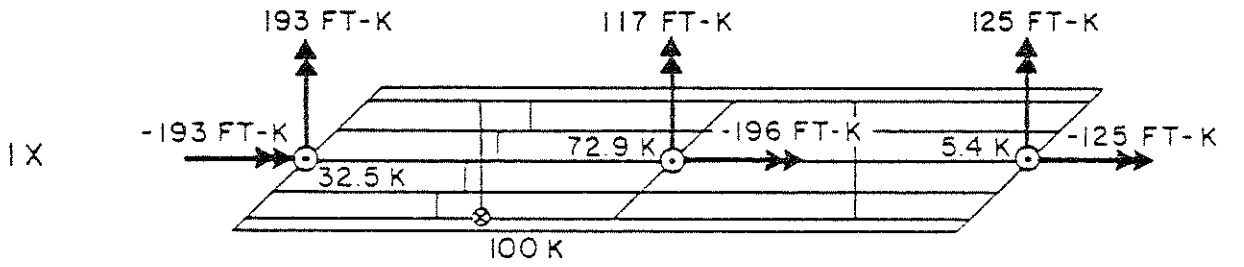

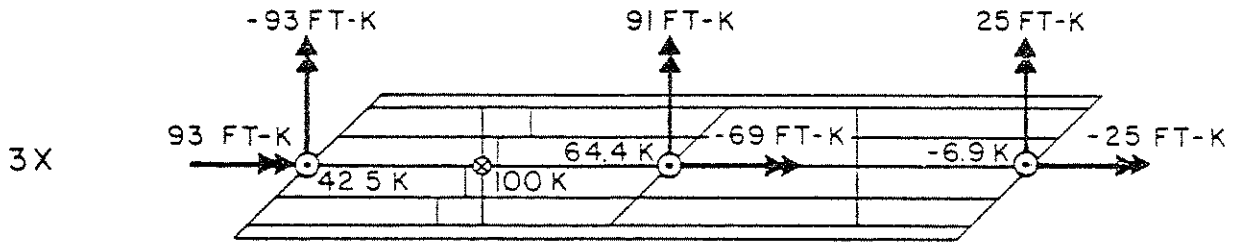

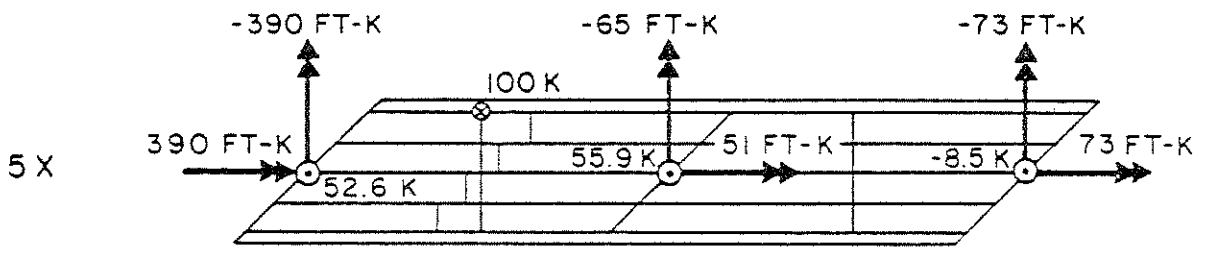

FIG. 3.3 CELL CENTERLINE REACTIONS FOR 100 KIP (445 kN) POINT LOADS AT 1X, 3X, 5X

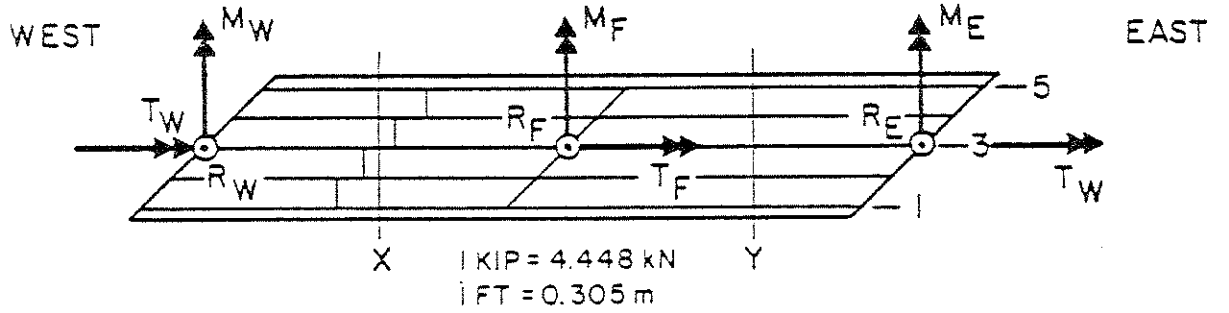

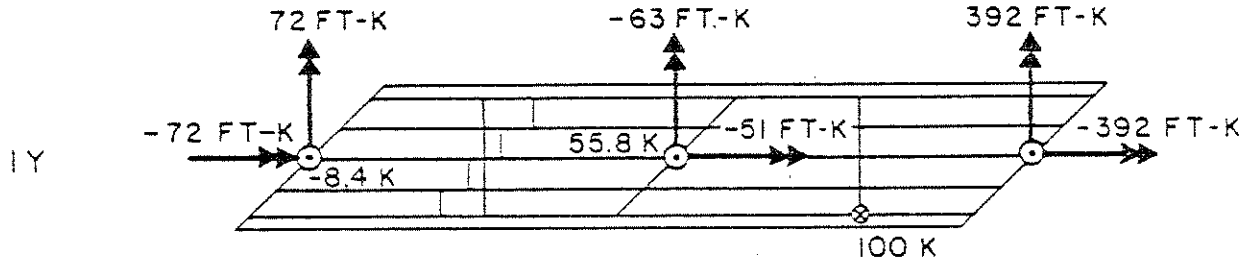

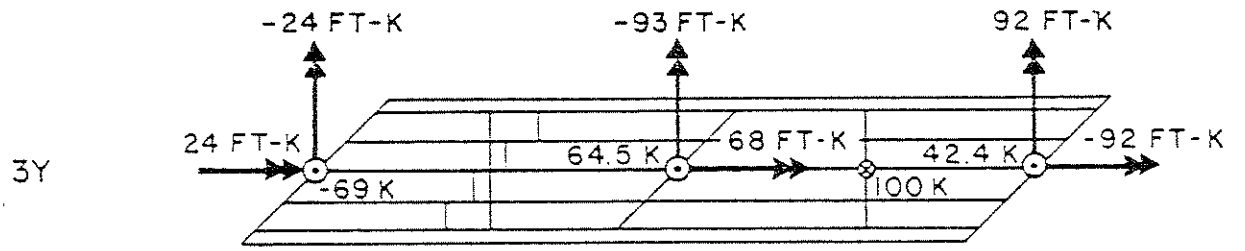

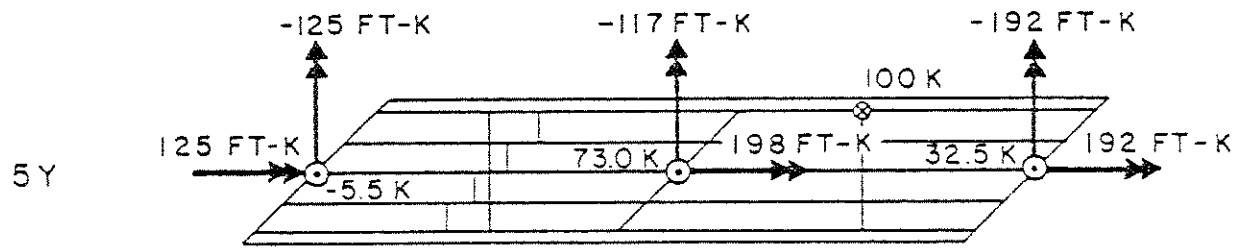

FIG. 3.4 CELL CENTERLINE REACTIONS FOR 100 KIP (445 kN) POINT LOADS AT 1Y, 3Y, 5Y

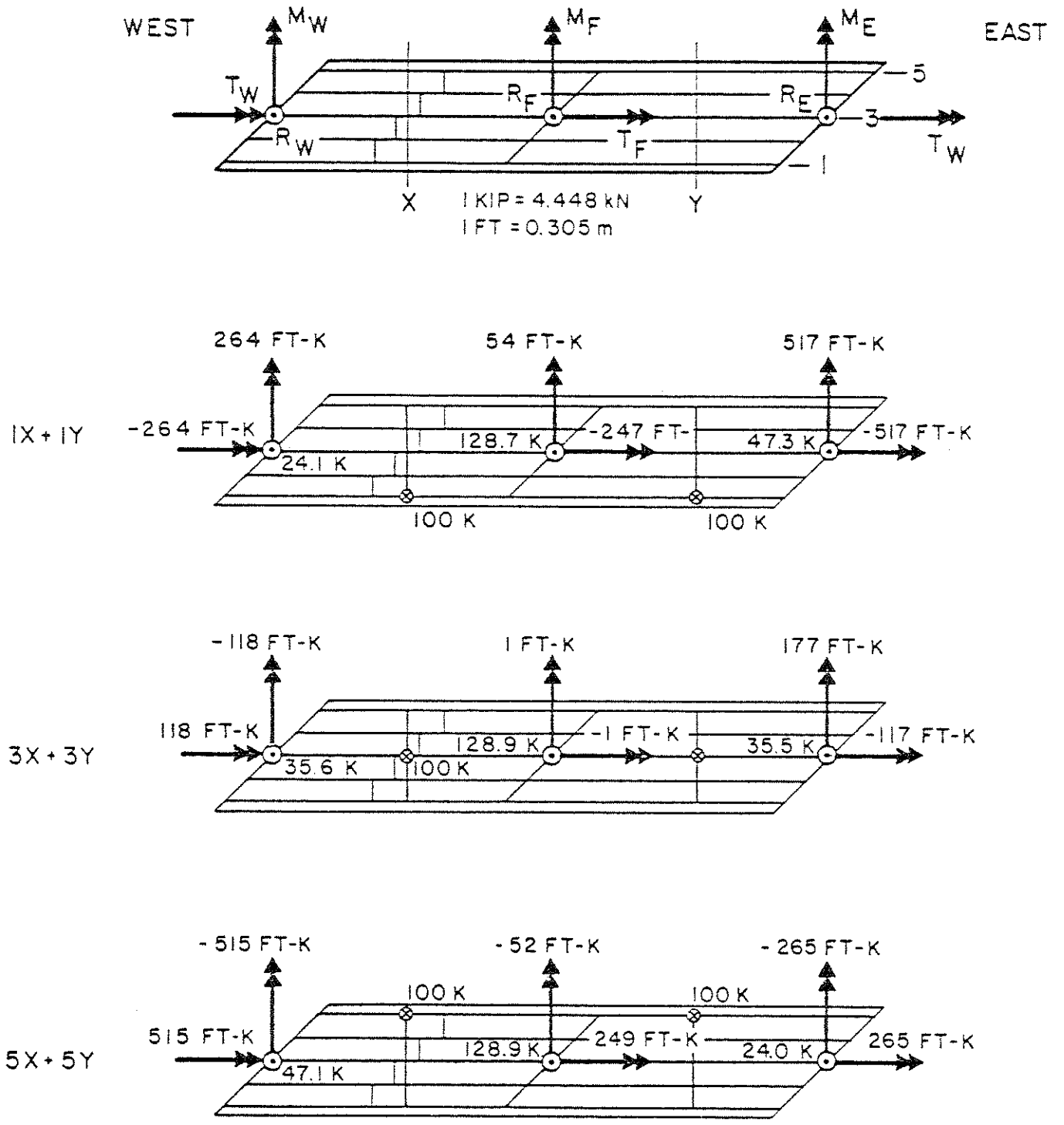

FIG. 3.5 CELL CENTERLINE REACTIONS FOR 100 KIP (445kN) POINT LOADS AT 1X + 1Y, 3X + 3Y, 5X + 5Y

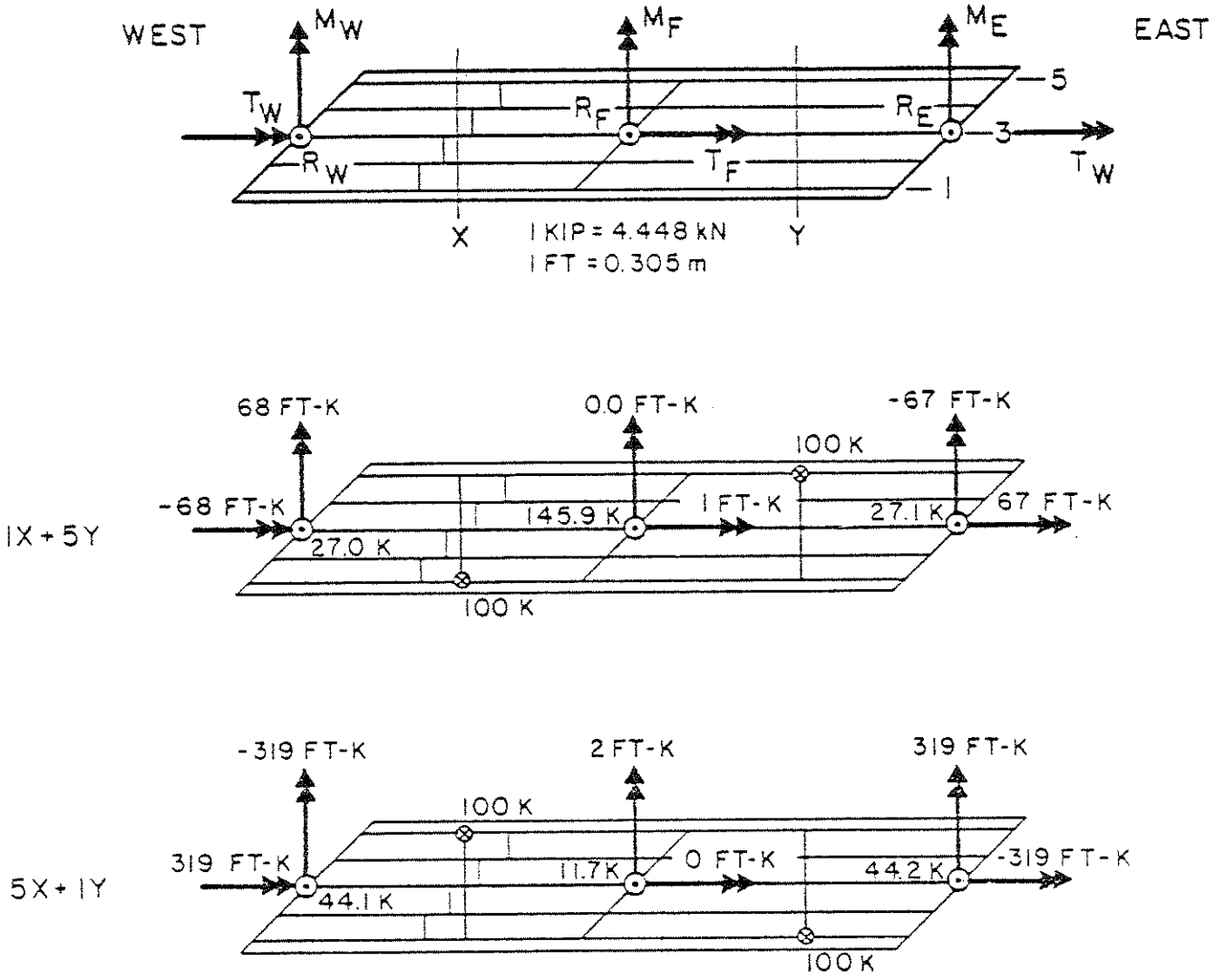

FIG. 3.6 CELL CENTERLINE REACTIONS FOR 100 KIP (445 kN) POINT LOADS AT 1X + 5Y, 5X + 1Y

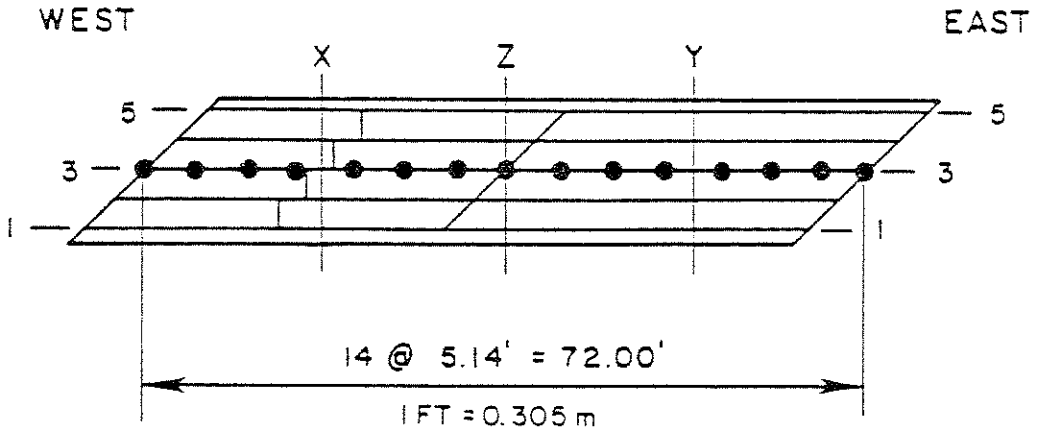

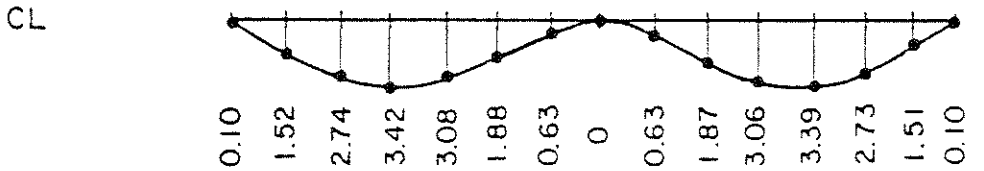

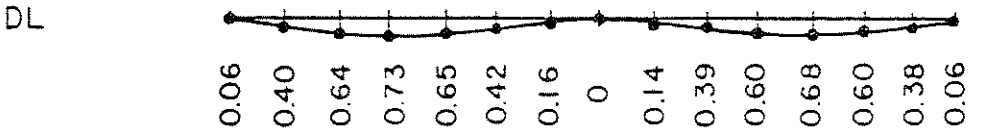

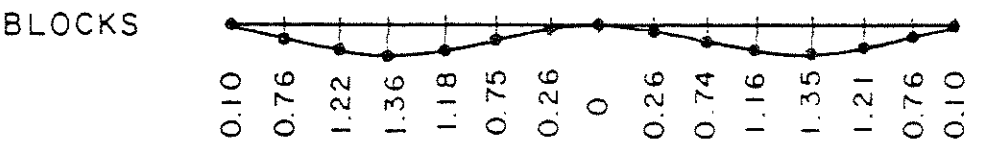

FIG. 3.7 LONGITUDINAL DISTRIBUTION OF DEFLECTIONS (FT x 10^{-2}) ALONG CENTER GIRDER 3 FOR CONDITIONING LOADS, DEAD LOAD AND BLOCK LOADING

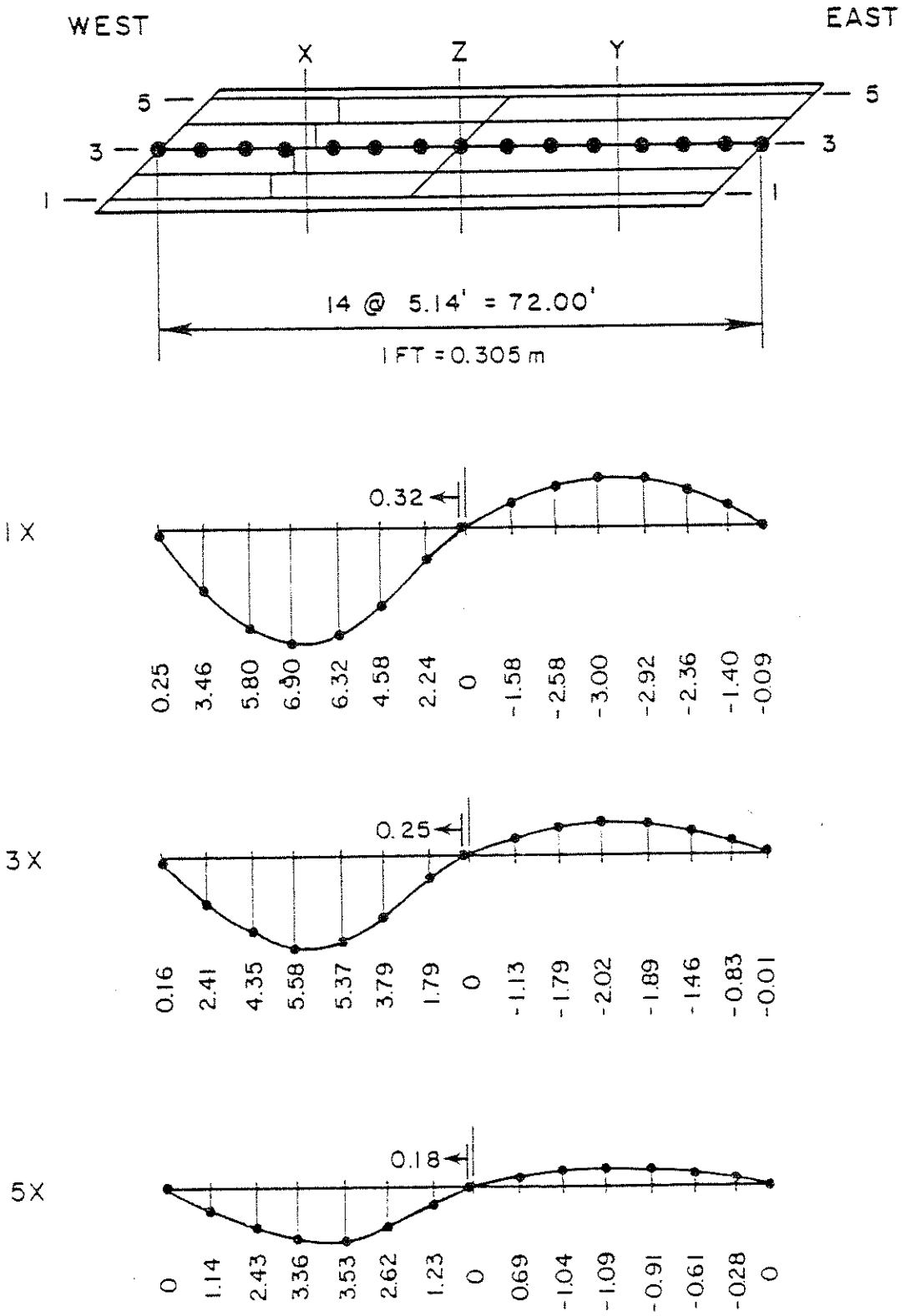

FIG. 3.8 LONGITUDINAL DISTRIBUTION OF DEFLECTIONS (FT x 10^{-3}) ALONG CENTER GIRDER 3 FOR 100 KIP (445 kN) POINT LOADS AT 1X, 3X, 5X

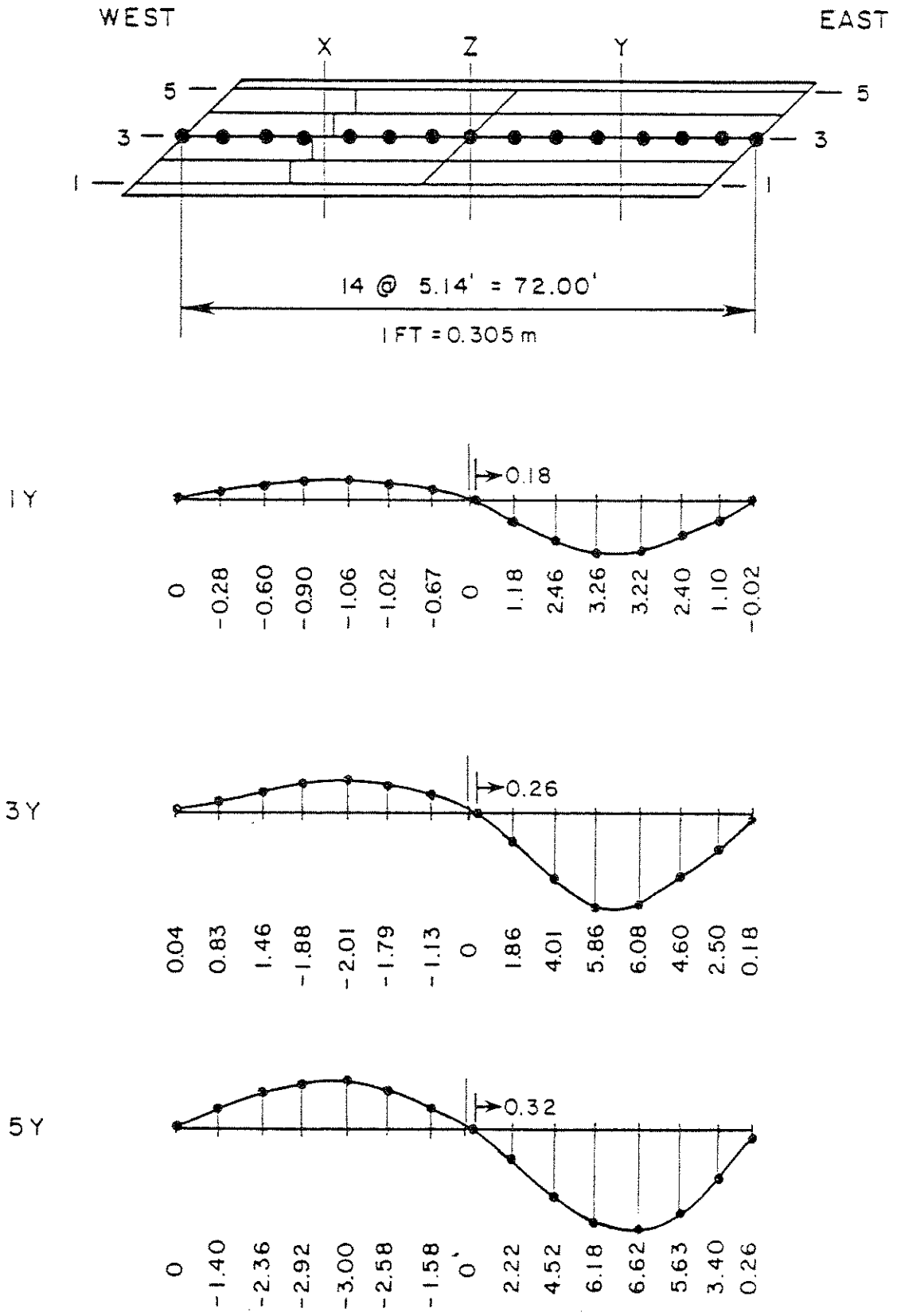

FIG. 3.9 LONGITUDINAL DISTRIBUTION OF DEFLECTIONS (FT x 10^{-2}) ALONG CENTER GIRDER 3 FOR 100 KIP (445 kN) POINT LOADS AT 1Y, 3Y, 5Y

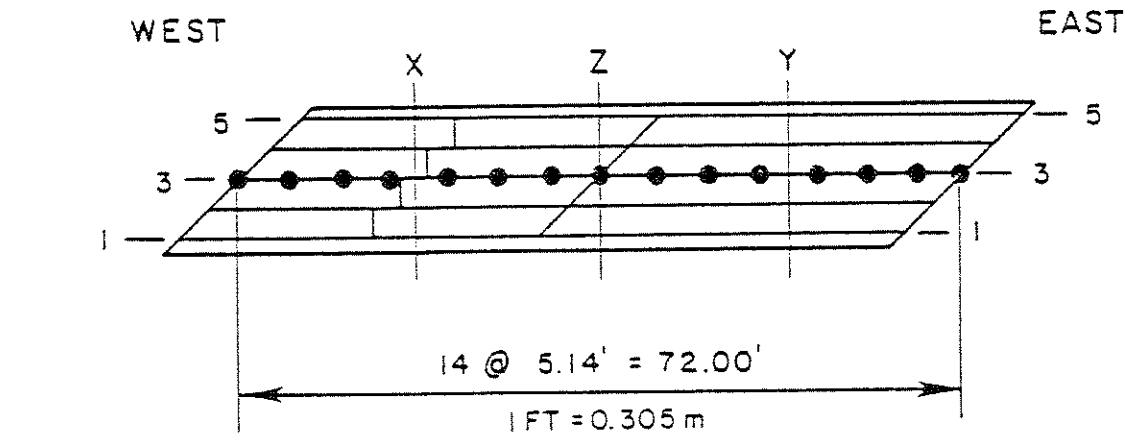

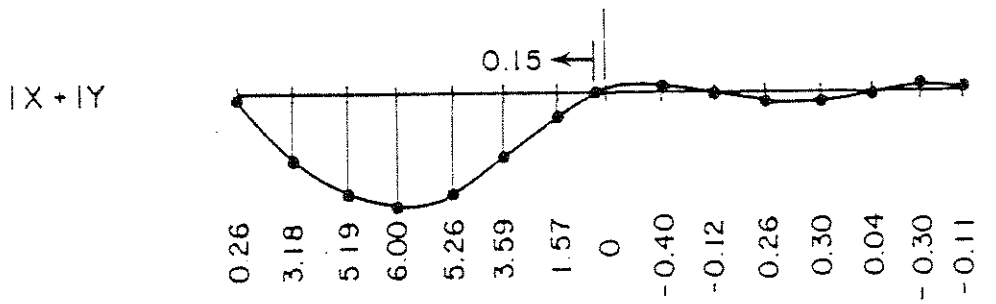

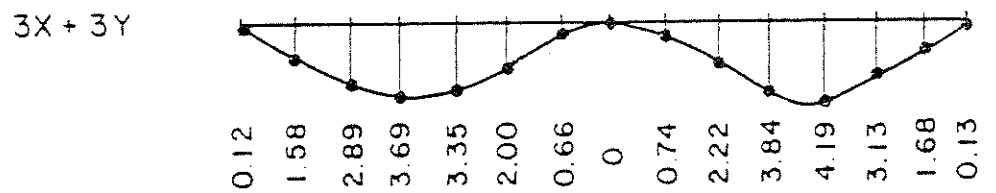

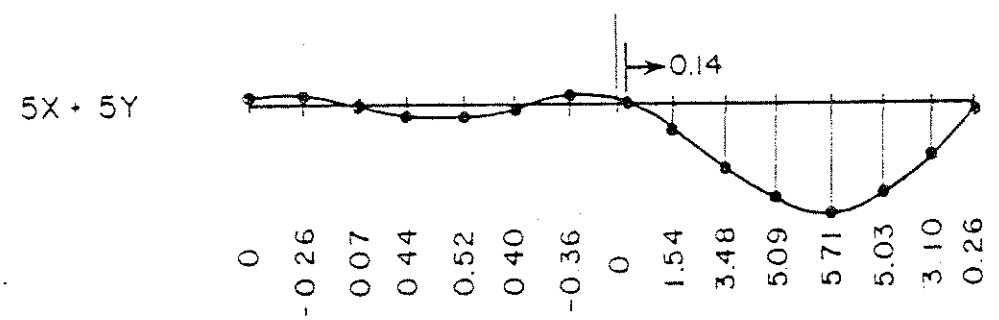

FIG. 3.10 LONGITUDINAL DISTRIBUTION OF DEFLECTIONS (FT x 10^{-3}) ALONG CENTER GIRDER 3 FOR 100 KIP (445 kN) POINT LOADS AT 1X + 1Y, 3X + 3Y, 5X + 5Y

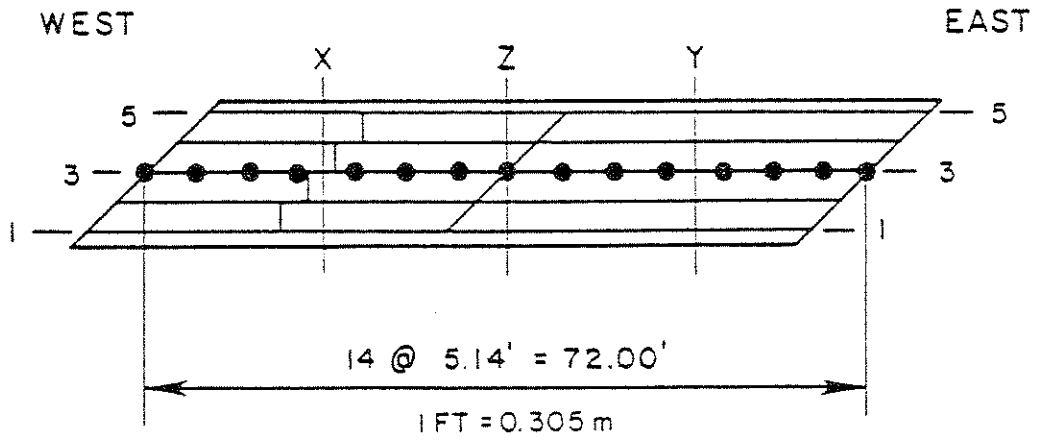

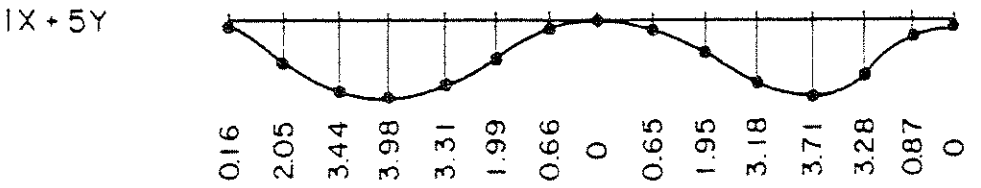

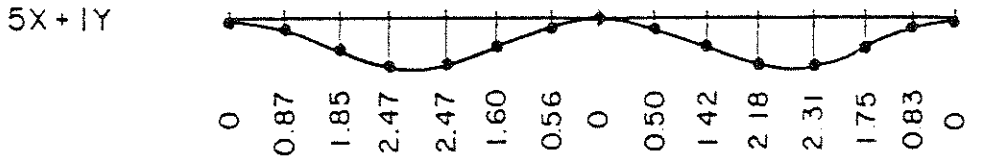

FIG. 3.11 LONGITUDINAL DISTRIBUTION OF DEFLECTIONS (FT x 10^{-2}) ALONG CENTER GIRDER 3 FOR 100 KIP (445 kN) POINT LOADS AT 5X + 1Y, 1X + 5Y

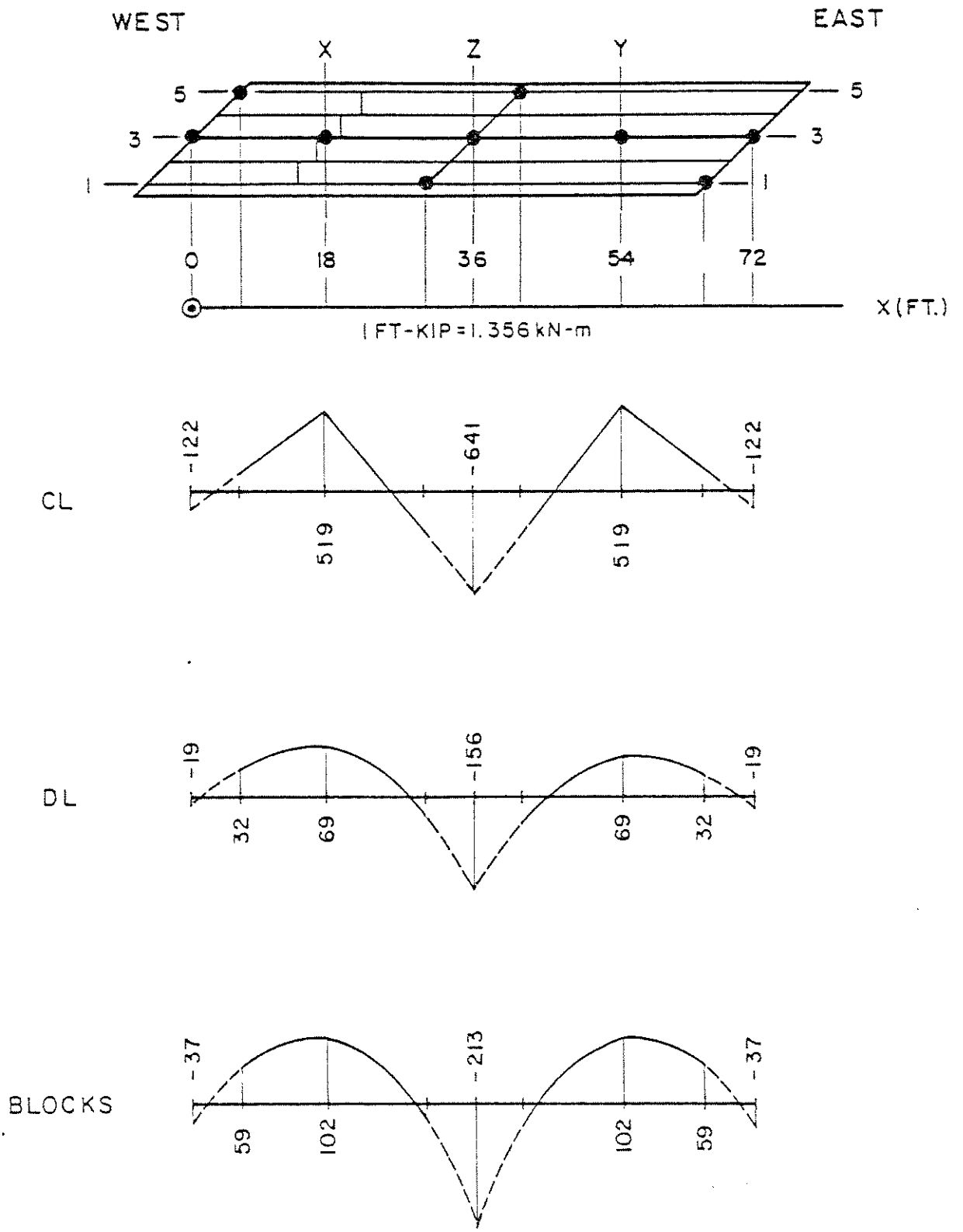

FIG. 3.12 LONGITUDINAL DISTRIBUTION OF EXTERNAL MOMENTS (FT-KIPS) FOR CONDITIONING LOADS, DEAD LOAD AND BLOCK LOADING

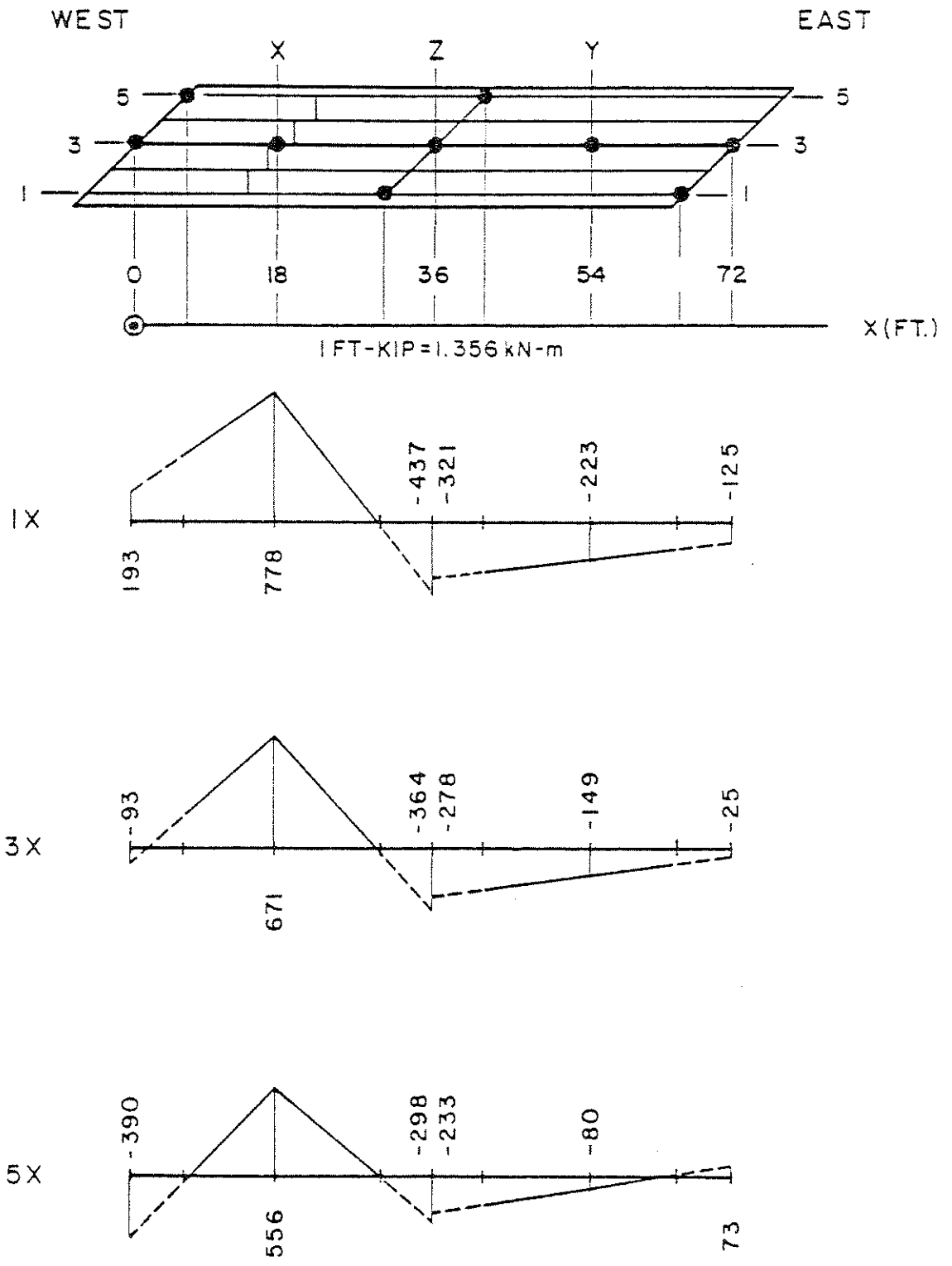

FIG. 3.13 LONGITUDINAL DISTRIBUTION OF EXTERNAL MOMENTS (FT-KIPS) FOR 100 KIP (445 kN) POINT LOADS AT 1X, 3X, 5X

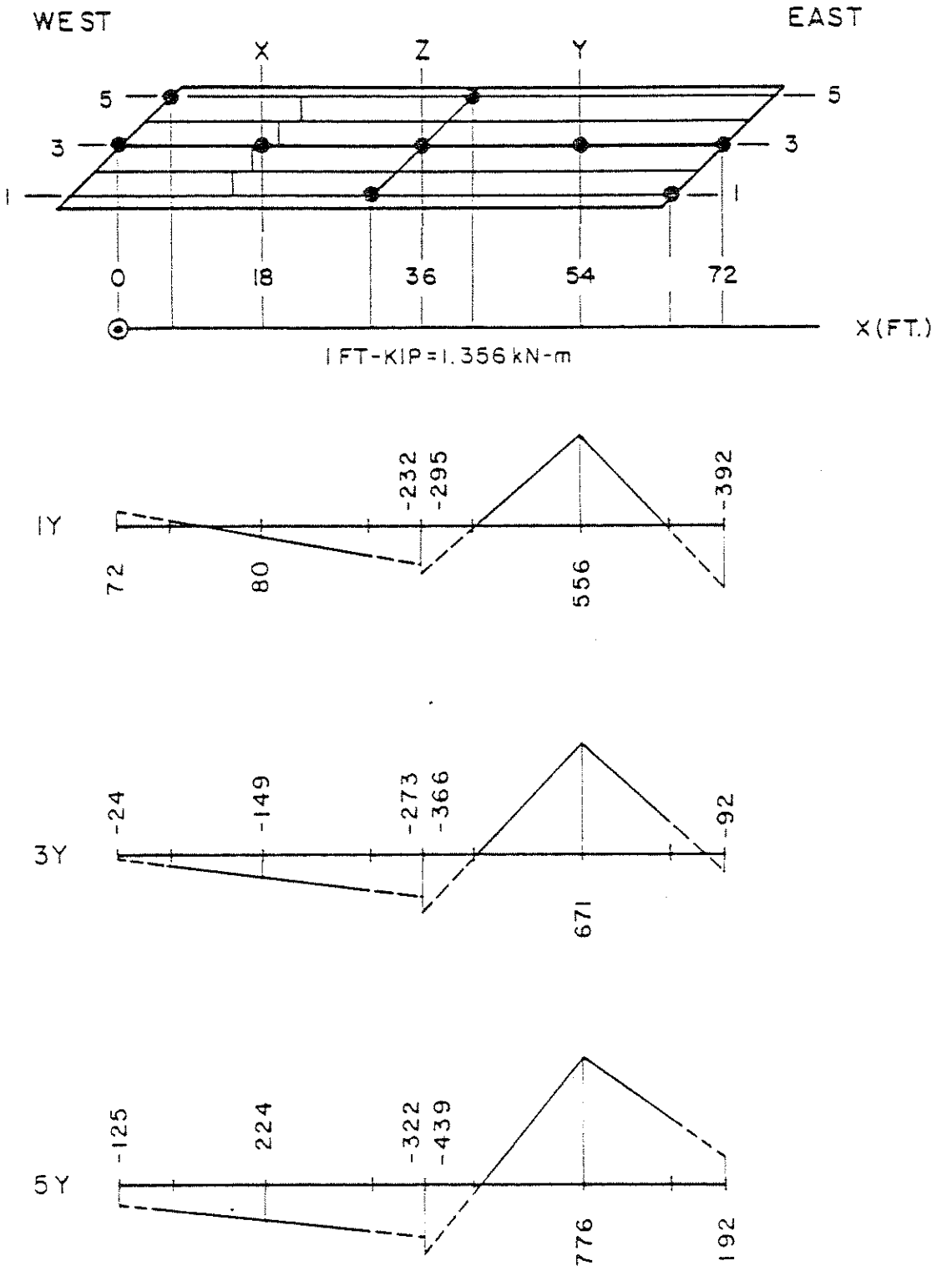

FIG. 3.14 LONGITUDINAL DISTRIBUTION OF EXTERNAL MOMENTS (FT-KIPS) FOR 100 KIP (445 kN) POINT LOADS AT 1Y, 3Y, 5Y

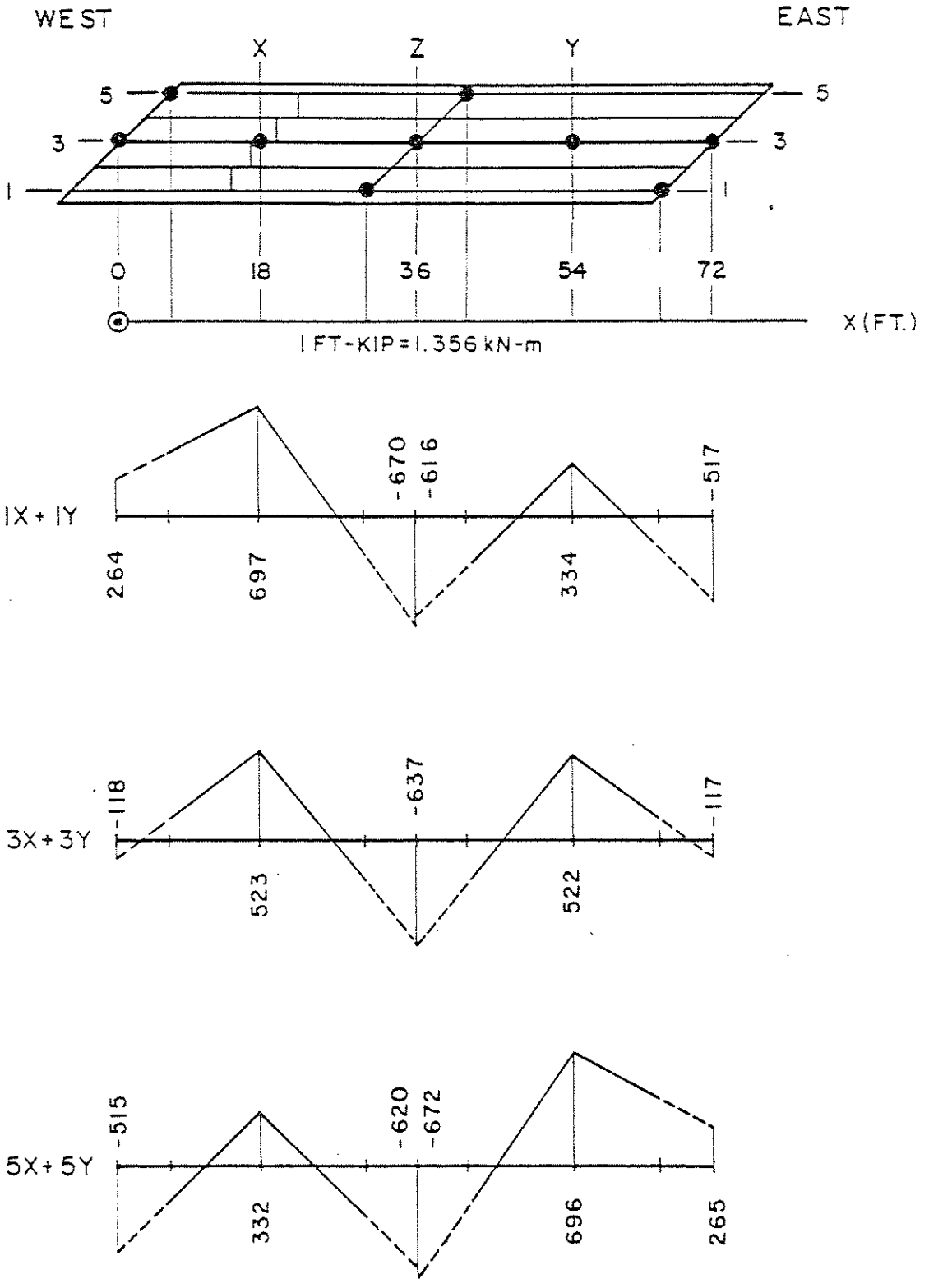

FIG. 3.15 LONGITUDINAL DISTRIBUTION OF EXTERNAL MOMENTS (FT-KIPS) FOR 100 KIP (445 kN) POINT LOADS AT 1X + 1Y, 3X + 3Y, 5X + 5Y

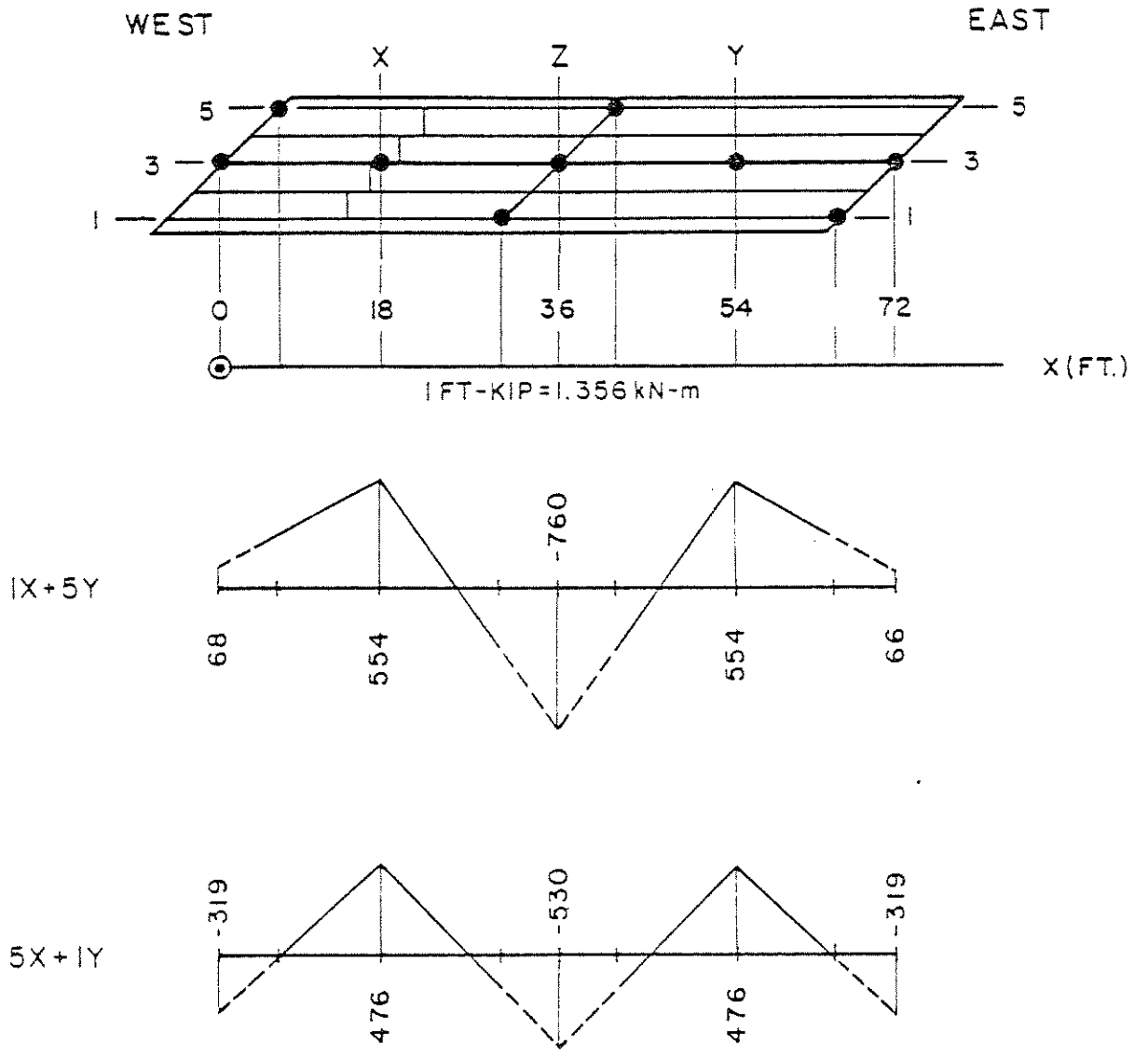

FIG. 3.16 LONGITUDINAL DISTRIBUTION OF EXTERNAL MOMENTS (FT-KIPS) FOR 100 KIP (445 kN) POINT LOADS AT 1X + 5Y, 5X + 1Y

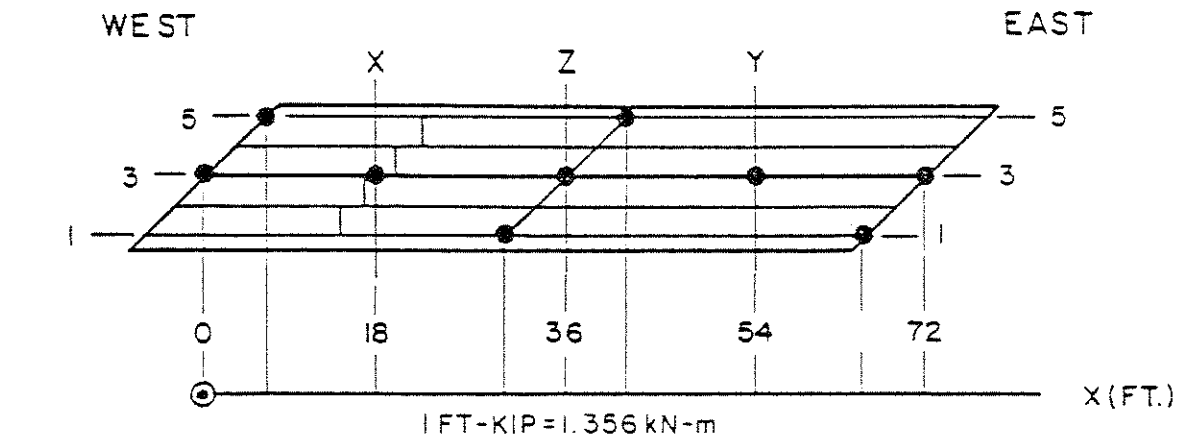

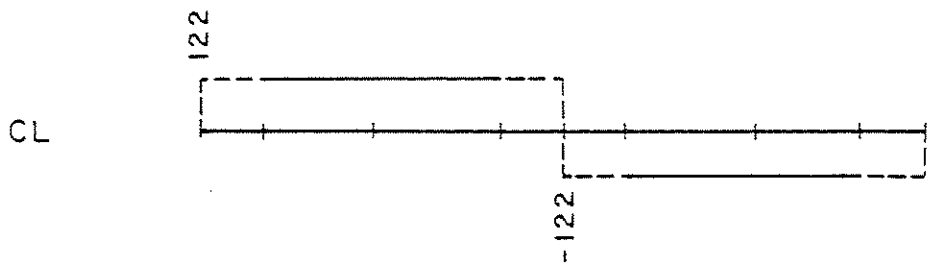

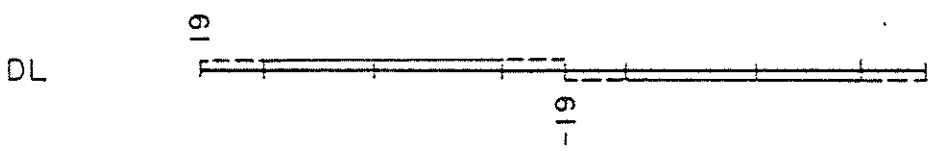

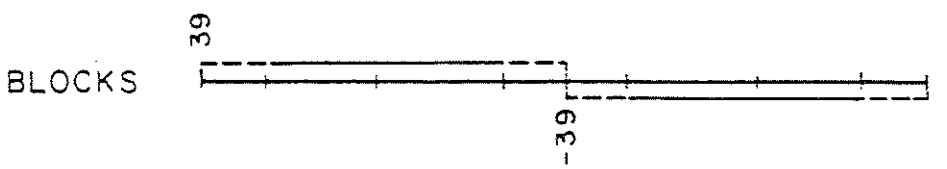

FIG. 3.17 LONGITUDINAL DISTRIBUTION OF EXTERNAL TORQUES (FT-KIPS) FOR CONDITIONING LOADS, DEAD LOAD AND BLOCK LOADING

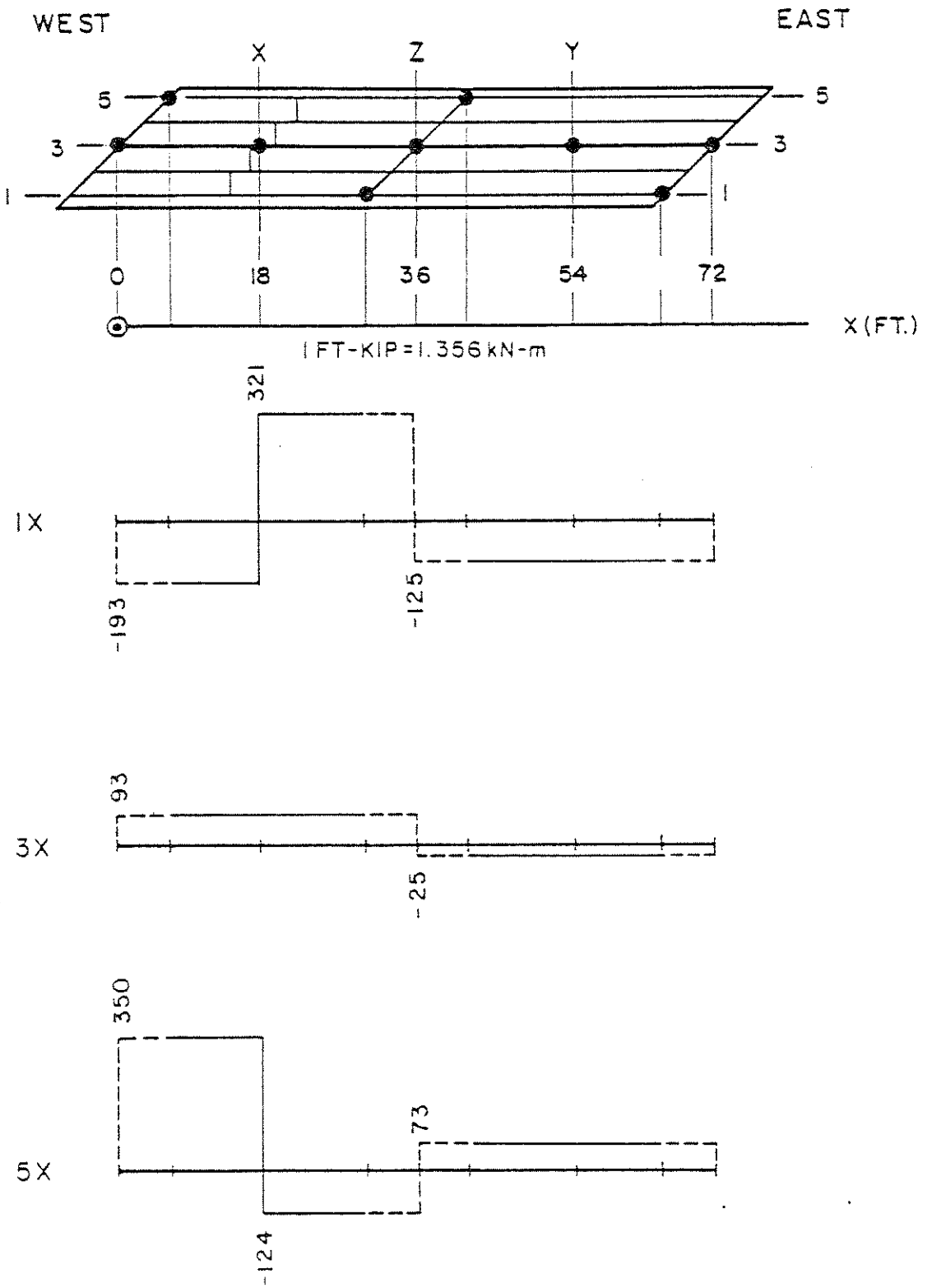

FIG. 3.18 LONGITUDINAL DISTRIBUTION OF EXTERNAL TORQUES (FT-KIPS) FOR 100 KIP (445 kN) POINT LOADS AT 1X, 3X, 5X

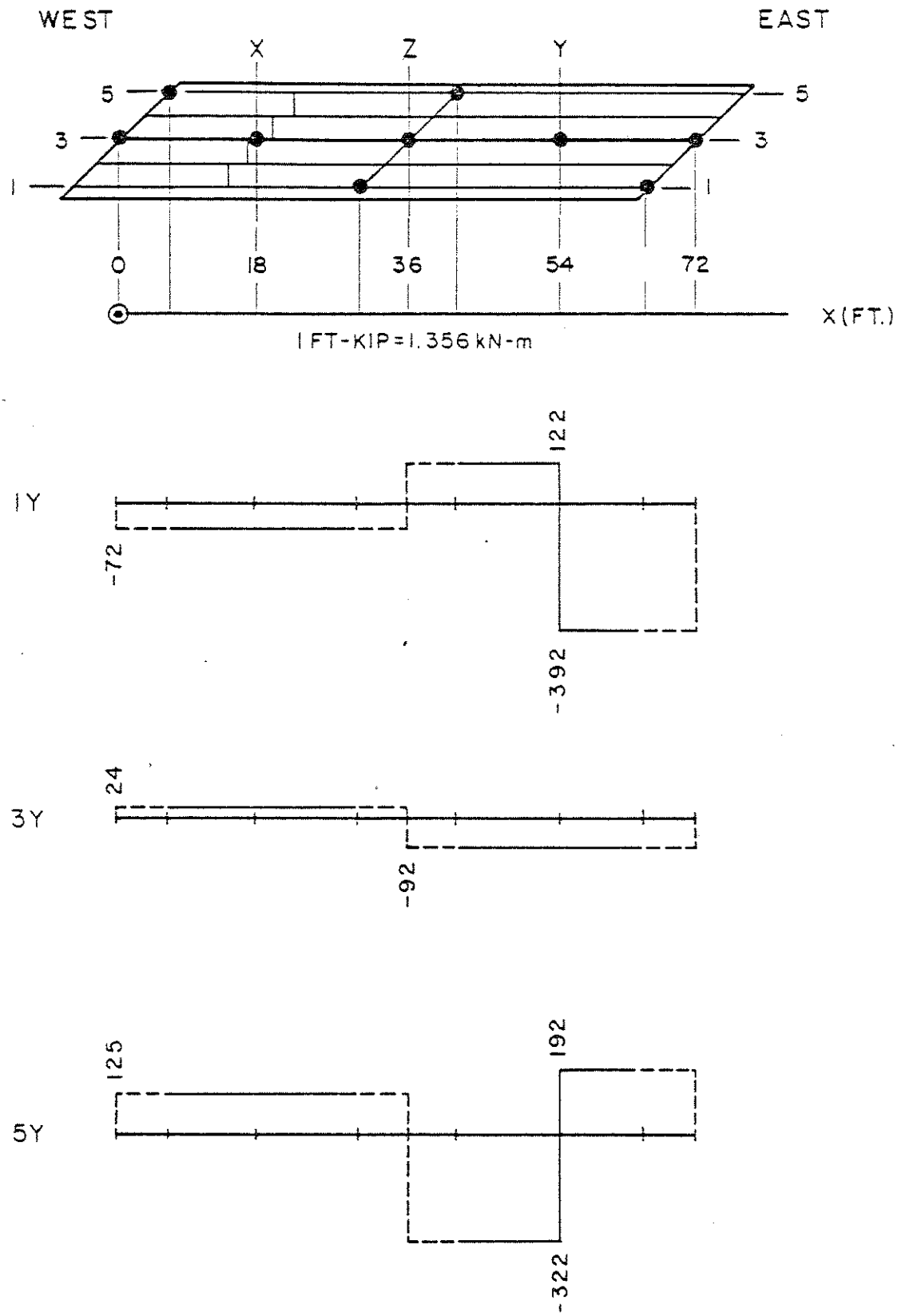

FIG. 3.19 LONGITUDINAL DISTRIBUTION OF EXTERNAL TORQUES (FT-KIPS) FOR 100 KIP (445 kN) POINT LOADS AT 1Y, 3Y, 5Y

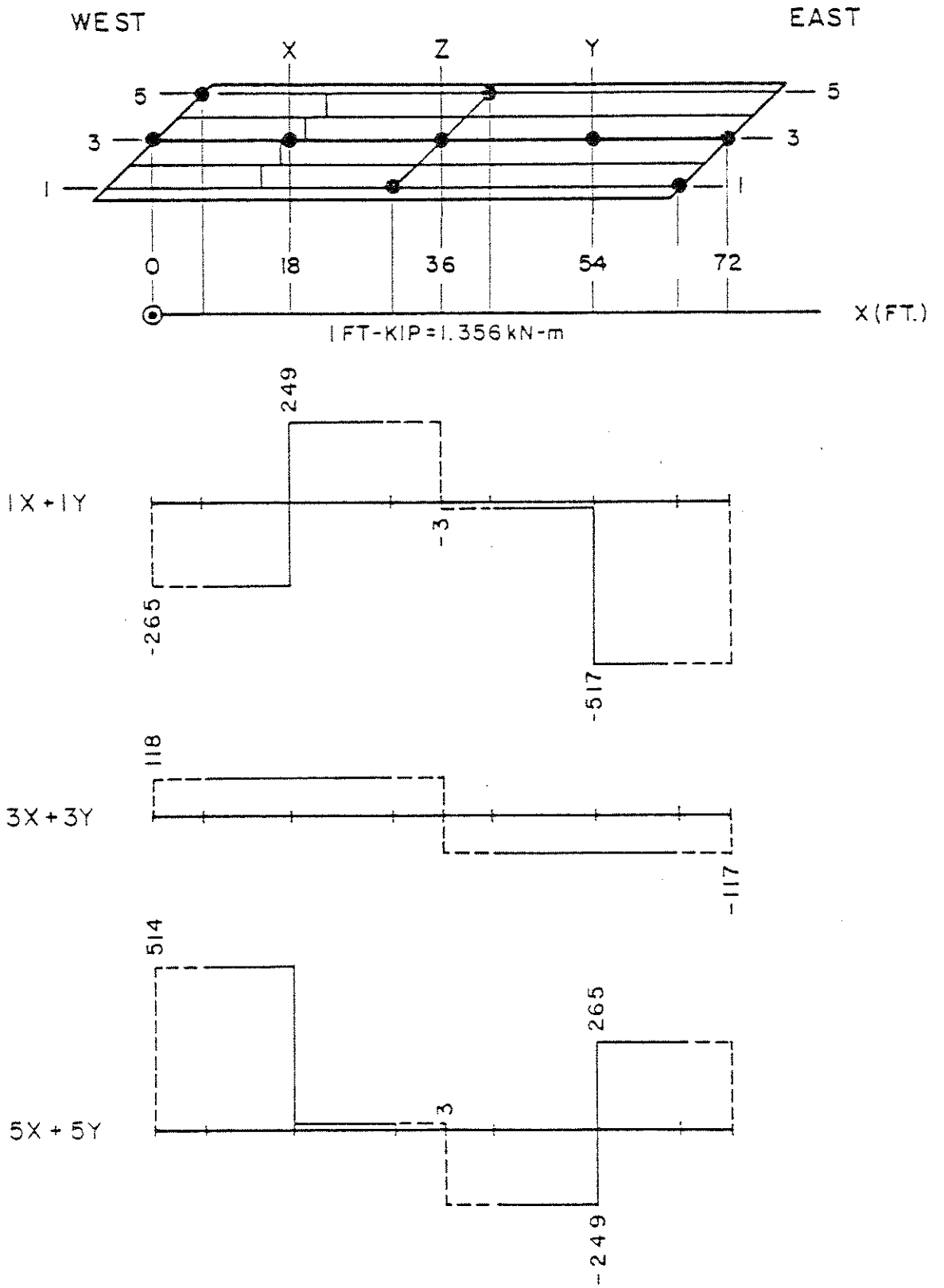

FIG. 3.20 LONGITUDINAL DISTRIBUTION OF EXTERNAL TORQUES (FT-KIPS) FOR 100 KIP (445 kN) POINT LOADS AT 1X + 1Y, 3X + 3Y, 5X + 5Y

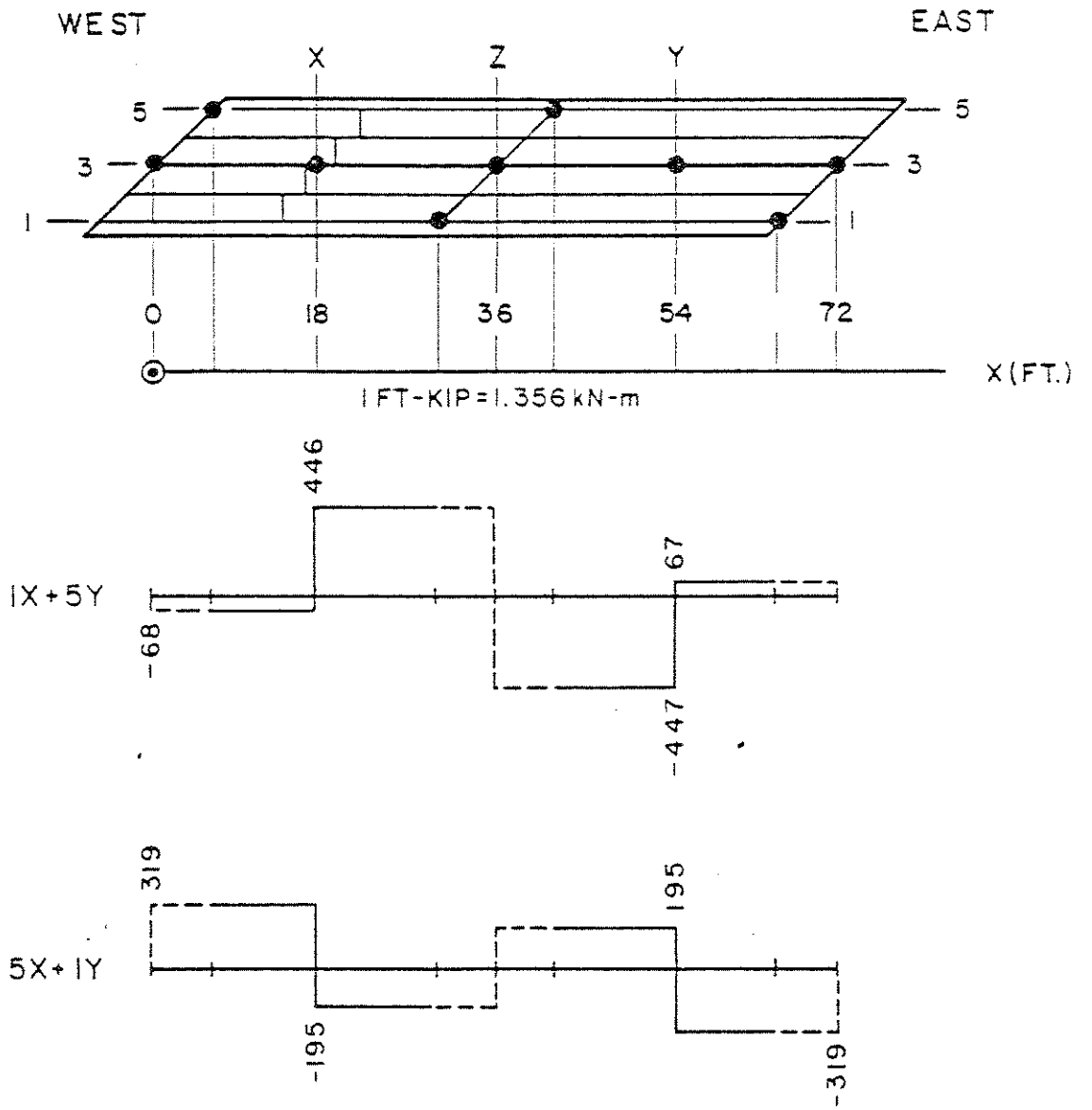

FIG. 3.21 LONGITUDINAL DISTRIBUTION OF EXTERNAL TORQUES (FT-KIPS) FOR 100 KIP (445 kN) POINT LOADS AT 1X + 5Y, 5X + 1Y

The influence of the skewness of the bridge can best be seen by observing the deflections along the centerline of the bridge for loads in successive transverse positions across the span. In Fig. 3.7 to 3.11 the deflections along the center girder are significantly larger for the load on the acute side of a span than for loads on the obtuse side.

The longitudinal distribution of external moments as calculated from the reactions is shown in Figs. 3.12 to 3.16. Of particular interest here are the midspan moments at sections X and Y and how they are influenced by the reaction moments at the end abutment. Again the midspan moment decreases as loads are shifted from the acute to the obtuse side of a span.

3.4 SAP Analysis - Beam Element Model

For a preliminary design of a skew box girder bridge, the sophisticated finite element analysis using the CELL program may be too elaborate and expensive. Thus from a practical design viewpoint a simple analytical model which can predict the most important design quantities within a reasonable accuracy would be very desirable.

Previous investigations at the University of California, Berkeley, have shown that the overall behavior of two span straight and curved box girder bridges [1,2,3] and [4,5,6] as well as skew single span box girders [16] can be predicted satisfactorily by using a standard direct stiffness analysis of a three dimensional frame made up of one dimensional beam and column elements having six degrees of freedom at each end. Such an analysis can be easily performed by any general purpose structural analysis program such as SAP [49].

The same concept was applied to analyze the skew two span box girder bridge shown in Fig. 3.22, which was modelled in the following manner.

For the SAP analyses the bridge was assumed to be a simple three dimensional frame made up of straight one dimensional beam and column members. The 72 ft. (22 m) long longitudinal box structure of the skew bridge was modelled by a single line of one dimensional beam elements. The section properties of each of these one dimensional members are obtained by considering the entire four cell bridge cross-section, Fig. 1.3, as an uncracked beam section. In calculating the section properties the fillets were ignored and the cantilever edges were taken as having a constant average thickness of 0.255 ft. (0.08 m). The center of bottom slab to center of top slab cross-sectional depth was 1.539 ft. (0.47 m). The centroid of the cross-section was found to be 0.852 ft. (0.26 m) above the mid-depth of the bottom slab or 0.687 ft. (0.21 m) below the mid-depth of the top slab. The section and material properties used for the bridge one dimensional members were taken as follows:

Axial Area = A_x = 5.62 ft.^{2} (0.52 m^2)

Shear Area = A_y shear deformations neglected as small

Shear Area = A_z shear deformations neglected as small

Torsion Constant = J_x = 7.67 ft.^{4} (0.066 m^4)

Moment of Inertia = I_y = 2.64 ft.^{4} (horizontal axis) (0.023 m^4)

Moment of Inertia = I_z = 66.83 ft.^{4} (vertical axis) (0.578 m^4)

Modulus of Elasticity = E = 432,000 ksf (20,700 MPa)

Poisson's Ratio = ν = 0.15

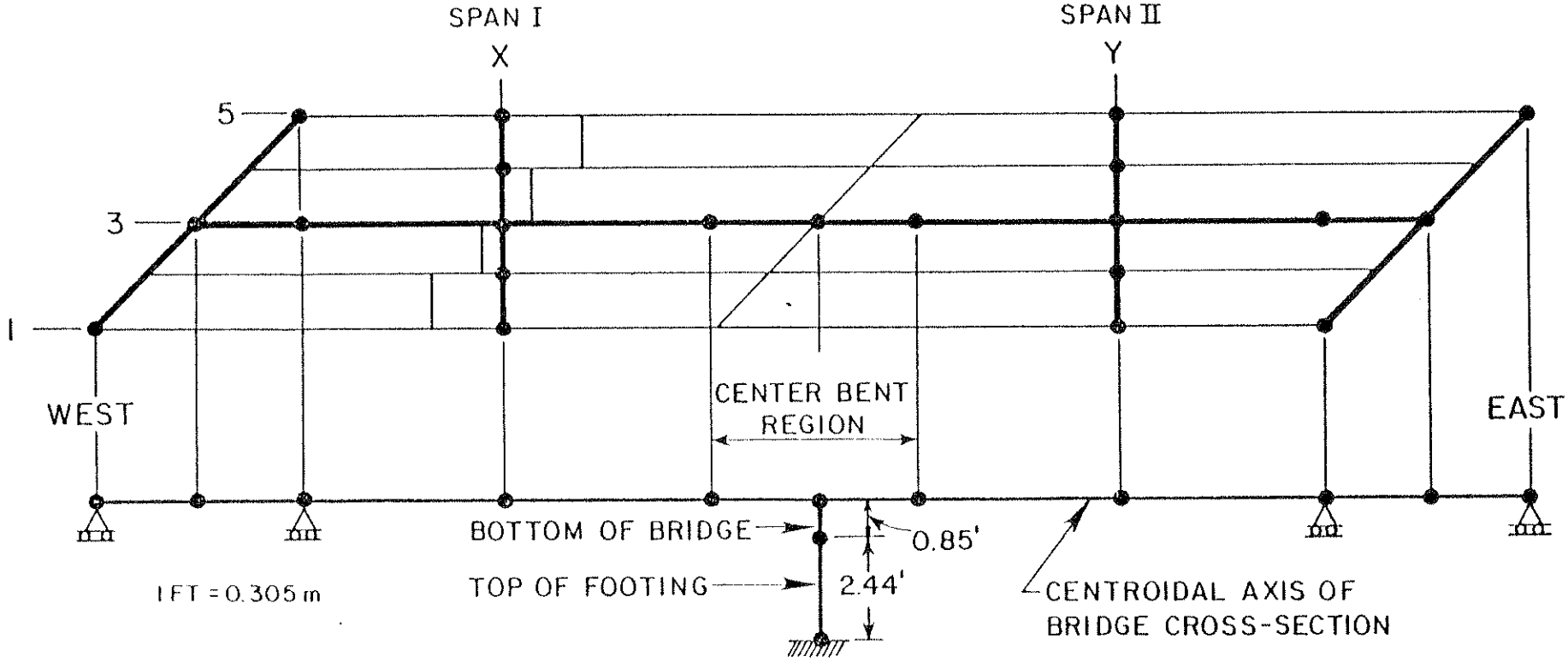

FIG. 3.22 BEAM ELEMENT MODEL

The above E was taken as an approximate average of the actual measured E values for the top and bottom slab concrete in the model.

The center bent column was idealized by two members. The first was a one dimensional member extending from the centroid of the bridge cross-section to the mid-depth of the bottom slab and was therefore 0.852 ft. (0.26 m) long. The second was a member, with a 1.5 ft. (0.46 m) diameter cross-section, extending from the mid-depth of the bottom slab to the top of the footing and was taken to be 2.441 ft. (0.74 m) long. This member's properties were taken as follows:

Axial Area	$= A_x = 1.767$ ft.^{2} (0.16 m^2)
Shear Area	$= A_y = A_z = 1.767$ ft.^{2} (0.16 m^2)
Torsion Constant	$= J_x = 0.498$ ft.^{4} (0.0043 m^4)
Moment of Inertia	$= I_y = I_z = 0.249$ ft.^{4} (0.0022 m^4)
Modulus of Elasticity	$= E = 432{,}000$ ksf (20,700 MPa)
Poisson's Ratio	$= \nu = 0.15$

The end abutments were modelled by one dimensional beam elements running at an angle of 45° to the longitudinal bridge axis in the horizontal plane and are vertically supported at the ends only. These elements were assumed to be rigid in bending since the actual end abutment was very stiff with supports at five points which restrained vertical deflections and also rigid in torsion since the abutment was monolithic with the four cell box. The end abutment elements were assumed to be rigidly connected to the longitudinal bridge elements.

Finally, as an aid to simulating the eccentric loading of the structure, rigid "outrigger" elements were assumed to be connected

perpendicular to the bridge axis at the two midspan sections X and Y so that eccentric point loads could be placed on them.

The derivation of the stiffness properties of the center bent region needs particular attention, Fig. 3.22, because these properties influence the force transmission in the structure considerably. Extensive studies on different representations of the center bent region indicate that the overall behavior of the model is primarily influenced by the column stiffness and the connection between the column and the bridge structure. Changes in bending and torsional stiffness of the longitudinal beam elements in the center bent region which were made to account for the skewness of the heavy center diaphragm, were found to have only little influence on the overall behavior of the bridge.

Another aspect which has to be considered in deriving the stiffness properties of the center bent region is that the actual four cell box structure has a certain transverse flexibility which also influences the longitudinal bending stiffness of the structure when the bridge is idealized as a one dimensional member along its longitudinal centroidal axis. This effect can be accounted for by increasing the bending flexibility of the center support, therefore by increasing the column length.

The above considerations as well as numerous trial calculations with different stiffness properties and the desire to retain the greatest simplicity possible, resulted in the following model. The layout of Fig. 3.22 was used with the stiffness properties given above. In addition the stiffness properties assigned to the connection element between the actual column and the centroid of the four cell box were taken as those of the actual column rather than as a rigid link which is equivalent to the previously discussed increase in column length.

The beam element model was tested for the following load cases: Dead Load, Blocks, Conditioning Load and Point Loads at locations 1X, 3X, 5X, 1Y, 3Y, 5Y, 1X+1Y, 3X+3Y, 5X+5Y, 1X+5Y and 5X+1Y. A comparison between the beam element model results for reactions and midspan deflections obtained using SAP and the CELL FINE results is given in Table 3.8. They show remarkable agreement for such a simplified model. The following observations can be made:

(1) The external vertical reactions of the beam element model are in very good agreement with the CELL FINE results. The fact that CELL gives a slightly higher center bent reaction and lower end abutment reactions than the beam element model is due to the elastic springs used in CELL but not in the beam element model.

(2) The internal moments and torques along the length of the bridge derived from the vertical end reactions as well as those calculated at the top of the column are also very close to the CELL values.

(3) The agreement of the midspan deflections is not quite as good as for reactions and moments but still acceptable. In general the deflections in the loaded span are slightly overestimated by the beam element model. The midspan deflection of the CELL FINE model was taken as the deflection under the center girder and not as an average of the deflections across the midspan section, which accounts partially for this effect.

TABLE 3.8 COMPARISON BETWEEN SAP BEAM ELEMENT MODEL AND CELL FINE RESULTS

LOAD CASE	PROGRAM	Reactions (KIPS or FT-KIPS)								Midspan Deflections ($\times 10^{-2}$ FT)	
		RW	RF	RE	Total R	MW	ME	MF	MT	3X	3Y
CL	CELL	35.6	128.9	35.6	200.1	-122	122	0	0	-3.42	-3.39
	SAP	36.1	127.8	36.1	200.0	-113	113	0	0	-3.66	-3.66
DL	CELL	16.7	48.2	16.4	81.3	-19	19	0	0	-0.71	-0.66
	SAP	17.7	47.1	17.7	82.5	-22	22	0	0	-1.07	-1.07
Blocks	CELL	25.0	46.7	25.0	96.7	-37	37	0	0	-1.07	-1.07
	SAP	23.3	50.0	23.3	96.6	-38	38	0	0	-1.03	-1.03
1X	CELL	32.5	72.9	-5.4	100.0	193	125	117	-196	-6.81	3.02
	SAP	33.0	71.6	-4.6	100.0	198	125	122	-191	-7.28	2.94
3X	CELL	42.5	64.4	-6.9	100.0	-93	25	91	-69	-5.77	1.99
	SAP	42.7	63.9	-6.6	100.0	-91	22	94	67	-5.65	1.99
5X	CELL	52.6	55.9	-8.5	100.0	-390	-73	64	51	-3.58	1.02
	SAP	52.4	56.2	-8.6	100.0	-380	-81	66	53	-4.02	1.04
1Y	CELL	-8.4	55.8	52.7	100.1	72	392	-63	-51	1.00	-3.35
	SAP	-8.6	56.2	52.4	100.0	81	380	-66	-53	1.04	-4.00
3Y	CELL	-6.9	64.5	42.4	100.0	-24	92	-93	68	1.99	-6.35
	SAP	-6.6	63.9	42.7	100.0	-22	91	94	69	1.99	-5.70
5Y	CELL	-4.8	72.0	32.8	100.0	-121	204	-122	189	2.93	-6.57
	SAP	-4.6	71.6	33.0	100.0	-125	198	-122	191	2.96	-7.28
1X + 1Y	CELL	24.1	128.7	47.3	200.1	264	517	54	-247	-5.81	-0.33
	SAP	24.4	127.8	47.8	200.2	279	505	56	-245	-6.24	-1.08
3X + 3Y	CELL	35.6	128.9	35.5	200.0	-118	117	-2	1	-3.78	-4.36
	SAP	36.1	127.8	36.1	200.0	-113	113	0	0	-3.66	-3.66
5X + 5Y	CELL	47.1	128.9	24.0	200.0	-515	-265	-52	249	-0.56	-5.55
	SAP	47.8	127.8	24.4	200.0	-505	-279	-56	245	-1.06	-6.24
1X + 5Y	CELL	27.0	145.9	27.1	200.0	68	-67	0	1	-3.78	-5.55
	SAP	28.4	143.2	28.4	200.0	73	-73	0	0	-4.34	-4.34
5X + 1Y	CELL	44.1	111.7	44.2	200.0	-319	319	2	0	-2.58	-2.33
	SAP	43.8	117.4	43.8	200	-299	299	0	0	-2.98	-2.98

1 KIP = 4.448 kN
1 FT = 0.305 m

(4) In general it can be observed that with this very simple beam element model the overall behavior of the actual bridge structure can be predicted quite accurately for the given conditions. However, it should be noted that extrapolations from these findings to skew box girder bridges with different span-to-width ratios, different angles of skewness, number of spans or support conditions at the center bent (e.g., several columns instead of one) would have to be checked very carefully in each individual case.

(5) Finally it should be remembered that the beam element model analyzed with SAP can only be used to give an indication of the longitudinal distribution of total reactions, moments and torques, but it gives no information about the transverse distribution of these quantities or the internal membrane forces and plate bending moments in each element, which are obtained from the more complex CELL program.

3.5 Comparison of Theoretical Results for Straight, Curved and Skew Box Girder Bridge Models

The influence of skewness of the box girder bridge can be best established by a direct comparison with the results of the straight and curved box girder bridge models investigated in previous studies [1,2,3] and [4,5,6] respectively. The theoretical results for the straight bridge were obtained using a finite element computer program entitled FINPLA 2 [Appendix of Research Reports, 5] while the curved bridge was also analyzed using CELL [14] as described above.

For all three models the boundary conditions were in general similar with the exception that flexible vertical end supports were used for the skew bridge instead of the rigid vertical end supports used for the straight and curved bridges and a horizontal transverse restraint at the end supports was used for the straight bridge. These differences however are not likely to influence the results considerably. A comparison of total reactions and distribution of moments as well as deflections and longitudinal membrane forces are presented in Tables 3.9 to 3.13.

In Table 3.9 the total reactions of the three different bridge types are compared. Considering first load cases where two spans are loaded and the loads are symmetrical about the center girder of the bridge (i.e., Dead Load, Conditioning Load and 3X+3Y) the vertical reactions for the straight and the curved bridge are virtually the same, whereas the skew bridge takes a larger portion of the load in the end abutments and relieves the center bent reaction.

For point loads in either or both spans as the loads shift transversely across the bridge from girder 1 to girder 3 to girder 5, the vertical reactions in the straight bridge do not change. The curved bridge shows a decrease in the vertical end reaction in the loaded spans while the center bent reaction increases accordingly. For the skew bridge the two spans have to be considered separately. The total vertical west abutment reaction increases significantly as the load moves from girder 1 to 3 to 5, while the corresponding reaction at the east end abutment decreases accordingly. Thus the vertical center bent reaction remains unchanged as in the straight bridge.

The skew bridge features the highest total vertical end abutment reactions as noted earlier for loads applied on the obtuse side of the

TABLE 3.9 COMPARISON OF THEORETICAL REACTIONS FOR STRAIGHT (ST), CURVED (CU) AND SKEW (SK) BRIDGE MODELS

LOAD CASE		REACTIONS (KIPS AND FT-KIPS)								
		R_W	T_W	M_W	R_F	T_F	M_F	R_E	T_E	M_E
DL + BL	ST	33.0	0	0	109.8	0	0	33.0	0	0
	CU	32.7	34	0	113.5	-4	-2	32.8	32	0
	SK	40.6	56	-56	94.3	0	1	40.1	-56	56
CL	ST	31.1	0	0	137.8	0	0	31.0	0	0
	CU	30.8	39	0	138.4	0	0	30.8	39	0
	SK	35.6	122	-122	128.9	0	0	35.6	-122	122
1X	ST	39.2	-355	0	69.0	-42	96	-8.2	-95	0
	CU	41.2	-283	0	64.5	-83	110	-5.7	-99	0
	SK	32.5	-193	193	72.9	-196	117	-5.4	-125	125
3X	ST	39.3	0	0	68.8	0	86	-8.1	0	0
	CU	38.8	57	0	69.1	0	122	-7.9	-17	0
	SK	42.5	93	-93	64.4	-69	91	-6.9	-25	25
5X	ST	39.2	335	0	69.0	42	96	-8.2	95	0
	CU	36.2	395	0	74.1	82	133	-10.2	63	0
	SK	52.6	390	-390	55.9	51	65	-8.5	73	-73
1X + 1Y	ST	31.0	-432	0	138.0	-84	0	31.0	-431	0
	CU	35.3	-382	0	129.3	-168	0	35.3	-382	0
	SK	24.1	-264	+264	128.7	-247	54	47.3	-517	517
3X + 3Y	ST	31.2	0	0	137.7	0	0	31.2	0	0
	CU	30.9	39	0	138.3	1	-3	30.8	39	0
	SK	35.6	118	-118	228.9	1	-2	35.5	-117	117
5X + 5Y	ST	31.0	432	0	138.0	84	0	31.0	431	0
	CU	26.0	458	0	147.9	166	3	26.1	458	0
	SK	47.1	515	-515	128.9	249	-52	24.0	265	-265

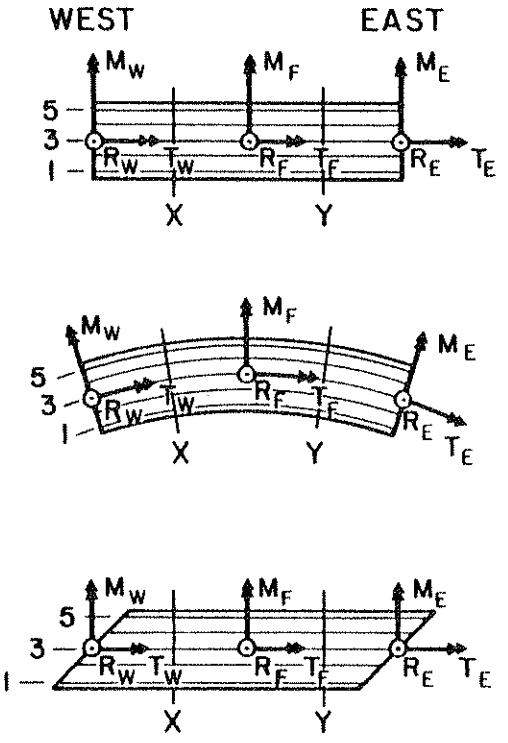

1 KIP = 4.448 kN
1 FT = 0.305 m

TABLE 3.10 COMPARISON OF THEORETICAL TOTAL INTERNAL MOMENTS (FT-KIPS) AT A SECTION FOR STRAIGHT, CURVED AND SKEW BRIDGE MODELS

LOAD CASE	BRIDGE MODEL	INTERNAL MOMENTS (FT-KIPS)					
		A	X	Z		Y	D
DEAD LOAD + BLOCKS	STRAIGHT	222	199	-395	-395	199	222
	CURVED	230	210	-378	-378	194	221
	SKEW	189	179	-304	-304	165	185
COND. LOAD	STRAIGHT	447	558	-674	-674	557	446
	CURVED	452	564	-700	-700	564	452
	SKEW	426	484	-545	-545	481	426
1X	STRAIGHT	565	705	-403	-295	-147	-118
	CURVED	557	695	-351	-242	-121	-97
	SKEW	561	*	*	*	*	-131
3X	STRAIGHT	561	700	-394	-290	-145	-116
	CURVED	569	710	-406	-290	-145	-116
	SKEW	561	*	*	*	*	-131
5X	STRAIGHT	565	705	-403	-295	-147	-118
	CURVED	582	726	-474	-347	-174	-139
	SKEW	420	*	*	*	*	-58
1X + 1Y	STRAIGHT	448	559	-678	-470	553	443
	CURVED	458	572	-596	-402	570	457
	SKEW	632	*	*	*	*	212
3X + 3Y	STRAIGHT	446	557	-670	-670	559	448
	CURVED	453	565	-694	-694	564	452
	SKEW	430	*	*	*	*	430
5X + 5Y	STRAIGHT	448	559	-678	-678	553	443
	CURVED	444	554	-812	-812	555	445
	SKEW	211	*	*	*	*	634

1 FT-KIP = 1.356 kN-m

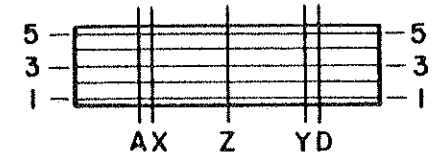

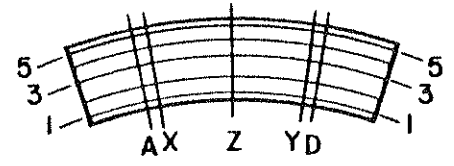

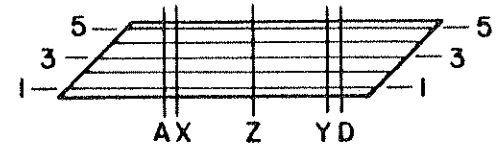

*Skew bridge values not shown were not computed.

TABLE 3.11 COMPARISON OF TRANSVERSE DISTRIBUTION OF DEFLECTIONS ($FT \times 10^{-2}$) AT MIDSPAN SECTIONS X AND Y FOR STRAIGHT, CURVED AND SKEW BRIDGE MODELS

LOAD CASE	BRIDGE MODEL	SECTION X					SECTION Y				
		GIRDERS					GIRDERS				
		1	2	3	4	5	1	2	3	4	5
1X + 1Y	STRAIGHT	6.86	5.27	3.88	3.59	1.61	8.00	5.30	3.50	2.25	1.36
	CURVED	5.79	4.61	3.41	2.40	1.50	4.77	4.77	3.18	2.01	1.33
	SKEW	11.69	8.30	5.81	3.99	1.32	5.75	2.63	0.33	-1.48	-3.04
3X + 3Y	STRAIGHT	3.86	3.98	4.13	3.98	3.86	3.50	3.89	4.90	3.89	3.50
	CURVED	3.44	3.72	4.04	4.07	4.12	3.15	3.67	4.81	3.95	3.71
	SKEW	3.78	3.77	3.78	3.16	2.56	2.36	3.06	4.36	3.65	3.55
5X + 5Y	STRAIGHT	1.61	2.68	3.88	5.28	6.86	1.36	2.25	3.50	5.30	8.00
	CURVED	1.56	2.78	4.15	5.72	7.49	1.27	2.30	3.69	5.63	8.46
	SKEW	-2.82	-1.18	.55	2.42	5.12	1.10	3.16	5.55	8.50	12.33
1X	STRAIGHT	8.29	6.97	5.85	4.93	6.17	-1.43	-1.71	-1.99	-].]8	-2.55
	CURVED	7.14	6.11	5.25	4.59	4.06	-1.16	-1.49	-1.81	-2.15	-2.50
	SKEW	12.46	9.18	6.80	4.60	2.56	-.76	-1.88	-3.02	-4.18	-5.37
3X	STRAIGHT	5.86	5.96	6.10	5.96	5.86	-1.98	-1.97	-1.97	-1.97	-1.98
	CURVED	5.25	5.61	6.01	6.13	6.31	-1.84	-1.91	-1.97	-2.06	-2.16
	SKEW	6.81	6.27	5.77	4.66	3.58	-.99	-1.48	-1.99	-2.51	-3.03
5X	STRAIGHT	4.17	4.94	5.86	6.97	8.30	-2.55	-2.28	-1.99	-1.71	-1.44
	CURVED	4.06	5.11	6.31	7.73	9.36	-2.55	-2.37	-2.18	-2.02	-1.87
	SKEW	2.59	3.01	3.58	4.30	5.90	-1.24	-1.12	-1.02	-.91	-.78

1 FT = 0.305 m

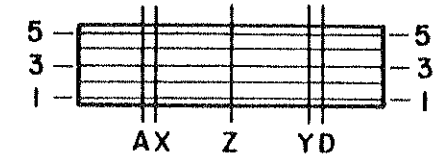

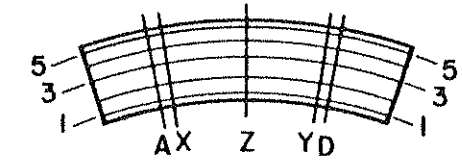

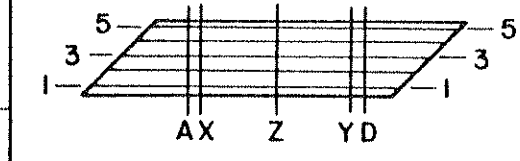

TABLE 3.12 COMPARISON OF TRANSVERSE DISTRIBUTION OF LONGITUDINAL MEMBRANE FORCES N_x (KIPS/FT) AT SECTION A FOR STRAIGHT CURVED AND SKEW BRIDGE MODELS

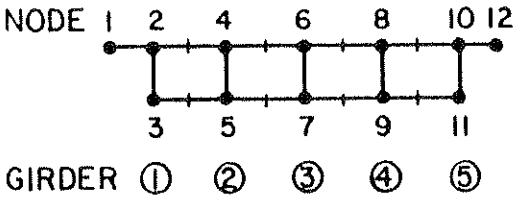

1 KIP = 4.448 kN
1 FT = 0.305 m

LOAD CASE	LOCATION	BRIDGE MODEL	TOP NODES							BOTTOM NODES				
			1	2	4	6	8	10	12	3	5	7	9	11
1X + 1Y	PLATE	STRAIGHT	-28.1	-26.2	-24.1	-22.1	-20.7	-21.6	-23.2	32.3	27.0	21.6	17.6	15.6
		CURVED	-41.6	-32.3	-24.7	-20.8	-18.0	-19.4	-22.5	32.5	26.7	21.8	18.6	17.2
		SKEW	-42.2	-37.2	-34.2	-32.5	-25.7	-28.0	-33.4	34.8	38.1	34.6	27.6	26.1
	WEB	STRAIGHT		-25.6	-24.5	-22.5	-20.9	-20.9		47.5	39.9	32.1	22.8	21.7
		CURVED		-32.0	-29.1	-24.6	-21.2	-19.3		48.0	39.5	32.2	27.0	25.4
		SKEW		-41.7	-46.2	-44.1	-34.7	-31.5		52.3	57.8	52.9	41.8	40.8
3X + 3Y	PLATE	STRAIGHT	-21.6	-22.1	-23.0	-23.8	-23.0	-22.1	-21.6	21.7	22.8	23.1	22.8	21.7
		CURVED	-27.2	-24.2	-20.1	-23.0	-21.8	-23.1	-24.7	22.8	23.3	23.5	23.0	21.2
		SKEW	-30.1	-25.4	-24.0	-20.4	-18.7	-18.6	-19.2	26.4	25.7	21.2	20.1	17.4
	WEB	STRAIGHT		-21.4	-22.9	-23.6	-22.9	-21.4		31.8	32.2	33.5	33.2	31.8
		CURVED		-23.9	-25.6	-26.4	-25.3	-22.9		33.4	34.0	34.2	33.6	31.1
		SKEW		-28.5	-31.4	-26.1	-24.1	-20.7		39.4	37.9	30.7	29.2	25.7
5X + 5Y	PLATE	STRAIGHT	-23.2	-21.6	-20.7	-22.1	-24.1	-26.2	-28.1	15.6	17.6	21.6	27.0	32.3
		CURVED	-24.3	-19.7	-18.0	-20.7	-23.8	-25.9	-37.3	18.1	18.6	21.5	25.6	29.3
		SKEW	-6.5	-5.2	-5.6	-5.3	-12.7	-26.0	-34.2	4.0	5.5	5.9	15.1	28.6
	WEB	STRAIGHT		-20.9	-20.9	-22.5	-24.5	-25.6		23.2	26.1	32.1	39.9	47.5
		CURVED		-19.6	-21.2	-24.6	-28.2	-29.3		26.8	27.6	32.0	38.0	43.3
		SKEW		-5.8	-7.4	-6.7	-16.6	-29.0		-6.0	7.9	8.1	21.9	42.9

TABLE 3.13 COMPARISON OF TRANSVERSE DISTRIBUTION OF TOTAL MOMENT AT SECTION A TO EACH GIRDER (FT-KIPS AND PERCENT) FOR STRAIGHT, CURVED AND SKEW BRIDGE MODELS

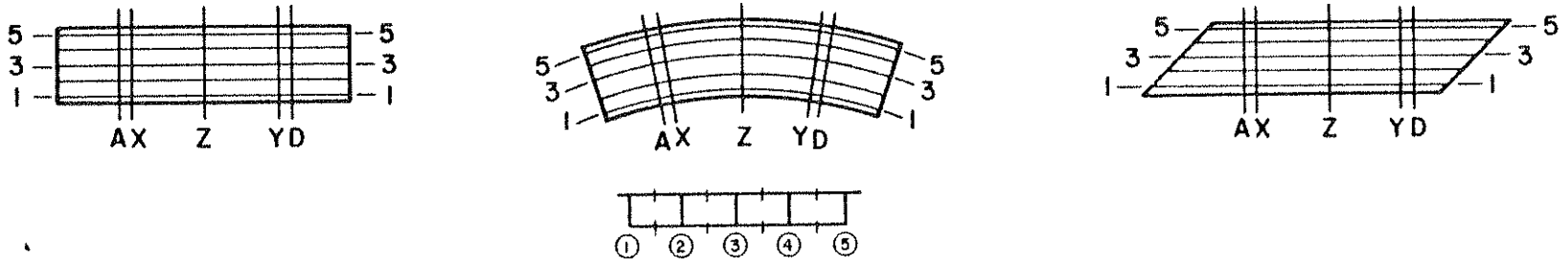

LOAD CASE	BRIDGE MODEL	INTERNAL MOMENTS (FT-KIPS)						PERCENTAGE OF TOTAL INTERNAL MOMENTS					
		GIRDERS					TOTAL	GIRDERS					TOTAL
		1	2	3	4	5		1	2	3	4	5	
1X + 1Y	STRAIGHT	89	116	99	86	59	448	19.8	25.9	22.1	19.2	13.1	100.0
	CURVED	100	118	97	84	58	458	21.8	25.8	21.3	18.4	12.6	100.0
	SKEW	115	164	149	123	84	634	18.1	25.9	23.5	19.4	13.3	100.0
3X + 3Y	STRAIGHT	68	103	105	103	68	446	15.2	23.0	23.5	23.0	15.2	100.0
	CURVED	73	104	105	102	69	453	16.2	22.9	23.1	22.5	15.3	100.0
	SKEW	79	110	97	88	56	430	18.3	25.5	22.7	20.6	13.0	100.0
5X + 5Y	STRAIGHT	59	86	99	116	89	448	13.1	19.2	22.1	25.9	19.8	100.0
	CURVED	60	84	96	113	91	444	13.4	19.0	21.6	25.4	20.5	100.0
	SKEW	15	23	28	65	80	211	6.9	11.1	13.4	30.8	37.9	100.0

1 FT-KIP = 1.356 kN-m

span. For only one span loaded, this effect is even more pronounced, and simultaneously the center bent reaction undergoes a substantial decrease while the small vertical end reaction in the unloaded span remains basically unchanged for loads shifting from the acute to the obtuse side of the span.

Observing the reaction torque values in Table 3.9 it should be noted that even loads applied along the centerline of the skew bridge cause considerable reaction torques due to the skew end abutments. The straight bridge has no torque for these load cases, while the curved bridge features torque values between the ones for the straight and skew bridge.

For the 45° skew bridge this torque at the end abutments is the same as the negative end moment, a condition which is not encountered in the straight or curved bridge. This negative end moment reaction contributes favorably to the midspan moment due to the vertical external reactions for loads on the obtuse side of the span. At the same time, however, it should be noted that this positive effect is reduced by an increase in the total vertical end reaction which results in increased midspan moments and that this reaction end moment acts unfavorably for loads on the acute side of the bridge.

The comparison of internal moments in Table 3.10 shows that for the important dead load and conditioning load cases substantially lower internal moments occur in the skew bridge. For the straight and curved bridges the midspan moment is virtually unchanged for point loads shifting transversely across the bridge. The skew bridge however shows higher midspan moments for loads on the acute side of the span and lower midspan moments for loads on the obtuse side of the span.

The negative moment over the center support is found to be smaller for the skew bridge than for the straight or curved bridges, independently of the load position on the bridge. The values of internal moments for the straight bridge in Table 3.10 have been adjusted from those given in references [2,5] to account for interpolations required by the mesh size used in the finite element analysis.

The transverse distribution of deflections at midspan sections X and Y is given in Table 3.11. Values for the deflections of the straight and curved bridge taken from the curved bridge report [5] have been multiplied by a factor of 400/438 = 0.91 to reflect the fact that the average values of the elastic modulus used in the curved bridge report and the present skew bridge analysis were 400,000 and 438,000 ksf (19,200 and 21,000 MPa) respectively. For standard point loads at 3X+3Y the skew bridge deflections are smaller than the corresponding deflections for the straight and the curved bridge. For a point load on the acute side of the span the skew bridge deflections are higher than for the straight or curved bridge, while for loads on the obtuse side of the bridge the opposite is the case.

The transverse distribution of longitudinal membrane forces N_x at the instrumented section A is shown in Table 3.12. It can be observed that for loads along the center girder the membrane forces in the longitudinal direction are of the same order of magnitude as for the straight and the curved bridges. It is interesting to note that higher membrane forces exist at section A on the acute side of the span than on the obtuse side. For loads along girder 1 the membrane forces N_x at section A are considerably higher for the skew bridge then the straight or the curved bridge models, while for loads along girder 5 the membrane forces at

section A of the skew bridge are much smaller than in the corresponding straight and curved bridge cases. This emphasizes the sensitivity of the skew bridge to transverse load position as compared to the straight or curved bridge.

A summary of a typical transverse distribution of internal moments to each girder at section A is given in Table 3.13. For loads shifting from girder 1 to 3 the distribution of internal moments is virtually the same for all three bridge types. For loads placed along girder 5 the distribution changes substantially. In the skew bridge the major portion of the load is transferred in the obtuse side of the bridge primarily by girder 5 while girder 1 at the acute side of the span contributes only a little.

3.6 Computer Times for Skew Bridge Model Analyses

Of particular interest in comparing solutions by various computer programs are the computer times and costs involved in obtaining the solutions. Table 3.14 summarizes a comparison of typical runs made on the CDC 6400 computer at the University of California Computer Center for analyses of the skew bridge model using SAP and CELL.

The half band width, Column (2), is equal to the number of degrees of freedom per node times the sum of the maximum difference in nodal point numbers of any element plus one. Proper numbering of the nodes will keep the band width to a minimum and thus reduce the computer time accordingly. The number of equations, Column (3), equals the total number of nodes times the degrees of freedom per node. For multiple load cases, Column (4), SAP and CELL reduce the stiffness matrix for the first load case, and this can then be also used for subsequent load cases. Thus additional load cases can be treated more economically than the first one.

TABLE 3.14 CDC 6400 CP AND PP COMPUTER TIMES (SECONDS) FOR SKEW BRIDGE MODEL ANALYSIS

PROGRAM	BAND WIDTH	NUMBER OF EQUATIONS	NUMBER OF LOAD CASES	FIRST LOAD CASE		NEXT LOAD CASE		TOTAL		COST ($)
				CP	PP	CP	PP	CP	PP	
(1)	(2)	(3)	(4)	(5)	(6)	(7)	(8)	(9)	(10)	(11)
SAP	24	128	9	3	9	0.5	0.4	7	12	2
CELL COARSE	90	2310	10	347	209	53	73	862	899	80
CELL FINE	130	6270	14	1692	1728	153	240	3670	4873	344

Columns (5) to (10) give the computer times in seconds. CP stands for central computer processing time and PP stands for peripheral unit processing time. For program CELL, which requires large core storage, PP time is charged at a rate of 0.9 to 1.6 times CP time. For comparative purposes only, Column (11) indicates actual costs charged by the University of California Computer Center for running the total number of load cases shown in Column (4). Actual costs on other computer systems would of course depend on the system and the rate schedule.

A study of Table 3.14 makes it evident that the cost for a SAP analysis is very small compared to a CELL analysis. The latter program of course involves a complete analysis of the multi-cell box structure.

In comparing computer times and cost, it must be recognized that additional time and costs involved in preparing the input data and interpreting the results from the output generally involve costs which are many times that of the computer cost itself.

3.7 Comments on Comparison of Theoretical Deflections and Strains with Experimental Values

Analytical methods used for comparison with experimental results, e.g., the finite element approach with the associated CELL program, or the three dimensional frame analysis used in the SAP program, are based on the linear elastic behavior of an uncracked, homogeneous, isotropic structure. The theoretical values given by these analyses for the deflection of a box girder bridge at a certain point or the strain at a cross-section are not immediately applicable to those experimentally obtained from the cracked reinforced concrete box girder bridge model. It is clear that the assumption of a completely uncracked section as made in the theories would result in underestimation of the actual deflection of the box girder bridge

model. Again, the strain values predicted by the theories in the part of the box girder cross-section subject to tension can not directly be compared with the experimental case where, due to concrete cracking, most of the stress was concentrated in the steel reinforcement.

Theoretical deflections based on an uncracked section should form a lower bound on the actual deflection in the model. An upper bound should be formed by assuming a fully cracked transformed section throughout, since it neglects participation of the concrete between cracks. Various empirical formulae have been proposed for interpolating between these two bounds, in calculating the deflection of straight reinforced concrete beams. For complex systems such as bridge decks, which involve transverse as well as longitudinal distributions of deflections, it will be important to ascertain whether a relatively uniform ratio of experimental to theoretical deflections (based on uncracked section using CELL) exists under various loadings and if so, what this ratio is for various stress levels. If these can be established then the deflections from analyses based on an uncracked section can be utilized to predict deflections in an actual reinforced concrete bridge structure under a given loading.

Direct comparisons between the longitudinal strains predicted by the CELL program, with its analytical model of homogeneous linear elastic material without cracking, and the actual experimental strains measured in the concrete and steel of the cracked box girder bridge model are difficult to make. If it is assumed that the force distribution over the width of the box girder model given by the CELL program is representative of the actual force distribution, then bearing in mind that each girder of the box girder bridge model essentially behaves like an I-beam with

the T-C couple acting in the flanges, approximate expressions for the strains in the girders can be derived.

Thus, for comparison with experimental values, compressive strains were obtained from the theoretical results given by the CELL program by dividing the values for the longitudinal compressive force N_x per unit length at each gaged location by the respective plate thickness and the concrete elastic modulus E_c. Theoretical steel strains were obtained by considering a fully cracked section and dividing the total longitudinal tensile force N_x per girder by the product of the steel area of the girder and the steel elastic modulus E_s.

As the contribution of the transverse membrane force N_y to the strains was found to be negligible it was ignored in the calculations.

Hereafter, comparisons for strains are based on theoretical strain values derived as above from the CELL analysis.

3.8 Summary

A comprehensive discussion of the various theoretical analyses made of the skew bridge model has been presented. Results obtained using various computer programs as well as for the straight and curved bridge models have been compared. The following important conclusions may be stated.

1. An analysis such as provided by the SAP program, in which the bridge system is assumed to be a simple three dimensional frame made up of one dimensional beam and column elements, can be used to accurately predict the longitudinal distribution of theoretical total reactions, moments and centerline deflections.

2. The finite element program CELL provides a solution of the bridge system as a true three dimensional cellular structure composed of a top and bottom plate system interconnected by vertical web elements. CELL can be used to accurately predict the longitudinal and transverse distribution of theoretical reactions, moments, deflections and internal membrane and plate bending forces. Henceforth, the CELL FINE solution will be used for all theoretical values to be compared with experimental results, unless otherwise stated.

3. A comparison of the theoretical results for the similar straight, curved and skew bridge models shows that while the straight and curved bridge behave quite similarly the skew bridge features substantial differences and is very sensitive to the type and position of the applied loads.

It should be emphasized that for the most important design load cases, such as dead load and conditioning load, substantially smaller internal moments occur in the midspan and center bent regions for the skew bridge as compared to the straight and curved bridge.

For all load cases, the negative moments in the center bent region are found to be smaller in the skew bridge than the corresponding moments in the straight and curved bridge models.

For positive midspan moments a beneficial effect of the skewness is dependent on the transverse position of the load. For point loads on the obtuse side of the span and along the center girder, the midspan moment in the skew bridge is smaller, whereas point loads on the acute

side of the span yield higher total midspan moments in the skew bridge than in the comparable cases for the straight and curved bridges. This behavior is especially important when the positioning of heavy concentrated overloads has to be considered.

4. REDUCTION OF EXPERIMENTAL DATA

4.1 General Remarks

In order to organize and process the large volume of experimental data obtained from the different loading cases, so as to evaluate the reactions, deflections, forces and moments, a sequence of six data reduction programs was developed. The computer programs, to be considered in detail below, were designated as MANFRED, REACT, DEFLECT, STRAINS, ROSETTE and TABLES. The data from the experimental program were categorized and different data sets used for each of the above programs. These operations were performed for each loading step, and all calculations necessary for theoretical comparisons, equilibrium checks and evaluation of important quantities were carried out and the results printed in desired formats.

4.2 MANFRED Program

The title of this program is a compound of (MAN)IP and (RED)UCE, two data reduction programs used for the experimental data of the curved box girder bridge model, described in detail in References 4-6.

The MANFRED program utilized the appropriate punched card decks obtained from the master magnetic tape of the experimental data for each loading case and catalogued the data under the following headings: Load cell reactions, applied loads, deflections, strain readings for weldable gages, concrete strain meters and concrete strain rosettes. In addition, there were two readings for standard resistors which provided a check on the stability of the recording equipment. As in the MANIP program, all faulty readings whether from over-range (i.e., unbalanced) or damaged

SERIAL NO.	NAME	CH.NO.	TYPE	READING
LOAD CELL REACTIONS IN KIPS				
1	W1	1	0	2.17
2	W2	2	0	3.32
3	W3	3	0	3.69
4	W4	8	0	.57
5	W5	9	0	-3.26
6	E1	10	0	2.64
7	E2	11	0	.66
8	E3	16	0	-.89
9	E4	17	0	-1.83
10	E5	18	0	-1.13
11	NET	19	0	.40
12	NEB	24	0	-6.69
13	SET	25	0	-.30
14	SEB	26	0	6.37
15	SWT	27	0	-.80
16	SWB	32	0	14.62
17	NWT	33	0	-.10
18	NWB	34	0	.20
APPLIED LOAD IN KIPS				
19	APL1	35	0	19.32
20	APL2	40	0	-.63
POTENTIOMETERS DEFLECTIONS IN INCHES				
21	P79	4	4	-.1799
22	P123	5	4	-.2837
23	P127	6	4	-.1512
24	P211X1	7	4	-.4054
25	P171	12	4	-.2151
26	P175	13	4	-.0759
27	P167	14	4	-.3667
28	P259	15	4	-.1753
29	P219X5	20	4	-.0990
30	P255	21	4	-.3157
31	P215X3	22	4	-.2227
32	P307	23	4	-.0181
33	P333	28	4	-.1044
34	P263	29	4	-.0711
35	P321	30	4	-.1564
36	P351	31	4	-.0127
37	P387	36	4	-.0461
38	P417	37	4	.1084
39	P411	38	4	-.0036
40	P435	39	4	.0570
41	P475	44	4	.0220
42	P479	45	4	.0792
43	P483	46	4	.1358
44	P519Y1	47	4	.0310
45	P523Y3	52	4	.0802
46	P527Y5	53	4	.1354
47	P563	54	4	.0241
48	P567	55	4	.0711
49	P571	60	4	.1242
50	P611	61	4	.0524
51	P615	62	4	.0988
52	P659	63	4	.0628

STEEL WELDABLE GAGES STRAINS IN MICRO-INCH PER INCH

BOTTOM SLAB GAGES				
53	AW100	64	1	309.
54	AW125	65	1	285.
55	AW150	66	1	239.
56	AW175	67	1	270.
57	AW200	68	1	291.
58	AW225	69	1	238.
59	AW250	70	1	198.
60	AW275	71	1	253.
61	AW300	72	1	285.
62	AW325	73	1	199.
63	AW350	74	1	178.
64	AW375	75	1	189.
65	AW400	76	1	206.
66	AW425	77	1	197.
67	AW450	78	1	168.
68	AW475	79	1	167.
69	AW500	80	1	81.
TOP SLAB GAGES				
70	BW000	81	1	66.
71	BW100	82	1	85.
72	BW125	83	1	61.
73	BW150	84	1	52.
74	BW175	85	1	48.
75	BW200	86	1	62.
76	BW225	87	1	55.
77	BW250	88	1	51.
78	BW275	89	1	56.
79	BW300	90	1	85.
80	BW325	91	1	94.
81	BW350	92	1	83.
82	BW375	93	1	61.
83	BW400	94	1	66.
84	BW425	95	1	40.
85	BW450	96	1	45.
86	BW475	97	1	37.
87	BW500	98	1	44.
88	BW600	99	1	39.
89	CW000	100	1	65.
90	CW100	101	1	64.
91	CW125	102	1	68.
92	CW150	103	1	81.
93	CW175	104	1	81.
94	CW200	105	1	69.
95	CW225	106	1	70.
96	CW250	107	1	40.
97	CW275	108	1	37.
98	CW300	109	1	60.
99	CW325	110	1	57.
100	CW350	111	1	38.
101	CW375	112	1	46.
102	CW400	113	1	55.
103	CW425	114	1	38.
104	CW450	115	1	75.
105	CW475	116	1	78.
106	CW500	117	1	59.
107	CW600	118	1	92.

FIG. 4.1 TYPICAL OUTPUT FROM MANFRED PROGRAM

BOTTOM SLAB GAGES

108	DW100	119	1	-60.
109	DW125	120	1	-59.
110	DW150	121	1	-50.
111	DW175	122	1	-69.
112	DW200	123	1	-64.
113	DW225	124	1	-62.
114	DW250	125	1	-65.
115	DW275	126	1	-54.
116	DW300	127	1	0.
117	DW325	128	1	-58.
118	DW350	129	1	-46.
119	DW375	130	1	-53.
120	DW400	131	1	-67.
121	DW425	132	1	-47.
122	DW450	133	1	-36.
123	DW475	134	1	-42.
124	DW500	135	1	-56.
125	FW100	136	1	81.
126	FW150	137	1	106.
127	FW200	138	1	207.
128	FW250	139	1	208.
129	FW350	140	1	214.
130	FW400	141	1	176.
131	FW450	142	1	200.
132	FW500	143	1	209.
133	GW100	144	1	-60.
134	GW150	145	1	-38.
135	GW200	146	1	-44.
136	GW250	147	1	-57.
137	GW350	148	1	-60.
138	GW400	149	1	-72.
139	GW450	150	1	-56.
140	GW500	151	1	-74.
141	HW100	152	1	24.
142	HW150	153	1	108.
143	HW200	154	1	117.
144	HW250	155	1	126.
145	HW300	156	1	144.
146	HW350	157	1	93.
147	HW400	158	1	91.
148	HW450	159	1	122.
149	HW500	160	1	154.
150	IW100	161	1	-27.
151	IW150	162	1	-27.
152	IW200	163	1	-44.
153	IW250	164	1	41.
154	IW300	165	1	-33.
155	IW350	166	1	-26.
156	IW400	167	1	-39.
157	IW450	168	1	-22.
158	IW500	169	1	-15.

TOP SLAB GAGES

159	JW100	170	1	-32.
160	JW150	171	1	-48.
161	JW200	172	1	-26.
162	JW250	173	1	-5.
163	JW300	174	1	13.
164	JW350	175	1	40.
165	JW400	176	1	21.
166	JW450	177	1	18.
167	JW500	178	1	33.
168	KW100	179	1	60.
169	KW150	180	1	80.
170	KW200	181	1	54.
171	KW250	182	1	82.
172	KW300	183	1	56.
173	KW350	184	1	56.
174	KW400	185	1	64.
175	KW450	186	1	50.
176	KW500	187	1	33.

CENTER BENT TOP GAGES

177	CBW1	188	1	35.
178	CBW2	189	1	97.
179	CBW3	190	1	114.
180	CBW4	191	1	34.

CONCRETE CARLSON METER STRAIN IN K.-INCH PER INCH

TOP SLAB GAGES

181	AK000	192	2	-311.
182	AK100	193	2	-123.
183	AK150	194	2	-107.
184	AK200	195	2	-85.
185	AK250	196	2	-78.
186	AK300	197	2	-86.
187	AK350	198	2	-85.
188	AK400	199	2	-66.
189	AK450	200	2	-68.
190	AK500	201	2	-67.
191	AK600	202	2	-16.

BOTTOM SLAB GAGES

192	BK100	203	2	-50.
193	BK150	204	2	-17.
194	BK200	205	2	-22.
195	BK250	206	2	-23.
196	BK300	207	2	-25.
197	BK350	208	2	-44.
198	BK400	209	2	-31.
199	BK450	210	2	-30.
200	BK500	211	2	-35.
201	CK100	212	2	-55.
202	CK150	213	2	-74.
203	CK200	214	2	-41.
204	CK250	215	2	-38.
205	CK300	216	2	-33.
206	CK350	217	2	-35.
207	CK400	218	2	-33.
208	CK450	219	2	-41.
209	CK500	220	2	-40.

FIG. 4.1 TYPICAL OUTPUT FROM MANFRED PROGRAM

TOP SLAB GAGES

210	DK000	221	2	18.
211	DK100	222	2	19.
212	DK125	223	2	19.
213	DK150	224	2	22.
214	DK175	225	2	18.
215	DK200	226	2	23.
216	DK225	227	2	25.
217	DK250	228	2	23.
218	DK275	229	2	19.
219	DK300	230	2	19.
220	DK325	231	2	20.
221	DK350	232	2	20.
222	DK375	233	2	21.
223	DK400	234	2	21.
224	DK425	235	2	18.
225	DK450	236	2	17.
226	DK475	237	2	21.
227	DK500	238	2	18.
228	DK600	239	2	23.
229	FK100	240	2	-51.
230	FK200	241	2	-82.
231	FK300	242	2	-77.
232	FK500	243	2	-51.
233	GK100	244	2	30.
234	GK200	245	2	25.
235	GK400	246	2	20.
236	GK500	247	2	13.
237	HK100	248	2	-22.
238	HK200	249	2	-36.
239	HK300	250	2	-42.
240	HK400	251	2	-61.
241	HK500	252	2	-55.
242	IK100	253	2	17.
243	IK200	254	2	17.
244	IK300	255	2	16.
245	IK400	256	2	13.
246	IK500	257	2	8.

BOTTOM SLAB GAGES

247	JK100	258	2	191.
248	JK200	259	2	37.
249	JK300	260	2	3.
250	JK400	261	2	-0.
251	JK500	262	2	-20.
252	KK100	263	2	-31.
253	KK200	264	2	-40.
254	KK300	265	2	-36.
255	KK400	266	2	-37.
256	KK500	267	2	-42.

CENTER BENT BOTTOM GAGES

257	CBK1	268	2	-65.
258	CBK2	269	2	-13.
259	CBK3	270	2	-67.
260	CBK4	271	2	-15.

CONCRETE STRAIN GAGES IN WEBS,STRAIN IN M.IN/IN

261	WS100	321	3	4.
262	WS190	322	3	-4.
263	WS145	323	3	5.
264	WS200	324	3	2.
265	WS290	325	3	-10.
266	WS245	326	3	-11.
267	WS300	327	3	11.
268	WS390	328	3	-2.
269	WS345	329	3	-9.
270	WS400	330	3	15.
271	WS490	331	3	0.
272	WS445	332	3	-6.
273	WS500	333	3	9.
274	WS590	334	3	-1.
275	WS545	335	3	10.
276	BS100	336	3	-26.
277	BS190	337	3	7.
278	BS145	338	3	-31.
279	BS200	339	3	-4.
280	BS290	340	3	52.
281	BS245	341	3	-16.
282	BS300	342	3	7.
283	BS390	343	3	-1.
284	BS345	344	3	-3.
285	BS400	345	3	0.
286	BS490	346	3	-6.
287	BS445	347	3	-5.
288	BS500	348	3	25.
289	BS590	349	3	-1.
290	BS545	350	3	9.
291	CS100	351	3	45.
292	CS190	352	3	-2.
293	CS145	353	3	19.
294	CS200	354	3	65.
295	CS290	355	3	-2.
296	CS245	356	3	2.
297	CS300	357	3	12.
298	CS390	358	3	1.
299	CS345	359	3	4.
300	CS400	360	3	7.
331	CS490	361	3	-5.
302	CS445	362	3	4.
303	CS500	363	3	0.
304	CS590	364	3	13.
305	CS545	365	3	-6.
306	ES100	366	3	-5.
307	ES190	367	3	1.
308	ES145	368	3	-9.
309	ES200	369	3	-2.
310	ES290	370	3	-1.
311	ES245	371	3	2.
312	ES300	372	3	-1.
313	ES390	373	3	3.
314	ES345	374	3	0.
315	ES400	375	3	-3.
316	ES490	376	3	1.
317	ES445	377	3	4.
318	ES500	378	3	-3.
319	ES590	379	3	-3.
320	ES545	380	3	3.

FIG. 4.1 TYPICAL OUTPUT FROM MANFRED PROGRAM

gages were screened by MANFRED and their values were set to zero. Alongside each valid data reading, the serial number, the channel number of the gage or device and the appropriate identification code consisting of the letter and number combination describing the type and location of the measuring device or quantity measured were also printed.

The MANFRED program incorporated the option of a "Normalization Factor" whereby it was possible to normalize all readings to a load of 100 kips (445 kN) per loaded span. This was carried out to facilitate comparison with theoretical values from the CELL program wherein a similar normalization was also made. Finally, the values of the catalogued data were rounded off by the MANFRED program as follows: strain values to the nearest micro inch per inch, reaction values to one-hundredths of a kip and deflections to one-ten thousandths of an inch.

A typical output from the MANFRED program is given in Fig. 4.1.

4.3 REACT Program

The REACT program was used to print the individual girder applied loads and reactions as well as the reactions at the four corners of the center column footing in a format that allowed immediate verification of experimental results for each loading case. A typical output from the REACT program is given in Fig. 4.2, wherein the girder reactions are printed at a skew angle and the general plan of the skew box girder bridge model is clearly visible. The total reactions at the east and west abutments and the center bent column as well as the reaction torques and bending moments at these locations have also been printed. Three different statics checks are carried out by the REACT program: the sum of the vertical forces and the sum of the moments about the bridge model

1 FILE 145 NET, OCT. 26, 78, TIME 9.15 AM, 1.0X 1X CL30

LOAD CELL REACTIONS IN KIPS

SUMMARY OF MEASURED APPLIED LOADS AND REACTIONS(KIPS)

```
         WEST                  L/2                      COLUMN                      L/2                   EAST

            -3.26 **********   0.  ****************************************   0.  ***************************   -1.13
               *               *                                              *                            *
           .57 **************  0.  ****************************************   0.  ***********************   -1.83
             *                 *                  .30**  -7.09                *                        *
       3.69 *****************  0.  ****************************************   0.  ******************    -.89
          *                    *                15.42**   5.67                *                      *
    3.32 ********************  0.  ****************************************   0.  **************     .06
        *                      *                                              *                  *
 2.17 ************************ -19.32**************************************   0.  **********    2.64
```

TOTALS MEASURED

WEST SUPPORT	LOADS	CENTER SUPPORT	LOADS	EAST SUPPORT
R3= 6.49	P3= -19.32	R3= 14.30	P3= 0.	R3= -1.15
M1= -34.97	M1= 99.40	M1= -41.82	M1= 0.	M1= -24.23
M2= 34.97		M2= 25.71		M2= 24.23

STATICS CHECK OF MEASURED APPLIED LOADS AND REACTIONS (KIPS)

(1) SUM OF APPLIED LOADS	-19.32
(2) SUM OF REACTIONS	19.64
(3) SUM OF (1)+(2)	.32

STATICS CHECK OF APPLIED AND MEASURED MOMENTS ABOUT LONGITUDINAL CENTERLINE - AXIS 1 (FT-KIPS)

(1) SUM OF MOMENTS DUE TO LOAD	99.40
(2) SUM OF MOMENTS DUE TO REACTIONS	-101.02
(3) SUM OF (1)+(2)	-1.62

STATICS CHECK OF APPLIED AND MEASURED MOMENTS ABOUT CENTER COLUMN - AXIS 2 (FT-KIPS)

(1) SUM OF MOMENTS DUE TO LOAD	-347.83
(2) SUM OF MOMENTS DUE TO REACTIONS	359.95
(3) SUM OF (1)+(2)	12.12

STATIC MOMENTS CALCULATED FROM APPLIED LOADS PLUS REACTIONS (FT-KIPS)

AT SECTION A	135.12
AT SECTION X	151.80
AT SECTION Z FROM WEST FORCES	-79.21
AT SECTION Z FROM EAST FORCES	-65.64
AT SECTION Y	-44.94
AT SECTION D	-41.98

FIG. 4.2 TYPICAL OUTPUT FROM REACT PROGRAM

longitudinal and transverse centerlines due to the applied loads and reactions are compared.

Lastly, the REACT program prints the external moments at different transverse sections of interest (e.g., A, D, X, Y and Z) from the experimental results for comparison with similar theoretical quantities.

4.4 DEFLECT Program

The deflections measured by the potentiometers at various locations on the bottom deck of the skew box girder bridge model were printed by the DEFLECT program in a format in which the experimental deflections were easy to read and verify. Figure 4.3 shows a typical output in the form of a skew table, in which the numerical value of each deflection is printed in its corresponding place on the plan view of the skew box girder model. For convenient orientation of the data the deflections at the end abutments and center bent column have also been printed as zero.

Using the graphical display option [PRINTR] of the CDC 6400 computer, the program DEFLECT was extended to include line printer plots of the deflected longitudinal configurations of girders 1, 3 and 5 for each load case. Such a line printer plot is given in Fig. 4.4. These were used as a qualitative visual check on the experimental results.

4.5 STRAINS Program

The STRAINS program comprised three parts, which can be considered as subprograms, with the following titles: STRNPLOT, ADJSTRN and MOMENT.

4.5.1 Subprogram STRNPLOT

Subprogram STRNPLOT was programmed to yield two outputs. The measured strains in the top and bottom slabs at all gaged sections

```
1 FILE 145 NET, OCT. 26, 78. TIME 9.15 AM, 1.0X  1X  CL30

POTENTIOMETERS DEFLECTIONS IN INCHES

      0.0    -.076  -.099  -.071  -.018  -.013   .108   .140   .135   .124   .099   .063   0.0
   0.0                                                                                   0.0
0.0    -.151  -.215  -.223  -.175  -.104   0.0    .057   .079   .080   .071   .052   0.0
   0.0                                                                                   0.0
0.0    -.180  -.284  -.367  -.405  -.316  -.156  -.046  -.004   .022   .031   .024   0.0
```

FIG. 4.3 TYPICAL OUTPUT FROM DEFLECT PROGRAM—SKEW TABLE

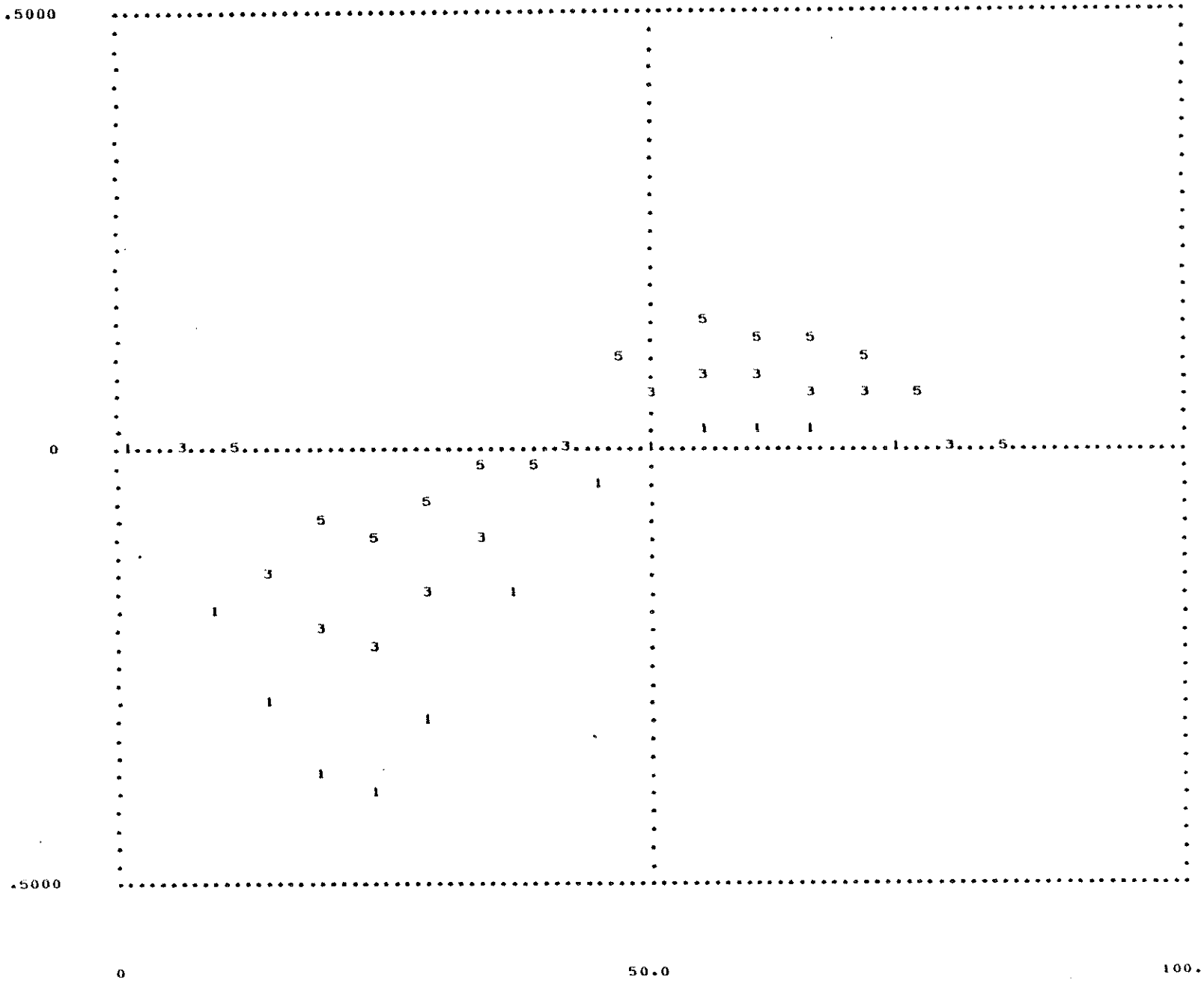

FIG. 4.4 TYPICAL OUTPUT FROM DEFLECT PROGRAM—LINE PRINTER PLOT

were printed as given in Fig. 4.5, in which is it observed that strain data for a typical loading case are presented for the right sections A and D, the skew sections B, C, F, G, H, I, J and for the gages embedded in the center bent. The sign convention adopted is that of a positive sign for tensile strains.

Subsequently, the top and bottom strains for all five girders were printed by means of the STRNPLOT and subprogram in a skew plan view to scale, Fig. 4.6. This pictorial representation of the major strain quantities enabled skew symmetric checks and other strain calculations to be carried out at a glance.

The STRNPLOT program incorporated the editing of faulty data from 8 gages which were either damaged or unstable. The identification codes for these gages, all of which were weldable gages measuring tensile strains in the steel reinforcement were W250A, W000B, W300B, W300D, W375D, W450F, W200I and W250I. In all strain tables, the experimental strain values at these locations as printed by the STRAINS program represent the average value of two stable gages in the vicinity.

4.5.2 Subprogram ADJSTRN

The box girder bridge model was instrumented at the right sections A and D and the skew sections B, C, E, G, H, I, J, and K (see Fig. 1.2). The arrangement of the tensile and compressive measuring devices at each of these sections may be seen in Fig. 4.5. The ADJSTRN subprogram was used only for the major sections A, B, C and D. The strain values at the other instrumented sections E, G, H, I, J and K were not adjusted by the ADJSTRN subprogram.

The object of the ADJSTRN subprogram was to ensure a smooth distribution of strain data across the width of each section by passing

1 FILE 145 NET, OCT. 26, 78. TIME 9.15 AM, 1.0X 1X CL30

STEEL AND CONCRETE STRAINS FOR SECTIONS A,B,C,D,F,G,H,I,J,K

MEASURED STRAINS IN MICRO-IN/IN

POSITION	000	100	125	150	175	200	225	250	275	300	325	350	375	400	425	450	475	500	600
SECTION		*		*		*		*		*		*		*		*		*	
A TOP	-311	-123		-107		-85		-78		-86		-65		-66		-60		-67	-16
A BOTTOM		309	285	239	270	291	238	245	253	285	199	178	139	206	197	168	167	31	
B TOP	85	85	61	52	48	62	55	51	56	75	94	63	61	69	40	45	37	44	39
B BOTTOM		-50		-17		-22		-23		-25		-44		-31		-36		-35	
C TOP	65	64	68	81	81	69	70	48	37	60	57	38	46	55	38	75	78	59	92
C BOTTOM		-55		-74		-41		-34		-33		-35		-33		-41		-40	
D TOP	18	19	19	22	18	23	25	23	19	19	20	20	21	21	18	17	21	18	23
D BOTTOM		-60	-59	-50	-69	-64	-62	-65	-54	-56	-59	-46	-56	-67	-47	-36	-42	-56	
F TOP		-51				-82								-77				-51	
F BOTTOM		81		106		207		208				214		176		192		209	
G TOP		30				25								20				13	
G BOTTOM		-60		-38		-44		-57				-60		-72		-56		-74	
H TOP		-22				-36				-42				-61				-55	
H BOTTOM		24		108		117		126		144		93		91		122		154	
I TOP		17				17				16				13				8	
I BOTTOM		-27		-27		-27		-33		-33		-26		-39		-22		-15	
J TOP		-32		-48		-26		-5		13		40		21		18		11	
J BOTTOM		191				37				3				0				-26	
K TOP		60		80		54		82		56		56		84		50		33	
K BOTTOM		-31				-40				-36				-37				-42	
CENTER BENT TOP								35		97		114		34					
CENTER BENT BOTTOM								-65		-13		-67		-15					

FIG. 4.5 TYPICAL OUTPUT FROM STRAINS PROGRAM—INSTRUMENTED SECTIONS

```
  1 FILE 145 NET, OCT. 26, 78. TIME 9.15 AM, 1.0X  1X  CL30

****************************************************************************************************

    TOP SLAB STRAINS IN GIRDERS 1 - 5

              ****     -55   -67      -51            33     44     59     33       18      13        8  ****
           ****     -61      -66  -77           21     69     55     84       21   20         13  ****
        ****     -42         -86           13     75     60     56       19         16  ****
     ****     -36      -82   -85      -26     62     69     54       25   23      17  ****
  ****     -22      -51   -123    -32    85     64     60          30     19   17  ****

    BOTTOM SLAB STRAINS IN GIRDERS  1 - 5

              ****     154    81      209           -26    -35    -40    -42      -56     -74      -15  ****
           ****     91       206  176            0    -31    -33    -37      -67  -72        -39  ****
        ****     144         285           3    -25    -33    -36      -56        -33  ****
     ****     117      207   291      37    -22    -41    -40      -44  -64     -27  ****
  ****      24      81    309     191   -50    -55    -31         -60     -60  -27  ****

****************************************************************************************************
```

FIG. 4.6 TYPICAL OUTPUT FROM STRAINS PROGRAM—SKEW TABLES

smooth curves through the measured data values. This adjustment was carried out for the sections A, B, C and D as follows: For the top slab at section A and bottom slabs at sections B and C wherein the number of gaged locations was 11 and 9, respectively, a polynomial expression of the sixth degree was used to provide a suitable fit to the observed, i.e. experimentally measured, data using the least squares method. The subroutine NLINEQ, to be described later in this section was employed for this strain adjustment.

For the bottom slab at section A, the top slabs at sections B and C and both slabs at section D where there were either 17 or 19 gages per slab, the same adjustment technique as used for the earlier tested straight and curved box girder bridge models was employed. At each of these sections, the strains in the top and bottom slabs were treated separately. The top slab in each case was divided into six regions, four corresponding to the bays of the box girder cells and two regions corresponding to the cantilever overhangs on either side. The bottom slab in each case was divided into four regions corresponding to the bays of the cells of the box girder model. For the locations described in the present paragraph, each cell bay of the top or bottom slab whether in tension or in compression was instrumented at 5 points (i.e., at the girder lines, midbays and quarter bays), the girder locations being common to contiguous bays. The cantilever overhangs were instrumented at two points (i.e., the exterior girder and the edge of the overhang). Reference may be made to Fig. 4.7.

The operation of the ADJSTRN subprogram for sections having 17 or 19 gages was as follows:

(a) The strain values at the edges of the cantilever overhangs of the top slab were compared with those at the girders nearest them. If the strain value at the edge of the overhang did not lie between 0.5 and 1.5 times the strain value for the adjacent girder, it was replaced by the strain value of the girder; otherwise it was retained as the actual value. A straight line was passed through the two points.

(b) For the five point strain values in a bay, a least squares parabola was passed in order to fit the five points. At each gaged location the adjusted value was compared with the observed (measured) value. If the absolute value of the difference of these two values exceeded 20% of the maximum measured strain value in this particular bay, the largest violating strain was discarded and a least squares parabola was passed to fit the remaining four points.

If two values out of five did not satisfy the 20% criterion described above, the two violating strain values were discarded and a parabola was passed through the three remaining points. If, as was usually the case, all observed values satisfied the established criterion, the first least squares parabola was accepted as the curve for strain-distribution in the bay and the ordinates for adjusted strains were printed out on this basis at several points in the bay.

4.5.2.1 Subroutine NLINEQ

The subroutine NLINEQ was employed for the adjustment of strains in the top slab at section A and the bottom slabs at sections B and C. As the number of gages at these sections was comparatively smaller than those at other instrumented sections it was decided

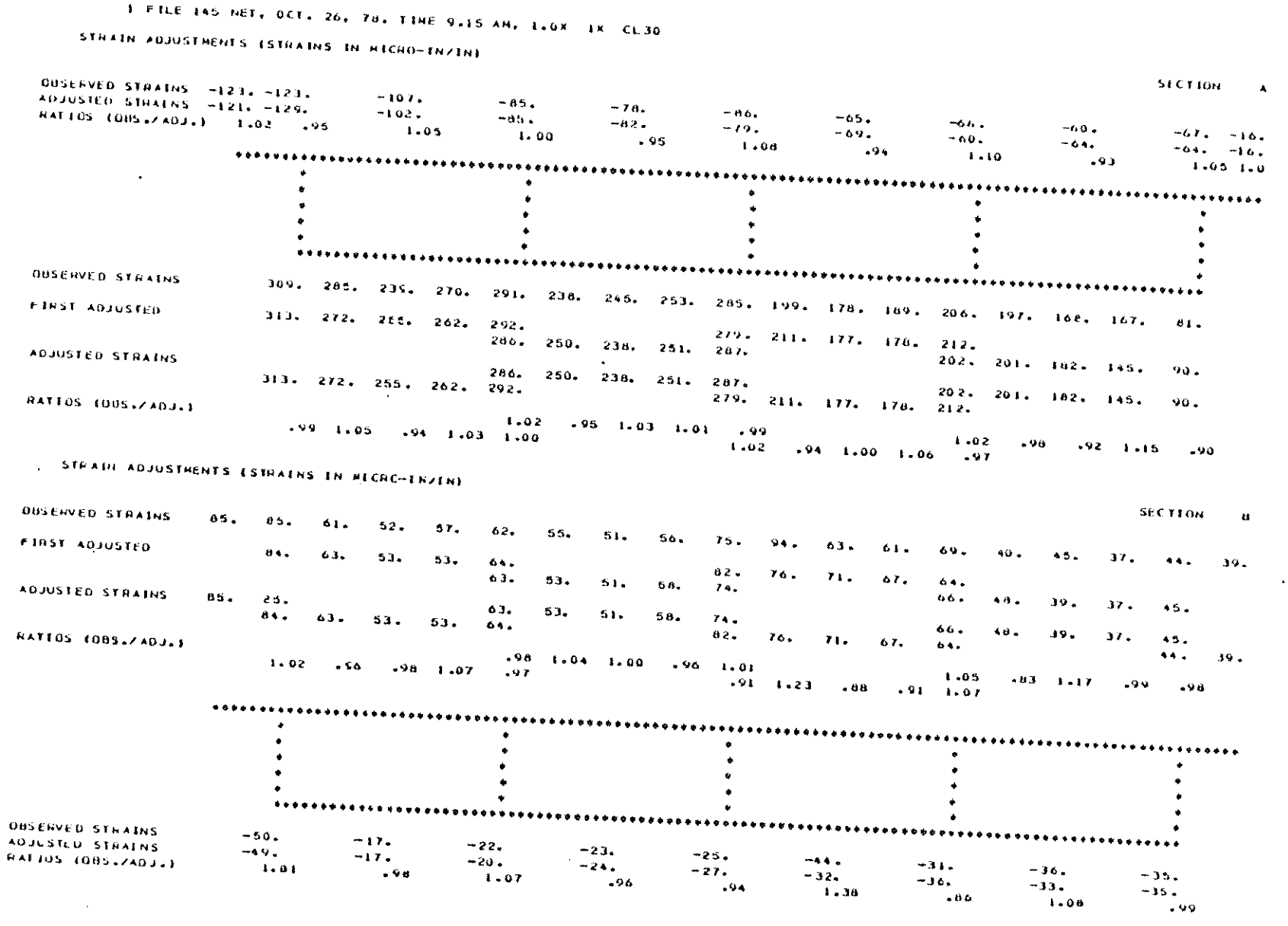

FIG. 4.7 TYPICAL OUTPUT FROM ADJSTRN SUBPROGRAM

STRAIN ADJUSTMENTS (STRAINS IN MICRO-IN/IN) SECTION C

OBSERVED STRAINS	65.	64.	68.	81.	81.	69.	70.	48.	37.	60.	57.	38.	46.	55.	38.	75.	78.	69.	59.
FIRST ADJUSTED		62.	74.	79.	78.	71.				63.	60.	44.	45.	54.					
						75.	58.	49.	48.	54.				46.	59.	66.	69.	65.	
ADJUSTED STRAINS	65.	64.				75.	58.	49.	48.	54.				55.	71.	78.	74.	60.	
		62.	74.	79.	78.	71.				63.	58.	44.	45.	54.				59.	59.
RATIOS (OBS./ADJ.)						.92	1.21	.98	.77	1.10				1.01	.53	.96	1.05	.98	
		1.04	.92	1.02	1.04	.97				.96	1.15	.87	1.01	1.01					

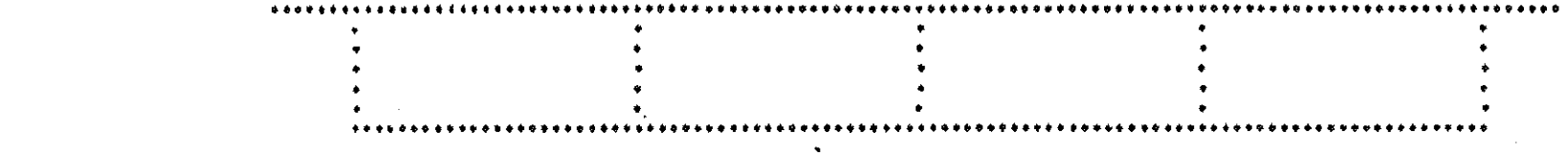

OBSERVED STRAINS		-55.		-74.		-41.		-38.		-33.		-35.		-33.		-41.		-40.	
ADJUSTED STRAINS		-55.		-70.		-44.		-34.		-35.		-34.		-33.		-41.		-40.	
RATIOS (OBS./ADJ.)		.99		1.05		.93		1.11		.94		1.02		1.01		.99		1.00	

STRAIN ADJUSTMENTS (STRAINS IN MICRO-IN/IN) SECTION D

OBSERVED STRAINS	18.	19.	19.	22.	18.	23.	25.	23.	19.	19.	20.	20.	21.	21.	18.	17.	21.	18.	23.
FIRST ADJUSTED		19.	19.	20.	21.	22.				19.	20.	20.	21.	21.					
						24.	24.	23.	21.	18.				20.	19.	18.	18.	19.	
ADJUSTED STRAINS	18.	19.				24.	24.	23.	21.	18.				20.	19.	18.	18.	19.	
		19.	19.	20.	21.	22.				19.	20.	20.	21.	21.				18.	23.
RATIOS (OBS./ADJ.)						.97	1.06	1.02	.91	1.05				1.03	.95	.93	1.14	.94	
		.99	.99	1.11	.87	1.04				1.00	1.01	.98	1.01	1.00					

OBSERVED STRAINS		-60.	-59.	-50.	-69.	-64.	-62.	-65.	-54.	-56.	-58.	-46.	-56.	-67.	-47.	-36.	-42.	-56.	
FIRST ADJUSTED		-60.	-57.	-58.	-61.	-67.				-58.	-52.	-51.	-56.	-66.					
						-64.	-63.	-61.	-58.	-55.				-67.	-46.	-37.	-41.	-56.	
ADJUSTED STRAINS						-64.	-63.	-61.	-58.	-55.				-67.	-46.	-37.	-41.	-56.	
		-60.	-57.	-58.	-61.	-67.				-58.	-52.	-51.	-56.	-66.					
RATIOS (OBS./ADJ.)						1.00	.98	1.06	.93	1.03				1.00	1.02	.96	1.03	.99	
		1.01	1.03	.87	1.14	.96				.96	1.12	.90	1.01	1.01					

FIG. 4.7 TYPICAL OUTPUT FROM ADJSTRN SUBPROGRAM

to use a polynomial expression of the sixth degree of the following form $y = \text{Function}\ (x,x^2,\ldots,x^6;\ b_1,b_2,\ldots,b_7)$ to provide an approximation to the observed strain data. The subroutine NLINEQ adjusted the parameters $b_1,b_2,\ldots,b_7$ of the polynomial by searching for those values of the parameters that minimized the sum of the squares

$$D = \sum_{i=1}^{i=N} \left[y_{i1} - y\left(x_i, x_i^2, \ldots, x_i^6;\ b_1,b_2,\ldots,b_7\right)\right]^2$$

where N indicates the number of measured data.

The minimization was done by setting $\partial D/\partial b$ equal to zero, resulting in a set of simultaneous non-linear equations which were solved by the subroutine using the Newton-Raphson method.

4.5.3 Subprogram MOMENT

The subprogram MOMENT took as its input data the adjusted strain values in the top and bottom slabs at right sections A and D only. By multiplying the strains by the appropriate elastic moduli and integrating over the concrete and steel areas, the internal forces were obtained. The multiplication of these forces by the corresponding lever arms resulted in the internal bending moment value. These moment values were calculated at the two right sections A and D only. However, for each of these sections the force equilibrium was checked and the moments were calculated about four different axes: the compression flange mid-depth; the line of main tensile reinforcement; the gross section neutral axis of the uncracked box girder; and the individual girder neutral axis

as obtained from the adjusted strains. The calculations were carried out in each case for the girders separately and for the total cross-section. Lastly, the internal moments were compared with external moment values obtained from the REACT program,. The above procedure was not carried out at skew sections B and C, because it is only valid for right sections such as A and D. A typical output for section A from the MOMENT subprogram is given in Fig. 4.8.

4.6 ROSETTE Program

As described in Chapter 8, strain rosettes were affixed to each girder web at four locations along its length. These locations were, respectively, 3.86 ft (1.18 m) east of the west abutment section W, west and east of the center bent diaphragm skew section T and west of the east abutment section E. The placing of these strain rosettes on each girder web at these fixed distances from the end abutments and the center bent diaphragm gave rise to four new skew sections L, M, N and O as may also be observed in Chapter 8.

Each rosette measured surface strains on the concrete at angles of 0°, 45° and 90° with the horizontal. These strains were converted into the shear forces transferred through the webs. Other quantities of interest such as the principal stresses were also evaluated. A typical output from the ROSETTE program is shown in Fig. 4.9.

The strain rosettes were not expected to function satisfactorily after the formation of cracks in the concrete and as such importance was attached only to shear force values obtained at and before the 30 ksi stress level.

RESULTS OF STRAIN INTEGRATION FOR SECTION A

1 FILE 145 NET, OCT. 26, 78, TIME 9.15 AM, 1.0X IX CL30

SECTION A
MODULUS OF ELASTICITY FOR CONCRETE....(KIPS/SQU.FT.)... 434000.

	GIRDER 1	GIRDER 2	GIRDER 3	GIRDER 4	GIRDER 5	ALL GIRDERS
LOCATION OF GIRDER EXPERIMENTAL NEUTRAL AXIS (FOOT)						
DISTANCE OF N.A. FROM LINE OF COMP. METERS	.45	.35	.34	.34	.64	
DISTANCE OF N.A. FROM LINE OF TENSILE STEEL	1.09	1.19	1.20	1.20	.90	
DETAILED SUMMARY OF INTERNAL FORCES (KIPS)						
COMPRESSIVE FORCES						
CONCRETE IN FLANGE	-24.20	-18.49	-16.23	-13.29	-10.48	
STEEL IN FLANGE	-5.26	-4.73	-4.15	-3.40	-2.28	
TOTAL IN FLANGE	-29.47	-23.21	-20.38	-16.69	-12.76	
CONCRETE IN WEB	-1.84	-.08	-.72	-.55	-.15	
STEEL IN WEB	-.42	-.20	-.18	-.14	-.27	
TOTAL IN WEB	-2.27	-.28	-.91	-.69	-.42	
TOTAL COMPRESSIVE FORCE	-31.73	-23.49	-21.29	-17.38	-13.18	-107.07
TENSILE FORCES						
STEEL IN FLANGE	12.10	15.68	14.26	12.49	6.11	
STEEL IN WEB	2.19	2.20	2.10	1.60	.52	
TOTAL TENSION FORCE	14.30	17.88	16.36	14.08	6.63	69.25
NET AXIAL FORCE	-17.43	-5.61	-4.93	-3.30	-6.55	-37.82
RATIO OF COMP. FORCE TO TENSILE FORCE	-2.22	-1.31	-1.30	-1.23	-1.99	-1.55
DETAILED SUMMARY OF INTERNAL MOMENTS (KIP-FT)						
ABOUT COMPRESSION FLANGE MID-DEPTH						
STEEL IN TENSION FLANGE	18.63	24.13	21.95	19.22	9.40	
STEEL IN TENSION WEB	2.57	2.53	2.42	1.84	.64	
CONCRETE IN COMPRESSION WEB	-.39	-.01	-.13	-.10	-.04	
STEEL IN COMPRESSION WEB	-.09	-.04	-.04	-.03	-.06	
TOTAL MOMENT ABOUT COMPRESSION FLANGE	20.71	26.61	24.20	20.93	9.54	102.40
PERCENT OF TOTAL MOMENT TAKEN BY GIRDERS	(20.23)	(25.99)	(23.64)	(20.44)	(9.31)	(100.00)
ABOUT TENSION FLANGE STEEL						
CONCRETE IN COMPRESSION FLANGE	37.25	28.45	24.98	20.46	16.13	
STEEL IN COMPRESSION FLANGE	8.10	7.28	6.39	5.23	3.51	
CONCRETE IN COMPRESSION WEB	2.44	.11	.99	.75	.19	
STEEL IN COMPRESSION WEB	.56	.26	.24	.18	.36	
STEEL IN TENSION WEB	-.81	-.85	-.81	-.62	-.16	
TOTAL MOMENT ABOUT TENSION FLANGE	47.55	35.25	31.78	26.00	20.02	160.60
PERCENT OF TOTAL MOMENT TAKEN BY GIRDERS	(29.61)	(21.95)	(19.79)	(16.19)	(12.47)	(100.00)

FIG. 4.8 TYPICAL OUTPUT FROM MOMENT SUBPROGRAM

ABOUT ENTIRE GROSS SECTION NEUTRAL AXIS (DISTANCE FROM TOP DECK FACE = 9.37 IN.)

STEEL IN TENSION FLANGE	10.31	13.36	12.15	10.64	5.21	
STEEL IN TENSION WEB	1.01	.97	.93	.70	.28	
CONCRETE IN COMPRESSION FLANGE	16.63	12.70	11.15	9.13	7.20	
STEEL IN COMPRESSION FLANGE	3.62	3.25	2.85	2.34	1.57	
CONCRETE IN COMPRESSION WEB	.07	.04	.37	.28	.06	
STEEL IN COMPRESSION WEB	.20	.09	.09	.06	.13	
TOTAL MOMENT ABOUT GROSS SECTION N.A.	32.64	30.41	27.53	23.15	14.43	128.18
PERCENT OF TOTAL MOMENT TAKEN BY GIRDERS	(25.47)	(23.73)	(21.48)	(18.06)	(11.26)	(100.00)

ABOUT GIRDER EXPERIMENTAL NEUTRAL AXIS

STEEL IN TENSION FLANGE	13.19	10.71	17.08	14.96	8.50	
STEEL IN TENSION WEB	1.59	1.77	1.71	1.30	.31	
CONCRETE IN COMPRESSION FLANGE	10.87	6.39	5.54	4.53	6.78	
STEEL IN COMPRESSION FLANGE	2.36	1.63	1.42	1.16	1.46	
CONCRETE IN COMPRESSION WEB	.44	.01	.12	.09	.05	
STEEL IN COMPRESSION WEB	.10	.03	.02	.02	.11	
TOTAL MOMENT ABOUT EXPERIMENTAL N.A.	28.55	28.55	25.88	22.05	14.13	119.16
PERCENT OF TOTAL MOMENT TAKEN BY GIRDERS	(23.96)	(23.96)	(21.72)	(18.51)	(11.86)	(100.00)

SUMMARY OF GIRDER FORCES AND MOMENTS

	GIRDER 1	GIRDER 2	GIRDER 3	GIRDER 4	GIRDER 5	ALL GIRDERS
LOCATION OF GIRDER EXPERIMENTAL NEUTRAL AXIS (FOOT)						
(1) DISTANCE OF N.A. FROM LINE OF COMP. METERS	.45	.35	.34	.34	.64	
(2) DISTANCE OF N.A. FROM LINE OF TENSILE STEEL	1.09	1.19	1.20	1.20	.90	
TOTAL INTERNAL FORCES (KIPS)						
(3) COMPRESSIVE FORCES	-31.73	-23.49	-21.29	-17.38	-13.18	-107.07
(4) TENSILE FORCE	14.30	17.88	16.36	14.08	6.63	69.25
(5) NET AXIAL FORCE	-17.43	-5.61	-4.93	-3.30	-6.55	-37.82
(6) RATIO OF COMP. FORCE TO TENSILE FORCE	-2.22	-1.31	-1.30	-1.23	-1.99	-1.55
TOTAL INTERNAL MOMENTS (KIP-FT)						
(7) ABOUT COMPRESSION FLANGE MID-DEPTH	20.71	26.61	24.20	20.93	9.94	102.40
(8) ABOUT TENSION FLANGE STEEL	47.55	35.25	31.78	26.80	20.02	160.60
(9) ABOUT ENTIRE GROSS-SECTION N.A.	32.64	30.41	27.53	23.15	14.43	128.18
(10) ABOUT GIRDER EXPERIMENTAL N.A.	28.55	28.55	25.88	22.05	14.13	119.16
MOMENT PERCENTAGES TAKEN BY EACH GIRDER						
(11) ABOUT COMPRESSION FLANGE MID-DEPTH	20.23	25.99	23.64	20.44	9.71	(100.00)
(12) ABOUT TENSION FLANGE STEEL	29.61	21.95	19.79	16.69	12.47	(100.00)
(13) ABOUT ENTIRE GROSS-SECTION N.A.	25.47	23.73	21.48	18.06	11.26	(100.00)
(14) ABOUT GIRDER EXPERIMENTAL N.A.	23.96	23.96	21.72	18.51	11.86	(100.00)

TOTAL SECTION MOMENTS

(15) CALCULATED FROM EXPERIMENTAL LOADS AND REACTIONS = 135.12

(16) RATIO (7) TO (15) = .76

(17) RATIO (8) TO (15) = 1.19

(18) RATIO (9) TO (15) = .95

(19) RATIO (10) TO (15) = .88

FIG. 4.8 TYPICAL OUTPUT FROM MOMENT SUBPROGRAM

1 FILE 145 NET, OCT. 26, 78. TIME 9.15 AM, 1.0X 1X CL30

SHEAR FORCES AND SHEAR FORCE TOTALS IN WEBS

STRESSES AND SHEAR FORCES IN WEBS OBTAINED FROM STRAIN GAGES IN WEBS

SECTION	GIRDER	SIGX PSI	SIGY PSI	TAUXY PSI	SIG1 PSI	SIG2 PSI	ALPHA DEG	SHEAR FORCE KIPS
SPAN 1								
W+3.86	1	11.0	-11.0	13.7	17.6	-17.6	-25.7	.7
W+3.86	2	1.6	-31.4	-19.2	10.5	-40.2	24.7	-1.2
W+3.86	3	34.6	-1.1	-37.1	57.9	-24.4	32.1	-2.5
W+3.86	4	48.5	7.3	-37.1	70.3	-14.6	30.5	-2.2
W+3.86	5	28.6	1.1	16.5	36.3	-6.6	-25.1	1.1
B-1.29	1	-80.6	10.0	-59.1	39.1	-109.8	-26.2	-4.7
B-1.29	2	12.3	166.1	-109.9	223.4	-44.9	-27.5	-8.6
B-1.29	3	21.2	-6.3	-13.7	26.9	-12.0	22.5	-1.4
B-1.29	4	13.3	-17.0	-12.4	17.7	-21.4	19.6	-1.0
B-1.29	5	80.3	8.9	-8.2	81.3	7.9	6.5	-.4
SPAN 2								
C+1.29	1	144.5	15.4	-6.9	144.8	15.0	3.0	-.4
C+1.29	2	209.1	25.0	-81.0	239.7	-5.5	20.7	-6.4
C+1.29	3	39.3	9.1	-6.9	40.8	7.6	12.2	-.7
C+1.29	4	20.2	-12.8	8.2	22.1	-14.7	-13.3	.6
C+1.29	5	25.7	44.9	-42.6	79.0	-8.3	-38.6	-3.4
E-3.86	1	-15.7	.8	-19.2	13.5	-28.4	-33.4	-1.3
E-3.86	2	-6.9	-4.2	9.6	4.1	-15.3	40.9	.6
E-3.86	3	-1.8	9.2	-2.7	9.9	-2.4	-13.3	-.2
E-3.86	4	-9.2	1.8	13.7	11.1	-18.5	34.1	.8
E-3.86	5	-11.2	-11.2	16.5	5.3	-27.6	90.0	.9

RECAPITULATION - SHEAR FORCE TOTALS

SECTION W+3.86	-4.1
SECTION B-1.29	-16.1
SECTION C+1.29	-10.1
SECTION E-3.86	.8

FIG. 4.9 TYPICAL OUTPUT FROM ROSETTE PROGRAM

4.7 TABLES Program

The main data reduction program and associated subprograms gave, in addition to the printed output, a deck of punched cards. This deck consisted of measured and adjusted strains, moments, deflections and reactions for selected cross-sections and girders for each load case.

These punched decks together with similar decks obtained from the theoretical finite element analysis results from CELL, were used as input for the TABLES Program. The TABLES program then printed summary tables of theoretical and experimental results for each load case. Each set of tables (for 2 or 3 load cases) consisted of theoretical and experimental reactions and statics checks, theoretical deflections in Spans I and II respectively, theoretical and experimental strains at all instrumented right and skew sections, and moments at sections A and D about the four axes described above, with theoretical values being obtained from the CELL postprocessing programs and experimental values being taken from the MOMENT subprogram. A typical output set of the TABLES program consisting of 12 pages of Tables A to L is given in Figs. 4.10 to 4.21. The complete tables for all load cases, consisting of 37 sets of 12 tables similar to Fig. 4.10 to 4.21, are presented in Vol. IV.

4.8 Modification of Experimental Data

After the scheme of experimental data reduction described in the previous sections was implemented for several loading cases, it was observed that the longitudinal compressive and tensile forces at a section as obtained from the MOMENT program did not balance as statics would require (see for example Fig. 4.8). The compressive forces were found to be generally larger than the tensile forces. An explanation for this discrepancy may be put forward as follows:

SUMMARY OF REACTIONS (KIPS OR FT-KIPS)

SEE FIGURE FOR POSITIVE DIRECTIONS
MF = MOMENT AT FOOTING ABOUT Z-AXIS
TF = MOMENT AT FOOTING ABOUT Y-AXIS

RESULTS FOR POINT LOADS
APPLIED AFTER 30 KSI COND. LOADING.
SIMPLY SUPPORTED, NO RESTRAINTS.

NORMALIZED POINT LOADS AT

REACTION OR LOAD	1X THEORY	1X EXPERM	1Y THEORY	1Y EXPERM	1X+1Y THEORY	1X+1Y EXPERM
1F	13.66	13.66	54.07	53.51	67.73	65.58
2E	.52	.31	16.81	19.88	17.33	21.14
3F	-5.56	-4.61	-.83	-2.47	-6.38	-6.76
4E	-7.24	-9.47	-7.39	-11.37	-14.63	-21.30
5E	-6.82	-5.85	-9.99	-6.71	-16.80	-11.42
1F	-33.98	-36.69	16.00	19.56	-17.97	-18.61
2F	31.48	29.34	32.96	36.10	64.44	65.25
3F	70.44	79.80	11.88	12.35	82.32	93.34
4F	4.98	1.55	-5.07	-9.97	-.09	-7.71
1W	13.87	11.21	2.33	2.80	16.20	13.50
2W	16.62	17.18	1.57	.76	18.19	17.95
3W	14.91	19.19	.06	.25	14.97	19.15
4W	4.77	2.95	-3.15	-3.49	1.62	-1.98
5W	-17.66	-16.87	-9.26	-9.30	-26.92	-24.00
RE	-5.42	-5.95	52.67	52.84	47.25	47.24
RF	72.92	74.00	55.77	58.04	128.69	132.27
RW	32.50	33.59	-8.44	-8.68	24.06	24.52
SUMR	100.00	101.64	100.00	102.20	199.99	204.03
PX	-100.00	-100.00	0.	0.	-100.00	-99.51
PY	0.	.18	-100.00	-100.00	-100.00	-100.50
SUMP	-100.00	-99.82	-100.00	-100.00	-200.00	-200.00
SUMR/SUMP	1.00	1.02	1.00	1.02	1.00	1.02
TW=-MW	-192.64	-191.11	-71.74	-71.61	-264.37	-243.85
MF	116.97	133.05	-63.23	-79.92	53.64	58.48
TF	-196.37	-216.41	-50.87	-58.29	-247.24	-277.36
TE=-ME	-125.27	-125.48	-391.67	-393.06	-516.95	-505.13
ACTUAL PX		-10.32		-0.		-10.40
ACTUAL PY		.21		-10.17		-10.63

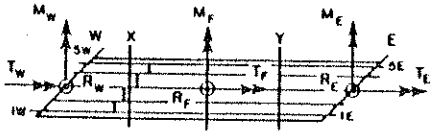

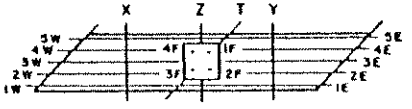

1 KIP = 4.448 kN
1 IN = 25.4 mm

FIG. 4.10 TYPICAL TABLE A FOR SUMMARY OF REACTIONS FROM TABLES PROGRAM

SUMMARY OF DEFLECTIONS (INCHES)

DEFLECTIONS POSITIVE DOWNWARDS

RESULTS FOR POINT LOADS
APPLIED AFTER 33 KSI COND. LOADING.
SIMPLY SUPPORTED, NO RESTRAINTS.

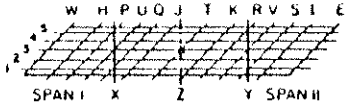

1 KIP = 4.448 kN
1 IN = 25.4 mm

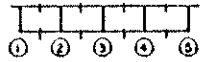

SPAN I — NORMALIZED POINT LOADS AT

DEFLECTION AT POINT	1X THEORY	1X EXPERM	1X E/T	1Y THEORY	1Y EXPERM	1Y E/T	1X+1Y THEORY	1X+1Y EXPERM	1X+1Y E/T
1H	-.735	-.931	1.27	.026	.058	2.19	-.709	-.981	1.24
3H	-.571	-.782	1.37	.053	.089	1.69	-.518	-.711	1.37
5H	-.274	-.393	1.43	.102	.167	1.64	-.172	-.245	1.43
1P	-1.113	-1.468	1.32	.053	.109	2.06	-1.060	-1.380	1.30
3P	-.784	-1.113	1.42	.091	.163	1.79	-.693	-.964	1.39
1X	-1.495	-2.098	1.40	.091	.162	1.78	-1.404	-1.977	1.41
2X	-1.102			.106			-.996		
3X	-.817	-1.152	1.41	.120	.207	1.73	-.697	-.972	1.39
4X	-.552			.134			-.419		
5X	-.307	-.512	1.67	.149	.231	1.55	-.158	-.264	1.67
1U	-1.371	-1.898	1.38	.077	.152	1.97	-1.294	-1.797	1.39
5U	-.200	-.368	1.84	.171	.268	1.57	-.029	-.104	3.64
3Q	-.668	-.907	1.36	.129	.205	1.59	-.539	-.720	1.34
5Q	.032	-.094		.158	.248	1.57	.160	.157	.98
1J	-1.258	-1.634	1.30	.085	.143	1.68	-1.174	-1.542	1.31
3J	-.413	-.540	1.31	.106	.157	1.48	-.306	-.386	1.26
5J	.239	-.066	-.28	.107	-.066	-.62	.346	-.040	-.12
1T	-.698	-.809	1.16	.007	.005	.71	-.691	-.809	1.17
2T	-.324			.005			-.320		
4T	.271			-.020			.251		
5T	.529	.561	1.06	-.044	-.087	1.98	.485	.497	1.03

FIG. 4.11 TYPICAL TABLE B FOR SUMMARY OF DEFLECTIONS IN SPAN I FROM TABLES PROGRAM

SUMMARY OF DEFLECTIONS (INCHES)

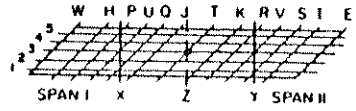

1 KIP = 4.448 kN
1 IN = 25.4 mm

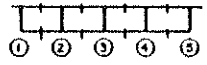

DEFLECTIONS POSITIVE DOWNWARDS

RESULTS FOR POINT LOADS
APPLIED AFTER 30 KSI COND. LOADING.
SIMPLY SUPPORTED, NO RESTRAINTS.

SPAN II

NORMALIZED POINT LOADS AT

DEFLECTION AT POINT		IX THEORY	IX EXPERM	IX E/T	IY THEORY	IY EXPERM	IY E/T	IX+IY THEORY	IX+IY EXPERM	IX+IY E/T
	1K	-.271	-.239	.88	-.229	-.294	1.28	-.500	-.533	1.07
	3K	.258	.295	1.14	-.221	-.324	1.46	.037	-.006	-.17
	5K	.651	.723	1.11	-.224	-.377	1.68	.427	.364	.85
	1R	-.079	-.019	.24	-.449	-.609	1.36	-.529	-.622	1.18
	3R	.343	.410	1.20	-.355	-.530	1.49	-.012	-.095	9.09
	1Y	.091	.160	1.76	-.781	-1.142	1.46	-.690	-.950	1.38
	2Y	.226			-.542			-.316		
	3Y	.363	.415	1.14	-.402	-.617	1.53	-.040	-.171	4.30
	4Y	.531			-.324			.177		
	5Y	.645	.701	1.09	-.281	-.497	1.77	.364	.239	.66
	1V	.040	.114	2.85	-.668	-.928	1.39	-.628	-.799	1.27
	5V	.591	.643	1.11	-.271	-.516	1.90	.319	.169	.54
	3S	.323	.368	1.14	-.345	-.571	1.66	-.022	-.168	7.79
	5S	.466	.511	1.10	-.204	-.414	2.03	.261	.122	.47
	1I	.092	.125	1.52	-.565	-.778	1.38	-.483	-.644	1.33
	3I	.231	.271	1.17	-.210	-.371	1.77	.021	-.084	-3.93
	5I	.308	.325	1.06	-.109	-.252	2.32	.199	.112	.57
LOAD	PX	-100.0	-100.0		0.	0.		-100.0	-99.5	
LOAD	PY	0.	.2		-100.0	-100.0		-100.0	-100.5	
ACTUAL	PX		-19.3			-0.			-19.4	
ACTUAL	PY		.0			-19.2			-19.6	

FIG. 4.12 TYPICAL TABLE C FOR SUMMARY OF DEFLECTIONS IN SPAN II FROM TABLES PROGRAM

SUMMARY OF STRAINS (MICRO IN/IN)

RESULTS FOR POINT LOADS
APPLIED AFTER 30 KSI COND. LOADING.
SIMPLY SUPPORTED, NO RESTRAINTS.

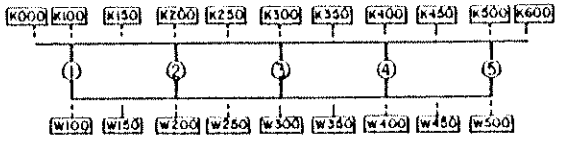

SECTION A

TENSION = +
COMPRESSION = -

K = CONCRETE STRAIN METERS
W = WELDABLE STRAIN GAGES

1 KIP = 4.448 kN
1 IN = 25.4 mm

		NORMALIZED POINT LOADS AT								
		IX			IY			IX+IY		
GAGE TYPE	GAGE LOC.	THEORY	MEASR	ADJUST	THEORY	MEASR	ADJUST	THEORY	MEASR	ADJUST
K	K000	-569	-1609	-626	43	315	73	-526	-1544	-591
K	K100	-501	-636	-667	38	74	79	-462	-599	-623
K	K150	-461	-553	-527	31	78	54	-430	-499	-483
K	K200	-456	-439	-439	30	28	33	-426	-406	-400
K	K250	-431	-403	-424	32	28	26	-399	-374	-392
K	K300	-438	-445	-408	34	53	25	-404	-397	-378
K	K350	-385	-336	-357	34	18	23	-350	-310	-324
K	K400	-356	-341	-310	35	42	22	-320	-297	-275
K	K450	-337	-310	-331	36	25	27	-301	-276	-296
K	K500	-393	-346	-331	43	29	29	-349	-310	-295
K	K600	-467	-82	-82	51	7	7	-416	-57	-57
W	W100	1130	1599	1619	-86	-157	-153	1044	1506	1550
W	W150	1470	1236	1319	-96	-124	-145	1373	1147	1235
W	W200	1608	1505	1495	-106	-103	-113	1501	1459	1431
W	W250	1564	1024	1231	-118	-254	-142	1446	909	1110
W	W300	1622	1474	1464	-131	-200	-199	1493	1337	1333
W	W350	1429	921	915	-133	-141	-129	1296	809	805
W	W400	1324	1066	1071	-136	-200	-198	1188	899	914
W	W450	1131	869	941	-124	-184	-177	1006	693	816
W	W500	1014	419	465	-115	-119	-115	899	317	366
LOAD	PX (KIPS)	-100.0	-100.0		0.	0.		-100.0	-99.5	
LOAD	PY (KIPS)	0.	.2		-100.0	-100.0		-100.0	-100.5	
ACTUAL	PX (KIPS)		-19.3			-9.			-19.4	
ACTUAL	PY (KIPS)		.0			-19.2			-19.6	

FIG. 4.13 TYPICAL TABLE D FOR SUMMARY OF STRAINS AT SECTION A FROM TABLES PROGRAM

SUMMARY OF STRAINS (MICRO IN/IN)

RESULTS FOR POINT LOADS
APPLIED AFTER 30 KSI COND. LOADING.
SIMPLY SUPPORTED. NO RESTRAINTS.

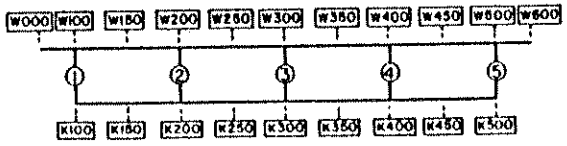

SECTION B

TENSION = + K = CONCRETE STRAIN METERS
COMPRESSION = - W = WELDABLE STRAIN GAGES

GAGE TYPE	GAGE LOC.	NORMALIZED POINT LOADS AT IX THEORY	IX MEASR	IX ADJUST	IY THEORY	IY MEASR	IY ADJUST	IX+IY THEORY	IX+IY MEASR	IX+IY ADJUST
W	W000	64	341	439	374	330	286	438	698	761
W	W100	64	439	437	374	286	282	438	761	754
W	W150	80	269	274	324	195	193	405	497	499
W	W200	166	320	328	337	222	228	503	555	564
W	W250	196	263	263	247	195	187	443	502	489
W	W300	242	439	403	158	195	173	400	640	597
W	W350	266	326	367	220	152	174	486	502	559
W	W400	290	357	336	224	249	247	504	619	599
W	W450	308	232	201	207	211	188	515	470	416
W	W500	430	227	230	224	184	183	655	444	445
W	W600	430	201	201	224	141	141	655	370	370
K	K100	-60	-258	-253	-147	-114	-115	-207	-369	-369
K	K150	-54	-87	-87	-149	-225	-203	-204	-321	-318
K	K200	-72	-113	-103	-145	-110	-123	-218	-221	-227
K	K250	-99	-119	-124	-131	-139	-115	-231	-258	-233
K	K300	-130	-129	-139	-98	-127	-134	-229	-249	-275
K	K350	-153	-227	-165	-132	-115	-122	-296	-336	-292
K	K400	-165	-160	-186	-132	-134	-121	-297	-294	-302
K	K450	-174	-186	-170	-116	-176	-186	-291	-353	-344
K	K500	-203	-181	-181	-106	-129	-128	-309	-301	-302
LOAD	PX (KIPS)	-100.0	-100.0		0.	0.		-100.0	-99.5	
LOAD	PY (KIPS)	0.	.2		-100.0	-100.0		-100.0	-100.5	
ACTUAL	PX (KIPS)		-19.3			-0.			-19.4	
ACTUAL	PY (KIPS)		.0			-19.2			-19.6	

FIG. 4.14 TYPICAL TABLE E FOR SUMMARY OF STRAINS AT SECTION B FROM TABLES PROGRAM

SUMMARY OF STRAINS (MICRO IN/IN)

RESULTS FOR POINT LOADS
APPLIED AFTER 30 KSI COND. LOADING.
SIMPLY SUPPORTED. NO RESTRAINTS.

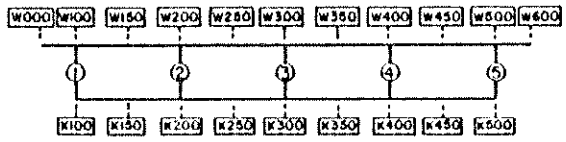

SECTION C

TENSION = +
COMPRESSION = -

K = CONCRETE STRAIN METERS
W = WELDABLE STRAIN GAGES

GAGE TYPE	GAGE LOC.	NORMALIZED POINT LOADS AT IX THEORY	IX MEASR	IX ADJUST	IY THEORY	IY MEASR	IY ADJUST	IX+IY THEORY	IX+IY MEASR	IX+IY ADJUST
W	W000	482	336	336	462	189	189	944	555	555
W	W100	482	331	326	462	357	357	944	703	701
W	W150	377	419	408	319	405	380	697	846	812
W	W200	376	357	377	286	465	466	663	856	872
W	W250	368	248	253	263	362	421	632	624	676
W	W300	329	310	302	269	259	267	598	587	588
W	W350	286	196	227	112	157	167	398	381	416
W	W400	444	284	282	57	130	123	501	428	420
W	W450	445	388	403	-40	16	21	404	418	442
W	W500	535	305	307	-131	-43	-39	404	259	265
W	W600	535	476	305	-131	-114	-43	404	349	349
K	K100	-241	-284	-284	-235	-178	-176	-476	-453	-452
K	K150	-214	-382	-362	-190	-167	-178	-405	-533	-539
K	K200	-224	-212	-227	-175	-201	-162	-399	-396	-391
K	K250	-219	-196	-175	-156	-165	-191	-375	-362	-360
K	K300	-210	-170	-181	-156	-191	-192	-367	-353	-365
K	K350	-179	-181	-175	-64	-150	-128	-244	-321	-302
K	K400	-187	-170	-170	-21	-45	-47	-209	-208	-214
K	K450	-198	-212	-213	17	-28	-28	-180	-225	-222
K	K500	-211	-206	-206	53	-6	-6	-158	-205	-205
LOAD	PX (KIPS)	-100.0	-100.0		0.	0.		-100.0	-99.5	
LOAD	PY (KIPS)	0.	.2		-100.0	-100.0		-100.0	-100.5	
ACTUAL	PX (KIPS)		-19.3			-0.			-19.4	
ACTUAL	PY (KIPS)		.0			-19.2			-19.6	

FIG. 4.15 TYPICAL TABLE F FOR SUMMARY OF STRAINS AT SECTION C FROM TABLES PROGRAM

SUMMARY OF STRAINS (MICRO IN/IN)

RESULTS FOR POINT LOADS
APPLIED AFTER 30 KSI COND. LOADING.
SIMPLY SUPPORTED, NO RESTRAINTS.

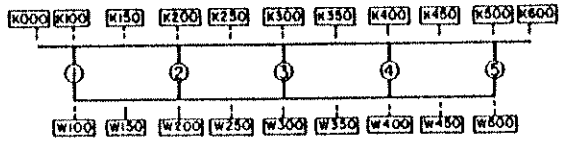

SECTION D

TENSION = +
COMPRESSION = -

K = CONCRETE STRAIN METERS
W = WELDABLE STRAIN GAGES

GAGE TYPE	GAGE LOC.	NORMALIZED POINT LOADS AT IX THEORY	IX MEASR	IX ADJUST	IY THEORY	IY MEASR	IY ADJUST	IX+IY THEORY	IX+IY MEASR	IX+IY ADJUST
K	K000	167	93	93	-584	-241	-241	-417	-172	-172
K	K100	144	98	98	-466	-279	-286	-321	-195	-196
K	K150	122	113	103	-353	-222	-276	-231	-118	-246
K	K200	121	119	119	-300	-235	-236	-178	-127	-127
K	K250	121	119	119	-245	-188	-210	-123	-68	-74
K	K300	121	98	95	-214	-178	-180	-93	-80	-78
K	K350	121	103	103	-185	-151	-153	-63	-46	-45
K	K400	121	108	106	-169	-146	-153	-48	-38	-39
K	K450	120	87	93	-155	-157	-159	-34	-74	-74
K	K500	140	93	95	-176	-171	-165	-35	-81	-81
K	K600	162	119	119	-198	-182	-182	-36	-61	-61
W	W100	-375	-310	-310	1378	1605	1649	962	1189	1248
W	W150	-415	-258	-330	1335	1113	1105	919	846	811
W	W200	-465	-331	-338	1197	1275	1242	732	936	892
W	W250	-453	-336	-315	954	875	884	492	555	579
W	W300	-461	0	-292	809	0	779	347	0	493
W	W350	-440	-238	-263	653	530	572	212	296	304
W	W400	-423	-346	-344	559	665	662	136	248	263
W	W450	-365	-186	-191	434	416	519	68	217	263
W	W500	-320	-289	-289	355	459	500	34	137	130
LOAD	PX (KIPS)	-100.0	-100.0		0.	0.		-100.0	-99.5	
LOAD	PY (KIPS)	0.	.2		-100.0	-103.0		-100.0	-100.5	
ACTUAL	PX (KIPS)		-19.3			-0.			-19.4	
ACTUAL	PY (KIPS)		.0			-19.2			-19.6	

FIG. 4.16 TYPICAL TABLE G FOR SUMMARY OF STRAINS AT SECTION D FROM TABLES PROGRAM

SUMMARY OF STRAINS (MICRO IN/IN)

RESULTS FOR POINT LOADS
APPLIED AFTER 30 KSI COND. LOADING.
SIMPLY SUPPORTED, NO RESTRAINTS.
LOADING SHOWN IN TABLES D,E,F,G

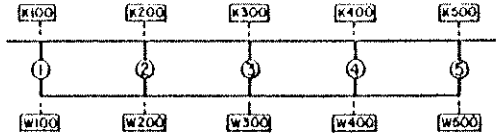

TENSION = + K = CONCRETE STRAIN METERS
COMPRESSION = - W = WELDABLE STRAIN GAGES

GAGE TYPE	GAGE LOC.	NORMALIZED POINT LOADS AT 1X THEORY	1X MEASR	1X ADJUST	1Y THEORY	1Y MEASR	1Y ADJUST	1X+1Y THEORY	1X+1Y MEASR	1X+1Y ADJUST
SECTION H										
K	K100	-194	-113		-9	2		-204	-103	
K	K200	-216	-186		-6	5		-223	-173	
K	K300	-265	-217		-3	1		-268	-209	
K	K400	-296	-315		6	5		-290	-297	
K	K500	-374	-284		25	16		-349	-253	
W	W100	244	124		13	-11		258	137	
W	W200	275	605		7	-16		282	629	
W	W300	321	745		1	5		322	798	
W	W400	363	470		-8	-76		354	434	
W	W500	408	796		-26	-130		381	719	
SECTION F										
K	K100	-339	-263		14	22		-325	-237	
K	K200	-440	-424		20	35		-420	-383	
K	K400	-348	-398		50	74		-298	-337	
K	K500	-319	-263		78	61		-240	-203	
W	W100	372	419		-15	-54		357	370	
W	W200	545	1071		-25	-65		519	1052	
W	W400	423	910		-63	-146		359	814	
W	W500	326	1081		-88	-249		238	914	

FIG. 4.17 TYPICAL TABLE II FOR SUMMARY OF STRAINS AT SECTIONS H AND F FROM TABLES PROGRAM

SUMMARY OF STRAINS (MICRO IN/IN)

RESULTS FOR POINT LOADS
APPLIED AFTER 30 KST COND. LOADING.
SIMPLY SUPPORTED, NO RESTRAINTS.
LOADING SHOWN IN TABLES D,E,F,G

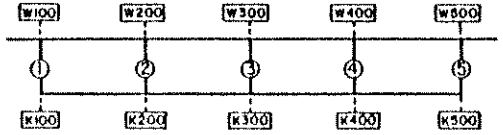

TENSION = + K = CONCRETE STRAIN METERS
COMPRESSION = − W = WELDABLE STRAIN GAGES

GAGE TYPE	GAGE LOC.	NORMALIZED POINT LOADS AT 1X THEORY	1X MEASR	1X ADJUST	1Y THEORY	1Y MEASR	1Y ADJUST	1X+1Y THEORY	1X+1Y MEASR	1X+1Y ADJUST
SECTION J										
W	W100	-332	-165		84	59		-248	-95	
W	W200	-156	-134		85	124		-71	-11	
W	W300	-61	67		90	259		29	349	
W	W400	7	108		86	195		94	344	
W	W500	71	170		104	222		175	444	
K	K100	743	988		-87	-253		256	824	
K	K200	196	191		-107	-107		88	81	
K	K300	80	15		-111	-99		-30	-76	
K	K400	-1	0		-105	-128		-107	-123	
K	K500	-72	-134		-106	-147		-178	-271	
SECTION K										
W	W100	179	310		100	211		280	545	
W	W200	162	270		31	108		194	396	
W	W300	151	289		-49	-70		101	211	
W	W400	150	434		-100	-232		50	174	
W	W500	167	170		-152	-168		14	12	
K	K100	-186	-160		-112	-198		-298	-323	
K	K200	-199	-206		-38	-1		-237	-197	
K	K300	-187	-186		61	70		-125	-112	
K	K400	-197	-191		121	104		-66	-81	
K	K500	-174	-217		150	172		-23	-38	

FIG. 4.18 TYPICAL TABLE I FOR SUMMARY OF STRAINS AT SECTIONS J AND K FROM TABLES PROGRAM

SUMMARY OF STRAINS (MICRO IN/IN)

RESULTS FOR POINT LOADS
APPLIED AFTER 30 KSI COND. LOADING.
SIMPLY SUPPORTED, NO RESTRAINTS.
LOADING SHOWN IN TABLES D,E,F,G

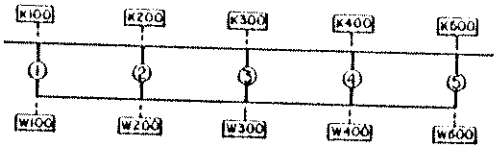

TENSION = + K = CONCRETE STRAIN METERS
COMPRESSION = - W = WELDABLE STRAIN GAGES

GAGE TYPE	GAGE LOC.	NORMALIZED POINT LOADS AT IX THEORY	IX MEASR	IX ADJUST	IY THEORY	IY MEASR	IY ADJUST	IX+IY THEORY	IX+IY MEASR	IX+IY ADJUST
SECTION G										
K	K100	160	155		-468	-509		-308	-334	
K	K200	134	129		-342	-334		-215	-211	
K	K400	111	103		-138	-137		-27	-34	
K	K500	117	67		-117	-128		0	-63	
W	W100	-172	-310		553	1183		380	814	
W	W200	-169	-227		450	946		289	714	
W	W400	-139	-372		168	676		28	280	
W	W500	-127	-382		124	594		-3	196	
SECTION I										
K	K100	133	87		-222	-18		-88	29	
K	K200	105	87		-86	-72		19	37	
K	K300	98	82		-22	8		75	92	
K	K400	84	67		-1	3		82	71	
K	K500	77	41		7	-15		85	32	
W	W100	-145	-139		225	368		80	222	
W	W200	-130	-227		111	400		-19	164	
W	W300	-117	-170		39	276		-77	111	
W	W400	-105	-201		8	54		-97	-137	
W	W500	-99	-77		-17	22		-116	-53	

FIG. 4.19 TYPICAL TABLE J FOR SUMMARY OF STRAINS AT SECTIONS G AND I FROM TABLES PROGRAM

DISTRIBUTION OF MOMENTS TO EACH GIRDER
(KIP-FT AND PERCENTAGE)

RESULTS FOR POINT LOADS
APPLIED AFTER 10 KSI COND. LOADING.
SIMPLY SUPPORTED, NO RESTRAINTS.

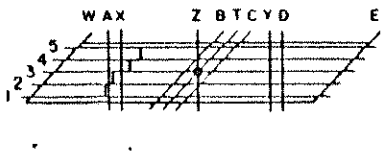

NORMALIZED POINT LOADS AT

1 KIP = 4.448 kN
1 FT = 0.305 m

1 FT-KIP = 1.356 kN-m
1 FT-KIP/FT = 4.448 kN-m/m

SECTION	GIRDER	IX THEORY K-FT	IX THEORY PCT	IX EXPERIMENTAL K-FT	IX EXPERIMENTAL PCT	IY THEORY K-FT	IY THEORY PCT	IY EXPERIMENTAL K-FT	IY EXPERIMENTAL PCT	IX+IY THEORY K-FT	IX+IY THEORY PCT	IX+IY EXPERIMENTAL K-FT	IX+IY EXPERIMENTAL PCT
MOMENTS ABOUT COMPRESSION FLANGE MID-DEPTH													
A	1	146.6	21.1	123.2	20.2	-11.0	18.8	-12.6	15.5	135.6	21.3	110.9	21.2
A	2	158.1	22.8	158.4	26.3	-10.8	18.5	-14.7	18.1	147.3	23.2	148.5	26.9
A	3	149.6	21.5	144.0	23.6	-11.8	20.2	-19.3	23.8	137.8	21.7	129.2	23.4
A	4	126.0	18.1	124.6	20.4	-12.4	21.1	-22.0	27.1	113.6	17.9	107.4	19.5
A	5	114.2	16.4	59.2	9.7	-12.5	21.4	-12.6	15.5	101.7	16.0	49.6	9.0
A	SUM	694.5		609.4		-58.6		-81.2		635.9		551.6	
D	1	-41.5	19.8	-29.9	18.9	130.8	31.0	138.5	28.6	89.3	42.0	108.9	33.7
D	2	-42.5	20.3	-42.0	26.5	104.3	24.7	144.4	29.9	61.7	29.0	102.3	33.2
D	3	-42.4	20.3	-34.6	21.8	75.3	17.9	89.4	18.5	32.9	15.5	54.9	17.8
D	4	-42.3	20.2	-30.9	19.5	59.8	14.2	66.1	13.7	17.5	8.2	30.0	9.7
D	5	-40.5	19.4	-20.9	13.2	51.7	12.3	45.0	9.3	11.2	5.3	16.8	5.5
D	SUM	-209.2		-158.4		421.9		483.5		212.7		308.1	
MOMENTS ABOUT TENSION FLANGE STEEL													
A	1	105.9	15.3	209.2	29.6	-7.5	12.9	-24.5	41.0	98.4	15.5	184.6	30.2
A	2	190.0	27.5	155.1	21.9	-12.9	22.1	-12.5	20.9	177.1	28.0	141.8	22.0
A	3	171.4	24.8	139.8	19.8	-14.1	24.2	-8.0	13.4	157.3	24.9	128.4	19.9
A	4	144.5	20.9	114.4	16.2	-14.8	25.4	-7.5	12.6	129.7	20.5	102.0	15.8
A	5	79.2	11.5	88.1	12.5	-8.9	15.3	-7.2	12.0	70.3	11.1	77.4	12.0
A	SUM	691.0		706.4		-58.2		-59.8		632.8		644.1	
D	1	-29.3	14.1	-38.5	18.2	102.5	24.5	100.7	25.5	73.2	34.7	76.2	36.5
D	2	-50.4	24.2	-47.4	22.4	131.4	31.4	94.8	24.0	81.0	38.4	56.7	27.1
D	3	-50.0	24.0	-43.1	20.4	97.7	20.9	72.3	18.3	37.7	17.9	25.5	12.2
D	4	-49.9	24.0	-42.6	20.2	65.8	15.7	61.5	15.6	15.8	7.5	19.3	9.2
D	5	-28.4	13.7	-39.6	18.8	31.6	7.5	65.5	16.6	3.2	1.5	31.4	15.0
D	SUM	-208.1		-211.3		419.0		394.8		211.3		209.0	
LOAD	PX (KIPS)	-100.0		-100.0		0.		0.		-100.0		-99.5	
LOAD	PY (KIPS)	0.		.2		-100.0		-100.0		-100.0		-100.5	
ACTUAL	PX (KIPS)			-19.3				-0.				-19.4	
ACTUAL	PY (KIPS)			.0				-19.2				-19.6	

FIG. 4.20 TYPICAL TABLE K FOR SUMMARY OF TRANSVERSE DISTRIBUTION OF SECTION MOMENTS TO EACH GIRDER FROM TABLES PROGRAM

DISTRIBUTION OF MOMENTS TO EACH GIRDER
(KIP-FT AND PERCENTAGE)

RESULTS FOR POINT LOADS
APPLIED AFTER 30 KSI COND. LOADING.
SIMPLY SUPPORTED, NO RESTRAINTS.

1 KIP = 4.448 kN
1 FT = 0.305 m

1 FT-KIP = 1.356 kN-m
1 FT-KIP/FT = 4.448 kN-m/m

NORMALIZED POINT LOADS AT

SECTION	GIRDER	IX THEORY K-FT	IX THEORY PCT	IX EXPERIMENTAL K-FT	IX EXPERIMENTAL PCT	IY THEORY K-FT	IY THEORY PCT	IY EXPERIMENTAL K-FT	IY EXPERIMENTAL PCT	IX+IY THEORY K-FT	IX+IY THEORY PCT	IX+IY EXPERIMENTAL K-FT	IX+IY EXPERIMENTAL PCT
MOMENTS ABOUT ENTIRE GROSS SECTION NEUTRAL AXIS													
A	1	123.8	17.9	167.2	25.5	-9.1	15.5	-18.7	26.9	114.7	18.1	156.6	26.2
A	2	176.0	25.4	155.8	23.7	-12.0	20.5	-13.5	19.4	164.0	25.9	144.2	24.2
A	3	161.9	23.4	141.0	21.5	-13.1	22.4	-13.3	19.2	148.8	23.5	128.1	21.5
A	4	136.3	19.7	118.6	18.1	-13.7	23.5	-14.4	20.6	122.6	19.3	104.0	17.4
A	5	94.6	13.7	73.9	11.3	-10.5	18.0	-9.7	13.9	84.1	13.3	63.9	10.7
A	SUM	692.6		656.7		-58.4		-69.6		634.2		596.8	
D	1	-34.6	16.6	-33.9	18.5	114.9	27.3	120.7	27.3	80.3	37.9	91.2	34.0
D	2	-46.9	22.5	-44.5	24.3	119.5	28.4	121.2	27.4	72.6	34.3	81.2	33.3
D	3	-46.7	22.4	-38.6	21.1	82.3	19.6	81.4	18.4	35.6	16.8	41.3	15.4
D	4	-46.6	22.3	-36.4	19.9	63.2	15.0	64.0	14.5	16.6	7.8	25.1	9.3
D	5	-33.7	16.2	-29.6	16.2	43.5	9.6	54.6	12.3	6.7	3.2	29.5	11.0
D	SUM	-208.6		-183.0		420.3		441.8		211.7		268.3	
MOMENTS ABOUT INDIVIDUAL GIRDER NEUTRAL AXIS													
A	1	124.0	17.9	146.3	24.0	-9.1	15.6	-16.9	22.8	114.9	18.1	136.7	24.6
A	2	175.8	25.4	146.3	24.0	-12.0	20.5	-13.1	17.7	163.9	25.9	135.9	24.5
A	3	161.5	23.3	132.6	21.7	-13.1	22.4	-15.8	21.4	148.5	23.4	119.9	21.6
A	4	136.1	19.7	113.0	18.5	-13.7	23.5	-17.9	24.2	122.4	19.3	98.4	17.7
A	5	94.8	13.7	72.4	11.9	-10.5	18.0	-10.3	14.0	84.3	13.3	63.9	11.5
A	SUM	692.3		610.5		-58.4		-74.0		633.9		554.9	
D	1	-34.7	16.6	-31.7	18.7	114.3	27.2	129.6	28.1	79.8	37.4	97.6	33.5
D	2	-46.9	22.5	-42.8	25.2	119.6	29.5	133.0	28.9	72.7	34.1	93.9	32.2
D	3	-46.6	22.4	-36.3	21.4	82.1	19.5	84.4	19.3	35.5	16.7	49.4	16.9
D	4	-46.5	22.3	-33.4	19.7	63.0	15.0	64.1	13.9	16.7	7.8	27.8	9.5
D	5	-33.8	16.2	-25.6	15.1	41.2	9.8	49.6	10.8	9.4	4.0	22.6	7.8
D	SUM	-209.5		-169.8		420.2		460.6		213.1		291.3	
LOAD PX (KIPS)		-100.0		-100.0		0.		0.		-100.0		-99.5	
LOAD PY (KIPS)		0.		.2		-100.0		-100.0		-100.0		-100.5	
ACTUAL PX (KIPS)				-19.3				-0.				-19.4	
ACTUAL PY (KIPS)				.0				-19.2				-19.6	

FIG. 4.21 TYPICAL TABLE L FOR SUMMARY OF TRANSVERSE DISTRIBUTION OF SECTION MOMENTS TO EACH GIRDER FROM TABLES PROGRAM

The adjusted strain values in steel and concrete were converted to stresses and forces through the use of their moduli of elasticity obtained from tests on control specimens. In the case of the concrete considerable uncertainty was expected in the determination of the modulus. Six by twelve inch (152 by 305 mm) cylindrical control specimens were here used to simulate the 2 1/4 in. (57.2 mm) thick, heavily reinforced compression flanges. The significant difference in the geometry of the control cylinders and the flanges of the model implied that the curing and drying would be different, and hence also the moduli.

The tensile forces were computed assuming the concrete to be cracked on the tension side, and all tensile forces taken by the reinforcement. The crack was assumed to pass through the gaged section, and the strain readings assumed to be those of the cracked section. However, even though a crack initiator was placed at the instrumented sections, it was clear that these assumptions were not satisfied in the bridge model. In many cases the strains measured were not the strains at the crack, but rather at a point somewhere between two cracks. Since the concrete was uncracked at this point, part of the tensile force was carried by the concrete, resulting in a reduction in the steel strains. The part of the tensile force carried by the concrete was larger the larger the spacing between the cracks, which accounted for the discrepancy between tensile and compressive forces as observed generally at sections A and D.

It was therefore decided to modify the tensile and compressive forces at all sections, rather than to attempt to modify the strains. The purpose of this modification was to ensure as much as possible that equilibrium was satisfied at all instrumented sections. Using the

measured reactions and applied loads and their respective lever arms, the gross external moments for the entire cross section were computed at sections A and D, for each load case.

Next an assessment of the value of the internal moment arm was made, keeping in view the fact that because of the presence of concrete and steel in the webs this moment arm would be somewhat less than the distance of 1.539 ft (0.47 m) between the mid-depths of the top and bottom slabs of the box girder model. As a representative example, the distances between the two forces of the T-C couple were calculated for the 30 ksi conditioning load case at sections A and D and the average of these experimental lever arms based on moments about the compression flange mid-depth, tensile flange steel and the gross sections neutral axis for both the total sectional and the individual girders was found to be 1.483 ft (0.45 m) and consequently this value was chosen as the internal lever arm for all load cases.

Using the value of 1.483 ft (0.45 m), a "theoretical" equilibrating force (tension T_E equal to compression C_E) was computed by dividing the gross external moment at the section by this lever arm. A set of modification factors was then obtained by dividing the "theoretical" force by the experimental tensile and compressive forces as computed by the MOMENT program, for sections A and D respectively. The factor $\alpha = T_E/T$ was used to modify the tensile force when moments were being taken about the compression flange mid-depth and the factor $\beta = C_E/C$ was used to modify the compressive force when moments were being taken about the tension steel. For the case of moments about the gross section or individual girder neutral axes, a factor γ, intermediate between α and β, was also calculated as described in detail in

Volume IV of the present sequence of research reports. Ideally these factors α for the tensile forces, β for the compressive forces and γ for the moments at a particular section would be the same for all load cases and load levels if the effective stiffness for converting the strains to stresses and thence to forces was a constant for each section force. Because of cracking under increasing stress levels, stress reversals and experimental variation, this does not occur. Only the results for α, β and γ obtained for each conditioning load case are plotted in Fig. 4.22 as a function of conditioning load stress level. It can be seen that the variation in the modification factors with stress level for these cases is quite smooth.

In essence, the curves of Fig. 4.22 represent the modification factors required to convert the moduli of elasticity of the concrete, and steel as obtained from control specimens, to effective stiffnesses. When these effective stiffnesses are used to convert measured strains to forces, longitudinal force equilibrium will be satisfied at the specified sections under the given conditioning loads shown in Fig. 4.22.

For the 24, 30, 40, 50 and 60 ksi conditioning load cases, the individual modification factors plotted in Fig. 4.22 were used to obtain experimental internal forces and moments at the sections indicated, thus satisfying equilibrium for these load cases.

For all other load cases, with the exception of dead load which is treated separately in Chapter 5, the modification factors obtained from the 30 ksi conditioning load were used. These other load cases (totalling to 144 cases) which have been described in Table 5.1 of Vol. I, included the point load combinations, designed to produce 24 to 30 ksi total stresses in the reinforcement, which were applied after

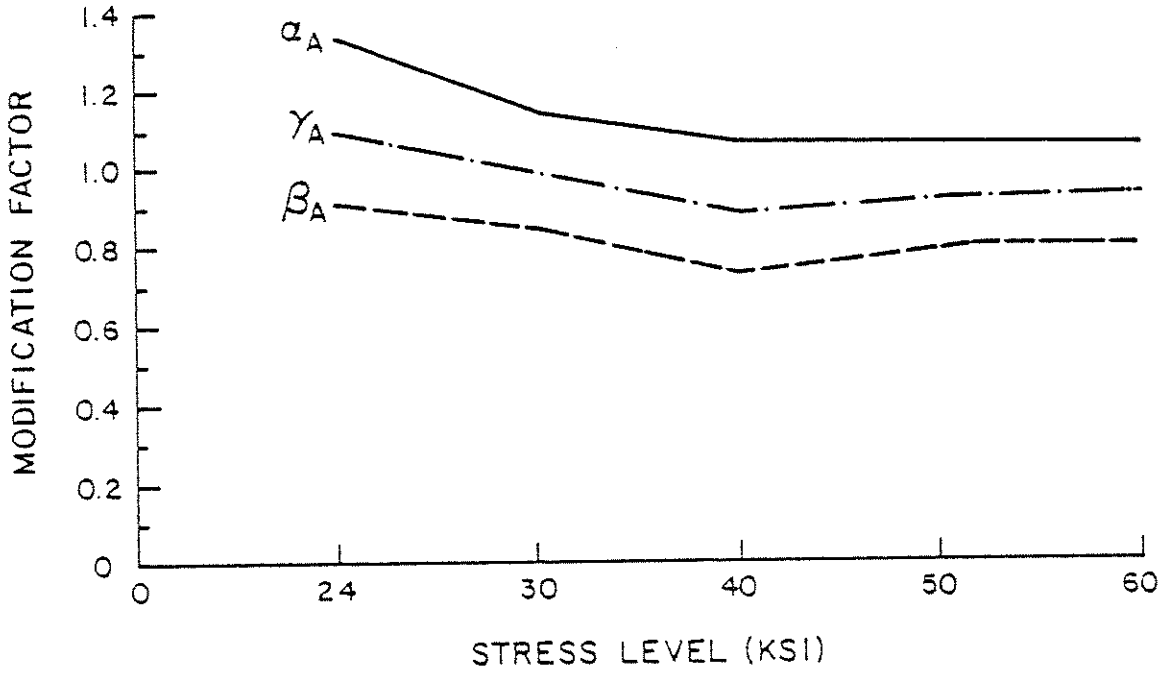

(a) MODIFICATION FACTORS FOR SECTION A

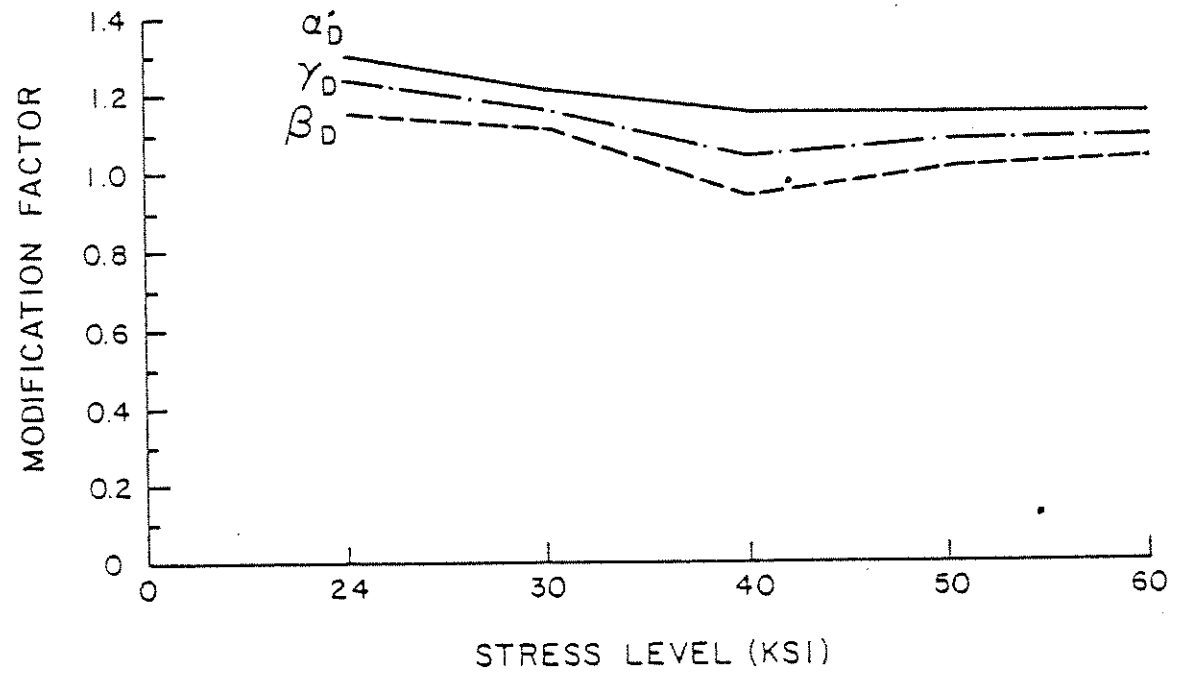

(b) MODIFICATION FACTORS FOR SECTION D

FIG. 4.22 VARIATION OF MODIFICATION FACTORS FOR INTERNAL FORCES FOR ALL CONDITIONING LOADS

each conditioning load, as well as truck load combinations and the moving fork lift loads applied after the 30 ksi conditioning load. All experimental results for internal forces and moments at a section presented in Vols. II and IV for these load cases have therefore been modified by these factors, which are taken from Fig. 4.22 and tabulated below in Table 4.1. The experimental strains, reactions and deflections, however, remain unchanged.

TABLE 4.1 MODIFICATION FACTORS FOR INTERNAL FORCES FROM 30 KSI CONDITIONING LOAD

Factor	Section A	Section D
α	1.15	1.20
β	0.85	1.11
γ	0.99	1.16

Since this common set of factors was used for a large number of different loading cases, perfect equilibrium could not be expected for all these cases. The effect of this modification procedure is shown in Table 4.2 for three typical point load cases after the 30 ksi conditioning load. A significant improvement in the result is obtained both for the ratio of compressive to tensile forces, and for the various moment ratios, particularly at the midspan sections of the loaded spans. These are section A for load case 1X, section D for load case 5Y and both sections A and D for load case 1X + 5Y.

Table 4.3 shows the same ratios for three point load combinations after the 60 ksi conditioning load. The first column within

TABLE 4.2 COMPARISON OF ORIGINAL AND MODIFIED FORCE AND MOMENT RATIOS FOR POINT LOADS AFTER 30 KSI CONDITIONING LOAD

LOAD CASE		SECTION A		SECTION D	
		ORIGINAL	MODIFIED	ORIGINAL	MODIFIED
1X	(15) MOMENT	699.4		-217.3	
	Ratio F_c/F_t	1.54	1.14	1.41	1.31
	Ratio (7)/(15)	0.76	0.87	0.61	0.73
	Ratio (8)/(15)	1.18	1.00	0.88	0.97
	Ratio (9)/(15)	0.95	0.94	0.73	0.84
	Ratio (10)/(15)	0.88	0.87	0.67	0.78
5Y	(15) MOMENT	-190.3		712.2	
	Ratio F_c/F_t	2.26	1.67	1.23	1.13
	Ratio (7)/(15)	0.61	0.71	0.73	0.88
	Ratio (8)/(15)	1.42	1.33	0.90	1.12
	Ratio (9)/(15)	0.97	1.03	0.80	1.00
	Ratio (10)/(15)	0.89	0.97	0.78	0.95
1X + 5Y	(15) MOMENT	493.9		508.9	
	Ratio F_c/F_t	1.44	1.06	1.16	1.07
	Ratio (7)/(15)	0.81	0.93	0.75	0.90
	Ratio (8)/(15)	1.18	1.00	0.88	0.98
	Ratio (9)/(15)	0.97	0.96	0.81	0.94
	Ratio (10)/(15)	0.92	0.91	0.80	0.93

F_c = compressive force; F_t = tensile force

(7) = internal moment about compression flange mid-depth

(8) = internal moment about tension flange mid-depth

(9) = internal moment about entire gross-section N.A.

(10) = internal moment about experimental N.A.

(15) = total external moment from experimental loads and reactions (kip-ft)

TABLE 4.3 COMPARISON OF ORIGINAL AND MODIFIED FORCE AND MOMENT RATIOS FOR POINT LOADS AFTER 60 KSI CONDITIONING LOAD

LOAD CASE		SECTION A			SECTION D		
		ORIGINAL	MOD. 60	MOD. 30	ORIGINAL	MOD. 60	MOD. 30
1X	(15) MOMENT	681.8			-204		
	Ratio F_c/F_t	1.75	1.33	1.29	1.55	1.39	1.43
	Ratio (7)/(15)	0.78	0.83	0.90	0.65	0.75	0.78
	Ratio (8)/(15)	1.40	1.13	1.19	1.02	1.05	1.13
	Ratio (9)/(15)	1.06	0.99	1.05	0.82	0.89	0.95
	Ratio (10)/(15)	0.97	0.90	0.96	0.75	0.82	0.87
5Y	(15) MOMENT	-188.1			697.3		
	Ratio F_c/F_t	2.40	1.83	1.77	1.37	1.23	1.27
	Ratio (7)/(15)	0.64	0.68	0.74	0.74	0.85	0.89
	Ratio (8)/(15)	1.59	1.29	1.35	1.03	1.06	1.14
	Ratio (9)/(15)	1.06	0.99	1.05	0.87	0.95	1.01
	Ratio (10)/(15)	1.00	0.93	0.99	0.83	0.91	0.96
1X + 5Y	(15) MOMENT	530.3			528.2		
	Ratio F_c/F_t	1.63	1.24	1.20	1.39	1.24	1.29
	Ratio (7)/(15)	0.81	0.86	0.93	0.70	0.81	0.84
	Ratio (8)/(15)	1.34	1.09	1.14	0.98	1.01	1.09
	Ratio (9)/(15)	1.04	0.97	1.03	0.82	0.89	0.95
	Ratio (10)/(15)	0.97	0.90	0.96	0.81	0.88	0.94

F_c = compressive force; F_t = tensile force

(7) = internal moment about compression flange mid-depth

(8) = internal moment about tension flange mid-depth

(9) = internal moment about entire gross-section N.A.

(10) = internal moment about experimental N.A.

(15) = total external moment from experimental loads and reactions (kip-ft)

each section represents the unmodified ratios, the second the ratios using the modification factors of the 60 ksi conditioning load, and the third those obtained using 30 ksi conditioning load. It can be seen that the differences in the modified results are not great and thus the simpler expedient of using the 30 ksi conditioning load modification factors for all of the point load cases after the 40, 50 and 60 ksi conditioning loads as well as those after the 24 and 30 ksi conditioning loads was adopted.

A more complete study of modification factors is made in Section 2.1 of Vol. IV, where the conditioning load cases and nine point load cases 1X, 1Y, 1X+1Y, 3X, 3Y, 3X+3Y, 5X, 5Y and 5X+5Y are studied. For stress levels at or after the 24, 20, 40, 50 and 60 ksi levels, unmodified tension and compression forces at sections A and D are tabulated to verify the consistency of the experimental data. These results are given in Tables 2.1, 2.2, 2.3 of Vol. IV, and then modification factors for each individual case are computed and tabulated in Tables 2.4, 2.5, 2.6 of Vol. IV. A study of these detailed tables indicates that the adopted procedure of using the modification factors from the 30 ksi conditioning load case described earlier is probably the best approach to use in reducing the data.

5. RESULTS FOR DEAD LOAD

5.1 Introduction

For the skew box girder bridge model of the present study the dead load case may be divided into two separate stages: (1) the self-weight of the bridge model, and (2) the extra weight of the concrete blocks subsequently placed on the bridge top deck for proper simulation of prototype dead load behavior. The experimental results for reactions, deflections, strains and moments for these two loadings as well as for their combined effect will be compared in this chapter with theoretical results obtained from the CELL computer program.

Significant aspects of the structural behavior of the skew box girder bridge model will be compared with earlier obtained results from the straight and curved box girder bridge models. Finally, the conclusions drawn from the dead load study of the skew box girder model will be presented in summarized form.

5.2 Dead Load Reactions

A complete summary of theoretical and experimental individual vertical end reactions, total vertical reactions and applied loads as well as total end moments and torques are given in Table 5.1 for the self-weight, block loading and combined total dead load case. The theoretical reactions are obtained from the CELL FINE analysis as described in Section 3.2.2

5.2.1 Reactions for Self-Weight of Skew Box Girder Model

For convenience of input, the box girder cross-section was modelled in the CELL program as shown in Fig. 5.1. Using the average

TABLE 5.1 SUMMARY OF BRIDGE MODEL DEAD LOAD REACTIONS (KIPS OR FT-KIPS)

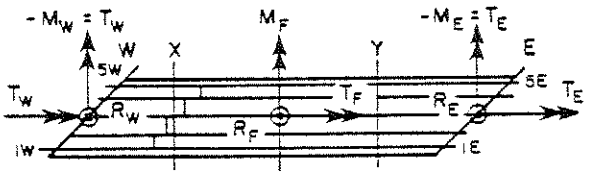

REACTION	SELF - WEIGHT		BLOCKS		TOTAL D.L.	
	THEORY	EXPT.	THEORY	EXPT.	THEORY	EXPT.
(1)	(2)	(3)	(4)	(5)	(6)	(7)
1W	1.6	1.4	1.6	0.8	3.2	2.1
2W	2.8	0	3.9	6.5	6.7	6.5
3W	3.6	7.0	5.5	4.8	9.1	11.7
4W	4.1	1.7	6.5	7.1	10.6	8.8
5W	4.7	5.3	7.4	6.7	12.1	12.0
TOTAL RW	16.7	15.3	25.0	25.9	41.7	41.1
1E	4.6	6.1	7.4	6.8	12.0	12.9
2E	4.0	3.3	6.5	6.6	10.5	9.9
3E	3.5	0.9	5.6	7.7	9.0	8.6
4E	2.7	5.3	3.9	1.4	6.6	6.7
5E	1.6	-0.1	1.6	3.1	3.2	2.9
TOTAL RE	16.4	15.5	25.0	25.5	41.4	41.0
RF	48.2	55.8	46.7	48.1	94.9	103.9
TOTAL R	81.2	86.5	96.7	99.5	178.0	186.0
TOTAL P	81.1	84.4	96.7	96.7	177.9	181.2
TW= -MW	19	25	37	32	56	57
TE= -ME	-19	-27	-37	-33	-56	-59

1 KIP = 4.448 kN
1 FT = 0.305 m

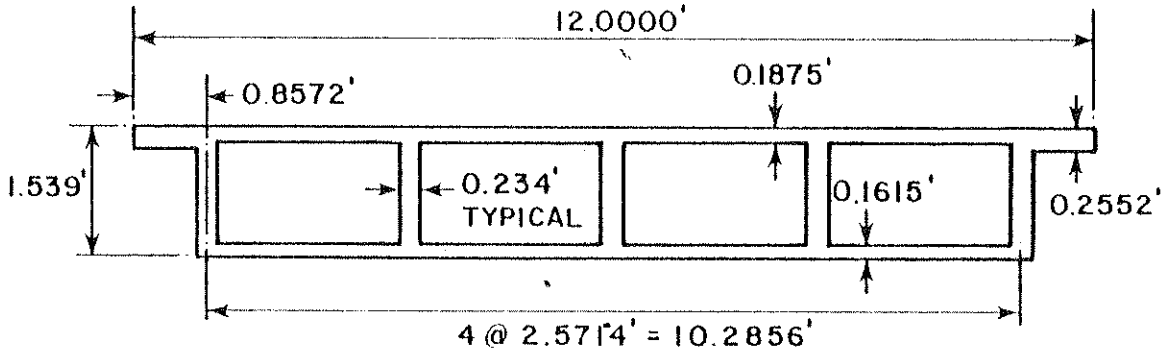

FIG. 5.1 TYPICAL BOX GIRDER CROSS-SECTION AS MODELLED IN CELL ANALYSIS

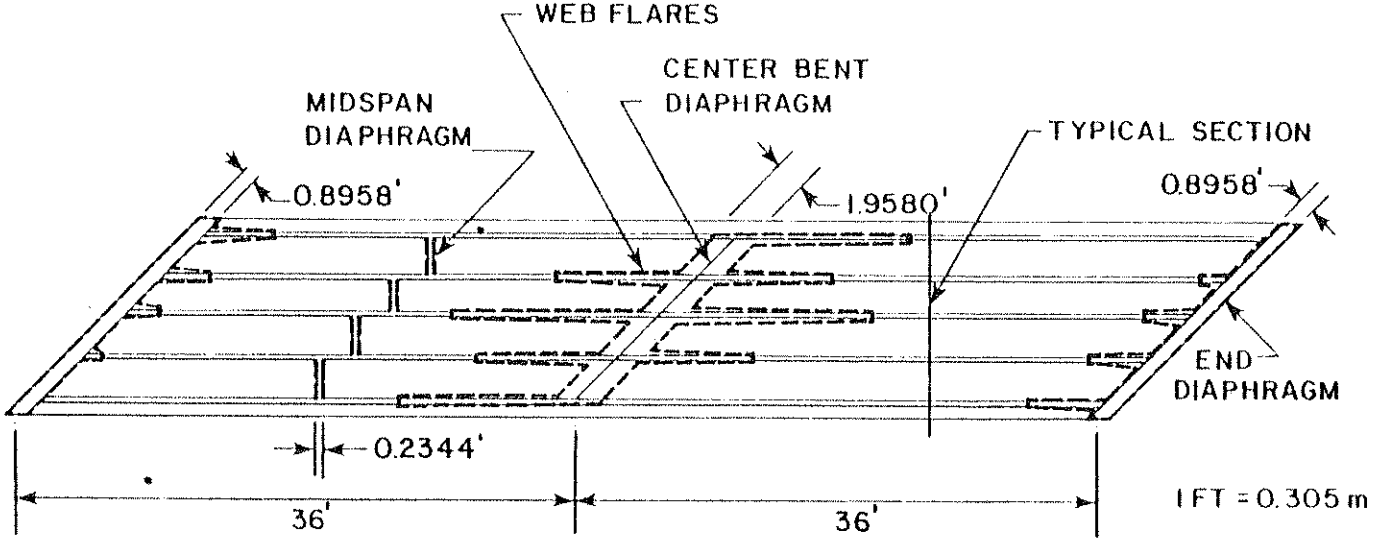

FIG. 5.2 ADDITIONAL BRIDGE PORTIONS MODELLED IN CELL ANALYSIS FOR SELF-WEIGHT CASE

thickness of 0.2552 ft (0.078 m) for the cantilever overhangs, the area of the box section may be calculated as 5.83 sq. ft (0.54 sq. m). Using the value of 0.156 kcf (24.5 kN/m^3) for the weight per unit volume of the reinforced concrete, the self-weight per unit length of the full box girder section is found to be 0.910 k/ft (13.3 kN/m).

The total self-weight of the box girder model as input into the CELL program can now be itemized thus:

	VOLUME ft^3 (m^3)	SELF WEIGHT kips (kN)
Cellular portion of bridge	419.82 (11.9)	65.52 (291.4)
Two end diaphragms	40.12 (1.12)	6.26 (27.8)
Flares in girder webs at abutments	1.94 (0.06)	0.30 (1.3)
Midspan diaphragm	3.71 (0.11)	0.58 (2.6)
Center bent diaphragm	43.85 (1.24)	6.84 (30.4)
Flares in girder webs at center bent	10.44 (0.30)	1.63 (7.3)
Total self-weight		81.13 (360.7)

In addition to the basic self-weight of the cellular portion of the cross-section, the weights of the two end diaphragms, the staggered midspan diaphragm and the skew center bent diaphragm, Fig. 5.2, were included in both the CELL COARSE and FINE analyses. The additional small weight of the flares in the girder webs, Fig. 5.2, was also included in the CELL FINE analyses but not in the CELL COARSE analyses.

From Table 5.1 column (2) it may be observed, that the self-weight of the bridge model as assessed above by considering the box

section, diaphragms and flares agrees within 0.1 kip (0.44 kN) with the total theoretical reaction R output by CELL.

Unlike the straight and curved box girder bridge models the load cells for the experimental determination of the girder and center bent reactions were placed in position and connected to the data acquisition system before the placing of the concrete for the bottom slab and girder webs. As such, it was possible to obtain the experimental reaction values due to the self-weight of the bridge model by subtracting the load cell readings immediately before the placing the bottom slab and girder web concrete from the load cell readings immediately after the removal of the shoring. By taking the difference of these two readings, it is possible to ignore the effects of the intermediate stages like the placing of the top slab concrete and also the transfer of part of the load by the shoring to the supports as a result of settlement of the shoring or creep and differential shrinkage in the concrete. The experimental reaction values are shown in Column (3) of Table 5.1.

Because of the nature of the self-weight loading, it is natural to expect some discrepancies between the theoretical and experimental values as listed in Columns (2) and (3) of Table 5.1 To begin with, the total experimental reaction R has been found to be 86.5 kips (385 kN) whereas the theoretical total is 81.2 kips (361 kN). However, the real difference between the two values is much smaller because of two items that have been neglected in the theoretical model:

(1) the weight of the wooden drop soffit top slab forms totalling about 2.0 kips (9 kN) which remained in the cells after casting the top slab;

and (2) the weight of 16 fillets (one at the corner of each cell) extending over the length of the bridge, totalling about 1.3 kips (6 kN).

When the above extra weight of 3.3 kips (15 kN) is added to the calculated input self-weight of 81.1 kips (361 kN), the value of P in Column (2) of Table 5.1 becomes 84.4 kips (376 kN) and the agreement between the theoretical and experimental values of R and P improves to acceptable limits. It is to be noted that the weight of one cubic foot of reinforced concrete in the theoretical model has been taken as 0.156 kips (0.694 kN). A small variation in this value can significantly affect the final results. Furthermore, the flares in the girder webs in the region of the abutments and center bent in each span have been modelled with their widths increasing stepwise rather than continuously as in the actual case. When all these factors are taken into account it is seen that the agreement between theoretical and experimental reaction values in Table 5.1 is quite good.

The same pattern of agreement is seen to exist between the theoretical and experimental reaction values for RW, RF and RE, i.e., the total reactions at the west abutement, center bent and east abutement respectively, when the differences between the theoretical model and the experimental input are recalled. As in the case of the curved bridge model, the experimental results indicate that a larger portion of the total self-weight reaction was taken by the center footing than the theory predicted. This is caused by the load transfer from the shoring to the bridge before removal of the shoring and by shrinkage effects.

The same effects make a comparison of the theoretical and experimental transverse distribution of the self-weight reactions at each end abutment unrealistic. In addition, the skewness of the bridge results in each girder of the bridge model having to undergo a different longitudinal displacement. Since the friction between the two teflon plates in each support assemblage was too large to accommodate this longitudinal displacement by relative sliding, this displacement was rather taken by shear deformations in the elastomeric pads and slight rotations of the load cells which were equipped with small rotation swivel heads. Because of the large vertical rigidity of the end diaphragm and the sensitivity to the different spring stiffnesses of the individual elastomeric pads (see Vol. I Sec. 6), it can be seen in Table 5.1 that the transverse distribution of the total experimental end reaction to the five individual end reactions cannot be predicted theoretically and the experimental values are not skew symmetrical for the two end abutments. However, Table 5.1 shows that the total east and west end vertical and moment reactions found in the experiment are in good agreement with respect to skew symmetry and can be adequately predicted theoretically.

5.2.2 Reactions for Block Loading

The extra weight required by the skew bridge model for proper simulation of prototype behavior was provided by 80 concrete blocks of total weight 96.74 kips (430.3 kN) placed on the bridge top deck. This loading was modelled by the CELL program in the form of concentrated loads at different nodes of the finite element mesh for the top deck in the locations in which the concrete blocks were actually placed. A comparison of the CELL results with those obtained from the experimentally

measured reactions may be observed in Table 5.1, in Columns (4) and (5) respectively. It can be seen that the CELL program accurately models the block loading. The agreement between theoretical and experimental values of the total vertical and moment reactions at the west and east abutments and at the center bent is seen to be quite good.

For the reasons stated in Section 5.2.1 where a comparison was made between theoretical and experimental reactions for the self-weight of the bridge, good agreement cannot be expected when, instead of the total abutment reactions at sections E and W, individual girder reactions are compared. Thus, the comparison of individual girder reactions in Columns (4) and (5) of Table 5.1 for the concrete block loading indicates only a general one-to-one agreement. However, this agreement is considerably superior to that between individual girder reactions for the self-weight case shown in Columns (2) and (3) of Table 5.1.

5.2.3 Reactions for Total Dead Load

The theoretical and experimental reaction values for the combined dead load composed of the self-weight of the bridge model and the concrete block loading are given in Columns (6) and (7) of Table 5.1. These values have been obtained by adding the relevant values from Columns (2) to (5).

The comparison of both total vertical and moment reactions at the east and west abutments and the center bent as well as the individual girder reactions shows much better agreement for the total dead load values in Table 5.1 than the agreement obtained for the separate components of dead load (i.e., the self-weight of the bridge model and the concrete block loading).

5.3 Deflections

Unlike the straight and curved bridges, in which the self-weight of the model and the extra dead load for proper simulation of prototype behavior (consisting of steel billets within the cells of the model) acted together simultaneously resulting in only one set of total dead load deflections, the dead load deflections for the skew box girder bridge model comprised two distinct components: deflections due to the self-weight of the model alone, and the deflections due to the concrete block loading. These will be treated separately below.

5.3.1 Deflections for Self-Weight of Skew Box Girder Model

Experimental and theoretical deflections are given in Table 5.2 for the sections H, U, J, T, K, V and I for the self-weight case. The experimental deflections were measured using scales attached to the outside girder webs as well as at 32 points on the top deck of the bridge using a high precision level instrument. The scales were graduated to 0.01 in. (0.25 mm), and readings were taken before and after removal of the shoring. The least count of the level reading was also 0.01 in. (0.25 mm).

The theoretical deflections in Column (3) are due to the self-weight of the model. There was no way of assesing any deflections due to creep of concrete or settlement of the formwork but these deflections should represent the effect of the removal of the shoring quite accurately for which the experimental deflections in Columns (4) and (5) were measured.

The ratio of experimental to theoretical deflections are given in Columns (6) and (7). As might be expected maximum deflections for both theory and experiment occur at the locations 1U and 5V, which are on the skew midspan sections U and V, and lie between an acute

TABLE 5.2 SUMMARY OF SELF-WEIGHT DEFLECTIONS (INCHES)

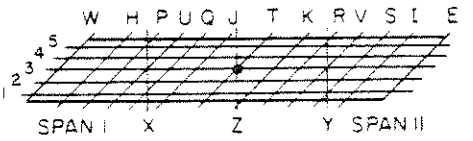

Note: Downward deflections are shown as positive

	SEC-TION	THEORY (CELL)	EXPERIMENT		E/T	
			MIRROR-SCALE READINGS	LEVEL READINGS	(4)/(3)	(5)/(3)
(1)	(2)	(3)	(4)	(5)	(6)	(7)
GIRDER 1	H	0.07	0.09	0.06	1.3	0.9
	U	0.11	0.15	0.12	1.4	1.1
	J	0.08	0.08	0.06	1.0	0.8
	T	0.03	-0.01	0	-	-
	K	0.02	-0.03	-0.03	-	-
	V	0.05	0.03	0.02	0.6	0.4
	I	0.05	0.05	0.04	1.0	0.8
GIRDER 5	H	0.06	0.06	0.06	1.0	1.0
	U	0.06	0.06	0.06	1.0	1.0
	J	0.02	-0.02	-0.01	-	-
	T	0.03	0.01	0.01	0.3	0.3
	K	0.07	0.09	0.09	1.3	1.3
	V	0.11	0.16	0.15	1.5	1.4
	I	0.07	0.07	0.07	1.0	1.0

1 IN = 25.4 mm

corner of the bridge model and the center bent. At these locations the E/T ratios have typical values of 1.4 and 1.5, which indicates that cracking of the concrete is significant in these areas. However, over the whole bridge, the stresses due to self-weight alone are less than 5 ksi (34 MPa) and therefore in the absence of significant cracking the E/T ratios are smaller in other regions. Certain inadmissable values of the E/T ratio are also obtained where both the theoretical and experimental values of the deflection are small and may even have opposite signs. This is partly due to the unavoidable lack of accuracy in the experimental values where the least count was 0.01 in. (0.25 mm) and an error of ±0.02 in. (0.51 mm) was not impossible.

5.3.2 Deflections for Concrete Block Loading

For the concrete block loading, the potentiometers were in place at 32 different locations. The theoretical deflection values from the CELL program and the experimental deflection values as obtained from the potentiometer readings have been listed in Table 5.3 The E/T ratios in Column (4) and (8) may be seen to have values in general between 1.5 and 2.0. This indicates that the addition of the concrete blocks on the top deck of the model results in additional cracking at all locations of the bridge model. Note that skew symmetry is generally satisfied for both theoretical and experimental results.

5.3.3 Deflections for Total Dead Load

A summary of deflections along outer girders 1 and 5 due to self-weight, blocks and total dead load is presented in Table 5.4. Values for self-weight and blocks in Columns (3) to (8) have been taken from Tables 5.2 and 5.3. However, for convenience the distinction between

TABLE 5.3 CONCRETE BLOCK LOADING DEFLECTIONS (INCHES)

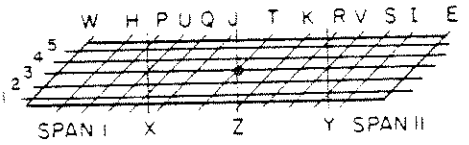

SPAN I				SPAN II			
LOCATION	THEORY	EXPT.	E/T	LOCATION	THEORY	EXPT.	E/T
(1)	(2)	(3)	(4)	(5)	(6)	(7)	(8)
1H	0.11	0.20	1.8	5I	0.11	0.04	0.4
3H	0.10	0.18	1.8	3I	0.10	0.17	1.7
5H	0.09	0.17	1.9	1I	0.09	0.14	1.6
1P	0.16	0.28	1.8	5S	0.16	0.25	1.6
3P	0.13	0.24	1.8	3S	0.13	0.21	1.6
1X	0.16	0.26	1.6	5Y	0.16	0.24	1.5
3X	0.13	0.23	1.8	3Y	0.13	0.18	1.4
5X	0.10	0.18	1.8	1Y	0.10	0.15	1.5
1U	0.18	0.30	1.7	5V	0.17	0.28	1.6
5U	0.08	0.14	1.8	1V	0.08	0.12	1.5
3Q	0.10	0.17	1.7	3R	0.10	0.15	1.5
5Q	0.05	0.08	1.6	1R	0.05	0.07	1.4
1J	0.11	0.18	1.6	5K	0.11	0.16	1.5
3J	0.05	0.09	1.8	3K	0.05	0.07	1.4
5J	0.02	0.05	2.5	1K	0.02	0.05	2.5
1T	0.03	0	-	5T	0.03	0.02	0.7

1 IN = 25.4 mm

TABLE 5.4 SUMMARY OF DEFLECTIONS FOR DEAD LOAD (INCHES)

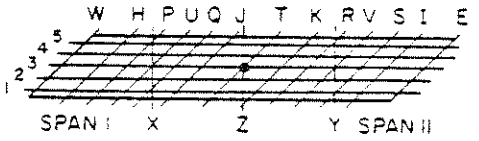

LOCATION		SELF - WEIGHT			BLOCKS			TOTAL DEAD LOAD		
		THEORY	EXPT.	E/T	THEORY	EXPT.	E/T	THEORY	EXPT.	E/T
(1)	(2)	(3)	(4)	(5)	(6)	(7)	(8)	(9)	(10)	(11)
GIRDER 1	H	0.07	0.08	1.1	0.11	0.20	1.8	0.18	0.27	1.5
	U	0.11	0.14	1.3	0.18	0.30	1.7	0.29	0.44	1.5
	J	0.08	0.07	0.9	0.11	0.18	1.6	0.19	0.25	1.3
	T	0.03	-0.01	-	0.03	0	-	0.06	0	-
	K	0.02	-0.03	-	0.02	0.05	2.5	0.04	0.02	0.5
	V	0.05	0.03	0.6	0.08	0.12	1.5	0.14	0.15	1.1
	I	0.05	0.05	1.9	0.09	0.14	1.6	0.14	0.18	1.3
GIRDER 5	H	0.06	0.06	1.00	0.09	0.17	1.9	0.14	0.23	1.6
	U	0.06	0.06	1.00	0.08	0.14	1.8	0.14	0.20	1.4
	J	0.02	-0.02	-	0.02	0.05	2.5	0.04	0.04	1.0
	T	0.03	0.01	0.33	0.03	0.02	0.7	0.06	0.03	0.5
	K	0.07	0.09	1.29	0.11	0.16	1.5	0.18	0.25	1.4
	V	0.11	0.16	1.45	0.17	0.78	1.6	0.28	0.43	1.5
	I	0.07	0.07	1.00	0.11	0.04	0.4	0.18	0.11	0.6

1 IN = 25.4 mm

the mirror-scale and level readings for the self-weight case has not been retained and an average of these readings has been added to the experimantal readings for the concrete block loading to obtain the final total dead load experimental values in Columns (9) and (10).

From Column (11) of Table 5.4 it can be observed that for the total dead load case the E/T ratios are now much more uniform and the experimental deflections in the highly stressed midspan region are approximately 1.5 times greater than those predicted by theory based on an uncracked section.

It is of interest to note that the maximum measured dead load deflection of 0.44 in. (11.2 mm) is approximately only 1/1000 of the 36 ft (11.0 m) span and because of similitude this ratio could be expected in a prototype structure.

5.4 Strains and Longitudinal Forces at a Section

The summary of tensile and compressive strains at the straight instrumented sections A and D in the diaphramed and undiaphramed spans respectively will be presented, for the case of self-weight of the bridge model and separately for the case of concrete block loading on the bridge top deck. Both theoretical and experimental strains will be given.

Theoretical strains and longitudinal forces at a section are based on the longitudinal membrane forces from the CELL analysis which assumes an uncracked concrete section. These are obtained using the procedure outlined below:

1. Theoretical longitudinal forces are obtained automatically from CELL by separately integrating the tensile and compressive longitudinal forces in the flanges and webs of the uncracked sections.
2. The compressive strains in the concrete (K gages) are the theoretical values at the points shown obtained by dividing the longitudinal forces (kips/ft) by the product of thickness of the slab times the modulus of elasticity of the concrete. The small effect of Poissions ratio is neglected.
3. The tensile strains in the steel (W gages) are obtained by dividing the longitudinal force in (kips/ft) at a node by the product of the area of the steel reinforcement in ($in.^2/ft$) in the vicinity times the modulus of elasticity of the steel. Thus it is assumed that the steel alone resists this tensile force.
4. The experimental results were obtained directly from the data processing programs described in Chapter 4.

5.4.1 Longitudinal Strains for Self-Weight of Model

A summary of the longitudinal strains in micro-inches per inch at sections A and D for the self-weight of the bridge model is given in Columns (3) and (4) of Tables 5.5 and 5.6. Both tensile and compressive strains are given, and the experimental strain data have been adjusted using the ADJSTRN program described in Chapter 4.

It is observed that the theoretical strain values for concrete are generally somewhat smaller than the experimental values at both sections A and D. The agreement between theoretical and experimental steel strains, which are tensile at sections A and D, is somewhat better.

TABLE 5.5 SUMMARY OF LONGITUDINAL STRAINS (MICRO INCH/INCH) AT SECTION A FOR DEAD LOAD

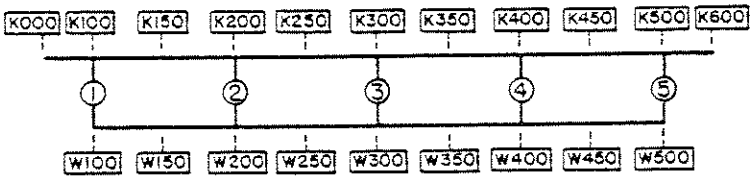

SECTION A

GAGE TYPE	LOCATION	SELF-WEIGHT		BLOCKS		TOTAL DEAD LOAD	
		THEORY	EXPT.	THEORY	EXPT.	THEORY	EXPT.
(1)	(2)	(3)	(4)	(5)	(6)	(7)	(8)
CONCRETE STRAIN METERS	K000	-55	-87	-93	-128	-148	-215
	K100	-49	-92	-81	-149	-130	-241
	K150	-42	-75	-67	-114	-109	-189
	K200	-43	-66	-68	-85	-111	-151
	K250	-43	-70	-67	-79	-110	-149
	K300	-44	-73	-69	-80	-113	-153
	K350	-42	-70	-66	-74	-108	-144
	K400	-42	-64	-67	-69	-109	-133
	K450	-40	-65	-63	-77	-103	-142
	K500	-48	-66	-75	-83	-123	-149
	K600	-54	-42	-84	-42	-138	-84
WELDABLE GAGES	W100	144	111	243	346	387	457
	W150	141	150	228	230	372	380
	W200	143	180	227	351	370	531
	W250	140	167	221	193	361	360
	W300	143	216	224	381	367	597
	W350	137	148	216	238	353	386
	W400	138	85	220	153	358	238
	W450	136	213	213	227	349	440
	W500	142	53	221	154	363	207

TABLE 5.6 SUMMARY OF LONGITUDINAL STRAINS (MICRO INCH/INCH) AT SECTION D FOR DEAD LOAD

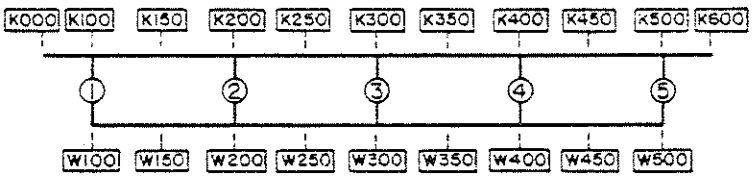

SECTION D

GAGE TYPE	LOCATION	SELF-WEIGHT		BLOCKS		TOTAL DEAD LOAD	
		THEORY	EXPT.	THEORY	EXPT.	THEORY	EXPT.
(1)	(2)	(3)	(4)	(5)	(6)	(7)	(8)
CONCRETE STRAIN METERS	K000	-51	-57	-85	-70	-136	-127
	K100	-45	-68	-75	-84	-120	-152
	K150	-38	-67	-64	-79	-102	-146
	K200	-40	-74	-67	-85	-107	-159
	K250	-39	-69	-67	-69	-106	-138
	K300	-41	-70	-70	-75	-111	-145
	K350	-40	-58	-68	-55	-108	-113
	K400	-41	-68	-69	-70	-110	-138
	K450	-40	-79	-67	-83	-107	-162
	K500	-47	-79	-79	-81	-126	-160
	K600	-54	-83	-89	-83	-143	-166
WELDABLE GAGES	W100	133	272	223	357	356	629
	W150	128	129	214	206	342	335
	W200	131	130	220	312	351	442
	W250	128	136	217	223	345	359
	W300	134	144	225	268	359	412
	W350	132	97	222	241	354	338
	W400	136	136	229	290	365	426
	W450	136	148	227	240	363	388
	W500	140	79	235	344	375	423

5.4.2 Longitudinal Strains for Concrete Block Loading

Columns (5) and (6) of Tables 5.5 and 5.6 also list the summary of longitudinal strains at sections A and D for the concrete block loading. With this loading the cracking of the concrete progresses considerably and the maximum tensile stress registered in the steel at sections A and D is 11 ksi (76 MPa). The experimental strains for both steel and concrete are now observed to be generally greater than the theoretical values.

5.4.3 Longitudinal Strains for Total Dead Load

The values for total dead load in Columns (7) and (8) of Tables 5.5 and 5.6 are obtained by adding those due to self-weight and the block loading. From Tables 5.5 and 5.6 it is noted that reasonable agreement exists in general for theoretical and experimental strains due to total dead load, except that the theoretical compressive strains at section A tend to be smaller than the adjusted experimental values. This is probably due to uneven cracking in the model.

A study of the experimental strains for total dead load in Tables 5.5 and 5.6 indicates average strain values in micro-inches per inch at sections A and D, respectively, of -159 and -147 in the concrete and +400 and +415 in the steel. The latter values correspond to a steel stress of about 12 ksi under total dead load. The average top and bottom strains also indicate a cracked section exists with the neutral axis being considerably higher than the gross uncracked section neutral axis used in the CELL theoretical analysis.

5.4.4 Longitudinal Forces for Self-Weight of Model

Table 5.7 shows theoretical and experimental values of the longitudinal membrane forces at the instrumented sections A and D for the self-weight of the model. Both "measured" and modified experimental

TABLE 5.7 INTERNAL LONGITUDINAL FORCES (KIPS) AT SECTIONS A AND D FOR SELF WEIGHT OF BRIDGE MODEL

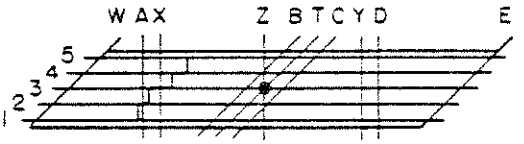

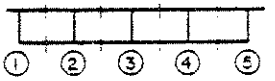

SECTION	GIRDER	THEORY		EXPERIMENTAL			
				MEASURED		MODIFIED	
		TENSILE	COMPRES.	TENSILE	COMPRES.	TENSILE	COMPRES.
(1)	(2)	(3)	(4)	(5)	(6)	(7)	(8)
A	1	7.4	- 9.9	6.3	-24.0	6.3	-11.6
	2	12.2	-10.6	11.3	-18.5	11.3	- 8.9
	3	12.1	-10.8	12.6	-19.9	12.6	- 9.6
	4	11.8	-10.3	9.8	-19.1	9.8	- 9.2
	5	7.3	- 9.6	6.8	-15.2	6.8	- 7.4
	Σ	50.9	-51.1	46.8	-96.7	46.8	-46.7
D	1	6.8	- 9.1	11.5	-15.1	11.5	- 7.3
	2	11.2	- 9.7	9.1	-18.4	9.1	- 8.9
	3	11.4	-10.1	8.6	-16.9	8.6	- 8.2
	4	11.7	-10.0	7.9	-17.5	7.9	- 8.4
	5	7.2	- 9.5	5.5	-20.6	5.5	- 9.9
	Σ	48.2	-48.5	42.6	-88.5	42.6	-42.6

1 KIP = 4.448 kN

results are given. Theoretical tensile and compressive forces on a section are practically equal as required by statics. The agreement between theoretical and measured experimental values of tensile forces on the sections is relatively good. However, the measured experimental compression forces are much higher than the theoretical values, and consequently also higher than the measured experimental values of tensile forces. This is due partly to the difficulty of determining the proper modulus of elasticity (effective stiffness) of the concrete to be used in converting strains to stresses and also to the lack of information about the internal stress distribution existing prior to the removal of the shoring.

The same pattern of high values for the experimental compression forces is also observed in the case of the concrete block loading on the bridge model deck (see Table 5.11 below). It was decided therefore to modify the forces on the cross-section at both sections A and D to eliminate the imbalance observed in the measured forces and to bring about longitudinal force equilibrium on each section, for the self-weight case as well as for the concrete block loading case. The modification procedure shall now be explained for the self-weight case.

The total measured tensile forces at sections A and D given in Table 5.7, which compare favorably with the theoretical values, were assumed to be correct and all measured experimental compressive forces were converted to modified experimental compressive forces by multiplying them by modification factors equal to the ratio of the total experimental tensile to compressive force at each section. The resulting modification factors are given in Table 5.8.

TABLE 5.8 FORCE MODIFICATION FACTORS FOR SELF WEIGHT OF BRIDGE MODEL

FORCE	Section A	Section D
TENSION	1.000	1.000
COMPRESSION	0.483	0.482

It is observed that for the self-weight case, the ratio of the tensile force to the compressive force at both sections A and D is almost exactly the same. This suggests that identical factors are responsible for the discrepancy between tensile and compressive forces on each section.

5.4.5 Longitudinal Forces for Concrete Block Loading

The internal longitudinal forces at sections A and D for the concrete block loading are shown in Table 5.11. Although not to the degree observed for the self-weight case, it is found that the measured compressive forces exceed the measured tensile forces at both the sections. A modification is therefore carried out by converting the measured compressive forces as before, i.e., by multiplying them by the ratio of the total experimental tensile force to the total experimental compressive force at each section, so as to restore the longitudinal force equilibrium at sections A and D. For the concrete block loading, the modification factors are given below in Table 5.9.

It is noted that for the block loading on the bridge top deck the discrepancy between the measured compression and tension forces is smaller. The difference between the measured values at sections A and D may result from the presence of the staggered diaphragm in Span I as opposed to no diaphragm in Span II.

TABLE 5.9 FORCE MODIFICATION FACTORS FOR CONCRETE BLOCK LOADING

FORCE	Section A	Section D
TENSION	1.000	1.000
COMPRESSION	0.642	0.913

5.4.6 Longitudinal Forces for Total Dead Load

For the sake of completeness of presentation of the dead load experimental data, the theoretical and experimental values for the internal longitudinal forces for the total dead load comprising the sum of the self-weight of the bridge model and the concrete block loading on the bridge top deck are given in Table 5.12. The experimental data are once again modified using the ratio of the total tensile force to the total compressive load force at sections A and D respectively. The modification factors for the total dead load are given below in Table 5.10.

TABLE 5.10 FORCE MODIFICATION FACTORS FOR TOTAL DEAD LOAD

FORCE	Section A	Section D
TENSION	1.000	1.000
COMPRESSION	0.571	0.700

In all the above comparisons between theoretical and experimental longitudinal forces, recourse has had to be made to a process of modification of the experimental values in order to ensure equilibrium of longitudinal forces on a section.

TABLE 5.11 INTERNAL LONGITUDINAL FORCES (KIPS) AT SECTIONS A AND D FOR CONCRETE BLOCK LOADING

SECTION	GIRDER	THEORY		EXPERIMENTAL			
				MEASURED		MODIFIED	
		TENSILE	COMPRES.	TENSILE	COMPRES.	TENSILE	COMPRES.
(1)	(2)	(3)	(4)	(5)	(6)	(7)	(8)
A	1	12.4	-16.3	14.3	-35.8	14.3	-23.0
	2	19.4	-16.7	18.4	-24.1	18.4	-15.4
	3	19.0	-16.9	20.2	-21.0	20.2	-13.5
	4	18.7	-16.3	13.9	-20.3	13.8	-13.0
	5	11.3	-15.1	9.7	-17.9	9.7	-11.5
	Σ	80.8	-81.3	76.4	-119.1	76.4	-76.4
D	1	11.4	-15.2	15.8	-18.3	15.8	-16.7
	2	18.7	-16.4	18.7	-19.5	18.7	-17.8
	3	19.1	-16.9	16.5	-16.5	16.5	-15.1
	4	19.5	-16.8	16.3	-16.8	16.3	-15.3
	5	12.1	-15.9	15.0	-19.1	15.0	-17.4
	Σ	80.8	-81.2	82.3	-90.1	82.3	-82.3

1 KIP = 4.448 kN

TABLE 5.12 INTERNAL LONGITUDINAL FORCES (KIPS) AT SECTIONS A AND D FOR TOTAL DEAD LOAD OF BRIDGE MODEL

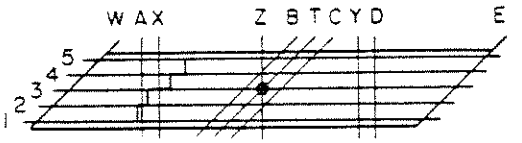

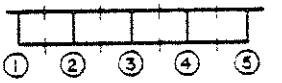

SECTION	GIRDER	THEORY		EXPERIMENTAL			
				MEASURED		MODIFIED	
		TENSILE	COMPRES.	TENSILE	COMPRES.	TENSILE	COMPRES.
(1)	(2)	(3)	(4)	(5)	(6)	(7)	(8)
A	1	19.8	-26.2	20.6	-59.8	20.6	-34.1
	2	31.6	-27.3	29.7	-42.6	29.7	-24.3
	3	31.1	-27.6	32.7	-41.0	32.7	-23.4
	4	30.5	-26.6	23.7	-39.4	23.7	-22.5
	5	18.6	-24.7	16.5	-33.2	16.5	-18.9
	Σ	131.6	-132.4	123.2	-215.8	123.2	-123.2
D	1	18.2	-24.2	27.2	-33.4	27.2	-23.3
	2	29.9	-26.1	27.8	-37.9	27.8	-26.5
	3	30.4	-27.0	25.2	-33.4	25.2	-23.4
	4	31.2	-26.8	24.2	-34.2	24.2	-23.9
	5	19.3	-25.5	20.5	-39.7	20.5	-27.7
	Σ	129.0	-129.6	124.9	-178.6	124.9	-124.9

1 KIP = 4.448 kN

5.5 Moments

Theoretical total moments at any right section of the box girder bridge model can be computed in one of two ways using the CELL program results: (1) external moments can be obtained by algebraically summing the moment contributions of the CELL reactions and the known applied self-weight or block loads, times their respective lever arms to the given right section; and (2) internal moments can be obtained by integrating the internal moment contribution of all the internal longitudinal forces at the given right sections. The theoretical external and internal moments calculated from the CELL program are normally almost exactly equal, as would be expected. Differences arise, however, in the region of the skew center bent because of the additional participation of the center bent diaphram in resisting the total longitudinal bending moment. This aspect is discussed in detail in Vol. III of the present sequence of research reports.

Experimental external moments at any right section can also be calculated from the experimental reactions and the applied loading. Differences between these and theoretical external moments will be a function of the agreement found between the experimental and theoretical reactions, Table 5.1, and the accuracy with which the type, distribution and magnitude of the applied loading is known. It should be noted that even small differences between experimental and theoretical end reactions may result in significant differences in the comparisons between the experimental and theoretical external moments at midspan sections X, Y and center bent section Z. However, it is important to remember that the total statical moment, defined as the simple beam midspan moment in each span, will always be the same and will equal one half of the moment found

at section Z plus the moment found at section X or Y respectively. Thus if sufficient reinforcement is provided at midspan sections X, Y and center support section Z to carry the total external statical moment, differences between individual moments at these sections can be accommodated by a redistribution of moments at high loads, if necessary.

Experimental internal moments were calculated only at sections A and D near midspan and they will be compared with the theoretical internal moments evaluated from the CELL program. These comparisons will be made for the self-weight, blocks and total dead load. The experimental values used, have in all cases been modified by the appropriate modification factors from Tables 5.8, 5.9 and 5.10.

5.5.1 Moments for Self-Weight of Bridge Model

Fig. 5.3 gives the theoretical moments due to the self-weight of the bridge model obtained from the CELL analysis. The points on the solid line represent calculated external moment values and the points within circles represent internal moment values. For the purposes of the present comparison, the moment diagram is assumed to be symmetrical about the transverse centerline section Z, although small differences do exist between the two spans as may be observed from Table 5.14.

It is observed from Fig. 5.3 that the agreement between the theoretical external and internal moments is excellent except over the range of the skew center bent diaphram, i.e. between 30.86 and 36.00 ft (9.41 and 10.97 m) where the participation of the skew center bent in the longitudinal bending reduces the internal moments of the box cross-section to those indicated by the broken lines in that region. The single experimental value of the internal moment at the instrumented section A, plotted in Fig. 5.3, has been obtained from measured values suitably modified by the factors shown in Table 5.8.

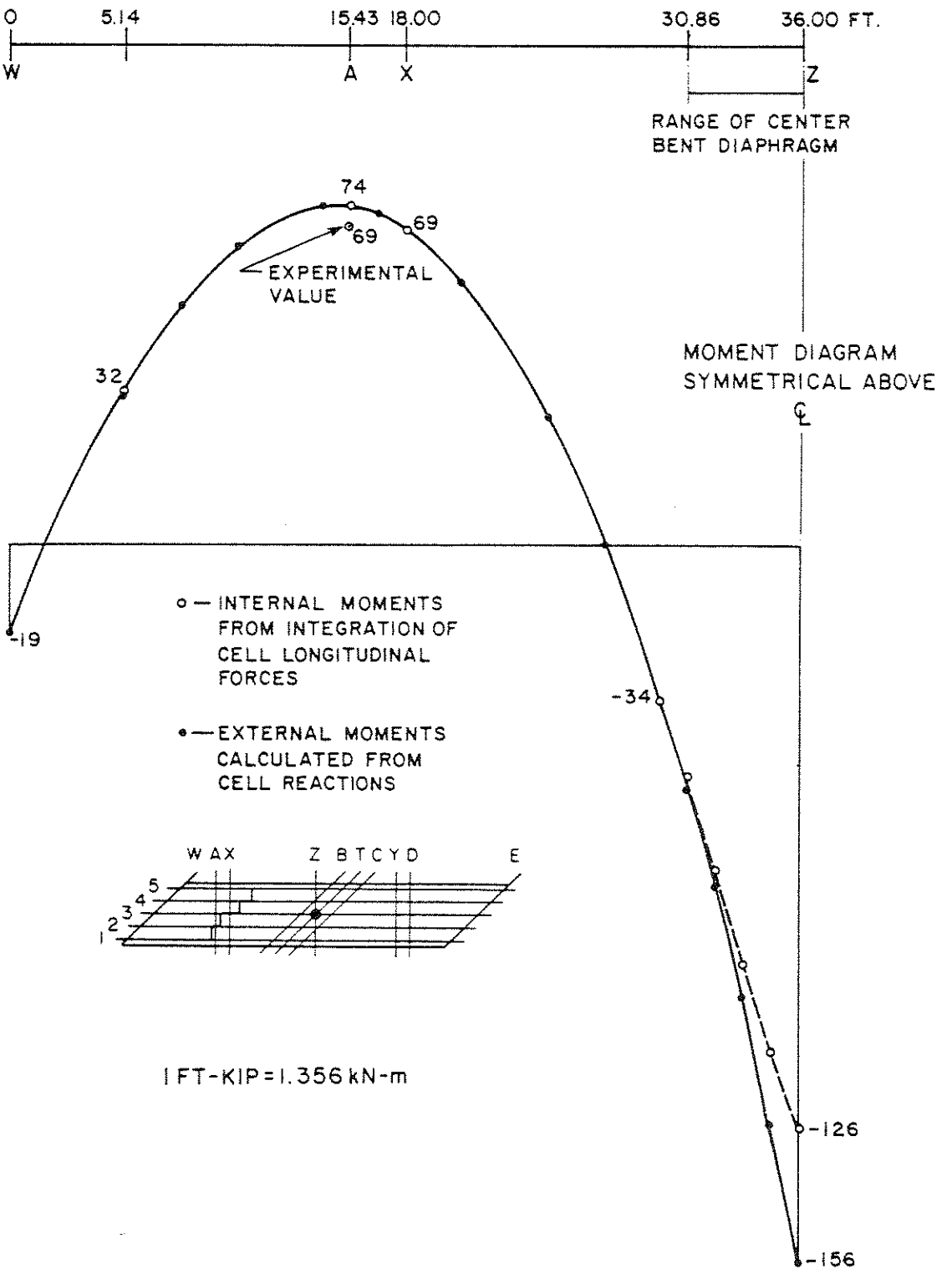

FIG. 5.3 LONGITUDINAL DISTRIBUTION OF THEORETICAL EXTERNAL AND INTERNAL MOMENTS IN SPAN 1 DUE TO SELF-WEIGHT

TABLE 5.13 DISTRIBUTION OF INTERNAL MOMENTS (KIP-FT AND %) TO EACH GIRDER FOR SELF-WEIGHT CASE

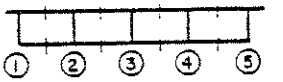

	SECTION	GIRDER	MOMEMTS BASED ON							
			COMPR. FLANGE MID-DEPTH		TENSION FLANGE STEEL		GROSS-SECTION NEUTRAL AXIS		INDIVID. GIRDER NEUTRAL AXIS	
			K-FT	%	K-FT	%	K-FT	%	K-FT	%
THEORY	A	1	14.2	19.3	10.4	14.2	12.0	16.4	12.0	16.4
		2	15.2	20.7	17.8	24.3	16.6	22.7	16.6	22.7
		3	15.5	21.1	17.6	24.1	16.7	22.8	16.6	22.8
		4	14.8	20.2	17.2	23.5	16.1	22.0	16.1	22.0
		5	13.8	18.8	10.2	13.9	11.8	16.1	11.7	16.1
		Σ	73.5	100.0	73.2	100.0	73.2	100.0	73.0	100.0
EXPT	A	1	9.2	13.2	17.0	24.6	12.8	18.4	12.8	18.0
		2	16.9	24.2	13.2	19.1	15.2	21.8	15.8	22.2
		3	18.6	26.6	14.1	20.4	16.6	23.9	17.5	24.6
		4	14.7	21.1	13.7	19.8	14.3	20.5	14.3	20.1
		5	10.4	14.9	11.2	16.2	10.7	15.4	10.8	15.2
		Σ	69.8	100.0	69.2	100.1	69.6	100.0	71.2	100.1
THEORY	D	1	13.0	18.7	9.5	13.8	11.0	15.9	11.0	15.9
		2	14.0	20.1	16.2	23.4	15.2	22.0	15.2	22.0
		3	14.5	20.9	16.5	23.8	15.6	22.5	15.6	22.5
		4	14.5	20.8	16.9	24.5	15.8	22.8	15.8	22.8
		5	13.7	19.6	10.1	14.5	11.7	16.8	11.6	16.8
		Σ	69.7	100.0	69.2	100.0	69.3	100.0	69.2	100.0
EXPT	D	1	16.8	26.8	10.3	16.4	13.9	22.2	15.5	23.9
		2	13.5	21.5	13.2	21.0	13.4	21.4	13.4	20.7
		3	12.8	20.4	12.1	19.2	12.4	19.8	12.5	19.3
		4	11.7	18.6	12.5	19.9	12.0	19.1	12.0	18.5
		5	8.0	12.7	14.8	23.5	11.0	17.5	11.4	17.6
		Σ	62.8	100.0	62.9	100.0	62.7	100.0	64.8	100.0

1 FT-KIP = 1.356 kN-m

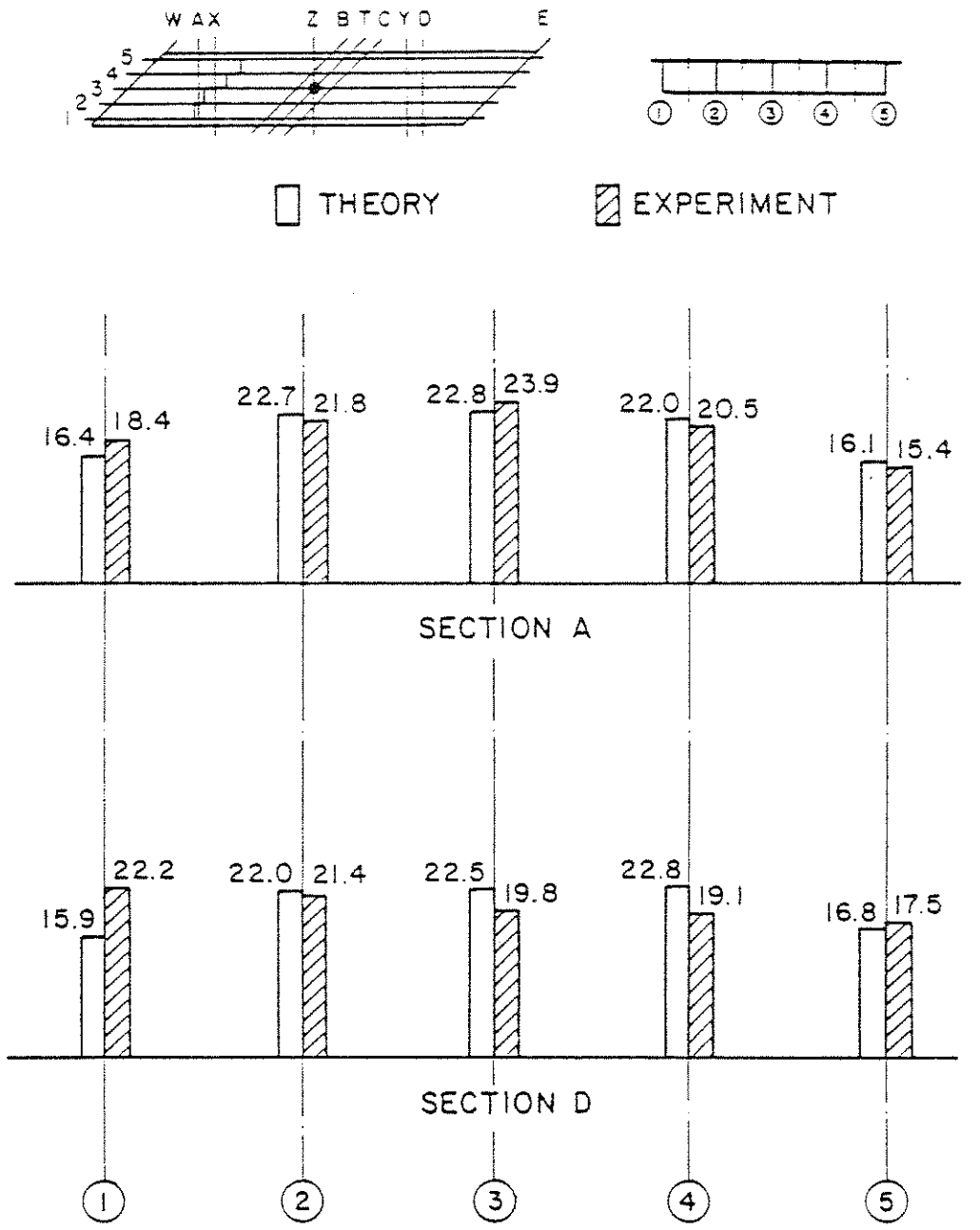

FIG. 5.4 PERCENTAGES OF TOTAL MOMENT AT A SECTION CARRIED BY EACH GIRDER FOR SELF-WEIGHT LOADING CASE

Table 5.13 gives a detailed breakdown of the transverse distribution of the internal moments to each girder. Theoretical results from CELL, and the experimental results are given about four different axes for comparison. The different values obtained for each girder moment about the four axes are due to the fact that the longitudinal compressive and tensile forces acting on each girder are not equal. Even though the total forces across a section are modified to give longitudinal equilibrium, this procedure does not result in equilibrium for each individual girder. However, the total internal moments at sections A and D about any section axis should be the same except for round off differences in the experimental results.

Fig. 5.4 compares theoretical and experimental percentage distribution to each girder for the moment about the entire gross cross-section neutral axis. It can be seen that the percentage distribution is generally within 1 - 3% of each other for all girders except girder 1 at section D. The overall agreement in the diaphramed span is better than in the undiaphramed span.

It should be noted that if the gross moments were distributed to each girder according to the ratios of their moment of inertia to that of the total section, the following percentages are obtained: 16.5, 22.4, 22.4, 22.4 and 16.5. The values in Fig. 5.4 indicate a rough approximation to this uniform stress distribution across the width of the section.

5.5.2 Moments for Bridge Model Concrete Block Loading

The detailed transverse distribution of internal moments at sections A and D for the concrete block loading on the bridge model top deck is given in Table 5.14 for theoretical and experimental moment values about four axes. As in the self-weight loading case, the percen-

TABLE 5.14 DISTRIBUTION OF INTERNAL MOMENTS (KIP-FT AND %) TO EACH GIRDER FOR CONCRETE BLOCK LOADING

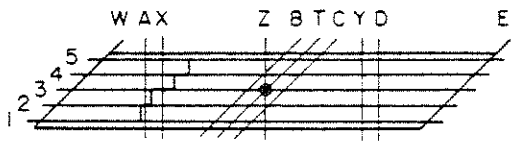

	SECTION	GIRDER	MOMENTS BASED ON							
			COMPR. FLANGE MID-DEPTH		TENSION FLANGE STEEL		GROSS-SECTION NEUTRAL AXIS		INDIVID. GIRDER NEUTRAL AXIS	
			K-FT	%	K-FT	%	K-FT	%	K-FT	%
THEORY	A	1	23.3	20.0	17.3	14.9	19.9	17.1	19.9	17.1
		2	24.0	20.6	28.2	24.3	26.4	22.7	26.3	22.7
		3	24.3	20.8	27.6	23.8	26.1	22.5	26.1	22.5
		4	23.5	20.2	27.1	23.4	25.5	22.0	25.5	22.0
		5	21.6	18.5	15.8	13.6	18.3	15.8	18.3	15.8
		Σ	116.7	100.0	116.0	100.1	116.2	100.0	116.1	100.0
EXPT	A	1	20.8	18.4	34.1	30.1	26.7	23.6	24.7	21.5
		2	27.3	24.2	22.7	20.1	25.2	22.3	26.4	23.0
		3	29.7	26.3	19.5	17.2	25.1	22.2	28.0	24.3
		4	20.7	18.3	19.5	17.2	20.2	17.9	20.4	17.7
		5	14.5	12.8	17.3	15.3	15.8	14.0	15.5	13.5
		Σ	113.0	100.0	113.1	99.9	113.0	100.0	115.0	100.0
THEORY	D	1	21.7	18.6	15.9	13.7	18.5	15.9	18.4	15.9
		2	23.6	20.2	27.2	23.4	25.6	22.0	25.6	22.0
		3	24.4	20.9	27.7	23.9	26.3	22.6	26.2	22.6
		4	24.3	20.8	28.4	24.4	26.6	22.8	26.5	22.8
		5	22.8	19.5	16.8	14.5	19.5	16.7	19.4	16.7
		Σ	116.8	100.0	116.0	100.0	116.5	100.0	116.1	100.0
EXPT	D	1	23.1	19.0	24.5	20.2	23.6	19.5	23.3	19.2
		2	27.7	22.9	26.3	21.7	27.0	22.3	27.4	22.6
		3	24.5	20.2	22.3	18.4	23.5	19.4	24.1	19.9
		4	24.1	19.9	22.6	18.6	23.4	19.3	23.8	19.6
		5	21.9	18.0	25.7	21.2	23.5	19.4	22.6	18.6
		Σ	121.3	100.0	121.4	100.1	121.0	99.9	121.2	99.9

1 FT-KIP = 1.356 kN-m

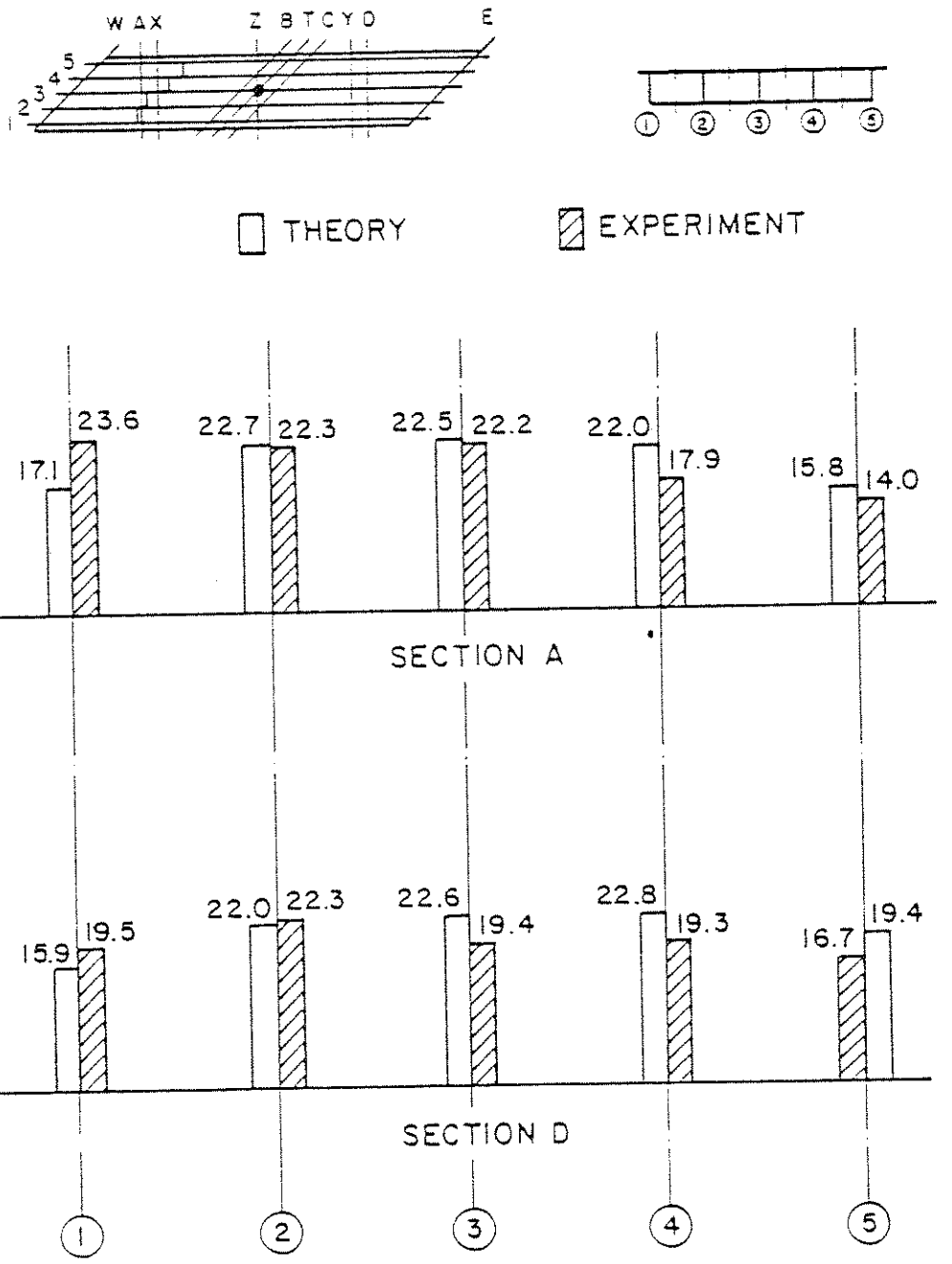

FIG. 5.5 PERCENTAGES OF TOTAL MOMENT AT A SECTION CARRIED BY EACH GIRDER FOR CONCRETE BLOCK LOADING

tage distribution to each girder for the moment about the entire gross cross-section neutral axis is shown in Fig. 5.5.

It is observed that the greatest discrepancy in percentage distribution is now at location 1A where the experimentally registered girder moment is 6.5% greater than the theoretical value. As seen in the key at the top of Fig. 5.5, location 1A, is very close to one of the staggered mid-span diaphrams which could distort both experimental and theoretical results.

5.5.3 Moments due to Total Dead Load

The internal moments due to the combined effect of the bridge model self-weight and the concrete block loading are tabulated in Table 5.16. Both the theoretical CELL results and the experimental moment values have been given about four different axes for comparison. It is to be recalled that the forces used for the evaluation of the experimental moments have been modified as per Table 5.12. Furthermore, the experimental moments for the gross-section and individual girder neutral axes have been recalculated because of the different contributions of the tensile and compressive forces to these moments after modification factors have been used. In other words, the experimental moment values for the gross-section neutral axis in Table 5.15 are not the simple sums of the corresponding values in Tables 5.13 and 5.14.

The percentages of section moment carried by each girder at sections A and D for the moment about the gross-section neutral axis are depicted in Fig. 5.6. It is observed that the experimental pattern does not change substantially; the experimental values of the moments at locations 1A and 1D continue to be higher than the theoretical values. Girder 2 continues to show the best agreement between theory and experiment.

TABLE 5.15 DISTRIBUTION OF MOMENTS (KIP-FT AND %)
TO EACH GIRDER FOR TOTAL DEAD LOAD CASE

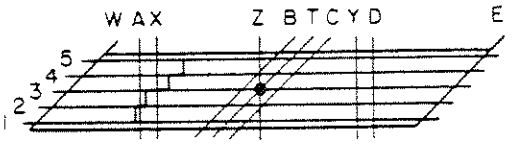

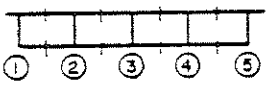

	SECTION	GIRDER	MOMENTS BASED ON							
			CO,PR. FLANGE MID-DEPTH		TENSION FLANGE STEEL		GROSS-SECTION NEUTRAL AXIS		INDIVID. GIRDER NEUTRAL AXIS	
			K-FT	%	K-FT	%	K-FT	%	K-FT	%
THEORY	A	1	37.5	19.7	27.7	14.6	31.9	16.8	31.9	16.9
		2	39.2	20.6	46.0	24.3	43.0	22.7	42.9	22.7
		3	39.8	20.9	45.2	23.9	42.8	22.6	42.7	22.6
		4	38.3	20.1	44.3	23.4	41.6	22.0	41.6	22.0
		5	35.4	18.6	26.0	13.7	30.1	15.9	30.0	15.9
		Σ	190.2	100.0	189.2	100.0	189.4	100.0	189.1	100.0
EXPT	A	1	29.9	16.4	50.7	27.8	39.2	21.5	37.9	20.2
		2	44.1	24.1	35.8	19.6	40.3	22.1	42.4	22.6
		3	48.4	26.5	34.0	18.6	41.8	22.9	45.8	24.4
		4	35.4	19.4	33.6	18.4	34.6	19.0	35.0	18.6
		5	24.9	13.6	28.6	15.7	26.6	14.6	26.8	14.3
		Σ	182.7	100.0	182.7	100.1	182.5	100.1	187.9	100.1
THEORY	D	1	34.7	18.6	25.4	13.7	29.5	15.9	29.4	15.9
		2	37.6	20.2	43.4	23.4	40.8	22.0	40.8	22.0
		3	38.9	20.9	44.2	23.9	41.9	22.6	41.8	22.6
		4	38.8	20.8	45.3	24.5	42.4	22.8	42.3	22.8
		5	36.5	19.6	26.9	14.5	31.2	16.8	31.0	16.7
		Σ	186.5	100.0	185.2	100.0	185.8	100.0	185.3	100.0
EXPT	D	1	39.8	21.5	33.9	18.4	37.0	20.2	38.7	20.3
		2	42.1	22.8	39.3	21.3	40.3	22.0	41.6	21.9
		3	37.3	20.2	34.6	18.8	36.0	19.6	37.2	19.6
		4	35.8	19.4	35.4	19.2	35.5	19.3	36.6	19.2
		5	29.7	16.1	40.9	22.2	34.7	18.9	36.1	19.0
		Σ	184.7	100.0	184.1	99.9	183.5	100.0	190.2	100.0

1 FT-KIP = 1.356 kN-m

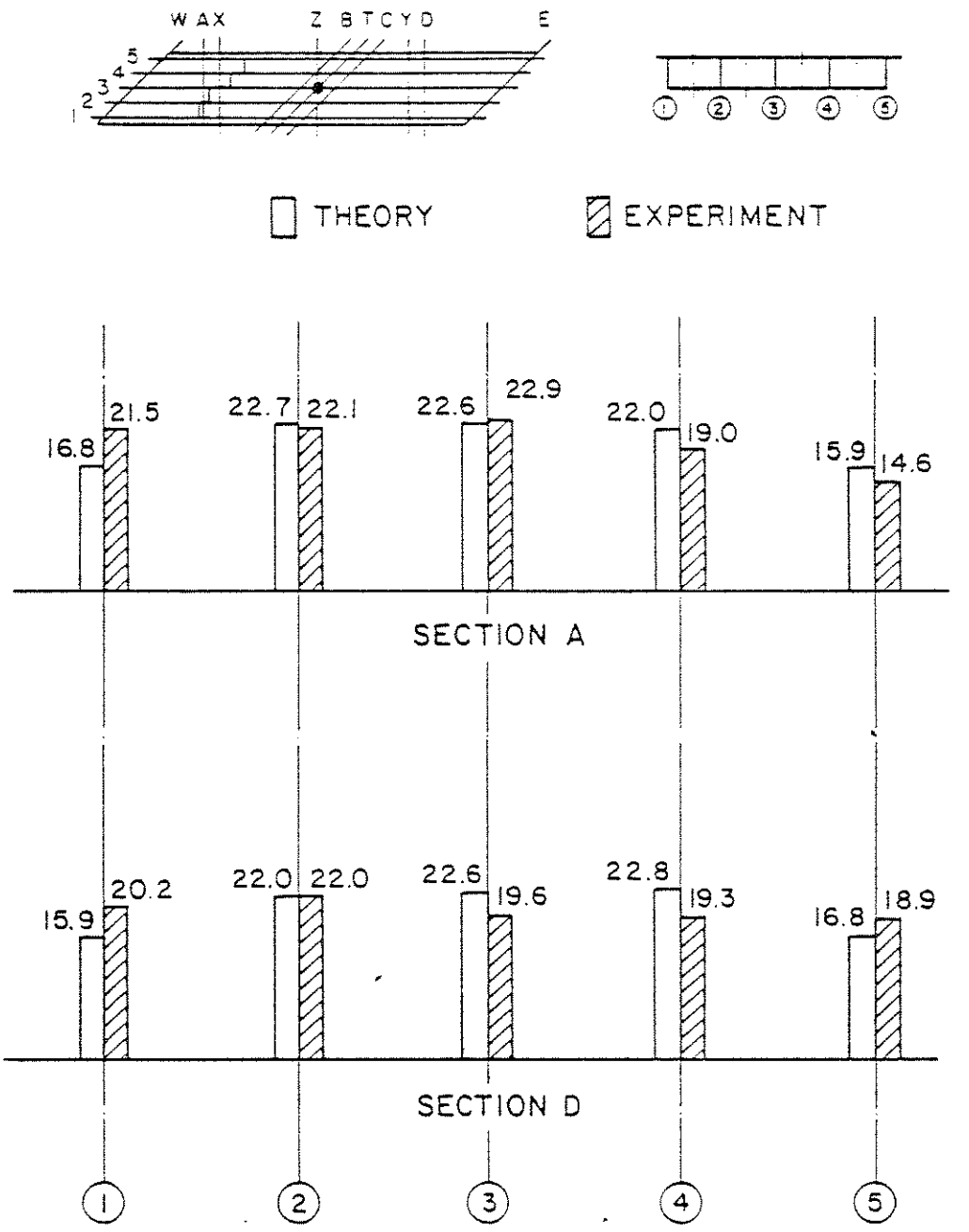

FIG. 5.6 PERCENTAGES OF TOTAL MOMENT AT A SECTION CARRIED BY EACH GIRDER FOR TOTAL DEAD LOAD CASE

5.6 Comparison of Experimental Results for Straight, Curved and Skew Bridge Models

Experimental results for reactions, deflections, strains and moments due to dead load on the straight and curved bridge models [1-10] and the skew bridge model reveal several differences in behavior.

The straight, curved and skew bridges had total measured dead loads of 199, 202 and 186 kips (886, 900 and 827 kN) respectively. The distribution of these total dead loads as vertical reactions between the east, center and west supports was 19.3%, 61.4% and 19.4% for the straight bridge; 18.0%, 63.3% and 18.7% for the curved bridge; and 22.0%, 55.9% and 22.1% for the skew bridge. The higher total vertical end reactions for the skew bridge are due to the nonuniform distribution of the individual girder end reactions resulting in a significant total negative end moment at the two end supports (Table 5.1) which does not exist for the straight or curve bridge models. The curved bridge has the lowest total vertical end reactions due to the eccentricity of the total dead load with respect to a line joining the middle of the east and west end supports, which eccentricity does not exist for the straight or skew bridge.

Vertical deflections at midspan sections X and Y were 0.38 and 0.44 in. (9.7 and 11.2 mm) respectively for the straight bridge and were uniform across the width of the bridge. For the curved bridge, deflections of outer girder 5 were slightly larger than those of inner girder 1 due to the longer span length of girder 5. At both sections X and Y deflections at girders 1 and 5 were 0.40 and 0.48 in. (10.2 and 12.2 mm) respectively, averaging 0.44 in. (11.2 mm) across the width, which is close to the straight bridge values. For the skew bridge, the maximum deflections in Spans I and II were 0.44 and 0.43 in. (11.2 and 10.9 mm)

at points 1U and 5V (Table 5.4) respectively, which are located at the midspans of the outer girders connecting the acute corners of the bridge with the center bent. These maximum values are close to those of the straight and curved bridges. The average deflection at right midspan sections X and Y can be found from Table 5.4 by interpolation to be about 0.30 in. (7.6 mm) which is substantially smaller than the straight or curved bridge values. Again it should be noted that a maximum dead load deflection of 0.44 in. (11.2 mm) represents a deflection to span ratio of only about 1/1000 and because of similitude, the same ratio could be expected in similar full scale prototype box girder bridges.

A comparison of experimental strains at the positive moment section D in the undiaphramed span for the total dead load is given in Fig. 5.7. Both the tensile and compressive strains for the skew bridge are somewhat lower than for the straight or curved bridges and appear to be fairly uniform across the width except for some shear lag effects in the midbay values.

Total dead load positive moments at midspan sections and negative moments near the center bent support, to be carried by the box girder section, are 10 to 15% smaller for the skew bridge than for the straight or curved bridge. This is due to effect of skewness of the end supports and the participation of the skew center bent diaphram as described earlier. A comparison of the transverse distribution of the total moments at section A and D in terms of percentage to each girder is given in Fig. 5.8. Some differences exist between the results for the skew bridge and those of the straight and curved bridges, but no definite trend can be ascertained. From a design standpoint an assumption of uniform stress distribution across the width resulting in a percentage distribution to

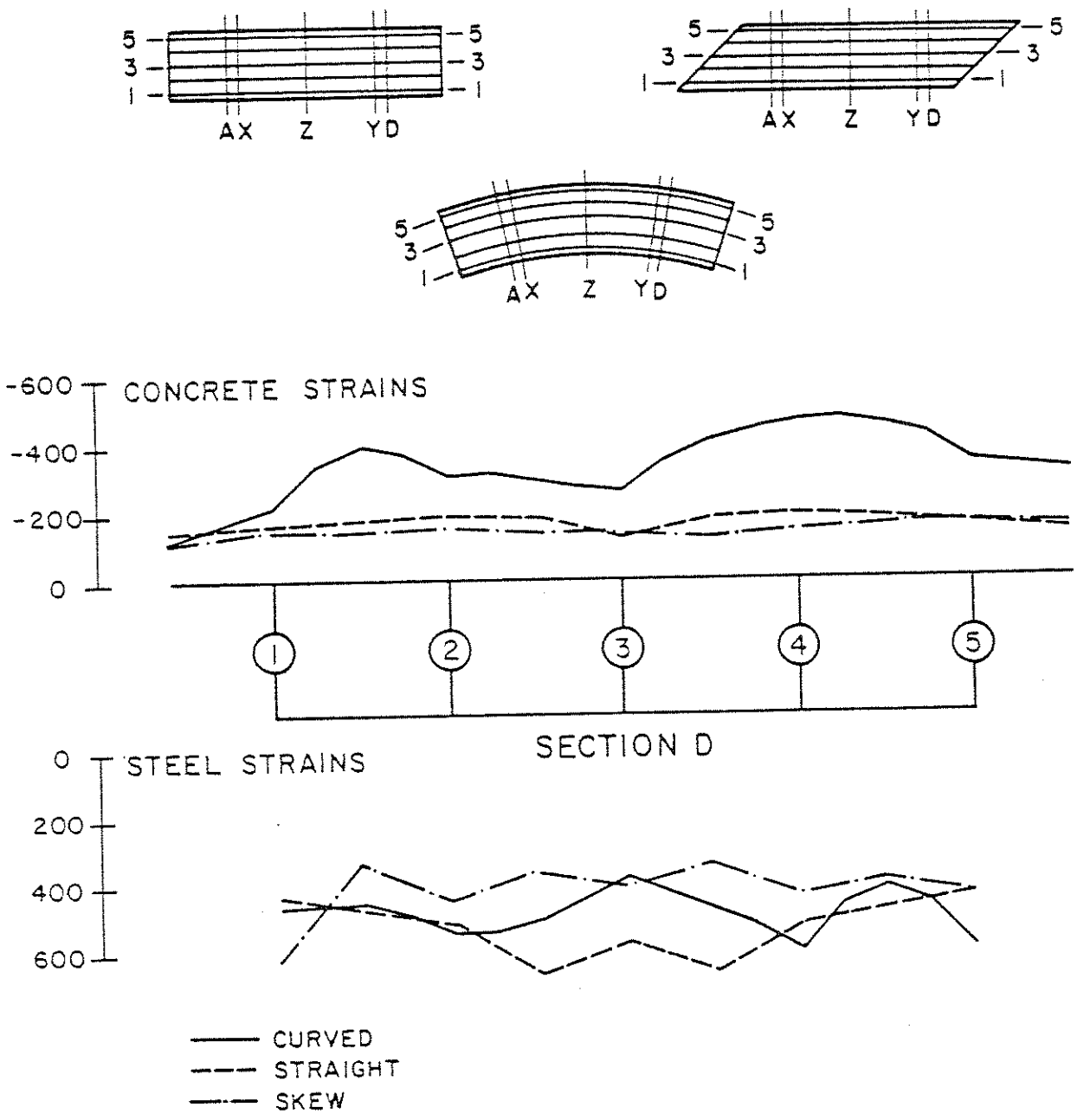

FIG. 5.7 TRANSVERSE DISTRIBUTION OF EXPERIMENTAL LONGITUDINAL STRAINS (MICRO INCH/INCH) AT SECTION D FOR TOTAL DEAD LOAD IN STRAIGHT, CURVED AND SKEW BRIDGE MODEL

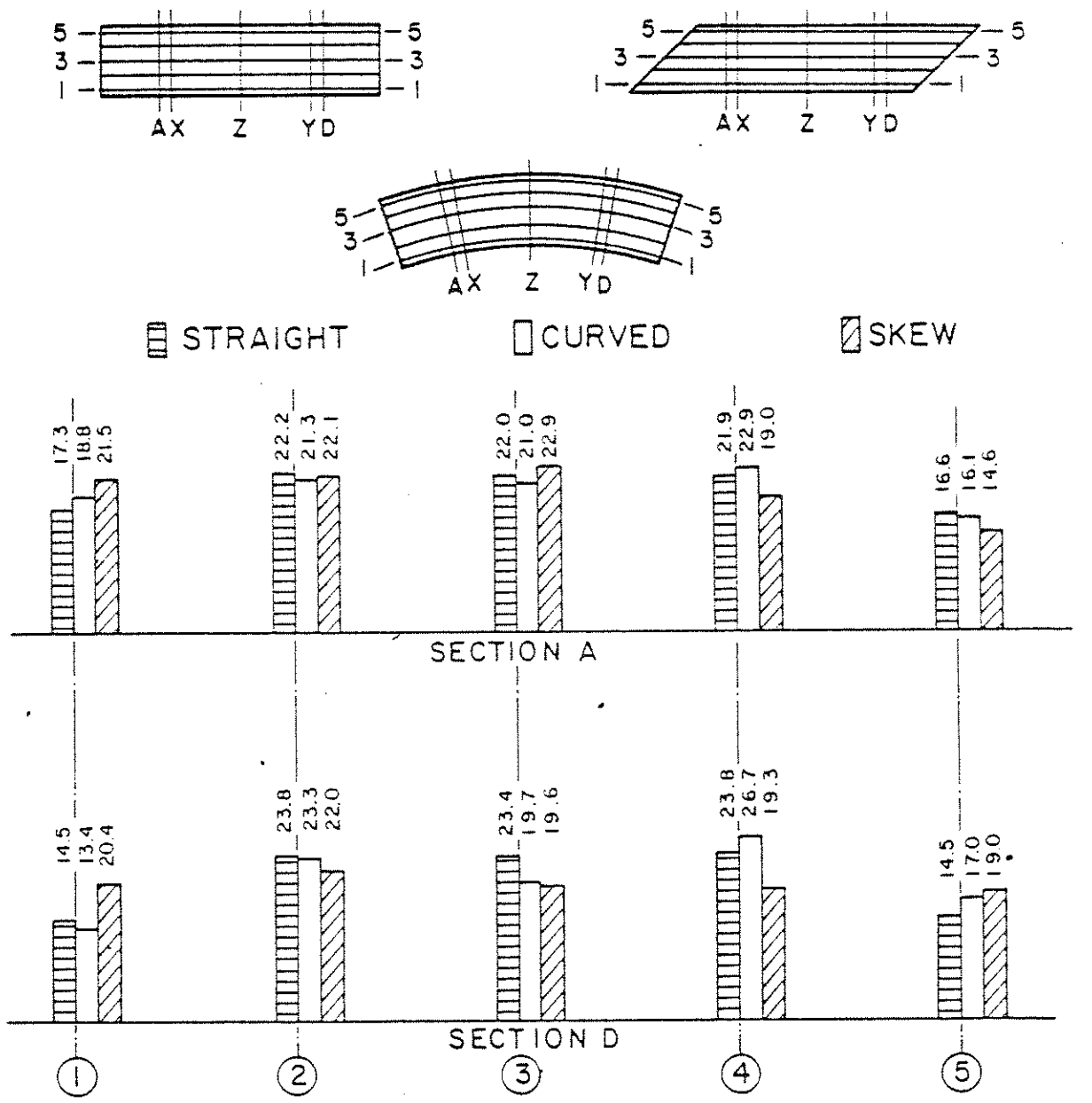

FIG. 5.8 EXPERIMENTAL PERCENTAGES OF TOTAL MOMENT AT A SECTION FOR TOTAL DEAD LOAD IN STRAIGHT, CURVED AND SKEW BRIDGE MODELS

five girders of 16.5, 22.4, 22.4, 22.4 and 16.5 would probably yield a satisfactory dead load design for all three bridges.

5.7 SUMMARY

Experimental measurements of response due to dead load are more difficult to evaluate than those due to live load, because they are dependent on the sequence and manner of construction, placing of instrumentation, design and installation of reaction supports and removal of shoring. Nevertheless after comparing theoretical and experimental results the following conclusions can be made with respect to the dead load case which consists of the self-weight loading of the skew bridge model and also the concrete block loading for proper simulation of prototype behavior.

1. Distribution of the total experimental reactions between east, center and west supports is accurately predicted by theory.
2. The transverse distribution of the total reactions at each end to the five reaction supports is highly dependent on the manner of design and installation of these supports and cannot be accurately predicted by theory. Because of the rigid end diaphragms, relative displacements due to support movements and differences in the spring constants of the support assemblies can totally change the transverse distribution of the reactions. However, the resultant of the five reactions at each end remains essentially unchanged. When the spring constants are known and are incorporated into the CELL analysis; as was done for the skew bridge model,

a significant improvement in the prediction of the individual experimental end reactions was obtained. In a prototype bridge, however, the constants would generally be unknown.

3. Maximum deflections occur in each span at the midspan of the outer girder lying between the acute corner of the bridge model and the center bent. Experimental deflections were 50 to 60% greater than theoretical deflections based on an uncracked section.
4. Experimental and theoretical values of tensile steel strains under total dead load were in relatively good agreement and the average experimental midspan strain indicated a steel stress of about 12 ksi (83 MPa).
5. The ratio of the average experimental top to bottom strain at midspan indicated that a cracked secyion existed. The experimental values of compressive strains in the concrete and thus the internal longitudinal forces and moments at a midspan section were not in good agreement with theory based on an uncracked section or statics. This was probably due to the fact that the assumed modulus of elasticity for the concrete used to convert strains to stresses, which was found from 6 x 12 inch cylinder tests, did not represent the true stiffness of the thin reinforced concrete top slab. When the experimental longitudinal compressive forces were modified to equal the measured tensile forces, as required by statics, the resulting internal experimental moments on a section were very close to those predicted by theory. However, the agreement between theory and experiment for the percentage of the

total moment at any section taken by each girder was less satisfactory and discrepancies of 5% were observed in a couple of cases.

6. The results of the concrete block loading, which was a uniformly distributed load of known magnitude were not noticeably in better agreement with theoretical values than the results of the self-weight loading case. This may be due to the fact that the block loading initiated extensive cracking in the bridge model.
7. Comparing the experimental response due to load of the skew bridge model with that of the straight and curved bridge models, significant differences exist with respect to the magnitude of the total vertical reactions at the end supports and the total moments at right sections with internal moments in the skew bridge being 10 to 15% smaller at critical sections. However, the magnitude of deflections and cracking under dead load was similar for the three bridge models.

6. RESULTS FOR WORKING STRESS LOADS

6.1 General Remarks

As described in Volume I the loading program was divided into several phases in which initial conditioning loads were applied to create total maximum tensile stresses in the reinforcement of 24, 30, 40, 50 and 60 ksi. Each of these initial conditioning loads was then followed by a detailed sequence of point loads on the bridge.

One of the prime objectives of the test program was to determine the bridge response at working stress levels. The loading phase involving the initial application of conditioning loads to produce a maximum tensile stress of 30 ksi was chosen to be representative of response at working stress from the point of view of assessing actual box girder bridge behavior for design purposes. An advantage of using the 30 ksi stress level instead of the 24 ksi stress level was that 50% higher values of live load stresses could be registered for a total increase in the bridge model tensile stresses of only 6 ksi. All subsequent point loads in this phase, however, were chosen to produce maximum stresses, where applied, of the order of the working stresses, i.e. 24 to 30 ksi total maximum tensile stress in the reinforcement.

The 30 ksi working load phase contained the most complete and detailed loading schedule of any phase (see Table 5.1 in Vol. I). In this chapter a presentation and evaluation of results will be made for this phase for the following loadings and conditions.

(1) Point loads on girder webs at midspan

(2) Effect of torsional restraint at center bent

(3) Truck and construction vehicle loads

(4) Moving fork lift load

6.2 Point Loads on Girder Webs at Midspans

Detailed tabulations of theoretical and experimental results related to reactions, deflections, strains and moments for each of the 19 point load combinations used are given in Vol. IV. All theoretical and experimental values have been normalized for purposes of comparison to loads of 100 kips (445 kN) per span. Theoretical values for these point load cases have been obtained using the CELL FINE computer model as described in Section 3.2.2.

Because of the voluminous amount of data, only nine point load cases will be treated in detail in the text of the present volume. These cases are: point loads at locations 1X, 3X or 5X; point load locations 1Y, 3Y or 5Y; point loads at locations 1X + 1Y, 3X + 3Y or 5X + 5Y. These cases have been chosen as typical of the 19 point load combinations, and comprise cases of loadings on the inner, center and outer girders of the bridge at the diaphragmed and undiaphragmed midspans. Loadings 1X, 3X and 5X produce maximum positive moments in diaphragmed Span I. Loadings 1Y, 3Y and 5Y produce maximum positive moments in undiaphragmed Span II. Loadings 1X + 1Y, 3X + 3Y and 5X + 5Y produce maximum negative moments at the center bent. Furthermore, these nine load cases lend themselves to comparisons of superposition which can be used as a check on the reliability of the experimental data.

In addition to a detailed discussion of the results for the nine load cases mentioned above, a special effort is made to show the transverse distribution of deflections, strains and moments at the two midspan sections.

6.2.1 Reactions (Point Loads)

Table 6.1 gives a comparison of theoretical and experimental total reactions due to point loads normalized to 100 kips (445 kN). The theoretical values of the applied loads and reactions shown precisely satisfy overall equilibrium defined by the sum of the vertical forces ($\Sigma V = 0$); the sum of moments about any transverse axis ($\Sigma M = 0$); and the sum of torques about the longitudinal center line of the bridge ($\Sigma T = 0$). Statics checks on experimental values were performed by summing the positive and negative contributions in each of the above equilibrium equations. The maximum percentage differences found for $\Sigma V = 0$ for example was about 6% with most load cases yielding much lower differences than this extreme value.

For vertical end reactions the agreement between theoretical and experimental values in Table 6.1 is generally quite good with differences ranging from 0.3 to 0.9, and 0 to 1.2 kips (1.3 to 4.0, and 0 to 5.3 kN). The experimental vertical reaction at the center footing shows for all cases slightly higher values than the theoretical reaction at R_F, which is one of the reasons for slight differences in the experimental statics check ($\Sigma V = 0$). However, since the agreement is still satisfactory no modification for the overestimated experimental vertical center footing reaction was performed.

For the 45° angle of skewness the end moments equal the end torques at both the west and east end supports. The agreement between theoretical and experimental torques and moments is good, considering the high sensitivity of the experimental values to slight differences in loading and reactions. The magnitude and sign of the end moment determines together with the total vertical end reaction the total mid-span moment and is therefore very important for the design of skew

TABLE 6.1 COMPARISON OF THEORETICAL AND EXPERIMENTAL REACTIONS (KIPS AND FT-KIPS) AT WORKING STRESS LEVEL

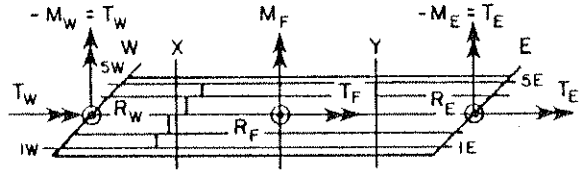

LOAD CASE	SOLUTION	REACTIONS (KIPS AND FT-KIPS)										LOAD (KIPS)		
		WEST END			CENTER FOOTING			EAST END			TOTAL	SEC. X	SEC. Y	TOTAL
		R_W	M_W	T_W	R_F	M_F	T_F	R_E	M_E	T_E	R	P_X	P_Y	P
1X	THEORY	32.5	193	-193	72.9	117	-196	-5.4	125	-125	100.0	100.0	0.0	100.0
	EXPER.	33.6	181	-181	74.0	133	-216	-6.0	125	-125	101.6	100.0	-0.2	99.8
1Y	THEORY	-8.4	72	- 72	55.8	- 63	- 51	52.7	392	-392	100.0	0.0	100.0	100.0
	EXPER.	-8.7	72	- 72	58.0	- 80	- 58	52.8	390	-390	102.2	0.0	100.0	100.0
1X+1Y	THEORY	24.1	264	-264	128.7	54	-247	47.3	517	-517	200.0	100.0	100.0	200.0
	EXPER.	24.5	244	-244	132.3	58	-277	47.2	505	-505	204.0	99.5	100.5	200.0
3X	THEORY	42.5	- 93	93	64.4	91	- 69	-6.9	25	- 25	100.0	100.0	0.0	100.0
	EXPER.	42.4	- 78	78	69.1	107	- 66	-8.1	10	- 10	103.3	100.0	0.0	100.0
3Y	THEORY	-6.9	- 24	24	64.5	- 93	68	42.4	92	- 92	100.0	0.0	100.0	100.0
	EXPER.	-7.3	- 9	9	69.4	-106	79	41.5	75	- 75	103.6	0.1	100.0	100.0
3X+3Y	THEORY	35.6	-118	118	128.9	- 2	- 1	35.5	117	-117	200.0	100.0	100.0	200.0
	EXPER.	36.0	- 90	90	137.6	3	9	35.9	85	- 85	209.5	99.3	100.7	200.0
5X	THEORY	52.6	-390	390	55.9	65	51	-8.5	- 73	73	100.0	100.0	0.0	100.0
	EXPER.	52.0	-373	373	62.3	91	68	-9.1	- 83	83	105.1	100.0	0.0	100.0
5Y	THEORY	-5.5	-125	125	73.0	-117	198	32.5	-192	192	100.0	0.0	100.0	100.0
	EXPER.	-6.2	- 95	95	78.6	-142	230	33.0	-203	203	105.4	0.0	100.0	100.0
5X+5Y	THEORY	47.1	-515	515	128.9	- 52	249	24.0	-265	265	200.0	100.0	100.0	200.0
	EXPER.	47.8	-475	475	140.1	- 49	300	24.0	-277	277	211.9	100.5	99.5	200.0

1 KIP = 4.448 kN
1 FT = 0.305 m

box girder bridges. This point will be emphasized in Section 6.5.1 where a comparison between straight, curved and skew box girder bridge models is presented.

Superposition can also be checked in Table 6.1 by comparing the sum of the results for point loads at section X and Y applied separately with those for the point loads applied simultaneously at sections X and Y. It can be seen that theoretical values satisfy superposition exactly, while experimental values show only very small differences.

Table 6.1 presents only the total end reactions R_W, M_W and T_W or R_E, M_E and T_E. These were obtained by summing the statical contributions to these quantities from each of the experimental or theoretical vertical reactions under the five girder supports at each end of the bridge. These individual girder reactions as well as the total reactions are given in detail in the tables of Vol. IV. The distribution of the total reaction to the five individual girders at each end is highly dependent on the type, installation and stiffness of the support assemblies as pointed out in Section 3.2.1 and cannot be accurately predicted by theory. Because the deep rigid end diaphragm rests on five supports, any slight change at an individual support point can change drastically the magnitude of the reaction at each point. However, it is very important to note, as shown in Table 6.1, that this does not affect the total R, M or T reactions at the end supports. Consequently, these total reactions are distributed by the rigid end diaphragm into the bridge in a similar way and thus the overall response of the bridge is not affected by small changes or displacements at individual girder reaction support points.

6.2.2 Deflections (Point Loads)

Vertical deflections for the nine point load cases are presented in Figs. 6.1 to 6.5. In each case, theoretical curves are given based on 1.0 and 1.5 times the theoretical values obtained from the CELL program, which assumes an uncracked gross concrete section. These curves may be compared with individually plotted experimental points.

The longitudinal variation of the deflection under the loaded girder is given in Figs. 6.1 to 6.3. It can be seen that the theoretical values based on an uncracked section and multiplied by a factor of 1.5 to account for cracking at this stress level, reflect the general deflected shape of the bridge model, as obtained from the experiment, quite satisfactorily. Especially Fig. 6.2 shows excellent agreement for load and deflections along center girder 3. For loads on the exterior girders 1 and 5 the factor of 1.5 used to modify the theoretical data slightly overestimates the extent of cracking on the acute side of the bridge model.

The tranverse distribution of vertical deflections under the loaded section is shown in Figs. 6.4 and 6.5. Except for the cases where the acute side of a span is loaded the agreement between experimental and 1.5 times theoretical values is very good. As noted for the longitudinal distribution of the vertical deflections in Figs. 6.1 to 6.3, the experimental deflections on the acute side of a span are smaller for loads on the acute side than the corresponding factored theoretical deflections; see Fig. 6.4 - Load of 1X and Load of 5Y and Fig. 6.5 - Load at 1X + 1Y and Load at 5X + 5Y.

Figs. 6.1 to 6.5 also show that superposition is valid for both theoretical and experimental values. At the 30 ksi stress level

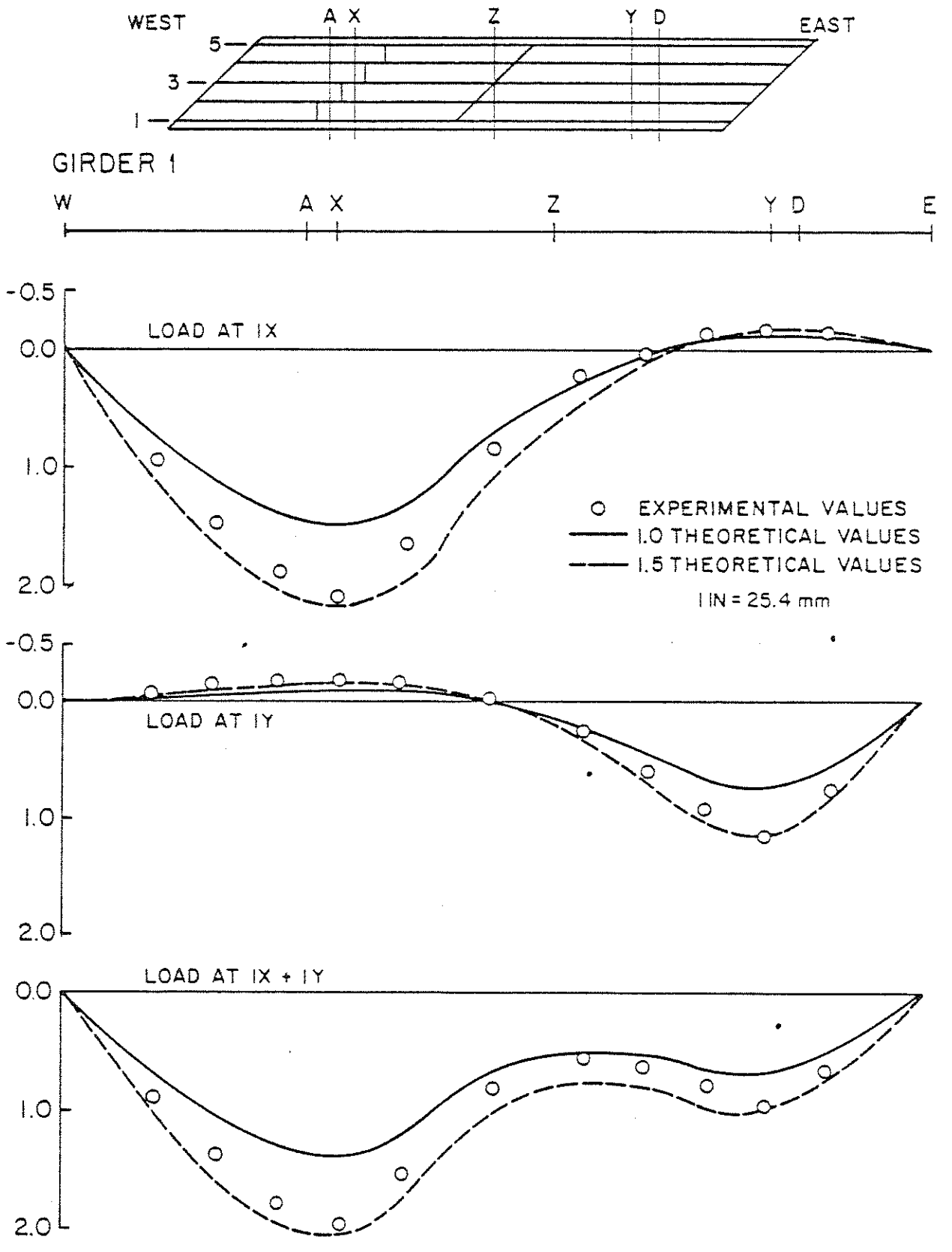

FIG. 6.1 VERTICAL DEFLECTIONS (INCHES) ALONG GIRDER 1 FOR 100 KIP (445 kN) POINT LOADS AT 1X, 1Y, 1X + 1Y

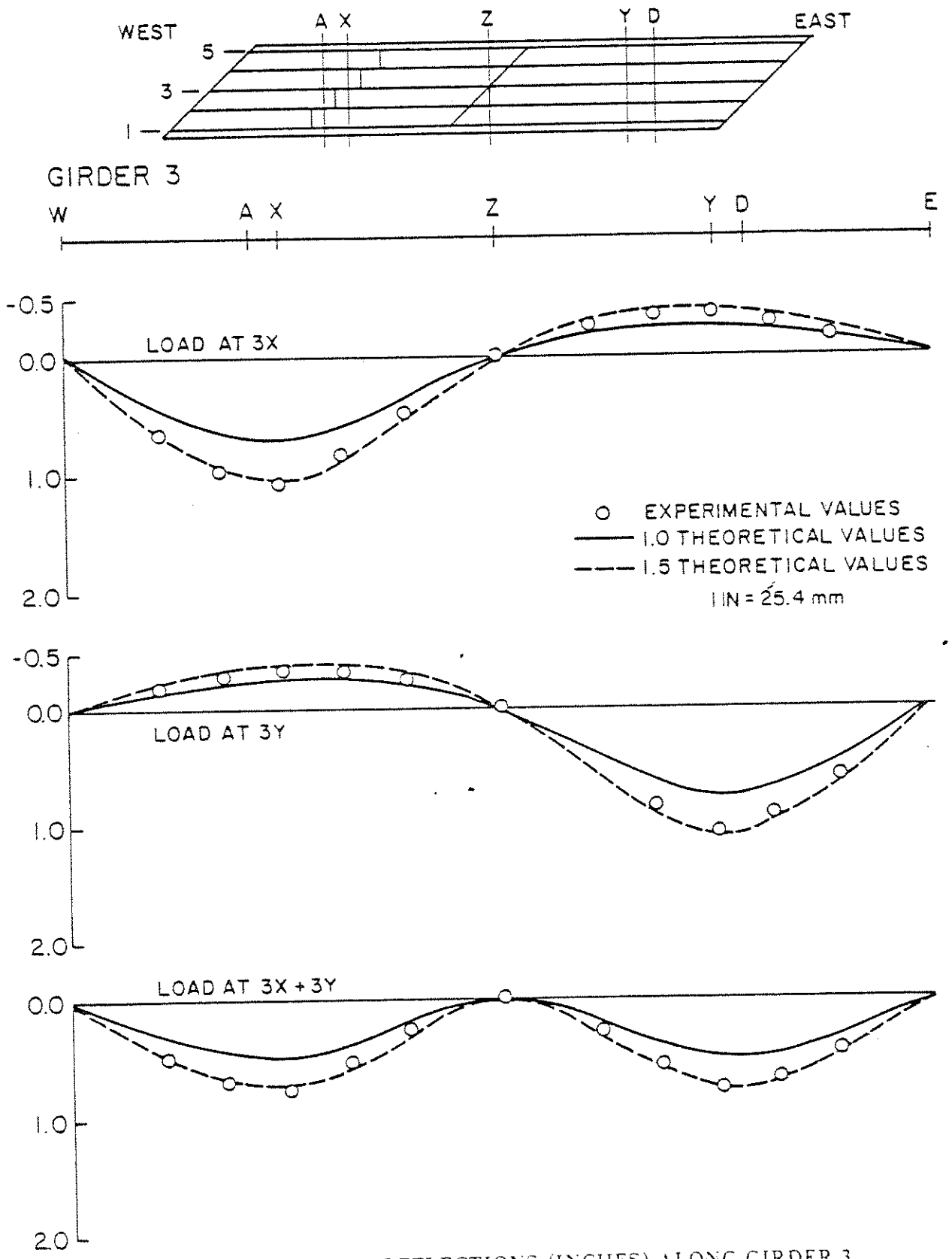

FIG. 6.2 VERTICAL DEFLECTIONS (INCHES) ALONG GIRDER 3 FOR 100 KIP (445 kN) POINT LOADS AT 3X, 3Y, 3X + 3Y

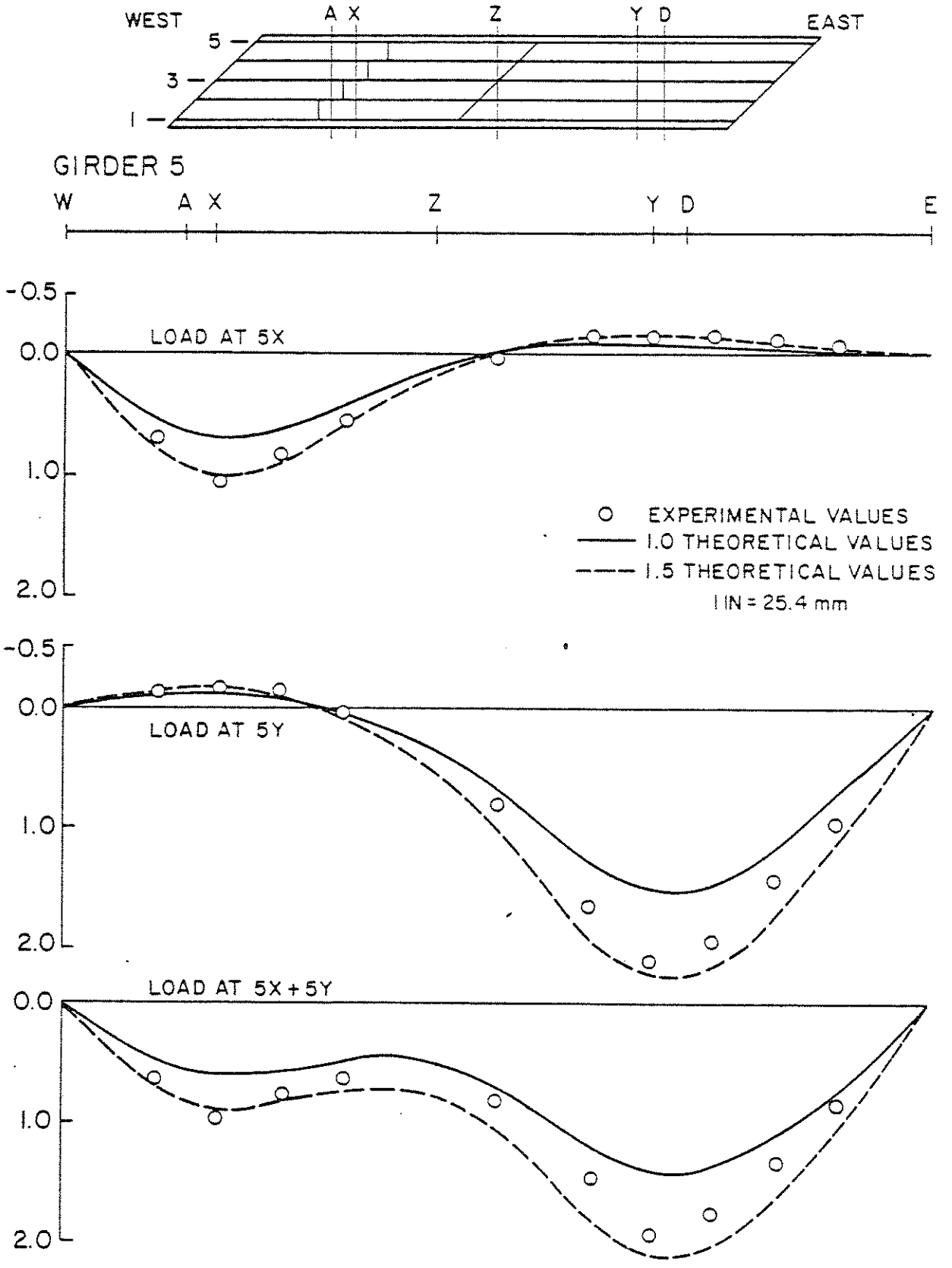

FIG. 6.3 VERTICAL DEFLECTIONS (INCHES) ALONG GIRDER 5 FOR 100 KIP (445 kN) POINT LOADS AT 5X, 5Y, 5X + 5Y

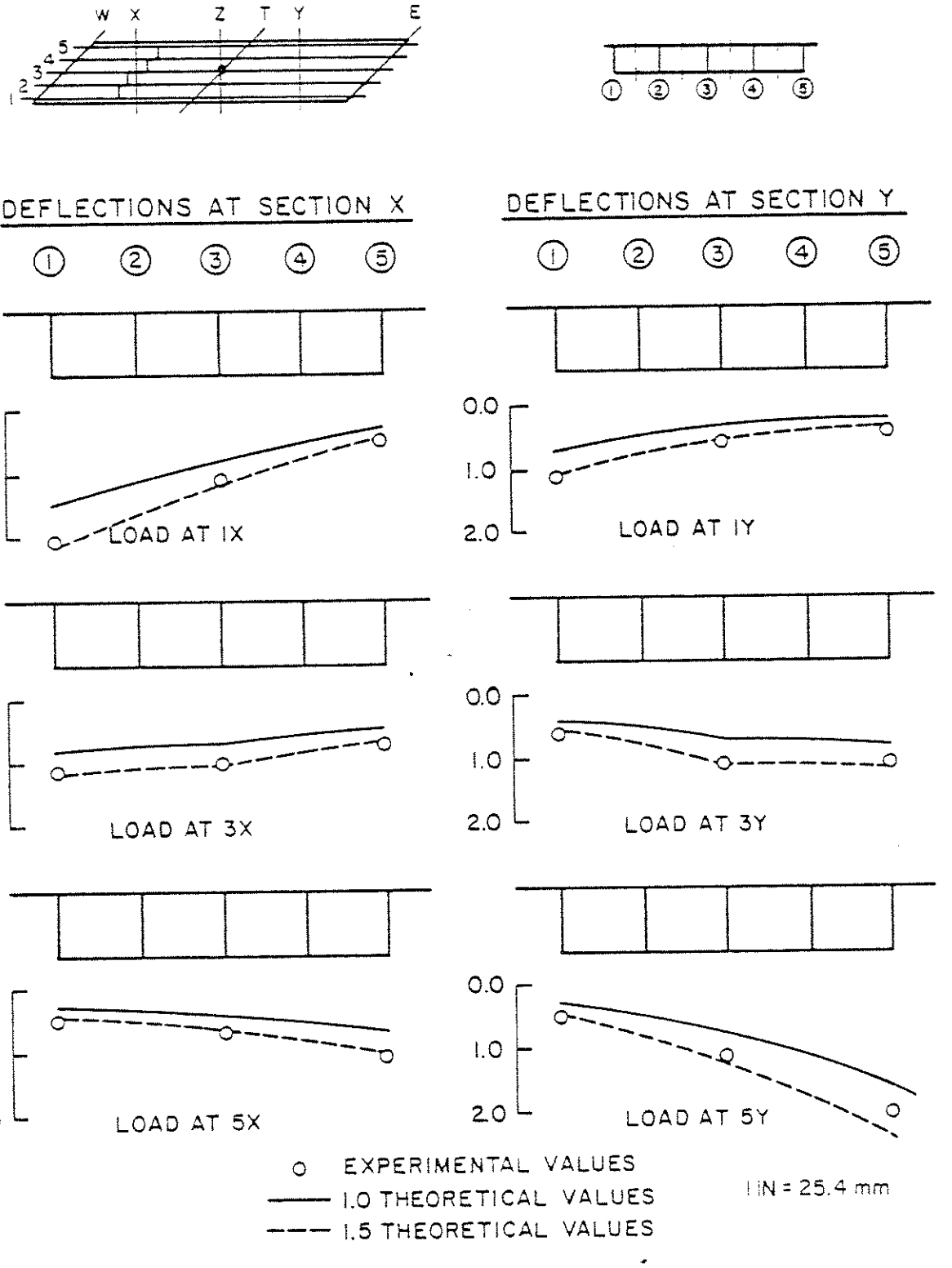

FIG. 6.4 VERTICAL DEFLECTIONS (INCHES) AT TRANSVERSE SECTIONS X AND Y FOR 100 KIP (445 kN) POINT LOADS AT 1X, 3X, 5X, 1Y, 3Y, 5Y

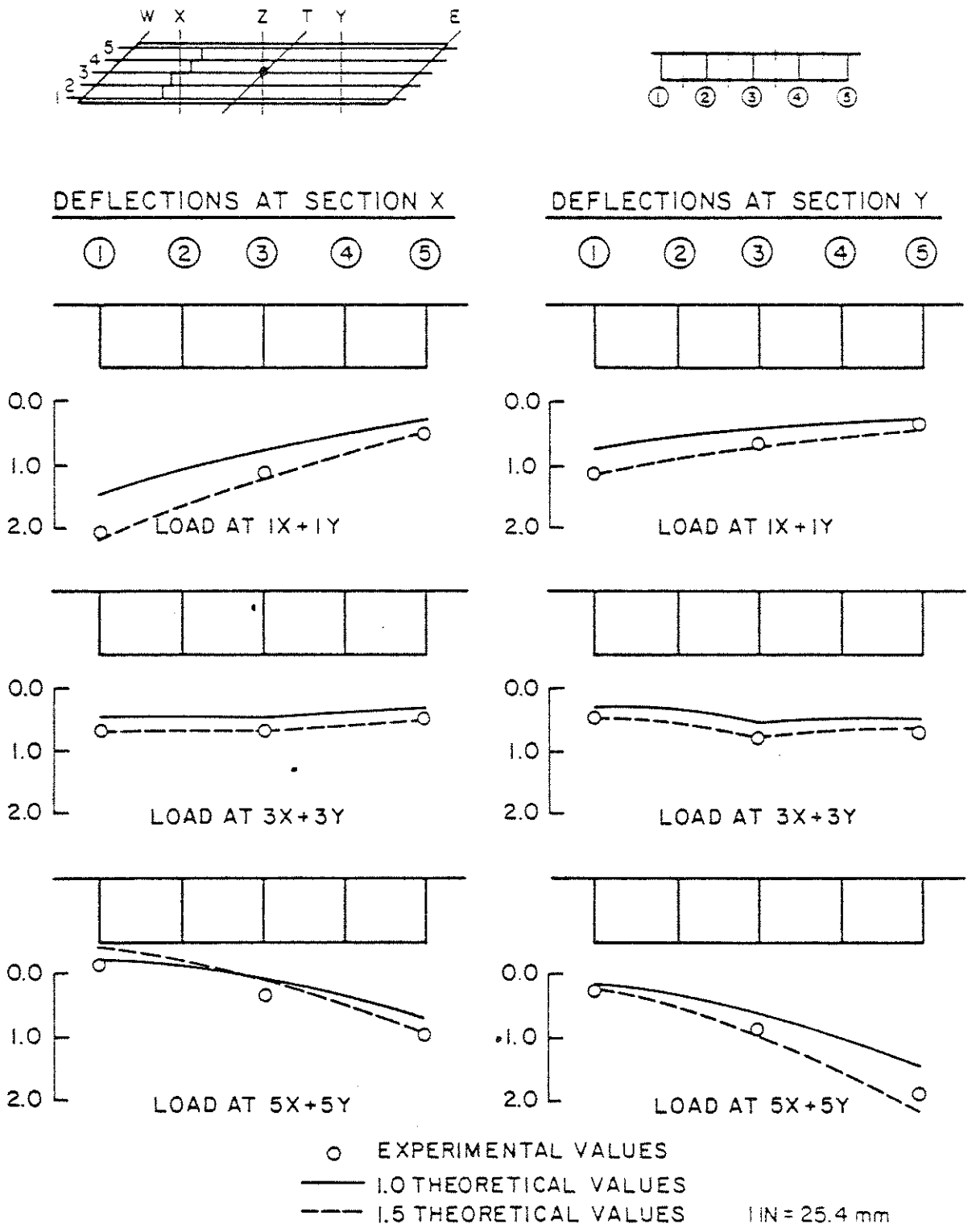

FIG. 6.5 VERTICAL DEFLECTIONS (INCHES) AT TRANSVERSE SECTIONS X AND Y FOR 100 KIP (445 kN) POINT LOADS AT 1X + 1Y, 3X + 3Y, 5X + 5Y

there is virtually no difference in the behavior of the diaphragmed Span I and the undiaphragmed Span II that is noticeable.

6.2.3 Strains (Point Loads)

The longitudinal distribution of experimental strains along girders 1, 3 and 5 is shown in Figs. 6.6 to 6.14 for the nine point load cases 1X, 3X, 5X, 1Y, 3Y, 5Y, 1X + 1Y, 3X + 3Y and 5X + 5Y. The strains plotted are the actually measured unadjusted strain values, with the exception of some unreliable or damaged gages which were replaced by the strain value measured in the neighboring gage.

Figs. 6.6 to 6.8 show the longitudinal strain distribution for point loads shifting transversely across the diaphragmed Span I. For loads on the exterior girders the highest measured strain values are also experienced in the loaded girder, while for a point load on center girder 3 slightly higher strains are measured on the acute side of the span which is due to the additional torque introduced by the skew end abutment. The maximum concrete strains in the loaded Span I occur in girder 1 for a point load at 1X. The maximum steel strains, which were also expected to occur in girder 1 for loads on the acute side of the span are slightly larger in girder 5 for a load at 5X. This shows the influence of the staggered skew midspan diaphragm. Loads on the obtuse side of the span are directly transfered through girder 5 to the obtuse corner of the end abutment, while loads on the acute side of the span are first transversely distributed by the midspan diaphragm.

For loads across the undiaphragmed Span II on section Y the longitudinal strain distributions are given in Figs. 6.9 to 6.11.

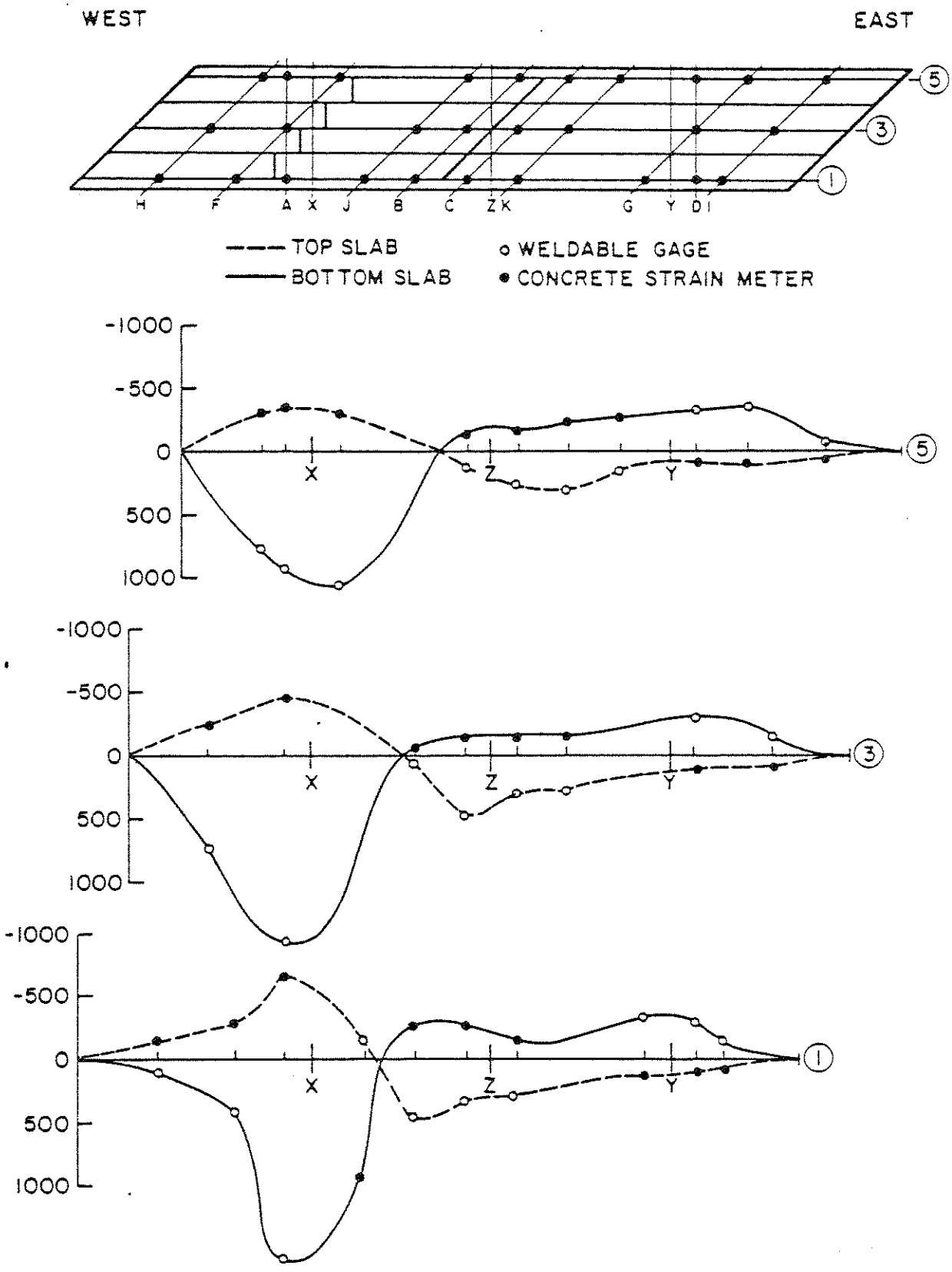

FIG. 6.6 EXPERIMENTAL LONGITUDINAL STRAINS (MICRO INCH/INCH) FOR 100 KIP (445 kN) POINT LOAD AT 1X

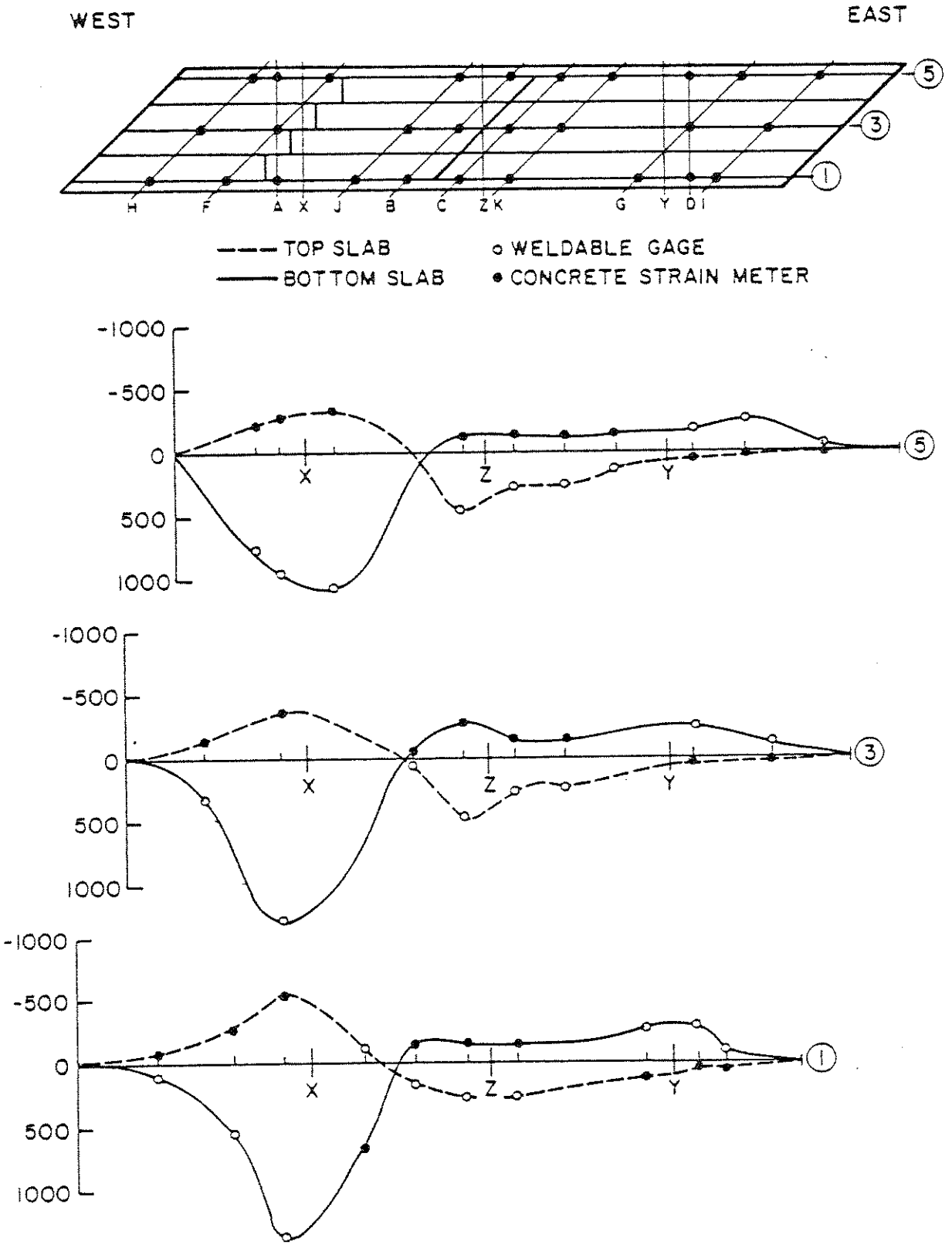

FIG. 6.7 EXPERIMENTAL LONGITUDINAL STRAINS (MICRO INCH/INCH) FOR 100 KIP (445 kN) POINT LOAD AT 3X

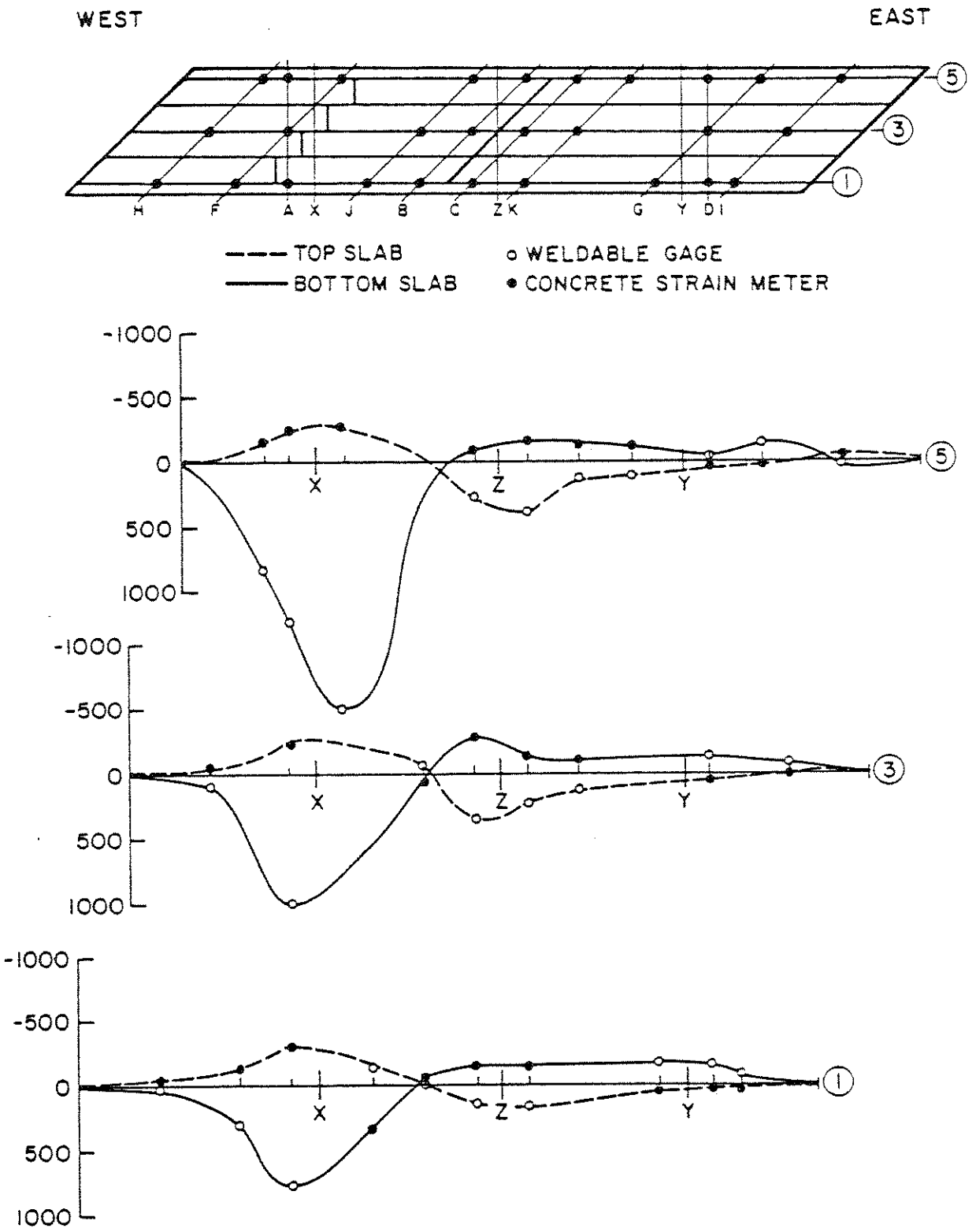

FIG. 6.8 EXPERIMENTAL LONGITUDINAL STRAINS (MICRO INCH/INCH) FOR 100 KIP (445 kN) POINT LOAD AT 5X

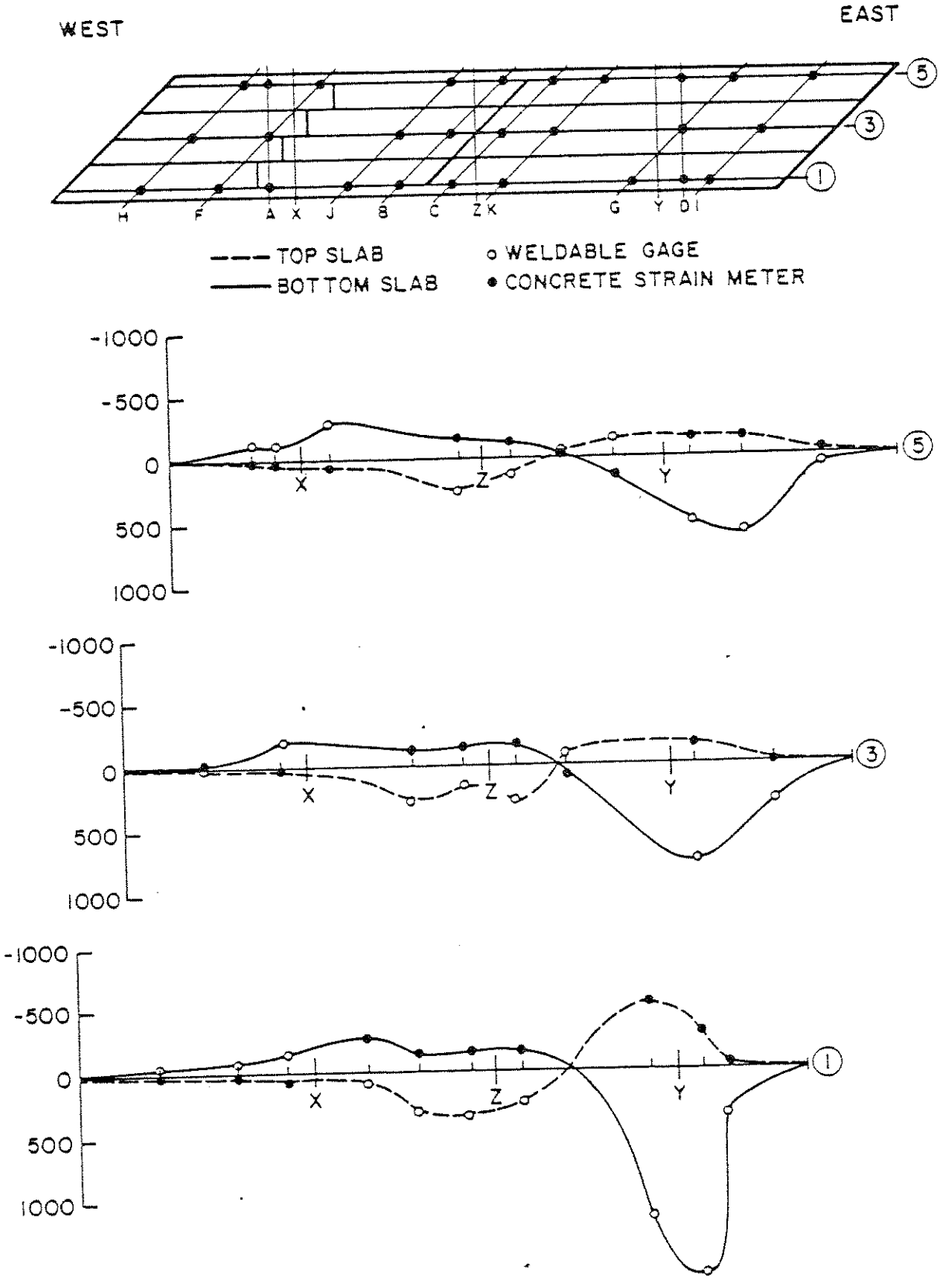

FIG. 6.9 EXPERIMENTAL LONGITUDINAL STRAINS (MICRO INCH/INCH) FOR 100 KIP (445 kN) POINT LOAD AT 1Y

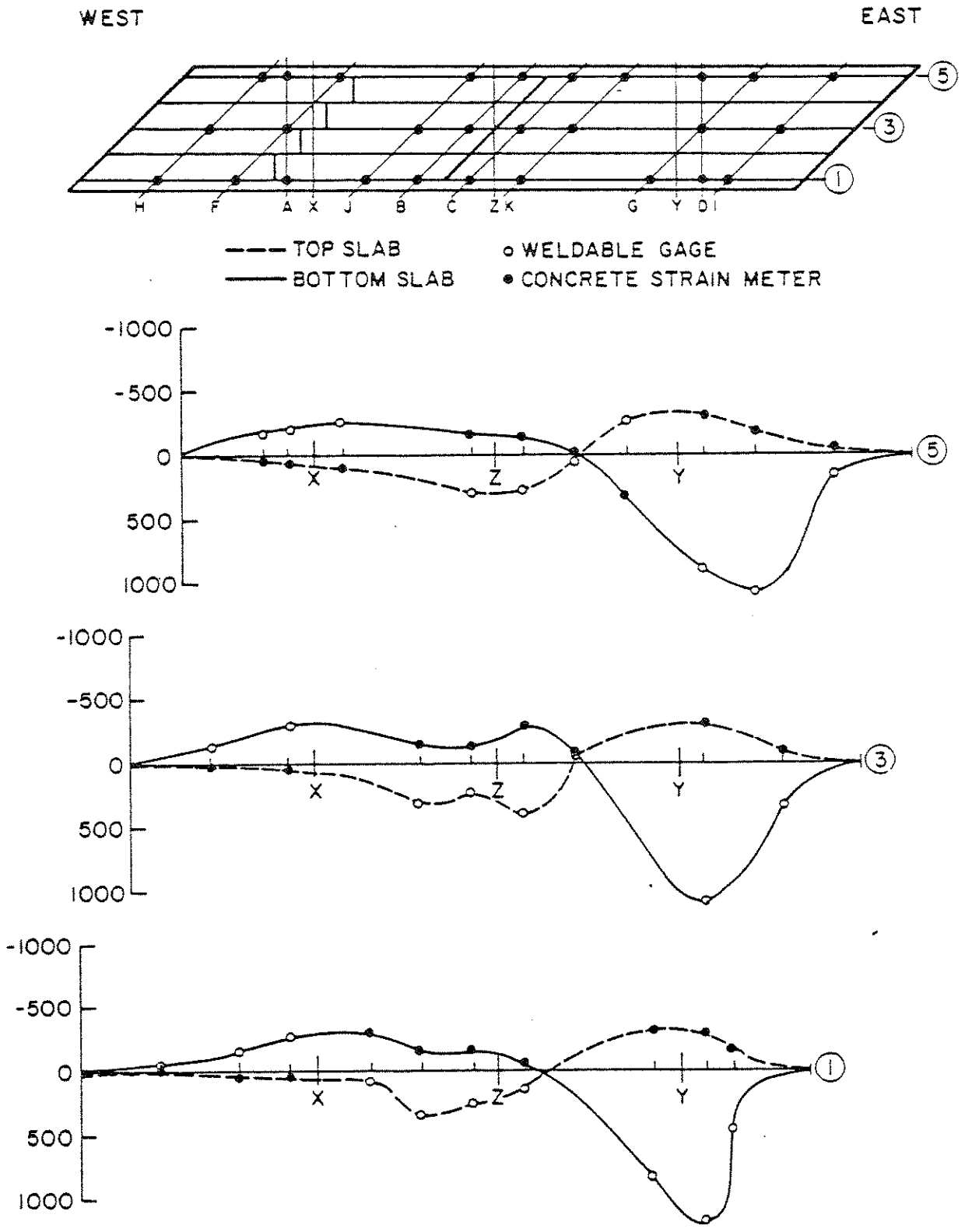

FIG. 6.10 EXPERIMENTAL LONGITUDINAL STRAINS (MICRO INCH/INCH) FOR 100 KIP (445 kN) POINT LOAD AT 3Y

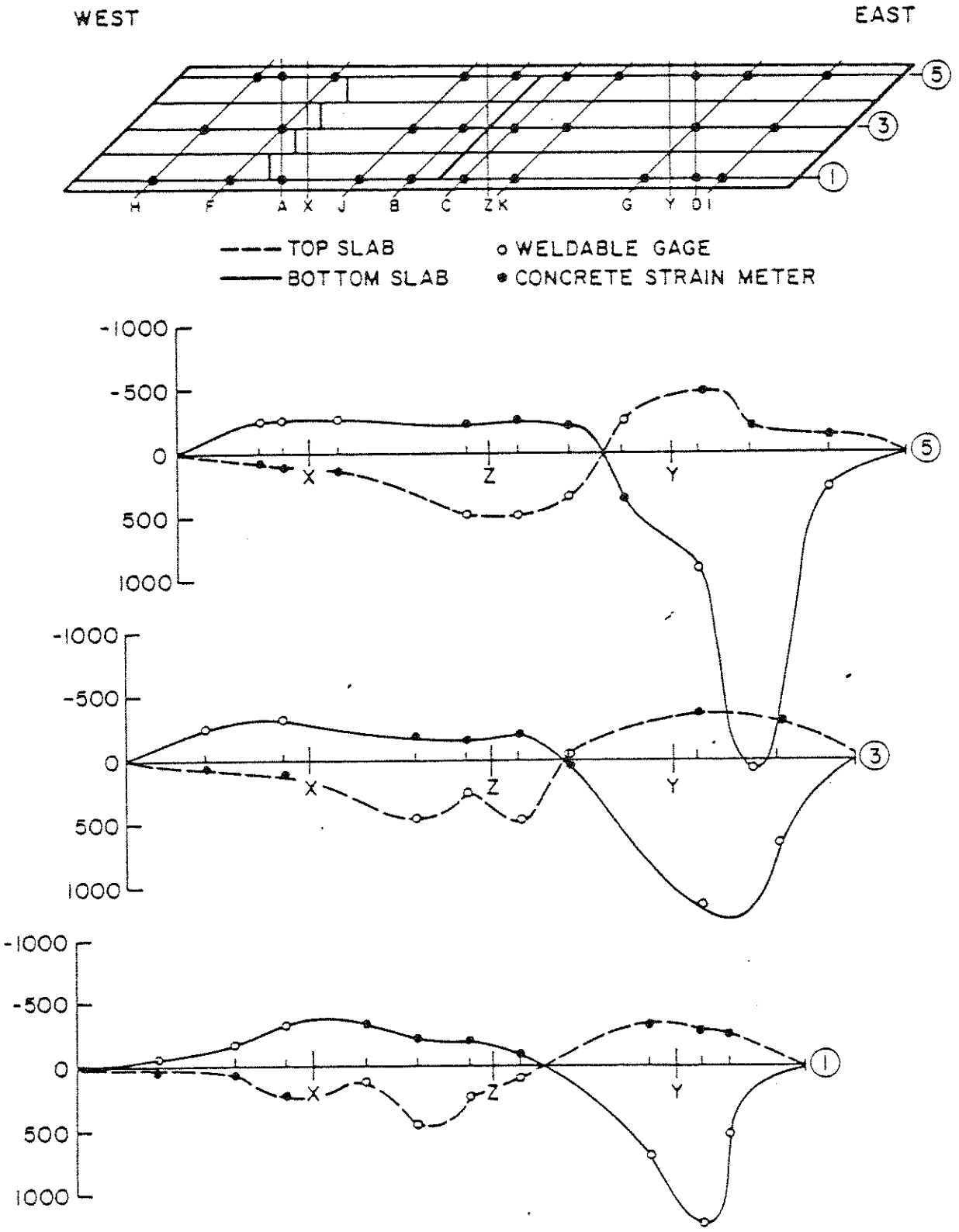

FIG. 6.11 EXPERIMENTAL LONGITUDINAL STRAINS (MICRO INCH/INCH) FOR 100 KIP (445 kN) POINT LOAD AT 5Y

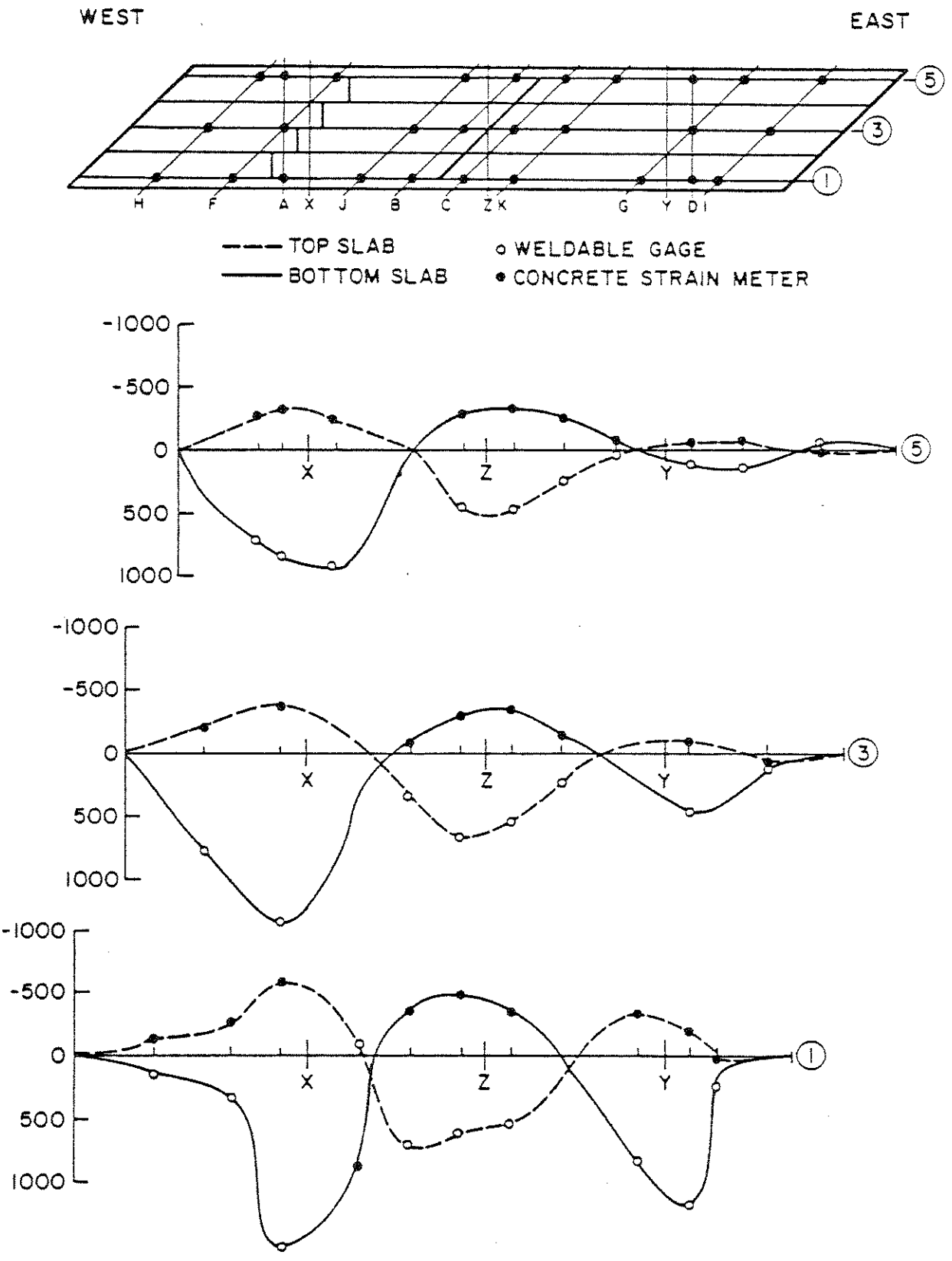

FIG. 6.12 EXPERIMENTAL LONGITUDINAL STRAINS (MICRO INCH/INCH) FOR 100 KIP (445 kN) POINT LOADS AT 1X + 1Y

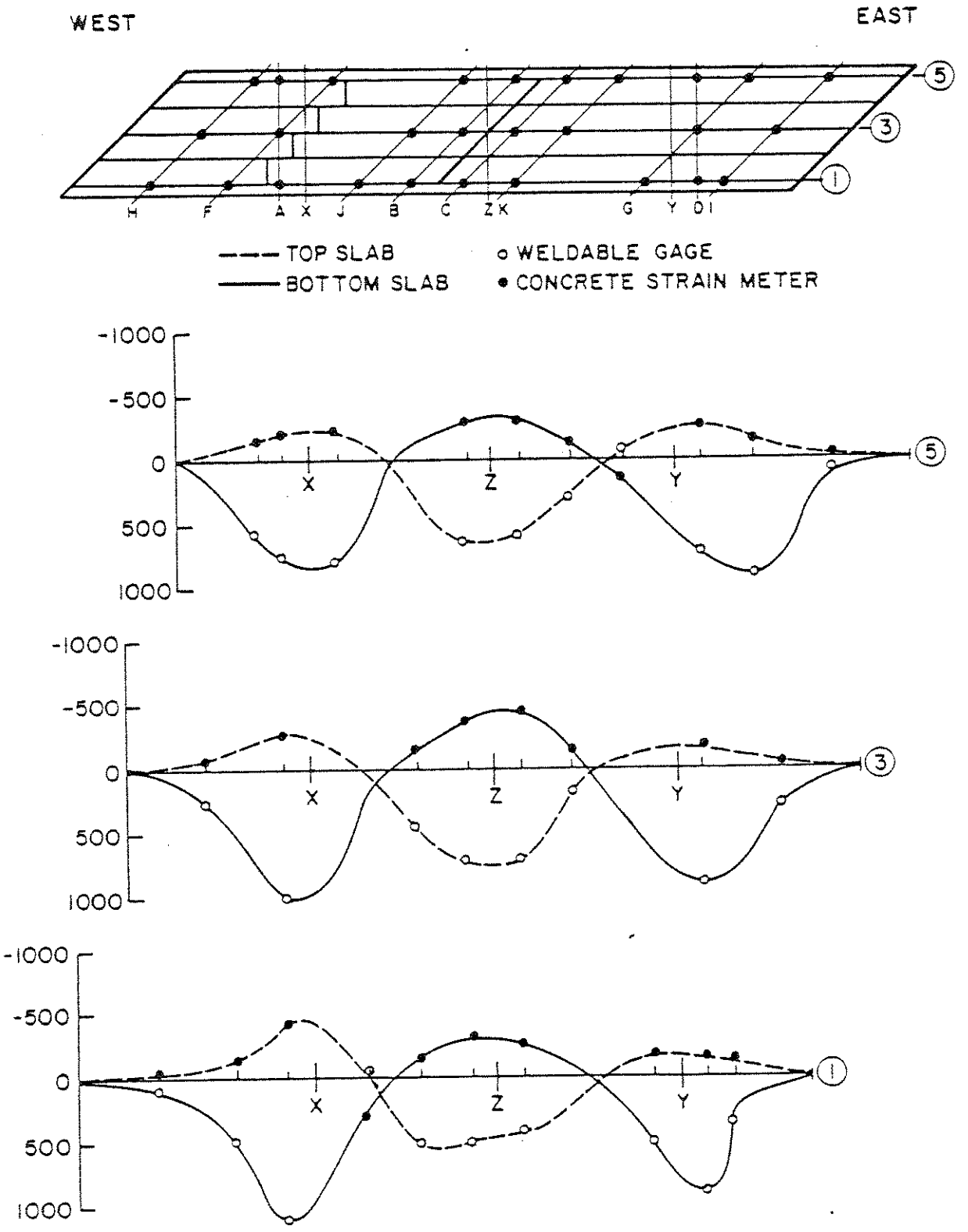

FIG. 6.13 EXPERIMENTAL LONGITUDINAL STRAINS (MICRO INCH/INCH) FOR 100 KIP (445 kN) POINT LOADS AT 3X + 3Y

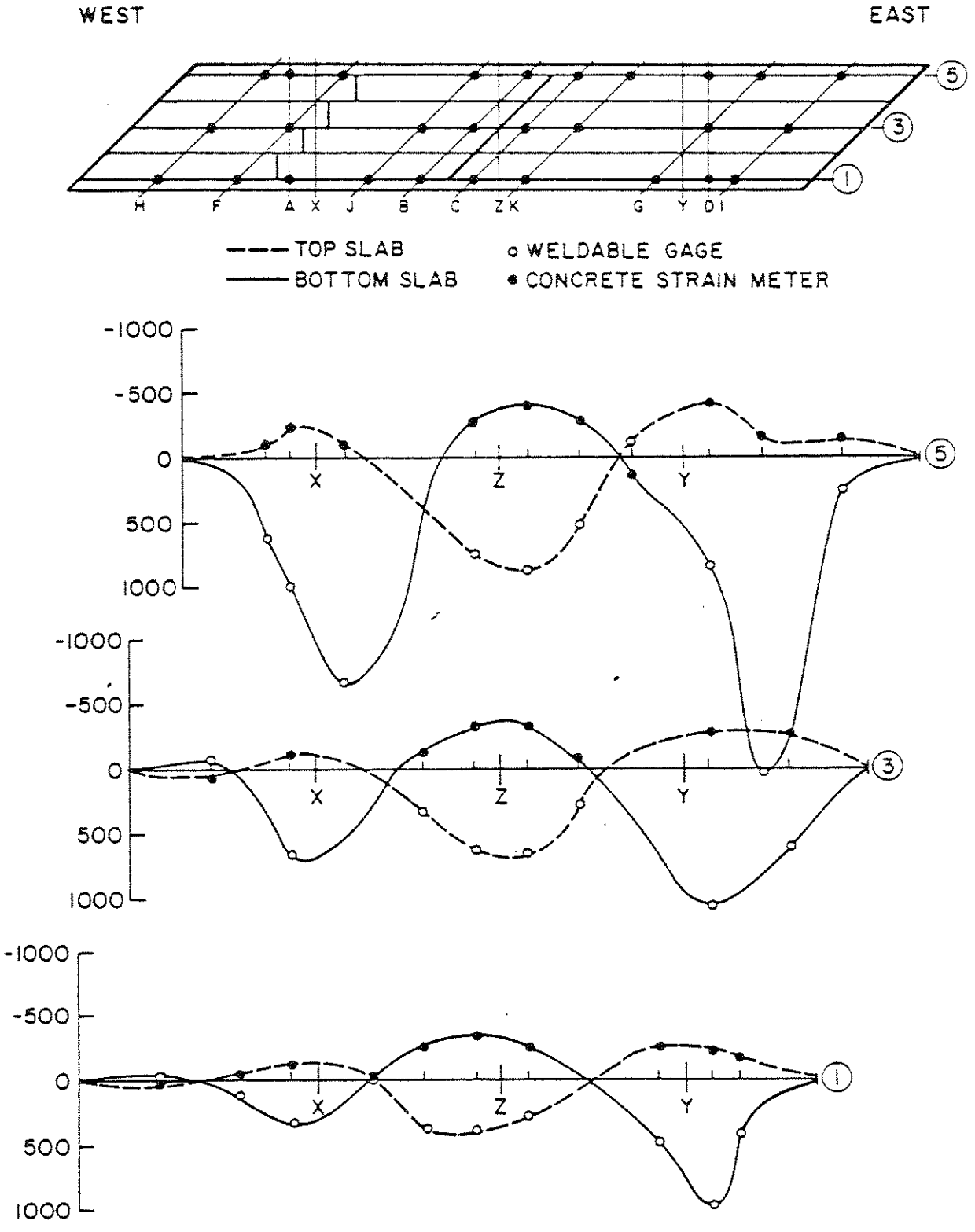

FIG. 6.14 EXPERIMENTAL LONGITUDINAL STRAINS (MICRO INCH/INCH) FOR 100 KIP (445 kN) POINT LOADS AT 5X + 5Y

Here the maximum experimental strains occur as expected on the acute side of the span for load case 5Y. The maximum measured strain value of about 2400 micro inches/inch at 5G for a point load normalized to 100 kips (445 kN) at 5Y corresponds to a steel stress of 13 ksi (89 MPa) in the bottom slab reinforcement for the actual point load of 19.3 kips (86 kN). When this is added to the nominal existing dead load stress of 12 ksi (83 MPa) a total stress of 25 ksi (172 MPa) is obtained, which was the desired stress level for the point load cases.

For point load cases where both spans are loaded simultaneously, the longitudinal strain distributions are given in Figs. 6.12 to 6.14 for loads shifting transversely from girder 1 to 3 to 5. The superposition of experimental strains due to the superposition of various load cases in Figs. 6.6 to 6.14 is generally satisfied indicating that the consistency of the data is good.

While for clarity the theoretical strain values are not plotted in Figs. 6.6 to 6.14, a careful study of these values in Vol. IV, which were calculated as described in Section 3.7, indicates general overall agreement between theoretical and experimental strains even though some differences do exist for certain points in some load cases. For the same 9 point load cases the transverse distribution of experimental strains in top and bottom slabs at sections A and S is given in Figs. 6.15 to 6.18. The bottom slab of section A as well as the top and bottom slabs at section D were instrumented at the girder points, half-bay points and quarter-bay points, while the top slab of section A was only instrumented at the girder and half-bay points.

Figs. 6.15 and 6.16 show the measured steel strains across the width of the bridge for sections in the loaded span. For all load

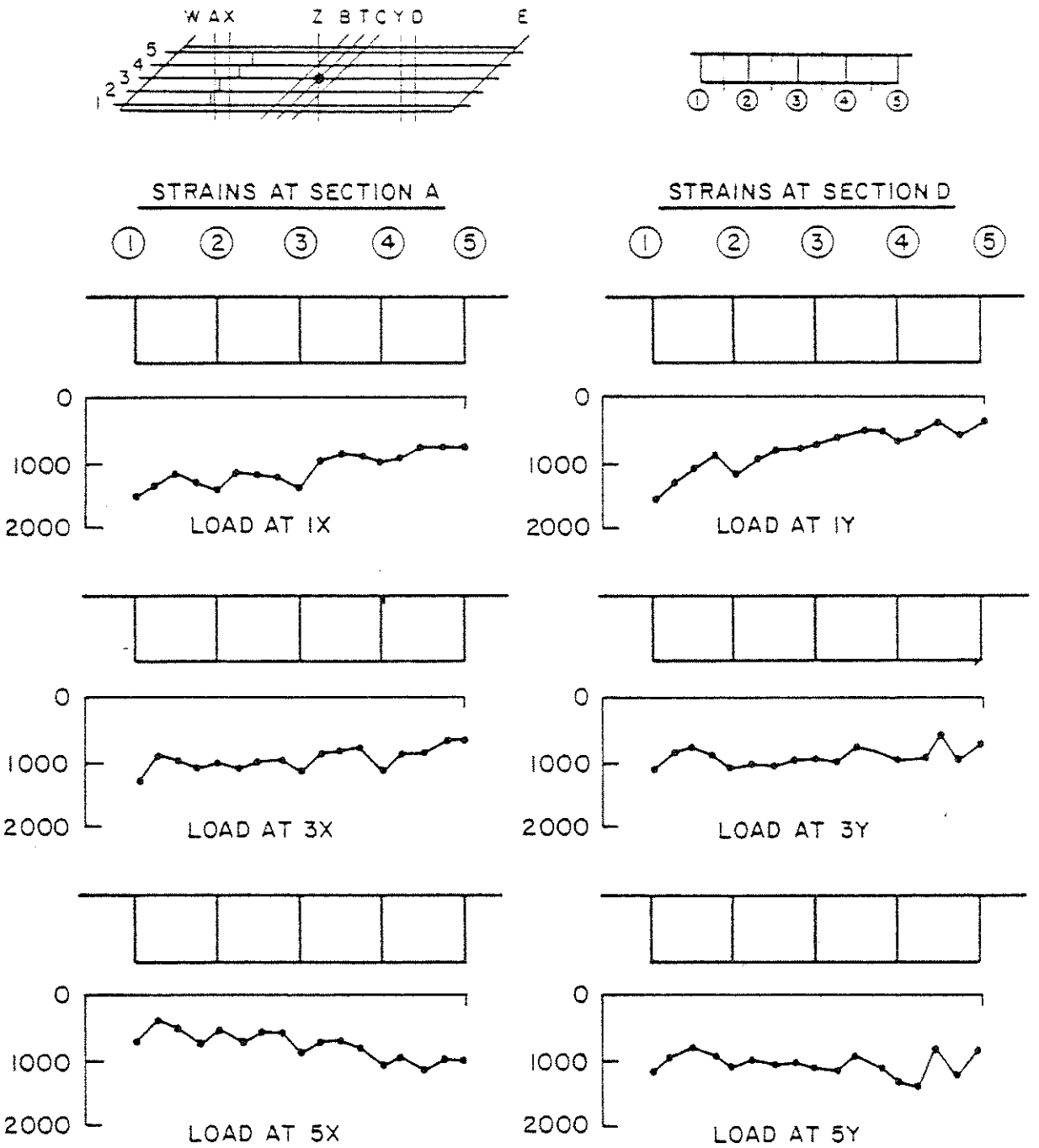

FIG. 6.15 EXPERIMENTAL STEEL STRAINS (MICRO INCH/INCH) AT TRANSVERSE SECTIONS A AND D FOR 100 KIP (445 kN) POINT LOADS AT 1X, 3X, 5X, 1Y, 3Y, 5Y

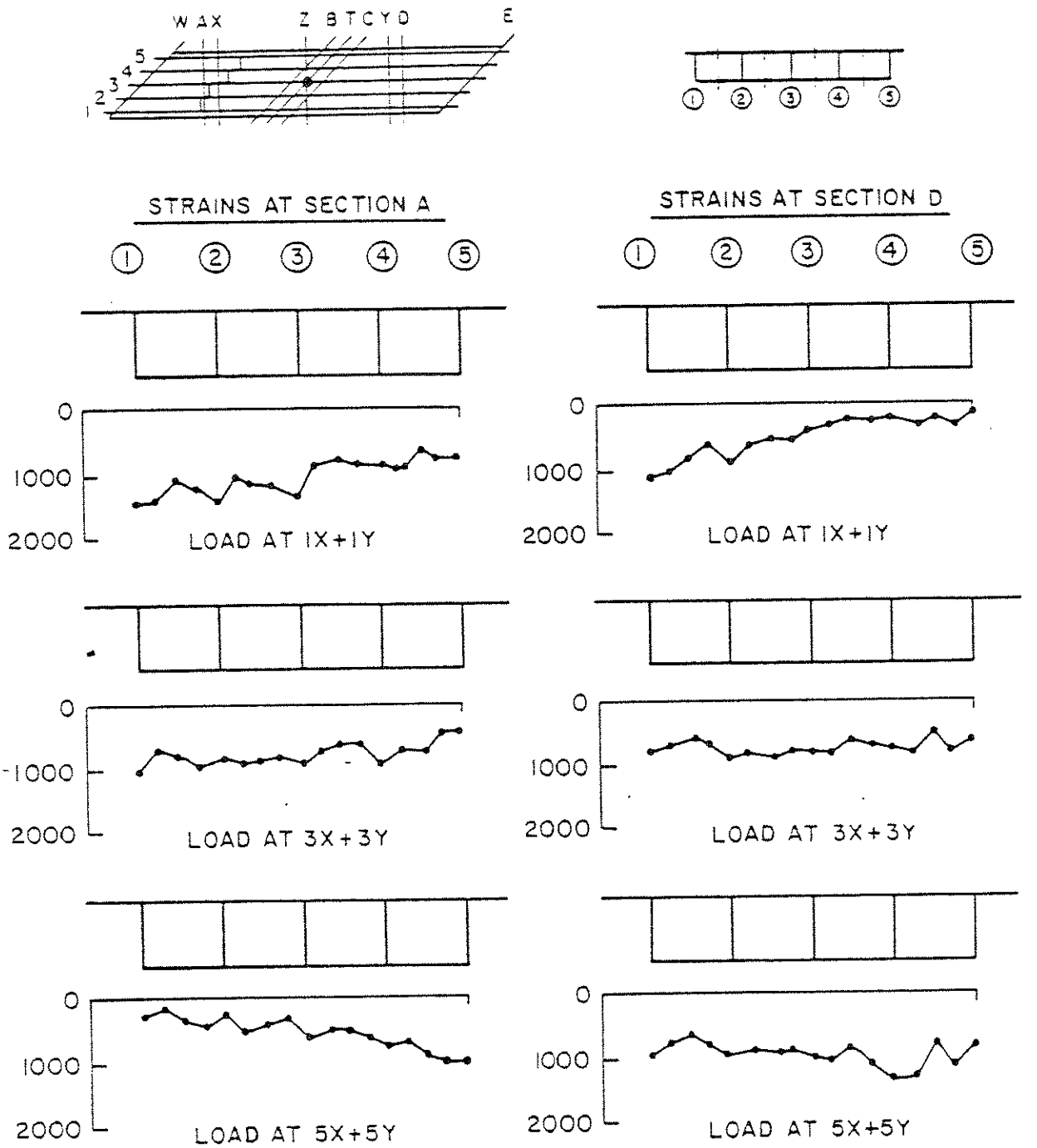

FIG. 6.16 EXPERIMENTAL STEEL STRAINS (MICRO INCH/INCH) AT TRANSVERSE SECTIONS A AND D FOR 100 KIP (445 kN) POINT LOADS AT 1X + 1Y, 3X + 3Y, 5X + 5Y

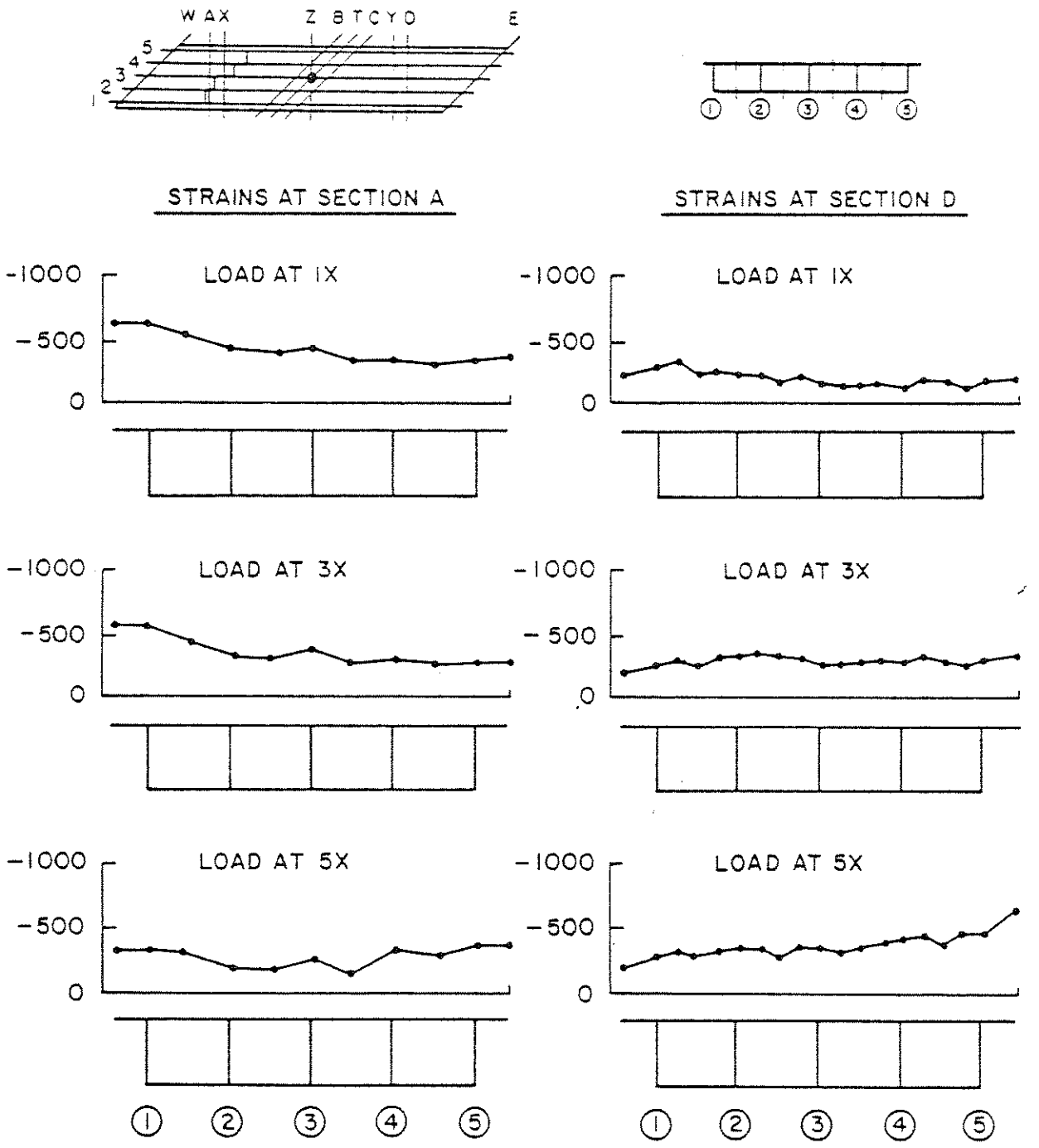

FIG. 6.17 EXPERIMENTAL CONCRETE STRAINS (MICRO INCH/INCH) AT TRANSVERSE SECTIONS A AND D FOR 100 KIP (445 kN) POINT LOADS AT 1X, 3X, 5X, 1Y, 3Y, 5Y

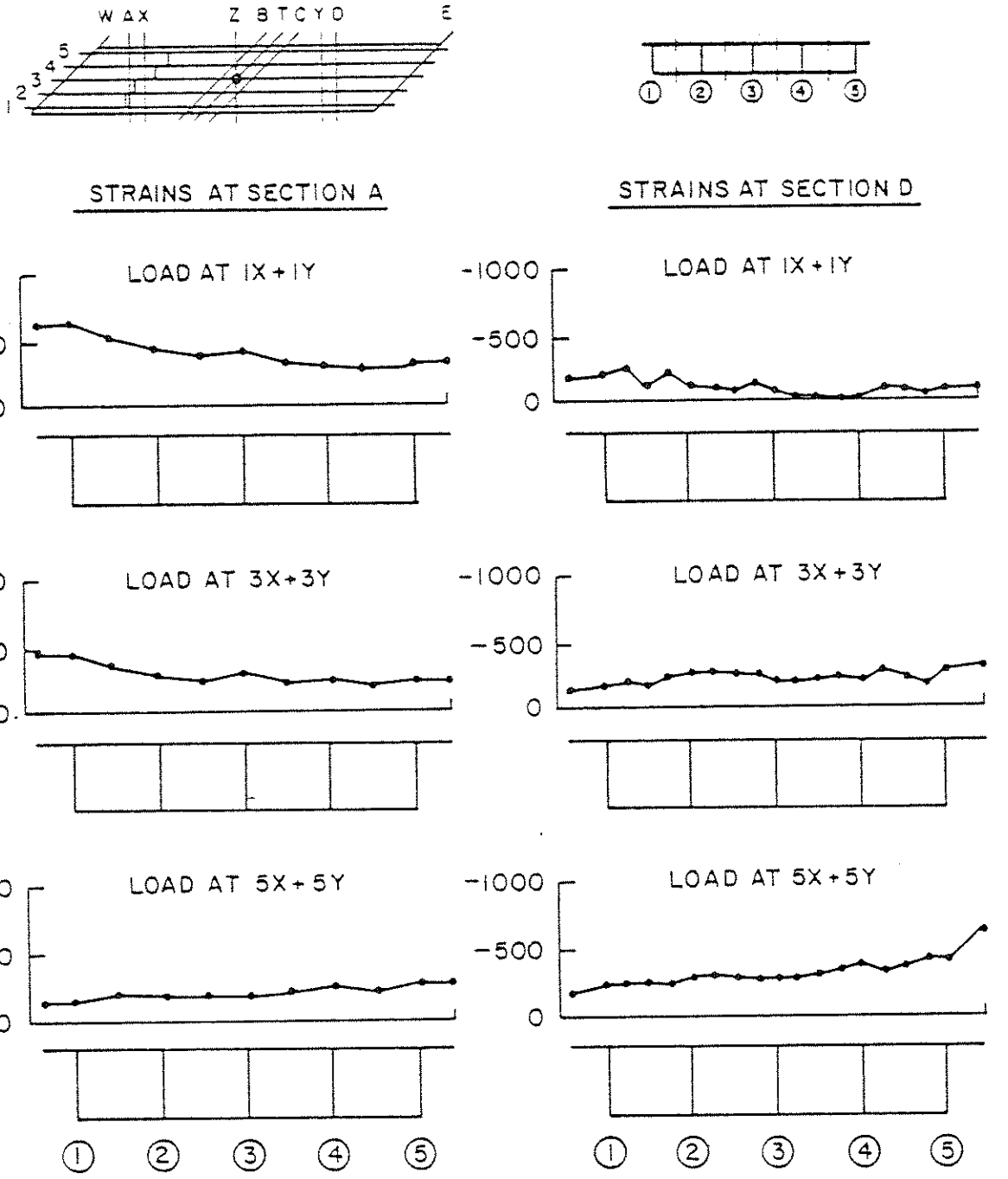

FIG. 6.18 EXPERIMENTAL CONCRETE STRAINS (MICRO INCH/INCH) AT TRANSVERSE SECTIONS A AND D FOR 100 KIP (445 kN) POINT LOADS AT 1X + 1Y, 3X + 3Y, 5X + 5Y

cases involving only loads on center girder 3 the steel strain distribution is fairly uniform with slight strain concentrations at the girder lines, which shows the small shear-lag effect in the multicell box girder. Skew symmetry checks and the influence of the midspan diaphragm in Span I can be observed by comparing the results at section A with section D for load cases 1X with 5Y, 5X with 1Y, 1X + 1Y with 5X + 5Y, and 5X + 5Y with 1X + 1Y. The concrete strains in the top slab at midspan sections A and D are presented in Figs. 6.17 and 6.18. While the general behavior of the concrete strains is very similar to the steel strains described above, it should be noted that girder 1 at section A generally features higher strains than would be expected from the skew symmetric values at section D. This can be seen most clearly by comparing results at section A with section D for load cases 3X with 3Y and 3X + 3Y with 3X + 3Y. These high concrete strains at point 1A may be accounted for by the proximity of the staggered midspan diaphragm to the instrumented section A at the acute side of the span. Note that, on the contrary, at point 5A the staggered midspan diaphragm is a considerable distance from the instrumented section A.

6.2.4 Moments (Point Loads)

For the bending moments in the skew box girder bridge model two questions arise besides the important effect of skewness on the longitudinal distribution of the total moment (see detailed discussion in Chapter 2):

1. How accurately can the total moment at a section be predicted by theoretical external or internal moments?

2. What is the transverse distribution of the total moment at a section to the individual girders?

A comparison between theoretical and experimental moments is given in Tables 6.2 to 6.5.

6.2.4.1 Total Moment at a Section

The total theoretical and experimental moments at the instrumented right sections A and D, near the midspans I and II, are given in Table 6.2 for all 19 point load cases. Both external moments based on external reactions and internal moments based on an integration of internal forces are given. The results are arranged so that results for skew symmetric loadings, for example 1X vs. 5Y, 2X vs. 4Y, etc., can be compared directly.

For theoretical moments, skew symmetry is almost perfectly satisfied, indicating that the staggered midspan diaphragm, only in Span I, has virtually no effect on total theoretical moments. In addition, theoretical external and internal moments are essentially identical as should be expected from the theoretical solution.

For experimental moments, skew symmetry is satisfied within 5% for more than half of the loadings, however, the discrepancy is between 10 to 13% for about one-fifth of the loadings. The latter larger discrepancies are generally for smaller moments in unloaded spans. Comparing experimental external and internal moments, which should be equal for a given loading, differences range from 1 to 10% for most cases, however, for about one-fifth of the loadings the discrepancies range from 10 to 16%. No definite pattern could be discerned regarding these experimental differences.

TABLE 6.2 SUMMARY OF THEORETICAL AND EXPERIMENTAL TOTAL MOMENTS (FT-KIPS) AT SECTIONS A AND D FOR ALL POINT LOAD (100 KIPS) POSITIONS.

SECTION A					SECTION D				
100 K LOAD AT	BASED ON EXTERNAL REACTIONS		BASED ON INTERNAL FORCES		100 K LOAD AT	BASED ON EXTERNAL REACTIONS		BASED ON INTERNAL FORCES	
	THEORY	EXPT.	THEORY	EXPT.		THEORY	EXPT.	THEORY	EXPT.
1X	694	699	693	657	5Y	693	712	692	663
2X	629	652	627	596	4Y	623	639	627	618
3X	562	573	561	556	3Y	562	565	561	543
4X	492	516	491	492	2Y	494	499	492	496
5X	420	429	420	407	1Y	421	425	420	441
1Y	- 59	- 62	- 58	- 70	5X	- 58	- 58	- 58	- 62
2Y	- 94	- 91	- 94	- 96	4X	- 94	- 99	- 94	- 88
3Y	-131	-122	-131	-125	3X	-131	-135	-131	-123
4Y	-163	-165	-169	-148	2X	-169	-170	-169	-147
5Y	-209	-190	-209	-183	1X	-209	-217	-209	-183
1X+1Y	635	622	634	597	5X+5Y	634	647	635	576
2X+2Y	535	544	533	515	4X+4Y	534	558	533	531
3X+3Y	431	465	430	433	3X+3Y	431	469	430	437
4X+4Y	323	367	322	348	2X+2Y	324	321	323	336
5X+5Y	211	262	211	273	1X+1Y	212	224	212	268
1X+5Y	484	494	484	476	1X+5Y	484	509	483	477
2X+4Y	460	495	459	458	2X+4Y	460	495	458	473
5X+1Y	362	384	362	336	5X+1Y	363	359	362	375
4X+2Y	398	418	397	391	4X+2Y	399	401	398	406

1 FT-KIP = 1.356 kN-m

TABLE 6.3 SUMMARY OF THEORETICAL AND EXPERIMENTAL TOTAL EXTERNAL MOMENTS (FT-KIPS) AT MIDSPAN SECTIONS X AND Y FOR ALL POINT LOAD (100 KIPS) POSITIONS.

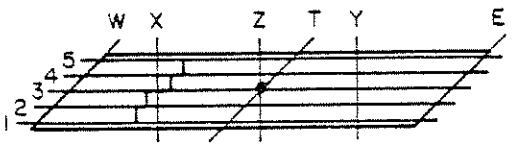

SECTION X			SECTION Y		
100 K LOAD AT	BASED ON EXTERNAL REACTIONS		100 K LOAD AT	BASED ON EXTERNAL REACTIONS	
	THEORY	EXPT.		THEORY	EXPT.
1X	778	786	5Y	776	797
2X	725	751	4Y	725	733
3X	671	681	3Y	671	672
4X	615	639	2Y	615	621
5X	556	563	1Y	556	561
1Y	- 80	- 85	5X	- 80	- 81
2Y	-114	-111	4X	-114	-122
3Y	-149	-141	3X	-149	-156
4Y	-185	-184	2X	-185	-187
5Y	-224	-206	1X	-223	-232
1X+1Y	697	685	5X+5Y	696	709
2X+2Y	612	621	4X+4Y	611	633
3X+3Y	523	558	3X+3Y	522	561
4X+4Y	430	474	2X+2Y	430	422
5X+5Y	332	386	1X+1Y	334	346
1X+5Y	554	562	1X+5Y	554	577
2X+4Y	584	577	2X+4Y	585	575
5X+1Y	476	498	5X+1Y	476	468
4X+2Y	501	518	4X+2Y	502	499

KIP = 1.356 kN-m

Comparing theoretical and experimental total moments at the instrumented sections A and D, as given in Table 6.2, quite good agreement within 5% is obtained for external moments based on external reactions for most of the load cases. Only 2 out of 38 comparisons show a difference greater than 10%. The differences between theoretical and experimental internal moments are somewhat larger, but still in general may be considered acceptable.

A careful study of Table 6.2 reveals the important influence on the total moment at a section near midspan of the transverse position of the normalized 100 kip (445 kN) point load. For point loads in one span only (i.e. at X or Y), the total moment decreases substantially as the transverse position of the point load moves from the acute side to the obtuse side of the span. This fact is even more pronounced for loads in both spans (i.e. at X + Y) on the same girder.

Since the maximum positive total moment for each of the 19 point load cases always occurs at the midspan loaded sections X or Y rather than at the internally strain instrumented sections A or D, the theoretical and experimental total external moments at section X and Y as calculated from external reactions are also presented in Table 6.3. Again here, the agreement between theoretical and experimental moments is quite good except for a couple of load cases.

6.2.4.2 Transverse Distribution of Total Moments

Theoretical and experimental percentages of the total moments at sections A and D carried by each girder are given in Tables 6.4 and 6.5 respectively for all 19 point load combinations. These tables are essentially influence tables, which at a glance enable one to determine the load distributing properties of the bridge. As shown in

Tables 6.2 and 6.3, maximum total moments are produced at section A for loads in Span I at section X only and at section D for loads in Span II at section Y only. For these critical loadings, Figs. 6.19 and 6.20 depict the data given in the tables in graphical form. It should be kept in mind that for a uniform stress distribution across the entire section, the percentage distributions to girders 1 to 5 respectively would be 16.5, 22.4, 22.4, 22.4 and 16..5%.

While a great deal of data is presented in Tables 6.4 and 6.5, a careful study of them reveals several important points.

The agreement between theoretical and experimental results is much better at the undiaphragmed section D than it is at the diaphragmed section A. At section A, the experimental results in Table 6.4 indicate a much greater tendency for girder 1 to take a larger percentage of the total moment than that obtained from theory. This tendency was observed not only for the 19 point load cases, but for almost all other loadings as well. It appears that a possible cause for this difference is the close proximity of the staggered midspan diaphragm to the instumented section A at the acute side of the span, which could influence the measured experimental strains in the vicinity of location 1A (see key in Fig. 6.19) in an unpredictable manner. Also the mesh size used in the theoretical finite element analysis, using the CELL program, may have been too coarse (only one element between section A and the staggered midspan diaphragm, see Fig. 3.1) to pick up the complex behavior at girders 1 and 2 on the acute side of the diaphragmed span. This emphasizes the need to carefully interpret theoretical results obtained from finite element analyses, especially in zones of steep stress gradients such as might be the case near location 1A.

TABLE 6.4 SUMMARY OF THEORETICAL AND EXPERIMENTAL PERCENTAGE DISTRIBUTION OF TOTAL MOMENT AT SECTION A FOR ALL POINT LOAD POSITIONS

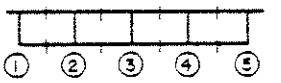

LOAD AT	THEORETICAL % TO GIRDERS					EXPERIMENTAL % TO GIRDERS				
	1	2	3	4	5	1	2	3	4	5
1X	18	25	23	20	14	26	24	22	18	11
2X	18	22	25	21	14	25	21	23	19	12
3X	18	25	23	21	14	25	22	21	20	12
4X	15	21	21	26	18	21	19	20	27	14
5X	11	17	18	27	27	20	17	19	25	20
1Y	16	21	22	23	18	27	19	19	21	14
2Y	16	22	23	23	17	27	20	20	20	13
3Y	16	22	23	23	17	27	20	20	19	13
4Y	16	22	23	23	17	26	21	20	19	14
5Y	16	22	22	23	17	26	21	20	19	13
1X+1Y	18	26	24	19	13	26	24	22	17	11
2X+2Y	19	22	25	20	13	26	21	23	19	11
3X+3Y	19	26	23	21	13	26	22	21	20	11
4X+4Y	14	20	20	28	18	22	18	20	23	16
5X+5Y	7	11	13	31	38	13	18	22	28	19
1X+5Y	19	27	24	18	12	26	25	22	17	10
2X+4Y	19	22	26	20	12	26	21	23	19	11
5X+1Y	11	16	17	27	29	18	16	19	27	20
4X+2Y	15	20	21	27	18	21	19	21	24	16

TABLE 6.5 SUMMARY OF THEORETICAL AND EXPERIMENTAL PERCENTAGE DISTRIBUTION OF TOTAL MOMENT AT SECTION D FOR ALL POINT LOAD POSITIONS.

LOAD AT	THEORETICAL % TO GIRDERS					EXPERIMENTAL % TO GIRDERS				
	1	2	3	4	5	1	2	3	4	5
1X	17	23	22	22	16	19	24	21	20	16
2X	17	23	22	22	16	18	25	21	18	18
3X	17	23	22	22	16	18	24	21	19	18
4X	17	23	22	22	16	18	23	21	17	22
5X	18	23	22	21	16	18	22	21	17	22
1Y	27	28	20	15	10	27	27	18	15	12
2Y	20	27	23	18	12	23	25	21	17	14
3Y	15	23	25	23	15	17	24	21	20	17
4Y	13	19	23	26	19	15	20	21	22	22
5Y	12	18	21	26	23	15	20	20	23	23
1X+1Y	38	34	17	8	3	34	30	15	9	11
2Y+2Y	22	29	23	16	10	24	26	22	16	17
3X+3Y	14	23	26	23	15	17	25	22	20	17
4X+4Y	12	18	23	27	20	14	20	21	23	22
5X+5Y	12	17	21	27	24	14	20	20	24	22
1X+5Y	10	16	20	28	26	13	18	19	25	25
2X+4Y	11	18	23	28	21	14	19	21	23	23
5X+1Y	29	29	19	14	9	29	29	18	14	10
4X+2Y	21	28	23	17	11	24	26	21	16	12

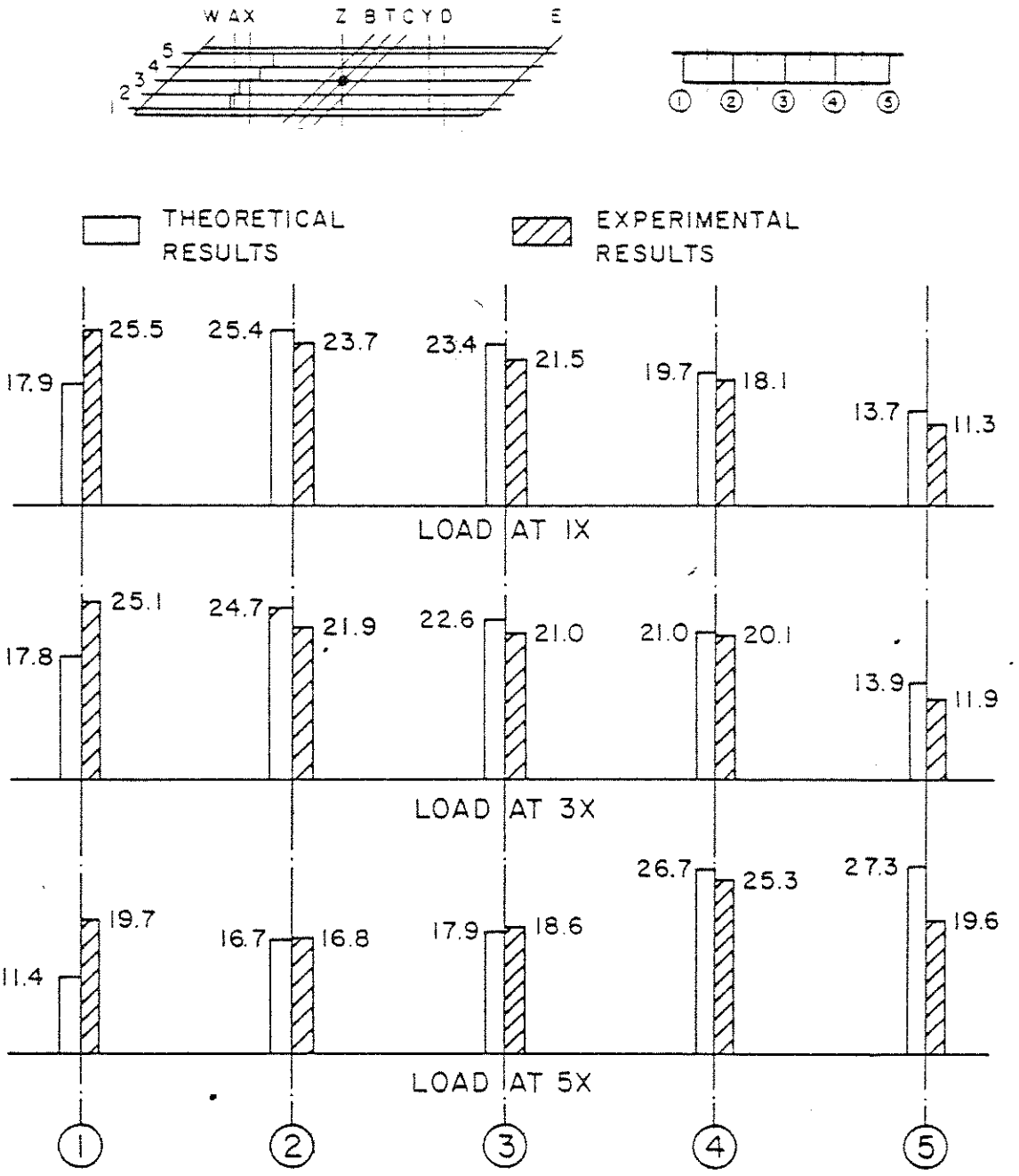

FIG. 6.19 PERCENTAGES OF TOTAL MOMENT AT SECTION A CARRIED BY EACH GIRDER FOR 100 KIP (445 kN) POINT LOADS AT 1X, 3X, 5X

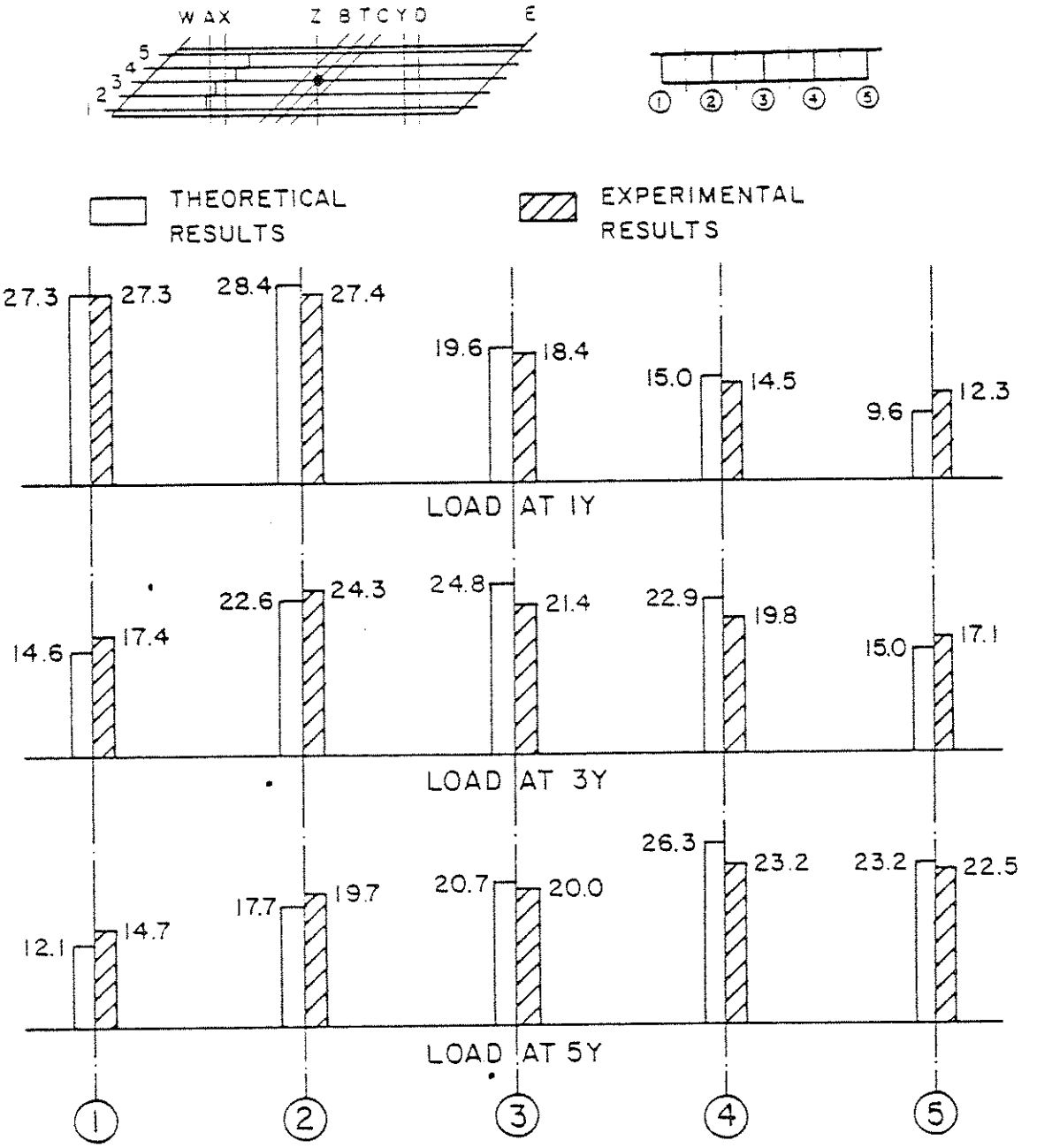

FIG. 6.20 PERCENTAGES OF TOTAL MOMENT AT SECTION D CARRIED BY EACH GIRDER FOR 100 KIP (445 kN) POINT LOADS AT 1Y, 3Y, 5Y

Note in Table 6.4 that at section A the agreement between theoretical and experimental values is generally much better for girders 4 and 5 as compared to girders 1 and 2.

The effect of the staggered diaphragm on one span can be seen clearly by studying the results in the loaded spans for load cases 3X, 3Y and 3X + 3Y. The theoretical results indicate at undiaphragmed section D a symmetrical distribution exists about the longitudinal bridge centerline, while at diaphragmed section A girders 1 and 2 take a higher percentage of the moment than do girders 4 and 5. The same trend is even more pronounced for the experimental results.

Next, consider the effect of moving the loads transversely across the width of the bridge. For only one span loaded, the distribution to each girder in the unloaded span remains virtually unchanged, while in the loaded span the contribution taken by any girder changes substantially as the load moves transversely. This effect is even more pronounced when both spans are loaded, however, it must be remembered that the total moments at sections A or D would be smaller for this loading then for only one span loaded. The maximum percentages found in Tables 6.4 or 6.5 for any of the point load cases shown are summarized below.

	Theoretical		Experimental	
	Interior Girder	Exterior Girder	Interior Girder	Exterior Girder
One Span Loaded				
Section A	27	27	25	26
Section D	28	28	27	27
Two Spans Loaded				
Section A	31	38	28	26
Section D	34	38	30	34

Theoretical and experimental maximum values given above are essentially the same for one span loaded, but not for both spans loaded by single point loads in each span. Actual design live loads consist of two or three lanes of trucks on the bridges instead of single point loads and for such conditions the maximum percentage of the total moment taken by an interior or exterior girder would be less than those given above. Such load conditions are discussed in Sections 6.3.3 and 7.2.4.

6.2.5 Effect of Torsional Restraint at Center Bent

As described in detail in Vol. I, most of the experimental program was carried out for the bridge model with normal support conditions which were termed "simply supported" and "no restraints". These consisted of simply supported end abutments and the center bent being supported by a single central column as shown in Figs. 1.2 and 1.3. Since in the practical application of skew multi-cell box girder bridges the support condition, where the heavy center bent diaphragm is supported by two or three columns or even a continuous wall element rather than just a single center column, is commonly encountered, the effect of a torsional restraint at the center bent was investigated for the 11 basic point load combinations (1X, 3X, 5X, 1Y, 3Y, 5Y, 1X + 1Y, 3X + 3Y, 5X + 5Y, 1X + 5Y and 5X + 1Y).

Torsional restraint at the center bent was provided by adding vertical supports under girders 1 and 5 at the skew center section T as described in Vol. I, Section 5.3.1.

Detailed tabulation of experimental results as well as theoretical results using the CELL program for the torsional restraint cases are given in Vol. IV for all 11 basic point load combination. In

this section the discussion will be limited to a comparison of the experimental data obtained from selected point load cases for the normal and the torsional restraint support conditions.

6.2.5.1 Reactions (Point Loads - Torsional Restraint)

Table 6.6 compares experimental reactions for the two support conditions for normalized 100 kip (445 kN) point loads on girder 1,3 and 5 respectively. It should be noted, that the total vertical reaction R now comprises R_W, R_E, R_F, R_{1T} and R_{5T}. The vertical reactions R_{1T} and R_{5T} which provided the torsional restraint along the center bent diaphragm are not listed in Table 6.6 since no corresponding reaction was present in the normal restraint case (values for R_{1T} and R_{5T} are given in Vol. IV).

The torsional restraint has only a small effect on the total vertical end reactions, R_W and R_E, while the vertical reaction at the center footing, R_F, decreases by the amount which is transfered to the vertical supports at the center bent under girder 1 and 5. The largest decrease in R_F is obtained for load cases where the acute side of a span is loaded, while for loads on the obtuse side of the span only small changes in R_F occur.

Considering the external moments and torques at the east and west end respectively (M_W, T_W and M_E, T_E), Table 6.6 shows that there is a substantial decrease in these reactions for the torsional restraint case for eccentric loadings on girder 1 or 5. This is again due to the vertical reactions developed under these girders at the center bent support, which aid in carrying the torque.

TABLE 6.6 EXPERIMENTAL REACTIONS FOR DIFFERENT SUPPORT RESTRAINTS

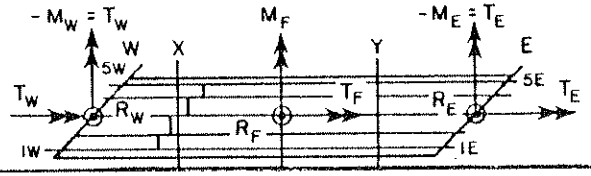

LOAD CASE	SUPPORT RESTRAINT	REACTIONS (KIPS AND FT-KIPS)										LOAD (KIPS)		
		WEST END			CENTER FOOTING			EAST END			TOTAL	SEC. X	SEC. Y	TOTAL
		R_W	M_W	T_W	R_F	M_F	T_F	R_E	M_E	T_E	R	P_X	P_Y	P
1X	NORMAL	33.6	181	-181	74.0	133	-216	-6.0	125	-125	101.6	100.0	-0.2	99.8
	TORSIONAL	31.3	72	- 72	19.0	54	- 32	-5.2	- 25	25	92.7	-100.0	0.0	-100.0
1Y	NORMAL	-8.7	72	- 72	58.0	- 80	- 58	52.8	390	-390	102.2	0.0	100.0	100.0
	TORSIONAL	-8.7	80	- 80	38.5	- 77	- 66	53.9	406	-408	97.8	- 0.1	-100.0	-100.1
1X+1Y	NORMAL	24.5	244	-244	132.3	58	-277	47.2	505	-505	204.0	99.5	100.5	200.0
	TORSIONAL	22.7	134	-134	45.5	- 22	- 89	48.2	369	-369	203.8	-100.7	- 99.3	-200.0
3X	NORMAL	42.2	- 78	78	69.1	107	- 66	-8.1	10	- 10	103.3	100.0	0.0	100.0
	TORSIONAL	41.5	-145	145	31.8	64	26	-7.4	- 60	60	98.5	-100.0	0.0	-100.0
3Y	NORMAL	-7.3	- 9	9	69.4	-106	79	41.5	75	- 75	103.6	0.1	100.0	100.0
	TORSIONAL	-6.8	30	- 50	33.6	- 61	- 15	40.4	140	-140	96.8	0.0	-100.0	-100.0
3X+3Y	NORMAL	36.0	- 90	90	137.6	3	9	35.9	85	- 85	209.5	99.3	100.7	200.0
	TORSIONAL	35.3	- 92	92	65.3	3	12	35.0	87	- 87	210.8	- 99.1	-100.9	-200.0
5X	NORMAL	52.0	-373	373	62.3	91	68	-9.1	- 83	83	105.1	100.0	0.0	100.0
	TORSIONAL	52.8	- 88	88	50.0	77	76	-9.2	- 88	88	184.6	-100.0	0.0	-100.0
5Y	NORMAL	-6.2	- 95	95	78.6	-147	230	33.0	-203	203	105.4	0.0	100.0	100.0
	TORSIONAL	-5.2	13	- 13	29.4	- 53	48	30.7	- 96	96	93.2	- 0.1	-100.0	-100.1
5X+5Y	NORMAL	47.8	-475	475	140.1	- 49	300	24.0	-277	277	211.9	100.5	99.5	200.0
	TORSIONAL	48.6	-357	357	60.0	33	102	21.4	-160	160	205.3	-101.1	- 98.9	-200.0

1 KIP = 4.448 kN
1 FT = 0.305 m

6.2.5.2 Deflections (Point Loads - Torsional Restraint)

The transverse distributions of the vertical deflections at the loaded sections are presented for nine point load cases in Figs. 6.21 and 6.22 for the two support conditions.

It is interesting to note that while in general the additional torsional restraints at the center bent tend to decrease the deflections at the midspan sections, simultaneous loads in both spans on the exterior girders feature slightly higher deflections for the torsional restraint case in the span which is loaded on the obtuse side.

A substantial decrease in deflections due to the torsional restraint can be observed on the acute side of a loaded span in all the cases where the loads are also on the acute side. For loads on the obtuse side of a span only small differences in the transverse distribution of the vertical deflections in this span are noticeable.

6.2.5.3 Strains (Point Loads - Torsional Restraint)

A comparison of the transverse distribution of experimental longitudinal strains for the different support conditions is given in Fig. 6.23 for one representative load case, 5X + 5Y, which yields very high midspan moments in the undiaphragmed Span II.

The general shape of transverse strain distribution is maintained for the two support conditions with larger changes in the positive steel strains in the bottom slab than in the negative concrete strains in the slab. Analogous to the findings for the transverse distribution of the vertical deflections, the load case 5X + 5Y (i.e. Span I is loaded on the obtuse side while Span II is loaded on the acute side) features higher strains for the obtuse loaded Span I

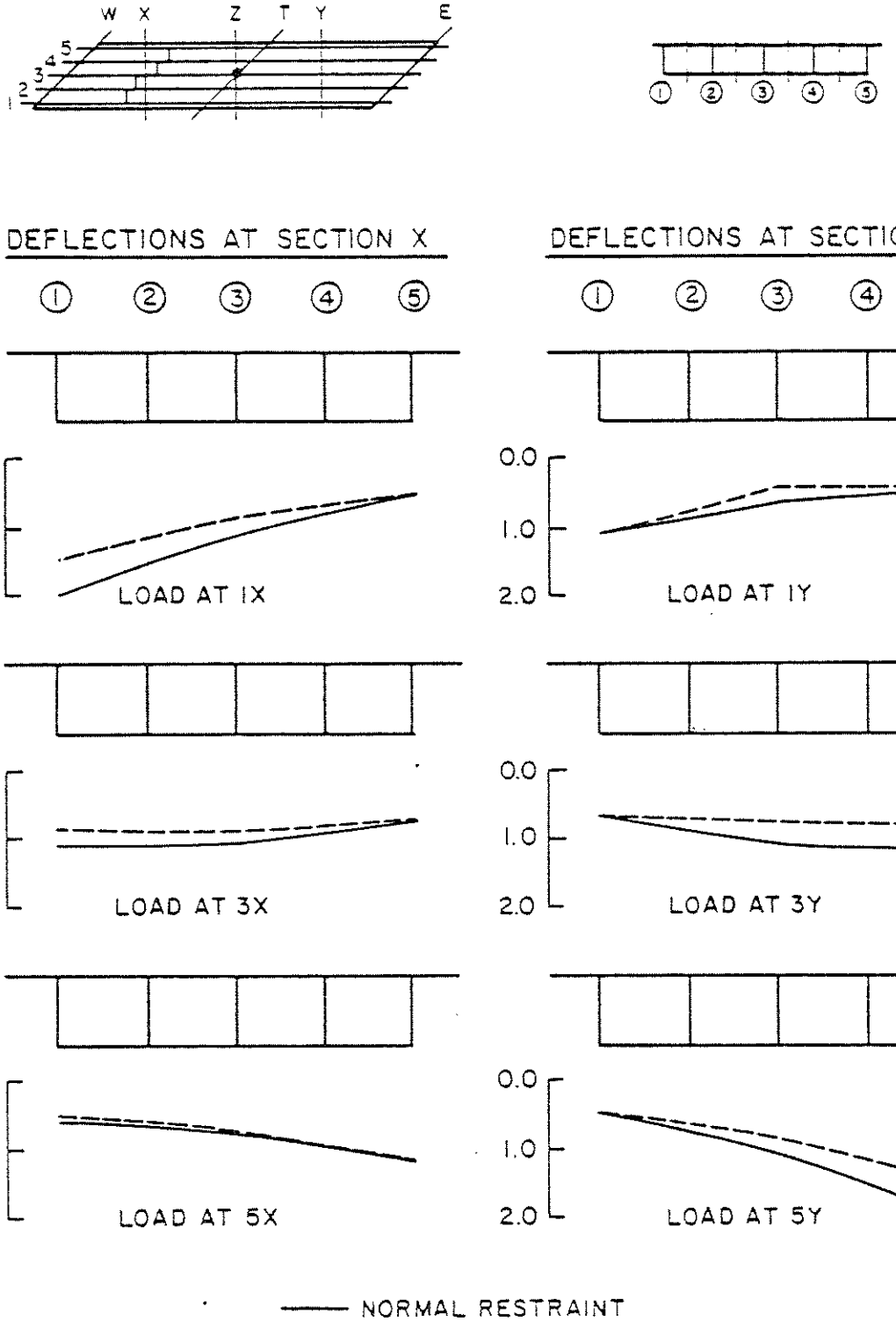

FIG. 6.21 EXPERIMENTAL DEFLECTIONS (INCHES) AT TRANSVERSE SECTIONS X AND Y WITH DIFFERENT SUPPORT RESTRAINTS FOR 100 KIP (445 kN) POINT LOADS AT 1X, 3X, 5X, 1Y, 3Y, 5Y

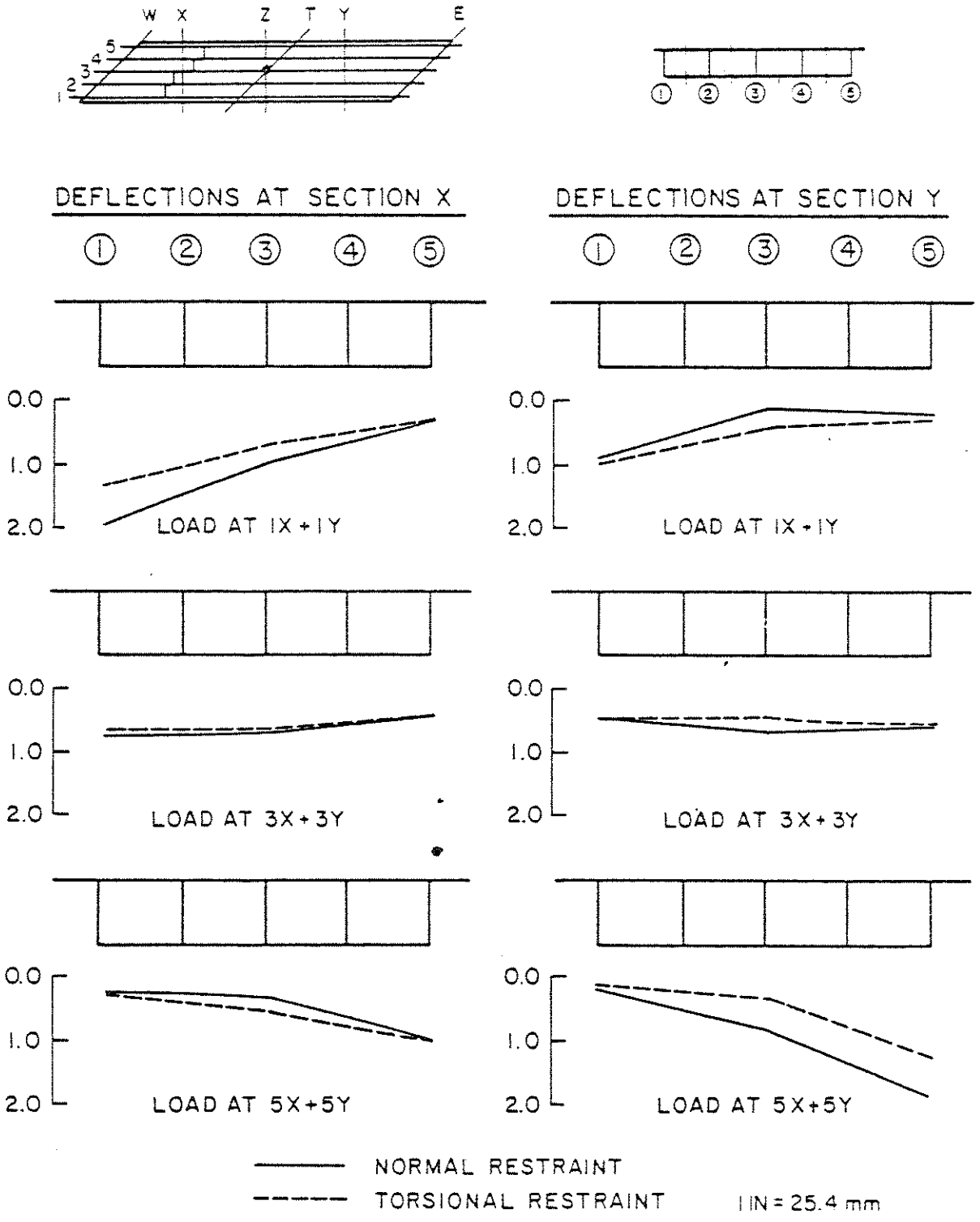

FIG. 6.22 EXPERIMENTAL DEFLECTIONS (INCHES) AT TRANSVERSE SECTIONS X AND Y WITH DIFFERENT SUPPORT RESTRAINTS FOR 100 KIP (445 kN) POINT LOADS AT 1X + 1Y, 3X + 3Y, 5X + 5Y

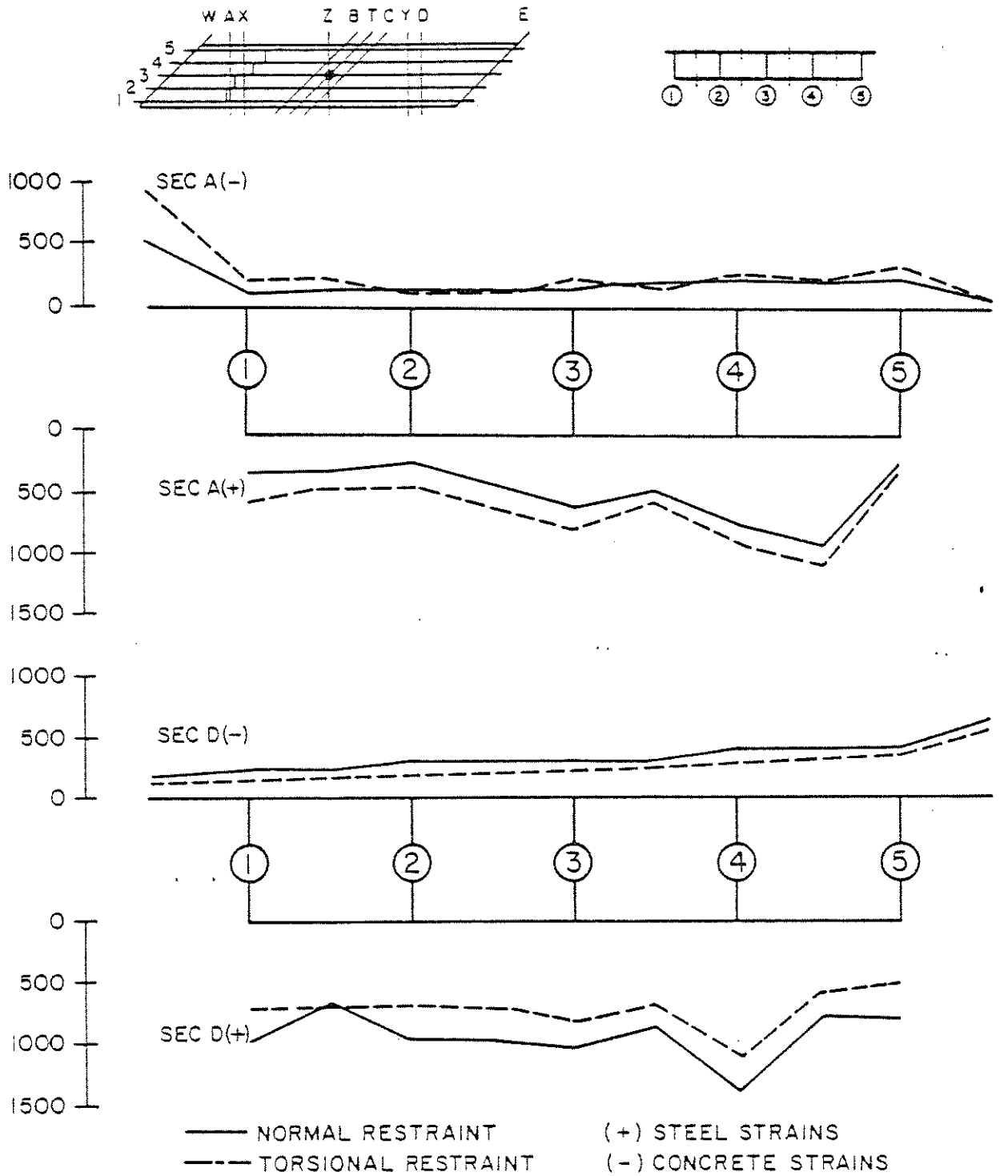

FIG. 6.23 EXPERIMENTAL LONGITUDINAL STRAINS (MICRO INCH/INCH) IN TOP AND BOTTOM SLABS AT SECTIONS A AND D WITH DIFFERENT SUPPORT RESTRAINTS FOR 100 KIP (445 kN) POINT LOADS AT 5X + 5Y

for the torsional restraint case, while Span II shows a decrease in strains from the normal restraint to the torsional restraint case.

6.2.5.4 Moments (Point Loads - Torsional Restraint)

The total moments at the instrumented midspan sections A and D for the two different support conditions are given in Table 6.7. The moments shown are based on experimental internal forces found from measured strains.

Comparing the values in Table 6.7 to ascertain the effect of the torsional restraint, the decrease in total midspan moment is quite substantial for loads on the acute side of the span (1X or 5Y), while in the cases where only the obtuse side of a span is loaded (5X or 1Y) virtually no change in total midspan moment occurs.

For loads along center girder 3 significant reductions in total midspan moments can be noticed for the cases where only one span is loaded (3X or 3Y) while no changes occur for both spans loaded (3X + 3Y).

For the load cases where both spans are loaded on an exterior girder (1X + 1Y and 5X + 5Y), the total moment in the acute loaded span decreases and in the obtuse loaded span increases when changing from the normal to the torsional restraint case.

The transverse distribution of the total moment at the midspan section is shown graphically in Figs. 6.24 to 6.27. For only one span loaded, Figs. 6.24 and 6.25 show only very small differences in the transverse moment distribution for the normal and the torsional restraint cases. As should be expected, the torsional restraint at the center bent tends to increase the percentages taken by an exterior girder when it is loaded.

TABLE 6.7 COMPARISON OF EXPERIMENTAL TOTAL INTERNAL MOMENTS (FT-KIPS) AT A SECTION FOR DIFFERENT SUPPORT RESTRAINTS

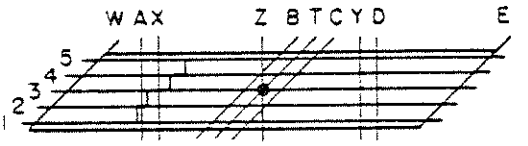

LOAD CASE	SUPPORT RESTRAINT	MOMENT AT SECTION	
		A	D
1X	NORMAL	657	-183
	TORSIONAL	528	- 50
1Y	NORMAL	-70	442
	TORSIONAL	-56	430
1X+1Y	NORMAL	597	268
	TORSIONAL	463	385
3X	NORMAL	556	-123
	TORSIONAL	473	- 51
3Y	NORMAL	-125	543
	TORSIONAL	- 60	472
3X+3Y	NORMAL	433	437
	TORSIONAL	435	422
5X	NORMAL	407	- 62
	TORSIONAL	405	- 58
5Y	NORMAL	-183	663
	TORSIONAL	- 65	532
5X+5Y	NORMAL	272	576
	TORSIONAL	356	441

1 FT-KIP = 1.356 kN-m

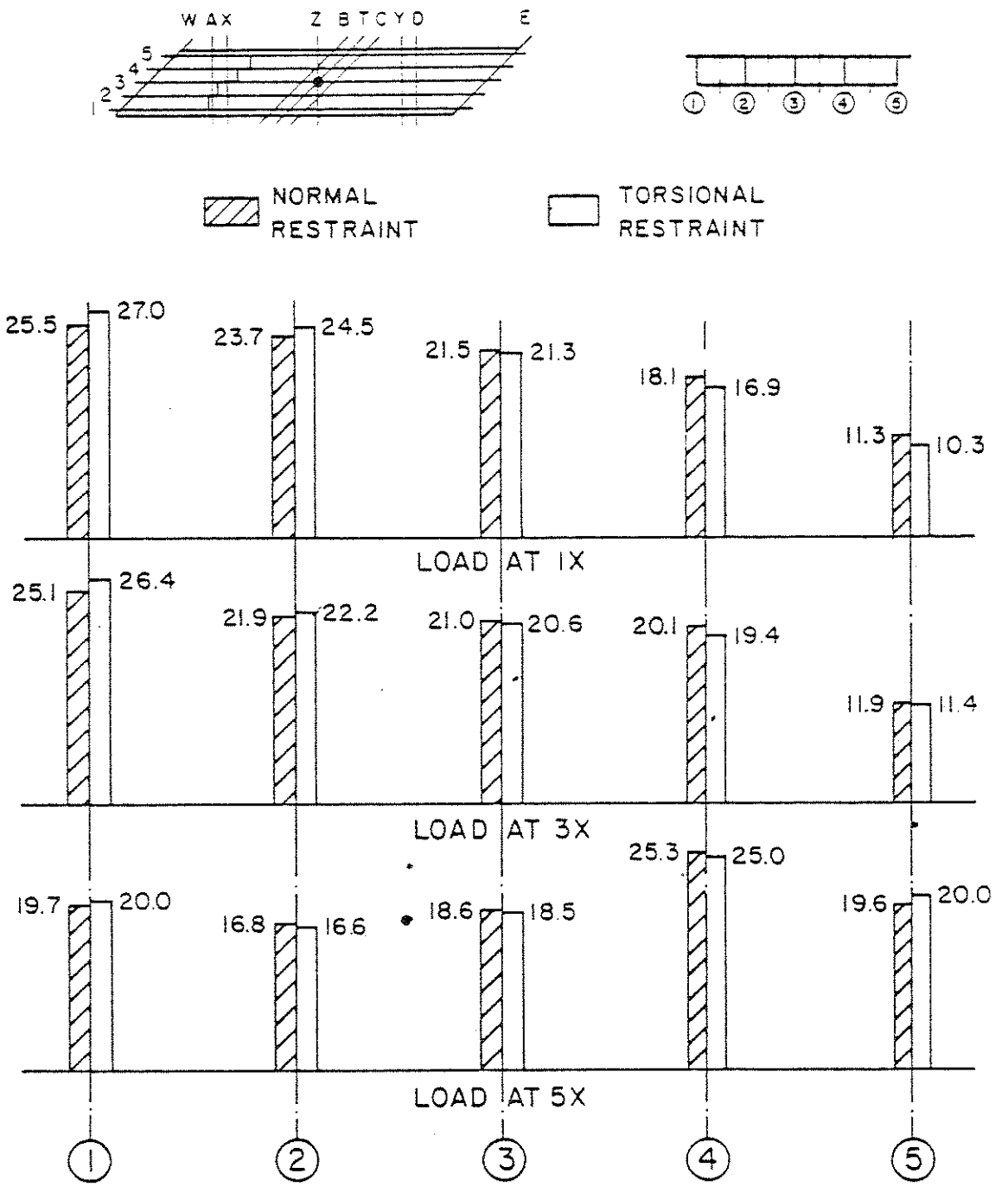

FIG. 6.24 PERCENTAGES OF TOTAL MOMENT AT SECTION A CARRIED BY EACH GIRDER FOR 100 KIP (445 kN) POINT LOADS AT 1X, 3X, 5X

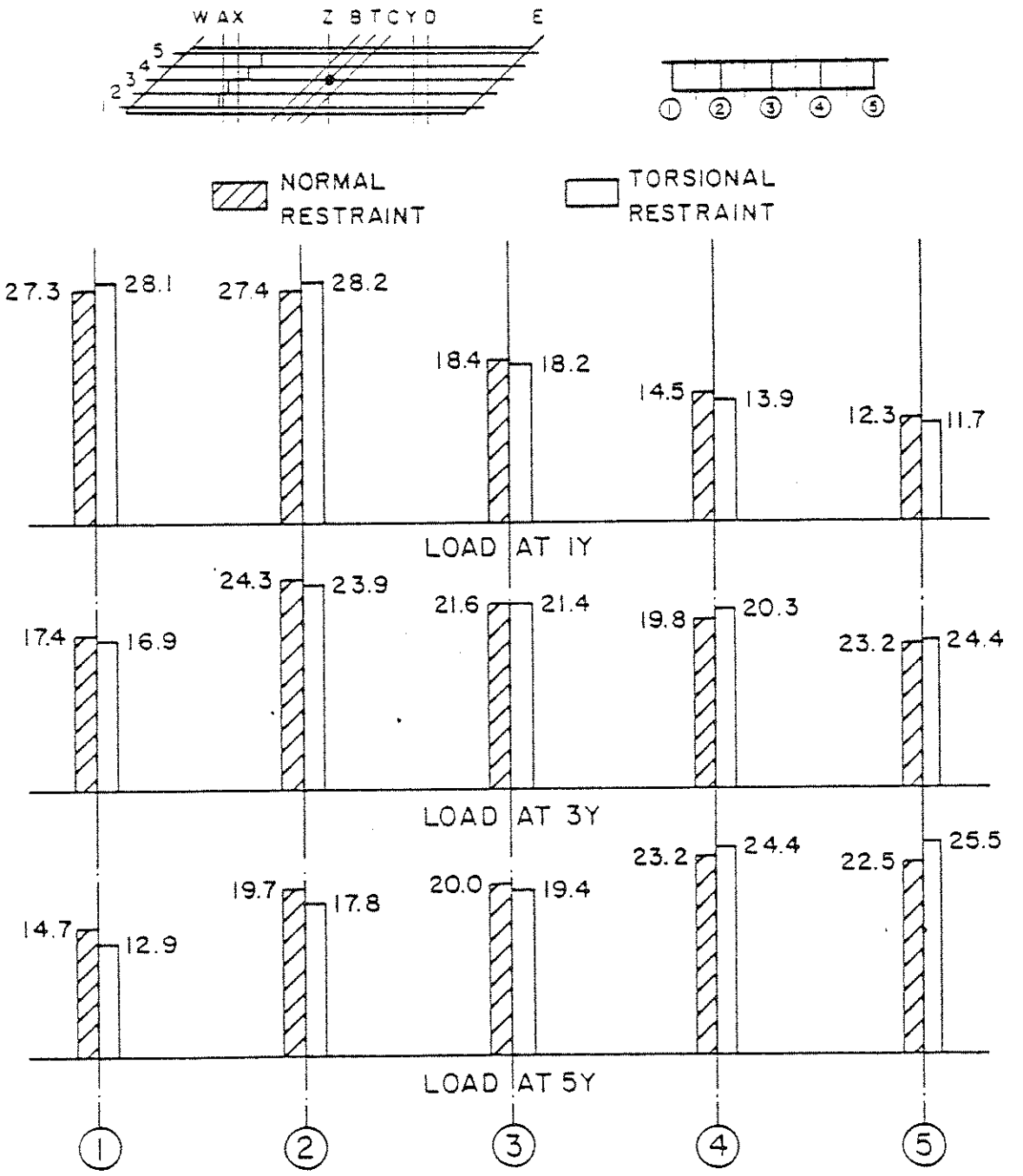

FIG. 6.25 PERCENTAGES OF TOTAL MOMENT AT SECTION D CARRIED BY EACH GIRDER FOR 100 KIP (445 kN) POINT LOADS AT 1Y, 3Y, 5Y

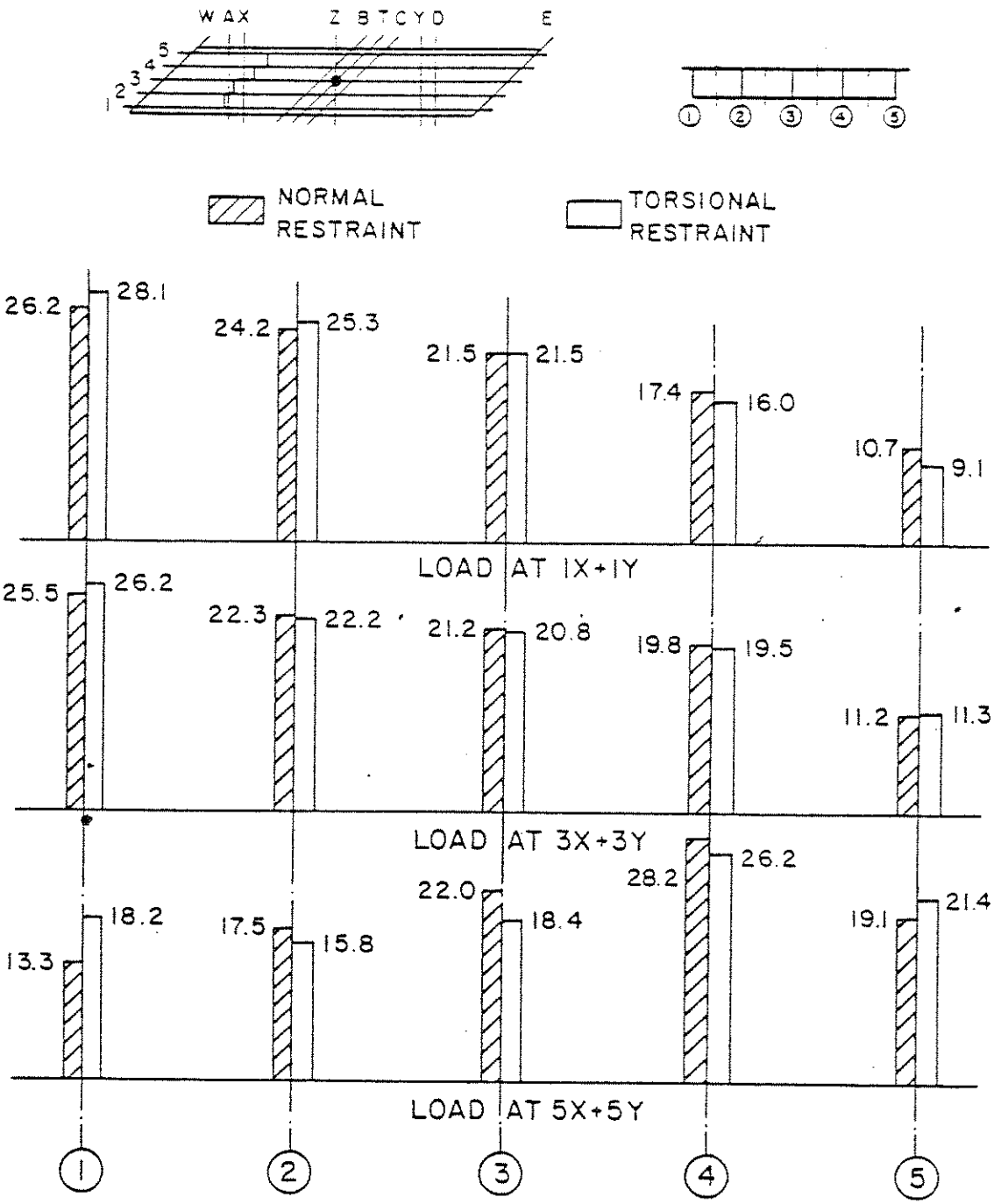

FIG. 6.26 PERCENTAGES OF TOTAL MOMENT AT SECTION A CARRIED BY EACH GIRDER FOR 100 KIP (445 kN) POINT LOADS AT 1X + 1Y, 3X + 3Y, 5X + 5Y

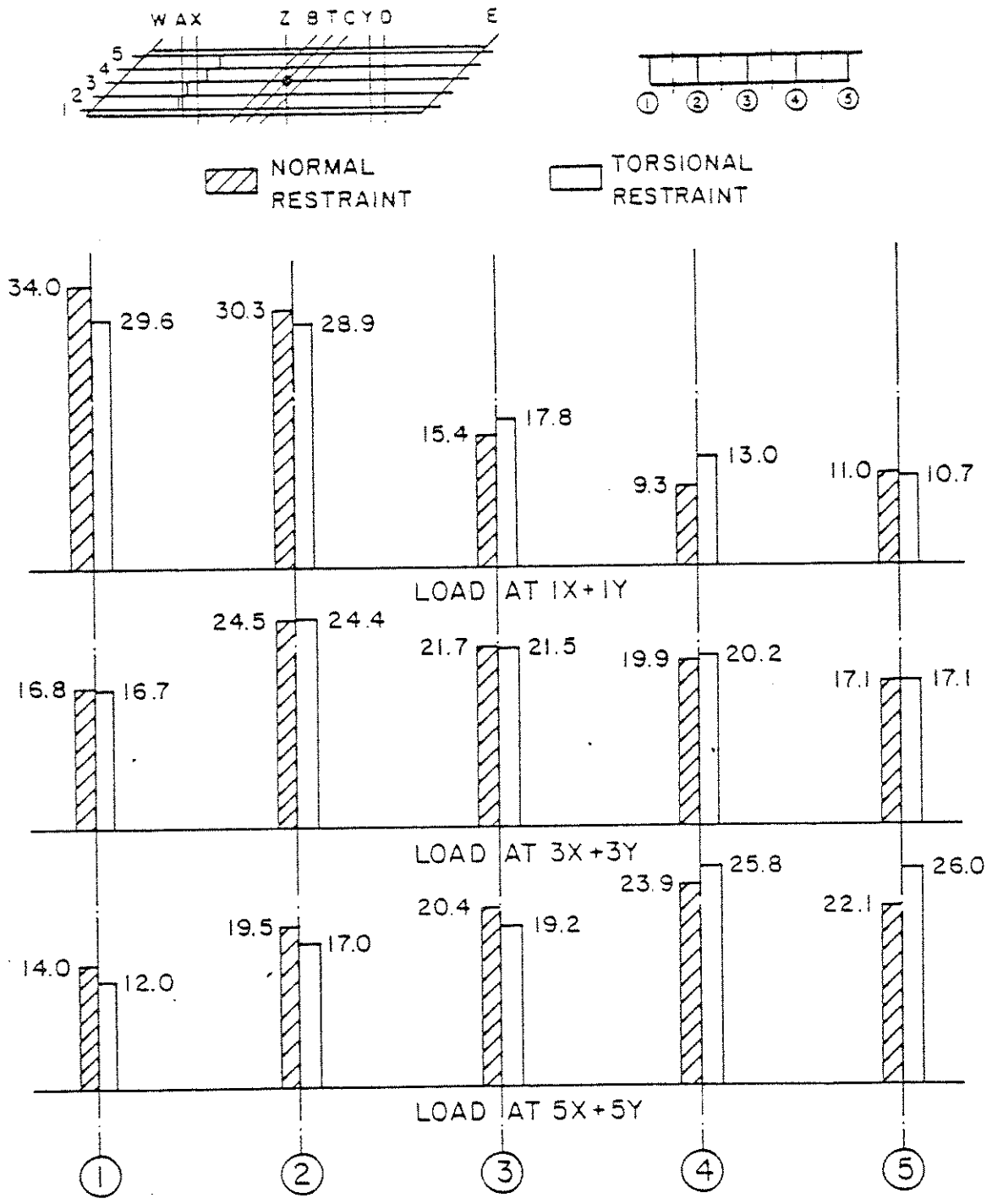

FIG. 6.27 PERCENTAGES OF TOTAL MOMENT AT SECTION D CARRIED BY EACH GIRDER FOR 100 KIP (445 kN) POINT LOADS AT 1X + 1Y, 3X + 3Y, 5X + 5Y

The differences in the transverse distribution of midspan moments increase for load cases where both spans are loaded and the loads are positioned on the exterior girders, while virtually no changes occur for loads along center girder 3.

6.3 Truck and Construction Vehicle Loads

As described in Vol. I, the model was loaded by scaled down versions of the standard AASHTO HS 20-44 truck [total load = 72 kips (320 kN)] and a proposed overload construction vehicle class II [total load = 330 kips (1470 kN)]. All linear dimensions were reduced by the scale factor 1: 2.82 and details of wheel positions in the model vehicles can be found in Vol. I. Similitude required that the loads be reduced by a factor of 1:8 to produce the same stresses in the model as in the prototype. Thus for the model the total load for each truck was 9.0 kips (40.0 kN) and for each construction vehicle 41.25 kips (183.5 kN). Using these loads, a study could be made of the bridge response due to actual design truck live loads placed at various positions on the bridge.

Fig. 6.28 shows the positions and directions of the truck and construction vehicle loads on the bridge. As described in Vol. I, a total of 11 combinations of two lane truck loadings, 3 combinations of three truck loadings, and 8 combinations of constuction vehicle loadings were used. Because all the vehicles were facing east and each vehicle had six wheels with the front wheels carrying smaller loads than the rear wheels, exact symmetry of loading about the bridge transverse center line, section Z, was not maintained, Fig. 6.28.

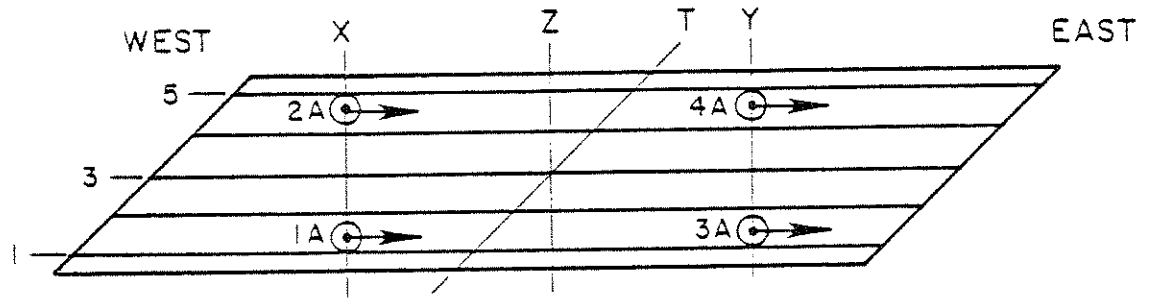

(a) TWO LANE TRUCK LOADING [EACH TRUCK = 9.0 KIPS (40.0 KN) NOMINAL]

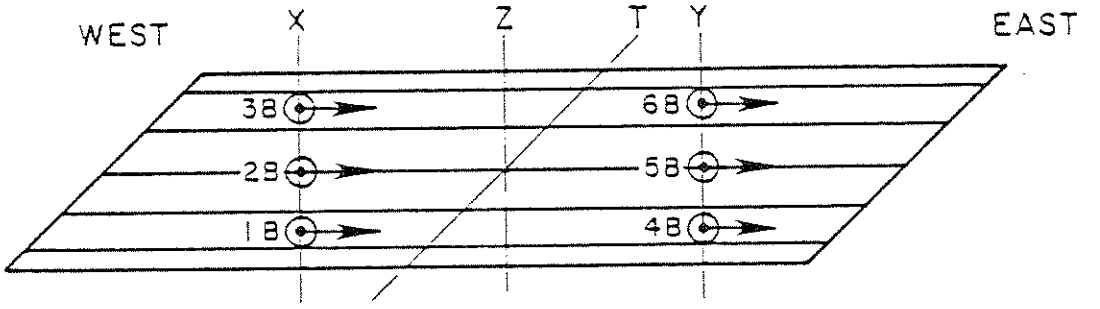

(b) THREE LANE TRUCK LOADING [EACH TRUCK = 9.0 KIPS (40.0 KN) NOMINAL]

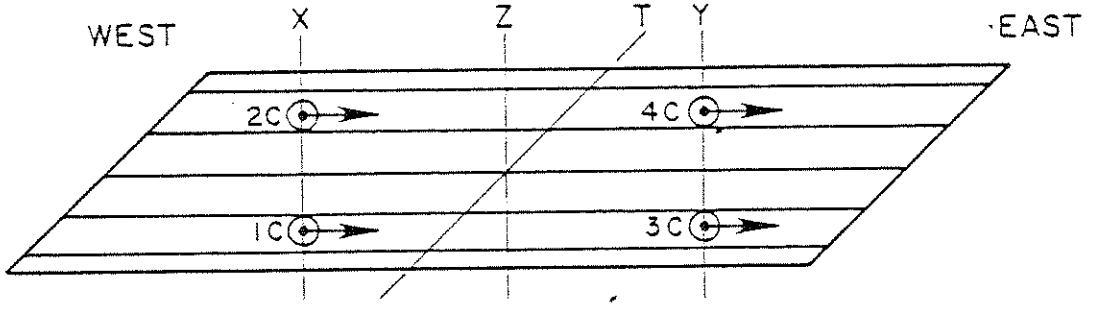

(c) CONSTRUCTION VEHICLE LOADING [EACH TRUCK = 41.25 (183.5 KN) NOMINAL]

(NOT TO SCALE)

FIG. 6.28 POSITIONS AND DIRECTIONS OF TRUCK AND CONSTRUCTION VEHICLE LOADINGS ON THE BRIDGE DECK

Detailed tabulations of theoretical and experimental results related to reactions, deflections, strains and moments for all of these loadings are given in Vol. IV. Theoretical values were obtained from computer analyses using CELL. Selected results will be discussed in the following sections.

6.3.1 Reactions (Truck and Construction Vehicle Loading)

A summary of theoretical and experimental reactions is given in Table 6.8 for various vehicle loadings. Excellent agreement exists between experiment and theory for the vertical end reactions R_W and R_E, while the vertical center footing reaction R_F turns out to be consistently slightly higher in the experiment than in the theoretical analysis. The moment and torque reactions show generally good agreement between experiment and theory except for a few load cases.

6.3.2 Deflections (Truck and Construction Vehicle Loading)

Experimental deflections are shown in Fig. 6.29 for vehicle loadings producing maximum values at diaphragmed section X and undiaphragmed section Y. For the two and three lane truck cases, the loading is relatively uniform across the width of the bridge, Fig. 6.28, resulting in an almost uniform distribution of deflections with slightly higher deflections towards the acute side of the span. For the construction vehicle, only one lane is loaded on the acute side of the span resulting in larger deflection at the loaded position. By comparing results at sections X and Y, these loadings also demonstrate the effect of the midspan diaphragm. Since deflections were only measured at girders 1, 3 and 5, a straight line connection between the three transverse displacements results in a kink at girder 3.

TABLE 6.8 COMPARISON OF THEORETICAL AND EXPERIMENTAL REACTIONS (KIPS & FT-KIPS) UNDER TRUCK (9 KIPS) AND CONSTRUCTION VEHICLE (41.25 KIPS) LOADS.

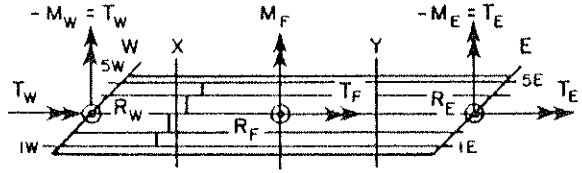

LOAD TYPE	LOAD CASE	SOLUTION	REACTIONS (KIPS & FT-KIPS)										LOAD (KIPS)		
			WEST END			CENTER FOOTING			EAST END			TOTAL	SEC. X	SEC. Y	TOTAL
			R_W	M_W	T_W	R_F	M_F	T_F	R_E	M_E	T_E	R	P_X	P_Y	P
TWO LANE TRUCK LOADING	4A	THEORY	-0.5	- 9	9	6.5	-10	15	3.1	-11	11	9.0	- 9.0	0.0	- 9.0
		EXPER.	-0.6	- 7	7	7.0	- 9	15	3.1	-14	14	9.6	- 9.0	0.0	- 9.0
	3A+4A	THEORY	-1.2	- 4	4	11.8	-16	12	7.5	17	-17	18.0	-18.0	0.0	-18.0
		EXPER.	-1.4	- 1	1	12.0	-17	11	7.3	12	-12	17.8	-18.0	0.0	-18.0
	2A+4A	THEORY	4.2	- 37	37	11.5	- 4	17	2.4	-15	15	18.0	- 9.0	- 9.0	-18.0
		EXPER.	4.0	- 34	34	12.7	- 2	20	2.5	-20	20	19.2	- 9.0	- 9.0	-18.0
	1A+2A +3A+4A	THEORY	6.7	- 22	22	23.0	0	0	6.3	21	-21	36.0	-18.0	-18.0	-36.0
		EXPER.	6.5	- 15	15	23.9	4	-1	6.2	16	-16	36.6	-17.8	-18.2	-36.0
THREE LANE TRUCK LOADING	4B+5B+6B	THEORY	-1.8	- 26	26	17.6	-24	18	11.2	7	- 7	27.0	0.0	-27.0	-27.0
		EXPER.	-2.0	- 1	1	18.1	-27	17	11.0	21	-21	27.1	0.0	-27.0	-27.0
	1B+2B+3B +4B+5B+6B	THEORY	10.1	- 32	32	34.5	0	0	9.4	31	-31	54.0	-27.0	-27.0	-54.0
		EXPER.	9.4	- 22	22	35.1	5	-1	9.1	22	-22	53.6	-27.1	-26.9	-54.0
CONSTR. VEHICLE LOADING	4C	THEORY	-2.1	- 35	35	28.5	-40	58	14.9	-39	39	41.2	0.0	-41.3	-41.3
		EXPER.	-2.5	- 27	27	30.5	-52	70	15.2	-52	52	43.2	0.0	-41.3	-41.3
	2C+4C	THEORY	18.9	-147	147	51.6	-14	64	12.0	-55	55	82.5	-41.3	-41.2	-82.5
		EXPER.	18.4	-138	138	56.5	-20	86	12.3	-69	69	87.1	-41.3	-41.2	-82.5

1 KIP = 4.448 kN
1 FT = 0.305 m

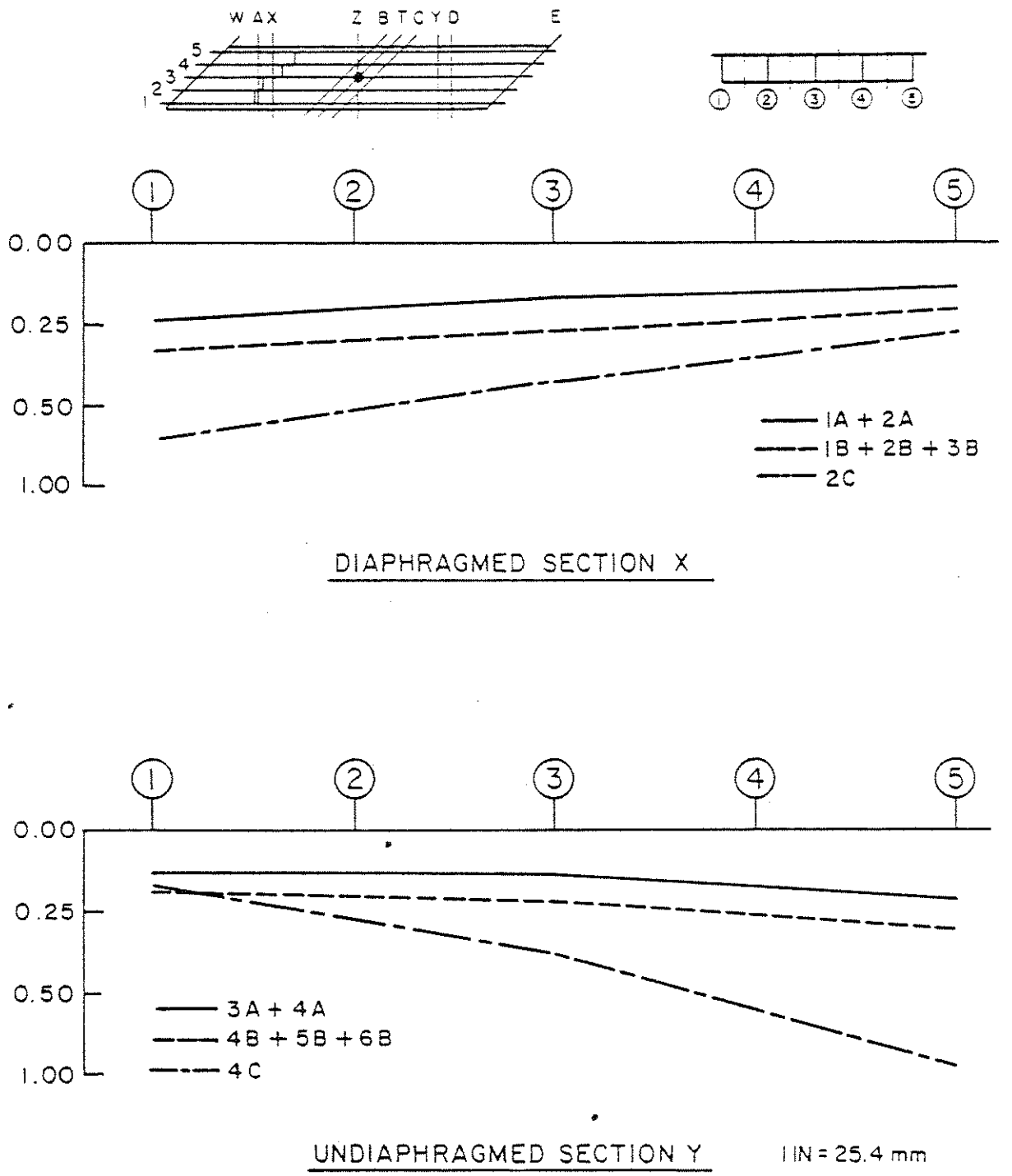

FIG. 6.29 EXPERIMENTAL DEFLECTIONS (INCHES) AT TRANSVERSE SECTIONS X AND Y FOR DIFFERENT VEHICLE LOADINGS

In the undiaphragmed Span II at section Y this kink appears to be slightly larger than for section X in the diaphragmed span. The differences in displacements between the acute girder and the obtuse girder at the loaded section are 0.736 in. - 0.195 in. = 0.541 in. (13.7 mm) and 0.703 in. - 0.209 in. = 0.495 in. (12.6 mm) for the undiaphragmed and diaphragmed span respectively, which shows that the transverse distribution of displacements is more uniform in the diaphragmed span while the transverse displacement gradient is larger in the undiaphragmed span.

It is of interest to compute the maximum deflection to span ratios for these design live load cases, since they would be the same in a full scale prototype structure because of similitude. For the two lane truck, three lane truck, and construction vehicle loadings results in Fig. 6.29, the maximum deflections are respectively 0.22, 0.33, and 0.74 in. (5.6, 8.4, and 18.8 mm) which when divided by the span of 432 in. equal to 36 ft. (11 m) give deflection to span ratios of 1/1960, 1/1300, and 1/580 all of which are quite small.

6.3.3 Loadings for Maximum Girder Moments

Tables 6.9 and 6.10 summarize the experimental girder moments and their transverse distributions for a variety of vehicle load combinations on the bridge involving 1, 2, 3, 4 or 6 vehicles simultaneously. Vehicle locations can be identified from Fig. 6.28. If one searches Tables 6.9 and 6.10 for maximum moments in interior girders 2, 3 and 4 and exterior girders 1 and 5 certain conclusions can be immediately reached regarding critical design loadings.

(1) As would be expected the maximum moments get progressively larger as one proceeds from the single truck load to two

TABLE 6.9 EXPERIMENTAL GIRDER MOMENTS (FT-KIPS) UNDER CRITICAL TRUCK (9.0 KIPS) AND CONSTRUCTION VEHICLE (41.3 KIPS) LOADS (MOMENTS ABOUT GROSS SECTION NEUTRAL AXIS).

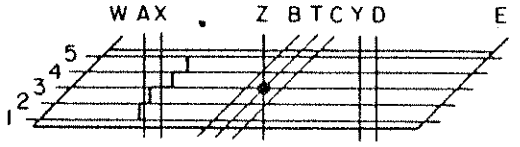

1 KIP = 4.448 kN
1 FT = 0.305 m

SECTION	GIRDER	SINGLE TRUCK		TWO LANE TRUCK LOADING			THREE LANE TRUCK LOADING		CONSTRUCTION VEHICLE LOADING			
		1A	2A	1A+2A	1A+3A	1A+2A+ 3A+4A	1B+2B+3B	1B+2B+3B+ 4B+5B+6B	1C	2C	1C+3C	1C+4C
A	1	16	7	23	14	18	37	27	53	32	44	35
	2	15	6	21	13	17	33	26	48	29	41	33
	3	12	7	20	11	16	33	26	48	29	41	34
	4	10	9	19	8	15	29	22	41	29	33	27
	5	5	7	12	5	9	18	13	24	20	19	15
	Σ	58	36	95	51	75	150	114	214	139	178	144
		4A	3A	4A+3A	4A+2A	1A+2A+ 3A+4A	4B+5B+6B	1B+2B+3B+ 4B+5B+6B	4C	3C	2C+4C	2C+3C
D	1	8	10	18	6	14	26	20	34	43	28	37
	2	11	11	21	10	16	33	25	48	48	41	42
	3	11	7	18	10	14	29	22	49	32	42	26
	4	13	7	19	12	13	28	20	56	27	50	22
	5	13	5	19	12	14	27	21	57	25	53	19
	Σ	56	40	95	50	71	143	108	244	175	214	146

TABLE 6.10 EXPERIMENTAL PERCENTAGE DISTRIBUTION OF TOTAL MOMENT AT SECTIONS A AND D FOR CRITICAL TRUCK AND CONSTRUCTION VEHICLE LOADINGS.

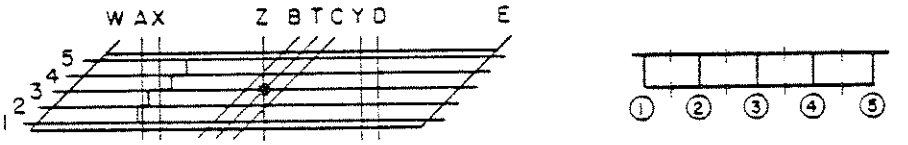

SECTION	GIRDER	UNIFORM STRESS DISTRIBUT.	2-LANE TRUCK	3-LANE TRUCK	CONSTR. VEHICLE
LOAD CASE			1A+2A	1B+2B+3B	1C
A	1	17	24	25	25
	2	22	22	22	22
	3	22	21	22	22
	4	22	20	19	19
	5	17	13	12	11
LOAD CASE			3A+4A	4B+5B+6B	4C
D	1	17	19	18	14
	2	22	22	23	20
	3	22	19	20	20
	4	22	20	20	23
	5	17	20	19	23

lane truck, three lane truck, and finally to the construction vehicle loading.

(2) Considering positive moment sections A and D, maximum moments for truck loadings are produced when loading only one span of the bridge with as many trucks as possible across the width of the bridge. However, a single construction vehicle in one span in an extreme eccentric position (on the acute side of the span) produces the largest total positive midspan moment of all the loadings. The case with two construction vehicles in one span was considered to be prohibited in practice and therefore not considered in the test program.

(3) The transverse distribution of the maximum positive moment due to two lane truck, three lane truck or construction vehicle loading is virtually the same for all three critical load cases in the diaphragmed span at section A (see Table 6.10). The high overload of a single construction vehicle on the acute side of the span is transversely distributed by the staggered midspan diaphragm in almost the same way as a two or three lane truck loading. In the undiaphragmed span at section D, however, the construction vehicle loading clearly shows a shift in the transverse distribution of the midspan moment to the acute side of the bridge.

A comparison of the transverse moment distribution for truck and construction vehicle loadings with the distribution of the midspan moment for the uniformly stressed cross-section (also shown in Table 6.10) shows again the high contribution of girder 1, section A, for all experimental cases due to the proximity of the staggered misdpan diaphragm to the instrumented section.

6.3.4 Strains and Maximum Stresses

Transverse distribution of experimental longitudinal strains at sections A, B, C and D for truck and construction vehicle loadings producing maximum effects are shown in Fig. 6.30. For the relatively uniform two and three lane truck loadings across the width of the bridge the strain distributions are also fairly uniform. For the heavy concentrated load of a construction vehicle on the acute side of the diaphragmed span only small changes in the general shape of the transverse strain distribution are noticeable at section A, while section D for loads in the undiaphragmed span features a shift of the transverse distribution of longitudinal strains towards the loaded (acute side) of the span.

An estimate of the maximum design live load stresses can be obtained by multiplying the maximum strain values from Fig. 6.30 by the unmodified modulus of elasticity values from Tables 6.5 and 6.9 of Vol. I for this loading phase. A summary of these stresses in the concrete and the steel is given in Table 6.11.

If one adds to the live load stresses for the steel in Table 6.11, the nominal average measured dead load steel stresses of 12,000 psi (83 MPa) at sections A and D (see Section 5.4.3), it can be seen that the total steel stresses for the two lane and three lane truck loadings would be below the allowable value of 24,000 psi (165 MPa). For the construction vehicle loading a maximum calculated total steel stress of about 27,000 psi (186 MPa) occurs.

It should be recognized that total stresses at midspan sections X and Y would be about 10% higher than those at the instru-

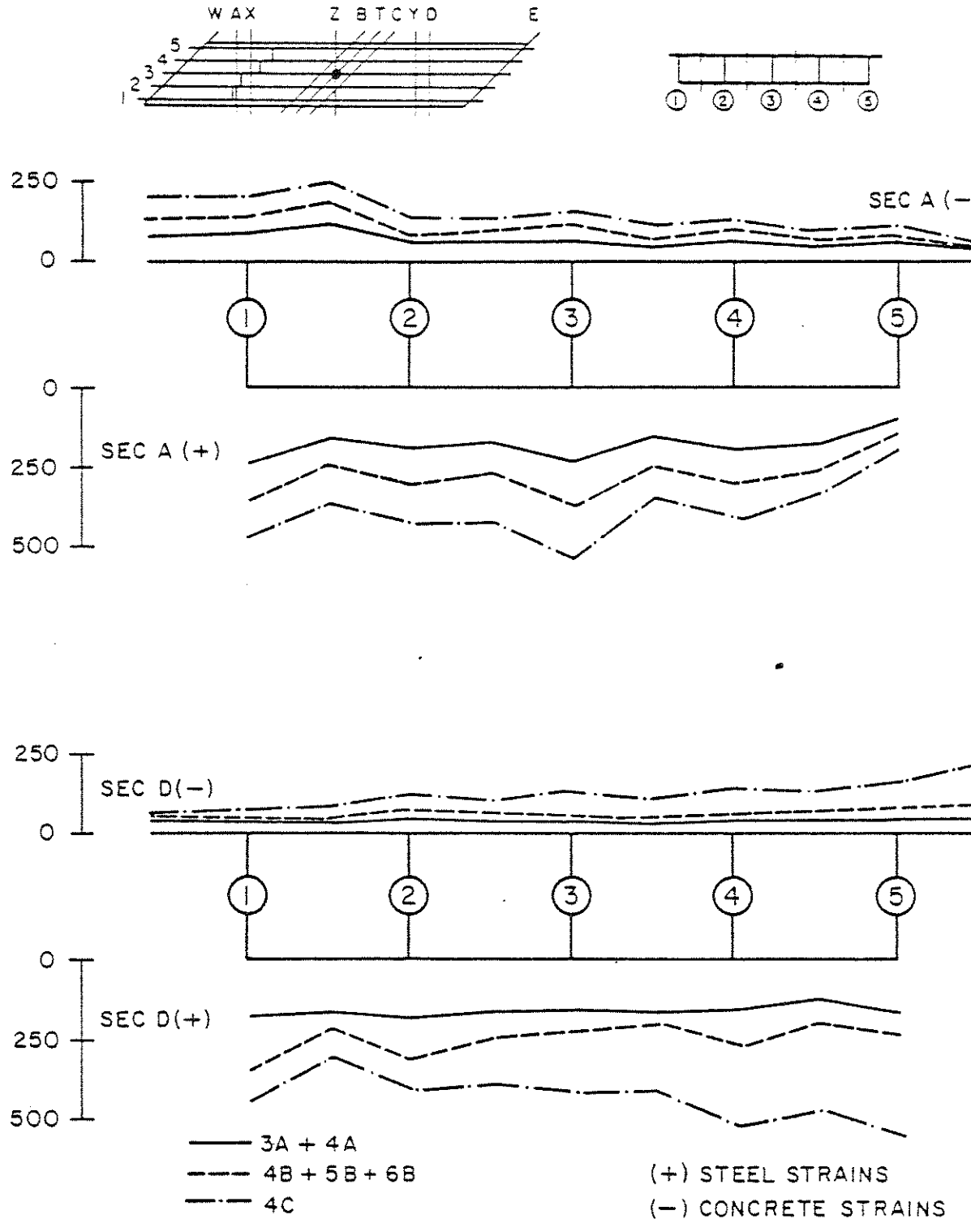

FIG. 6.30 EXPERIMENTAL LONGITUDINAL STRAINS (MICRO INCH/INCH) AT SECTIONS A AND D FOR DIFFERENT VEHICLE LOADINGS

TABLE 6.11 MAXIMUM LIVE LOAD EXPERIMENTAL STRESSES (PSI) UNDER TRUCK AND CONSTRUCTION VEHICLE LOADS

MATERIAL	SECTION	TWO LANE TRUCK LOADING	THREE LANE TRUCK LOADING	CONSTRUCTION VEHICLE LOADING
CONCRETE	A	348	525	747
	B	309	435	525
	C	264	387	675
	D	201	294	690
STEEL	A	6450	10100	14600
	B	3440	5130	6900
	C	3410	5070	9370
	D	4820	9420	14400

1 PSI = 0.006895 MPa

mented sections A and D each of which are 2.57 ft (0.78 m) away from midspan sections X and Y respectively.

Live load concrete stresses in Table 6.11 are quite low and would be well within the allowable when added to the nominal dead load stresses.

6.4 Moving Fork Lift Truck Loads

6.4.1 General Remarks

For highway bridges the most important live loads are moving concentrated loads in the form of vehicles travelling across the bridge. Therefore an extensive theoretical and experimental study was performed to obtain information about the behavior of the two span ekw box girder bridge under moving concentrated loads.

The results of both experimental and analytical studies are represented in the form of influence lines for total vertical end reactions, total end moments, midspan deflections and longitudinal membrane forces at midspan.

6.4.2 Experimental Influence Lines

A fork lift truck with two concrete blocks on the fork was used as a total moving load of about 10.3 kips (45.8 kN). Three longitudinal passes were made from west to east and static readings were taken at 2 different transverse sections, in order to obtain an approximately continuous record from which experimental influence ordinates could be determined. Details on the truck dimensions, wheel loads, loading paths and transverse sections at which measurements were taken may be found in Section 5.5 of Vol. I.

6.4.3 Theoretical Influence Lines

The theoretical influence lines were obtained using the CELL COARSE analytical model as described in Section 3.2.1. Point loads representing the front wheel axle and the back wheel axle loads of the forklift were applied to the analytical model as shown in Fig. 6.31.

Three longitudinal passes, a North, Center and South Pass along girder lines 4, 3 and 2 respectively were simulated by considering a total of 40 different load positions as indicated in Fig. 6.31.

The mesh spacing of the CELL COARSE mesh which is based on a 1.27 ft (0.39 m) module and the axle spacing of the fork lift truck of 3.8 ft (1.16 m) allows a simple positioning of the total fork lift load by placing the front wheel axle directly on a nodal point and distributing the back wheel load equally to the two adjacent nodes. In the transverse direction the entire load was concentrated along girder lines 2, 3 and 4 for the three passes respectively and no adjustment was made for the small eccentricity of the experimental forklift pass to the girderline as shown in Fig. 5.10 in Section 5 of Vol. I.

6.4.4 Results For Moving Fork Lift Truck Loads

Fig. 6.32 to 6.41 show theoretical influence lines obtained using the CELL program and plotted experimental points for the three passes of the fork lift truck. In each figure results are given for a pass near girder 4 (North Pass), a pass near girder 3 (Center Pass) and a pass near girder 2 (South Pass). In each case

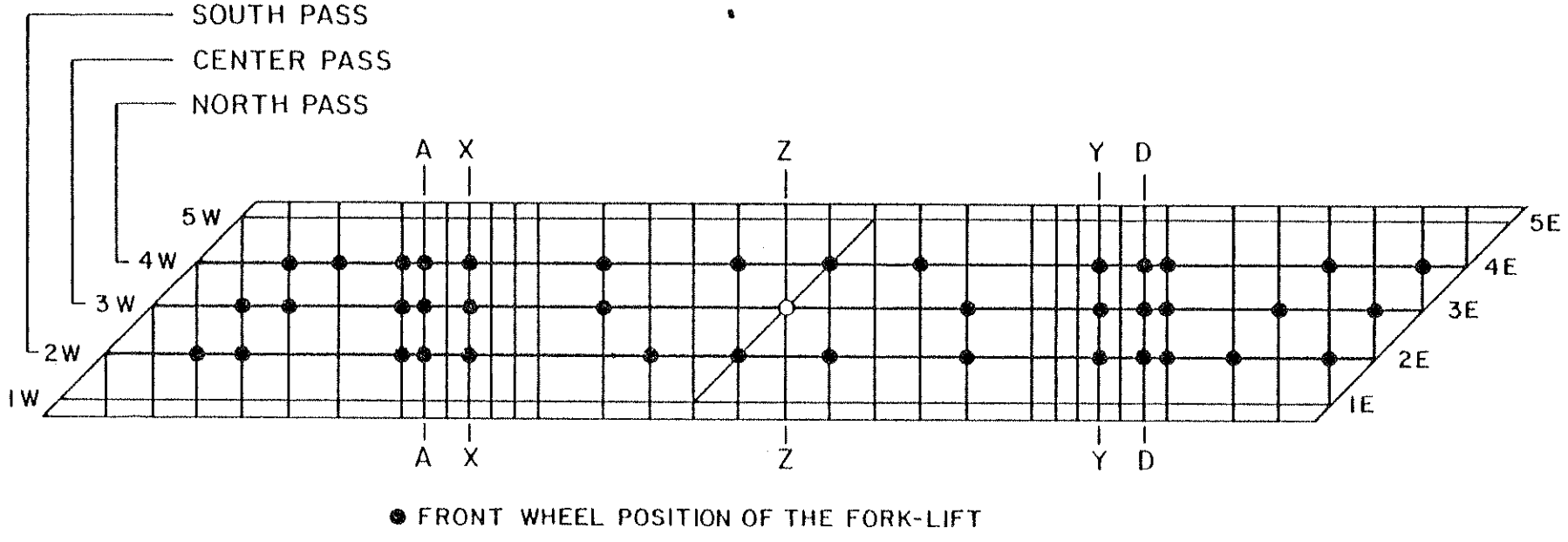

FIG. 6.31 POSITIONS AND PATHS OF THE FORK LIFT TRUCK FOR CELL COARSE ANALYSIS

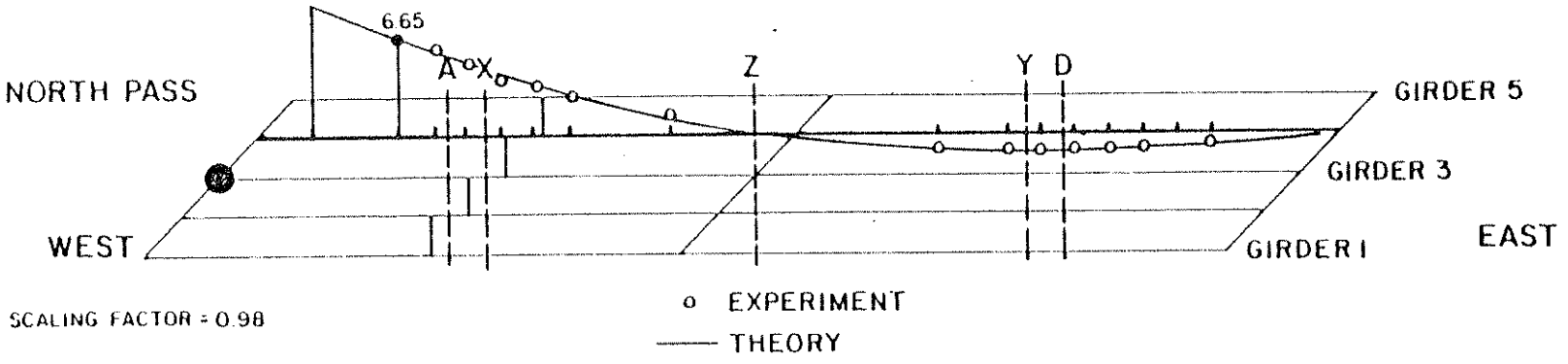

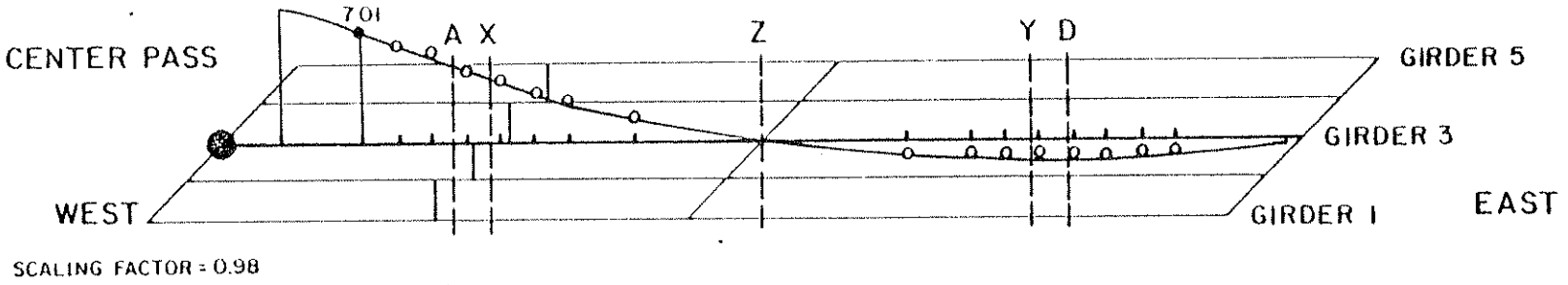

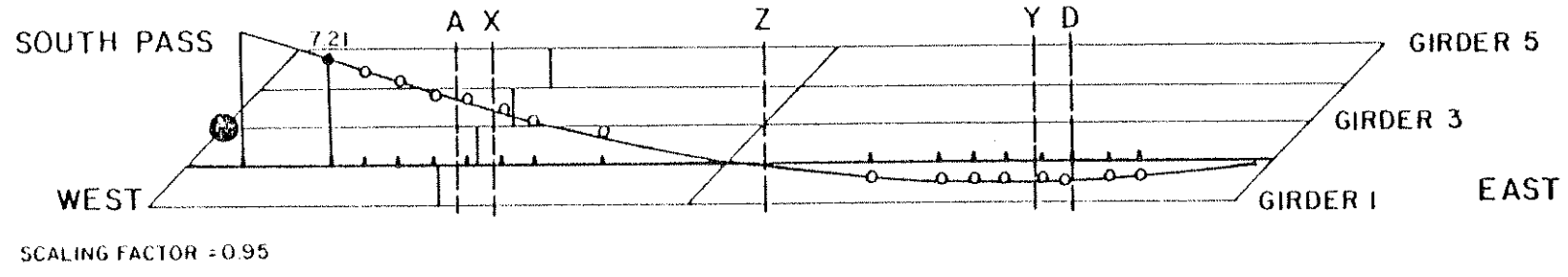

FIG. 6.32 INFLUENCE LINES FOR TOTAL VERTICAL WEST REACTION (KIPS) UNDER MOVING FORK LIFT TRUCK LOAD

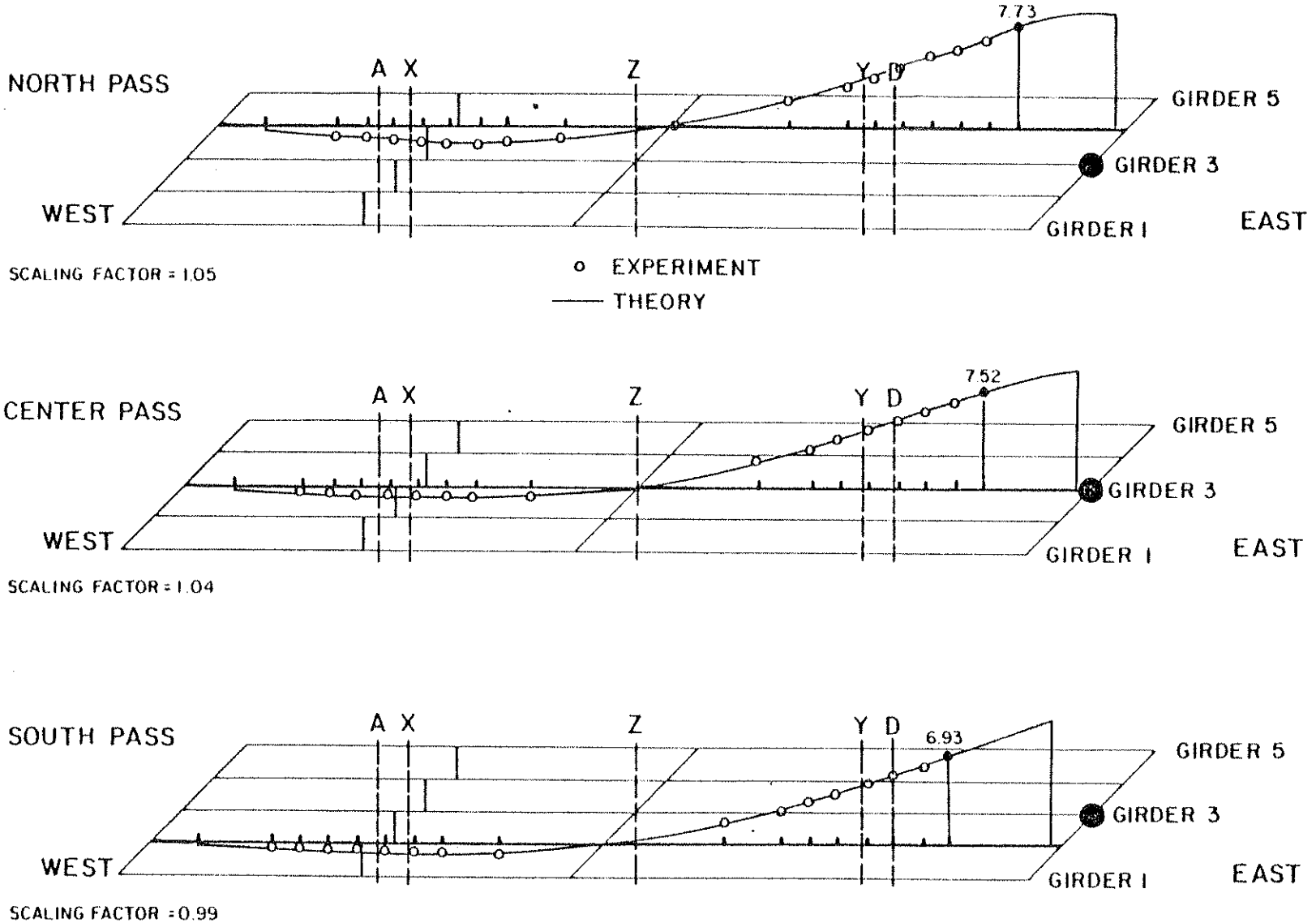

FIG. 6.33 INFLUENCE LINES FOR TOTAL VERTICAL EAST REACTION (KIPS) UNDER MOVING FORK LIFT TRUCK LOAD

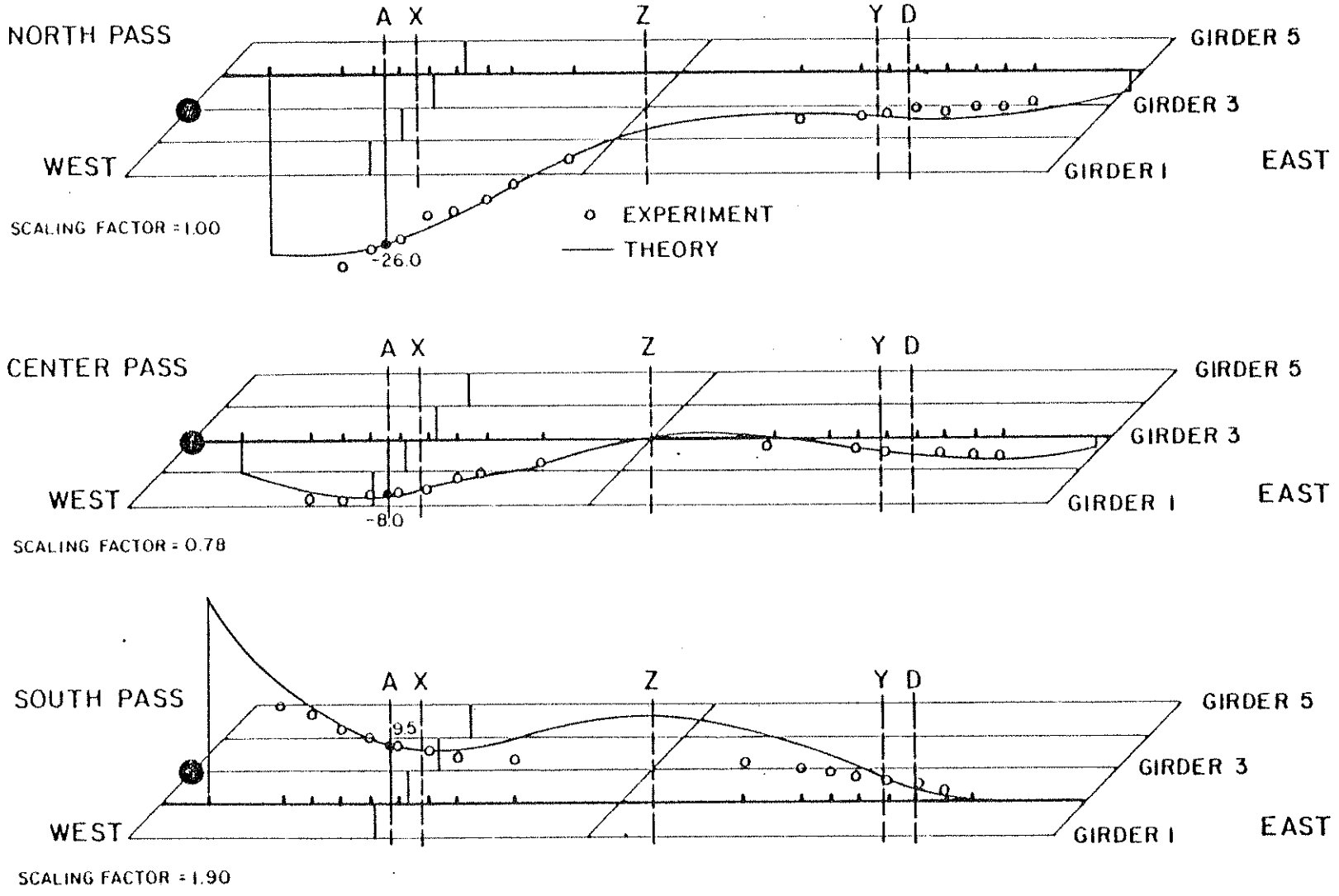

FIG. 6.34 INFLUENCE LINES FOR WEST END MOMENT (FT-KIPS) UNDER MOVING FORK LIFT TRUCK LOAD

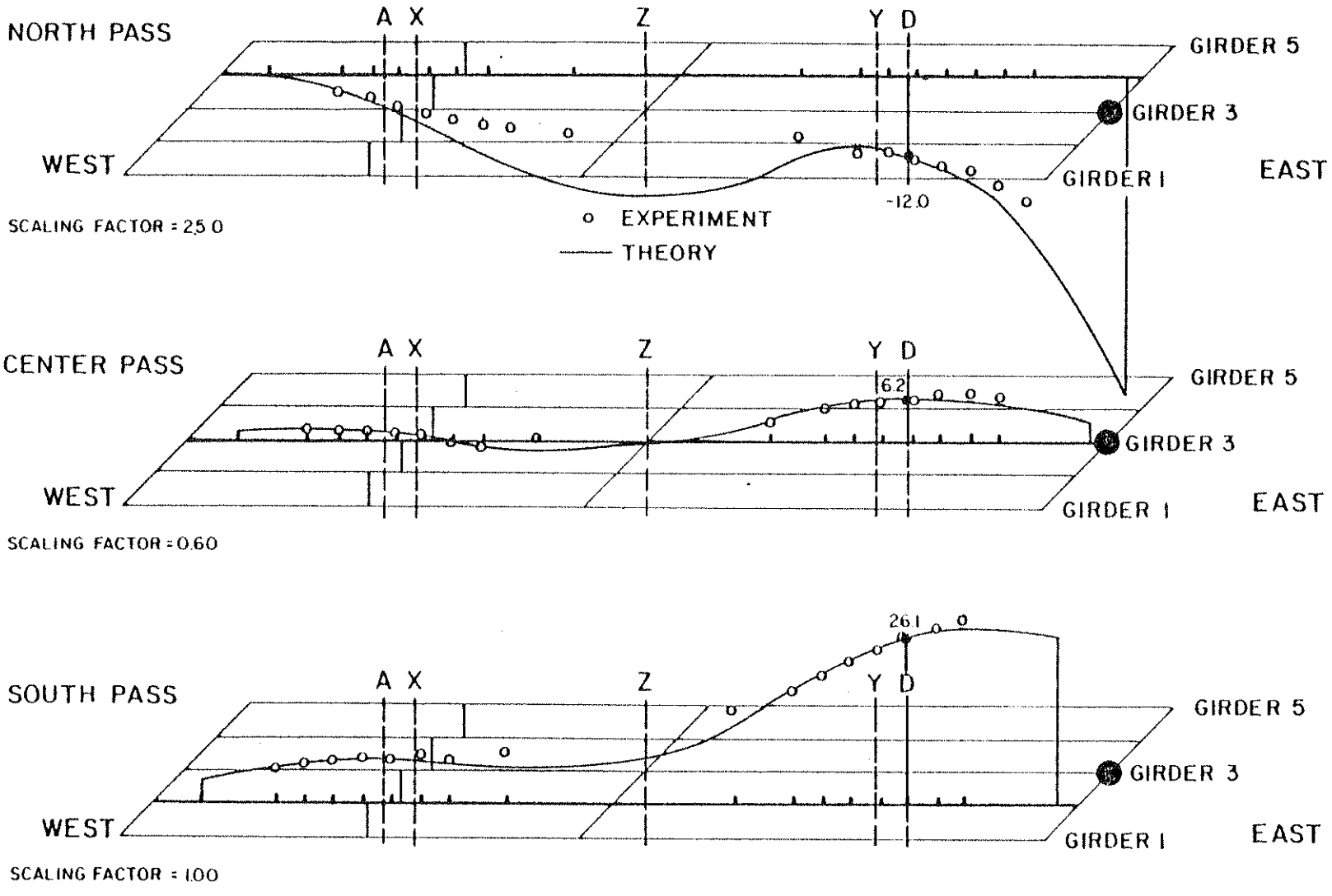

FIG. 6.35 INFLUENCE LINES FOR EAST END MOMENT (FT-KIPS) UNDER MOVING FORK LIFT TRUCK LOAD

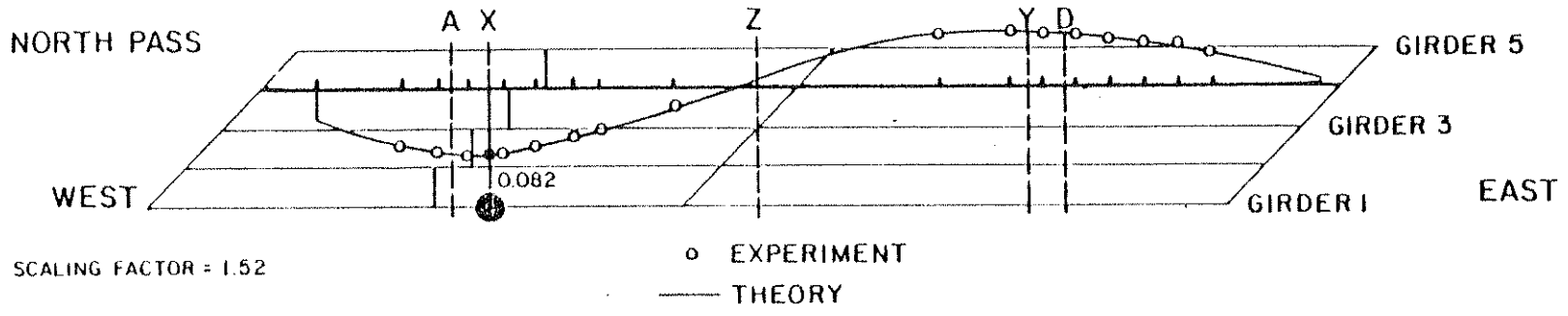

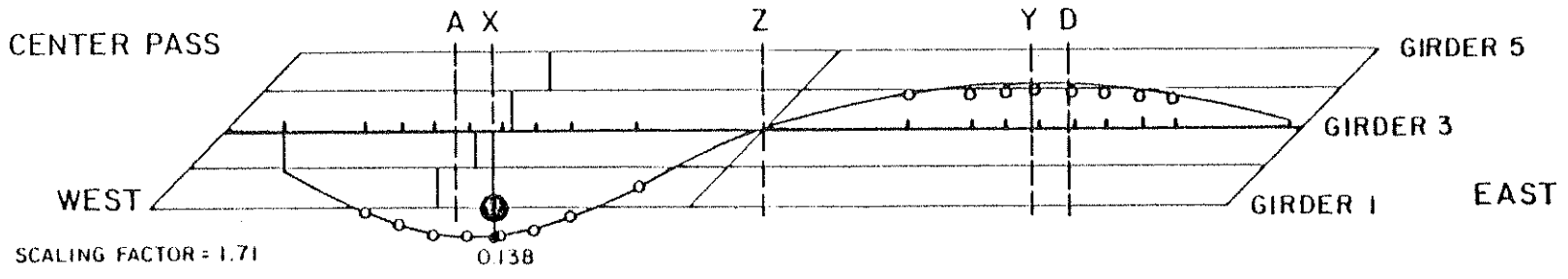

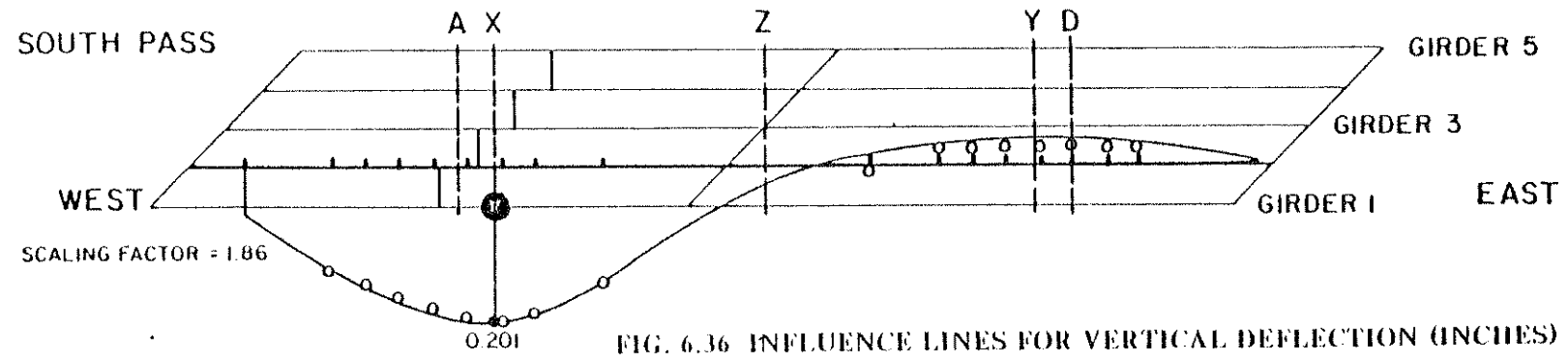

FIG. 6.36 INFLUENCE LINES FOR VERTICAL DEFLECTION (INCHES) AT IX UNDER MOVING FORK LIFT TRUCK LOAD

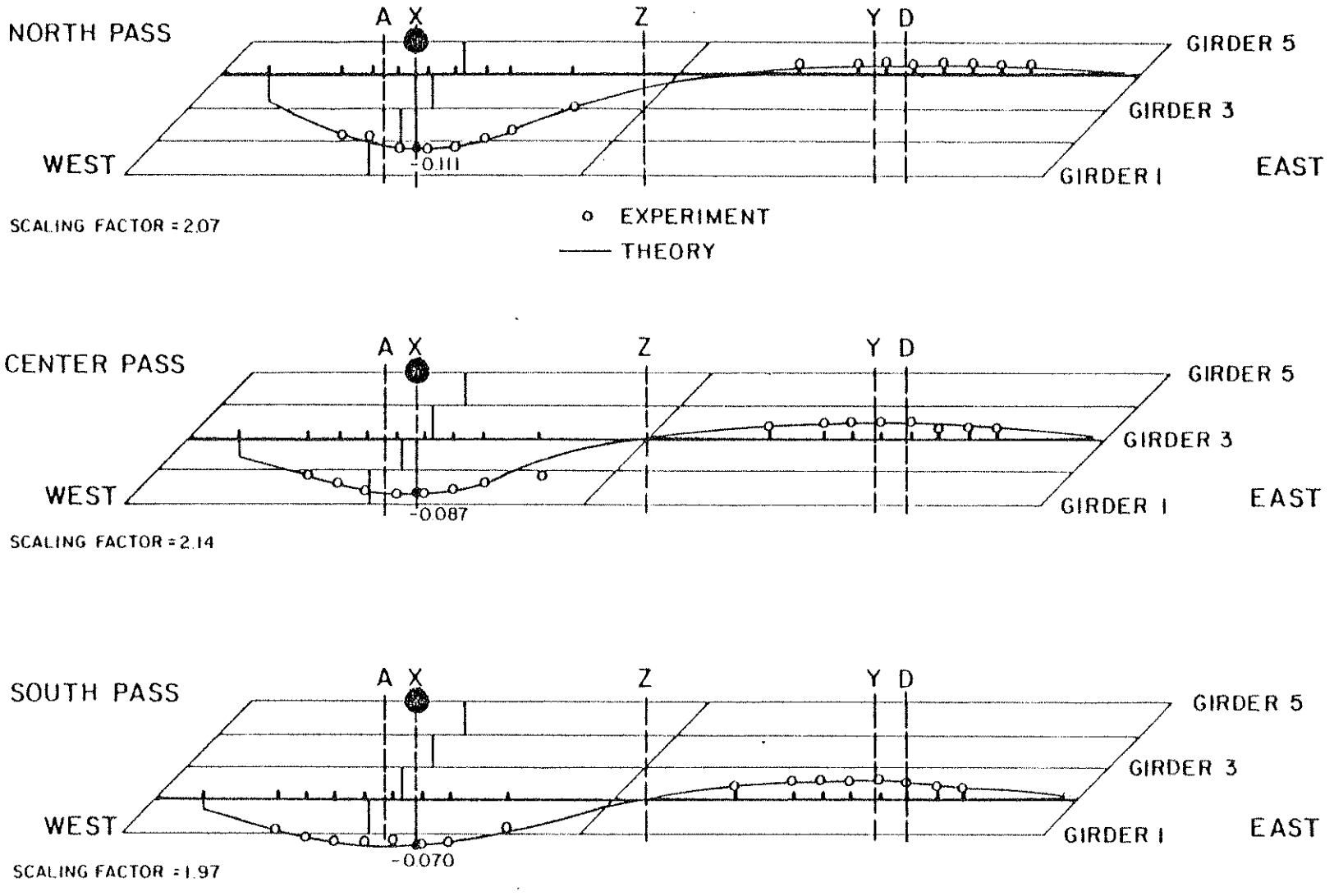

FIG. 6.37 INFLUENCE LINES FOR VERTICAL DEFLECTION (INCHES) AT 5X UNDER MOVING FORK LIFT TRUCK LOAD

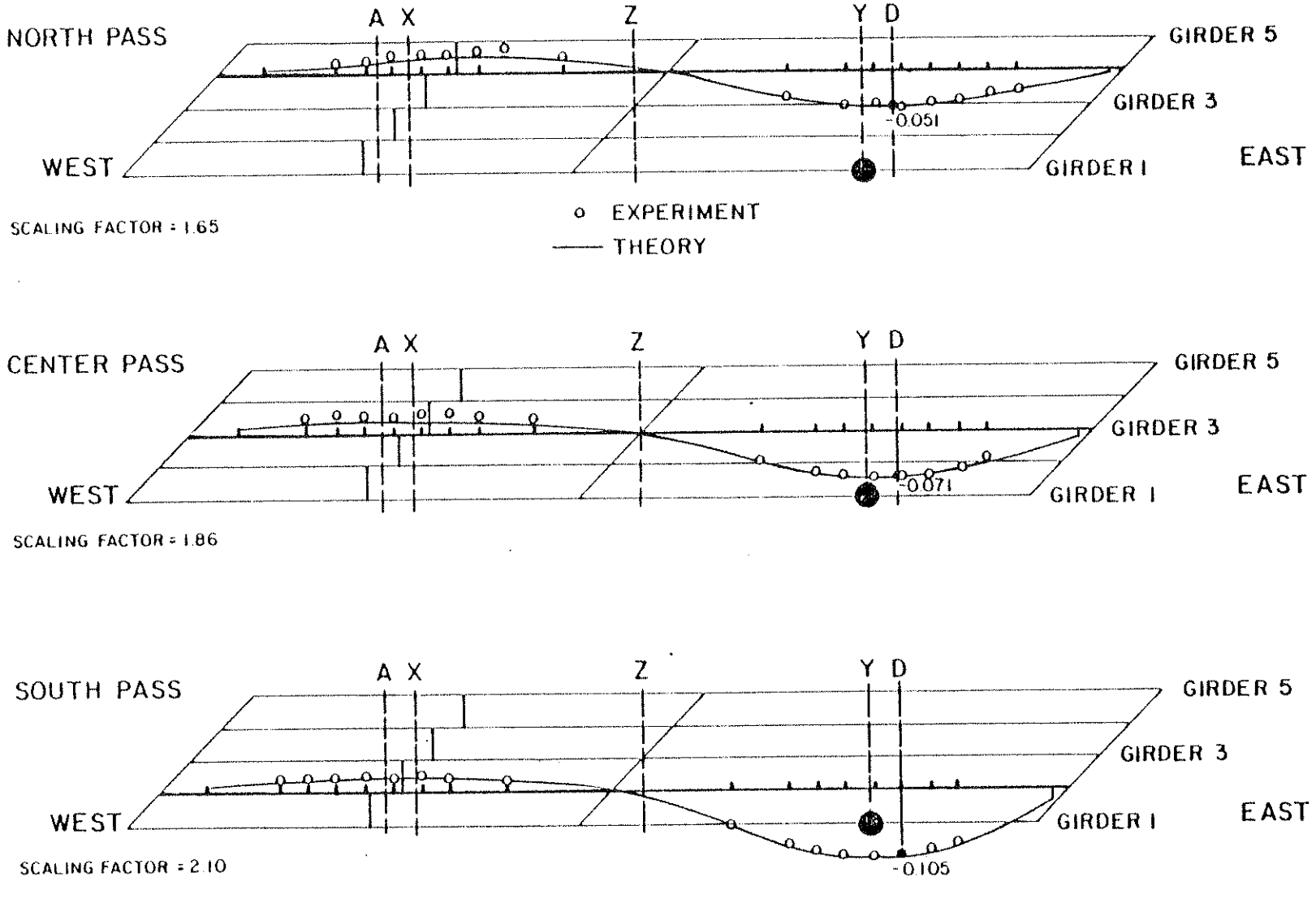

FIG. 6.38 INFLUENCE LINES FOR VERTICAL DEFLECTION (INCHES) AT IY UNDER MOVING FORK LIFT TRUCK LOAD

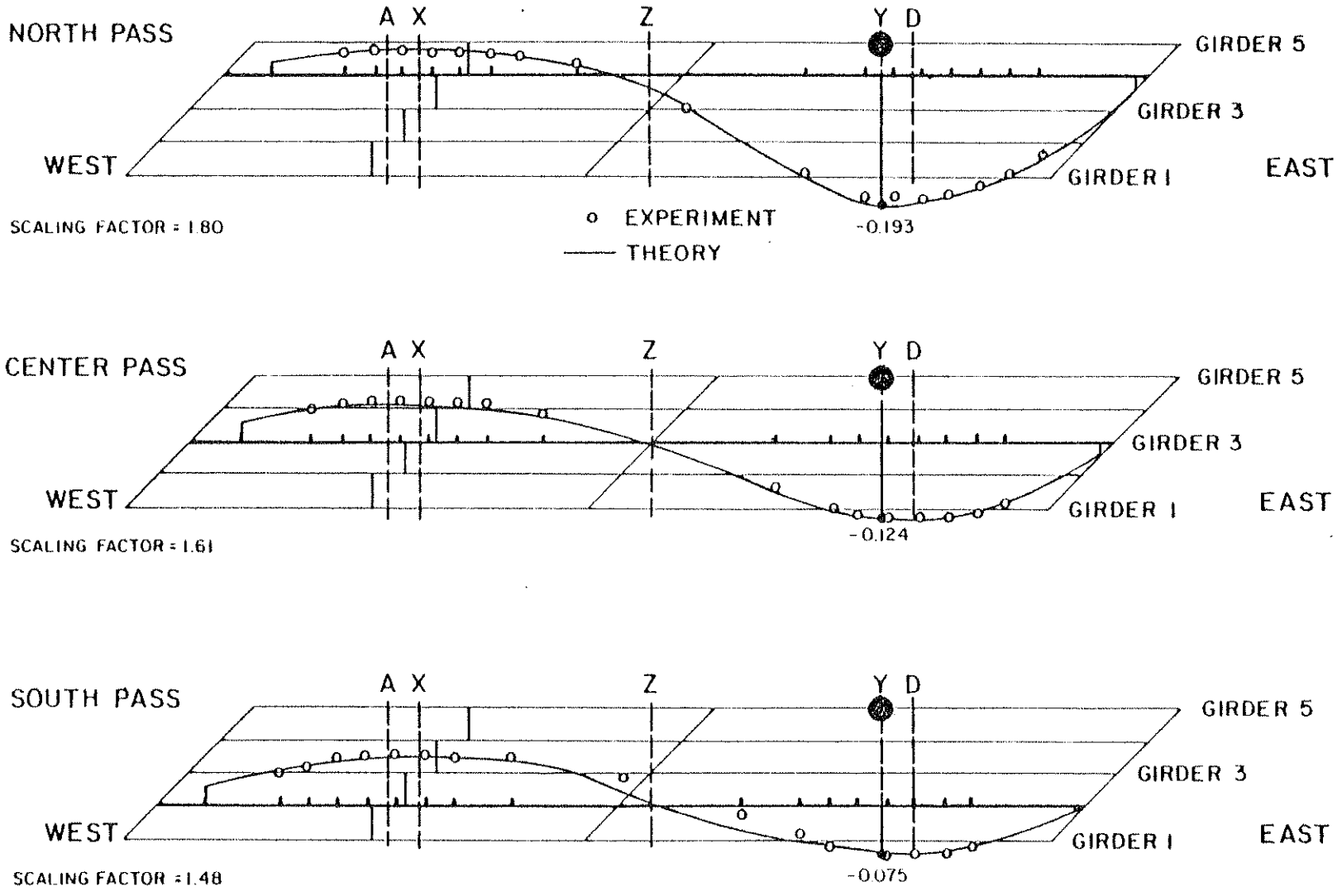

FIG. 6.39 INFLUENCE LINES FOR VERTICAL DEFLECTION (INCHES) AT 5Y UNDER MOVING FORK LIFT TRUCK LOAD

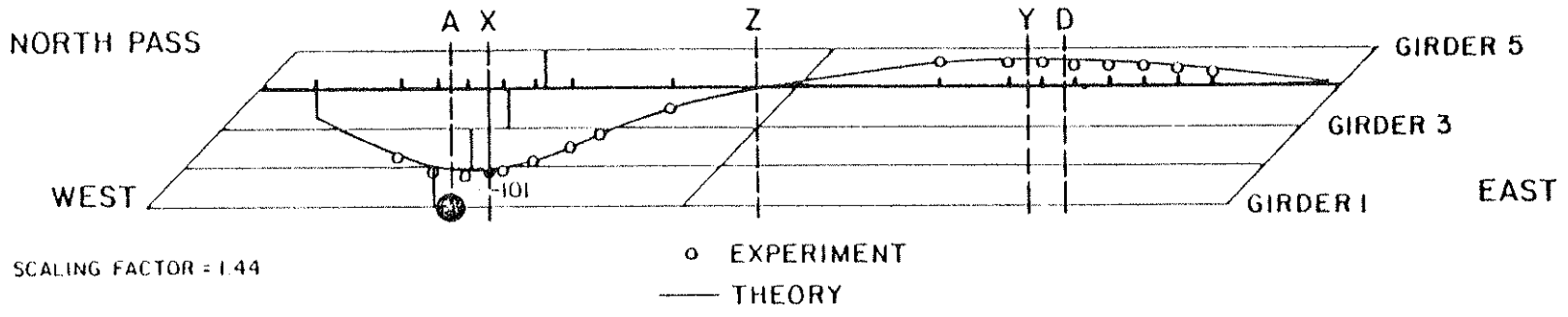

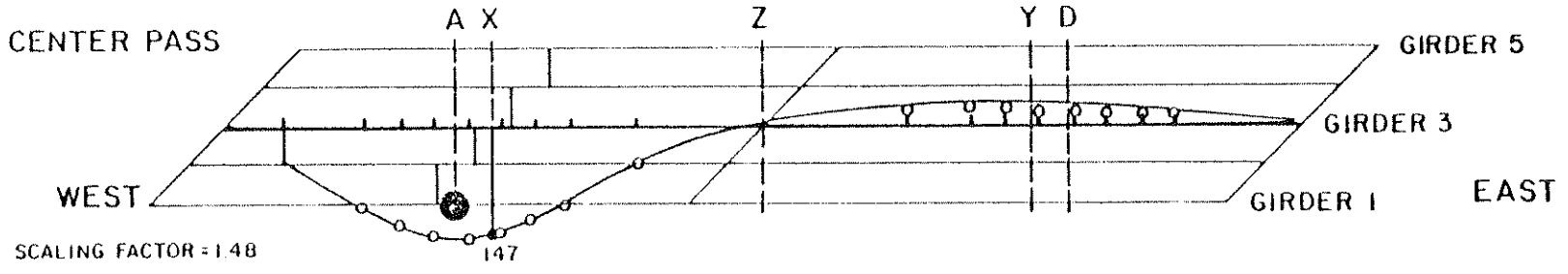

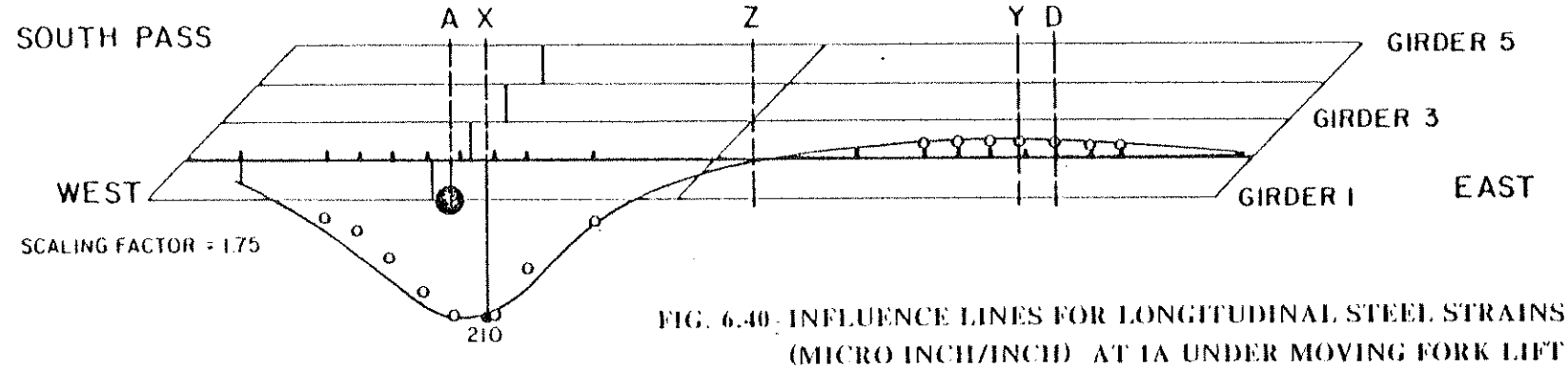

FIG. 6.40 INFLUENCE LINES FOR LONGITUDINAL STEEL STRAINS (MICRO INCH/INCH) AT 1A UNDER MOVING FORK LIFT TRUCK LOAD

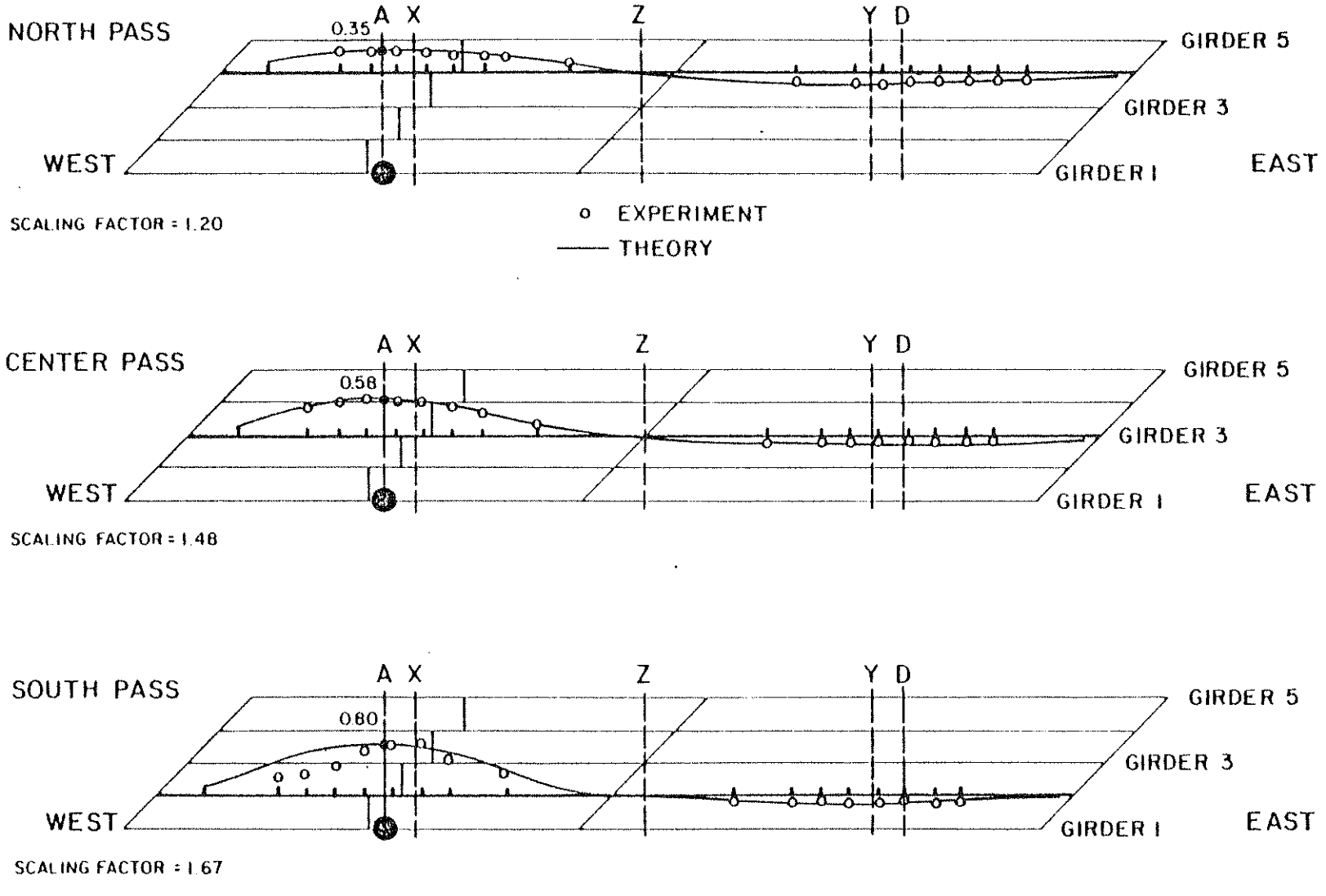

FIG. 6.41 INFLUENCE LINES FOR LONGITUDINAL CONCRETE STRAINS (MICRO INCH/INCH) AT 1A UNDER MOVING FORK LIFT TRUCK LOAD

the experimental influence ordinates are plotted for the center of gravity of the fork lift truck at the given position on the bridge. Theoretical values have been scaled so that the experimental and theoretical ordinates at a selected location are identical. In this way a comparison between the shapes of the experimental and theoretical influence lines can be made directly. The scaling factors and the location of the reference values as well as the ordinates are given in Figs. 6.32 to 6.41. The scaling factor equals the ratio of the experimental to theoretical value of the reference location.

For the total vertical end reaction excellent agreement exists between theory and experiment as can be seen in Fig. 6.32 and 6.33. The influence lines for the total end moments are given in Fig. 6.34 and 6.35. The high scaling factors as well as differences in the shape of experimental and theoretical curves show the difficulty of obtaining exact influence lines for the total end moments which are dependent on the distribution of the 5 vertical reactions along each end abutment. However, general tendencies encountered also for single midspan point loads can be extracted. For example, the change in sign of the end moment for loads shifting transversely across the bridge can be observed in Fig. 6.34 and 6.35. Since this end moment is primarily responsible for the reduction of the total midspan and center support moment in a skew bridge as compared to a straight box girder bridge, Fig. 6.34 and 6.35 can be used to determine for which load positions a beneficial effect of the end moment can be expected.

Influence lines for vertical deflections at 1X, 5X, 1Y and 5Y are shown in Fig. 6.36 to 6.39 respectively. Again excellent

agreement in the shape of theoretical and experimental influence lines can be noticed. The high scaling factors used for the theoretical values are due to the fact that the theoretical analysis was carried out using an uncracked linear elastic model which significantly underestimates the actual deflections occuring in a cracked reinforced concrete structure.

Finally a representative set of influence lines for strains at location 1A is given in Fig. 6.40 and 6.41. While the agreement between the shape of the theoretical and experimental influence lines show slight differences in the direct vicinity of the influence location 1A, excellent agreement can be observed for the rest of the bridge structure.

In general the shapes of influence lines obtained by the theoretical analysis using CELL, based on an uncracked homogeneous cross-section, predict the shape of the influence lines found from experiment quite satisfactorily. The amount of cracking in the model at specific locations can be accounted for by using scaling factors as shown in Figs. 6.32 to 6.41 for the theoretical influence ordinates.

6.5 Comparison of Results for Straight, Curved and Skew Bridge Models

The influence of skewness in the skew multicell box girder bridge model can best be seen by comparison with the similar straight bridge model [1,2,3] and curved bridge model [4,5,6] tested earlier. In this section, a comparison will, in general, only be made of the experimental results for the straight, curved and skew bridge models. Comparisons of theoretical results have already been made and discussed in Chapter 3.

6.5.1 Reactions (Straight, Curved and Skew Bridge)

A comparison of experimental reactions under point loads is given in Table 6.12. The total vertical reactions R_W, R_F and R_E change only very insignificantly for point loads moving transversely across the straight or curved bridge. The skew bridge, however, shows significant changes in the vertical reactions depending on the transverse positioning of the load. While for load cases where the acute side of a span is loaded the adjacent end reaction is smaller than for the corresponding straight and curved bridge cases, this reaction increases to a value much larger than for the straight and curved bridge models as the loads shift from the acute to the obtuse side of the skew span. For the load cases where only the center girder 3 is loaded, the skew bridge features slightly higher end reactions and slightly lower vertical center-bent reactions than the curved or straight bridge. In addition to this, however, a significant negative end moment can also be noted for the skew bridge which decreases the total positive midspan moment. This negative end moment increases in magnitude as the loads move towards the obtuse side of the span, but decreases and even changes sign for loads moving towards the acute side of the span. Note that there is no end moment for the simply supported straight or curved bridges and that the end moment for the skew bridge is only introduced by the skewness of the simply supported end abutment.

The torque at the end abutments of the skew bridge has the same magnitude but opposite sign as the end moment and is smaller for loads on the acute side but larger for loads on the obtuse side of the skew span than its corresponding straight or curved bridge cases.

TABLE 6.12 COMPARISON OF EXPERIMENTAL REACTIONS (KIPS & FT-KIPS) FOR STRAIGHT, CURVED AND SKEW BRIDGE MODELS DUE TO 100 KIP (445 kN) POINT LOADS.

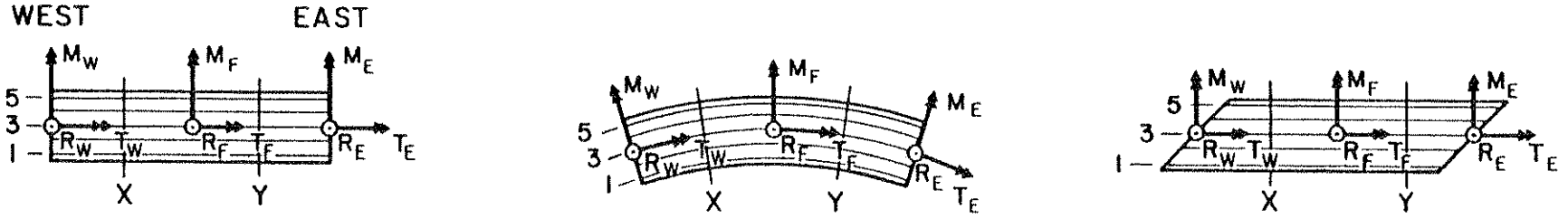

LOAD CASE	BRIDGE MODELS	REACTIONS (KIPS AND FT-KIPS)										LOAD (KIPS)		
		WEST END			CENTER FOOTING			EAST END			TOTAL	SEC X	SEC Y	TOTAL
		R_W	M_W	T_W	R_F	M_F	T_F	R_E	M_E	T_E	R	P_X	P_Y	P
1X	STRAIGHT	38.0	0	-300	69.0	135	- 66	-8.3	0	-122	98.7	-100.0	- 0	-100.0
	CURVED	41.2	0	-280	68.1	24	- 78	-7.1	0	- 96	102.2	-100.0	- 0.1	- 99.9
	SKEW	33.6	181	-181	74.0	133	-216	-6.0	126	-126	101.6	-100.0	- 0.2	- 99.8
1Y	STRAIGHT	-8.0	0	- 86	70.1	-126	- 69	38.3	0	-343	100.5	0	-100.0	-100.0
	CURVED	-7.2	0	-110	68.9	- 15	- 84	39.5	0	-256	101.2	0.3	-100.0	-100.3
	SKEW	-8.7	72	- 72	58.0	- 78	- 58	52.8	390	-390	102.2	0	-100.0	-100.0
1X+1Y	STRAIGHT	30.1	0	-374	139.2	14	-140	30.4	0	-458	199.7	-100.0	- 99.7	-199.7
	CURVED	35.5	0	-381	132.5	- 54	-149	33.2	0	-346	201.3	-100.0	- 99.1	-199.1
	SKEW	24.5	244	-244	132.3	58	-277	47.2	505	-505	204.0	- 99.5	-100.5	-200.0
3X	STRAIGHT	38.1	0	5	70.3	135	3	-8.3	0	- 2	100.1	-100.0	0	-100.0
	CURVED	40.0	0	67	69.7	103	9	-7.2	0	-20	102.5	-100.0	0	-100.0
	SKEW	42.2	- 78	78	69.1	107	- 65	-8.1	10	-10	103.3	-100.0	0	-100.0
3Y	STRAIGHT	-8.0	0	- 2	70.9	-125	3	38.4	0	2	101.3	0	-100.0	-100.0
	CURVED	-8.0	0	-27	71.3	-146	- 3	36.1	0	54	99.4	- 0.1	-100.0	- 99.9
	SKEW	-7.3	- 9		69.4	-106	79	41.5	75	- 75	103.6	- 0.1	-100.0	-100.1
3X+3Y	STRAIGHT	29.7	0	2	138.4	9	5	30.5	0	1	198.8	-100.0	-100.2	-200.2
	CURVED	31.3	0	37	141.1	72	7	30.1	0	35	202.4	-100.0	- 99.7	-199.7
	SKEW	36.0	- 41	99	137.6	3	9	35.9	85	- 85	209.5	- 99.3	-100.7	-200.0

1 KIP = 4.448 kN
1 FT = 0.305 m

TABLE 6.12 (CONT.) COMPARISON OF EXPERIMENTAL REACTIONS (KIPS & FT-KIPS) FOR STRAIGHT, CURVED AND SKEW BRIDGE MODELS DUE TO 100 KIP (445 kN) POINT LOADS.

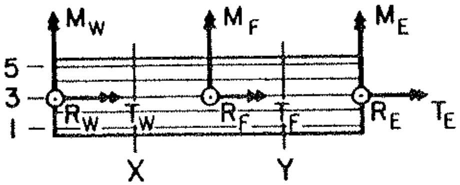

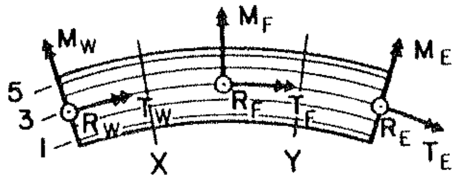

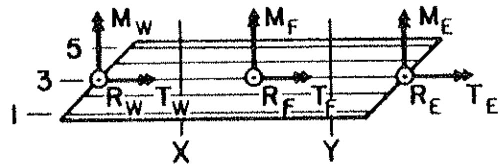

LOAD CASE	BRIDGE MODELS	REACTIONS (KIPS AND FT-KIPS)										LOAD (KIPS)		
		WEST END			CENTER FOOTING			EAST END			TOTAL	SEC X	SEC Y	TOTAL
		R_W	M_W	T_W	R_F	M_F	T_F	R_E	M_E	T_E	R	P_X	P_Y	P
5X	STRAIGHT	37.9	0	306	69.5	128	-72	-8.3	0	116	99.1	-100.0	0	-100.0
	CURVED	36.4	0	400	76.0	145	74	-9.7	0	45	107.6	-100.0	0	-100.0
	SKEW	57.0	-373	373	62.3	91	68	-9.1	-83	83	105.1	-100.0	0	-100.0
5Y	STRAIGHT	-8.4	0	79	69.7	-131	69	39.0	0	347	100.2	0	-100.0	100.0
	CURVED	-9.2	0	59	72.2	-130	98	36.6	0	366	99.6	-0.1	-100.0	100.1
	SKEW	-6.2	-95	95	78.6	-142	230	33.0	-203	203	105.4	-0.1	-100.0	-100.1
5X+5Y	STRAIGHT	30.3	0	389	140.2	-2	144	31.5	0	468	201.9	-100.0	-101.3	-201.3
	CURVED	28.7	0	461	151.4	-31	162	27.1	0	417	207.1	-100.0	-103.5	-203.5
	SKEW	47.8	-475	475	190.1	-49	300	24.0	-277	277	211.9	-100.5	-97.5	-200.0

1 KIP = 4.448 kN
1 FT = 0.305 m

6.5.2 Deflections (Straight, Curved and Skew Bridge)

The transverse distribution of experimental deflections at midspan sections X and Y for nine point load cases is given in Figs. 6.42 and 6.43. No modifications have been made in the plotted experimental results to reflect the fact that the modulus of elasticity of the concrete was slightly different for the straight, curved and skew bridge models.

Considering the deflection under the application point of the load, Figs. 6.42 and 6.43 show that the skew bridge features the highest deflections at the acute side of a span and the lowest deflections of all three bridge types at the obtuse side of the span.

The influence of the midspan diaphragm in Span I can also be seen by comparing the deflections at section X and section Y. While the transverse distribution of deflections for all three bridge types shows an almost straight line in the diaphragmed Span I at section X, the undiaphragmed Span II features larger changes in displacement gradients at section Y.

6.5.3 Moments (Straight, Curved and Skew Bridge)

Table 6.13 gives a comparison of experimental total maximum moments at the instrumented midspan sections A and D for single point loads normalized to 100 kips (445 kN). Moments based on external reactions, as well as on internal forces, are presented.

While the total moments for the straight and curved bridge change only a little for point loads moving from girder 1 to girder 5, the skew bridge total midspan moments vary significantly. For loads on the acute side of the skew span, the total moments are much higher, and

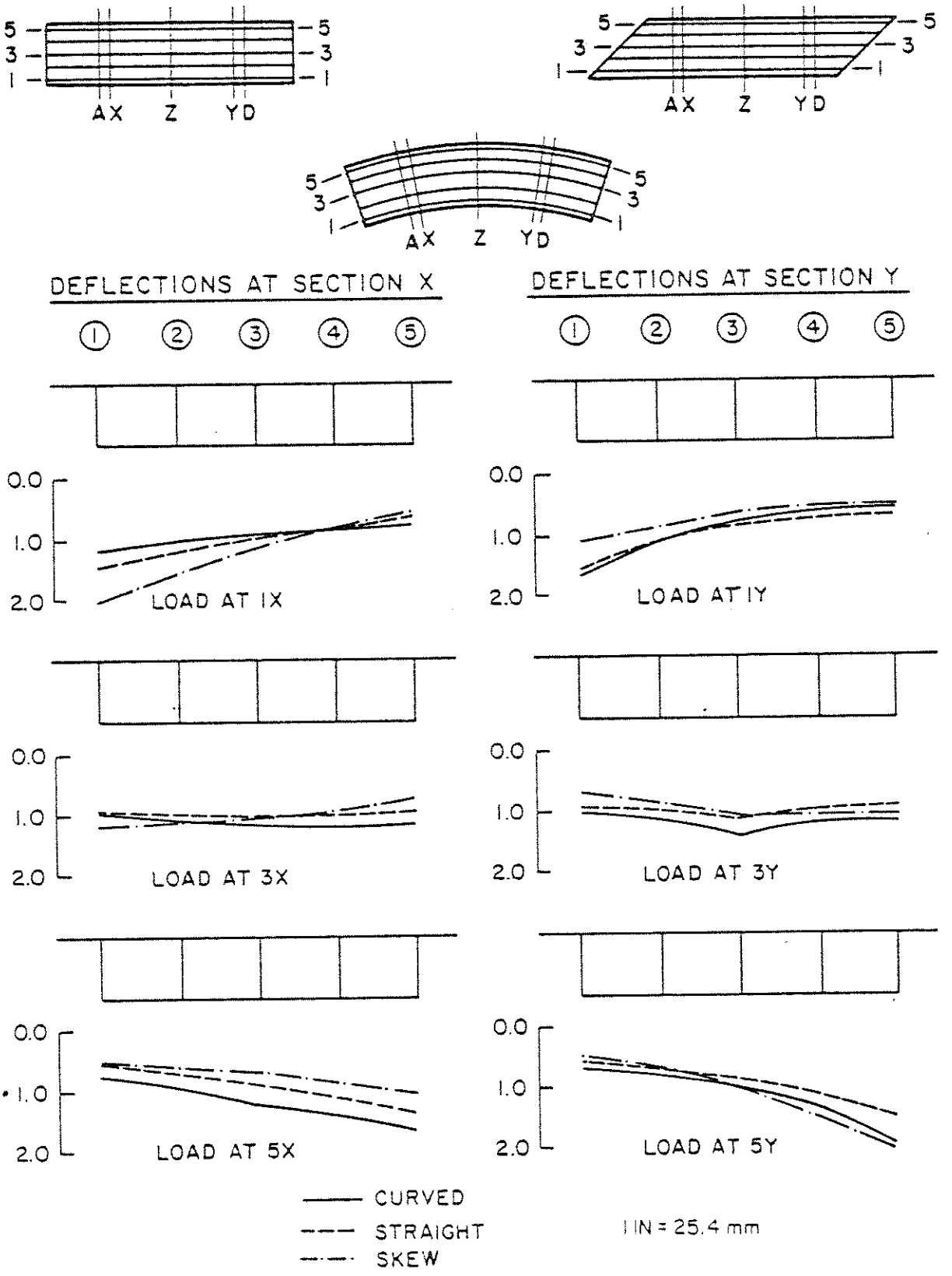

FIG. 6.42 EXPERIMENTAL VERTICAL DEFLECTIONS (INCHES) AT TRANSVERSE SECTIONS X AND Y FOR STRAIGHT, CURVED AND SKEW BRIDGE MODELS FOR 100 KIP (445 kN) POINT LOADS AT 1X, 3X, 5X, 1Y, 3Y, 5Y

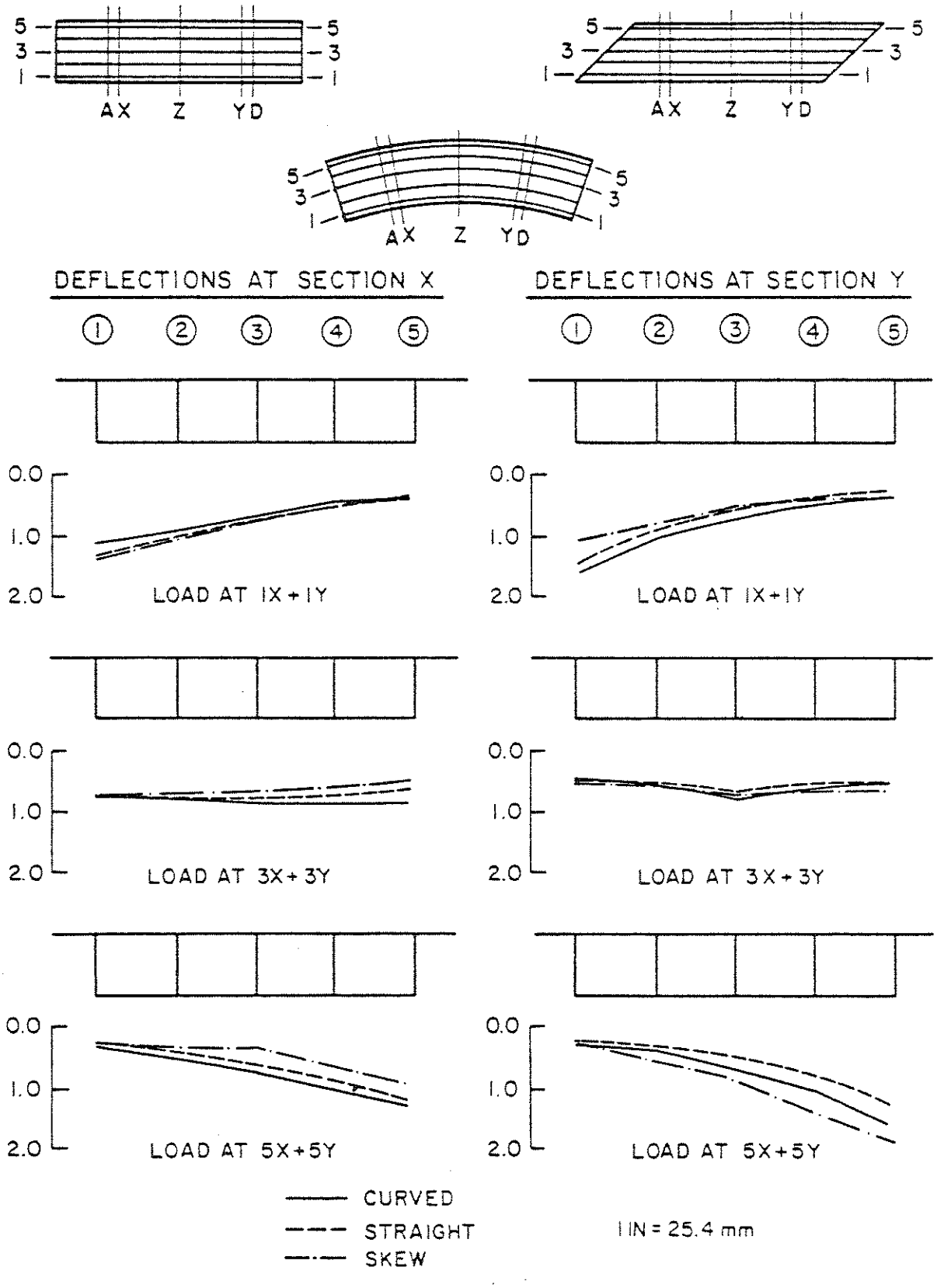

FIG. 6.43 EXPERIMENTAL VERTICAL DEFLECTIONS (INCHES) AT TRANSVERSE SECTIONS X AND Y FOR STRAIGHT, CURVED AND SKEW BRIDGE MODELS FOR 100 KIP (445 kN) POINT LOADS AT 1X + 1Y, 3X + 3Y, 5X + 5Y

TABLE 6.13 COMPARISON OF EXPERIMENTAL MAXIMUM TOTAL MOMENTS (FT-KIPS) AT A SECTION FOR STRAIGHT, CURVED AND SKEW BRIDGE MODELS DUE TO 100 KIP (445 kN) POINT LOADS.

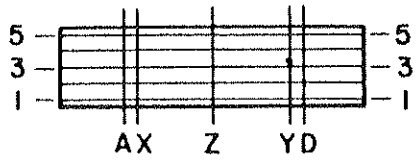

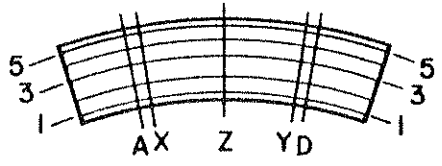

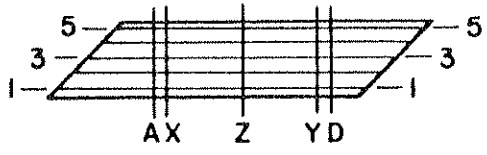

100 K LOAD AT	BASED ON EXTERNAL REACTIONS			BASED ON INTERNAL FORCES			100 K LOAD AT	BASED ON EXTERNAL REACTIONS			BASED ON INTERNAL FORCES		
	STR	CUR	SKW	STR	CUR	SKW		STR	CUR	SKW	STR	CUR	SKW
	MAXIMUM MOMENT AT SECTION A							MAXIMUM MOMENT AT SECTION D					
1X	546	551	694	524	515	693	1Y	553	531	421	572	474	420
2X	547	573	629	525	526	627	2Y	544	526	493	586	536	492
3X	550	585	562	535	538	561	3Y	553	527	562	574	554	561
4X	547	588	493	532	544	692	4Y	558	534	629	581	572	627
5X	546	580	421	542	586	420	5Y	562	578	693	598	563	692

1 FT-KIP = 1.356 kN-m

for loads on the obtuse side of the span much lower than for the straight or curved bridges. This is especially important for the positioning of high concentrated live loads like the construction vehicle used in this investigation.

A comparison of the transverse distribution of maximum total positive moments for the straight, curved and skew bridge models is given in Table 6.14. While the straight and curved bridge distributions of maximum total moments to individual girders are almost identical at Section A for the diaphragmed Span I and only slightly different at Section D for the undiaphragmed Span II, they differ from those of the skew bridge which shows larger percentages being taken by the exterior girders. This is especially true in the vicinity of location 1A near the staggered midspan diaphragm in the skew bridge.

6.5.4 Maximum Strains and Stresses (Straight, Curved and Skew Bridge)

A final comparison of results for the straight, curved and skew bridge models is made in Table 6.15 for maximum live load experimental strains and stresses under truck and construction vehicle loadings described in Section 6.3. Strains are the maximum values recorded at any point under the loadings shown. Concrete stresses are obtained by multiplying the strains by the appropriate modulus of elasticity for the concrete at the instrumented location for straight, curved and skew bridges, respectively. Steel stresses are obtained by multiplying strains in the straight, curved and skew bridge models by 29.0, 27.5 and 27.7×10^6 psi (2.0, 1.9 and 1.9×10^5 MPa), respectively, which were the average moduli of elasticity of no. 4 steel reinforcement bars in the three bridges.

TABLE 6.14 COMPARISON OF EXPERIMENTAL PERCENTAGE DISTRIBUTION OF TOTAL MAXIMUM MOMENTS AT A SECTION FOR STRAIGHT, CURVED AND SKEW BRIDGE MODELS DUE TO 100 KIPS (445 kN) POINT LOADS.

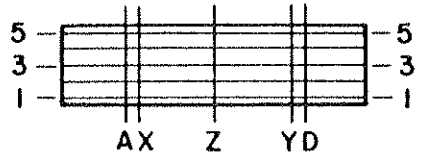

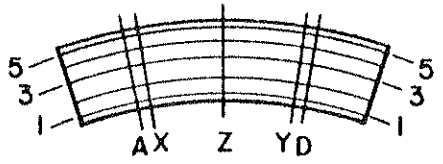

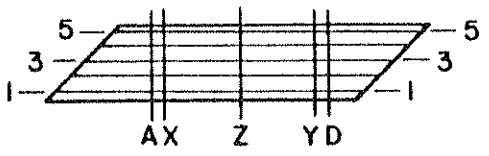

100 K LOAD AT	STRAIGHT BRIDGE % TO GIRDERS					CURVED BRIDGE % TO GIRDERS					SKEW BRIDGE % TO GIRDERS				
	1	2	3	4	5	1	2	3	4	5	1	2	3	4	5
	DISTRIBUTION OF MAXIMUM MOMENT AT SECTION A														
1X	21	24	23	21	12	21	24	21	21	13	26	24	22	13	11
2X	18	23	23	22	13	18	23	22	22	14	25	21	23	14	12
3X	17	22	23	23	15	16	22	23	24	16	25	22	21	20	19
4X	14	20	23	24	18	15	20	22	25	17	21	19	20	27	14
5X	13	18	23	26	20	14	19	22	25	19	20	17	19	25	20
	DISTRIBUTION OF MAXIMUM MOMENT AT SECTION D														
1Y	16	29	23	20	12	20	30	20	18	13	27	27	18	15	12
2Y	16	25	27	21	11	17	26	22	21	14	23	25	21	17	14
3Y	13	25	24	25	13	13	24	23	24	17	17	24	22	20	17
4Y	11	22	26	25	16	11	20	23	27	20	15	20	21	22	22
5Y	14	18	23	28	17	10	19	21	29	21	15	20	20	23	23

TABLE 6.15 COMPARISON OF MAXIMUM LIVE LOAD EXPERIMENTAL STRAINS (MICRO INCH/INCH) AND STRESS (PSI) FOR STRAIGHT, CURVED AND SKEW BRIDGE MODELS UNDER TRUCK AND CONSTRUCTION VEHICLE LOADS.

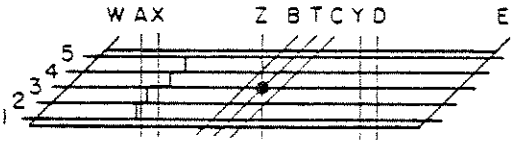

MATERIAL	SEC.	TWO LANE TRUCK LOADING			THREE LANE TRUCK LOADING			CONSTRUCTION VEHICLE LOADING		
		STR	CUR	SKW	STR	CUR	SKW	STR	CUR	SKW
		EXPERIMENTAL STRAINS (MICRO INCH/INCH)								
CONCRETE	A	59	110	116	72	138	175	135	191	249
	B	81	67	103	123	99	145	176	154	175
	C	83	70	88	119	110	129	177	155	225
	D	65	83	67	100	127	98	115	178	230
STEEL	A	276	221	233	344	306	365	586	565	527
	B	128	123	124	202	195	185	352	303	249
	C	133	125	123	201	200	183	324	324	338
	D	229	197	174	369	290	340	448	450	519
		EXPERIMENTAL STRESS (PSI)								
CONCRETE	A	207	297	348	276	373	525	516	516	747
	B	235	178	309	351	263	435	510	408	525
	C	241	186	264	346	292	387	514	411	675
	D	249	254	201	383	387	294	440	543	690
STEEL	A	8030	6080	6450	9980	8420	10100	17000	15500	14600
	B	3710	3380	3440	5850	5360	5130	10200	8330	6900
	C	3860	3440	3410	5830	5500	5070	9380	8910	9360
	D	6690	5420	4820	10700	7980	9420	13000	12400	14400

1 PSI = 0.006895 MPa

Table 6.15 shows that live load concrete strains and stresses are relatively low for all three bridge types. The order of magnitude for concrete and steel strains and stresses is about the same for straight, curved and skew bridge models, with the concrete stresses in the skew bridge being slightly higher at almost all instrumented sections.

6.6 Summary

A detailed discussion of the results for working stress loads has been presented. The most important conclusions under various categories are summarized below.

1. Comparison of theoretical results from CELL with experimental results.
   a. The total reactions at the east, center and west supports are accurately predicted by theory.
   b. Total end moments arising from the skewness of the end abutment can be predicted satisfactorily by the CELL program.
   c. Theory predicts the distribution and magnitude of deflections quite well (within 10 to 20%) if theoretical values based on an uncracked section are multiplied by a factor of 1.5 to account for cracking at this stress level.
   d. While theory predicts the general distribution of strains, significant differences can exist with experimental values at certain points.

e. Maximum total midspan moments as computed either from external reactions or from internal forces can be adequately predicted by theory for design purposes.

f. The transverse distribution of these moments to individual girders can be predicted with sufficient accuracy for the undiaphragmed span, section D, for almost all the load cases considered. In the diaphragmed span, the same range of accuracy applies to the interior girders, while the exterior girders show larger discrepancies. Experimental values for girder 5 on the obtuse side of the span are generally slightly smaller than those predicted by theory, while girder 1 on the acute side of the span features consistently higher values. This may be caused by the close proximity of the staggered midspan diaphragm to the instrumented section A at the acute side of the span which makes it difficult to monitor the complex structural behavior of the skew bridge model in this vicinity, both theoretically and experimentally.

2. Effect of torsional restraint.

a. Vertical reactions at the end supports are virtually not influenced by the torsional restraint of the center bent.

b. End moments and torques decrease due to additional center bent supports at girders 1 and 5.

c. High strains and deflections at the acute side of a span are decreased due to the torsional center bent restraint.

3. From the study of 19 different midspan point load combinations, it can be concluded that the total moment at a midspan section depends strongly on the transverse positioning of the loads. Loads on the obtuse side of a span benefit from the negative end moment introduced by the skewness of the end abutment and result in low positive design moments, while loads on the acute side of the span create a positive end moment which results in higher positive design moments.

4. The above response is especially important for the positioning of heavy concentrated loads, such as the construction vehicle loading. A construction vehicle on the acute side of a span also yields the highest deflection to span ratio for live loads of 1/580 which is still quite small.

5. The general response of the skew bridge model was different from the straight or curved bridge model in that the transverse positioning of concentrated live loads affects the design quantities like moments and deflections considerably. Load distribution factors for a straight bridge which assume a uniformly stressed cross-section no longer apply to the skew bridge.

7. RESPONSE AT OVERLOAD STRESS LEVELS

7.1 General Remarks

As described in Vol. I, the experimental program was divided into two parts to study the response of the bridge under the following loadings:

Part 1 - Dead load and working loads

Part 2 - Overloads and loading to failure

Responses to dead load and working loads have been discussed in Chapters 5 and 6. Response to overloads will be discussed in this chapter and loading to failure will be discussed in Vol. III of the present sequence of research reports.

The overload sequence was divided into several phases, in each of which initial conditioning loads were applied to create total maximum tensile stresses in the reinforcement of 40, 50 and 60 ksi. Each of these was then followed by a detailed sequence of 11 point load cases, having magnitudes in all cases identical to those used after the 30 ksi working stress conditioning load. These point load magnitudes were chosen to produce total maximum stresses or the order of 24 to 30 ksi in the reinforcement. In this manner, the response of the bridge at working stress level could be studied assuming it had been subjected to an overload of increasing magnitude, which would accentuate the maximum amount of cracking, deflection and stress in the bridge.

Of particular interest was how much, if any, would these overloads change the distribution and magnitude of reactions, deflections,

strains, total moments at a section and percentage distribution of the total moment at a section to each girder. Of additional interest was the degree of linearity of response and the change in stiffness of the bridge during and after each of the conditioning overloads.

In this chapter the results for the above will be discussed and compared for the following cases: (1) during each of the conditioning loads to bring the stress level to 24, 30, 40, 50 and 60 ksi; and (2) for a working stress point load at 1Y or 5Y after each of the conditioning loads to bring the stress level to 30, 40, 50 and 60 ksi was applied.

7.2 Results for Conditioning Loads

Detailed tabulations of theoretical and experimental results related to reactions, deflections, strains and moments for each of the conditioning loads are given in Vol. IV. Conditioning loads were obtained by applying equal loads over each of the five girders at both midspan sections X and Y. All theoretical values obtained from the computer analysis using the CELL program are for total loads of 100 kips (445 kN) per span. Experimental values have been normalized to an average total load of 100 kips (445 kN) at midspan sections X and Y.

During each of the conditioning load cases a specific sequence of loading as follows was used.

(1) Take sustained dead load readings relative to the absolute zero readings.

(2) Take zero readings on all gages and meters.

(3) Apply load in several increments to reach the full conditioning load and take readings after each increment.

(4) Remove load in several increments to reach zero load and take readings after each increment.

(5) Cycle eight times from zero to full load to zero.

(6) Take zero readings on all gages and meters.

(7) Apply full load in one increment and take readings.

(8) Unload to zero in one increment and take readings.

(9) Take sustained dead load readings relative to absolute zero readings.

A series of graphs is given in Figs. 7.1 to 7.9 for the total vertical and moment reactions at the end supports, deflections at 1Y and 5Y, and steel and concrete strains produced by the conditioning loads. Figures 7.1, 7.4, 7.6 and 7.7 depict for each conditioning load separately the response for the initial complete load cycle (zero, full load, zero) as dotted lines, together with the response during the final load cycles as solid lines. These plots enable one to study the linearity of response and the permanent sets encountered in each conditioning load sequence. Figures 7.2 and 7.3 superimpose on a single plot the unnormalized response for the final load cycle only, for all conditioning loads. The same procedure is used also for Figs. 7.5, 7.8 and 7.9, where this information is given for both inner girder 1 and outer girder 5. These plots permit an evaluation of

TABLE 7.1 COMPARISON OF EXPERIMENTAL AND THEORETICAL REACTIONS (KIPS AND FT-KIPS) FOR CONDITIONING LOADS.

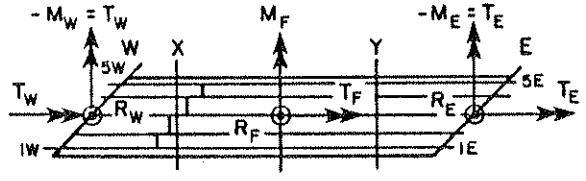

LOAD CASE	SOLUTION	REACTION (KIPS AND FT-KIPS)									TOTAL	LOAD (KIPS)		
		WEST END			CENTER FOOTING			EAST END			TOTAL	SEC X	SEC Y	TOTAL
		R_W	M_W	T_W	R_F	M_F	T_F	R_E	M_E	T_E	R	P_X	P_Y	P
ALL CASES	THEORY	35.6	-122	122	128.9	0	0	35.6	122	-122	200.0	-100.0	-100.0	-200.0
24 KSI	EXPER.	36.3	-105	105	135.2	2	5	35.5	104	-104	207.0	-101.5	- 98.5	-200.0
30 KSI	THEORY	35.8	- 86	86	135.0	6	-1	34.9	83	- 83	205.7	-100.0	-100.0	-200.0
40 KSI	EXPER.	34.2	- 65	65	132.5	17	-9	32.5	71	- 71	199.2	-102.5	- 97.5	-200.0
50 KSI	THEORY	34.5	- 71	71	135.4	9	-1	32.9	64	- 64	202.8	-101.1	- 98.9	-200.0
60 KSI	EXPER.	34.3	- 60	69	137.0	10	7	33.6	61	- 61	204.9	- 99.2	-100.8	-200.0

1 KIP = 4.448 kN
1 FT = 0.305 m

change in response to load for increasing values of maximum conditioning load.

7.2.1 Reactions

Table 7.1 gives a comparison of theoretical and experimental reactions for conditioning loads normalized to 100 kips (445 kN) at sections X and Y. One set of theoretical values applies for all conditioning load levels. Table 7.1 shows that for vertical end reactions R_W and R_E experimental values for all conditioning load levels are close to the theoretical reactions. For increasing conditioning load levels it can be observed that the total vertical center footing reaction R_F increases slightly with a corresponding slight decrease in the end vertical end reactions R_W and R_E. The changes, however, are small.

Experimental external end moments and torques are in good agreement with theory as long as the bridge model is in an almost uncracked condition (24 ksi level). Increased cracking in the bridge model due to higher conditioning loads results in a rapid decrease of the external end moment and torque values between the 24 and 30 ksi conditioning loads and then a more gradual change up to the 60 ksi conditioning load. The 60 ksi load case, for example, features experimental end moments which have only half the magnitude of the theoretical end moments obtained for the homogeneous uncracked linear elastic structure. Thus, the theoretical effects of the end moment, due to the skewness of the bridge model, on the total positive midspan moments diminish with increased cracking of the bridge model.

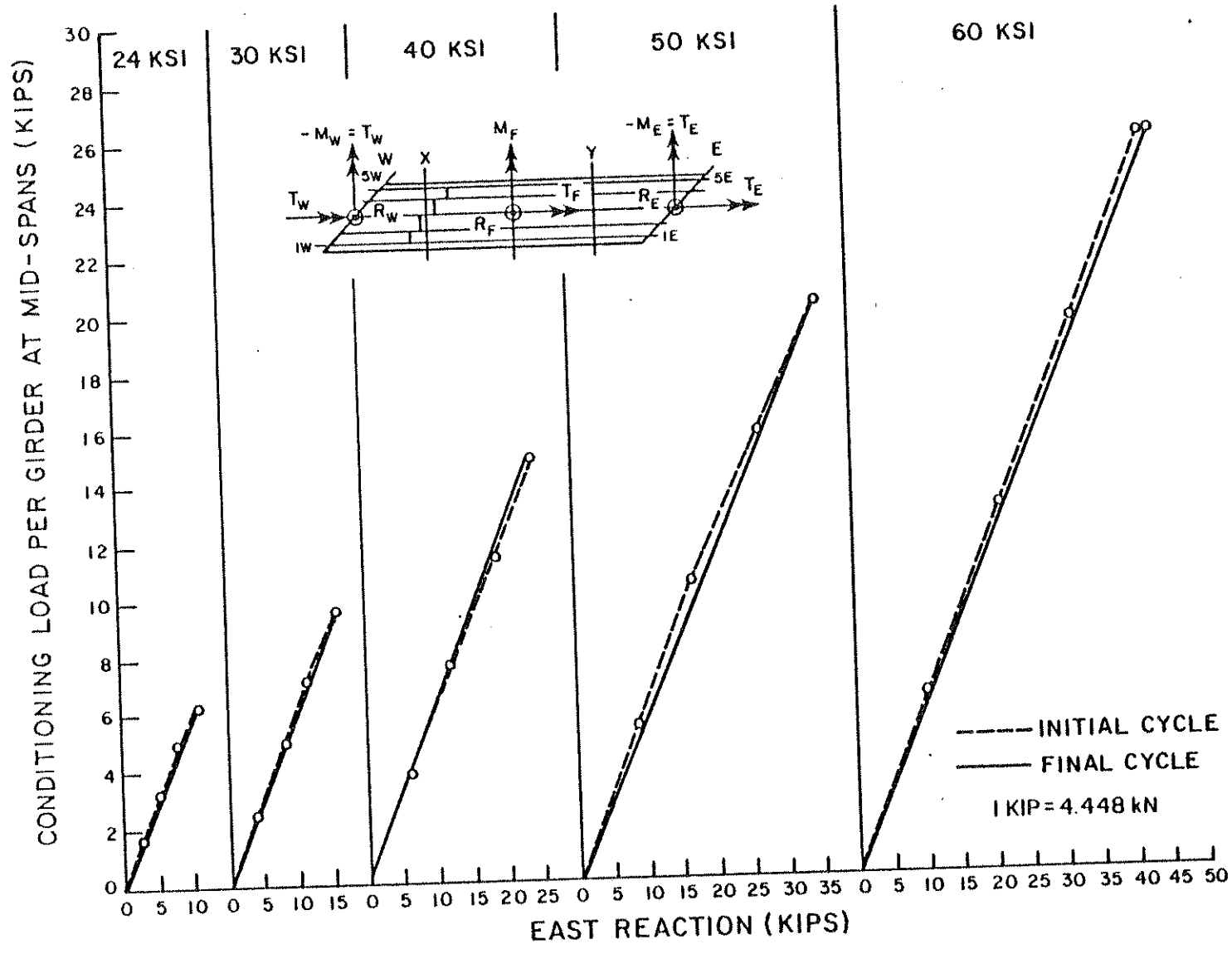

FIG. 7.1 EXPERIMENTAL TOTAL EAST REACTION (KIPS) DURING CONDITIONING LOAD CYCLES

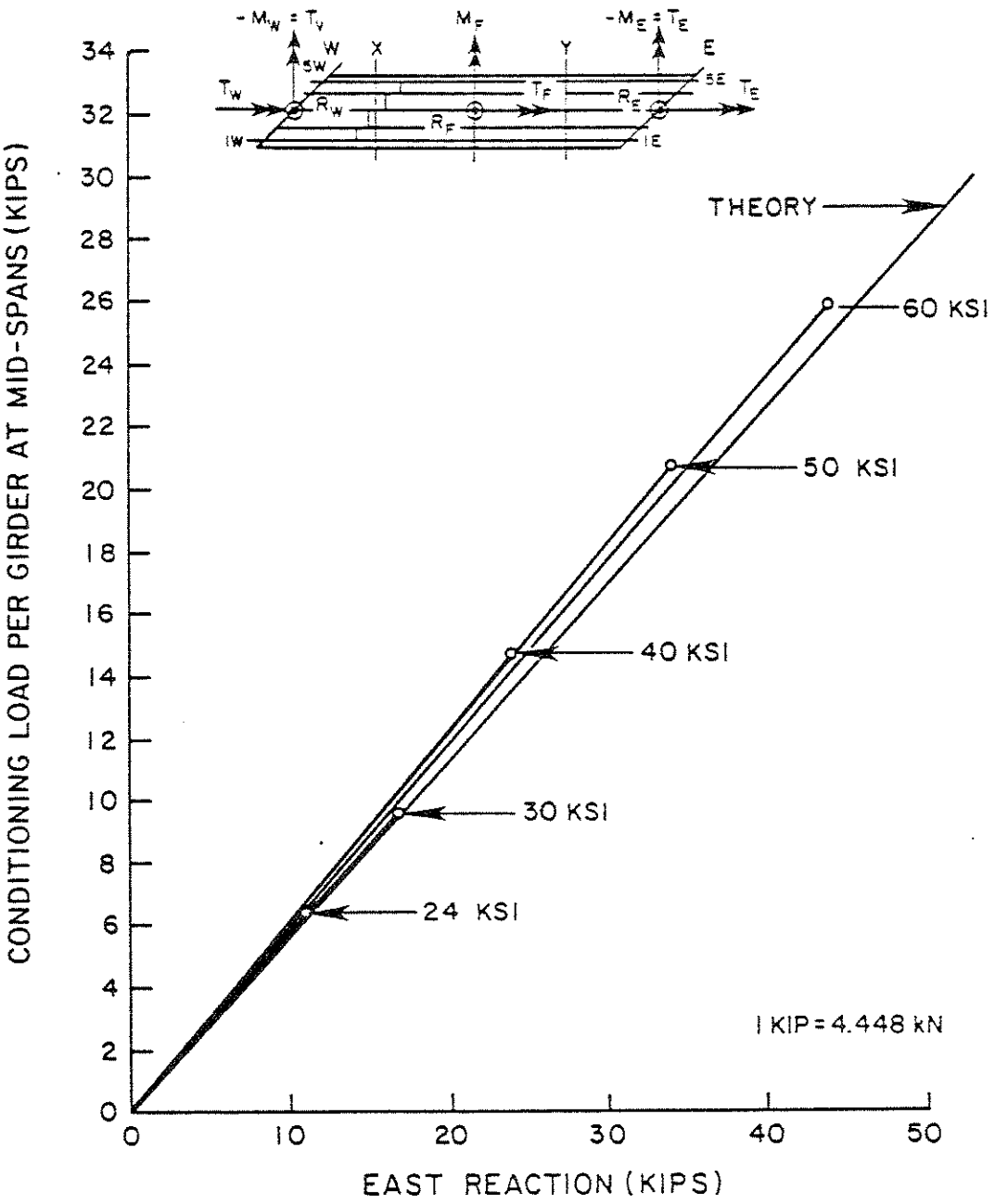

FIG. 7.2 TOTAL VERTICAL EAST REACTION (KIPS) FOR DIFFERENT CONDITIONING LOADS

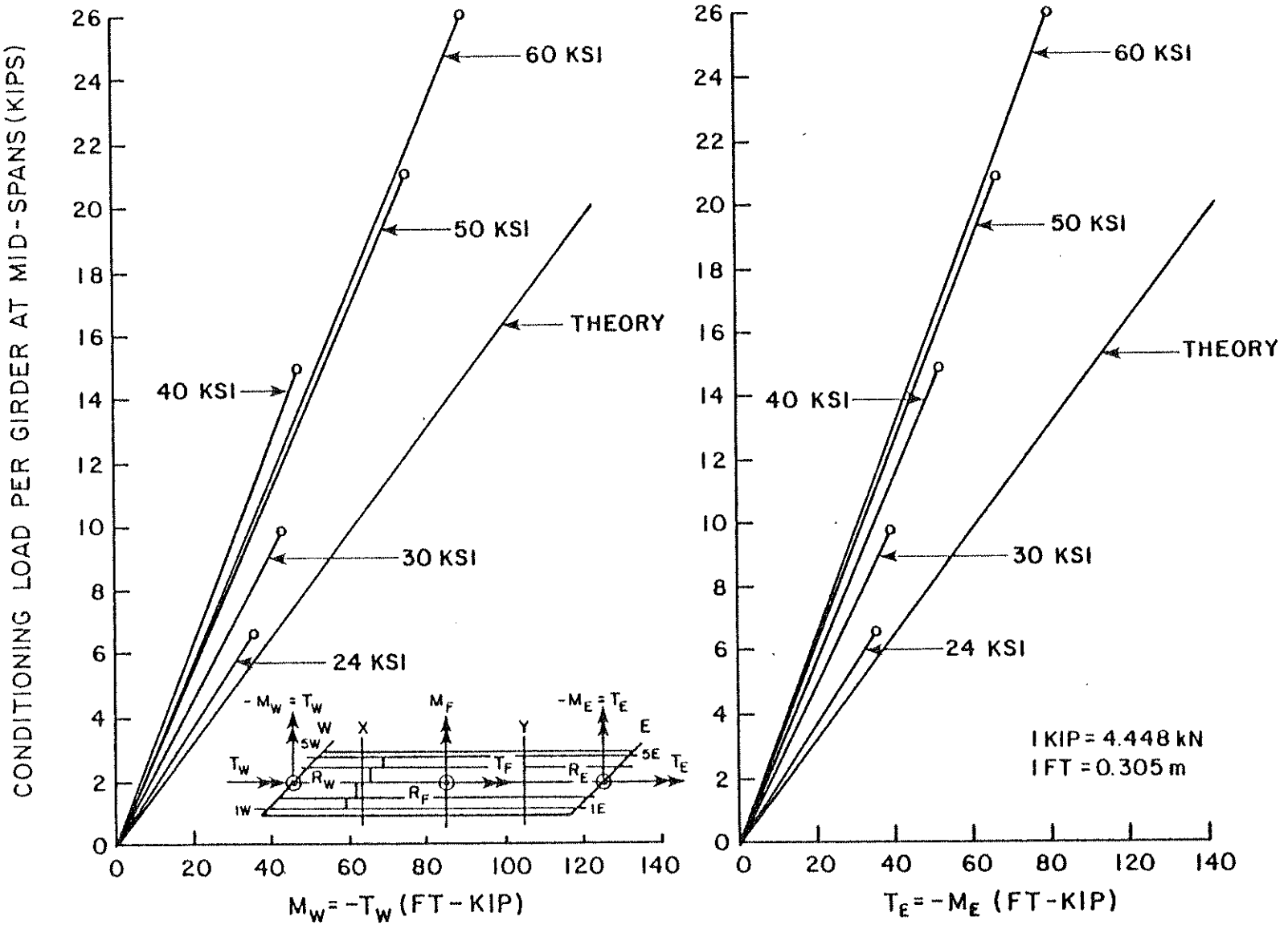

FIG. 7.3 TOTAL WEST AND EAST MOMENTS (FT-KIPS) FOR DIFFERENT CONDITIONING LOADS

Figures 7.1 and 7.2 depict graphically the results for the t tal east reaction in which the values have not been normalized. Figure 7.1 indicates that this reaction is linearly related to load for all load levels and little difference exists between the first and last cycle of loading. Figure 7.2 shows that theory accurately predicts this reaction response and that there is very little change under increasing conditioning load levels.

Figures 7.3 shows the unnormalized external end moments at the east and west end abutments, where the decrease in total end moment and torque with increasing crack development between the 24 and 40 ksi conditioning load levels can be clearly seen.

7.2.2 Deflections at 1Y and 5Y

Figure 7.4 indicates that some residual deflection exists at 5Y after the first cycle of loading in each case due to an increased level of cracking. A comparison of the unloading path during the first cycle with the loading path during the final cycle of loading, indicates that the slopes are almost identical and little additional permanent deflection occurs between the first cycle and the last (tenth) cycle of loading.

Figure 7.5 shows the decrease of structural stiffness (increasing deflections) under increasing conditioning loads due to the advancement of the concrete cracking.

Comparing the experimental values with those from theory based on an uncracked section, one finds similar ratios of experimental to theoretical deflections for girders 1 and 5 on the obtuse and acute side of Span II. These ratios are approximately 1.4, 1.8, 2.2,

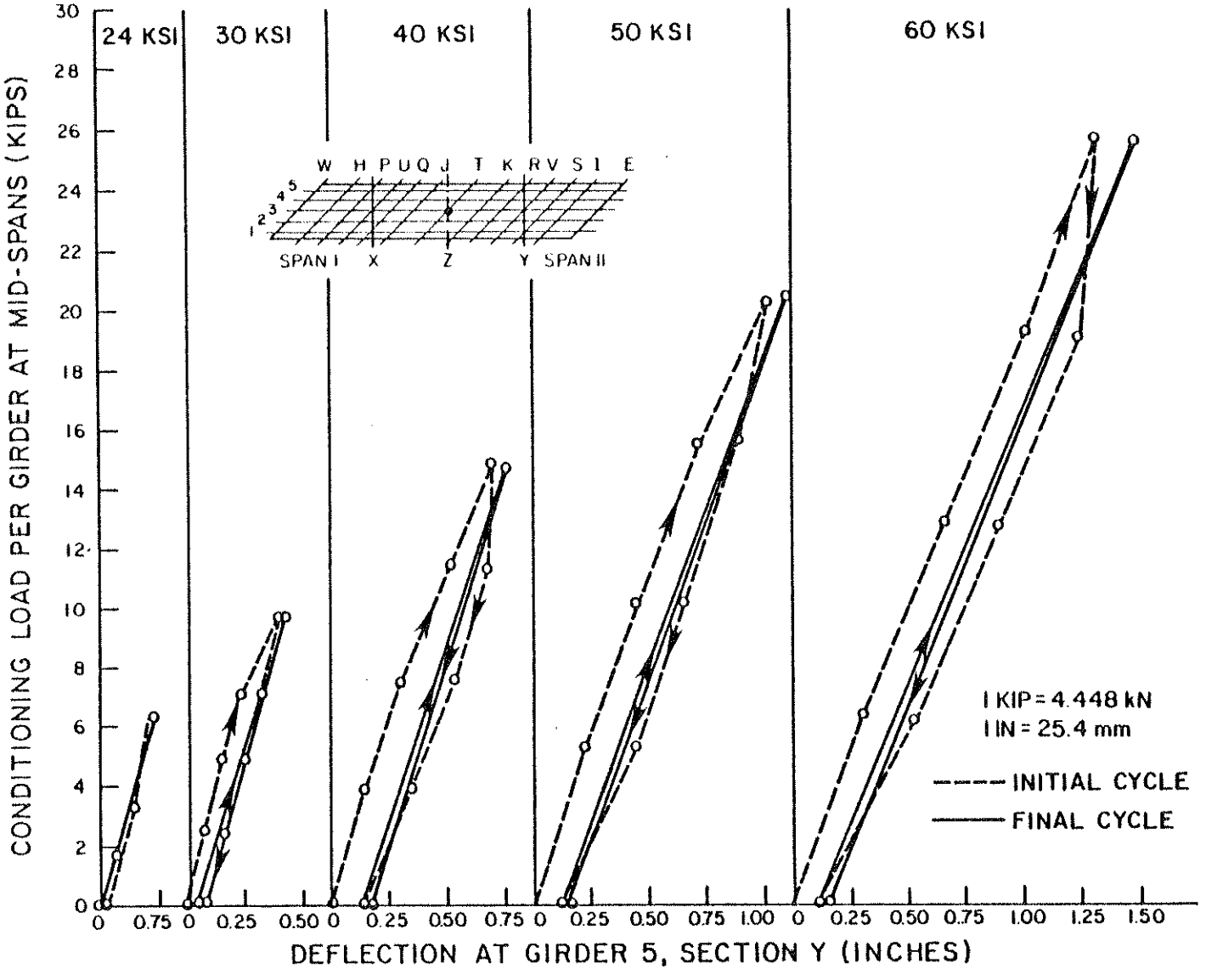

FIG. 7.4 EXPERIMENTAL DEFLECTIONS (INCHES) AT 5Y DURING CONDITIONING LOAD CYCLES

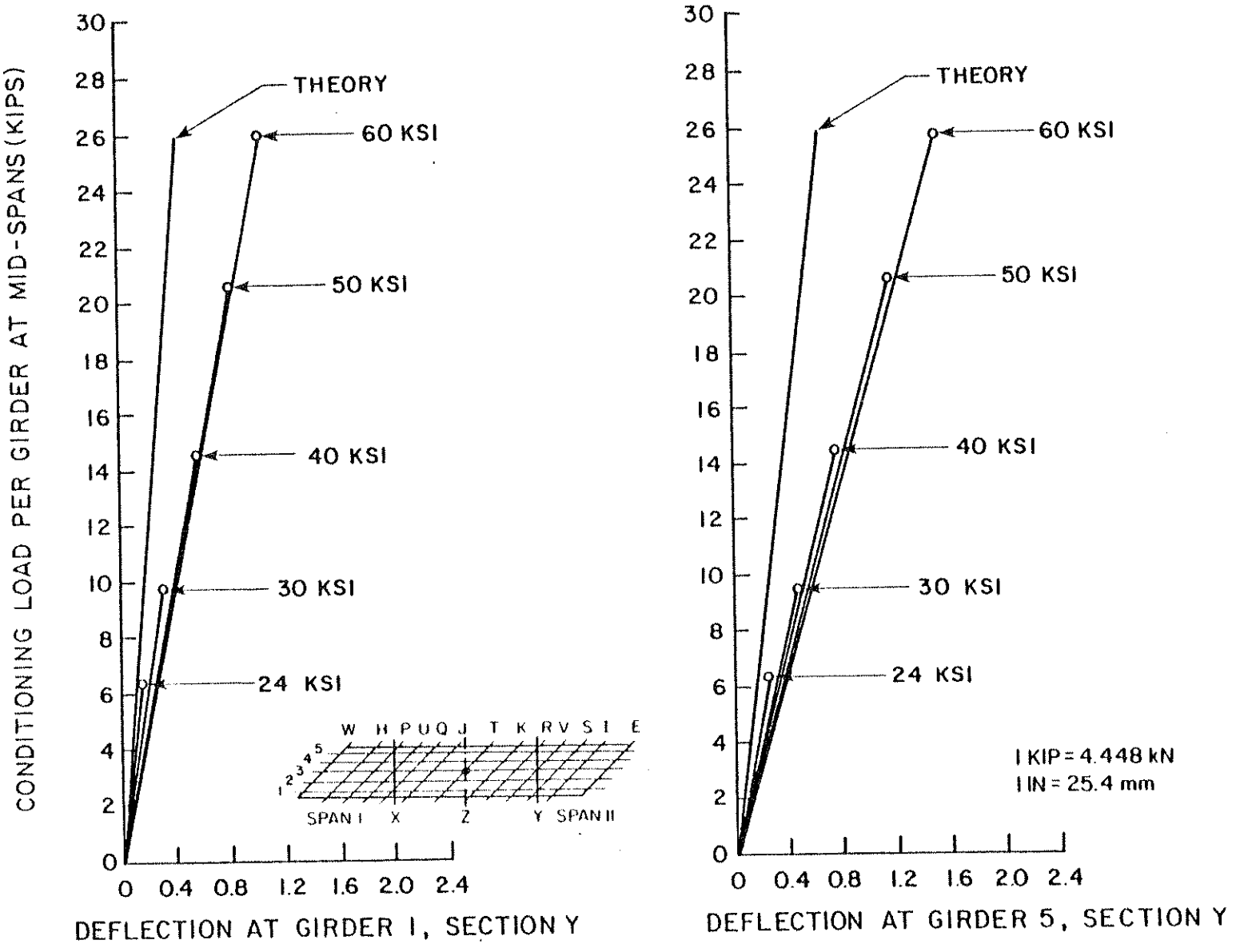

FIG. 7.5 EXTERIOR GIRDER DEFLECTIONS AT SECTION Y FOR DIFFERENT CONDITIONING LOADS

2.3 and 2.4 for the 24, 30, 40, 50 and 60 ksi conditioning loads respectively.

7.2.3 Steel and Concrete Strains

As indicated in Figs. 7.6 and 7.7, steel and concrete strains at 5D on the acute side of the undiaphragmed Span II, exhibit a similar response to that of deflections with respect to linearity and residual deformation. Linearity seems to be quite good even at high load levels.

Figures 7.8 and 7.9 show that the response for concrete and steel strains per unit load is virtually the same at all load levels. Only the steel strain on the acute side of the span at 5D seems to increase slightly with higher levels of conditioning loads.

The longitudinal distributions of normalized steel and concrete strains along girders 1, 3 and 5 for the 30 and 60 ksi conditioning loads are given in Fig. 7.10. It can be observed that there are only very small differences in the results between the 30 and 60 ksi load levels. This means that the shape of the longitudinal strain distribution can be reproduced at different load levels and is only insignificantly influenced by increased cracking in the bridge model between the 30 and 60 ksi load levels.

7.2.4 Moments

Experimental total moments at a section for each conditioning load normalized to 100 kips (445 kN) per span are compared to theoretical values in Table 7.2. Moments obtained from external reactions and loads are given for sections A, Z, and D while moments obtained from internal forces are only given at instrumented midspan sections A

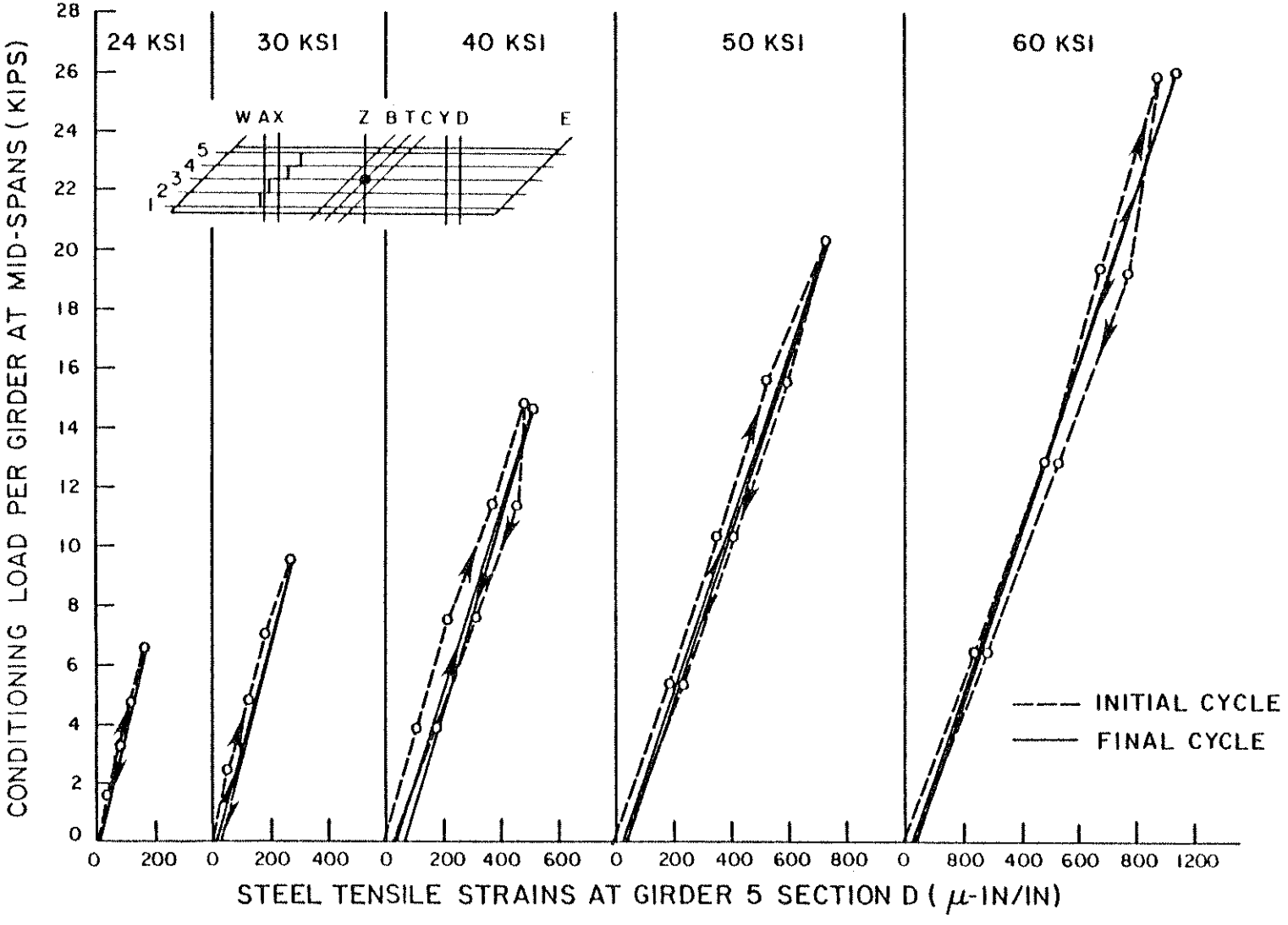

FIG. 7.6 EXPERIMENTAL LONGITUDINAL STEEL STRAINS (MICRO INCH/INCH) AT 5D DURING CONDITIONING LOAD CYCLES

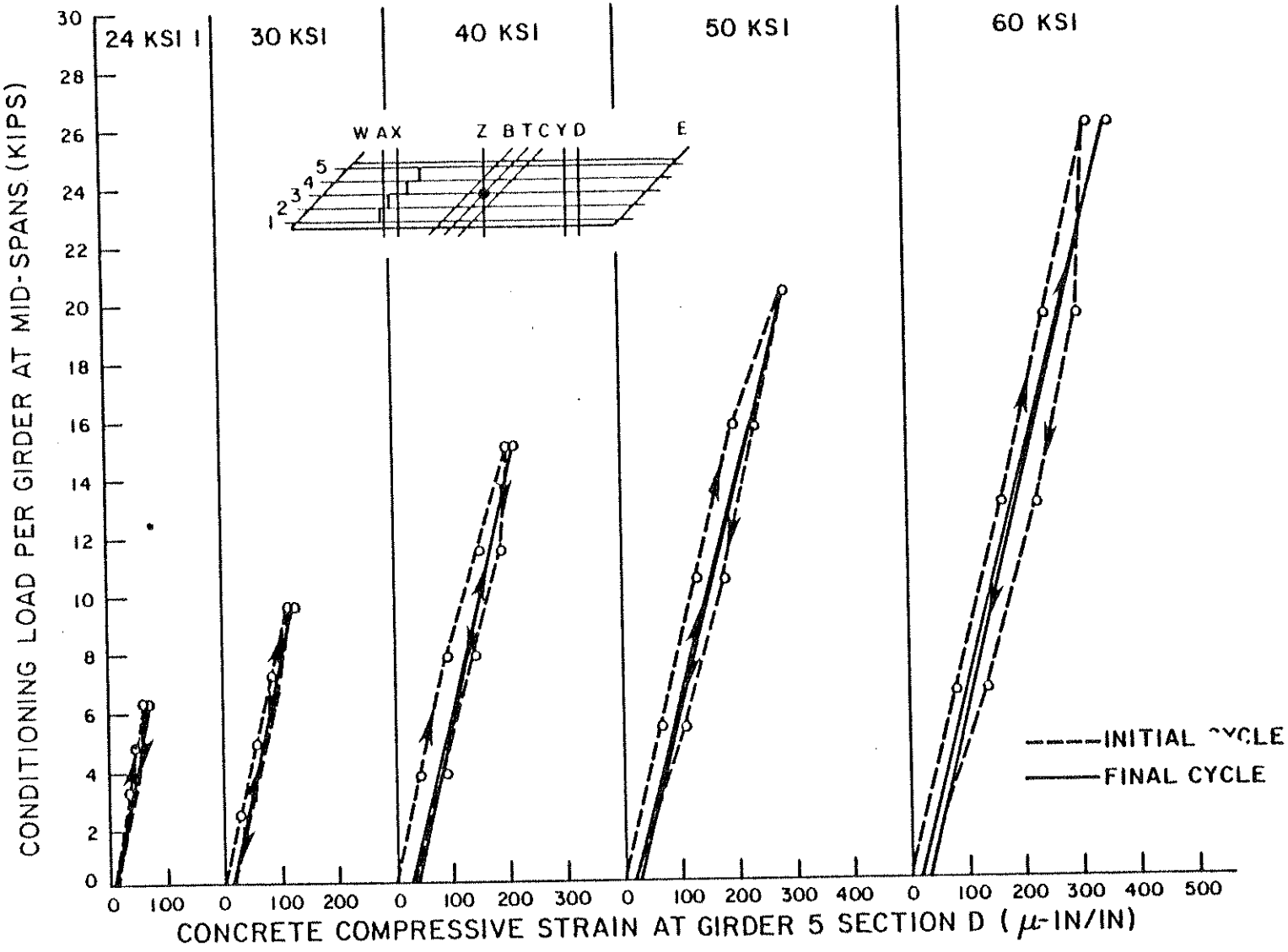

FIG. 7.7 EXPERIMENTAL LONGITUDINAL CONCRETE STRAINS (MICRO INCH/INCH) AT 5D DURING CONDITIONING LOAD CYCLES

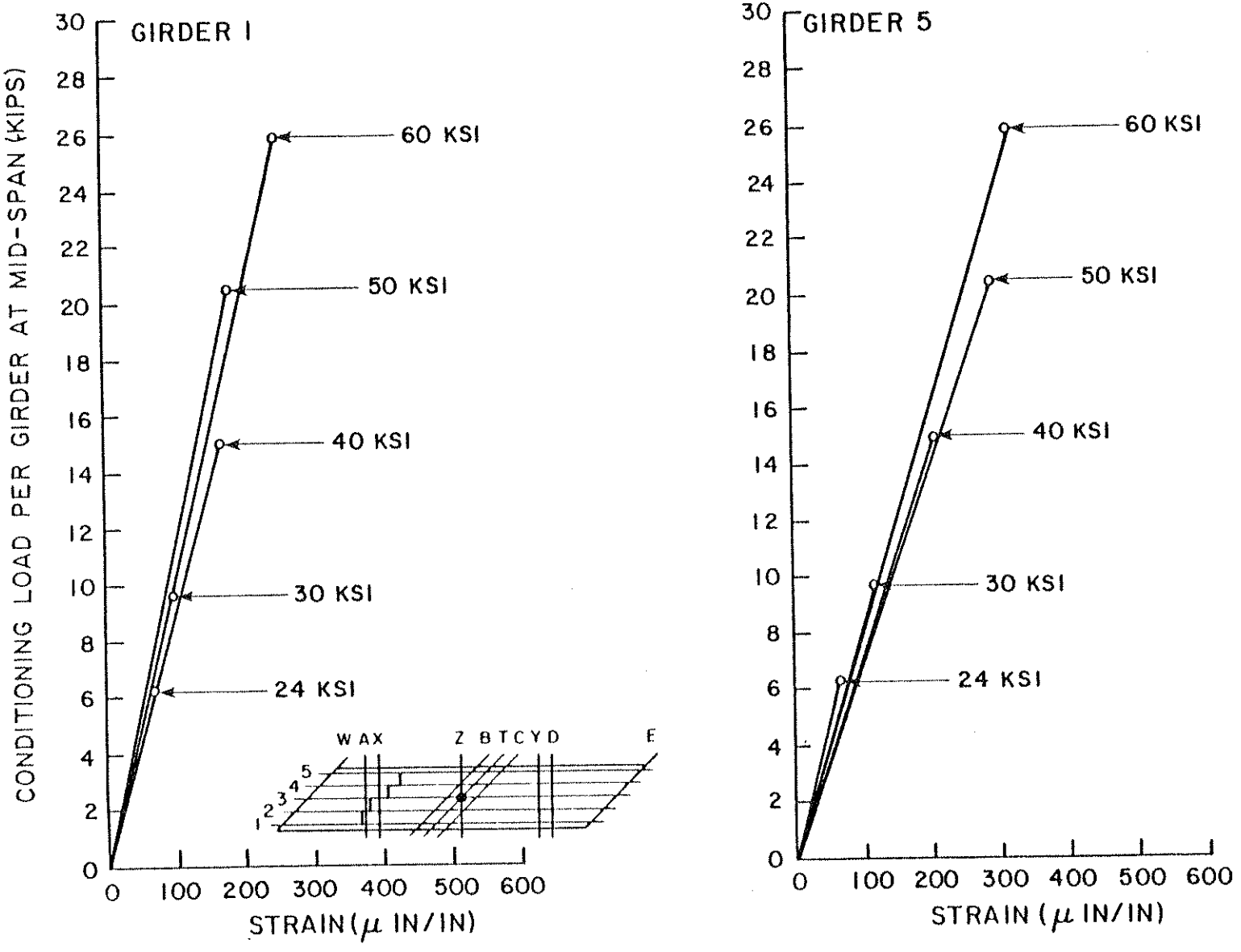

FIG. 7.8 EXPERIMENTAL LONGITUDINAL CONCRETE COMPRESSIVE STRAINS (MICRO INCH/INCH) AT 1D AND 5D FOR DIFFERENT CONDITIONING LOADS

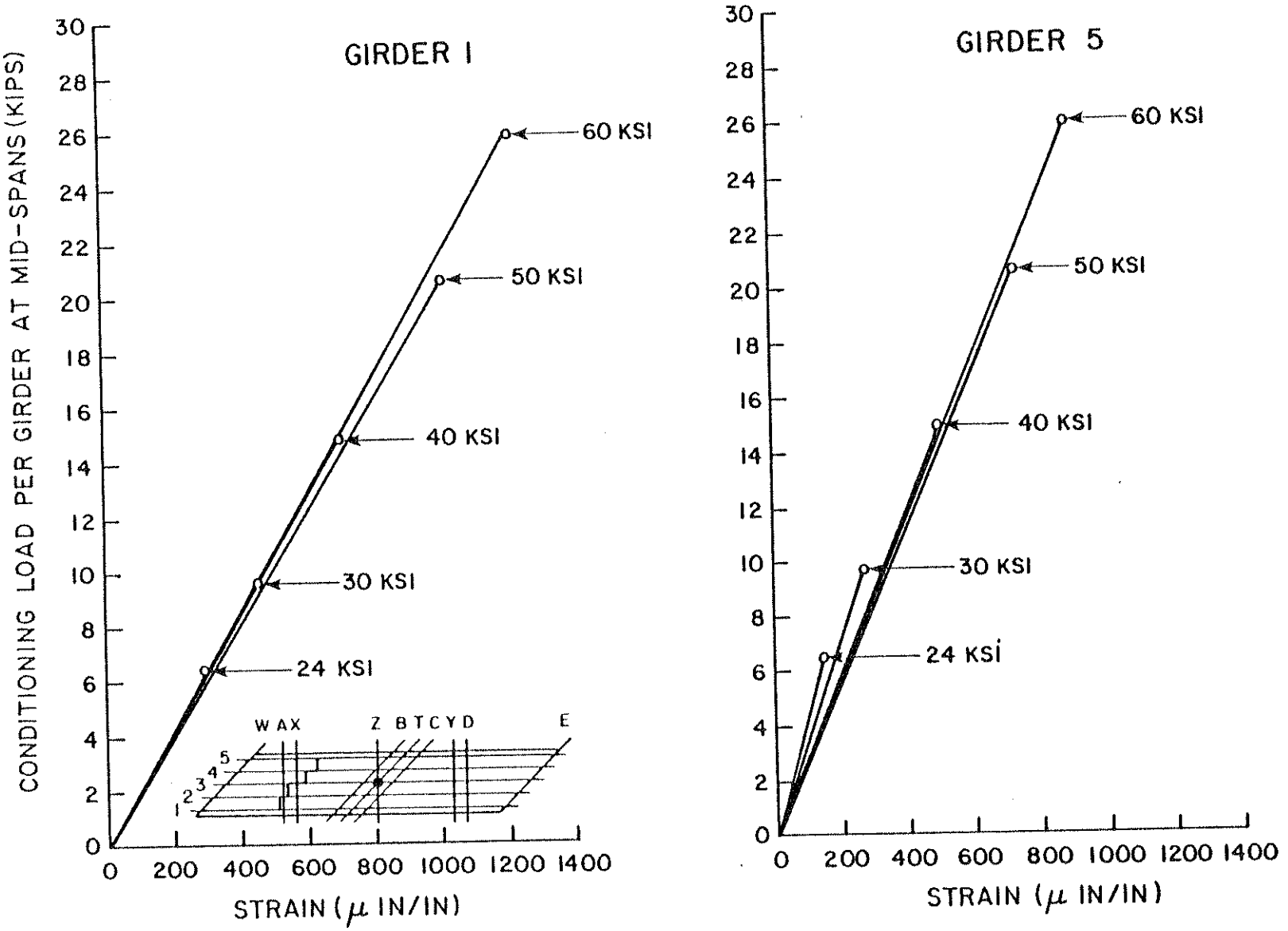

FIG. 7.9 EXPERIMENTAL LONGITUDINAL STEEL TENSILE STRAINS (MICRO INCH/INCH) AT 1D AND 5D FOR DIFFERENT CONDITIONING LOADS

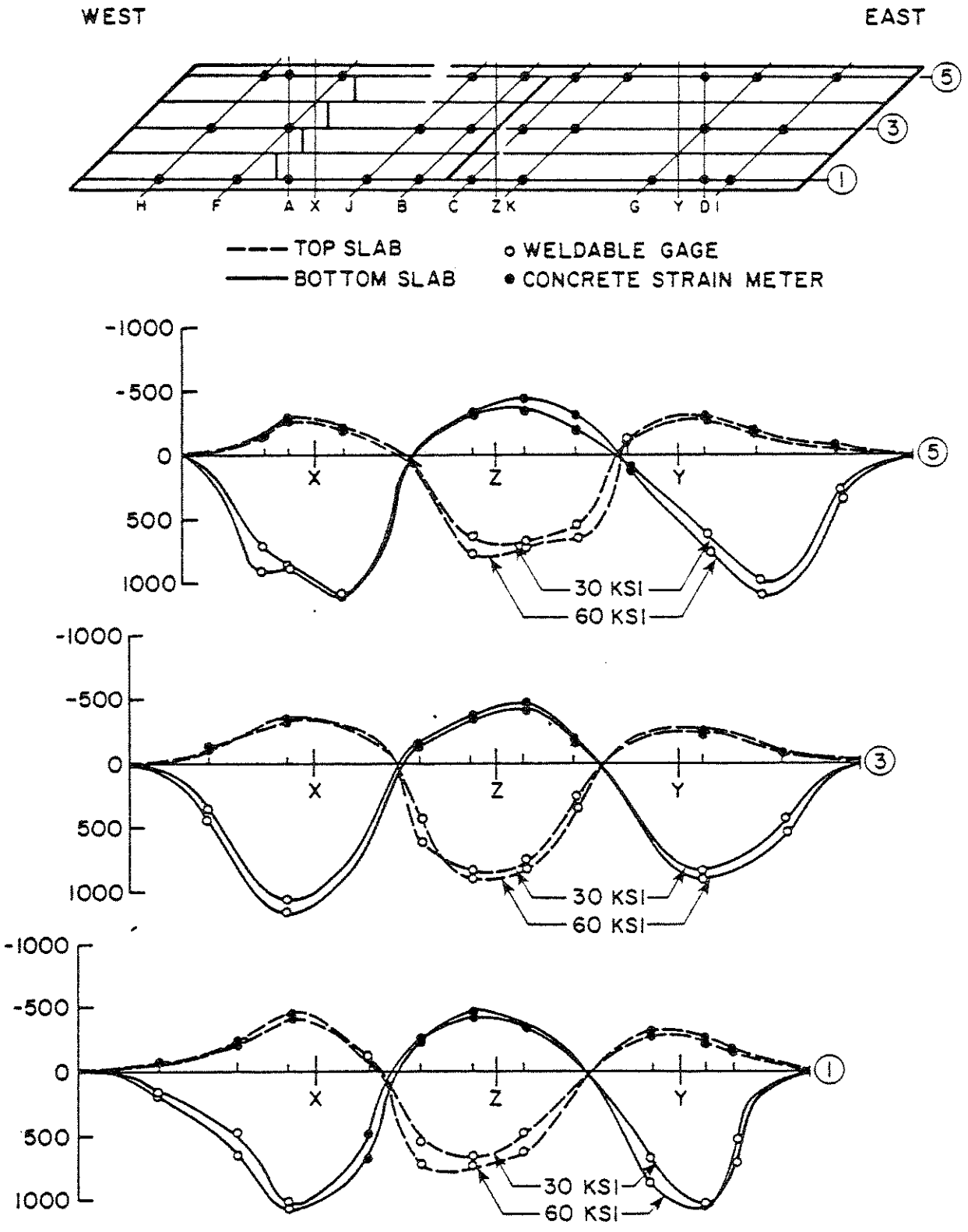

FIG. 7.10 EXPERIMENTAL LONGITUDINAL STRAINS (MICRO INCH/INCH) FOR 30 AND 60 KSI CONDITIONING LOADS

TABLE 7.2 SUMMARY OF THEORETICAL AND EXPERIMENTAL TOTAL MOMENTS (FT-KIPS) AT SECTIONS A, D AND Z FOR ALL CONDITIONING LOADS.

100 K COND. LOADS PER SPAN	SECTION A				SECTION Z		SECTION D			
	BASED ON EXTERNAL REACTIONS		BASED ON INTERNAL FORCES		BASED ON EXTERNAL REACTIONS		BASED ON EXTERNAL REACTIONS		BASED ON INTERNAL FORCES	
	THEORY	EXPT.	THEORY	EXPT.	THEORY	EXPT.	THEORY	EXPT.	THEORY	EXPT.
24	427	454	426	457	-641	-599 -626	427	444	426	443
30	427	467	426	464	-641	-597 -625	427	456	426	455
40	427	463	426	463	-641	-634 -702	427	430	426	428
50	427	461	426	460	-641	-631 -678	427	444	426	443
60	427	460	426	460	-641	-635 -652	427	457	426	454

1 FT-KIP = 1.356 kN-m

and D. The total moment at all sections can be predicted by theory within 9% for all conditioning load cases. It should be noted that under increasing experimental conditioning loads, the decrease in total end moment has only a small effect on the total positive midspan moment since the accompanying slight decrease in the vertical end reaction for higher load levels has a reverse effect on the midspan moments. Therefore, the positive midspan moments remain almost unchanged with increasing conditioning loads. The same holds also for the negative moment at the center support. Experimental results indicate slightly larger positive midspan moments and smaller negative support moments in diaphragmed Span I compared to undiaphragmed Span II.

The transverse distributions of the positive midspan moments are given in Table 7.3 and shown graphically in Fig. 7.11. It can be seen that the theoretical values at sections A and D are identically skew symmetric, indicating no effect of the staggered midspan diaphragm near section A. In addition the theoretical values are essentially the same as those for a uniform stress distribution across the entire section, that is, 16.5, 22.4, 22.4, 22.4 and 16.5% for girders 1 to 5.

The experimental values in Table 7.3 and Fig. 7.11 indicate that at both sections A and D very little change, 0 to 2%, occurs in the distribution of the total moment to each girder under increasing conditioning loads from 24 to 60 ksi. The agreement with theoretical distributions is good at the undiaphragmed section D, but not at the diaphragmed section A. Experimental values at section D range from 2 to 3% higher than theory in the outer girders 1 and 5. At section A, experimental values are 5 to 7% higher than theory in

TABLE 7.3 SUMMARY OF THEORETICAL AND EXPERIMENTAL PERCENTAGE DISTRIBUTION OF TOTAL MOMENT AT SECTIONS A AND D FOR ALL CONDITIONING LOADS

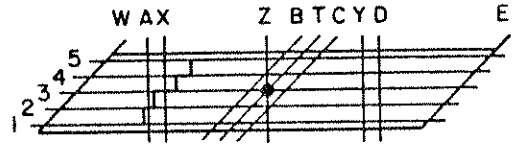

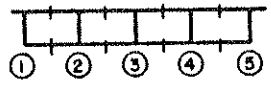

100 K COND LOAD PER SPAN	SECTION A										SECTION D									
	THEORY					EXPERIMENT					THEORY					EXPERIMENT				
	% TO GIRDERS					% TO GIRDERS					% TO GIRDERS					% TO GIRDERS				
	1	2	3	4	5	1	2	3	4	5	1	2	3	4	5	1	2	3	4	5
24	17	23	22	22	16	23	21	21	21	13	16	22	22	23	17	19	23	21	19	19
30	17	23	22	22	16	23	20	21	22	14	16	22	22	23	17	19	23	21	19	19
40	17	23	22	22	16	24	20	21	21	14	16	22	22	23	17	18	23	20	19	20
50	17	23	22	22	16	23	20	21	22	15	16	22	22	23	17	18	23	21	20	19
60	17	23	22	22	16	22	21	21	22	15	16	22	22	23	17	18	23	21	20	19

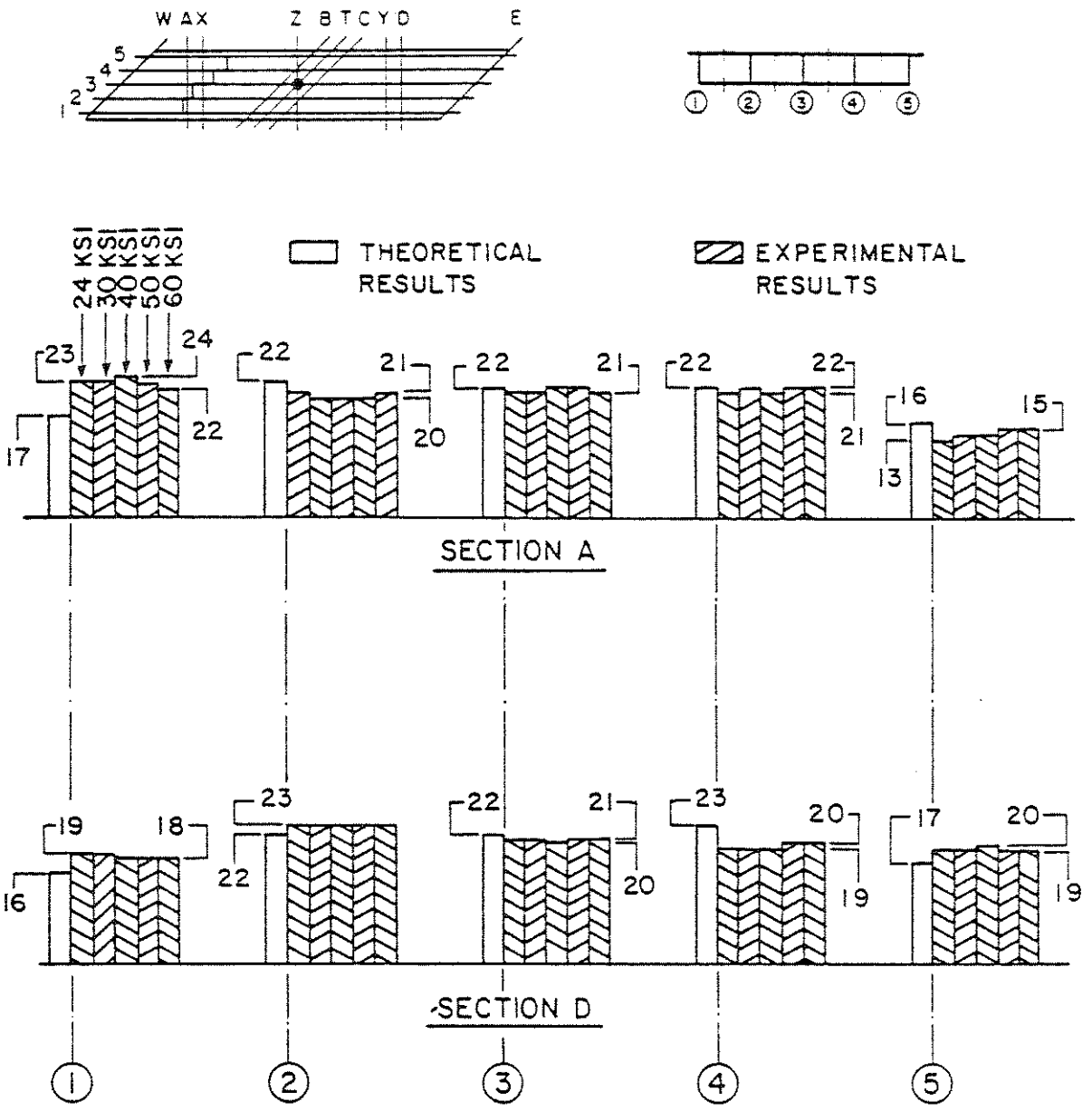

FIG. 7.11 PERCENTAGES OF TOTAL MOMENT AT A SECTION CARRIED BY EACH GIRDER FOR DIFFERENT CONDITIONING LOADS

girder 1 and 1 to 3% lower in girder 5. Thus the same concentration of moment in girder at section A found for all other load cases, due to the close proximity of the staggered midspan diaphragm (see key in Fig. 7.11), exists for the conditioning load cases.

7.3 Results for Point Loads After Conditioning Overloads

Detailed tabulation of theoretical and experimental results related to reactions, deflections, strains and moments are given in Vol. IV for the basic eleven point load combinations. These point loads were designed to give a total maximum stress of 24 to 30 ksi (165 to 207 MPa) in the reinforcement in each case, subsequent to the application of the conditioning loads which brought the maximum stress level to 24, 30, 40, 50 and 60 ksi. All theoretical and experimental values have been normalized for purposes of comparison to total loads of 100 kips (445 kN) per span.

During each of the cases of application of a point load at 1X or 5Y following the 24, 30, 40, 50 and 60 ksi conditioning load a special sequence was followed.

(1) Take zero readings on all gages and meters.

(2) Apply load in four increments (1/4, 1/2, 3/4, 1) to reach the full load and take readings after each increment.

(3) Remove full load in one increment to reach zero load and take readings.

For point loads at the exterior girder position in the undiaphragmed span, (1Y and 5Y), reactions, deflections at 1Y and 5Y, strains at 1D and 5D, the longitudinal distribution of strains in girders 1, 3 and 5 are presented in Figs. 7.12 to 7.21.

7.3.1 Total East and Center Reactions

Figure 7.12 and 7.13 indicate that the east and center vertical reactions are linearly related to load for all cases shown and little difference exists between the results for the cycles after 30 and 60 ksi conditioning loads.

Figure 7.14 shows that the relation between reactions and applied point load remains essentially unchanged after all conditioning overloads up to 60 ksi. It can also be seen that while theory predicts the vertical end reaction exactly, the experimental center footing reaction tends to be consistently higher which was also found and discussed for working stress loads in Chapter 6.

7.3.2 Deflections at 1Y and 5Y

Figure 7.15 indicates that very little permanent deflection exists after each point load cycle. For the point load case 5Y which was applied in 4 increments it can be seen that the deflection is fairly linear after all conditioning load levels.

Figure 7.16 shows that the deflections directly under a point load of 19.3 kips (86 kN) at 5Y or at 1Y increase if the load is applied after successively higher conditioning loads. This is due to larger amount of cracking produced by the higher conditioning loads. Comparing the experimental values with those from theory based on an uncracked section, Fig. 7.16, indicates that the ratios of experimental

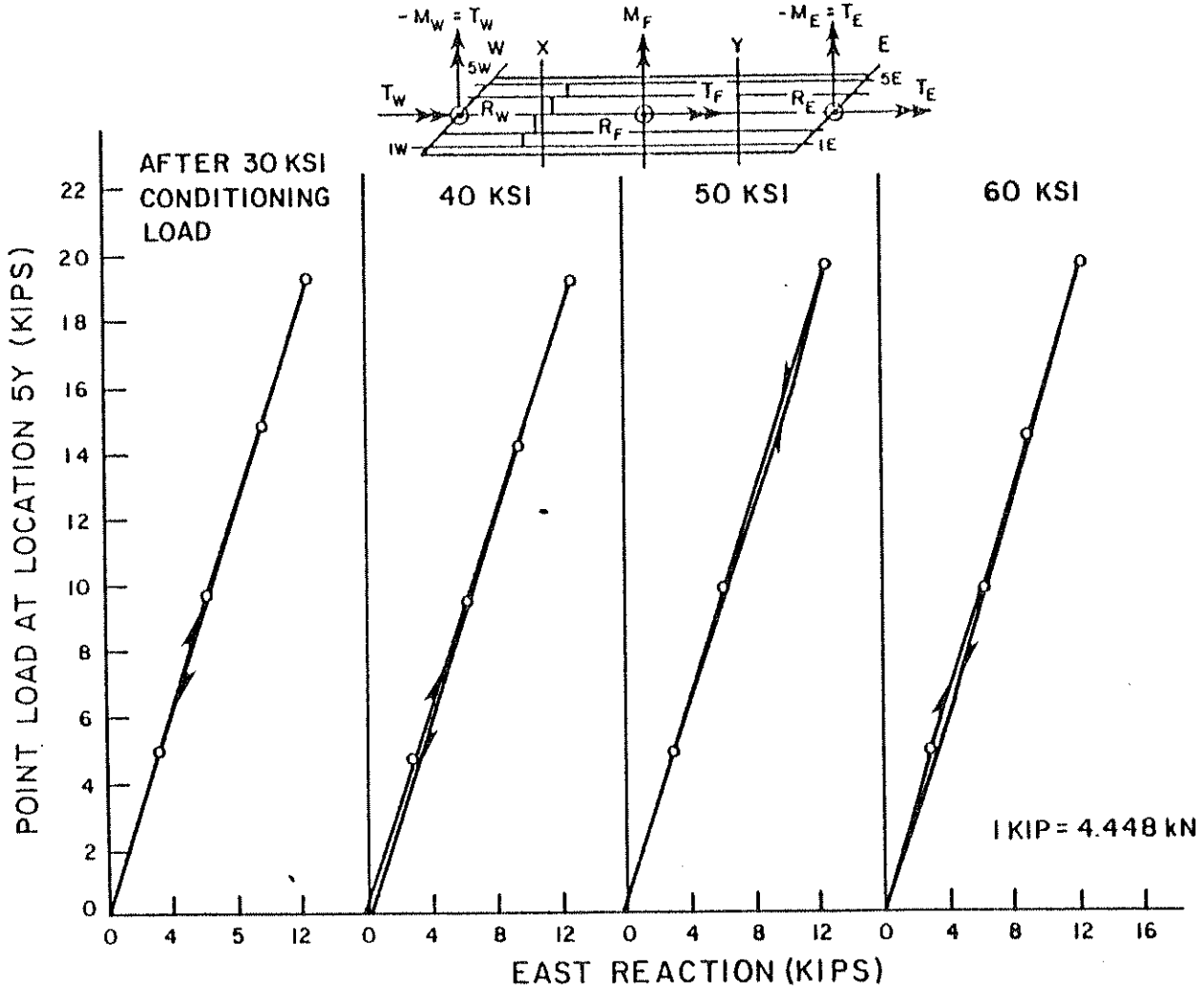

FIG. 7.12 EXPERIMENTAL TOTAL VERTICAL EAST REACTION (KIPS) FOR A POINT LOAD AT 5Y AFTER DIFFERENT CONDITIONING LOADS

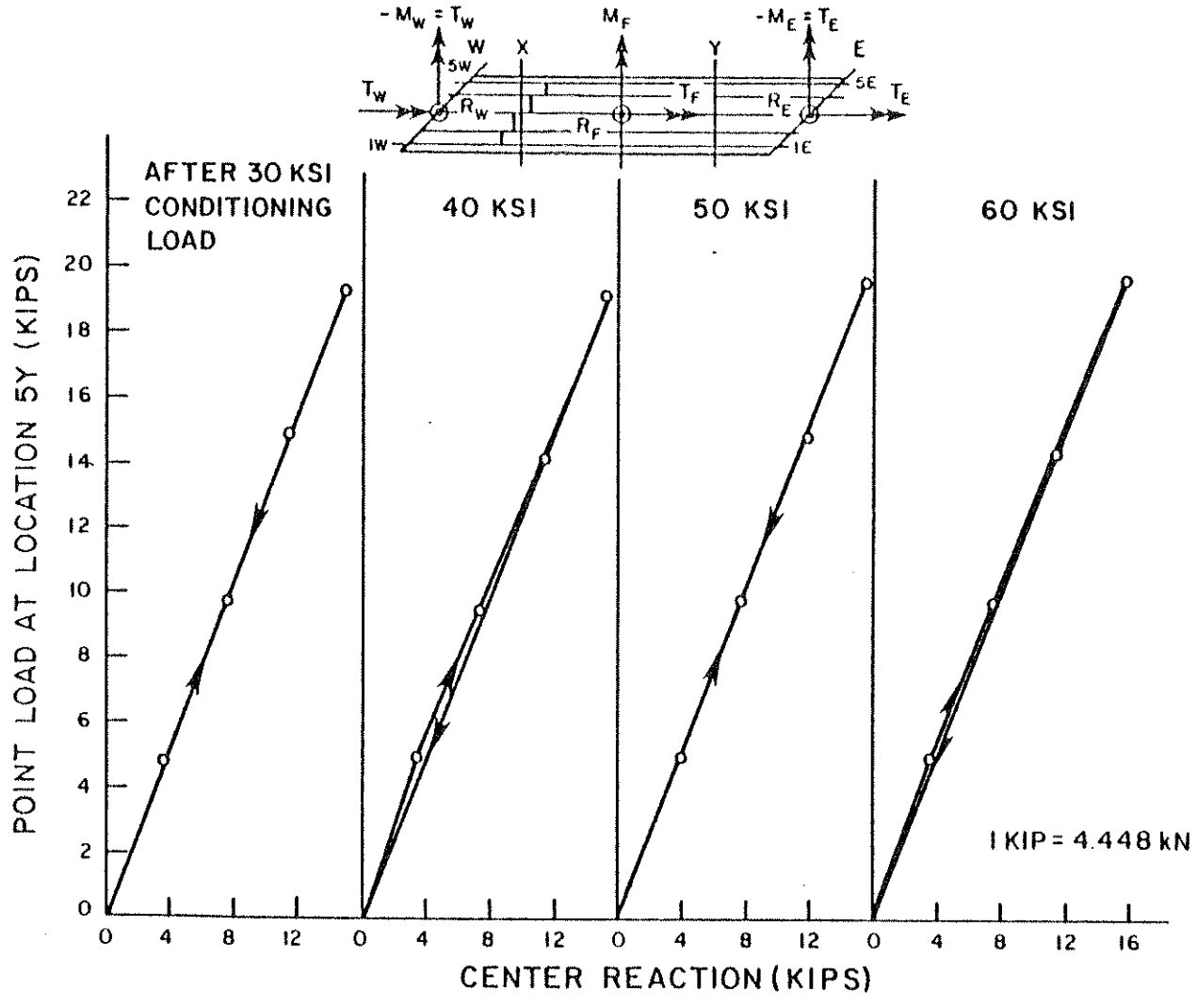

FIG. 7.13 EXPERIMENTAL TOTAL VERTICAL CENTER FOOTING REACTION (KIPS) FOR A POINT LOAD AT 5Y AFTER DIFFERENT CONDITIONING LOADS

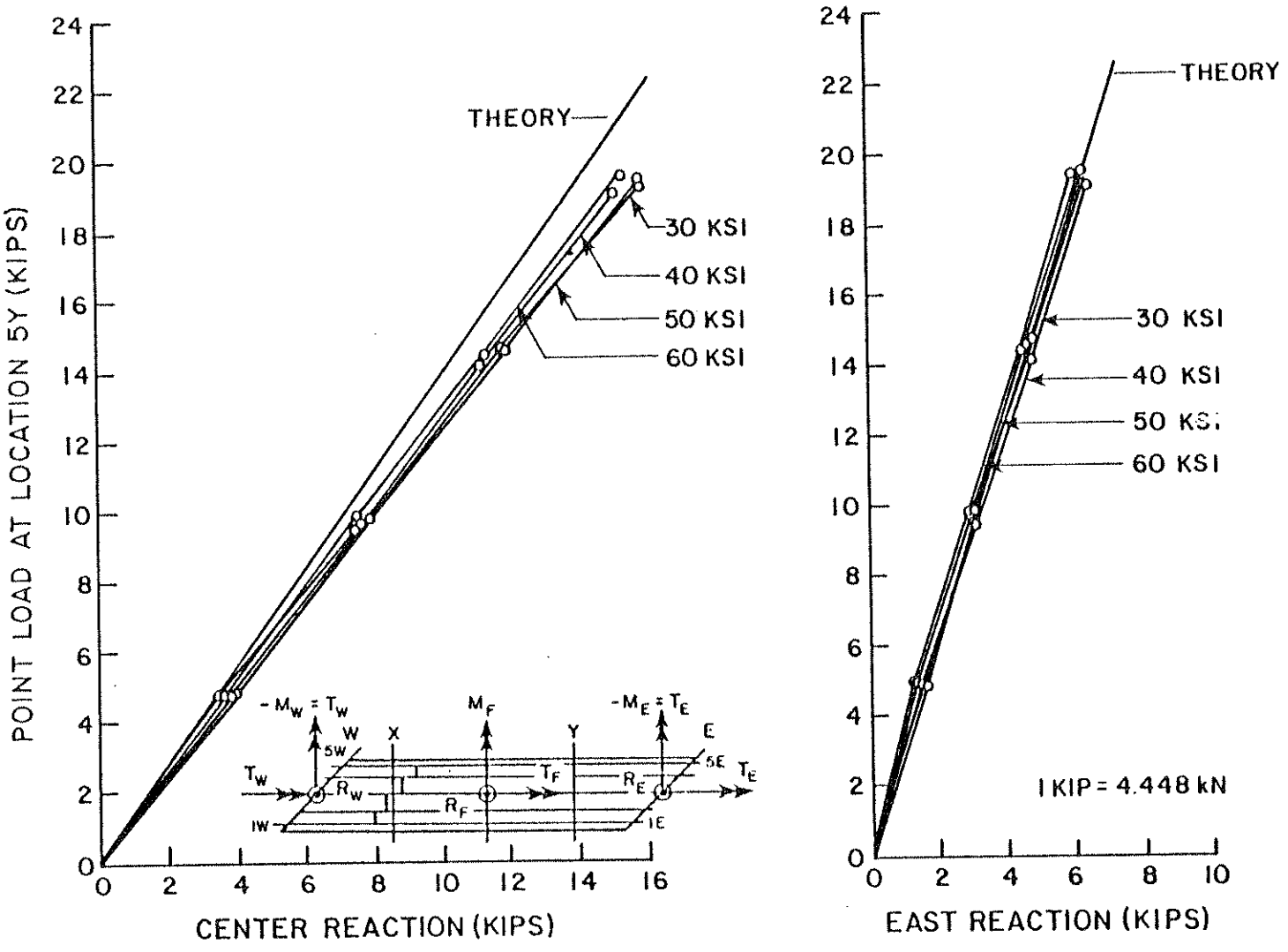

FIG. 7.14 COMPARISON OF THEORETICAL AND EXPERIMENTAL VERTICAL REACTIONS (KIPS) AT EAST END AND CENTER FOOTING FOR A POINT LOAD AT 5Y AFTER DIFFERENT CONDITIONING LOADS

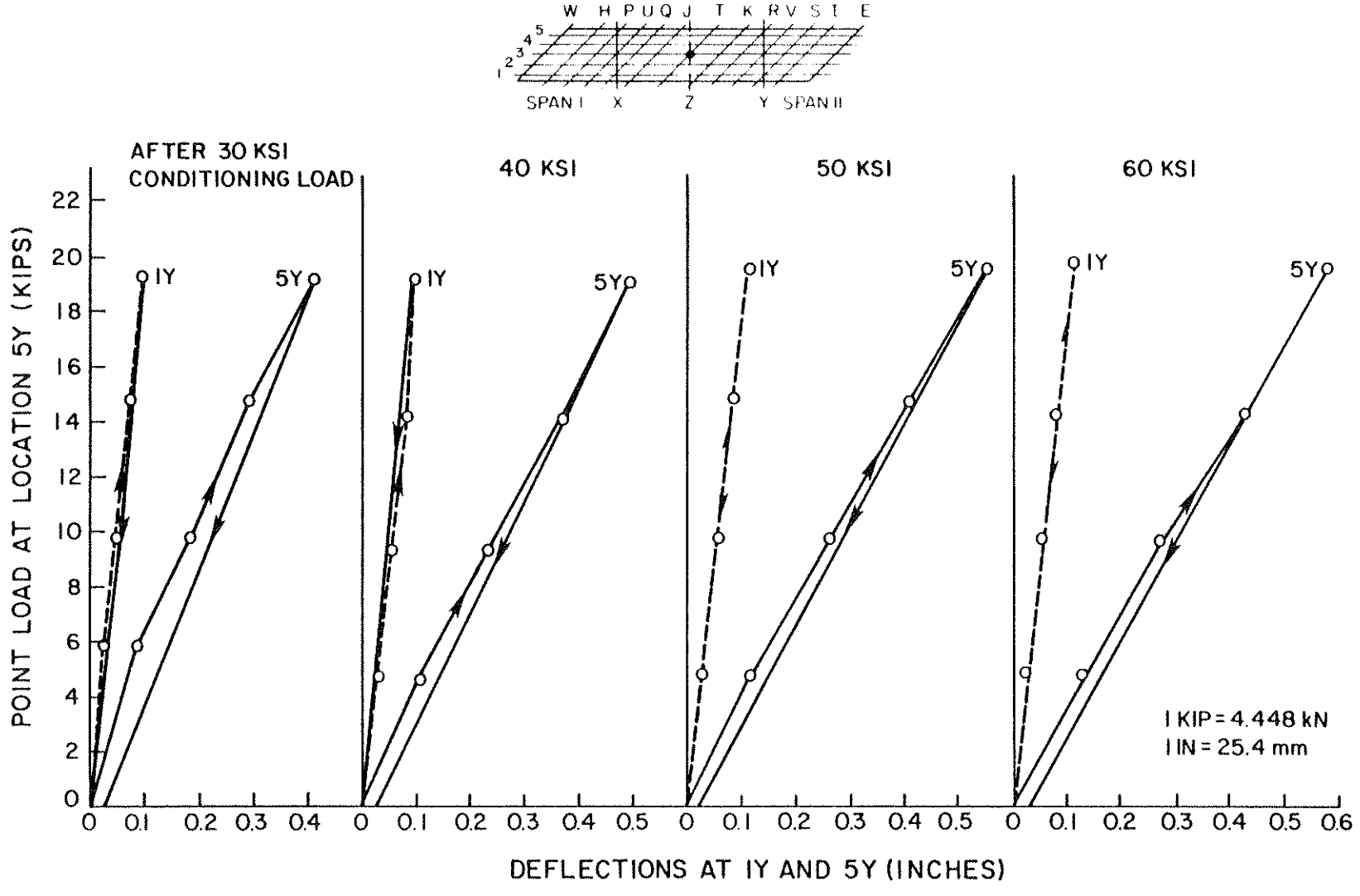

FIG. 7.15 EXPERIMENTAL EXTERIOR GIRDER DEFLECTIONS (INCHES) AT SECTION Y FOR A POINT LOAD AT 5Y FOR DIFFERENT CONDITIONING LOAD CYCLES

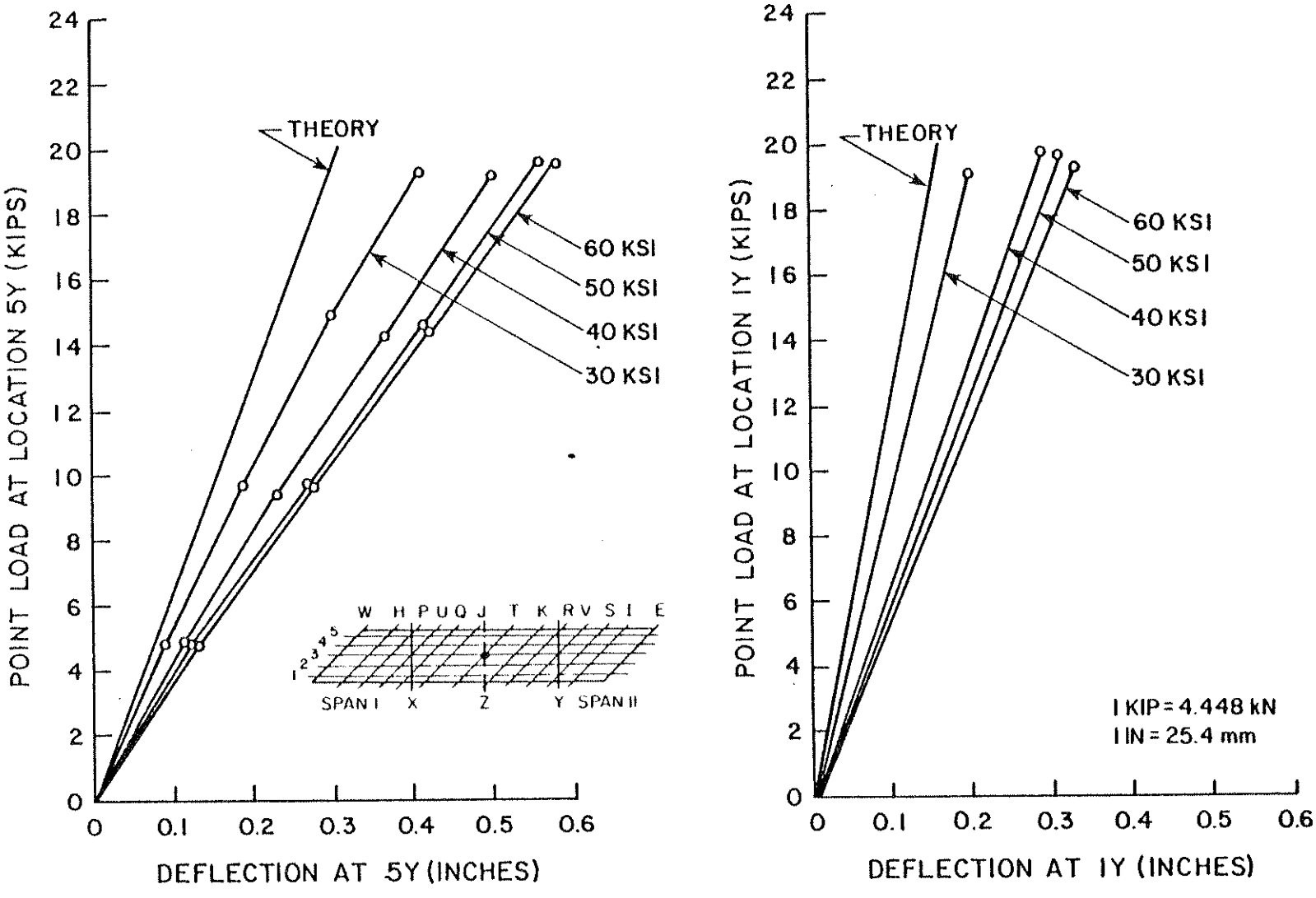

FIG. 7.16 EXTERIOR GIRDER DEFLECTIONS (INCHES) UNDER POINT LOADS AT 5Y AND 1Y AFTER DIFFERENT CONDITIONING LOADS

to theoretical deflections are higher for deflections and loads on the obtuse side of the span (1Y) than they are on the acute side of the span (5Y). These ratios are for the former 1.46, 1.83, 2.00, 2.16 and for the latter 1.36, 1.66, 1.80, 1.89, for point loads of 19.3 kips (86 kN) applied after the 30, 40, 50 and 60 ksi conditioning loads respectively. Similar increases in deflections after the 30, 40, 50 and 60 ksi conditioning loads occur also for the deflection at 1Y or 5Y due to a point load at 5Y or 1Y. The ratios for these cases are 1.86, 1.95, 2.08, 2.05 for the deflection at 1Y due to a point load at 5Y and 1.77, 1.93, 2.12, 2.16 for the deflection at 5Y due to a point load at 1Y after the four conditioning load cases respectively.

From the above, it can be seen, that it is very difficult to predict the experimental deflections after higher conditioning load levels by multiplying the theoretical values with a single magnification factor to account for the stiffness deterioration due to cracking. While no uniform magnification factor can be found for all conditioning load levels, it can be seen that for each individual load level a magnification factor could be found which would give an approximate theoretical deflection to predict the experimental results. These magnification factors would range from 1.5 for the 30 ksi level to about 2.2 for the 60 ksi level.

7.3.3 Steel and Concrete Strains at 1D and 5D

For the extreme point load position 5Y on the acute side of the undiaphragmed span, Figs. 7.17 to 7.20 depict the strains at 5D, near the point load and at 1D on the obtuse side of the loaded span. It can be seen that both steel and concrete strains vary linearly for point loads after all conditioning load levels and the

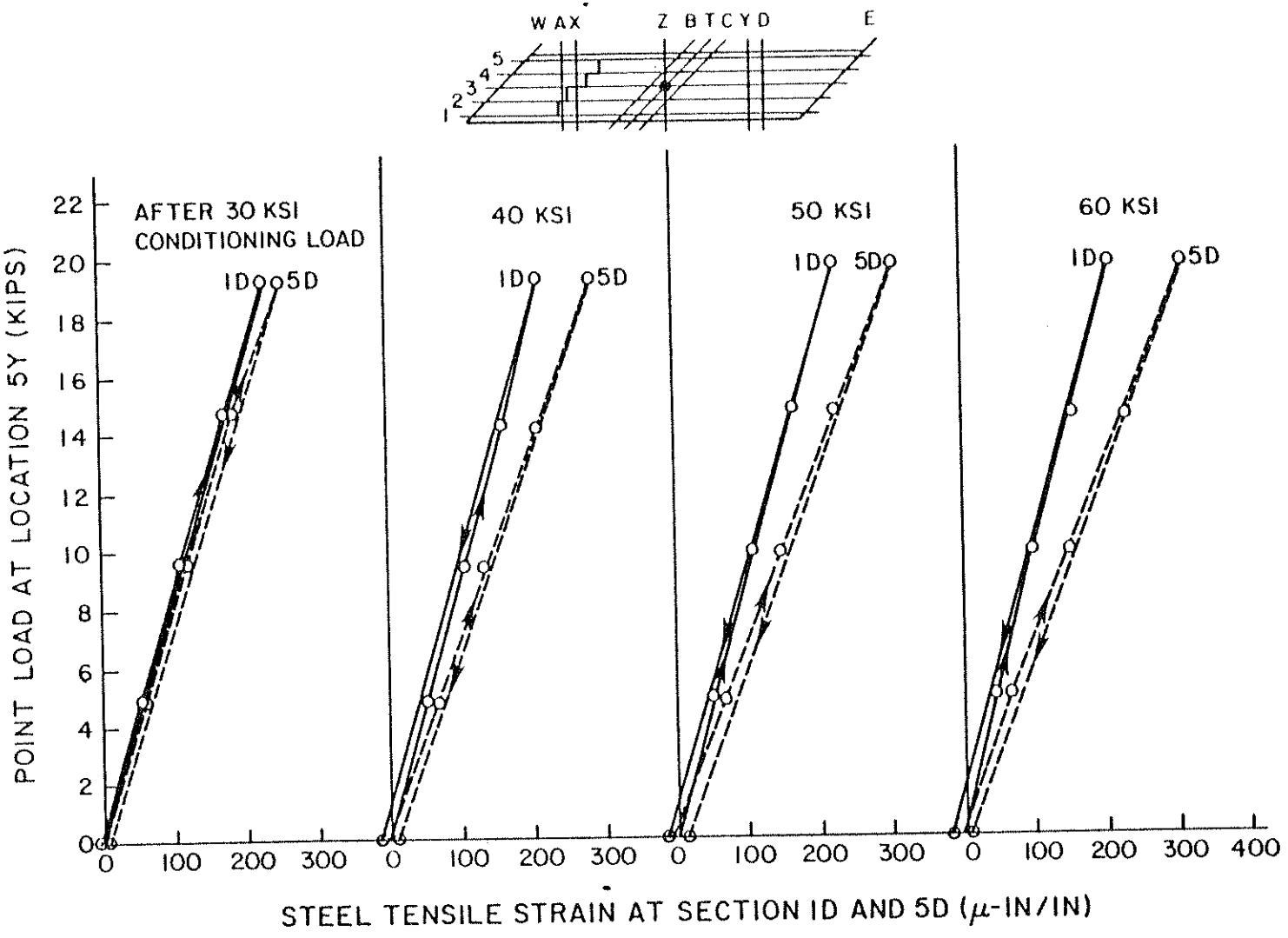

FIG. 7.17 EXPERIMENTAL LONGITUDINAL STEEL STRAINS (MICRO INCH/INCH) AT 1D AND 5D FOR A POINT LOAD AT 5Y AFTER DIFFERENT CONDITIONING LOAD CYCLES

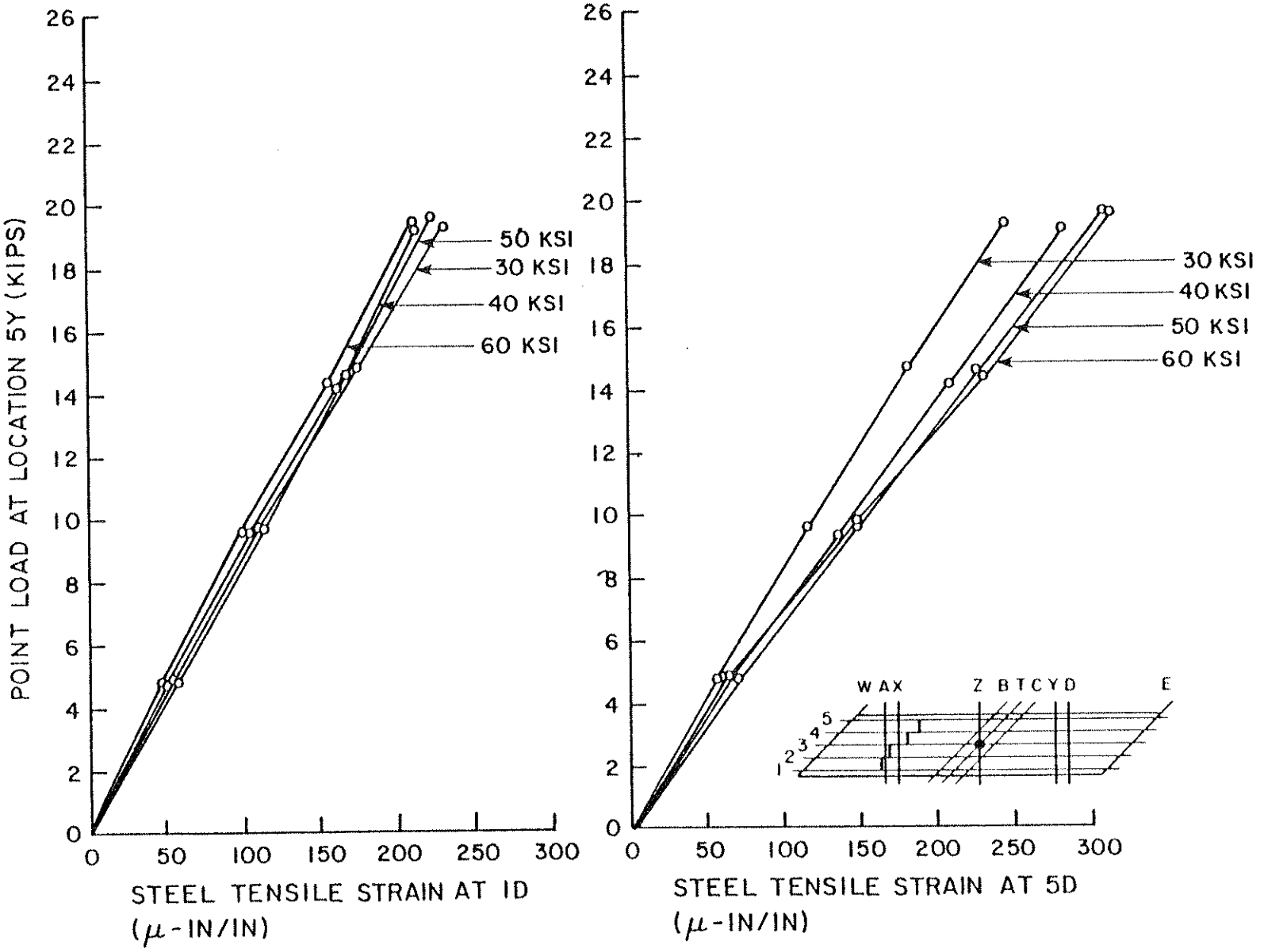

FIG. 7.18 EXPERIMENTAL LONGITUDINAL STEEL STRAINS (MICRO INCH/INCH) AT 1D AND 5D FOR A POINT LOAD AT 5Y AFTER DIFFERENT CONDITIONING LOADS

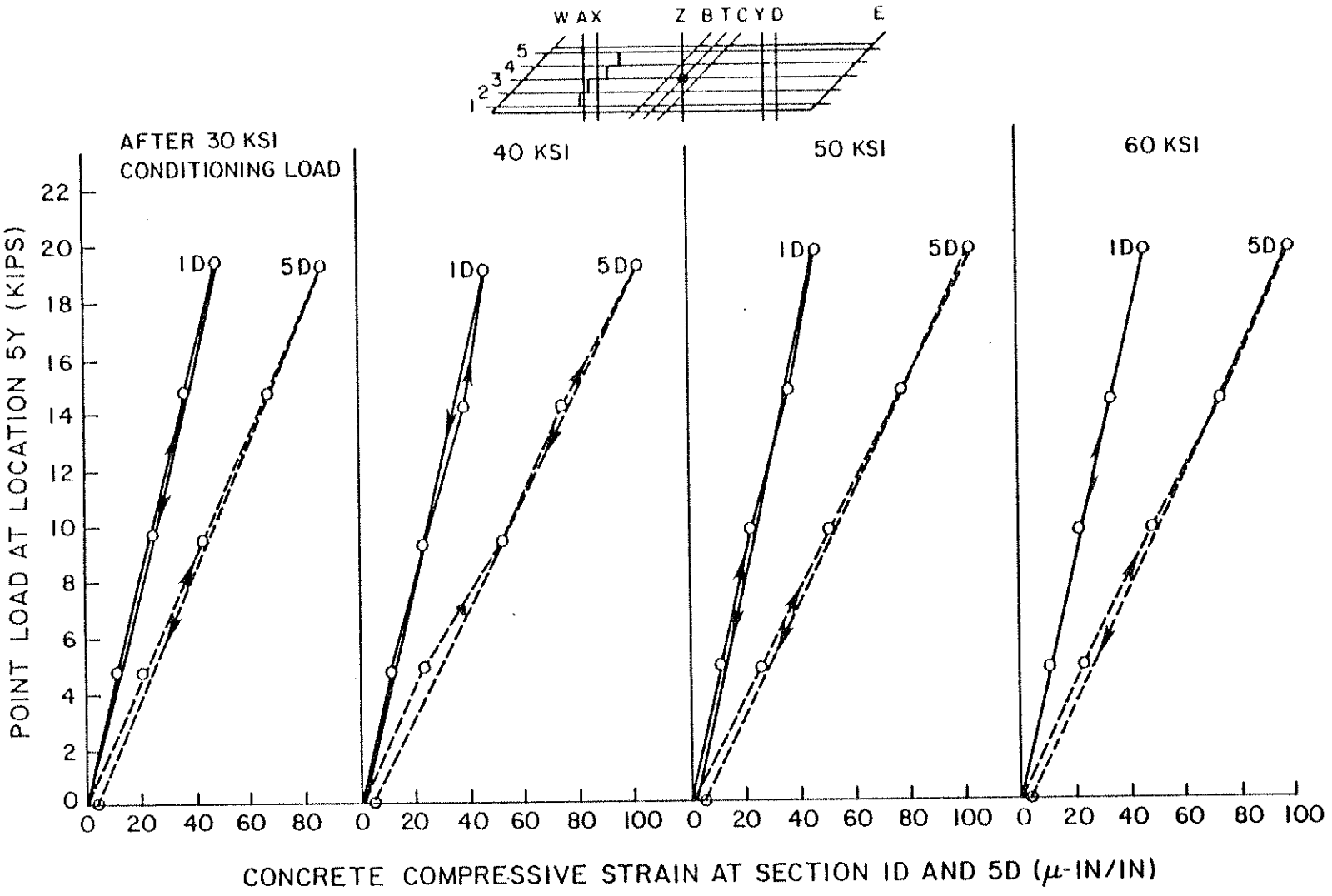

FIG. 7.19 EXPERIMENTAL LONGITUDINAL CONCRETE STRAINS (MICRO INCH/INCH) AT 1D AND 5D FOR A POINT LOAD AT 5Y AFTER DIFFERENT CONDITIONING LOAD CYCLES

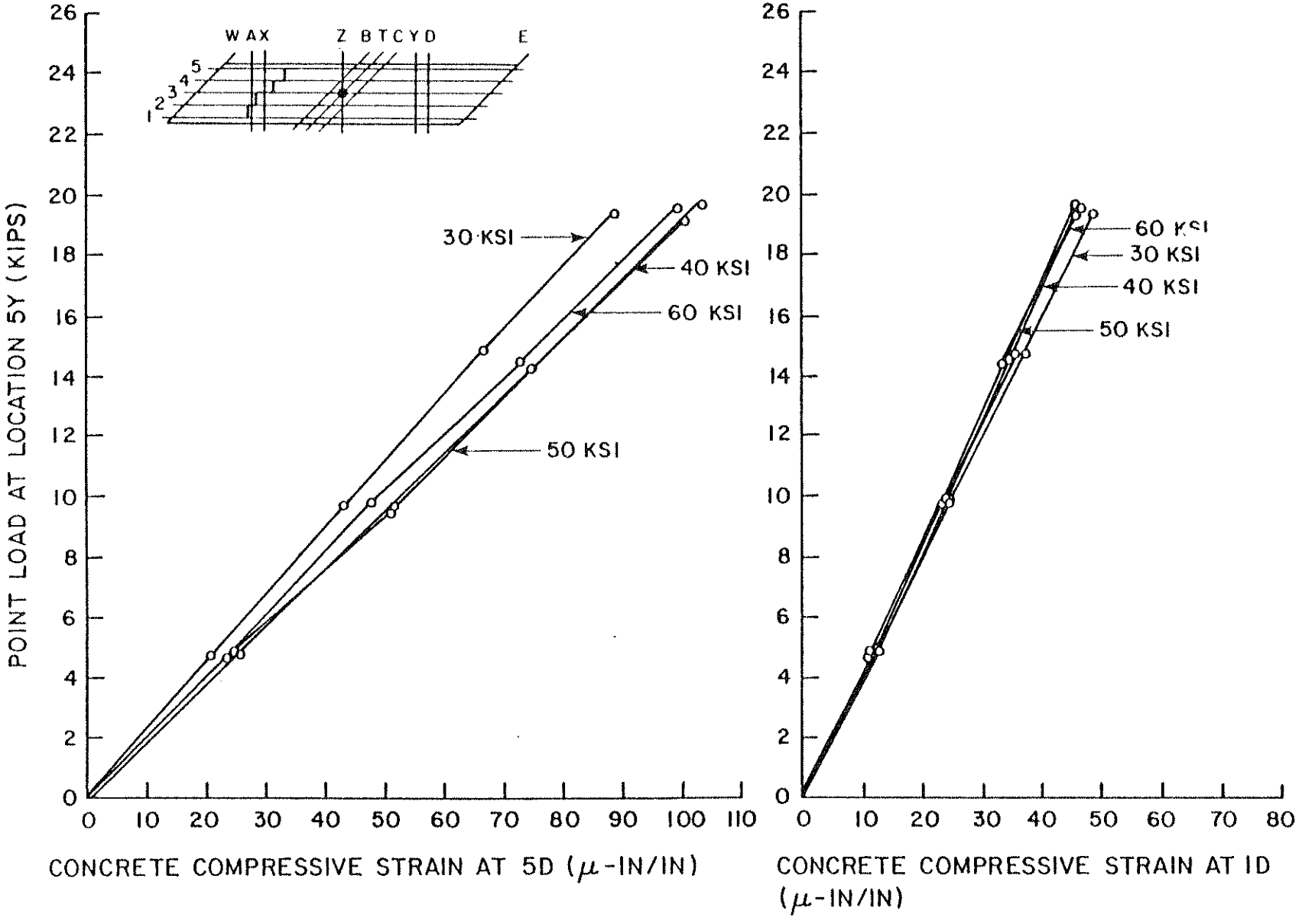

FIG. 7.20 EXPERIMENTAL LONGITUDINAL CONCRETE STRAINS (MICRO INCH/INCH) AT 1D AND 5D FOR A POINT LOAD AT 5Y AFTER DIFFERENT CONDITIONING LOADS

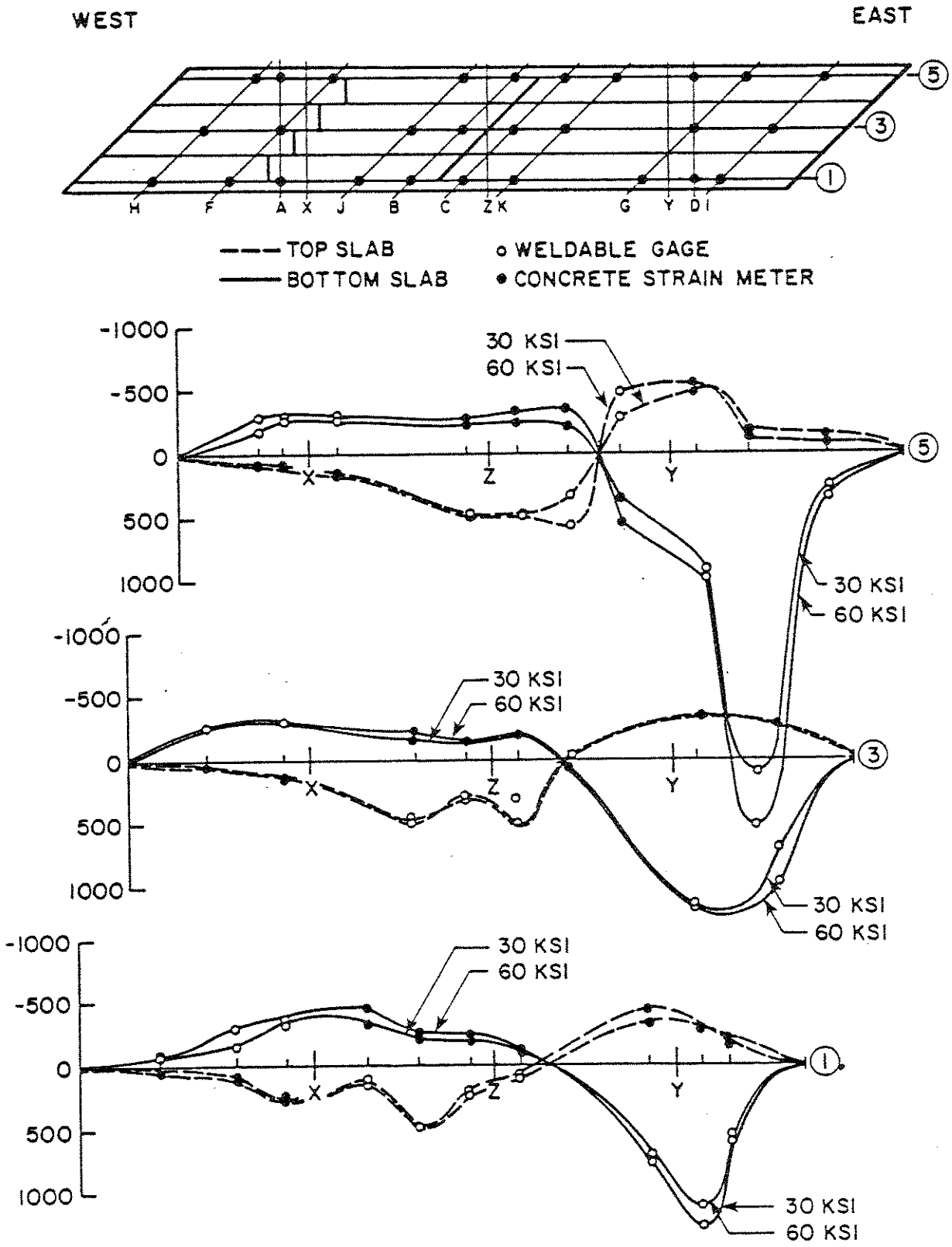

FIG. 7.21 EXPERIMENTAL LONGITUDINAL STRAINS (MICRO INCH/INCH) FOR 100 KIP (445 kN) POINT LOAD AT 5Y AFTER 30 AND 60 KSI CONDITIONING LOADS

residual deformations are very small. The steel and concrete strains per unit point load remain relatively constant at 1D and 5D for all conditioning load levels. Only the steel strain at 5D tends to increase slightly after higher conditioning loads.

Similar conclusions can also be drawn fron the longitudinal experimental strain distribution along girders 1, 3 and 5 for a normalized point load of 100 kips (445 kN) at 5Y after 60 ksi conditioning load level which are plotted in Fig. 7.21. The general shape of the longitudinal strain distribution remains virtually unchanged with slightly higher strains after higher conditioning load levels on the acute side of the loaded span and slightly lower strains at the obtuse side of the loaded span.

7.3.4 Moments

The transverse distributions of the total moments at instrumented sections A and D for point loads at 1X or 5Y (point load on the acute side of the span) after 24 to 60 ksi conditioning loads are depicted graphically in Fig. 7.22.

The experimental values indicate that changes of 1 to 2% at section D and 1 to 5% at section A occur in the distribution of the total moment to each girder under increasing conditioning loads from 24 to 60 ksi. The agreement with theoretical distributions is relatively good at undiaphragmed section D, but not at section A due to the proximity of the staggered midspan diaphragm. Experimental values at section D range from 1 to 2% higher in exterior girders 1 and 5 and 3 to 4% lower in girder 4. Experimental values at section A for girder 1 are from 8 to 13% higher than theory while in girder 5 they are 2 to 6% lower than theory.

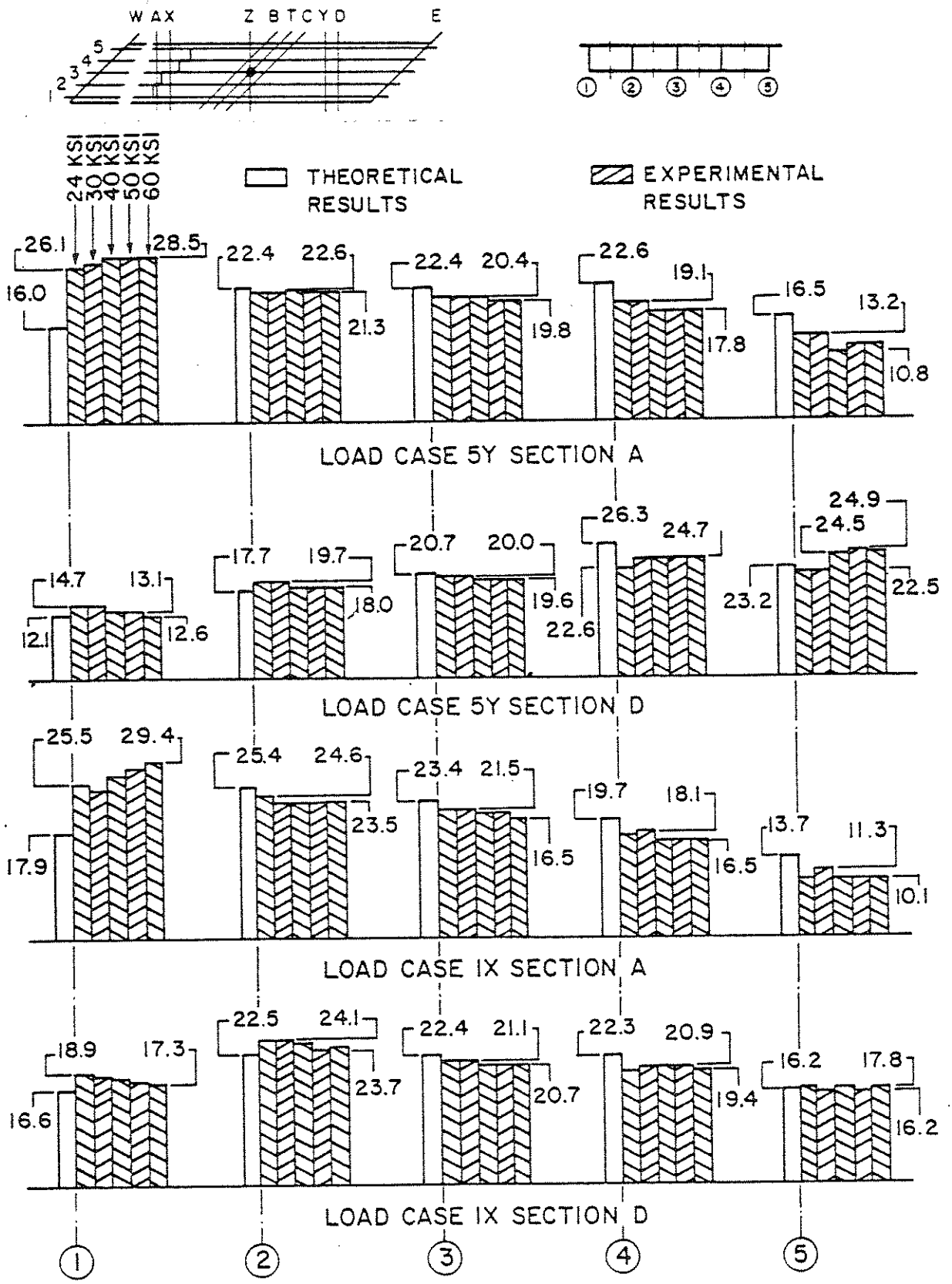

FIG. 7.22 PERCENTAGES OF TOTAL MOMENT AT A SECTION CARRIED BY EACH GIRDER FOR POINT LOADS AT 1X AND AT 5Y AFTER DIFFERENT CONDITIONING LOADS

7.4 Comparison of Results for Straight, Curved and Skew Bridge Models

A comparison of results found for the skew bridge model with those of the straight and curved bridge models [1 to 6] for selected reactions, deflections, and transverse moment distributions is given in Figs. 7.23 to 7.27.

In Fig. 7.23 a comparison is made between the three bridge types for 30 and 60 ksi conditioning loads and the theoretical conditioning load case. Unnormalized results are plotted for the total east reaction and for the maximum deflection at location 5Y on the acute side of the undiaphragmed Span II. For the total vertical east reaction excellent agreement between theoretical and experimental values can be observed for all three bridges. The skew bridge model features higher end reactions than the two other bridge models which show similar values.

Deflections in Fig. 7.23 have not been adjusted to account for the different concrete modulus of elasticity in the three bridge models. The average moduli of elasticity of the concrete at section D for top and bottom slabs at the 60 ksi loading stage were 3725, 2850 and 3025 ksi (25,700, 19,700 and 20,900 MPa) for the straight, curved and skew bridge respectively. Ratios of experimental to theoretical deflections for 30 ksi and 60 ksi conditioning loads are 1.6 and 2.2 for the straight bridge, 1.4 and 2.0 for the curved bridge and 1.8 to 2.4 for the skew bridge indicating similar decreases in stiffness due to cracking in the three bridges.

Percentages of total moment at a section carried by each girder for conditioning loads are shown in Fig. 7.24. For experimental results the maximum and minimum value found for each girder during

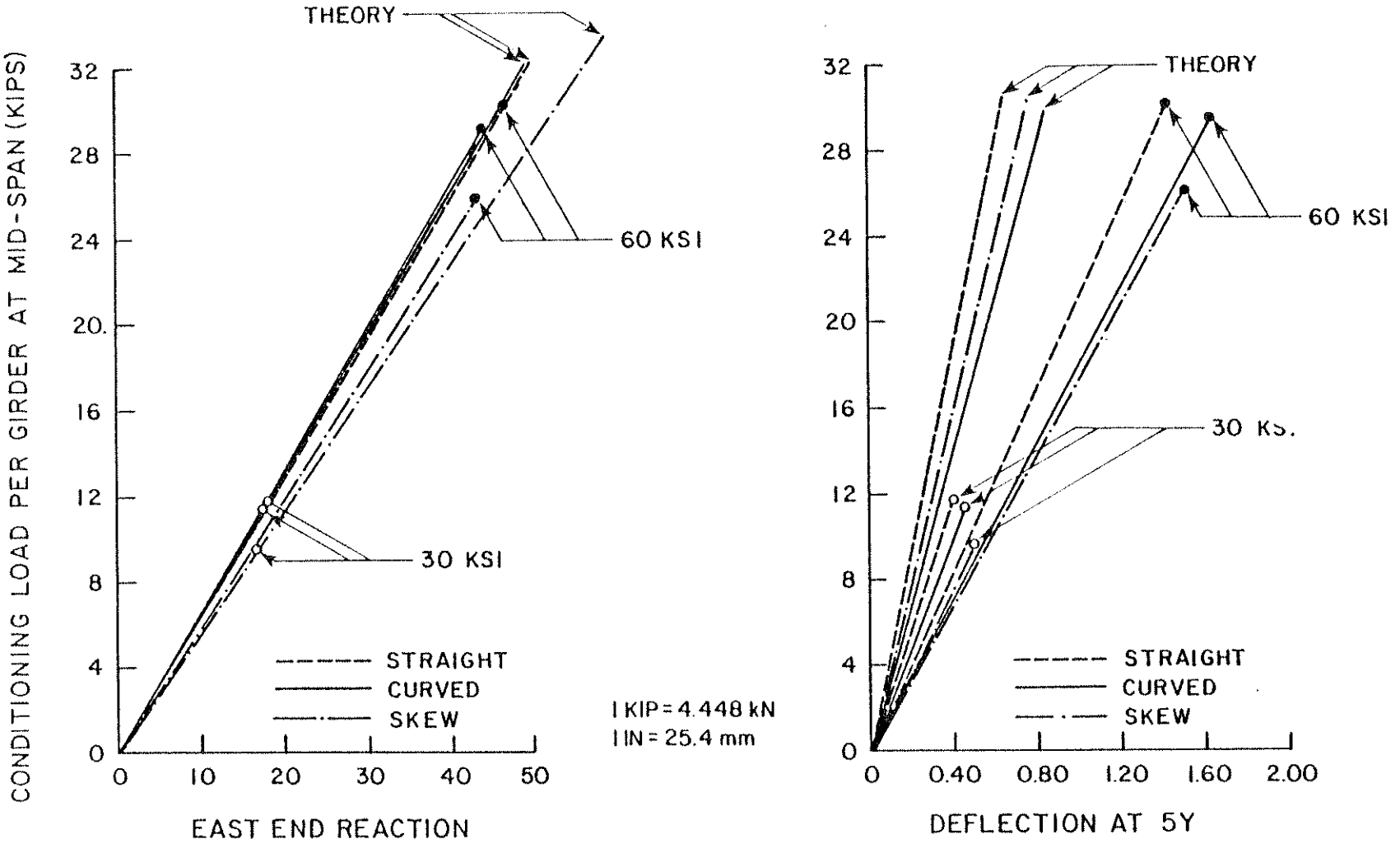

FIG. 7.23 TOTAL VERTICAL EAST END REACTION (KIPS) AND DEFLECTIONS (INCHES) AT 5Y FOR STRAIGHT, CURVED AND SKEW BRIDGE MODELS FOR 30 AND 60 KSI CONDITIONING LOADS

the 24, 30, 40, 50 and 60 ksi conditioning loads is given. These differ by only 0 to 2% of the total moment for all three bridges indicating little change under increased cracking. While the theoretical results shown for all three bridge types approach the 16.5, 22.4, 22.4, 22.4, 16.5% distribution to girders 1 to 5, which would be obtained for a uniform stress distribution across the entire cross-section, the experimental values for the skew bridge do not follow this pattern. In the diaphragmed Span I at section A, girder 1 takes a much larger portion and girder 5 takes a slightly smaller portion of the total moment in the skew bridge model as compared to the straight or curved bridges, while in the undiaphragmed Span II at section D both exterior girders take slightly larger portions of the total moment in the skew bridge.

Results of selected point load cases after 30 and 60 ksi conditioning loads are shown in Figs. 7.25 to 7.27 for the straight, curved and skew bridge models. The influence of skewness becomes quite obvious by comparing load case 1Y. Figure 7.25, with load case 5Y, Fig. 7.26. For loads on the obtuse side of the span (1Y), the total vertical end reaction is substantially higher for the skew bridge case in experiment and theory, while smaller total end reactions are registered in the skew bridge model for loads on the acute side of the span (5Y) than for the equivalent loadings on the straight or curved bridge models.

Deflections of the bridge models obtained at the location of the point load application show the same behavior. While for load case 1Y the deflections at 1Y for the skew bridge are smallest in theory and

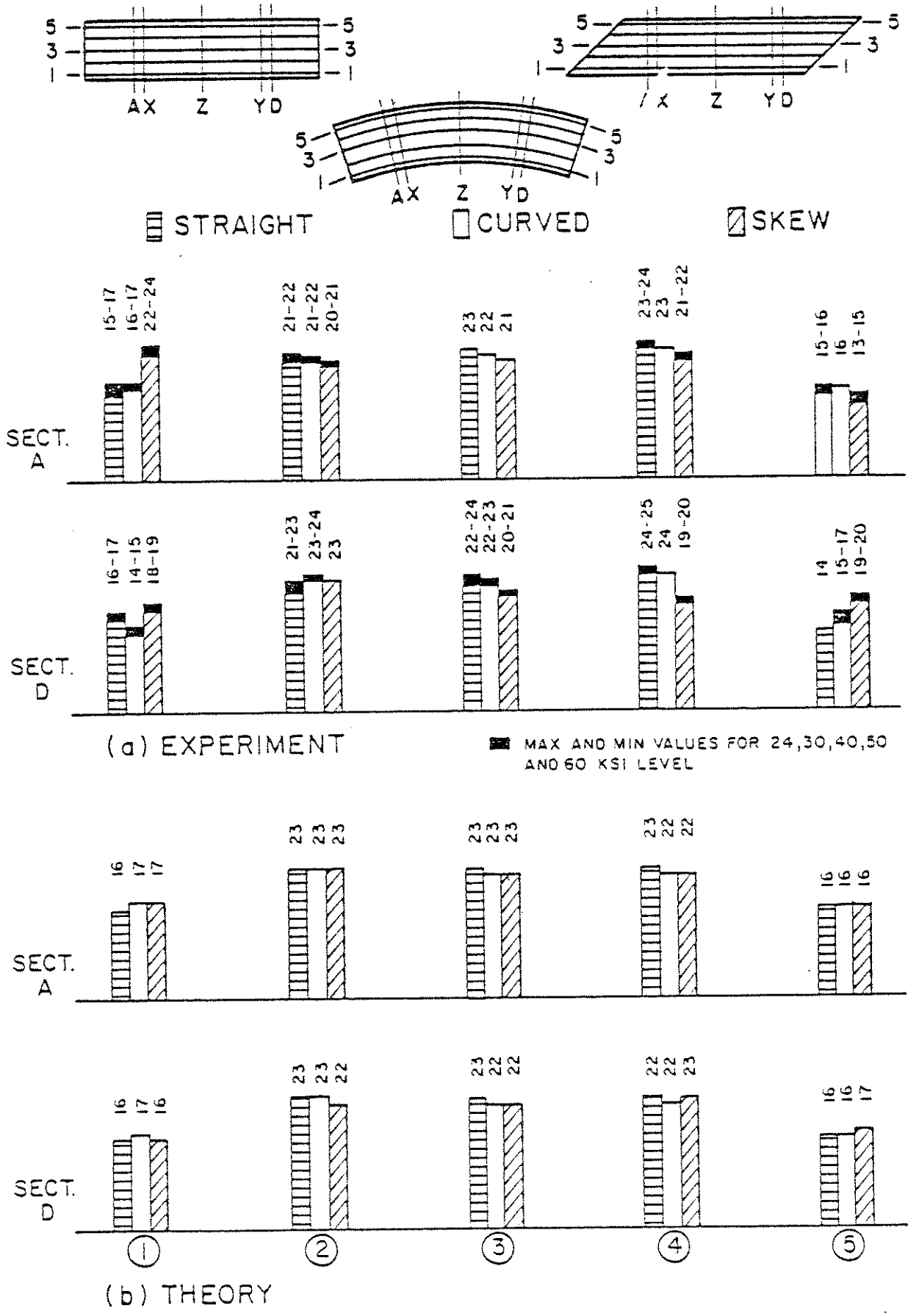

FIG. 7.24 PERCENTAGES OF TOTAL MOMENT AT A SECTION CARRIED BY EACH GIRDER FOR CONDITIONING LOAD—STRAIGHT VS. CURVED VS. SKEW BRIDGE MODELS

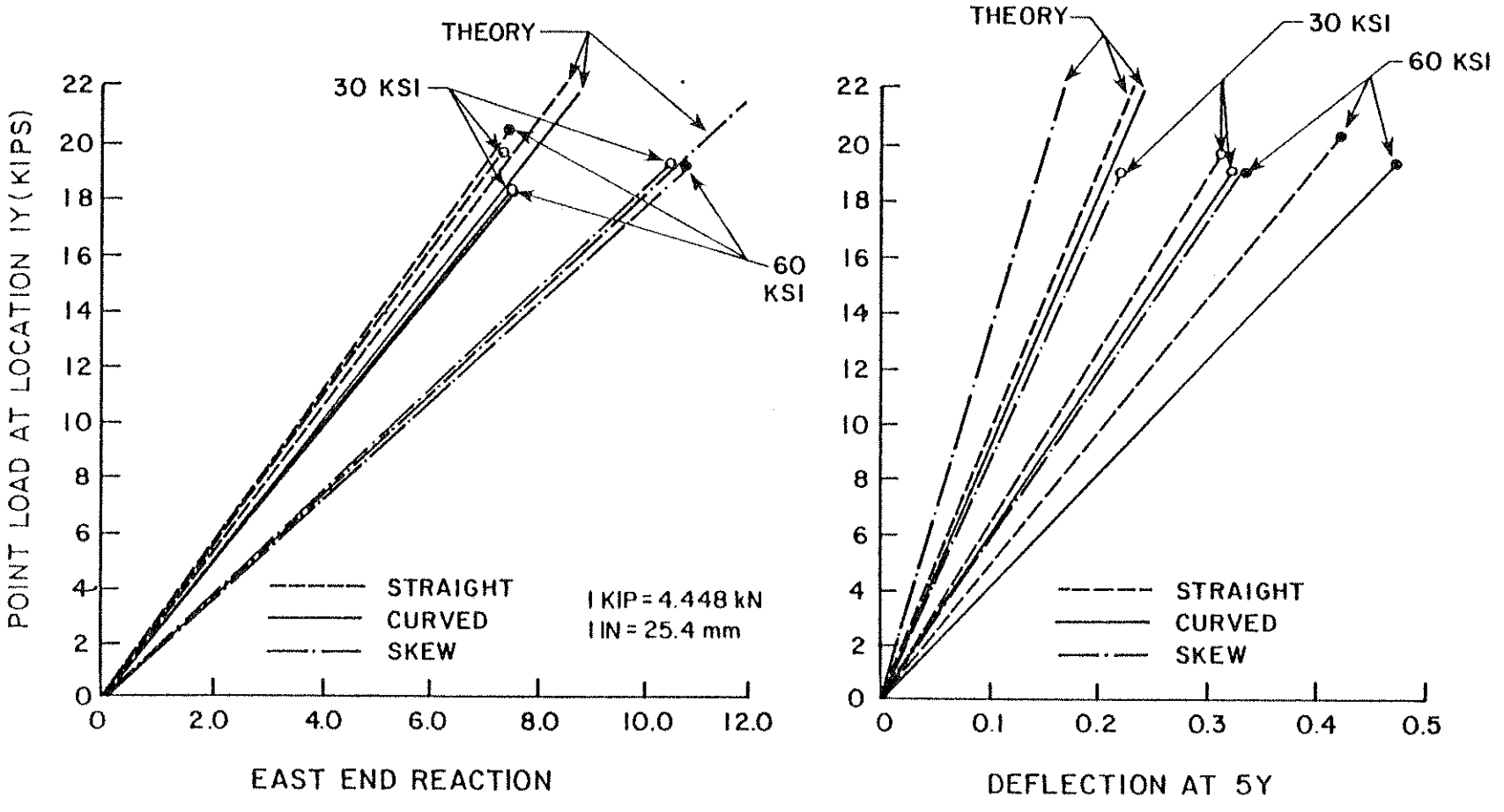

FIG. 7.25 TOTAL VERTICAL EAST REACTION (KIPS) AND DEFLECTION (INCHES) AT 5Y FOR A POINT LOAD AT 1Y AFTER 30 AND 60 KSI CONDITIONING LOADS —STRAIGHT VS. CURVED VS. SKEW BRIDGE MODELS

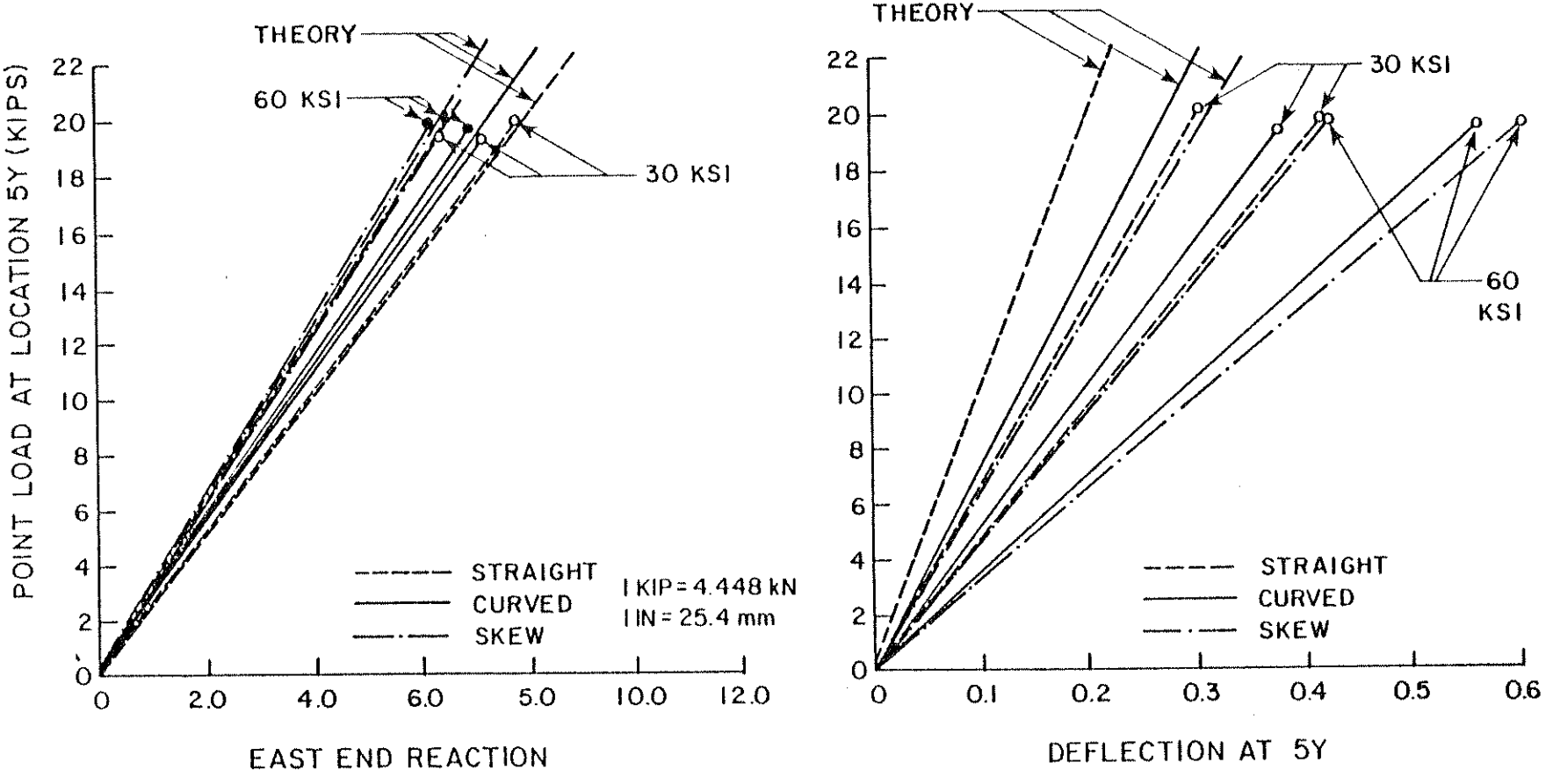

FIG. 7.26 TOTAL VERTICAL EAST REACTION (KIPS) AND DEFLECTION (INCHES) AT 5Y FOR A POINT LOAD AT 5Y AFTER 30 AND 60 KSI CONDITIONING LOADS —STRAIGHT VS. CURVED VS. SKEW BRIDGE MODELS

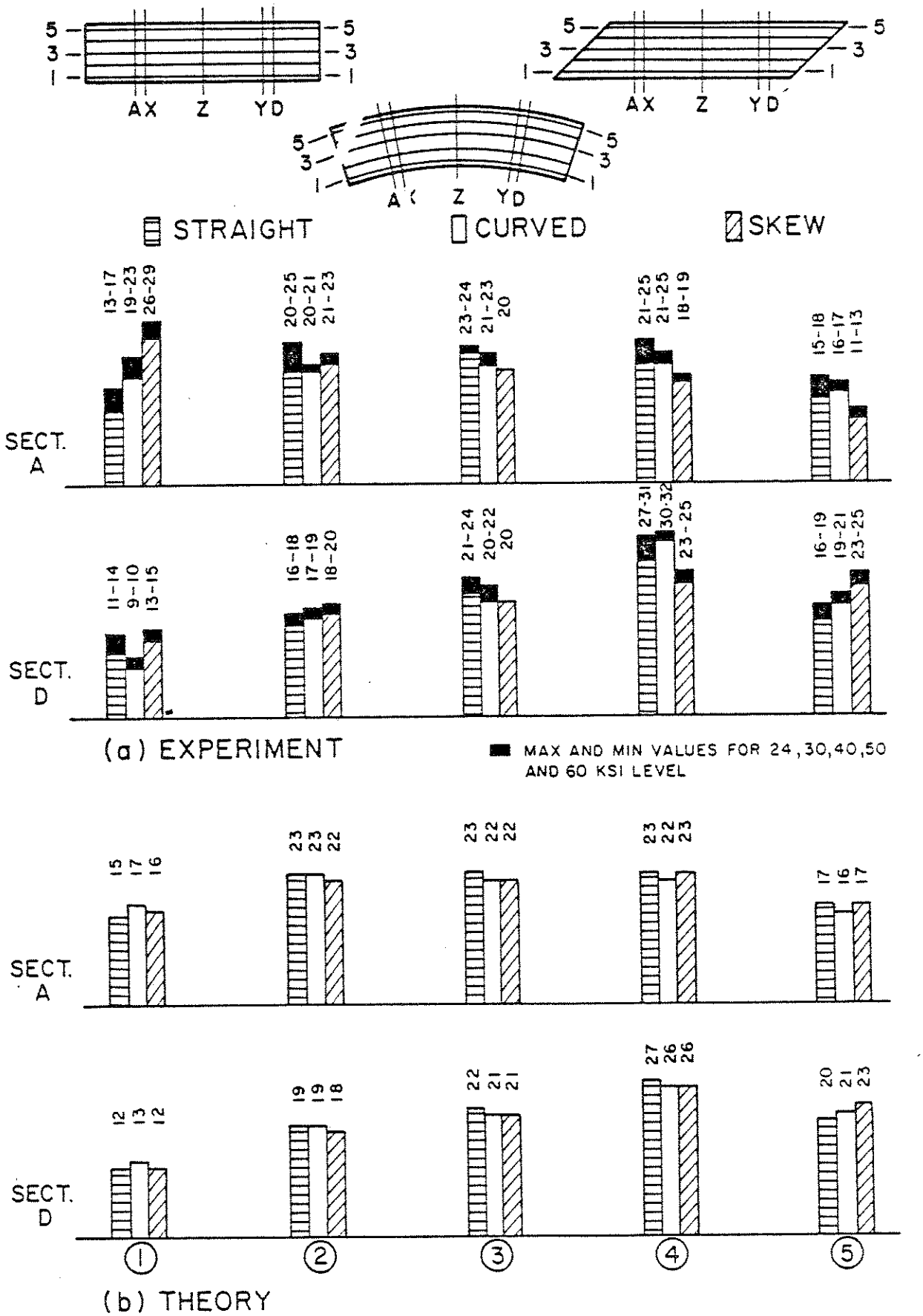

FIG. 7.27 PERCENTAGES OF TOTAL MOMENT AT A SECTION CARRIED BY EACH GIRDER FOR A POINT LOAD AT 5Y AFTER 24 TO 60 KSI CONDITIONING LOADS—STRAIGHT VS. CURVED VS. SKEW BRIDGE MODELS

after the 30 and 60 ksi experimental cases, the skew bridge features the highest deflections at location 5Y for load case 5Y.

The transverse moment distribution for a point load at 5Y after 24 to 60 ksi conditioning loads is given in Fig. 7.27. Again it can be noticed that experimentally, the skew bridge takes larger portions of the total moment in the loaded span in the exterior girders 1 and 5 as compared to the straight or curved bridges.

7.5 Summary

Detailed discussions of the results for the overload stress levels produced by increasing conditioning loads and for working stress point loads applied after each successively higher conditioning load have been presented. The most important conclusions for the skew bridge model studied are summarized below.

1. Total measured vertical reactions at the end abutments and at the center column of the bridge can be predicted with sufficient accuracy by theory for all load levels. For increasing conditioning load levels a slight decrease in the total vertical end reactions along with a small increase in the center footing reactions can be observed.

2. The total measured end moment (and torque) decreases considerably with increasing conditioning loads but remains virtually unchanged for the same working stress point loads after different conditioning load levels.

3. The increase in total experimental midspan moment due to the decrease in end moment is compensated by the simultaneous decrease in the total vertical end reaction under increasing conditioning load levels, so that little change occurs in the total midspan moment.

4. Theory can be used to adequately predict the magnitude and distribution of deflections at each conditioning load level provided a proper magnification factor is used to account for the progressive cracking of the bridge under increasing conditioning loads. These magnification factors would range from 1.4 to over 2.2 for 24 to 60 ksi conditioning load levels.

5. Concrete and steel strains show essentially a linear load vs. strain behavior and the strains per unit load are almost the same for all load levels.

6. Total moments obtained from internal forces at the instrumented midspan sections A and D can be predicted within 9% by theory for all conditioning load cases. The same margin of accuracy can be achieved for the total moments at sections A, D and Z calculated from external reactions.

7. Changes in the transverse distribution of moments at a section under uniform load across the width of the bridge such as the conditioning loads are small (less than 2% generally) for all overload stress levels.

These changes are much greater for single point loads applied after the above conditioning overloads and can range generally from 1 to 5% and 1 to 2% of the total moment at sections A and D respectively.

8. Theoretical calculations based on the CELL program predict the transverse distribution of the total moment with sufficient accuracy at undiaphragmed section D. At section A, near the staggered midspan diaphragm much higher experimental values were found for exterior girder 1 on the acute side of the span than the ones predicted by theory. This is probably due to close proximity of the staggered diaphragm to the instrumented section in girder 1.

9. Some differences in the response of the skew bridge model as compared to the similar straight or curved bridge models were observed. Under conditioning loads, end vertical reactions were larger and total midspan moments were smaller for the skew bridges. The experimental distribution of these total moments to individual girders showed higher percentages for the skew bridge going to exterior girders 1 and 5 at section D and especially to girder 1 at section A. Theoretical distributions did not exhibit such differences and were essentially the same for all three bridges. Decreases in stiffness due to cracking resulting in higher deflections under increasing

conditioning loads appeared to be about the same for all three bridge types. Effects of skewness under certain working point loads after successively higher overloads are even more pronounced than that of the uniform conditioning loads, when comparing the response of the three bridge types.

8. SHEAR RESPONSE OF BOX GIRDER MODEL

8.1 General Remarks

In the design of box girder bridges, the distribution of the total bending moment at a given section among the individual girders is of major importance. Values for shear forces are generally of interest near supports, i.e., at the end abutments or in the region of the center bent if the bridge is continuous. The effects of the introduction of skewness on the bridge bending moments has been treated in detail in Chapter 2, wherein it is illustrated how midspan moments are changed as a result of skew supports and diaphragms. The effect of skewness on shears is mainly to bring about a different shear distribution because of the manner in which skewness modifies the distribution of the girder reactions at the abutments. As a result, the shear force is increased at the obtuse corners of skew structures and in the vicinity of intermediate supports of continuous skew bridges.

The skew box girder bridge model of the present study has been analyzed by the finite element computer program CELL, using both coarse and fine mesh discretizations. From the CELL program, the theoretical shear force in a girder web at any section is calculated by averaging the values of the internal forces N_{xy} as output by CELL at the top and bottom nodes of each web and multiplying by the overall depth of the web.

The investigation of shear forces for the skew box girder model was directed towards the following objectives:

(1) Evaluation of the total shear force at a section and the transverse distribution of this force to individual

girders as well as the longitudinal variation of the individual girder shears as indicated by their shear force diagrams;

(2) An assessment of the accuracy with which the CELL program predicts the shear forces in box girder bridges;

(3) The feasibility of using an approximate method for the calculation of shear forces.

Three load cases were chosen for the detailed study of shear force effects: the dead load, conditioning load and the 1X load cases. These represent a range of important cases covering distributed as well as highly concentrated and eccentrically positioned loads. The CELL values given in the figures in this chapter are taken mainly from the CELL FINE analyses.

8.2 Theoretical Results from CELL Analyses

The shear forces in individual girders as obtained from the CELL program for the dead load, conditioning load and the 1X load cases are plotted in Figs. 8.1, 8.2 and 8.3. The dead load case comprises only the self weight of the bridge model; the conditioning load case has been normalized to a load value of 100 kips (445 kN) per span and the 1X load case to a load of 100 kips (445 kN) at the location 1X in Span I. As CELL does not output reliable values for the shears at the supports and at the diaphragms, such values have been extrapolated and indicated in the figures in each case.

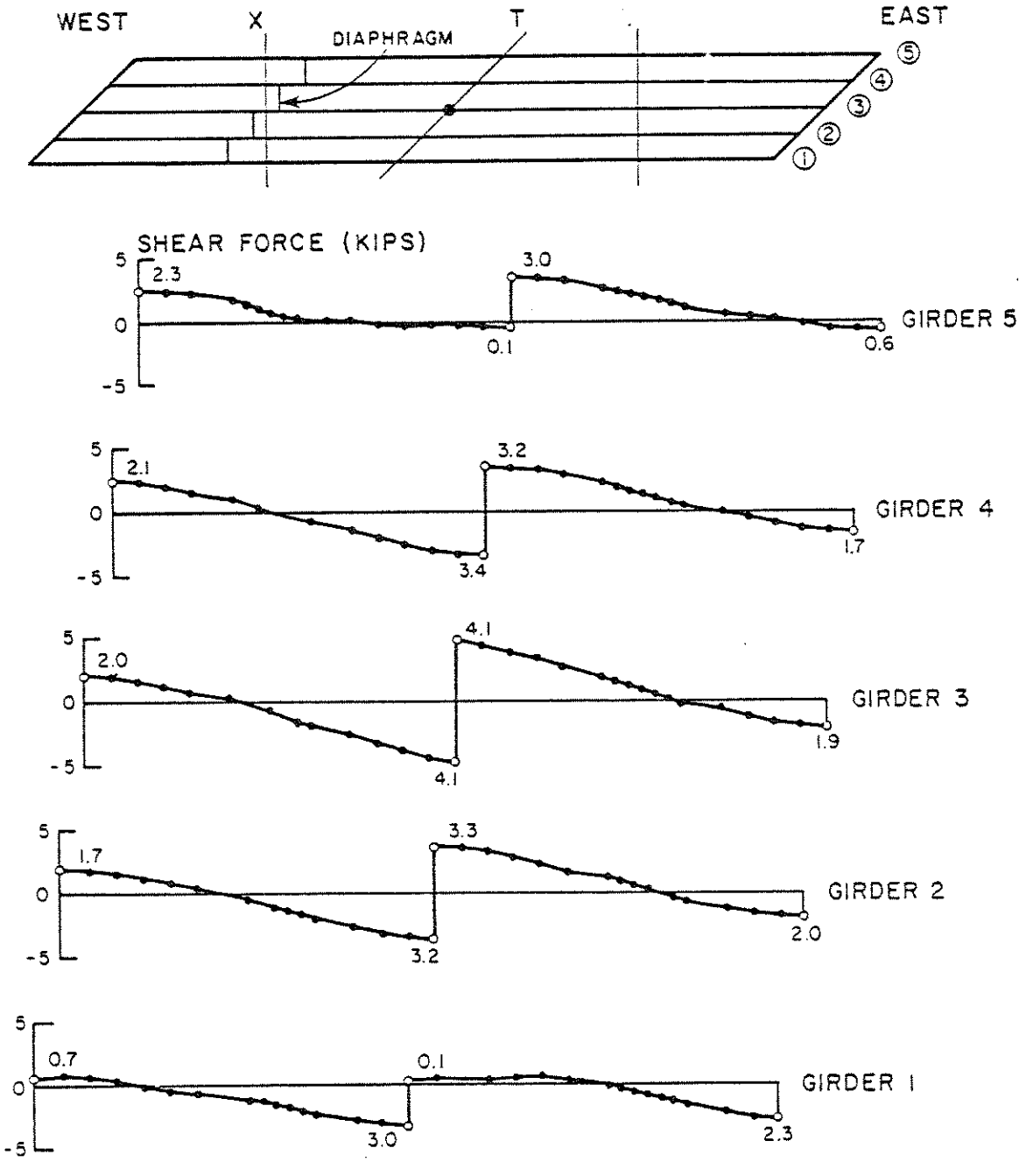

FIG. 8.1 THEORETICAL INTERNAL SHEAR FORCES IN INDIVIDUAL GIRDERS DUE TO SELF-WEIGHT OF BRIDGE MODEL

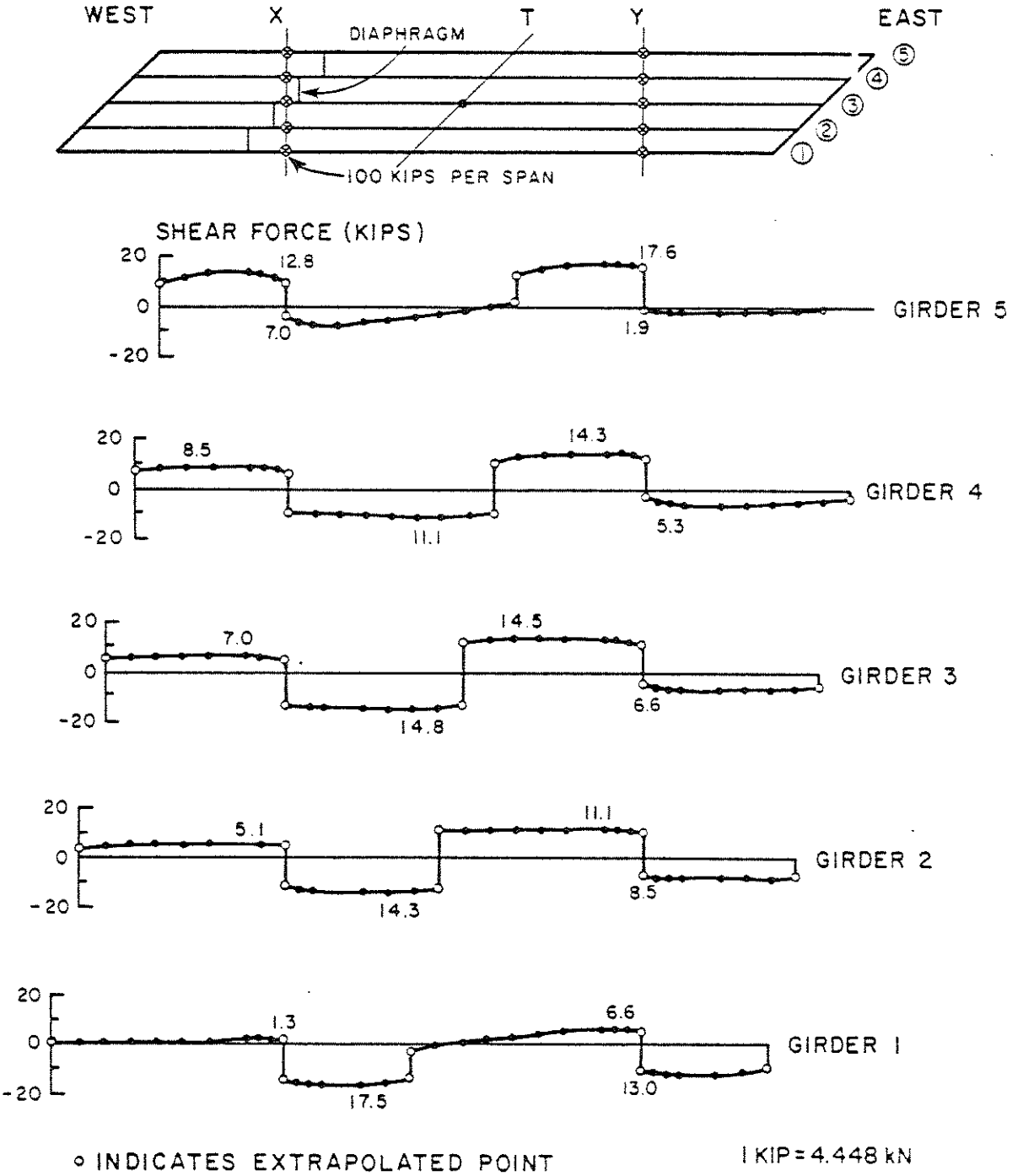

FIG. 8.2 THEORETICAL INTERNAL SHEAR FORCES IN INDIVIDUAL GIRDERS DUE TO CONDITIONING LOADS

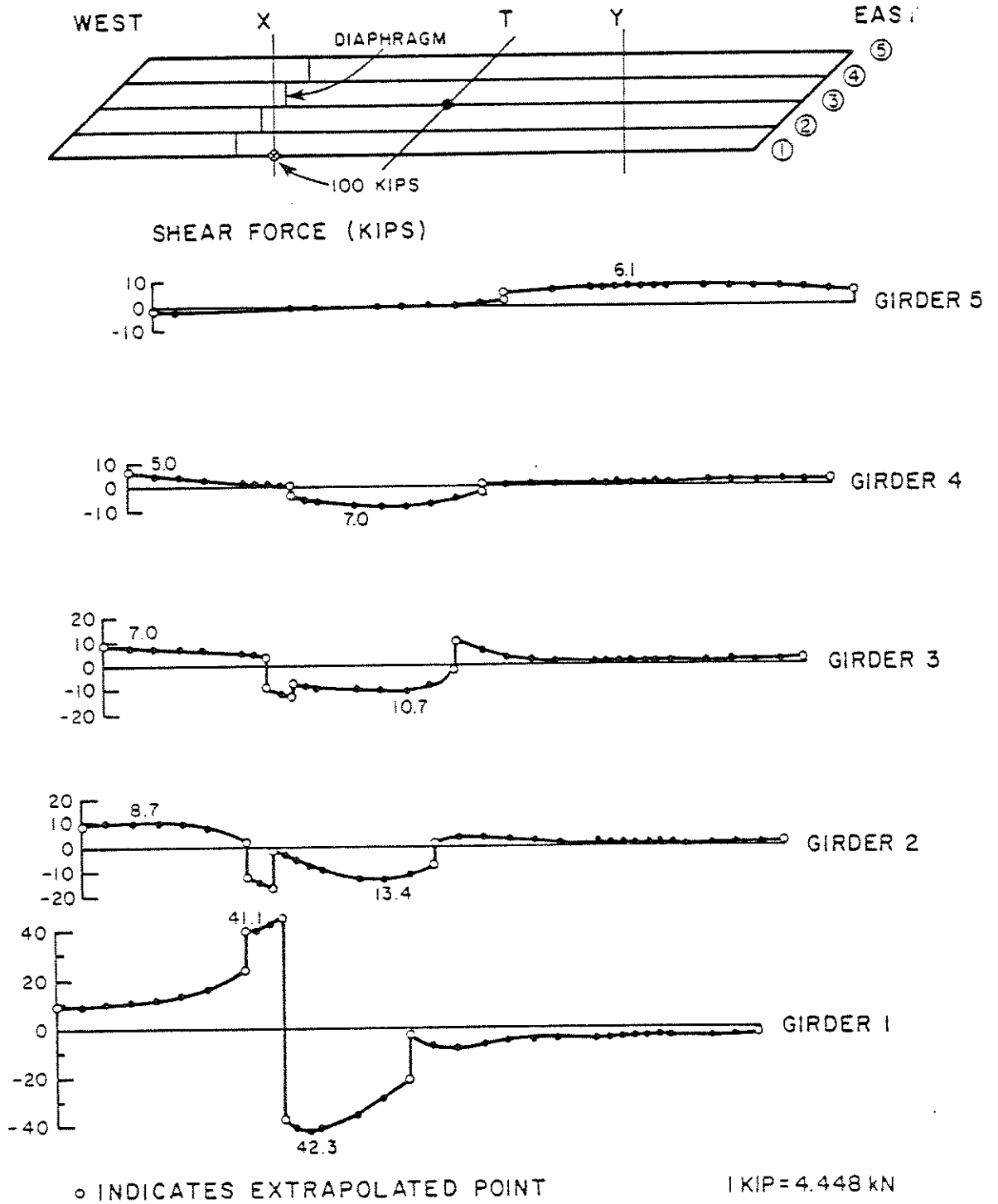

FIG. 8.3 THEORETICAL INTERNAL SHEAR FORCES IN INDIVIDUAL GIRDERS DUE TO 100 KIP (445 kN) POINT LOAD AT 1X

From Fig. 8.1 for the dead load case it is observed that the shear at the obtuse corners (1E and 5W) is greater than at the acute corners (1W and 5E), but this effect is much less marked than for the conditioning and 1X load cases, shown in Figs. 8.2 and 8.3. It may also be noted from Fig. 8.1 that in the region of the center bent the largest share of the total shear force is carried by girder 3, i.e., the middle girder. This is because girders 1 and 2 are elastically supported by the thick center bent diaphragm whereas there is a column support under the center bent diaphragm at girder 3. A greater local slope in the girder shear force diagrams is observed for each girder in Fig. 8.1 in the midspan region of Span I because of the effect of the additional weights of the midspan diaphragms in this span.

The internal shear forces in individual girders corresponding to the conditioning load, Fig. 8.2, show a pronounced concentration at the obtuse corners of the bridge model. The explanation lies in the fact that all loading for the conditioning load case is at the midspans from where it can feed more directly into the obtuse corners, as opposed to the distributed loading corresponding to the dead load case, in which the individual girders carry their self weights along their whole lengths. In Fig. 8.3 the shear force diagrams for individual girders, corresponding to the highly eccentric concentrated loading case 1X are shown. Note the large shear force carried by girder 1 and that there are breaks in the curves in the locations where the transverse midspan diaphragms frame into the girders.

The total shear forces at right sections in the box girder bridge model for the dead load, conditioning and 1X load cases are plotted in Figs. 8.4, 8.5 and 8.6. In each figure, the solid line indicates the

shear forces calculated from the external forces and reactions (as obtained from CELL) and the broken line indicates the sum over the section of the internal shear forces in the individual girders as calculated from CELL and plotted in Figs. 8.1, 8.2 and 8.3. On the whole, close agreement between the shear forces calculated from the external and internal forces is observed, especially in regions where there are no load concentrations or connections with diaphragms. It is to be noted that the shear values in Figs. 8.2, 8.5 and 8.6 in the region of the center bent consist mainly of extrapolated ordinates and that the center bent skew diaphragm participates with the girder webs in carrying the total external shear.

8.3 Theoretical Results at Skew Sections

In order to investigate the agreement between the shear forces as calculated from the external forces and reactions with those calculated from internal forces more thoroughly, especially in the vicinity of the end support abutments and in the region of the center bent, it was decided to study the shear behavior at the skew sections L, M, N and O as shown in Fig. 8.7. These sections were chosen so as to coincide with the positions of strain gage rosettes attached to the girder webs for the measurement of shearing strains, and thus to provide a check on the experimentally obtained values.

Figure 8.8 shows the distribution of theoretical abutment reactions and shear forces at sections L and O due to dead load as calculated by CELL. It is observed that the shear forces are considerably smaller in magnitude than the corresponding reactions. This discrepancy is due to two reasons.

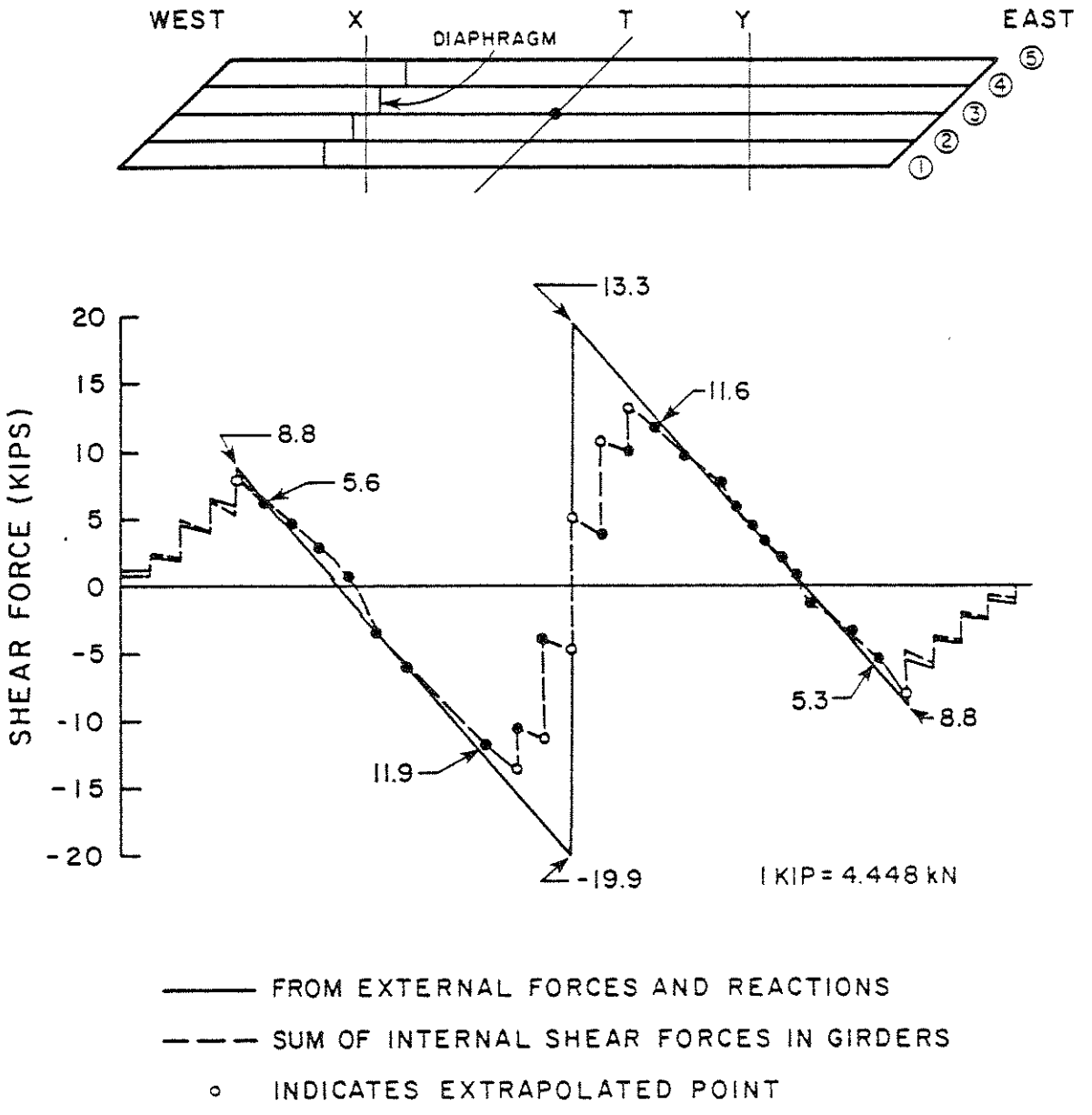

FIG. 8.4 TOTAL EXTERNAL AND INTERNAL THEORETICAL SHEAR FORCES AT RIGHT SECTIONS DUE TO SELF-WEIGHT OF BRIDGE MODEL

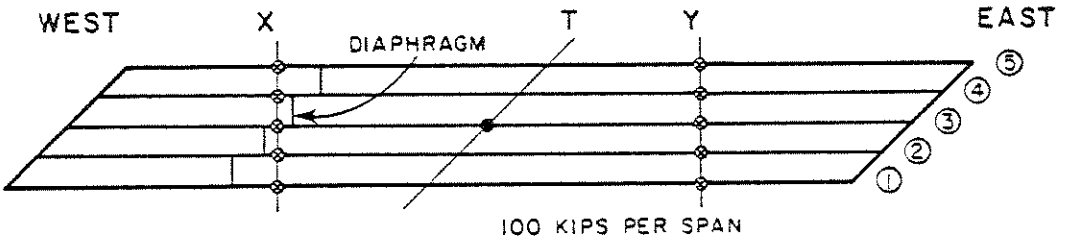

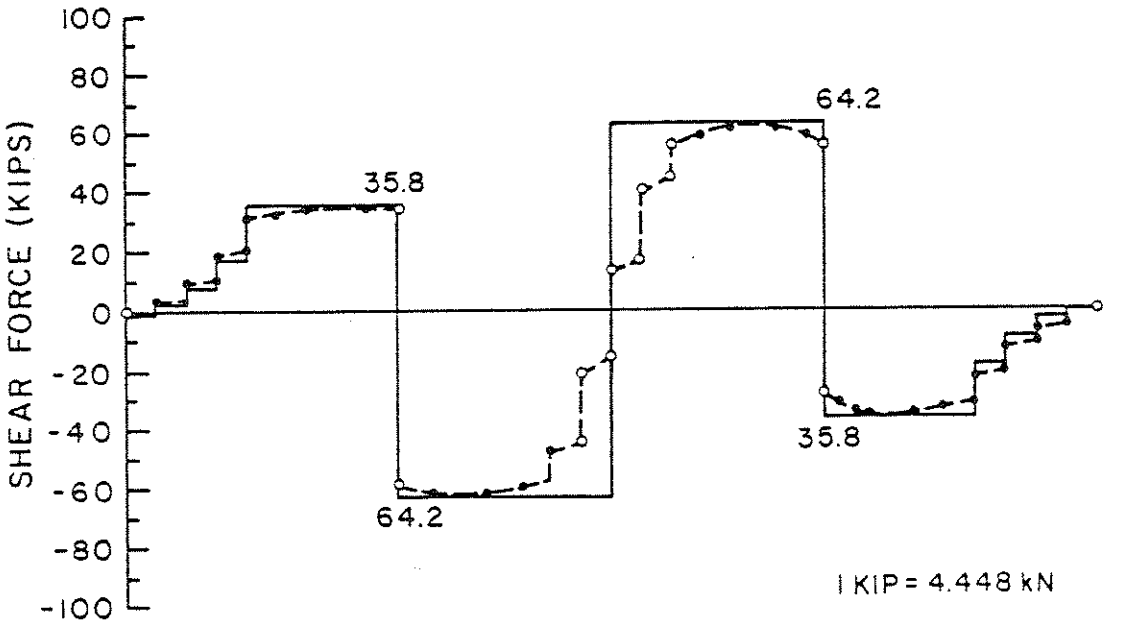

——— FROM EXTERNAL FORCES AND REACTIONS

— — — SUM OF INTERNAL SHEAR FORCES IN GIRDERS

○ INDICATES EXTRAPOLATED POINT

FIG. 8.5 TOTAL EXTERNAL AND INTERNAL THEORETICAL SHEAR FORCES AT RIGHT SECTIONS FOR CONDITIONING LOADS

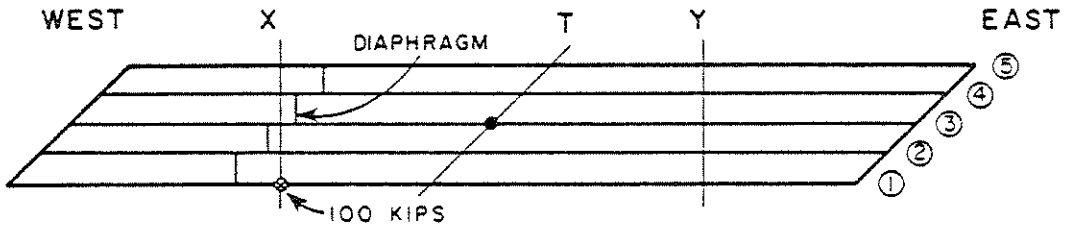

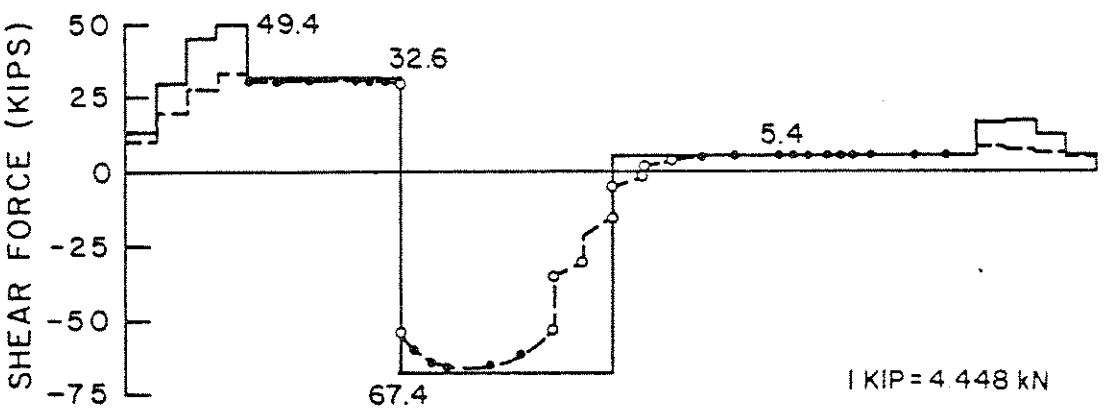

——— FROM EXTERNAL FORCES AND REACTIONS

— — — SUM OF INTERNAL SHEAR FORCES IN GIRDERS

o INDICATES EXTRAPOLATED POINT

FIG. 8.6 TOTAL EXTERNAL AND INTERNAL THEORETICAL SHEAR FORCES AT RIGHT SECTIONS DUE TO 100 KIP (445 kN) POINT LOAD AT 1X

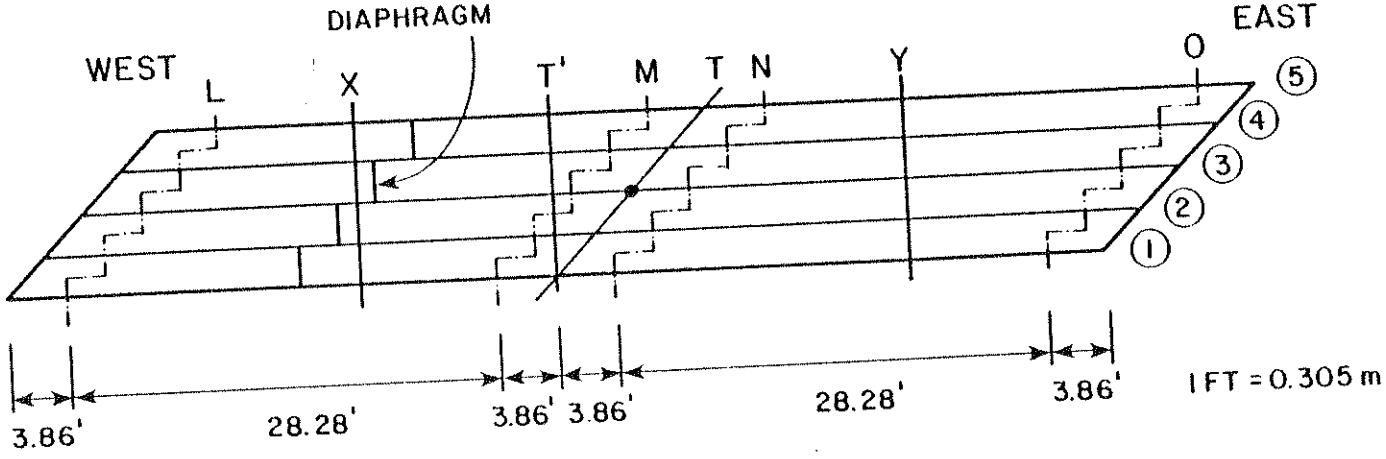

FIG. 8.7 LOCATIONS OF SKEW SECTIONS INSTRUMENTED WITH STRAIN GAGE ROSETTES ON GIRDER WEBS

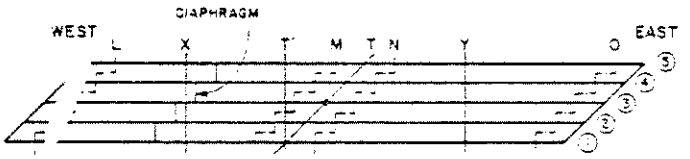

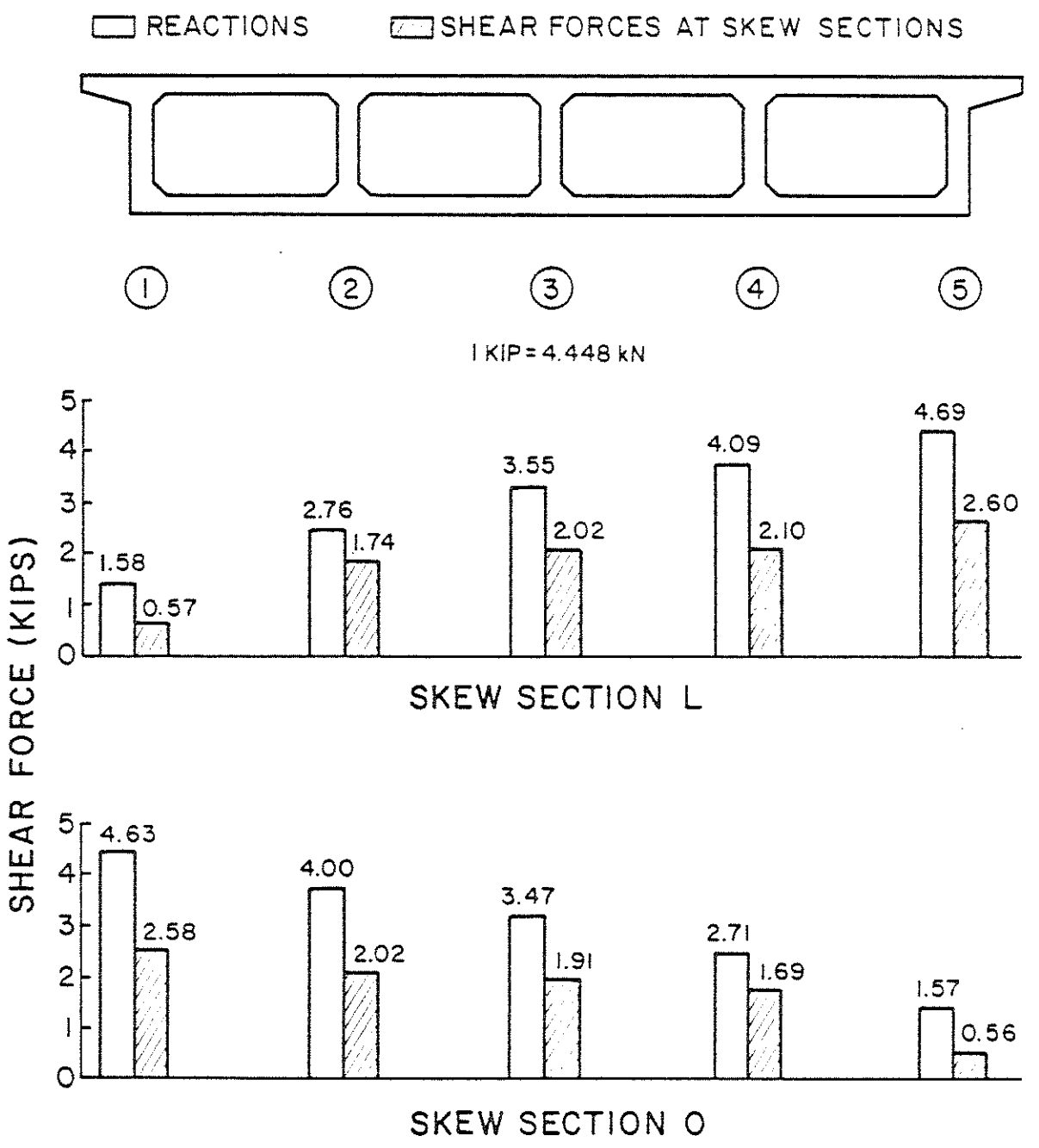

FIG. 8.8 COMPARISON OF THEORETICAL INTERNAL GIRDER SHEAR FORCES (KIPS) AT SKEW SECTIONS L AND O AND CORRESPONDING EXTERNAL REACTIONS (KIPS) DUE TO SELF-WEIGHT OF BRIDGE MODEL

(1) the dead load acts between skew sections W and L, also between O and E, causing the shear values to be smaller than the reactions by the amount of the dead load, and

(2) part of the difference between the reactions and the shear forces is carried by the slabs as transverse slab shears.

In Fig. 8.9 the distribution of shear forces in individual girders over the skew sections M and N on either side of the center bent as obtained from CELL internal forces is given for the dead load case. The greatest amount of shear is seen to be carried by the middle girder. Figure 8.10 contains a bar chart comparison between the total external reactions due to dead load and the total internal shear forces at the skew sections L, M, N and O as given by CELL for the dead load case.

Figures 8.11, 8.12 and 8.13 are similar to Figs. 8.8, 8.9 and 8.10 but apply to the conditioning load case. In Fig. 8.11, the external reactions as obtained from CELL are compared with the girder internal shear forces calculated from CELL for the skew sections L and O. The discrepancy between the reactions and the shear forces is smaller for the conditioning load case than for the dead load case because the conditioning load acts only at the midspans and no distributed load is involved. However, the transverse shear in the slabs, not included in the girder shears, results in the reactions having higher values than the girder shear forces. Figure 8.12 shows the shear force distribution as obtained from CELL internal forces at the skew sections M and N for the individual girders. The total internal values of shear forces are

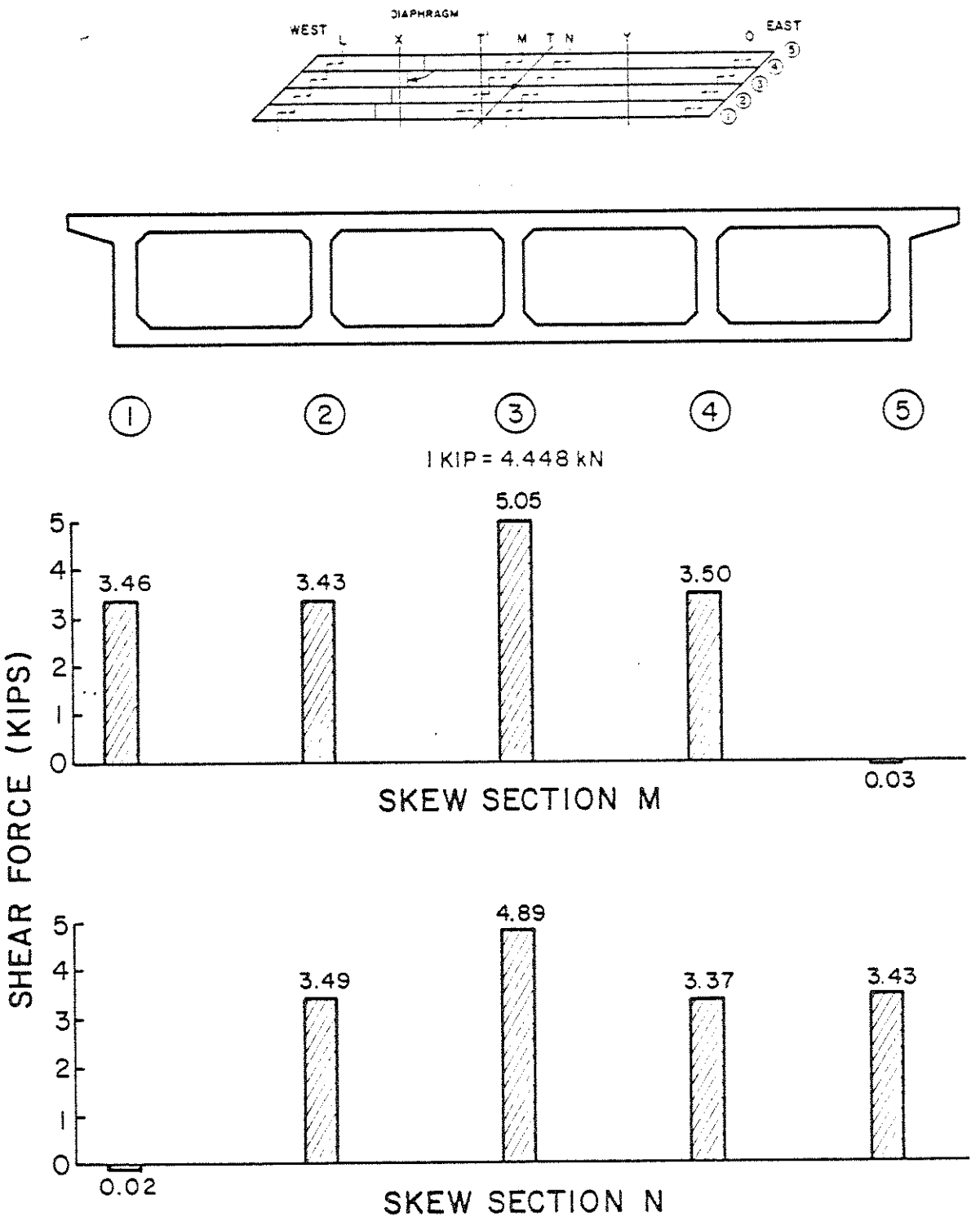

FIG. 8.9 THEORETICAL INTERNAL GIRDER SHEAR FORCES (KIPS) AT SKEW SECTIONS M AND N DUE TO SELF-WEIGHT OF BRIDGE MODEL

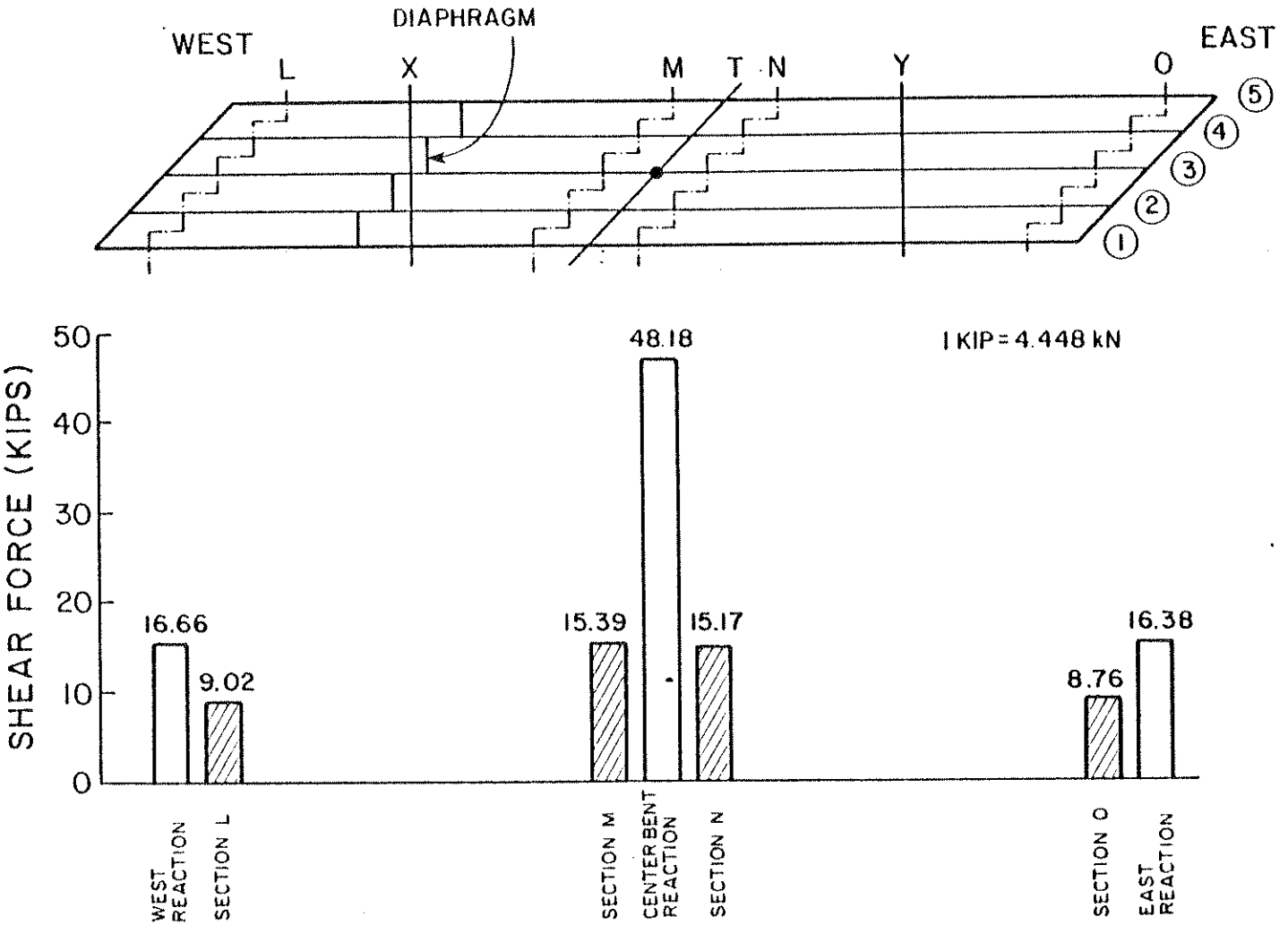

FIG. 8.10 TOTAL THEORETICAL INTERNAL SHEAR FORCES (KIPS) AT SKEW SECTIONS L, M, N AND O AND TOTAL EXTERNAL REACTIONS DUE TO SELF-WEIGHT OF BRIDGE MODEL

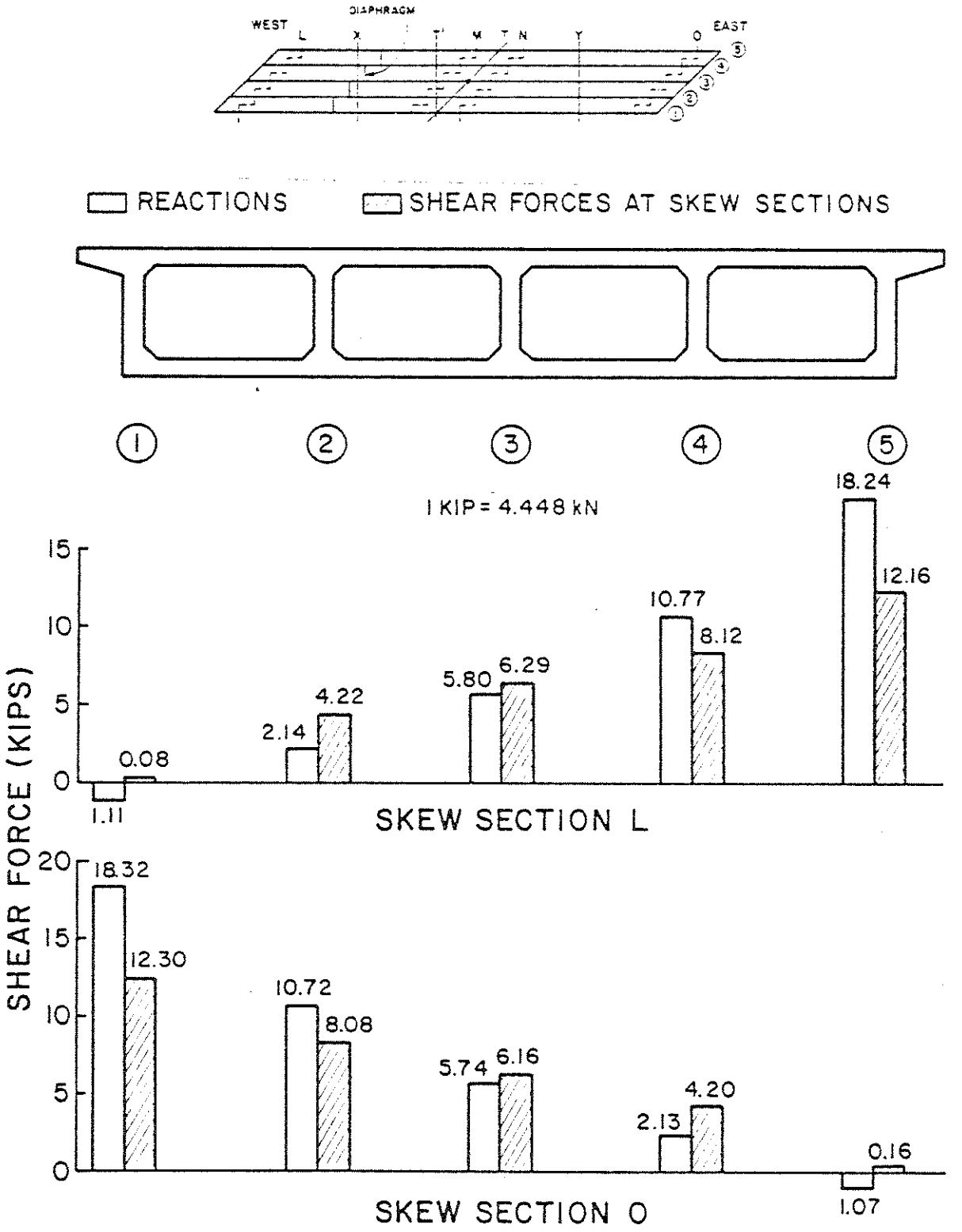

FIG. 8.11 COMPARISON OF THEORETICAL INTERNAL GIRDER SHEAR FORCES (KIPS) AT SKEW SECTIONS L AND 0 AND CORRESPONDING EXTERNAL REACTIONS (KIPS) FOR CONDITIONING LOADS

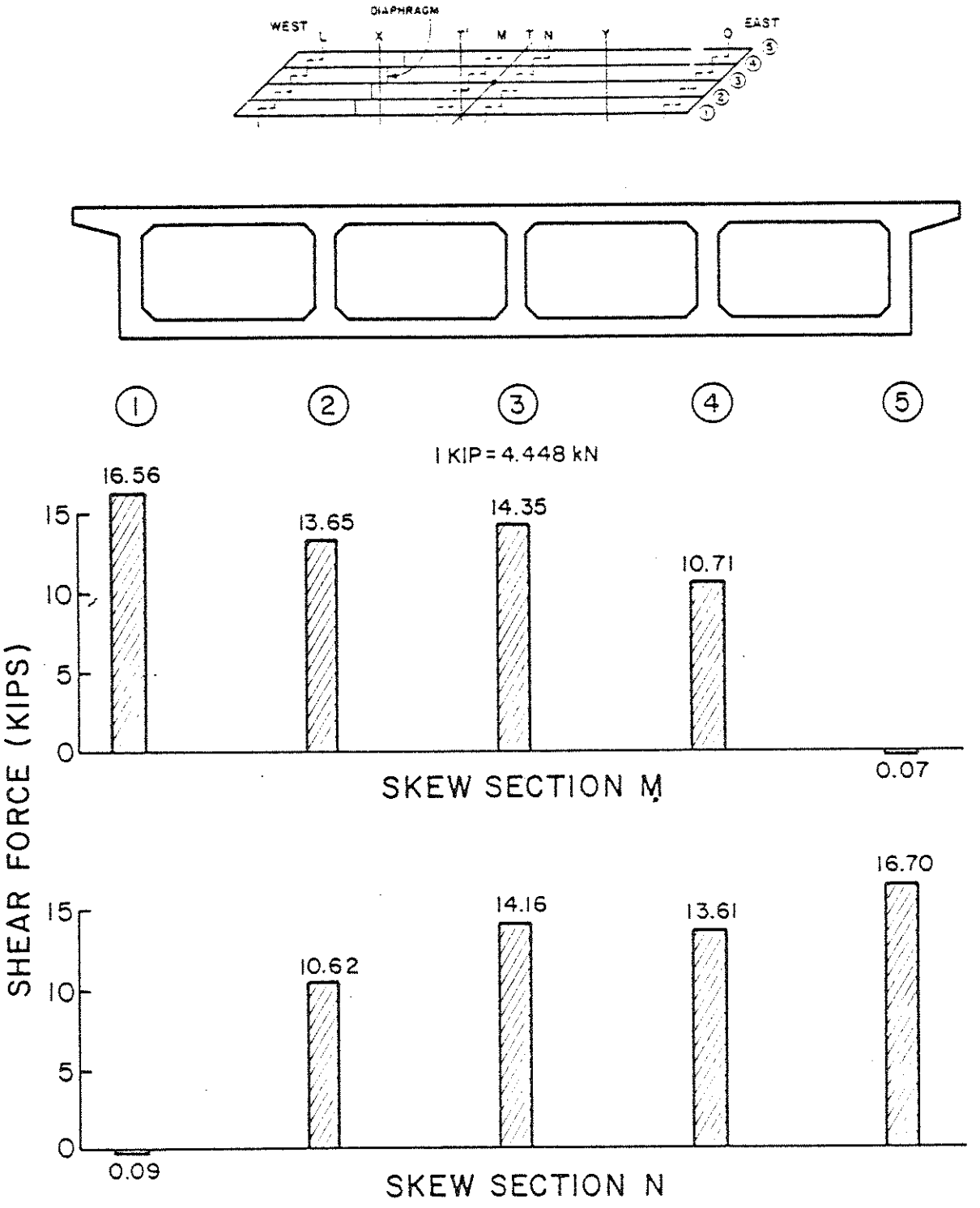

FIG. 8.12 THEORETICAL INTERNAL GIRDER SHEAR FORCES (KIPS) AT SKEW SECTIONS M AND N FOR CONDITIONING LOADS

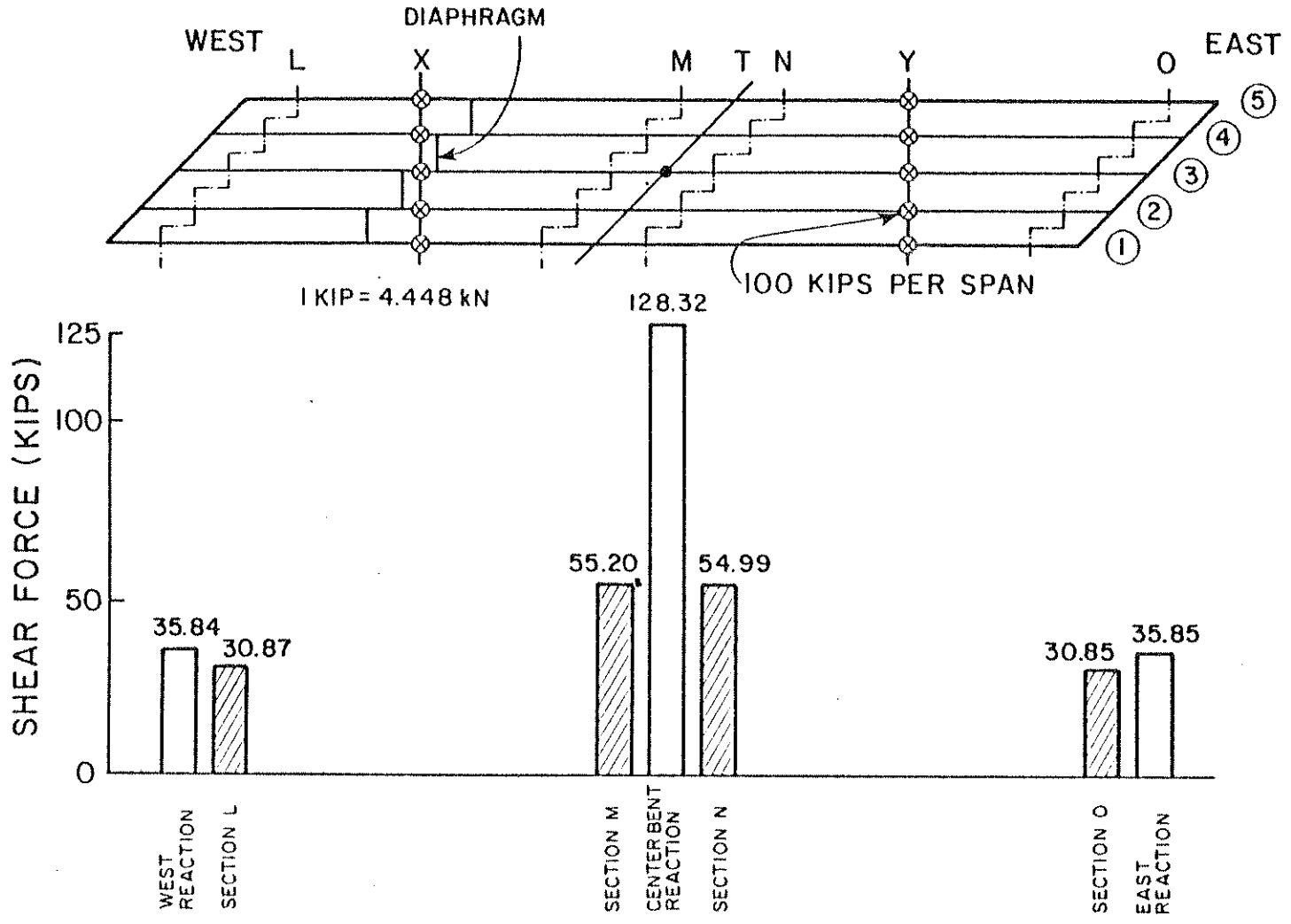

FIG. 8.13 TOTAL THEORETICAL INTERNAL SHEAR FORCES (KIPS) AT SKEW SECTIONS L, M, N AND O AND TOTAL EXTERNAL REACTIONS FOR CONDITIONING LOADS

compared in a bar chart (Fig. 8.13) with the total external reactions due to conditioning load, both sets of values having been obtained from CEL..

Figure 8.14 shows the external and internal total shear diagrams due to the conditioning load obtained by summing the shear forces at the skew sections, parallel to the end abutments and the center bent girder.

From the above figures it is observed that there are considerable differences in the vicinities of the skew abutments and the center bent between total shears calculated as the sum of the shear forces in individual girders and those obtained from the external loads and reactions. These differences are occasioned by the redistribution of loads transversely between girders and by the direct transfer of a part of the load into the diaphragms and supports in the transverse direction. Both these effects result from the high transverse distortional resistance of the box section. Shear forces per unit length Q_{yy} resulting from the transverse flexural effect contribute to transverse loading transfer, as is shown for the skew section M in Fig. 8.15. This beneficial effect, while reducing the girder web shear force values in the most stressed areas of the structure considerably, also necessitates the investigation of the stresses in the transverse direction, particularly the transverse distortional slab bending moments in the flanges and webs.

Figure 8.16.a shows the transverse slab distortional bending moment diagram due to the conditioning load for the right section T' at a distance of 5.14 ft (1.57 m) from section Z and passing through one end of the center bent diaphragm. Transverse shear forces Q_{yy} corresponding to these distortional moments are plotted in Fig. 8.16.b.

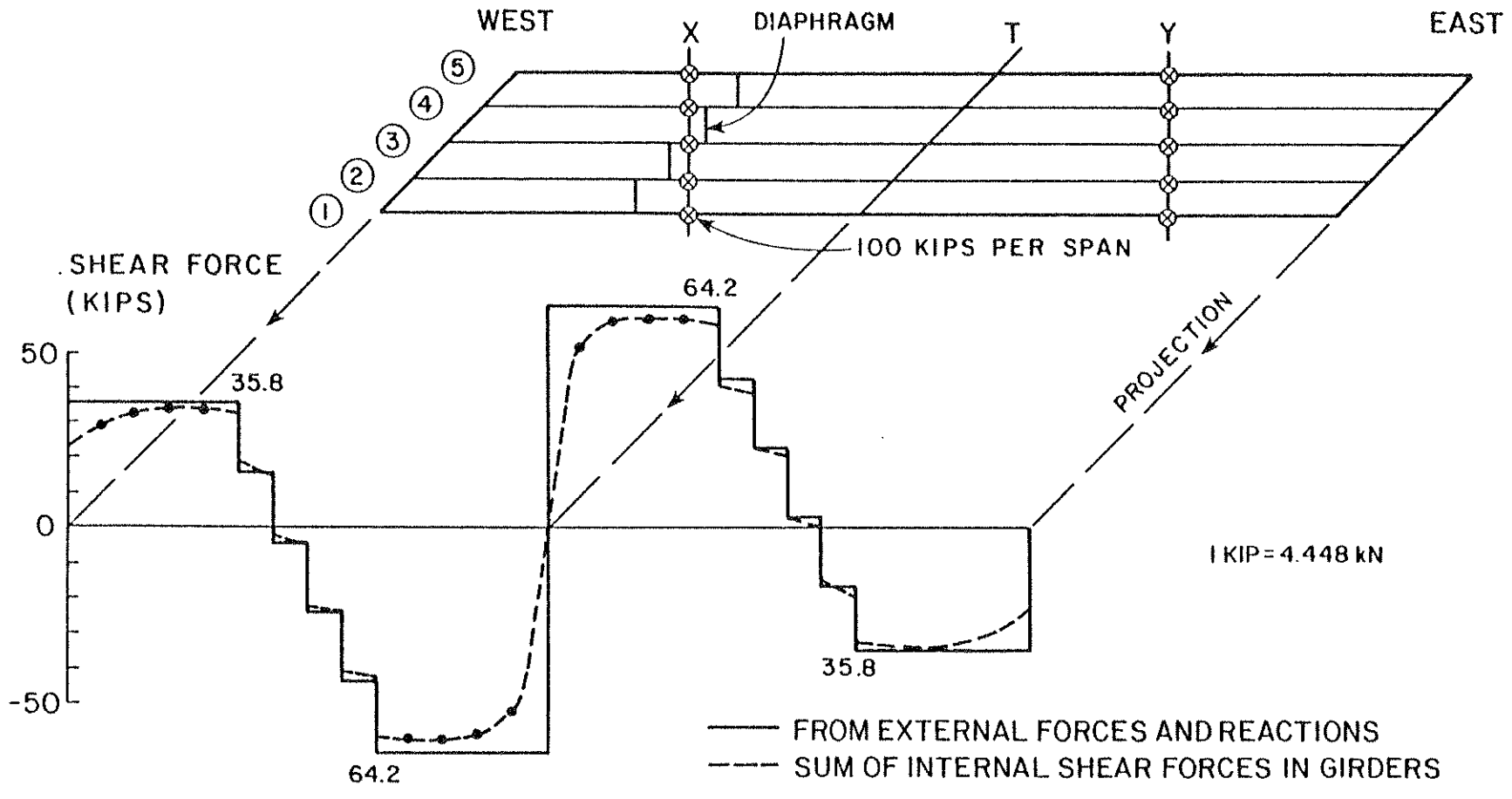

FIG. 8.14 TOTAL THEORETICAL EXTERNAL AND INTERNAL SHEAR FORCES (KIPS) AT SKEW SECTIONS FOR CONDITIONING LOADS

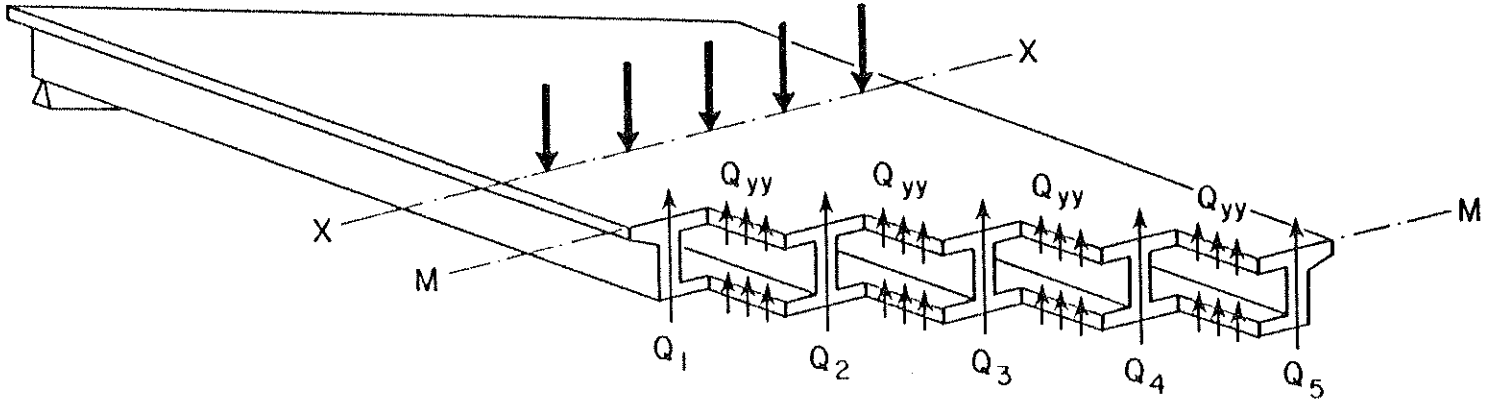

FIG. 8.15 TRANSVERSE LOAD TRANSFER AT SKEW SECTION M FOR CONDITIONING LOADS

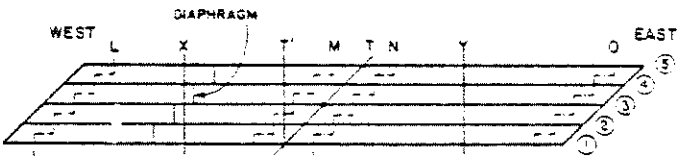

(a) M_{yy}

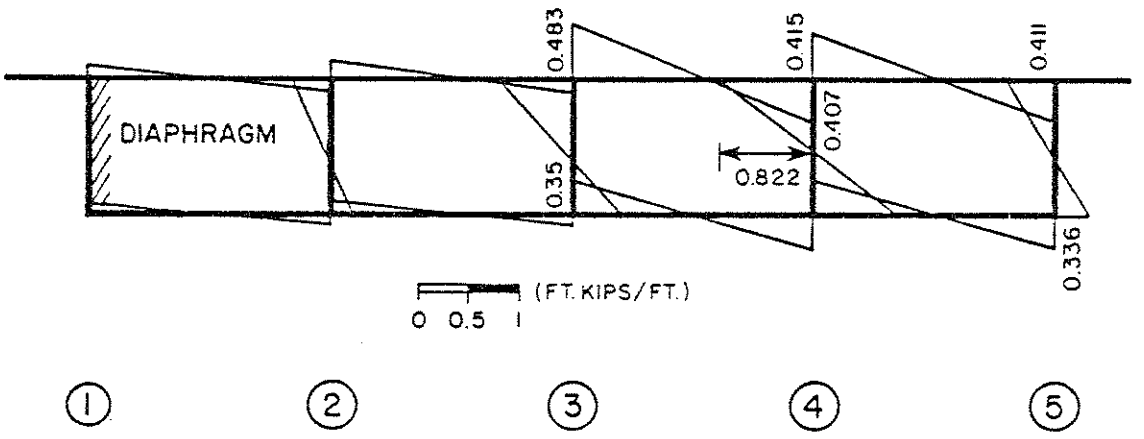

1 FT-KIP/FT = 4.448 kN-m/m

(b) Q_{yy}

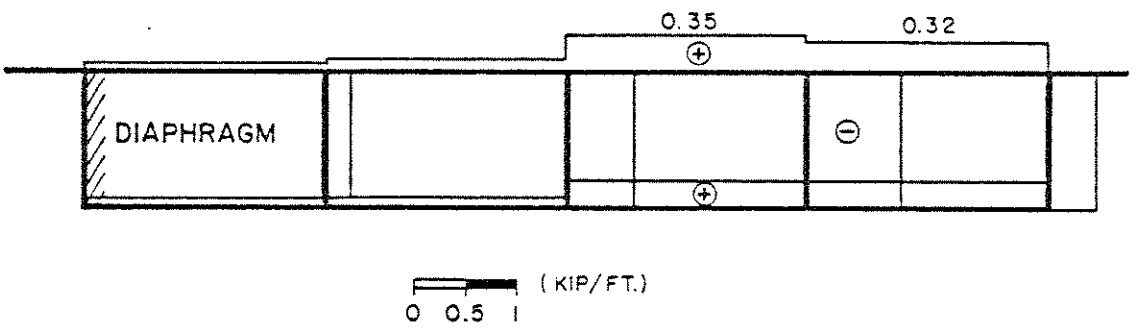

SECTION T'

FIG. 8.16 THEORETICAL TRANSVERSE SLAB DISTORTIONAL MOMENTS AND CORRESPONDING SHEAR FORCES AT RIGHT SECTION *T* FOR CONDITIONING LOADS

It is thus evident that it would be incorrect to investigate the vertical equilibrium of girder shears at skew sections with external reactions if the additional slab shears due to the secondary transverse distributing effect are ignored.

Taking into account the actual behavior of a box girder structure, it may therefore be stated as a result of the present study that with proper interpretation, the finite element program CELL is probably the best available analytical tool for the prediction of the complex distribution of shear forces in continuous skew bridge structures and may, accordingly, be recommended as an aid in establishing design values.

8.4 Simplified Approximate Analytical Method

Adequate evaluation of shear behavior in box girder bridges, e.g., by means of the computer program CELL, may also be supplemented by the use of simpler models of shear distribution.

The simplest approach is to consider that the total torsional moments in the structure, induced by the reactions as well as by the transverse position of the loads are carried by the multi-cellular cross-section in the same manner as in pure torsion of the cross-section. The assumptions in this approach are as follows:

(1) Beam theory is considered valid

(2) The cross-section does not distort transversely

The pattern of the shear flow circulation along the median line of a four-cell cross-section is shown in Fig. 8.17.a. Two components of the shear flow, q_1 and q_2, can be calculated from the following equations of the warping compatability of the cross-section:

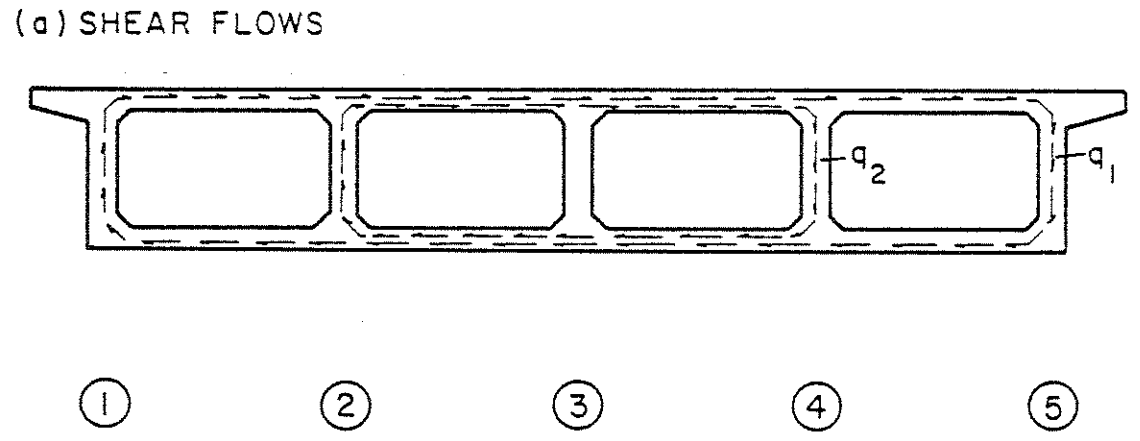

FIG. 8.17 SHEAR FLOW AND SHEAR FORCES DUE TO PURE TORSION

$$\oint \frac{\partial u}{\partial s} ds = 0 \qquad (8.1)$$

$$\oint \frac{\partial u}{\partial s} ds = 0 \qquad (8.2)$$

in which u is the cross-sectional warping and the s coordinate is measured along the median line of the cross section.

Shear force contributions in the outermost webs (girders 1,5) due to pure torsion, Fig. 8.17.b, are as follows:

$$Q_{t(1,5)} = q_1 \, h \qquad (8.3)$$

and the shear force contributions in the inner webs (girders 2,4) are:

$$Q_{t(2,4)} = q_2 \, h \qquad (8.4)$$

where h is the depth of the girder webs.

Now if the total shear forces at any section of the box girder bridge are divided equally among the individual girders and then adjusted by the torsional contributions derived in Eqs. (8.3) and (8.4) above, then approximate theoretical values of the shear forces in the girders are obtained. Shear force diagrams for the individual girders as obtained by the above approximate method for the dead load, conditioning load and 1X load cases are plotted in Figs. 8.18, 8.19 and 8.20 with

solid lines. For purposes of comparison, the shear forces as obtained from the CELL program are also plotted in these figures with broken lines. From an observation of Figs. 8.18, 8.19 and 8.20 it follows that the approximate method yields adequate results for the conditioning load case and approximate results for the dead load case, but the results for the highly eccentric 1X concentrated load case are generally unsatisfactory. The assumption that the cross-section does not distort transversely and the other assumptions which are made in the approximate method are obviously not valid for general loadings on this type of structure.

8.5 Comparison between Experimental and Analytical Results

During the construction of the box girder bridge model, strain gage rosettes were mounted on the web surfaces at the skew sections L, M, N and O as shown in Fig. 8.7 so that some information on shear forces in the neighborhood of the end abutments and the center bent might be obtained. It was recognized at the outset that the shear force values yielded by surface strain gage rosettes would not be wholly reliable for two main reasons:

(1) the individual gages are fragile and cease to give accurate results after cracking occurs in the concrete;

(2) the malfunctioning of one gage in the rosette results in erroneous values.

In Fig. 8.21 the values of the shear forces in the girder webs at skew section L as calculated from the strain gage rosettes are plotted for the 24, 30 and 40 ksi conditioning load levels. Results

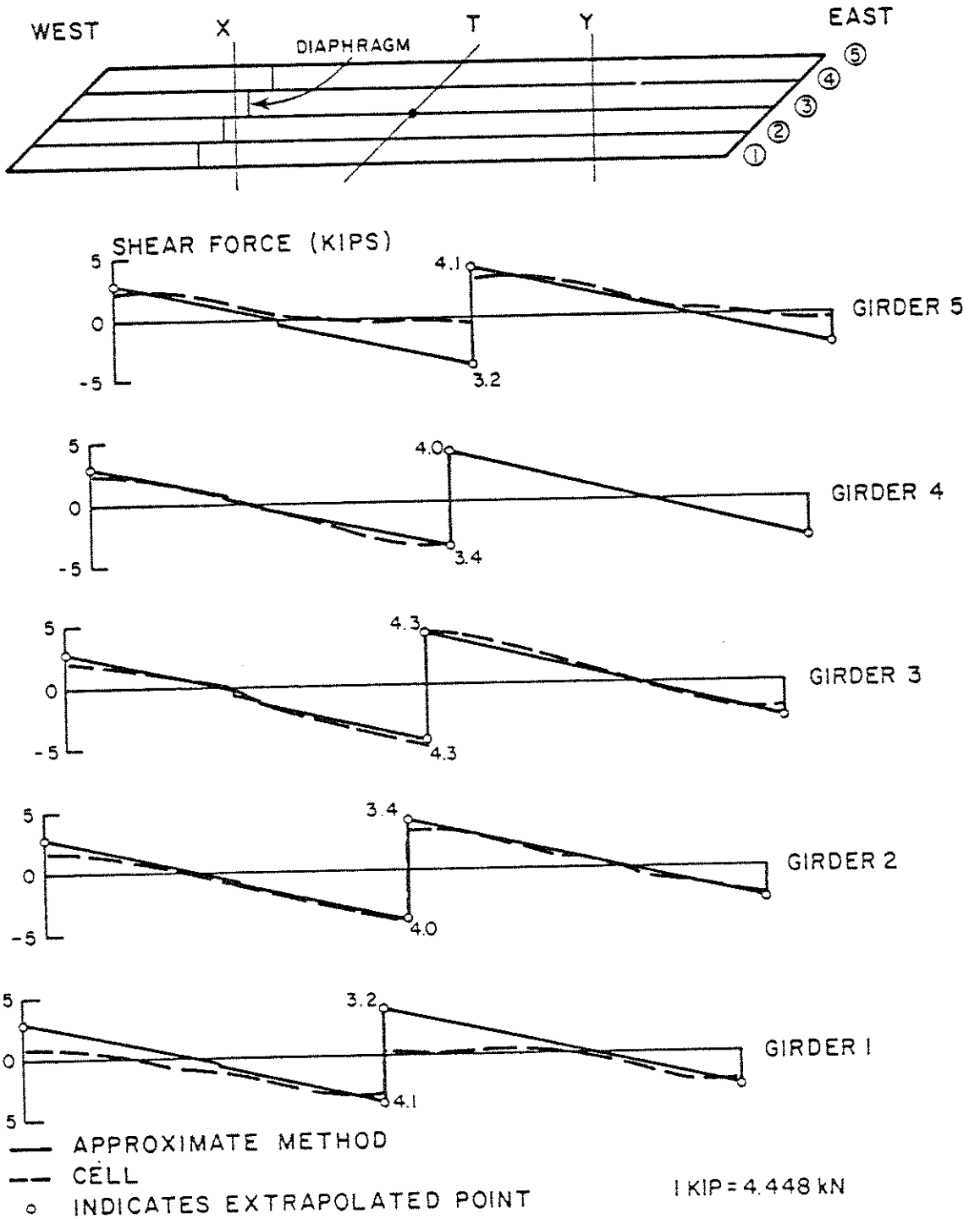

FIG. 8.18 COMPARISON OF THEORETICAL GIRDER SHEAR FORCES (KIPS) FROM APPROXIMATE METHOD WITH CELL RESULTS FOR SELF-WEIGHT OF BRIDGE MODEL

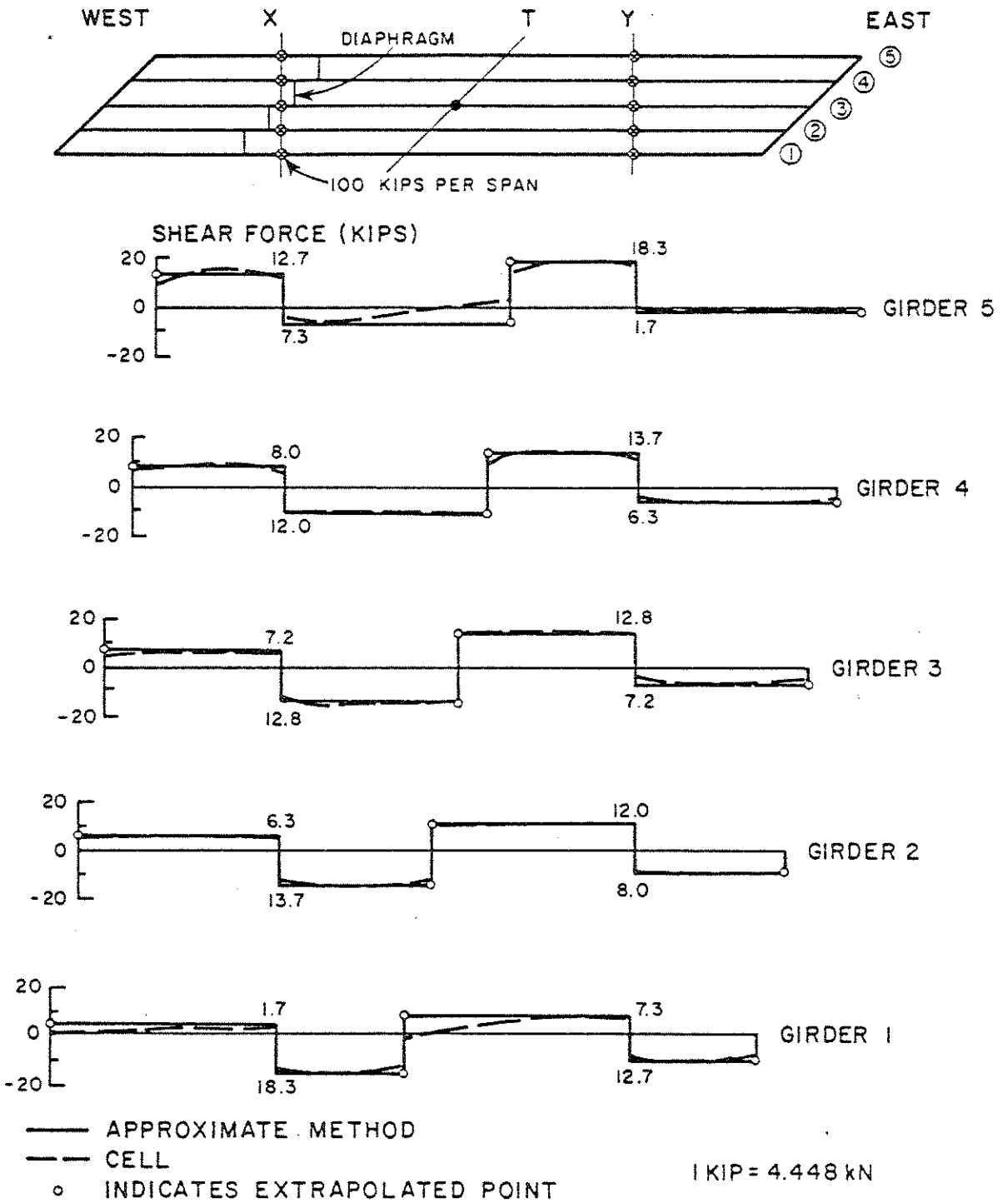

FIG. 8.19 COMPARISON OF THEORETICAL GIRDER SHEAR FORCES (KIPS) FROM APPROXIMATE METHOD WITH CELL RESULTS FOR CONDITIONING LOADS

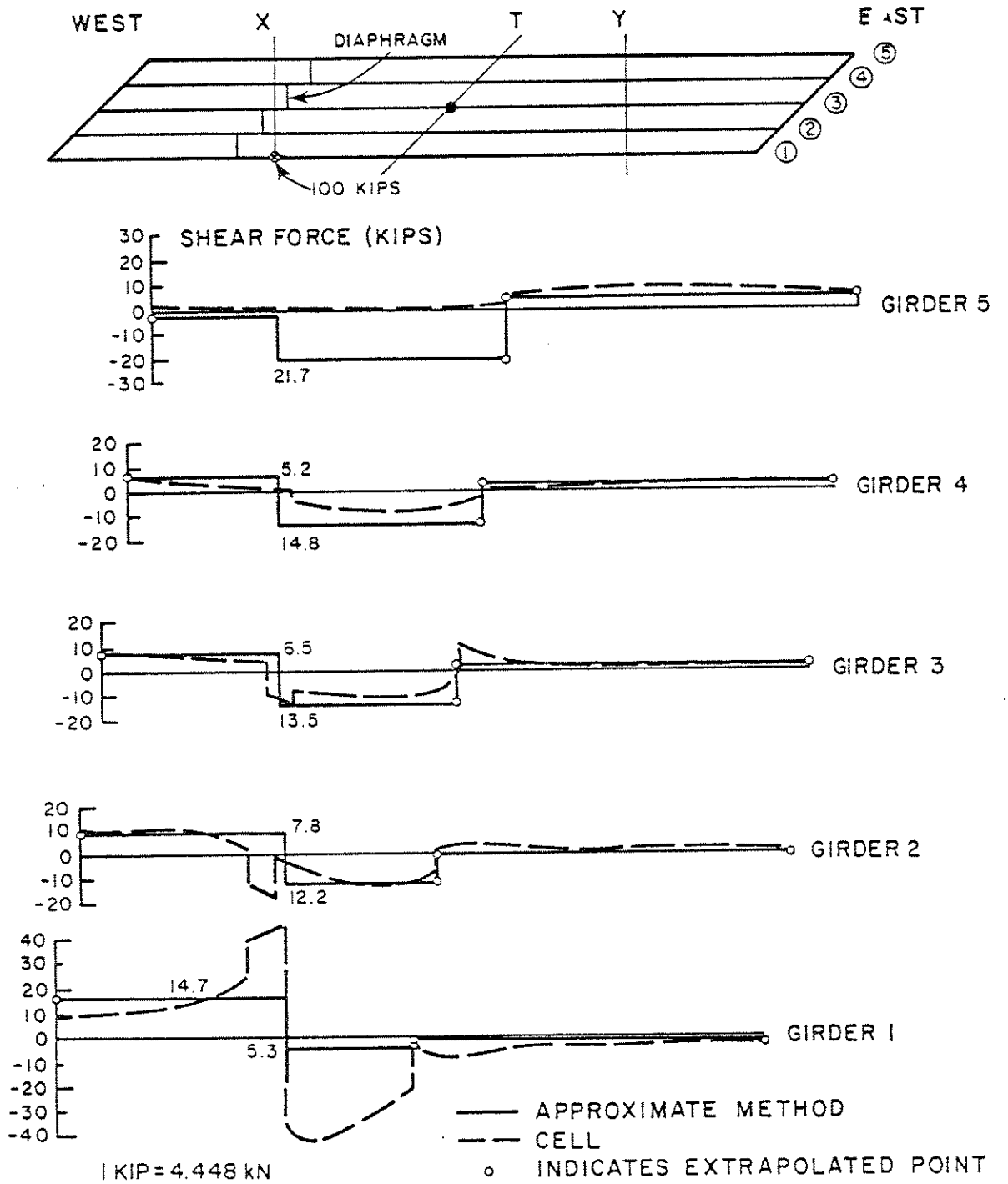

FIG. 8.20 COMPARISON OF THEORETICAL GIRDER SHEAR FORCES (KIPS) FROM APPROXIMATE METHOD WITH CELL RESULTS FOR 100 KIP (445 kN) POINT LOAD AT 1X

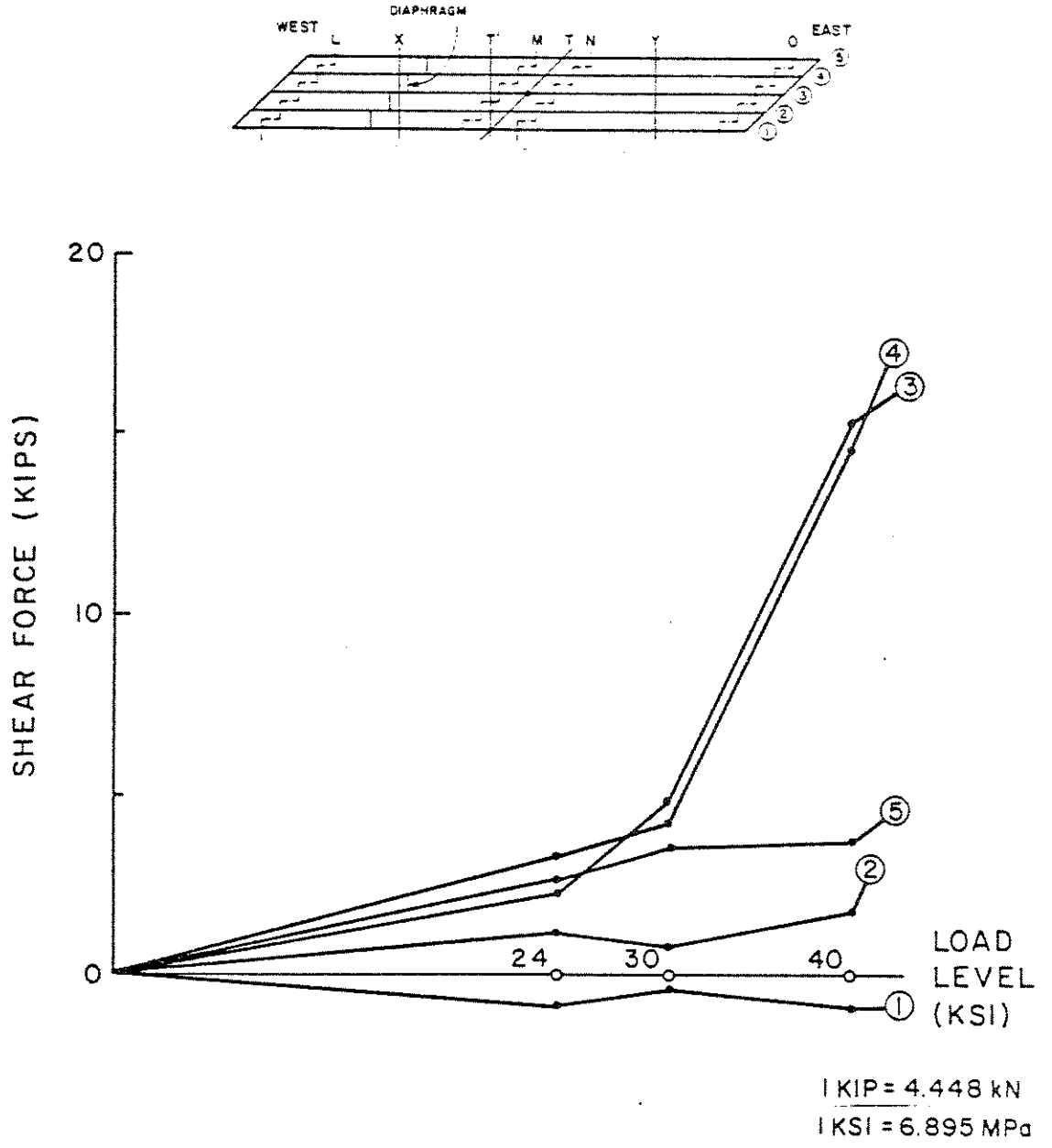

FIG. 8.21 EXPERIMENTAL INTERNAL GIRDER SHEAR FORCES (KIPS) AT SKEW SECTION L AS MEASURED FROM STRAIN GAGE ROSETTES

obtained after the 30 ksi load level are not reliable. Inaccurate results were obtained from the rosettes at skew sections M and N in the neighborhood of the center bent, and they are not plotted. It is surmised that, because the rosettes at all four skew sections were placed in the upper part of the webs, the negative moments in the center bent region caused cracks to form at the skew sections M and N in the initial stages of the loading, rendering the rosette measurements unreliable.

Figure 8.22 contains a bar chart comparison of the reactions obtained from the CELL program for the 24 ksi conditioning load case and the experimental values were calculated after averaging the load cell readings at the skew symmetric locations 1E and 5W for the obtuse corner, 1W and 5E for the acute corner, 2E and 4W, 3E and 3W, and 4E and 2W respectively. The agreement between the two sets of reactions is observed to be good.

In Fig. 8.23 a bar chart comparison is made for shear forces for individual girders near the end abutments, i.e., at the skew sections L and O. The experimental shear values have been calculated from the strain gage rosettes and the stippled bars indicate shear forces that have been calculated from the CELL internal forces. The hatched bars represent the CELL values multiplied by the factor obtained by dividing the ratio (External Measured Reactions/External Theoretical Reactions) by the ratio (Internal Shear/CELL Shear). Ideally this factor should be equal to 1 and in the present case it is 1.08, which provides a measure of the overall accuracy of the experimental results.

The results of Fig. 8.23 show satisfactory agreement and indicate that experimental results do provide confirmation for the shear forces calculated from CELL. However the CELL shear forces are smaller in

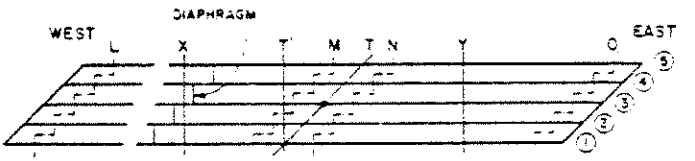

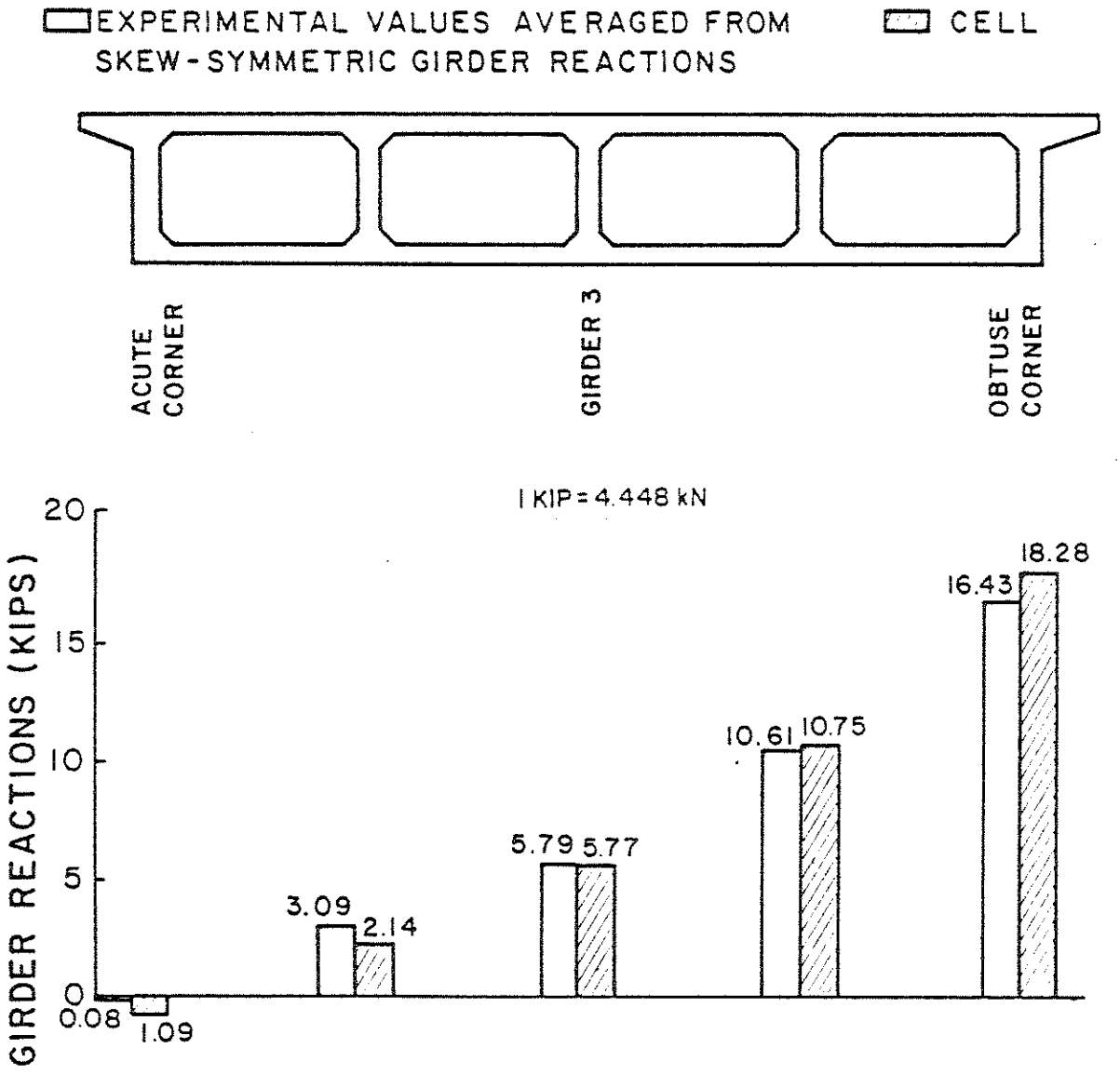

FIG. 8.22 COMPARISON OF THEORETICAL AND AVERAGE EXPERIMENTAL REACTIONS (KIPS) AT END ABUTMENTS FOR 24 KSI CONDITIONING LOADS

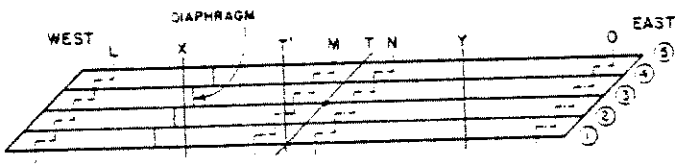

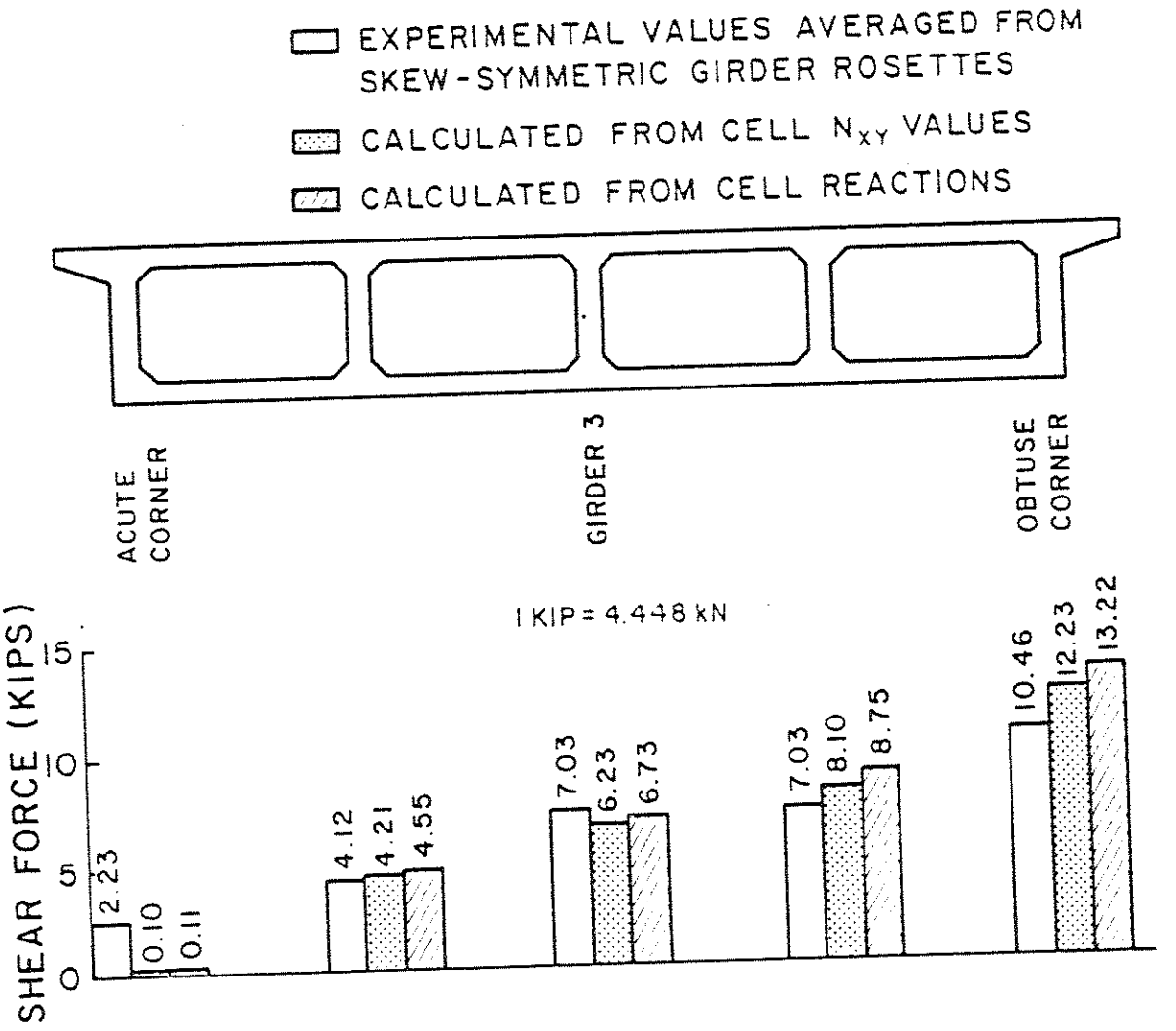

FIG. 8.23 COMPARISON OF THEORETICAL AND AVERAGE EXPERIMENTAL SHEAR FORCES (KIPS) NEAR END ABUTMENTS FOR 24 KSI CONDITIONING LOADS

magnitude than the reaction values, and this is due to the secondary transverse distribution effects in the structure as discussed in Section 8.3.

8.6 Summary

A discussion of the shear response of the skew box girder bridge model has been presented. The following conclusions can be drawn.

1. While the total external reactions at the east, center and west supports can be accurately predicted theoretically by CELL, the distribution of the internal shear forces to individual girder webs is complex and can only be predicted approximately.

2. For skew box girder bridges the total end support or center bent vertical reactions are balanced not only by the girder web shears, but also by significant transverse slab shears due to the high transverse distortional resistance of the box section.

3. While simplified methods may be used to predict the distribution of girder shears for certain loading conditions on skew box girder bridges, for general loadings they cannot be employed and thus the finite element program CELL should be used to estimate or develop design values.

9. REVIEW OF STRUCTURAL RESPONSE DURING LOAD HISTORY OF BRIDGE MODEL

9.1 Strain History During Construction Phase

With the intent of monitoring the concrete and steel strains during the construction phase up to the time the dead load was applied, strains in a number of concrete strain meters and weldable strain gages were registered by means of the Low Speed Scanner Unit. The readings provide an unbroken record of steel and concrete strains from the casting of the bottom slab to the loading to failure.

The steel strain data during the construction phase for the weldable gages on the steel reinforcement are presented in Figs. 9.1 and 9.2 for the bottom slab and top slab respectively. The patterns at sections A and D in the bottom slab, as well as the comparisons between skew symmetric locations show good general agreement indicating a reliability of the data. At section D the gage at girder 1 was damaged during construction and gave unreliable results. At this section the results from girder 2 are therefore plotted, which agree especially during the period of the first 50 days with the strains recorded at section A, girder 5. From Fig. 9.2 it is observed that, although similarities exist in the pattern, the strains in the top slab at the skew sections B and C show less agreement. The values of steel strains registered at sections B and C in the top slab are, however, significantly lower than at sections A and D in the bottom slab. This is caused by the constraints imposed on the top slab by the bottom slab and webs which were cast 60 days prior to the top slab.

Figures 9.3 and 9.4 give the strain data for the concrete meters in girders 1 and 5 at the major instrumented sections A, B, C and D.

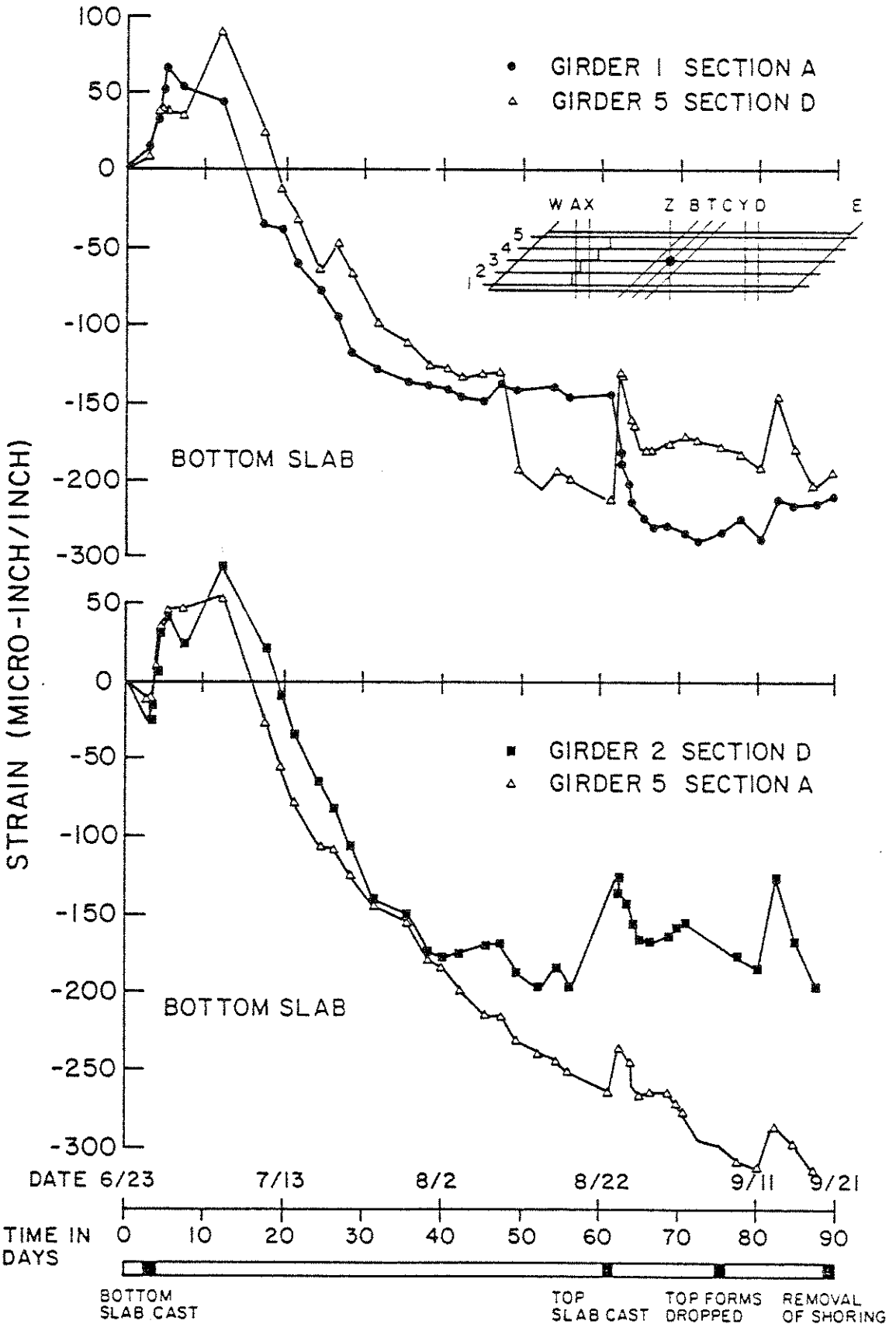

FIG. 9.1 HISTORY OF STEEL STRAINS PRIOR TO REMOVAL OF SHORING (BOTTOM SLAB)

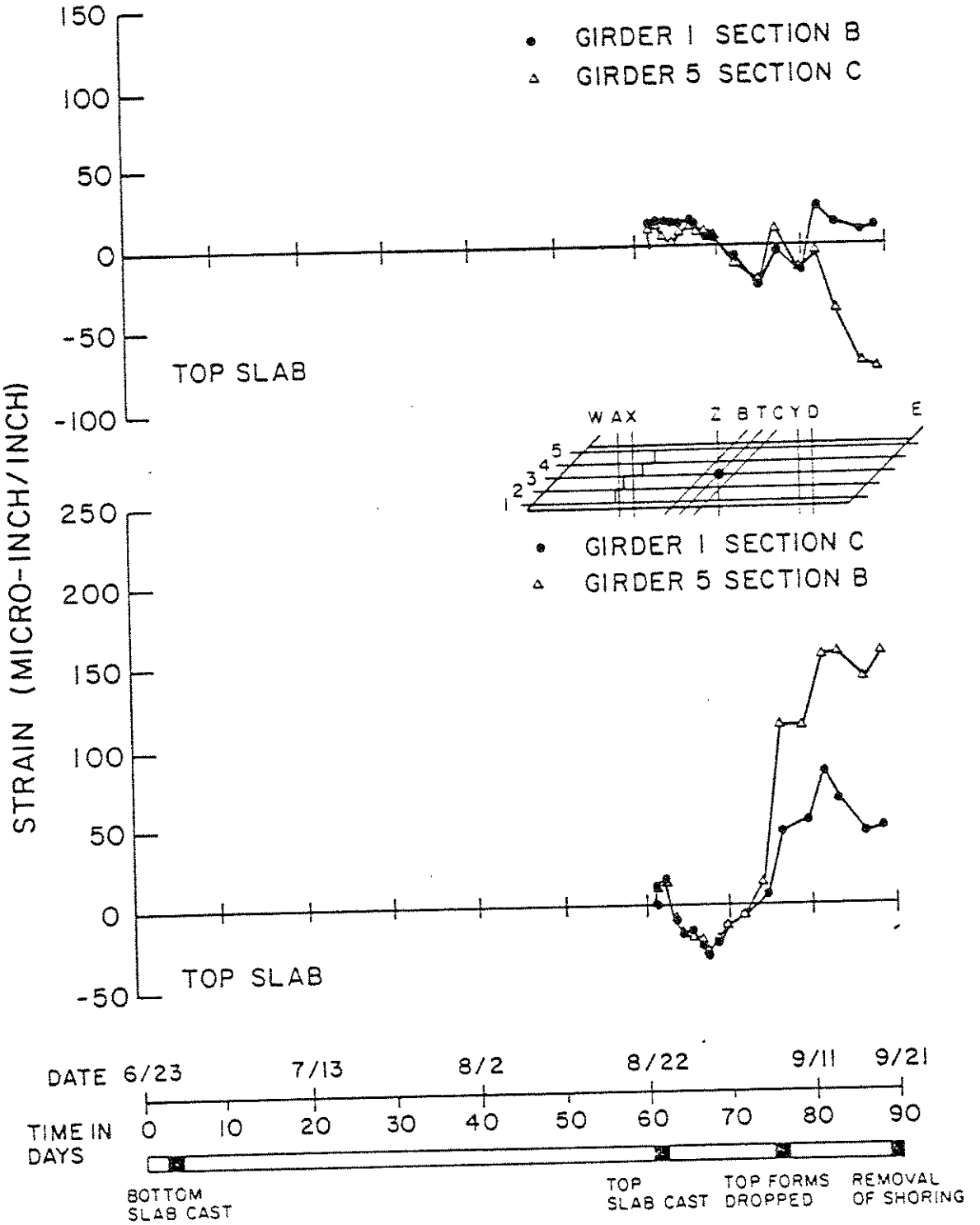

FIG. 9.2 HISTORY OF STEEL STRAINS PRIOR TO REMOVAL OF SHORING (TOP SLAB)

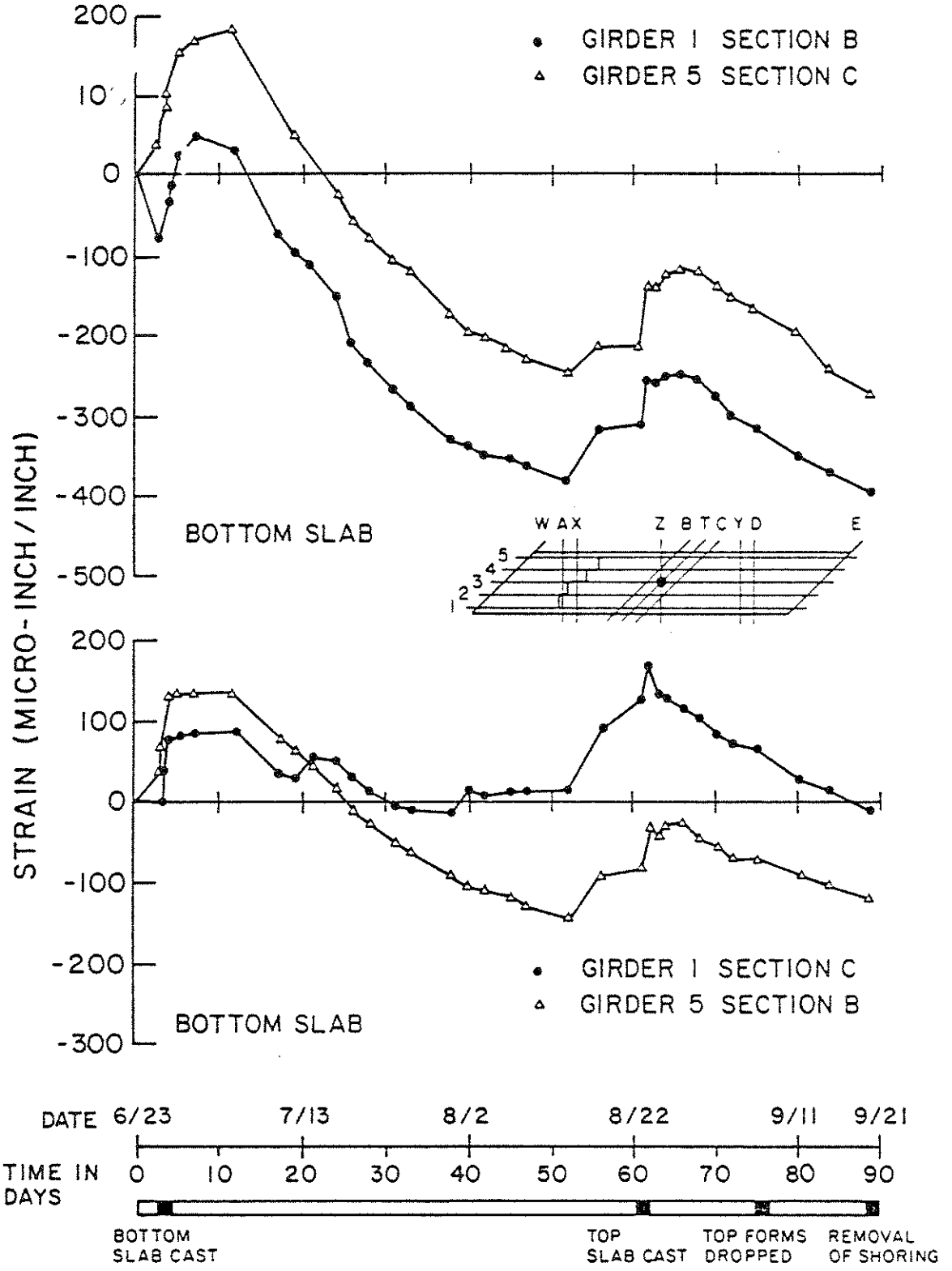

FIG. 9.3 HISTORY OF CONCRETE STRAINS PRIOR TO REMOVAL OF SHORING (BOTTOM SLAB)

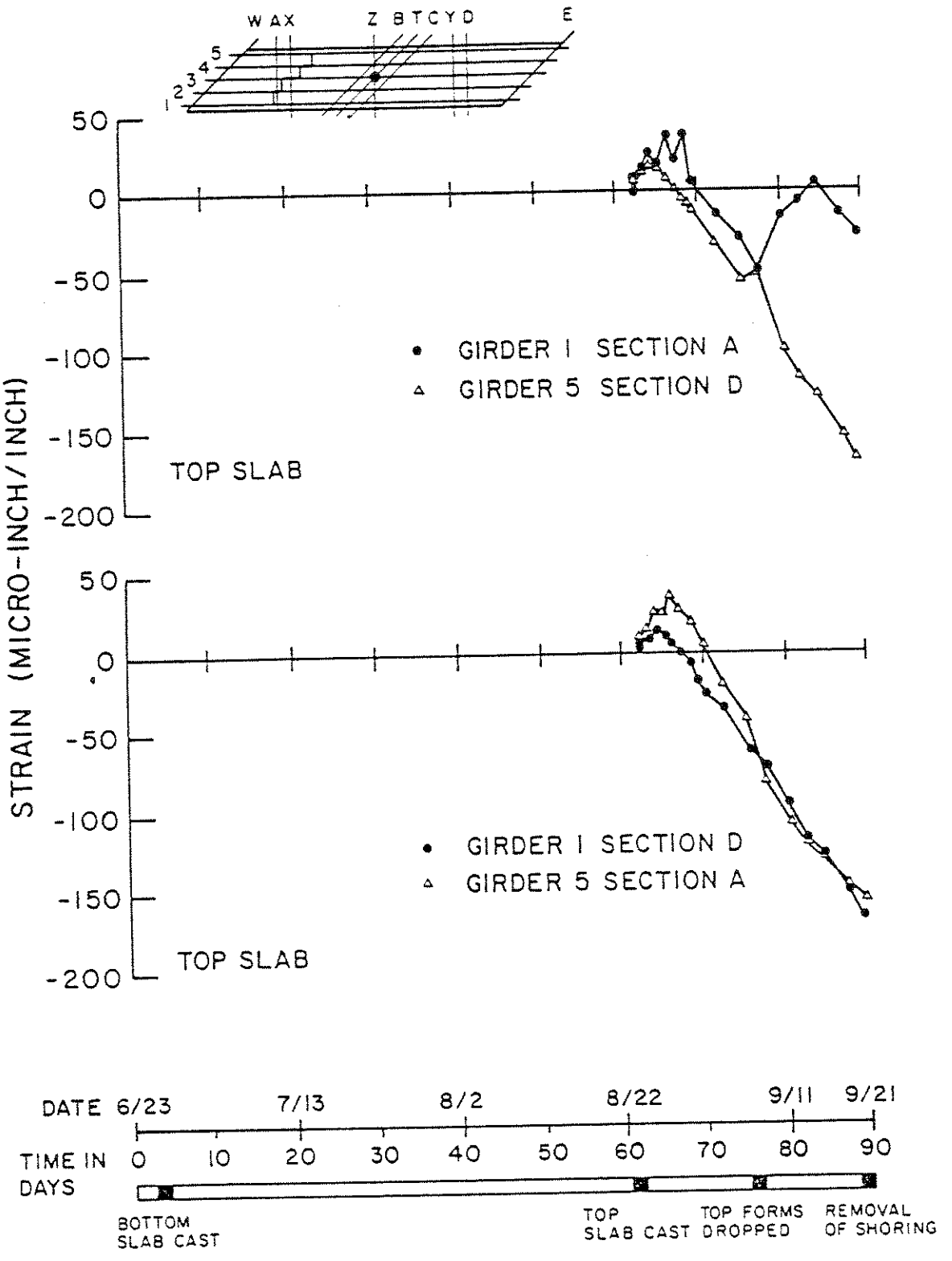

FIG. 9.4 HISTORY OF CONCRETE STRAINS PRIOR TO REMOVAL OF SHORING (TOP SLAB)

The strain histories for concrete show remarkable similarity of behavior, especially for the bottom slab. The strain in the concrete at location 1B agrees fairly well with the strain in the concrete at the skew-symmetric location 5C. The variation of strain at location 5B resembles that at the skew-symmetric location 1C. A higher magnitude of strain is again observed in the bottom slab at sections B and C than in the top slab at sections A and D. Higher strains are also registered at the locations 1B and 5C which are near the obtuse corners in the center bent region than at 5B and 1C which are near the acute corners in the center bent region. The maximum strain readings for the concrete, Fig. 9.3, are about 1.3 times as large as those in the steel reinforcement.

A study of the strains in Figs. 9.1 to 9.4 seems to indicate a relatively similar behavior in the two spans during the 90 day time period covered. The effect of the transverse diaphragm at section X does not significantly influence the strain distribution due to differential shrinkage.

9.2 Strain History Under Sustained Dead Load

The variation of the dead load strains with time was monitored using the Low Speed Scanner Unit. Before and after each load phase a set of dead load readings was taken relative to the condition immediately prior to the removal of the shoring and formwork. This latter condition was taken as a reference absolute zero for all subsequent readings. Thus, total dead load strains are plotted in Figs. 9.5 to 9.6 for the entire 110 day period from removal of shoring to ultimate failure loading.

The steel strain data for the undiaphragmed east span are given for the bottom slab, girders 2 and 5 at section D and for the top slab,

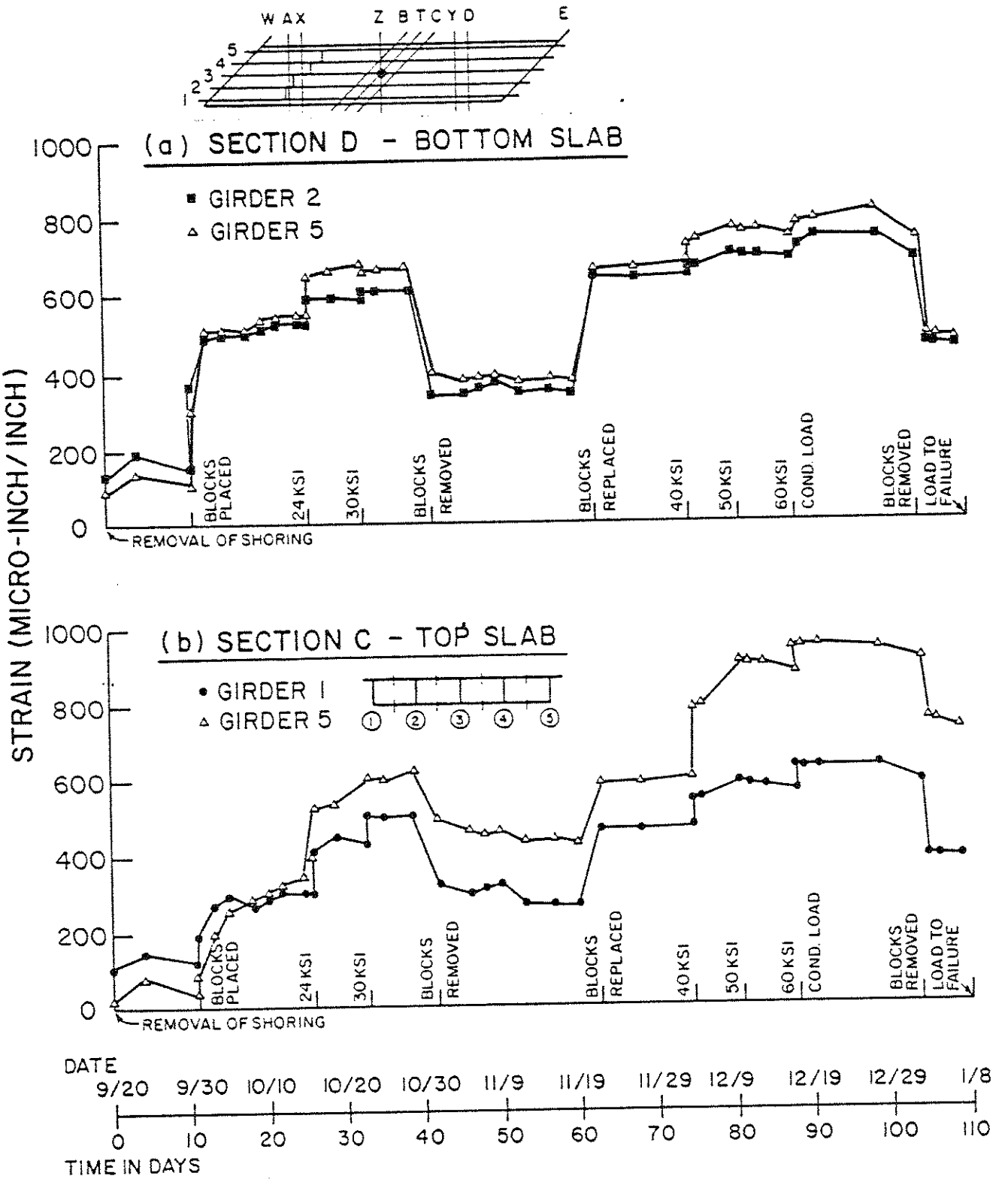

FIG. 9.5 HISTORY OF STEEL STRAINS UNDER SUSTAINED DEAD LOAD

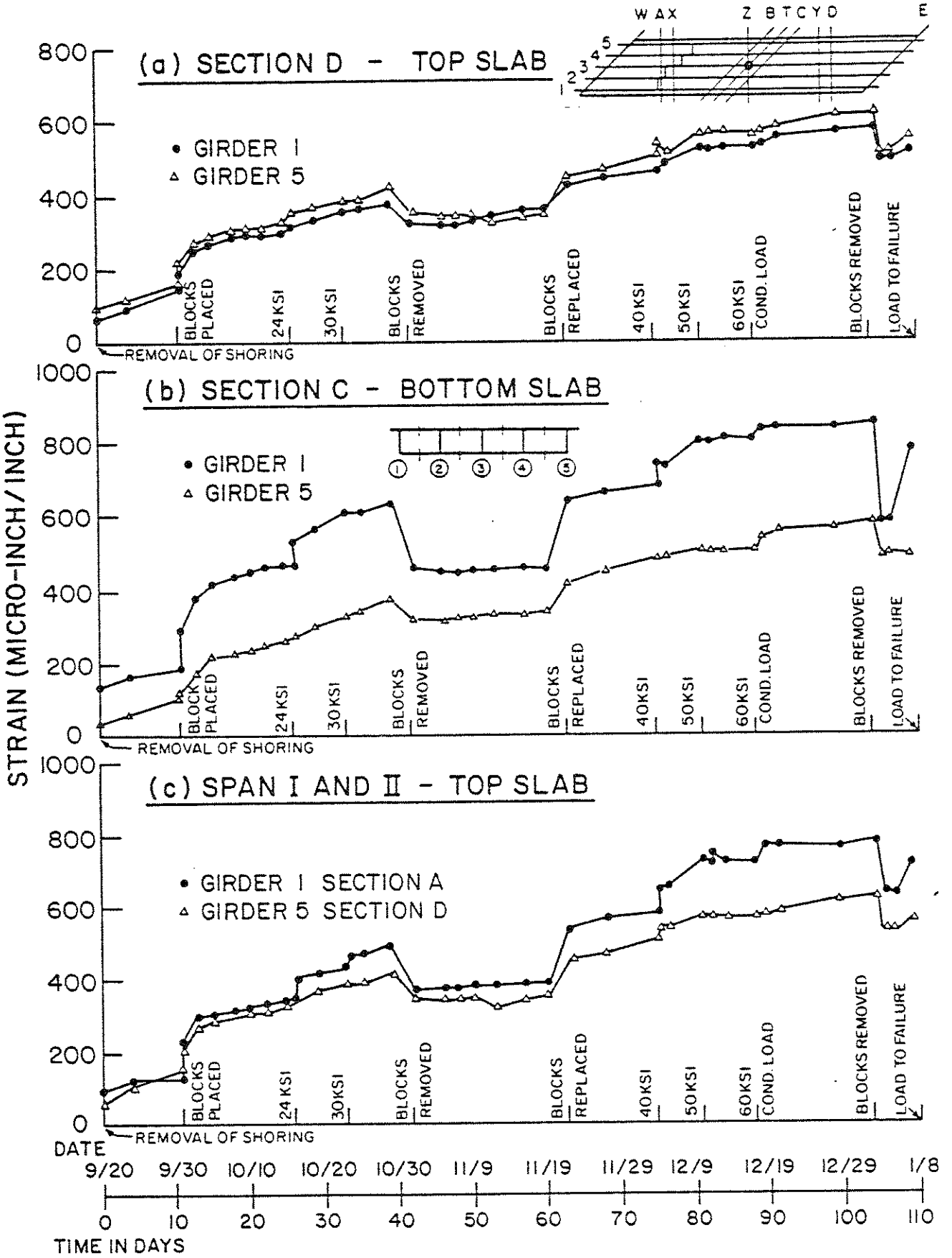

FIG. 9.6 HISTORY OF CONCRETE STRAINS UNDER SUSTAINED DEAD LOAD

girders 1 and 5 at section C. The jump in the values between the dates 10/2/1978 and 10/4/1978 is due to the fact that the concrete blocks for proper simulation of prototype behavior were placed on the bridge deck during this period. The blocks were removed on 11/2/1978 when truck loads, construction vehicle loads and the fork lift loads were applied and replaced on 11/23/1978 after completion of these loadings. A drop in the strain values is noticeable on 1/3/1979 when the blocks were finally removed from the bridge deck in preparation for the loading to failure.

From Fig. 9.5 it is observed that the steel strains across the right section D are fairly uniform over the transverse section. As opposed to this the strains across the skew section C are not uniform over the section, and the strains at the obtuse location 5C are much higher than those at the acute location 1C. At all locations, however, the strains increase significantly over the period of testing. Much of this increase is caused by additional strains accumulated after each conditioning cycle, when the cracking gets successively more extensive and the concrete participates less and less in carrying any of the tensile stress. However, the stress redistribution in the bridge due to the creep in the concrete has little influence on the steel strains. This is clearly indicated by the near constant value of the strain between each of the conditioning load cycles.

Figure 9.6 gives the concrete strains for girders 1 and 5, also at sections C and D. Here the increase in strain over the test period of 110 days is more uniform than for the steel strains. The final concrete strain values are about two to four times greater than the initial values. In contrast to the steel strains, the residual concrete strains

caused by each of the conditioning load cycles are negligible. The major part of the increase is caused by the creep in the concrete, while the progressive cracking and deterioration of the bridge model have a smaller influence.

From Figs. 9.6(a) and 9.6(b) it is observed once again that the concrete strains across the right section D are almost constant over the transverse section. The concrete strains across the skew section C are not uniform over the section, with higher values at the obtuse location 5C.

It can be concluded from Figs. 9.6(a) and 9.6(b) that the rate of change of the concrete strains decreases somewhat with time, as would be expected.

A comparison of the behavior of the diaphragmed and undiaphragmed spans is made in Fig. 9.6(c), giving the history for the concrete strains at location 1A and the skew symmetric location 5D. Remarkably similar behavior is observed under sustained dead load for the concrete strains at both locations.

9.3 Deflections Under Sustained Dead Load

While the instantaneous deflections of the bridge model due to dead load were measured using scales and a precise surveyor's level, the deflections due to sustained dead load were measured using linear potentiometers and the Low Speed Scanner. A set of readings was taken before and after each load application for every load phase to determine any residual displacements.

The displacement data for the deflections under sustained dead load at the skew symmetric locations 1U and 5V, and at 1V and 5V are

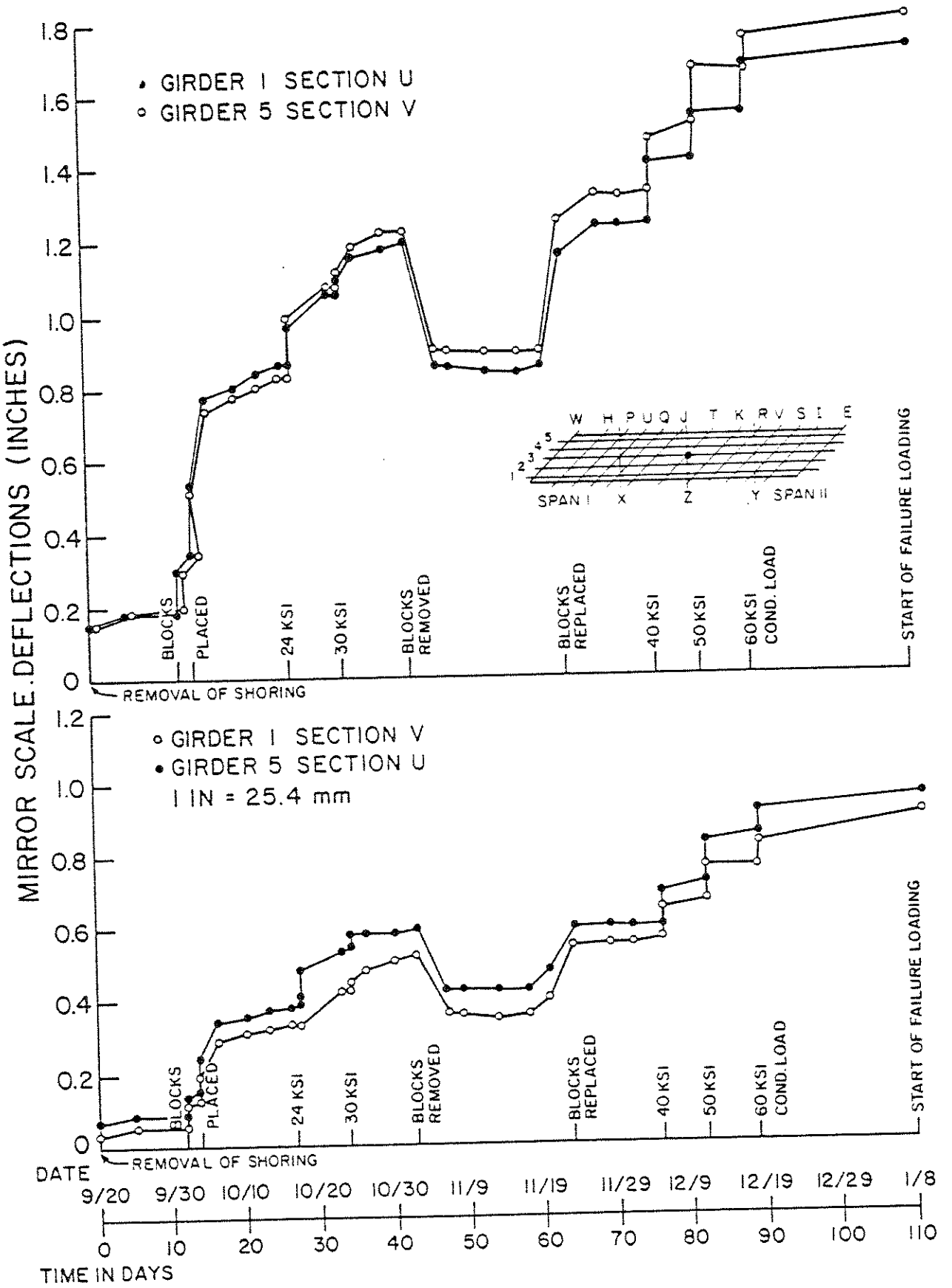

FIG. 9.7 DEFLECTION HISTORY AT SECTIONS U AND V UNDER SUSTAINED DEAD LOAD

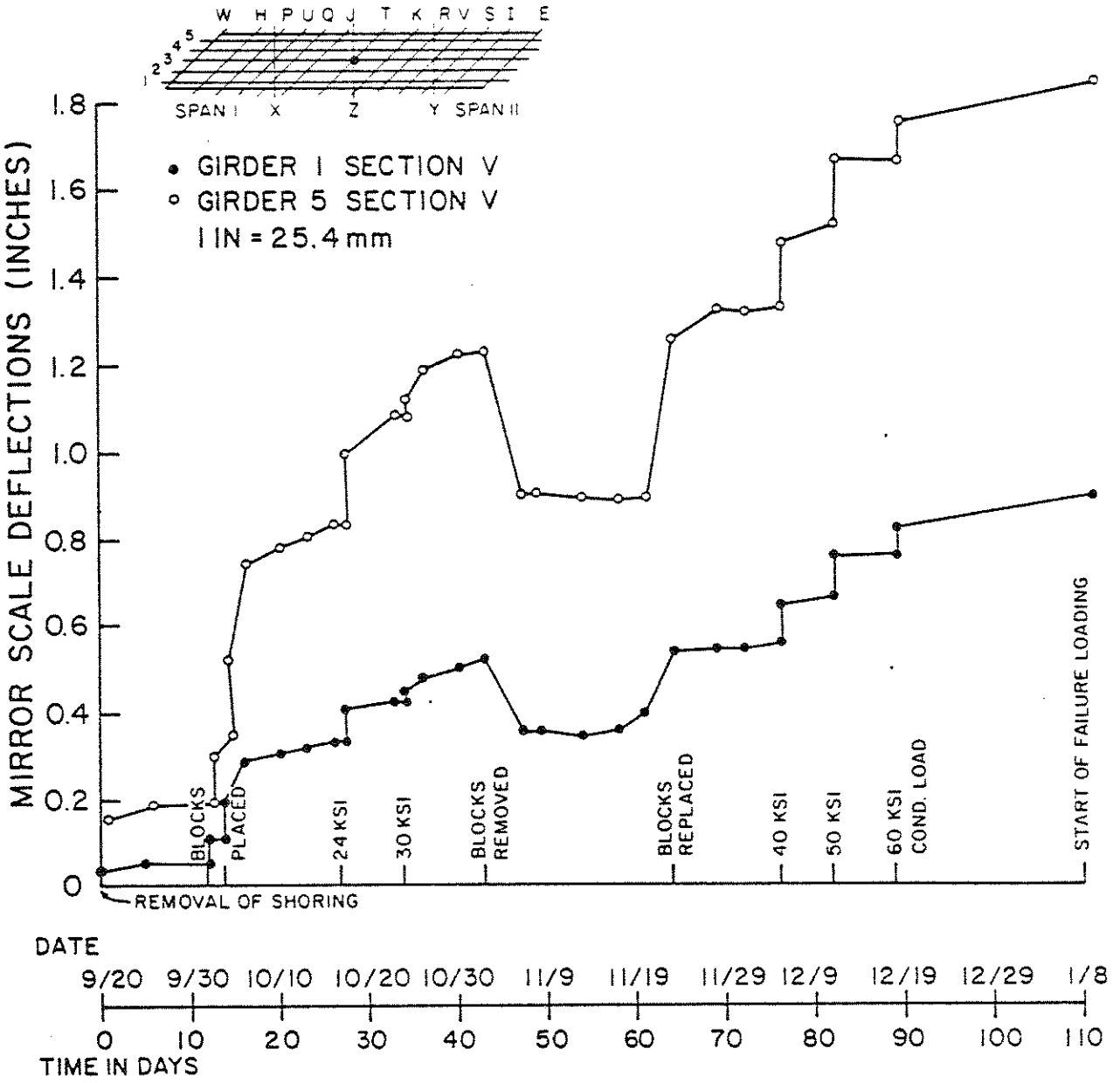

FIG. 9.8 DEFLECTION HISTORY AT SECTION V, UNDIAPHRAGMED SPAN, UNDER SUSTAINED DEAD LOAD

presented in Fig. 9.7. Good agreement is observed between the residual deflection data at 1V and 5', 1V and 5U. It is noted, furthermore, that the deflection values under sustained dead load are higher at locations 1U and 5V than at 1V and 5U. One explanation for the difference is that the effective "span" for 1U is larger than the effective "span" for 5U because 5V is closer to the center bent column support than 1U.

A comparison of the behavior of girders 1 and 5 in the undiaphragmed Span II at the skew section V as shown in Fig. 9.8 brings out the difference between the deflections at the two locations more clearly. Girder 5 at section V not only has a larger instantaneous deflection, but also shows a slightly larger rate of increase with time.

9.4 Crack Development After Conditioning Loads

After removal of the shoring and following each application of the conditioning loads the cracks in the girders 1 and 5 (south and north side respectively) and in the top and bottom slabs were recorded and are presented in Figs. 9.9 to 9.13.

The crack patterns as presented for blocks required for simulation of prototype dead load, which resulted in a total nominal stress of 12 ksi, and the 24, 30, 40, 50 and 60 ksi conditioning loads are basically self explanatory. However, a couple of observations are particularly pertinent in evaluating the bridge model under design stress conditions and successively increasing overloads. It is satisfying to note that under combined dead and design live loads, the crack pattern consisted virtually exclusively of hair-line cracks.

The crack patterns in the girder 5 and girder 1 webs as presented in Figs. 9.9 and 9.10 show progressively the development of bending

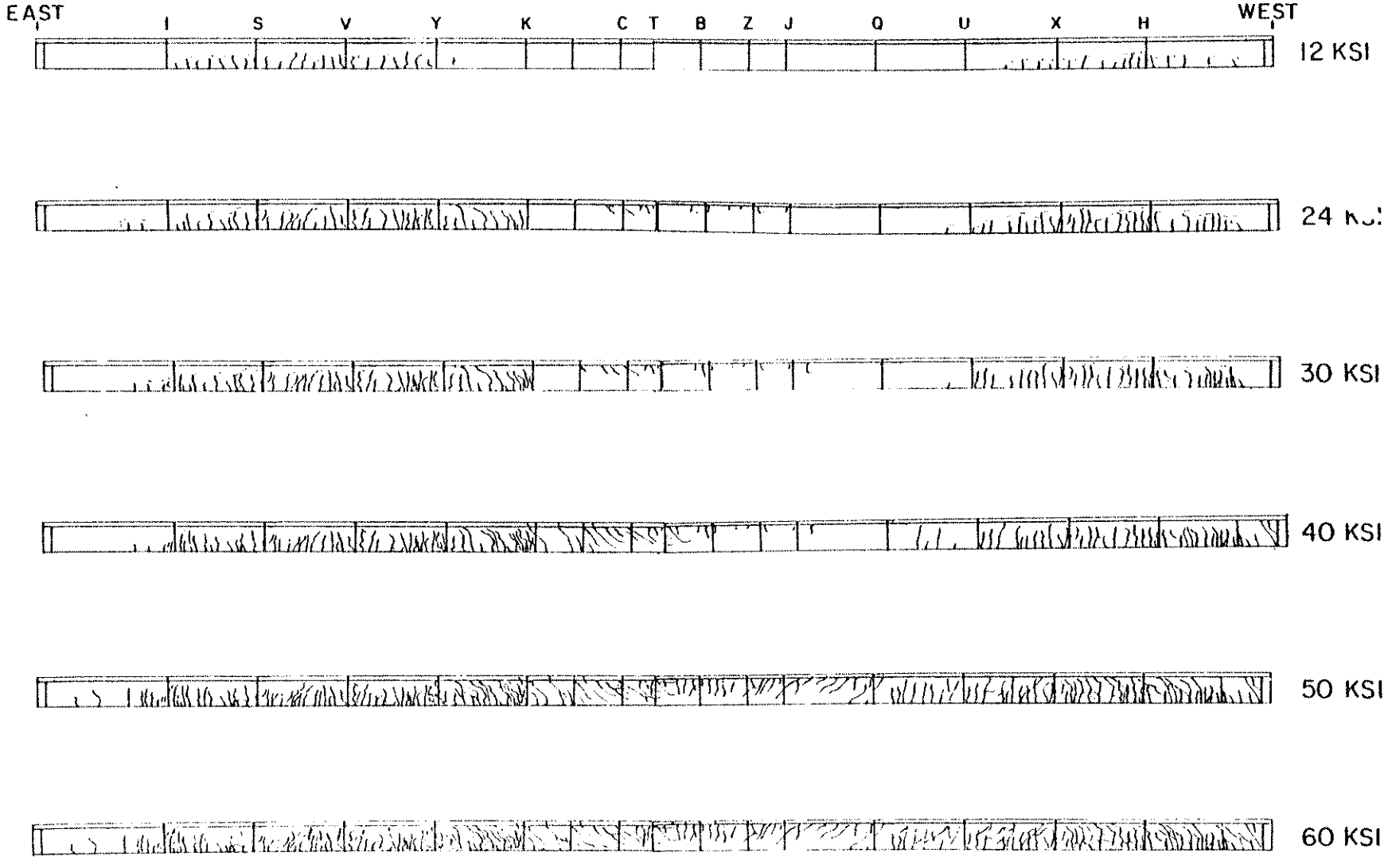

FIG. 9.9 CRACK HISTORY FOR GIRDER 5 (NORTH FACE)

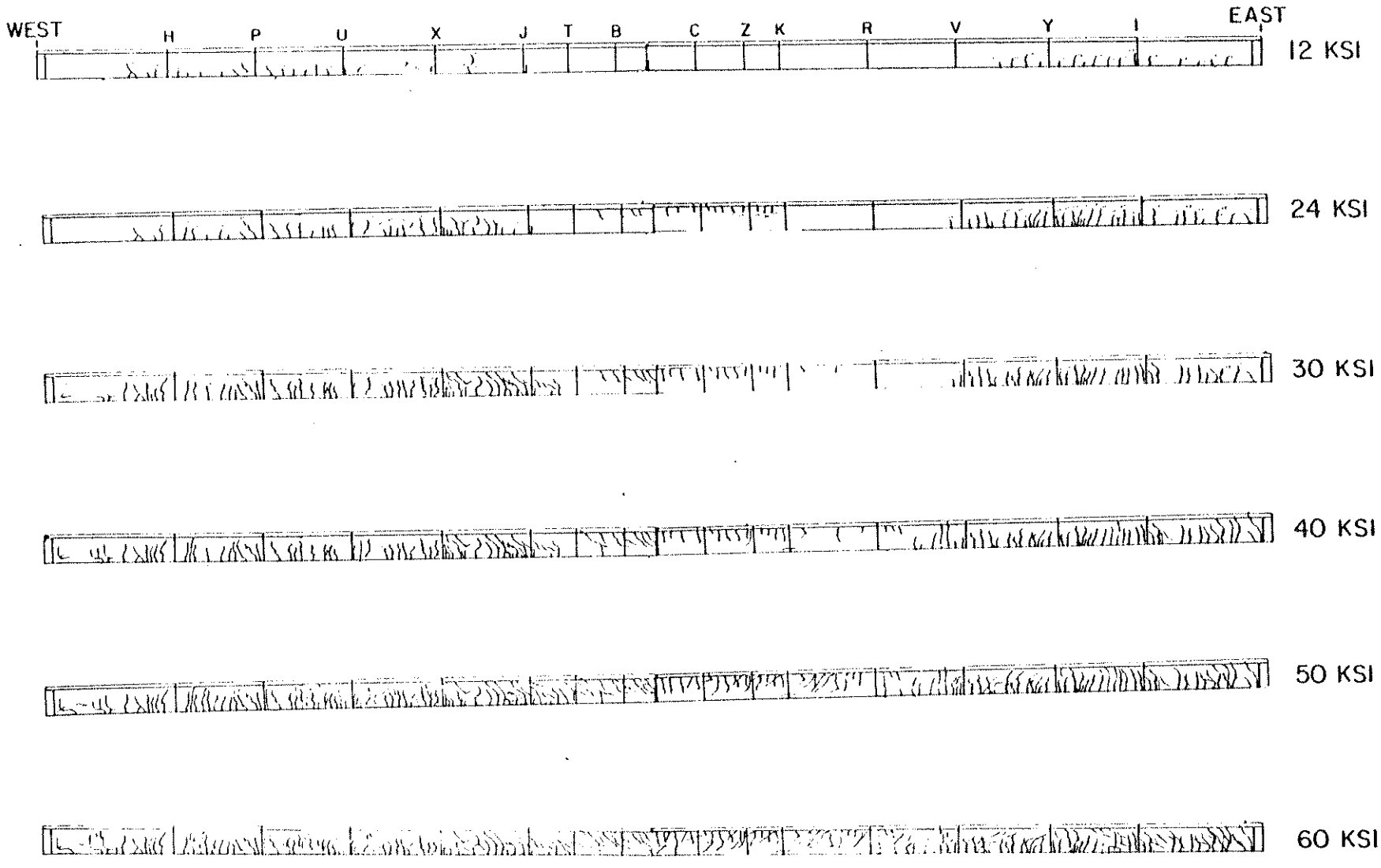

FIG. 9.10 CRACK HISTORY FOR GIRDER 1 (SOUTH FACE)

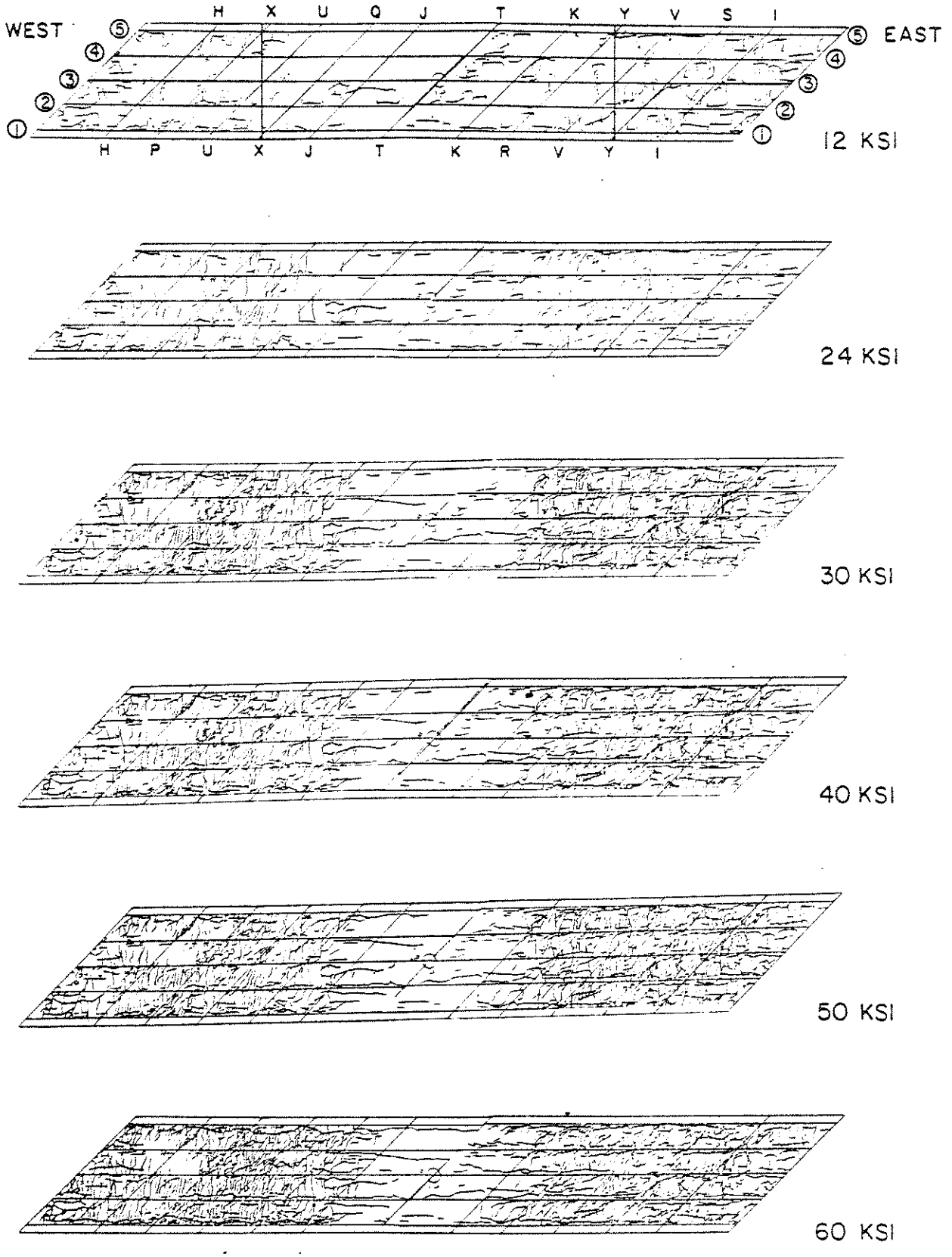

FIG. 9.11 CRACK HISTORY FOR BOTTOM SLAB

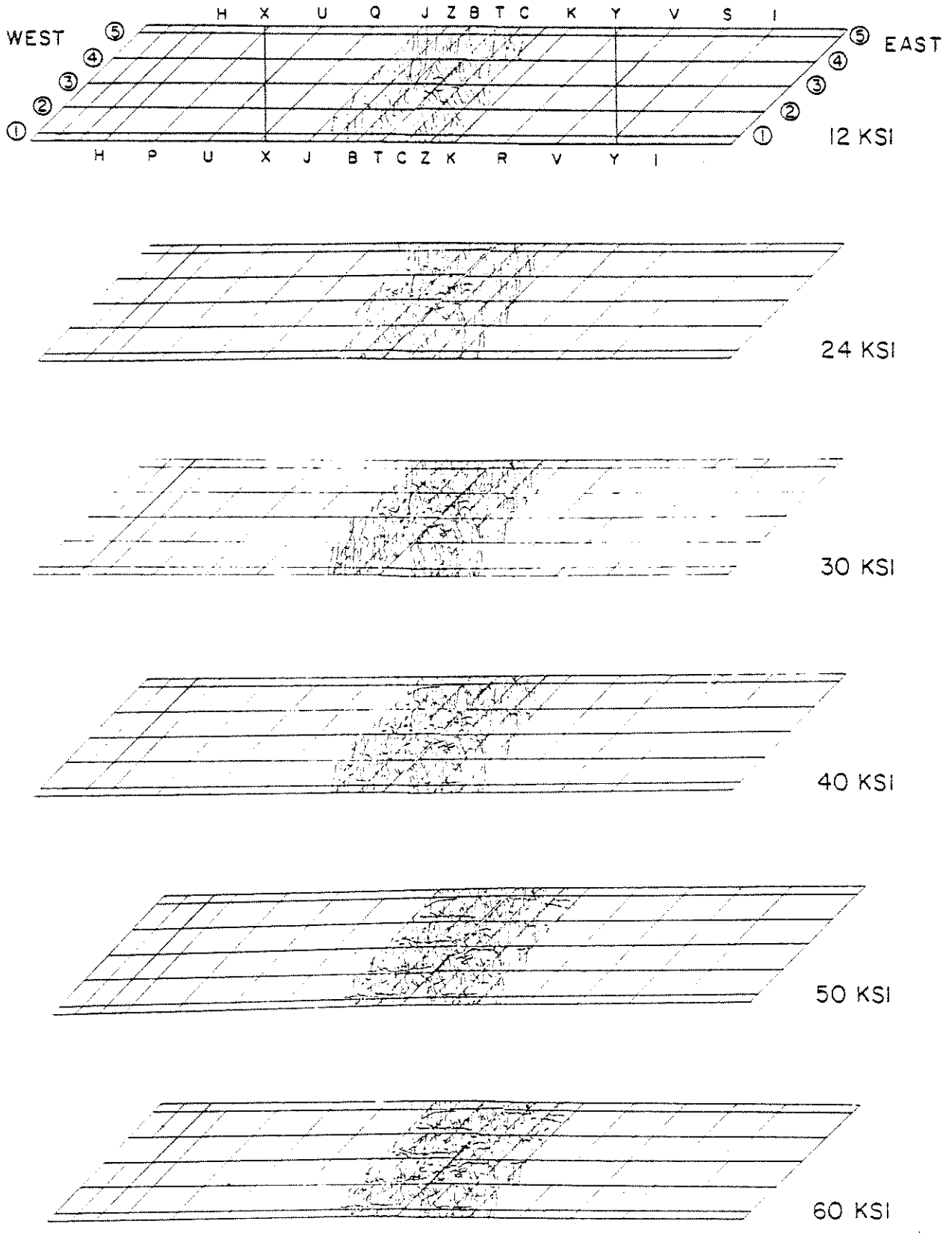

FIG. 9.12 CRACK HISTORY FOR TOP SLAB

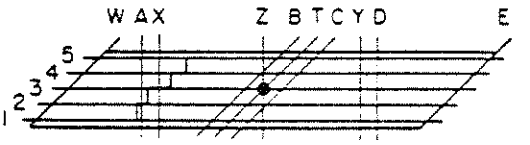

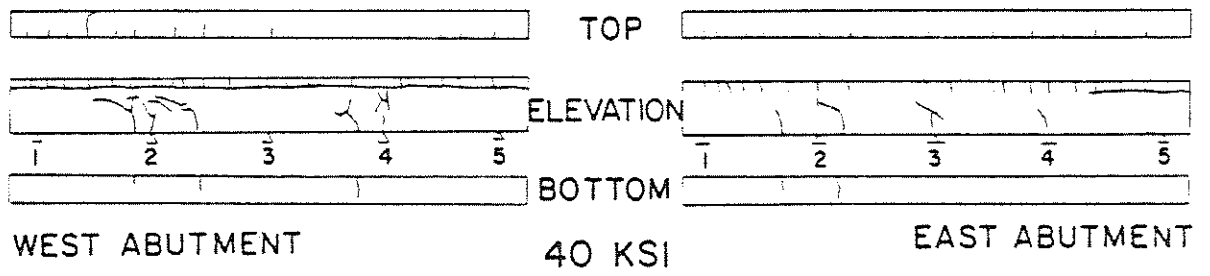

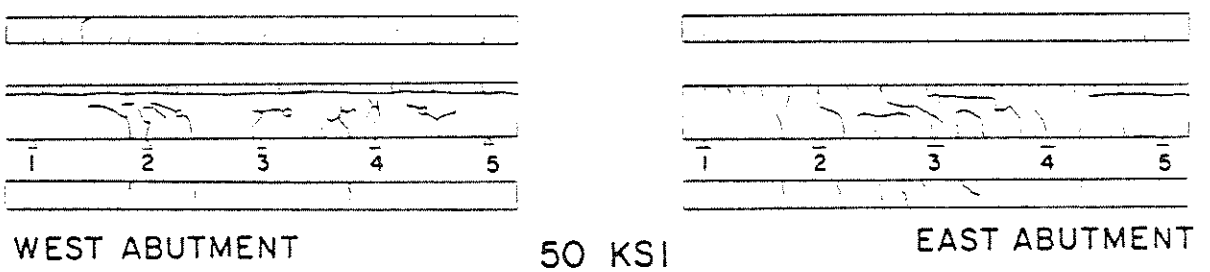

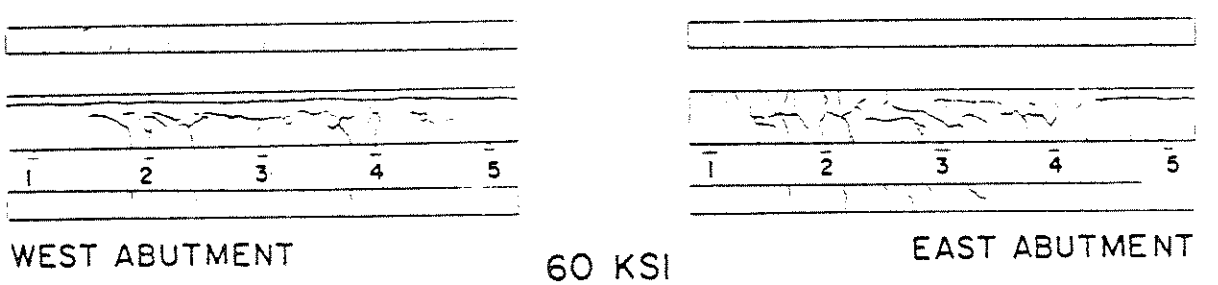

FIG. 9.13 CRACK HISTORY FOR END ABUTMENTS

moment cracks from the early stages of loading followed by the development of typical shear cracks after applications of the 30 ksi conditioning loads.

The crack patterns for the bottom slab are shown in in Fig. 9.11 and for the top slab in Fig. 9.12. The bottom slab shows quite extensive hair-line cracking already at the dead load stage, except for the center support region. The pattern does not change significantly until the 40 ksi stage, when the number of longitudinal cracks increases in both spans. An uncracked region in the bottom slab between girders 3 and 4 in the neighborhood of section H in Fig. 9.11 indicates the location where the bottom slab was patched with epoxy after the removal of the shoring. For the top slab, even after the conditioning load stress level of 60 ksi the cracking was restricted to the center support region.

9.5 Comparison Between Straight, Curved and Skew Bridge Models

Due to the lack of an absolute zero reading for the strain history during the construction phase, only the deflections under sustained dead load can be compared for the three structures. While the crack patterns were of a similar nature for the three models, the records appear to indicate somewhat more extensive cracking at lower levels in the curved bridge. However, the development of cracking after each conditioning load cannot be compared directly since the crack recording schemes were quite subjective.

A comparison between the displacements of the three models is given in Fig. 9.14 for outer girder 5. It can be seen that the final total displacement of the curved bridge is about 20% larger than that of the straight one. This is of course not surprising considering the

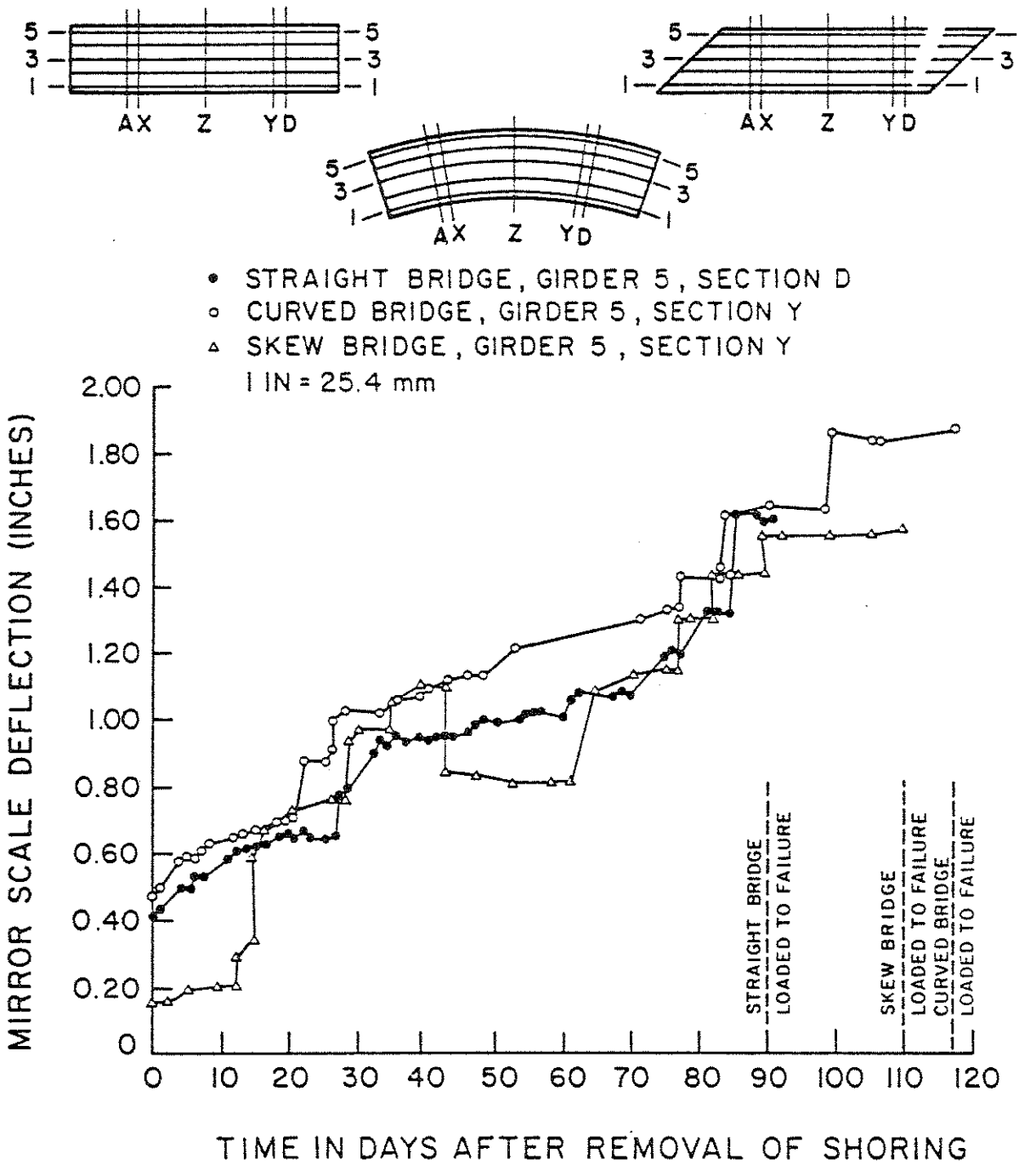

FIG. 9.14 COMPARISON OF DEFLECTION HISTORY OF STRAIGHT, CURVED AND SKEW BRIDGE MODELS UNDER SUSTAINED DEAD LOAD

difference in this outer girder's total length in the two bridges. The results of the skew box girder bridge are somewhat more difficult to compare with those of the straight and curved bridges because the extra dead load required by the skew model for proper simulation of prototype behavior was not put into the cells in the form of steel billets as in the case of the straight and curved models, but in the form of concrete blocks of the required weight on the top deck of the skew bridge. From Fig. 9.14 it may be observed that on completion of the placing of the concrete blocks (in two stages, on the 12th and 14th day respectively after the removal of shoring, the dead load deflections for the skew bridge model agree very well with those of the straight and curved models, and are, in fact, closer to the deflections of the curved bridge.

For an interim period of about 20 days between the 43rd and 64th days after the removal of shoring the concrete blocks were removed again, to allow for the truck and construction vehicle loadings and replaced at the end of this period. Finally the concrete blocks were removed from the bridge deck on the 105th day in preparation for the loading to failure of the skew bridge on the 110th day after removal of the shoring.

If the drop in values due to the removal of the concrete blocks is ignored, it is observed that over the whole deflection history, good agreement is obtained between the skew bridge results and the results of the straight and curved bridges. There is also a tendency for the skew bridge residual deflection values to approach those of the straight bridge and move slightly away from those of the curved bridge as the bridge testing progresses. Considering the various parameters influencing the behavior, such as time lag between the casting of top and

bottom flanges, duration of the total test program, etc., there appears to be no significant differences in the way the three structures behave under sustained dead load.

10. SUMMARY AND CONCLUSIONS FOR VOLUME II

10.1 General Remarks

In the present volume, the reduction, analysis and interpretation of the theoretical and experimental results obtained for a large (1:2.82) scale, 45° skew, continuous, two span, four cell, reinforced concrete box girder bridge model, subjected to working and overload stress levels have been presented. The loading cases discussed have included dead load, point live loads singly or in combination, AASHTO standard truck loads, construction vehicle overloads, and a moving fork lift truck load. In addition to these short time loads the strain, cracking and deflection history of the bridge model prior to the removal of shoring and subsequently under sustained dead load have been presented. The response during ultimate loading to failure is treated separately in Volume III.

The skew bridge model of the present study contained about 9% less main longitudinal reinforcement area at midspan and 17% less main longitudinal reinforcement area over the center support than the earlier tested straight and curved bridge models. This was in accordance with the reduction in longitudinal moments envisaged by the proposed design methods developed from previous research at the University of California and by engineers from the State of California. Possible adoption of the proposed procedure is contingent upon the satisfactory performance of the skew bridge model at the working and overload stress levels, as well as during its ultimate loading to failure. In this regard, the most important conclusion to be advanced based on the results of this research program is that the skew box girder bridge

model performed very satisfactorily under all phases of the loading program from the removal of shoring to the final ultimate loading to failure.

In the following sections, conclusions related to the theoretical analyses, dead load, working stress loads, and overloads will be given, followed by some final general observations.

10.2 Theoretical Analyses

The finite element program CELL, which provides a solution of the skew bridge model as a three dimensional cellular structure composed of top and bottom plates interconnected by vertical web elements, is an accurate and versatile program. It can be used to predict the longitudinal and transverse distribution of theoretical reactions, deflections, internal membrane and plate bending forces and individual girder moments in a skew, continuous box girder bridge structure, assuming it to be a linearly elastic, homogeneous, isotropic and uncracked concrete structure. Conclusions regarding its accuracy in predicting the experimental results for the reinforced concrete model which experienced cracking under dead load, working stress loads, and overloads are discussed later in this chapter.

For the present study, the CELL program was extended to include spring supports under each girder and under the center bent, in consequence of which it was possible to model the actual behavior of the bridge more closely. A SAP analysis using a beam element model, in which the skew box girder bridge system is modelled analytically as a simple three-dimensional frame made up of one-dimensional beam and column elements, can be performed at a small fraction of the time and

cost of a CELL analysis using a finite element model. A SAP analysis gives results for the longitudinal distrib tion of the theoretical total reactions, moments and centerline ceflections which compare quite well with those found from a CELL analysis. However, the SAP analysis gives no information on the transverse distribution of these quantities or the internal membrane forces and plate bending moments which are obtained from the more complex and expensive CELL finite element analysis.

Both of the above analytical models are valuable tools for making theoretical studies and comparisons of various complex bridge systems. Such a detailed comparison of the theoretical results for the similar straight, curved and skew bridge models indicated that while the straight and curved bridges show similar behavior the skew bridge features substantial differences and is sensitive to the type and position of the applied loads.

10.3 Dead Load

Experimental values of total vertical reactions, moments and torques at the end abutments and center bent were well matched with theoretical values obtained from the finite element CELL program. The maximum internal moments in the midspan and center bent regions were smaller for the skew bridge as compared to the straight and curved bridges. The midspan strains in the skew bridge under total dead load indicated an average steel stress of about 12 ksi (83 MPa).

Maximum total dead load deflections occurred in each span at the midspan of the outer girder lying between the acute corner of the bridge model and the center bent. These deflections equalled 0.44 in. (11.2 mm) or about 1/1000 of the span. Over a period of three months

during which the bridge was subjected to numerous live load cycles, under increasing overloads, the sustained dead load deflection increased fourfold due to a combination of creep and increased cracking.

10.4 Working Stress Loads

Theory can be used to predict the total magnitudes of the reactions almost exactly, but the transverse distributions only very approximately, unless the spring constants of the supports are known and included in the analytical model. For deflections, multiplying the theoretical values by magnification factors to take account of cracking, e.g. 1.5 at working stress levels, results in good agreement with measured values.

For point loads along the center girder and on the obtuse side of the span it is found from the CELL analysis and from integration of the forces obtained from strains measured over the box section that the midspan moment in the skew bridge is smaller than would be the case in a similarly loaded straight or curved bridge. However, for point loads on the acute side of the span, the midspan moment in the skew bridge is larger than in the comparable cases for the straight and curved bridges. This behavior is especially important when the positioning of heavy concentrated overloads has to be considered. Load distribution factors for a straight bridge which assume a uniformly stressed cross-section no longer apply to the skew bridge.

Theoretical calculations based on the CELL program predict the transverse distribution of the total moment with sufficient accuracy at undiaphragmed midspan section D. In the other span at section A,

near the staggered midspan diaphragm, much higher experimental values were found for exterior girder 1 on the acute side of the span than the ones predicted by theory. This is probably due to close proximity of the staggered diaphragm to the instrumented section in girder 1.

The vertical experimental reactions at the end supports are virtually uninfluenced when torsional restraint of the center bent is introduced by the addition of supports at locations 1T and 5T at the two ends of the skew center bent. However, it is observed that end moments and torques are diminished by the introduction of the torsional restraint. Theory adequately predicts the effect of the torsional restraint as far as the total east, west and center bent reactions are concerned.

The bridge response under various simulated AASHTO HS 20-44 truck loads [72 kips (320 kN)] and overload construction vehicles [330 kips (1470 kN)] was excellent with maximum measured live load steel stresses of about 6.5 and 10.1 ksi (45 and 70 MPa) for the two and three lane AASHTO truck loads and 14.6 ksi (101 MPa) for the one lane construction vehicle overload. Maximum live deflection registered under the construction vehicle loading was only 0.74 in. (18.8 mm) or about 1/580 of the span.

A study of the shear response of the skew box girder bridge model indicates that the distribution of the internal shear forces to individual girder webs is complex and can be predicted by the CELL program only approximately. For skew box girders the total end support or center bent vertical reactions are balanced not only by the girder web shears, but also by significant transverse slab shears due to the

high transverse distortional resistance of the box section. However, the latter caused no distress in the bridge model.

For all point load cases, skew-symmetry and superposition checks on experimental results were found to be satisfactory, indicating reliability in the measured values.

10.5 Overloads

The total experimental end vertical reactions arising from the skewness of the end abutments continue to be predicted satisfactorily by theory for the stress range 40 to 60 ksi. The total measured end moments and torques decrease considerably with increasing conditioning loads indicating that the eccentricity of the resultant west and east abutment vertical reactions decreases with loads causing overload stresses. This tendency is also noticed in the loading to failure (Volume III) and suggests that the effects of skewness deteriorate somewhat with very high loads. The increase in the total experimental midspan moment due to the abovementioned decrease in end moments is, however, compensated by a simultaneous small decrease in the total vertical end reaction under increasing, conditioning load levels, so that little change occurs in the total midspan moment.

Under all overloads, up to 60 ksi, concrete and steel experimental strains show essentially a linear load vs. strain behavior, and the strains per unit load are almost the same at all load levels. However, a decreasing stiffness occurs due to progressive cracking under increasing overloads, such that the magnification factor relating experimental to theoretical deflections increases from 1.4 at 24 ksi to 2.2 at 60 ksi loadings.

10.6 General Observations

The proximity of the staggered midspan diaphragm in Span I to the instrumentation near location 1A (and also 2A) resulted in an influence on the measured strains for these girders and all experimental results indicate that a larger percentage of the total moment is taken by girder 1 than is estimated by theory. The finite element mesh size used in the CELL FINE analysis allowed only one element between the diaphragm and section A at girders 1 and 2 and emphasizes the need for refined meshes in such critical regions for the estimation of structural behavior. In the undiaphragmed span at section D the agreement between theory and experiment was much better. No apparent need of a midspan diaphragm for the working stress dead and live loads and the construction vehicle overloads was evidenced.

The structural behavior of the skew box girder bridge model makes it possible to decrease certain percentages of the main longitudinal steel reinforcement areas in the regions of maximum positive moment at the midspans and maximum negative moment over the center bent support. However this reduction in steel may only comprise a small amount of the total volume of steel reinforcement in the bridge. The amount of the reduction in required steel for a skew bridge as compared to a similar straight bridge is dependent on a number of factors such as angle of skew; span to width ratio; simple versus continuous bridge; and live to dead load ratios.

For the skew bridge model tested in this investigation it should again be emphasized that its response under all working stress dead and live loads was excellent and it was able to carry increasingly higher

overloads up to the 60 ksi stress level with only increased cracking and some residual deflections, but no signs of any serious distress.

ACKNOWLEDGEMENTS

This investigation was sponsored by the Business and Transportation Agency, Department of Transportation, State of California, and the Federal Highway Administration, United States Department of Transportation.

The contents of this report reflect the views of the authors who are responsible for the facts and the accuracy of the data presented herein. The contents do not necessarily reflect the official views or policies of the State of California or the Federal Highway Administration. This report does not constitute a standard, specification or regulation.

The planning, preparation, construction, supervision, testing, control, analysis and data reduction for a research project of the scope and size of the skew box girder bridge model of the present study necessitate the cooperative assistance and teamwork of all involved.

From the State of California Division of Highways, R. E. Davis, Senior Bridge Engineer of the Research and Development Section, maintained a close and keen interest in the project in all its stages.

R. M. Stephen, Principal Development Engineer, Structural Engineering and Structural Mechanics Division, actively participated in the preliminary planning, design, instrumentation and construction of the box girder bridge model, and deserves special thanks for his assistance and interest.

Of primary importance to the success of the project were the hard work and enthusiasm of the various Research Assistants, Students and Staff working for different periods on the research investigation.

Special acknowledgement should be given to F. Seible, Graduate Research Assistant, who particpated in all phases of the research program

from its inception to the publication of the final reports. Noteworthy were his efficient handling of the CELL computer program for the production of analytical data, and his work on the beam element model.

The smooth conduct of the extensive testing program was made possible by S. J. Thoman and H. Mashhoon, Graduate Research Assistants. W. W. Lau was instrumental in the preparation by computer of the Tables of Experimental Data in Volume IV. J. van Greunen and E. Chan provided assistance at different stages of the work. A. Hafeez was involved with data reduction and preparation of figures and charts.

Dr. Vladimir Kristek from the Technical University of Prague, Czechoslovakia, spent about three months in 1979 as a Visiting Associate Research Engineer on the skew box girder project. He made significant contributions to the study of the shear behavior of the box girder bridge model.

The support provided by the S.E.S.M. Laboratory Staff was excellent and indispensable. D. Wasley gave generous help in the trouble-shooting of the S.E.S.M. Data Acquisition System. A. D. Lawrence, A. Costa, R. Parsons and H. Williams enabled full utilization of the skills and resources of the Mechanical and Electronics Shops. R. Knowles helped in matters dealing with purchases and supplies, xerox reductions, etc.

Last but not least, the visual appearance of this set of reports owes much to the skillful efforts of the Graphics staff composed of A. Klash, G. Feazell and A. Pertschuk, to the typing staff composed of J. Kono and E. Dwyer, and to the photographs produced by E. Caine.

REFERENCES

1. Bouwkamp, J. G., Scordelis, A. C., and Wasti, S. T., "Structural Behavior of a Two Span Reinforced Concrete Box Girder Bridge Model, Volume I," Structural Engineering and Structural Mechanics Report No. UC SESM 71-5, University of California, Berkeley, April 1971.

2. Scordelis, A. C., Bouwkamp, J. G., and Wasti, S. T., "Structural Behavior of a Two Span Reinforced Concrete Box Girder Bridge Model, Volume II," Structural Engineering and Structural Mechanics Report No. UC SESM 71-16, University of California, Berkeley, October 1971.

3. Scordelis, A. C., Bouwkamp, J. G., and Wasti, S. T., "Structural Behavior of a Two Span Reinforced Concrete Box Girder Bridge Model, Volume III," Structural Engineering and Structural Mechanics Report, No. UC SESM 71-17, University of California, Berkeley, October 1971.

4. Scordelis, A. C., Bouwkamp, J. G., and Larsen, P. K., "Structural Behavior of a Curved Two Span Reinforced Concrete Box Girder Bridge Model Volume I,"Structural Engineering and Structural Mechanics Report No. UC SESM 74-5, University of California, Berkeley, September 1974.

5. Scordelis, A. C., Bouwkamp, J. G., and Larsen, P. K.,"Structural Behavior of a Curved Two Span Reinforced Concrete Box Girder Bridge Model, Volume II," Structural Engineering and Structural Mechanics Report No. UC SESM 74-6, University of California, Berkeley, September 1974.

6. Scordelis, A. C., Bouwkamp, J. G., and Larsen, P. K., Structural Behavior of a Curved Two Span Reinforced Concrete Box Girder Bridge Model, Volume III," Structural Engineering and Structural Mechanics Report No. UC SESM 74-7, University of California, Berkeley, September 1974.

7. Scordelis, A. C., Bouwkamp, J. G., and Wasti, S. T., "Structural Response of Concrete Box Girder Bridge," Journal of the Structural Division, Proceedings of the American Society of Civil Engineers, Volume 99, No. ST10, October 1973.

8. Bouwkamp, J. G., Scordelis, A. C., and Wasti, S. T., "Ultimate Strength of Concrete Box Girder Bridge," Journal of the Structural Division, Proceedings of the American Society of Civil Engineers, Vol. 100, No. ST 1, January 1974.

9. Scordelis, A. C., and Larsen, P. K., "Structural Response of Curved RC Box Girder Bridge," Journal of the Structural Division, Proceedings of the American Society of Civil Engineers, Vol. 103, No. ST8, August 1977.

10. Scordelis, A. C., Larsen, P. K., and Elfgren, L. G., "Ultimate Strength of Curved RC Box Girder Bridge," Journal of the Structural Division, Proceedings of the American Society of Civil Engineers, Vol. 103, No. ST8, August 1977.

11. Bouwkamp, J. G., Scordelis, A. C., and Wasti, S. T., "Structural Behavior of a Reinforced Concrete Box Girder Bridge," Proceedings, Conference on Modern Developments in Bridge Design and Construction, Cardiff, Great Britain, April 1971.

12. Scordelis, A. C., Bouwkamp, J. G., and Wasti, S. T., "Study of AASHO Loadings on a Concrete Box Girder Bridge," Highway Research Record No. 428, Highway Research Board, Washington, D. C., 1973.

13. Scordelis, A. C., Elfgren, L. G., and Larsen, P. K., "Time-Dependent Behavior of Concrete Box Girder Bridges," Journal of the American Concrete Institute, Title No. 76-9, January 1979.

14. Willam, K. J., and Scordelis, A. C., "Computer Program for Cellular Structures of Arbitrary Plan Geometry," Structural Engineering and Structural Mechanics Report No. UC SESM 70-10, University of California, Berkeley, September 1970.

15. Willam, K. J., and Scordelis, A. C., "Cellular Structures of Arbitrary Plan Geometry," Journal of the Structural Division, Proceedings of American Society of Civil Engineers, Volume 98, No. ST 7, July 1972.

16. Comartin, C. D., and Scordelis, A. C., "Analysis and Design of Skew Box Girder Bridges," Structural Engineering and Structural Mechanics Report No. UC SESM 72-14, University of California, Berkeley, December 1972.

17. Scordelis, A. C., "Analytical Solutions for Box Girder Bridges," Proceedings, Conference on Modern Developments in Bridge Design and Construction, Cardiff, Great Britain, April 1971.

18. Scordelis, A. C., "Analytical and Experimental Studies of Multi-Cell Concrete Box Girder Bridges," Bulletin of the International Association for Shell and Spatial Structures, Madrid, No. 58, August 1975.

19. Scordelis, A. C., and Meyer, C., "Wheel Load Distribution in Concrete Box Girder Bridges," Structural Engineering and Structural Mechanics Report No. SESM 69-1, University of California, Berkeley, January 1969.

20. Lin, C. S., and Scordelis, A. C., "Computer Program for Bridges on Flexible Bents," Structural Engineering and Structural Mechanics Report No. UC SESM 71-24, University of California, Berkeley, December 1971.

21. Godden, W. G., and Aslam, M., "Model Studies of Skew Box Girder Bridges," Structural Engineeri g and Structural Mechanics Report No. UC SESM 71-26, University of California, Berkeley, December 1971.

22. Godden, W. G., and Aslam, M., "Model Studies of Skew Multicell Girder Bridges," Journal of the Engineering Mechanics Division, Proceedings of the American Society of Civil Engineering, Volume 99, No. EM 1, February 1973.

23. "Standard Specifications for Highway Bridges," American Association of State Highway and Transportation Officials [AASHTO], Twelfth Edition, Washington, D. C., 1977.

24. Davis, R. E., Kozak, J. J., and Scheffey, C. F., "Structural Behavior of Concrete Box Girder Bridge," National Research Council - Highway Research Report No. 1976, 1965.

25. Kennedy, J. B., and Tamberg, K. G., "Problems of Skew in Concrete Bridge Design," Department of Highways, Ontario, Report No. RR 144, March 1969.

26. Mehrain, M., "Finite Element Analysis of Skew Composite Girder Bridges," Structural Engineering and Structural Mechanics Report No. UC SESM 67-28, University of California, Berkeley, California, November 1967.

27. Powell, G. H., Bouwkamp, J. G., and Buckle, I. G., "Behavior of Skew Highway Bridges," Structural Engineering and Structural Mechanics Report No. UC SESM 69-9, University of California, Berkeley, California, February 1969.

28. Clark, L. A., "The Provision of Reinforcement in Simply Supported Skew Bridge Slabs in accordance with Elastic Moment Fields," Technical Report 42.450, Cement and Concrete Association, London, November 1970.

29. Clark, L. A., "The Service Load of Short-Span Skew Slab Bridges Designed by Yield Line Theory," Technical Report 42.464, Cement and Concrete Association, London, May 1972.

30. Clark, L. A., "Tests on Slab Elements and Skew Slab Bridges Designed in Accordance with the Factored Elastic Moment Field," Technical Report 42.474, Cement and Concrete Association, London, September 1972.

31. Hallbjörn, L., "Continuous Reinforced Concrete Skew Slabs Supported on Columns," Publication 72:5, Division of Structural Engineering and Bridge Building, Royal Institute of Technology, Stockholm, 1972.

32. Meades, P. and Green, R., "Model Studies for Voided Post-tensioned Concrete Slab Bridges," Research Report RR 195, Ministry of Transportation and Communications, Ontario, Canada, 1974.

33. Green, R., "Voided Two-Span Skew Slab - A Model Study," RTAC Forum, Vol. 2, No. 1, Canada, 1978.

34. Panak, J. J., "Skewed Multi-Beam Bridges with Precast Box Girders," Report No. 206 IF, Texas State Department of Highways and Public Transportation, Austin, Texas, September 1977.

35. Ghali, A., "Analysis of Continuous Skew Concrete Birder Bridges," Proceedings of the ACI First International Symposium on Concrete Bridge Design, ACI Special Publication No. SP-23, Detroit, Michigan, 1969.

36. Sisodiya, R. G., Cheung, Y. K., and Ghali, A., "Finite Element Analysis of Skew, Curved Box Girder Bridge," IABSE Mémoires, Vol. 30-II, Zürich, 1970.

37. Sisodiya, R. G., Ghali, A., and Cheung, Y. K., "Diaphragms in Single and Double-Cell Box Girder Bridges with Varying Angle of Skew," University of Calgary Report No. CE-71-21, Calgary, Canada, September 1971.

38. Pama, R., Nimityongskul, P., Pribadi, D., and Lee, S-L., "Model Studies of Double-Cell Box Girder Bridge with Intermediate Diaphragms," Bridge Engineering, Vol. 2, Transportation Research Board No. 665, National Academy of Sciences, Washington, D. C., 1978.

39. Billington, C. J., and Dowling, P. J., "The Influence of Skew Supports on the Behaviour of Multibox Bridges," Mémoires, IABSE No. 36-I, Zürich, 1976.

40. Maisel, B. I., Rowe, R. E., and Swann, R. A., "Concrete Box-Girder Bridges," The Structural Engineer, Vol. 51, No. 10, London, October 1973.

41. Maisel, B. I., and Roll, F., "Methods of Analysis and Design of Concrete Boxbeams with Side Cantilevers, Technical Report No. 42.494, Cement and Concrete Association, London, November 1974.

42. Swann, R. A., "A Feature Survey of Concrete Box Spine-Beam Bridges," Cement and Concrete Association Technical Report No. 42.469, London, June 1972.

43. Wallace, M. R., "Studies of Skewed Concrete Box-Girder Bridges," Transportation Research Record 607 - "Bridge Design, Testing and Evaluation," Transportation Research Board, National Academy of Sciences, Washington, D. C., 1976.

44. Carpenter, J. E., Hanson, J. M., Fiorato, A. E., Russell, H. G., Meinheit, D. F., Rosenthal, I., Corley, W. G., and Hognestad, E., "Analysis and Design of Bridge Bents," Final Report Draft, Vols. I and II, Portland Cement Association, Skokie, Illinois, October 1973.

45. Sanders, W. W., and Elleby, H. A., "Distribution of Wheel Loads on Highway Bridges," National Cooperative Highway Research Program Report 83, Highway Research Board, Washington, D. C., 1970.

46. Leonhardt, F., and Walther, R., "Shear Tests on T-Beams with Varying Shear Reinforcement" (Schubversuche an Plattenbalken mit unterschiedlicher Schubbewehrung. In German). Deutscher Ausschuss für Stahlbeton, Heft 156, Berlin 1963, 84 pp.

47. Leonhardt, F., Walther, and Dilger, W., "Shear Tests on Continuous Beams" (Schubversuche an Durchlaufträgern. In German). Deutscher Ausschuss für Stahlbeton, Heft 163, Berlin 1964, 138 pp.

48. Elfgren, L., "Reinforced Concrete Beams Loaded in Combined Torsion, Bending and Shear. A Study of the Ultimate Load-Carrying Capacity," Division of Concrete Structures, Publication 71:3, Chalmers University of Technology, 2nd Ed., Göteborg 1972, 230 pp.

49. Wilson, E. L., "SOLID SAP - A Static Analysis Program for Three Dimensional Solid Structures," Structural Engineering and Structural Mechanics Report No. UC SESM 71-19, University of California, Berkeley, September 1971, Revised December 1972.

50. Davis, R. E., "Structural Behavior of a Skew, Reinforced Concrete, Box Girder Model, Vol. 1, Design," Report No. FHWA-CA-ST-487-78-01, Office of Structures Design, Division of Project Development, California Department of Transportation, January 1978.

APPENDIX OF RESEARCH RFPORTS AND TECHNICAL PAPERS

Research Reports and Techn.cal Papers that have been published on the research on Box Girder Bridges carried out in the Division of Structural Engineering and Structural Mechanics, University of California, Berkeley are catalogued in this appendix under two headings: List A for Research Reports and List B for Technical Papers.

Almost all the research reports (List A) have been placed on file with the U. S. Department of Commerce and may be obtained on request for cost of reproduction by writing to the following address:

National Technical Information Service
Operations Division
Springfield, Virginia 22151

The accession number (shown in parentheses on reference List A) should be specified when ordering a particular report.

RESEARCH REPORTS AND TECHNICAL PAPERS PUBLISHED ON BOX GIRDER BRIDGE RESEARCH PERFORMED AT THE UNIVERSITY OF CALIFORNIA, BERKELEY

A. Research Reports

1. Scordelis, A. C., "Analysis of Simply Supported Box Girder Bridges," Structural Engineering and Structural Mechanics Report No. SESM 66-17, University of California, Berkeley, October 1966 (PB 175 646).

2. Scordelis, A. C., "Analysis of Continuous Box Girder Bridges," Structural Engineering and Structural Mechanics Report No. SESM 67-25, University of California, Berkeley, November 1967 (PB 178 355).

3. Scordelis, A. C., and Meyer, C., "Wheel Load Distribution in Concrete Box Girder Bridges," Structural Engineering and Structural Mechanics Report No. SESM 69-1, University of California, Berkeley, January 1969 (PB 183 923).

4. Willam, K. J., and Scordelis, A. C., "Analysis of Orthotropic Folded Plates with Eccentric Stiffeners," Structural Engineering and Structural Mechanics Report No. SESM 70-2, University of California, Berkeley, February 1970 (PB 191 051).

5. Meyer, C., and Scordelis, A. C., "Computer Program for Prismatic Folded Plates with Plate and Beam Elements," Structural Engineering and Structural Mechanics Report No. SESM 70-3, University of California, Berkeley, February 1970 (PB 191 050).

6. Meyer, C., and Scordelis, A. C., "Analysis of Curved Folded Plate Structures," Structural Engineering and Structural Mechanics Report No. UC SESM 70-8, University of California, Berkeley, June 1970 (PB 193 535).

7. Willam, K. J., and Scordelis, A. C., "Computer Program for Cellular Structures of Arbitrary Plan Geometry," Structural Engineering and Structural Mechanics Report No. UC SESM 70-10, University of California, Berkeley, September 1970 (PB 196 143).

8. Meyer, C., "Analysis and Design of Curved Box Girder Bridges," Structural Engineering and Structural Mechanics Report No. UC SESM 70-22, University of California, Berkeley, December 1970 (PB 197 289).

9. Bouwkamp, J. G., Scordelis, A. C., and Wasti, S. T., "Structural Behavior of a Two Span Reinforced Concrete Box Girder Bridge Model, Volume I," Structural Engineering and Structural Mechanics Report No. UC SESM 71-5, University of California, Berkeley, April 1971 (PB 199 187).

10. Scordelis, A. C., Bouwkamp, J. G., and Wasti, S. T., "Structural Behavior of a Two Span Reinforced Concrete Box Girder Bridge Model, Volume II," Structural Engineering and Structural Mechanics Report No. UC SESM 71-16, University of California, Berkeley, October 1971 (PB 210 431).

11. Scordelis, A. C., Bouwkamp, J. G., and Wasti, S. T., "Structural Behavior of a Two Span Reinforced Concrete Box Girder Bridge Model, Volume III," Structural Engineering and Structural Mechanics Report No. UC SESM 71-17, University of California, Berkeley, October 1971.

12. Meyer, C., and Scordelis, A. C., "Computer Program for Non-Prismatic Folded Plates with Plate and Beam Elements," Structural Engineering and Structural Mechanics Report No. UC SESM 71-23, University of California, Berkeley, December 1971 (PB 220 197).

13. Lin, C. S., and Scordelis, A. C., "Computer Program for Bridges on Flexible Bents," Structural Engineering and Structural Mechanics Report No. UC SESM 71-24, University of California, Berkeley, December 1971 (PB 210 171).

14. Godden, W. G., and Aslam, M., "Model Studies of Skew Box Girder Bridges," Structural Engineering and Structural Mechanics Report No. UC SESM 71-26, University of California, Berkeley, December 1971 (PB 223 120).

15. Comartin, C. D., and Scordelis, A. C., "Analysis and Design of Skew Box Girder Bridges," Structural Engineering and Structural Mechanics Report No. UC SESM 72-14, University of California, Berkeley, December 1972 (PB 226 793).

16. Godden, W. G., and Aslam, M., "Model Studies of Curved Box Girder Bridges," Structural Engineering and Structural Mechanics Report No. UC SESM 73-5, University of California, Berkeley, March 1973 (PB 226 842/AS).

17. Scordelis, A. C., Bouwkamp, J. G., and Larsen, P. K., "Structural Behavior of a Curved Two Span Reinforced Concrete Box Girder Bridge Model, Volume I," Structural Engineering and Structural Mechanics Report No. UC SESM 74-5, University of California, Berkeley, September 1974 (PB 242 523/AS).

18. Scordelis, A. C., Bouwkamp, J. G., and Larsen, P. K., "Structural Behavior of a Curved Two Span Reinforced Concrete Box Girder Bridge Model, Volume II," Structural Engineering and Structural Mechanics Report No. UC SESM 74-6, University of California, Berkeley, September 1974 (PB 242 524/AS).

19. Scordelis, A. C., Bouwkamp, J. G., and Larsen, P. K., "Structural Behavior of a Curved Two Span Reinforced Concrete Box Girder Bridge Model, Volume III," Structural Engineering and Structural Mechanics Report No. UC SESM 74-7, University of California, Berkeley, September 1974 (PB 242 525/AS).

20. Kabir, A. F., and Scordelis, A. C., "Computer Programs for Curved Bridges on Flexible Bents," Structural Engineering and Structural Mechanics Report No. UC SESM 74-10, University of California, Berkeley, September 1974 (PB 242 470/AS).

21. Van Zyl, S., "Analysis of Curved Segmentally Erected Prestressed Concrete Box Girder Bridges," Structural Engineering and Structural Mechanics, Report No. UC SESM 78-2, University of California, Berkeley, January 1978 (PB 284 939/AS).

B. Technical Papers

1. DeFries-Skene, A., and Scordelis, A. C., "Direct Stiffness Solution for Folded Plates," Journal of the Structural Division, Proceedings of American Society of Civil Engineers, Volume 90, No. ST-3, June 1964.

2. Scordelis, A. C., Davis, R. E., and Lo, K. S., "Load Distribution in Concrete Box Girder Bridges," ACI Proceedings of First International Symposium on Concrete Bridge Deisgn, Toronto, Canada, April 1967, ACI Publication SP-23, 1969.

3. Scordelis, A. C., and Davis, R. E., "Stresses in Continuous Concrete Box Girder Bridges," ACI Proceedings of Second International Symposium on Concrete Bridge Design, Chicago, April 1969, ACI Publication SP-26, 1971.

4. Lo, K. S., and Scordelis, A. C., "Finite Segment Analysis of Folded Plates," Journal of the Structural Division, Proceedings of American Society of Civil Engineers, Volume 95, No. ST5, May 1969.

5. Willam, K. J., and Scordelis, A. C., "Analysis of Eccentrically Stiffened Folded Plates," Proceedings of IASS Symposium on Folded Plates and Prismatic Structures, Vienna, September 1970.

6. Scordelis, A. C., "Analytical Solutions for Box Girder Bridges," Proceedings, Conference on Modern Developments in Bridge Design and Construction, Cardiff, Great Britain, April 1971.

7. Bouwkamp, J. G., Scordelis, A. C., and Wasti, S. T., "Structural Behavior of a Reinforced Concrete Box Girder Bridge," Proceedings, Conference on Modern Developments in Bridge Design and Construction, Cardiff, Great Britain, April 1971.

8. Meyer, C., and Scordelis, A. C., "Analysis of Curved Folded Plate Structures," Journal of the Structural Division, Proceedings of American Society of Civil Engineers, Volume 98, No. ST1, January 1972.

9. Willam, K. J., and Scordelis, A. C., "Cellular Structures of Arbitrary Plan Geometry," Journal of the Structural Division, Proceedings of American Society of Civil Engineers, Volume 98, No. ST7, July 1972.

10. Godden, W. G., and Aslam, M., "Model Studies of Skew Multicell Girder Bridges," Journal of the Engineering Mechanics Division, Proceedings of the American Society of Civil Engineers, Volume 99, No. EM 1, February 1973.

11. Scordelis, A. C., Bouwkamp, J. G., and Wasti, S. T., "Study of AASHO Loadings on a Concrete Box Girder Bridge," Highway Research Record No. 428, Highway Research Board, Washington, D. C., 1973.

12. Scordelis, A. C., Bouwkamp, J. G., and Wasti, S. T., "Structural Response of a Concrete Box Girder Bridge," Journal of the Structural Division, Proceedings of the American Society of Civil Engineers, Volume 99, No. ST10, October 1973.

13. Scordelis, A. C., Bouwkamp, J. G., and Wasti, S. T., "Ultimate Strength of a Concrete Box Girder Bridge," Journal of the Structural Division, Proceedings of the American Society of Civil Engineers, Vol. 100, ST1, January 1974.

14. Aslam, M., and Godden, W. G., "Model Studies of Multicell Curved Box-Girder Bridges," Journal of the Engineering Mechanics Division, Proceedings of the American Society of Civil Engineering, Vol. 101, No. EM3, June 1975.

15. Scordelis, A. C., "Folded Plates for Bridges," Bulletin of the International Association for Shell and Spatial Structures, Madrid, No. 57, April 1975.

16. Scordelis, A. C., "Analytical and Experimental Studies of Multi-Cell Concrete Box Girder Bridges," Bulletin of the International Association for Shell and Spatial Structures, Madrid, No. 58, August 1975.

17. Scordelis, A. C. and Larsen, P. K., "Structural Response of Curved RC Box Girder Bridge," Journal of the Structural Division, Proceedings of the American Society of Civil Engineers, Vol. 103, No. ST8, August 1977.

18. Scordelis, A. C., Larsen, P. K. and Elfgren, L. G., "Ultimate Strength of Curved RC Box Girder Bridge," Journal of the Structural Division, Proceedings of the American Society of Civil Engineers, Vol. 103, No. ST8, August 1977.

19. Scordelis, A. C., Elfgren, L. G. and Larsen, P. K., "Time-Dependent Behavior of Concrete Box Girder Bridges," Journal of the American Concrete Institute, Vol. 76, No. 76-9, January 1979.

20. Van Zyl, S., and Scordelis, A. C., "Analysis of Curved Prestressed Segmental Bridges," Journal of the Structural Division, Proceedings of the American Society of Civil Engineers, Vol. 105, No. ST 11, November 1979.